

## THÈSE

en cotutelle internationale

entre l'Université Lille 1 et l'Université d'État de Saint Pétersbourg (Russie)

présentée en vue de l'obtention du grade de

**DOCTEUR DE L'UNIVERSITÉ LILLE 1**

discipline : Chimie

spécialité : Molécules et Matière condensée

soutenue publiquement par

**Vadim M. KOVRUGIN**

à l'Université d'État de Saint Pétersbourg

le 22 septembre 2015

---

# Cristallochimie de Nouveaux Composés d'Oxyde du $\text{Se}^{4+}$ et du $\text{Se}^{6+}$

---

### Membres du jury :

<b>Dr. Olivier HERNANDEZ</b>	MdC, Institut des Sciences Chimiques, Université Rennes 1, France	Rapporteur
<b>Dr. Dmitri O. CHARKIN</b>	Associate Professor, Faculté de Chimie, Université d'État de Moscou, Russie	Rapporteur
<b>Dr. Igor V. PEKOV</b>	Professor, Faculté de Géologie, Université d'État de Moscou, Russie	Examineur
<b>Dr. Vladimir G. KRIVOVICHEV</b>	Professor, Institut des Sciences de la Terre, Université d'État de Saint Pétersbourg, Russie	Examineur
<b>Dr. Olivier MENTRÉ</b>	DR CNRS, Unité de Catalyse et de Chimie du Solide, Université Lille 1, France	Directeur de thèse
<b>Dr. Sergey V. KRIVOVICHEV</b>	Professor, Institut des Sciences de la Terre, Université d'Etat de Saint Pétersbourg, Russie	Co-Directeur de thèse
<b>Dr. Marie COLMONT</b>	MdC ENSCL, Unité de Catalyse et de Chimie du Solide, Université Lille 1, France	Co-Encadrant

Thèse préparée au sein du lab. UCCS (UMR 8181) et du dépt. de cristallographie (SPbSU)  
École doctorale Sciences de la Matière, du Rayonnement et de l'Environnement



# ABSTRACT

This work deals with the synthesis and characterization of novel oxide materials containing selenium in the oxidation states of +4 or +6. The structural types occurring in 33 known oxoselenite minerals have an amazing variety, and cover the whole field from *0D* isolated complexes to *3D* frameworks, which offer unexploited potentialities in terms of physical properties. This thesis aims to synthesize and investigate new Se based compounds, using methods inspired by mineralogical processes.

Information based on original building units assembled into original architectures have been deduced and compared to related inorganic phases of the literature. In the present study, our innovative so-called “geo-inspired” approach is applied in order to obtain complex novel crystalline compounds. This approach assumes emulation and modelling of natural crystal growth processes.

Herein, we used either a traditional descriptive procedure based on consideration of the crystal structures in terms of coordinations of cations, or the modern theory of anion-centered tetrahedra developed by the St. Petersburg school of crystallography and the UCCS group of solid-state chemistry in Lille, in cases when the traditional structural interpretation does not reflect basic principles of crystal chemistry. Thus, several metal-oxide chemical systems with  $\text{Se}^{4+/6+}$  and various metals ( $\text{Cu}^{+/2+}$ ,  $\text{Ni}^{2+}$ ,  $\text{Co}^{2+}$ ,  $\text{V}^{4+/5+}$ ,  $\text{Mn}^{2+}$ ,  $\text{Fe}^{3+}$ ,  $\text{Pb}^{2+}$ ,  $\text{Bi}^{3+}$ ,  $\text{U}^{6+}$ ) were studied in the context of the present work.

The thesis contains results of synthetic procedures, and crystal chemical characterization of 39 new metal selenites, selenates, and selenite-selenates. The analogy of selenite groups with phosphites was also investigated. Main results are described with references to more detailed publications given in the appendices.

**Keywords:** selenite, selenate, uranyl, vanadate, phosphite, copper, nickel, cobalt, manganese, lead, bismuth, iron, synthesis, crystal structure, single crystal X-ray analysis, oxo-centered tetrahedra

# RÉSUMÉ

Ce manuscrit est consacré à la synthèse et la caractérisation de nouveaux matériaux d'oxyde à base de sélénium dans les états d'oxydation +4 ou +6. Les types structuraux rencontrés parmi les 33 oxy sélénites minéraux montrent une diversité structurale étonnante, et couvrent le champ des dimensionnalités  $0D$  à  $3D$ , offrant ainsi des potentialités inexploitées en termes des propriétés physiques. Cette thèse a visé la synthèse de l'étude de nouveaux composés du Se, en utilisant des méthodes de synthèse essentiellement inspirées des conditions de croissance des minéraux.

Les informations basées sur l'assemblage de briques élémentaires originales dans des architectures structurales ont été déduites et comparées aux données de la littérature sur des phases proches.

Lors de ce travail, notre approche « géo-inspirée » innovante a été appliquée afin d'obtenir de nouveaux polytypes complexes. Nous avons donc utilisé des procédés simulant les conditions de croissance des minéraux. En termes de description, nous avons également utilisé soit le modèle « standard » basé sur l'examen des structures cristallines en termes de coordinations de cations, soit des outils plus modernes basés sur l'assemblage de tétraèdres anions-centrés développée par l'école de la cristallographie de Saint-Petersbourg et par le groupe de chimie du solide de l'UCCS, à Lille, et ce dans les cas où l'interprétation structurale traditionnelle ne reflète pas les principes de base de la cristallographie. Finalement, plusieurs systèmes chimiques métal-oxyde avec du  $\text{Se}^{4+/6+}$  et divers métaux ( $\text{Cu}^{+2+}$ ,  $\text{Ni}^{2+}$ ,  $\text{Co}^{2+}$ ,  $\text{V}^{4+/5+}$ ,  $\text{Mn}^{2+}$ ,  $\text{Fe}^{3+}$ ,  $\text{Pb}^{2+}$ ,  $\text{Bi}^{3+}$ ,  $\text{U}^{6+}$ ) ont été étudiés dans le cadre de ce manuscrit.

La thèse contient les résultats des procédures synthétiques et de la caractérisation cristallographique des 39 nouveaux sélénites, sélénates et sélénite-sélénates des métaux. Les principaux résultats sont donnés et font référence aux publications plus détaillées données en annexe.

**Mots-clés:** sélénite, sélénate, uranyle, vanadate, phosphite, cuivre, nickel, cobalt, manganèse, fer, plomb, bismuth, synthèse, structure cristalline, analyse sur monocristal par diffraction des Rayons-X, tétraèdres oxo-centrés

**Supervisors**

Prof. Dr. Olivier Mentré  
Unité de Catalyse et de Chimie du Solide  
UMR 8181 CNRS  
Université Lille 1, France

Prof. Dr. Sergey V. Krivovichev  
Department of Crystallography  
Institute of Earth Sciences  
Saint-Petersburg State University, Russia

**Co-Encadrant**

Ass. Prof. Dr. Marie Colmont  
Unité de Catalyse et de Chimie du Solide  
UMR 8181 CNRS  
Université Lille 1, France

## Jury

Ass. Prof. Dr. Olivier Hernandez (rapporteur)  
Institut des Sciences Chimiques de Rennes  
UMR 6226 CNRS  
Université Rennes 1, France

Ass. Prof. Dr. Dmitri O. Charkin (rapporteur)  
Department of Inorganic Chemistry  
Faculty of Chemistry  
Moscow State University, Russia

Prof. Dr. Igor V. Pekov (examinateur)  
Department of Mineralogy  
Faculty of Geology  
Moscow State University, Russia

Prof. Dr. Vladimir G. Krivovichev (examinateur)  
Department of Mineralogy  
Institute of Earth Sciences  
Saint-Petersburg State University, Russia

Prof. Dr. Olivier Mentré (directeur de thèse)  
Unité de Catalyse et de Chimie du Solide  
UMR 8181 CNRS  
Université Lille 1, France

Prof. Dr. Sergey V. Krivovichev (co-directeur de thèse)  
Department of Crystallography  
Institute of Earth Sciences  
Saint-Petersburg State University, Russia

Ass. Prof. Dr. Marie Colmont (co-encadrant)  
Unité de Catalyse et de Chimie du Solide  
UMR 8181 CNRS  
Université Lille 1, France

## Opponents

Prof. Dr. Anatoly N. Zaitsev  
Department of Mineralogy  
Institute of Earth Sciences  
Saint-Petersburg State University, Russia

Prof. Dr. Igor V. Pekov  
Department of Mineralogy  
Faculty of Geology  
Moscow State University, Russia

Prof. Dr. Vladimir G. Krivovichev  
Department of Mineralogy  
Institute of Earth Sciences  
Saint-Petersburg State University, Russia

Prof. Dr. Olivier Mentré  
Unité de Catalyse et de Chimie du Solide  
UMR 8181 CNRS  
Université Lille 1, France

Ass. Prof. Dr. Olivier Hernandez  
Institut des Sciences Chimiques de Rennes  
UMR 6226 CNRS  
Université Rennes 1, France

Ass. Prof. Dr. Dmitri O. Charkin  
Department of Inorganic Chemistry  
Faculty of Chemistry  
Moscow State University, Russia

Ass. Prof. Dr. Sergey N. Britvin  
Department of Crystallography  
Institute of Earth Sciences  
Saint-Petersburg State University, Russia

## ACKNOWLEDGEMENTS

First, I would like to express my sincere gratitude to my supervisors, Prof. Dr. Sergey V. Krivovichev and Prof. Dr. Oliver Mentré. I am extremely thankful and indebted to them for sharing valuable expertise, encouragement extended to me. They gave me an incredible opportunity to work and write this thesis under their High-level guidance.

A heartfelt, special word of my thanks goes to Ass. Prof. Dr. Marie Colmont, my French co-encadrant, for insightful discussions, her genuine caring and concern, and devoting so much time to me during this international co-tutorial project.

Besides my mentors, I would also like to thank the members of the defence committee: Ass. Prof. Dr. Olivier Hernandez, Ass. Prof. Dr. Dmitri O. Charkin, Prof. Dr. Igor V. Pekov, Prof. Dr. Vladimir G. Krivovichev, Prof. Dr. Anatoly N. Zaitsev, and Ass. Prof. Dr. Sergey N. Britvin, for their acceptance to be in the jury, and for having critically reviewed my work.

I wish to express my sincere thanks to Ass. Prof. Dr. Vladislav V. Gurzhiy, who was always willing to help and to give his helpful advice. I started with him my undergraduate research work dealing with the uranyl compounds, which has been evolved into this Ph.D. thesis.

I am also very thankful to Ass. Prof. Dr. Oleg I. Siidra for his excellent scientific suggestions, knowledge, professionalism, and our common publications. He visited annually the UCCS laboratory to work on joint projects with French colleagues, when I was staying in France, and helped me in practice with my research in the lab.

My gratitude is also extended to the personnel of the UCCS laboratory in Lille, Frédéric Capet, Maxence Vandewalle, Nora Djelal, Laurence Burylo, Prof. Sylvie Daviero-Minaud, Prof. Marrielle Huvé, and Prof. Pascal Roussel. Their work was of high quality and efficient. I would like to emphasize my comrades, Almaz and Jacob, with whom I was collaborating in Lille at the beginning of my work. I am also thankful to all my international friends, PhD students, who are (or have been) working in the lab for creating a jovial atmosphere in the workplace: Anne-Lise, Annie, Blaise, Clément, Denys, Esperanza, Florence, Florent, Frédérique, Guillaume, Guiliano, Manon, Margot, Marine, Nacho, Nathalie, Nicolas, Raynald, Rénaud, Tanguy, Xavier.

The present co-tutorial research work would not have been possible without the scholarship doctoral program of the Embassy of France in Russia: *la bourse de doctorat en cotutelle de thèse en Fédération de Russie (la bourse doctorale Vernadski)*. This co-tutorial research project allows students to be enrolled simultaneously at each involved institution and be awarded a double doctoral degree by the two institutions in the case of a successful defence of the thesis. I am very grateful to the French Government for creating this outstanding doctoral program allowing students to gain invaluable international experience.

I would like also to thank my parents for supporting and helping me throughout my life. I should especially thank my mom, Svetlana, for being so caring, responsible, loving and having great faith in my abilities.

Last, but certainly not least, I would like to give my thanks to my cat, Belka, who inspired me from the beginning of my education started in school and still to this day.



The present work was carried out under the framework of the international co-tutorial thesis project between St. Petersburg State University (Russia) and University of Lille 1 (France) supported by the Embassy of France in Russia, the French Government, and managed by the Agency Campus France.

Financial support was also provided through the Multi-InMaDe project (grant ANR 2011-JS-0800301), the Federal Target Program “Scientific and Scientific-Pedagogical Personnel of the Innovative Russia” (grant 02.740.11.0326), Russian Science Foundation (grant 14-17-00071), Russian Foundation for Basic Research (grant 12-05-33097), and the St. Petersburg State University (internal grants 3.37.84.2011, 3.38.136.2014).

The experimental work including X-ray diffraction studies were performed predominantly in the Unité de catalyse et de chimie du solide of the University of Lille 1, and in the X-ray Diffraction Resource Centre of the St. Petersburg State University. The Fonds Européen de Développement Régional (FEDER), CNRS, Région Nord Pas-de-Calais, and Ministère de l’Education Nationale de l’Enseignement Supérieur et de la Recherche are acknowledged for funding the X-ray diffractometers in the University of Lille 1.

## LIST OF FIGURES

FIGURE 2.1	General scheme of the CVT method – (a), the source zone of the tube – (b), the crystals of $K[Cu_5O_2](SeO_3)_2Cl_3$ ( <b>c2.1</b> ) picked out from the source zone – (c), and a common view of the sealed silica tube after the CVT synthesis – (d). .....	9
FIGURE 2.2	The crystal structures of $A[Cu_5O_2](SeO_3)_2Cl_3$ ( $A^+ = K^+$ ( <b>c2.1</b> ), $Na^+$ ( <b>c2.2</b> )) in two different projections featuring side and top view of the $[O_2Cu_5]^{6+}$ sheet of oxocentered $(OCu_4)^{6+}$ tetrahedra highlighted by red colour. ....	10
FIGURE 2.3	The crystal structures of $K[Cu_5O](SeO_3)_2Cl$ ( <b>c2.3</b> ) and $Na_2[Cu_7O_2](SeO_3)_4Cl_4$ ( <b>c2.4</b> ). The $(OCu_4)^{6+}$ tetrahedra are highlighted by red colour. ....	11
FIGURE 2.4	Projections of the $[Cu(HSeO_3)_2]^0$ sheet (a) and the crystal structure of $[NaCl][Cu(HSeO_3)_2]$ ( <b>c2.5</b> ) featuring two-dimensional $[Cu(HSeO_3)_2]^0$ sheets with intercalated ...-Na-Cl-... chains. ....	12
FIGURE 2.5	Projections of the structures of $[Cu^+Cl_2][Pb_2Cu_9O_4](SeO_3)_4Cl_5$ ( <b>c2.6</b> ) – (a) and (b), $[Cu^+Cl_2][PbCu_5O_2](SeO_3)_2Cl_3$ ( <b>c2.7</b> ) – (c), and $K_{(1-x)}[Cu^+Cl_2][Pb_xCu^{2+(6-x)}O_2](SeO_3)_2Cl_{(4-x)}$ , $x = 0.20$ ( <b>c2.8</b> ) – (d). ....	13
FIGURE 2.6	Coordination environment of the dimers composed of oxo-centered tetrahedra in the crystal structures of different minerals and synthetic compounds listed in Table 2.3. 15	
FIGURE 3.1	Experimental crystallization diagram of the $PbO-NiO-SeO_2-H_2O$ system at 200 °C with the pH zones shown in background by grey colors – (a); series of the experiments with a $PbO / NiO / SeO_2$ molar ratio of 5 : 3 : 10 corresponding to the $P_I$ point with various pH values – (b). ....	17
FIGURE 3.2	General projection of the crystal structures of $\alpha-PbM(SeO_3)_2$ ( $M = Ni^{2+}$ ( <b>c3.1</b> ), $Co^{2+}$ ( <b>c3.4</b> )) along the $b$ -axis – (a), and the corresponding black-and-white graph – (b), $M^{2+}$ $Se^{4+}$ are black and white circles, respectively. ....	19
FIGURE 3.3	The crystal structure of $\beta-PbNi(SeO_3)_2$ ( <b>c3.2</b> ) in two different projections – (a) and (b), and the black-and-white graph corresponding to the Ni-Se sheet in the structure– (c). ....	20

FIGURE 3.4	General projection of the crystal structure of $\text{PbNi}_2(\text{SeO}_2\text{OH})_2(\text{SeO}_3)_2$ ( <b>c3.3</b> ) along the <i>b</i> and <i>c</i> -axis – (a) and (b), respectively; its black-and-white graph – (c); and more detailed fragment of the structure – (d). .....	21
FIGURE 4.1	Experimental crystallization diagram of the $\text{PbCl}_2\text{--V}_2\text{O}_5\text{--SeO}_2\text{--H}_2\text{O}$ (a) and $\text{PbO--V}_2\text{O}_5\text{--SeO}_2\text{--H}_2\text{O}$ (b) systems at 200 °C with the pH zones shown in the background by gray colors. ....	23
FIGURE 4.2	Projections of the structures and optical images of the crystals of <b>c4.1</b> , <b>c4.2</b> , <b>c4.3</b> , and $\alpha\text{-Pb}_4(\text{V}_3\text{O}_8)_2(\text{SeO}_3)_3(\text{H}_2\text{O})$ . $\text{VO}_6$ octahedra, $\text{VO}_5$ square pyramids, $\text{SeO}_3$ triangular pyramids, and $\text{Pb}^{2+}$ cations are blue, green, orange, and grey, respectively. ....	24
FIGURE 4.3	Vanadate tetrameric structural units in the structures of $\alpha\text{-(V}_2\text{O}_3)(\text{SeO}_3)_2$ and $\beta\text{-(V}_2\text{O}_3)(\text{SeO}_3)_2$ ( <b>c4.1</b> ) – (a) and (b), respectively. ....	25
FIGURE 4.4	Structural units in the crystal structure of $\beta\text{-Pb}_4(\text{V}^{5+}_3\text{O}_8)_2(\text{SeO}_3)_3(\text{H}_2\text{O})$ ( <b>c4.3</b> ). ....	27
FIGURE 4.5	Mode of stacking of the vanadate selenite ribbons in the crystal structures of $\alpha\text{-Pb}_4(\text{V}_3\text{O}_8)_2(\text{SeO}_3)_3(\text{H}_2\text{O})$ – (a) and $\beta\text{-Pb}_4(\text{V}_3\text{O}_8)_2(\text{SeO}_3)_3(\text{H}_2\text{O})$ ( <b>c4.3</b> ) (b). ....	28
FIGURE 5.1	View of the crystal structure of $\text{Mn}(\text{SeO}_4)(\text{H}_2\text{O})_2$ ( <b>c5.1</b> ) projected along the <i>a</i> -axis – (a); heteropolyhedral sheet parallel to the (001) plane – (b) and its black-and-white graph with symbols designating the direction of bonds to adjacent sheets – (c). ....	31
FIGURE 5.2	Projection of the crystal structure of $\text{Mn}_2[\text{Bi}_2\text{O}](\text{SeO}_3)_4$ ( <b>c5.2</b> ) (b) composed of $[\text{MnO}_4]^{6-}$ (a) and $[\text{Bi}_2\text{O}]^{4+}$ chains (c). ....	31
FIGURE 5.3	General projections of the crystal structure of $\text{MnBi}(\text{SeO}_3)_2\text{Cl}$ ( <b>c5.3</b> ) along [010] – (a) and [001] – (b) (disordered O sites are omitted for clarity); anionic arrangement of metal cations in the structure – (c). ....	32
FIGURE 5.4	Projection of the crystal structure of $\text{Mn}_4(\text{Mn}_5\text{Bi})(\text{SeO}_3)_8\text{Cl}_5$ ( <b>c5.4</b> ) along [100] – (c), the sheet of square antiprisms – (a), the tetrameric unit – (d), and their arrangement in the structure – (b). ....	33
FIGURE 5.5	Projection of the crystal structure of $\text{Bi}_6(\text{SeO}_3)_4\text{Cl}_{10}$ ( <b>c5.5</b> ) on the (010) plane, showing $\text{BiO}_x\text{Cl}_y$ polyhedra (yellow) and $\text{SeO}_3$ groups (orange) sharing their edges and corners. ....	34

FIGURE 5.6	Projection of the crystal structure of $\beta$ -Bi(SeO <sub>3</sub> )Cl ( <b>c5.6</b> ) along [100] – (a). An alternation of three different parallel layers: [Bi <sub>14</sub> (SeO <sub>3</sub> ) <sub>24</sub> ] <sup>6-</sup> – (b), [Bi <sub>12</sub> Cl <sub>32</sub> ] <sup>4+</sup> – (c), and [Bi <sub>8</sub> Cl <sub>16</sub> ] <sup>8+</sup> – (d). .....	35
FIGURE 5.7	Projection of the crystal structure of PbBi <sub>10</sub> (SeO <sub>3</sub> ) <sub>12</sub> Cl <sub>8</sub> ( <b>c5.7</b> ) along the a axis – (b), two parallel cationic and anionic layers: [(Pb,Bi) <sub>14</sub> (SeO <sub>3</sub> ) <sub>24</sub> ] <sup>n-</sup> – (a) and [(Pb,Bi) <sub>8</sub> Cl <sub>16</sub> ] <sup>n+</sup> – (c). .....	36
FIGURE 6.1	Topological diversity of inorganic structural units in the crystal structures of novel compounds. Uranyl pentagonal bipyramids and selenate/selenite groups are shown by yellow and orange in polyhedral representation and by black and white vertices in graphs. ....	40
FIGURE 6.2	Dimensional fields on the compositional diagram of the UO <sub>2</sub> TO <sub>4</sub> – A <sub>2</sub> TO <sub>4</sub> – H <sub>2</sub> O (A = monovalent cation, T = S, Se, Cr, Mo) system. ....	43
FIGURE 7.1	Lewis structures and simplified artistic representation of orbital models of (ESeO <sub>3</sub> ) <sup>2-</sup> (a) and (HPO <sub>3</sub> ) <sup>2-</sup> (b) anions, which highlight the similar role of H <sub>HPO3</sub> and E <sub>SeO3</sub> from the geometrical point of view. ....	44
FIGURE 7.2	View of the crystal structures of Fe <sub>2</sub> (SeO <sub>3</sub> ) <sub>3</sub> ( <b>c7.1</b> ) and Fe <sub>2</sub> (HPO <sub>3</sub> ) <sub>3</sub> ( <b>c7.2</b> ) along the c-axis – (a) and (c), respectively; mode of linkage of iron (brown) and selenite (orange) polyhedra in <b>c7.1</b> – (b). ....	45

## LIST OF TABLES

TABLE 2.1	Crystallographic data and refinement parameters for <b>c2.1</b> , <b>c2.2</b> , <b>c2.3</b> , <b>c2.4</b> , <b>c2.5</b> , <b>c2.6</b> , <b>c2.7</b> , and <b>c2.8</b> . ....	8
TABLE 2.2	Experimental details of the CVT syntheses of <b>c2.1</b> , <b>c2.2</b> , <b>c2.3</b> , <b>c2.4</b> , <b>c2.5</b> , <b>c2.6</b> , <b>c2.7</b> , and <b>c2.8</b> . ....	9
TABLE 2.3	Crystallographic data for minerals and inorganic copper compounds based upon dimers composed of oxo-centered tetrahedra. ....	14
TABLE 3.1	Crystallographic data and refinement parameters for $\alpha$ -PbNi(SeO <sub>3</sub> ) <sub>2</sub> ( <b>c3.1</b> ), $\beta$ -PbNi(SeO <sub>3</sub> ) <sub>2</sub> ( <b>c3.2</b> ), PbNi <sub>2</sub> (SeO <sub>2</sub> OH) <sub>2</sub> (SeO <sub>3</sub> ) <sub>2</sub> ( <b>c3.3</b> ), and $\alpha$ -PbCo(SeO <sub>3</sub> ) <sub>2</sub> ( <b>c3.4</b> ). ....	16
TABLE 4.1	Crystallographic data and refinement parameters for $\beta$ -(V <sub>2</sub> O <sub>3</sub> )(SeO <sub>3</sub> ) <sub>2</sub> ( <b>c4.1</b> ), Pb <sub>2</sub> (VO)(SeO <sub>3</sub> ) <sub>3</sub> ( <b>c4.2</b> ), and $\beta$ -Pb <sub>4</sub> (V <sub>3</sub> O <sub>8</sub> ) <sub>2</sub> (SeO <sub>3</sub> ) <sub>3</sub> (H <sub>2</sub> O) ( <b>c4.3</b> ). ....	22
TABLE 5.1	Crystallographic data and refinement parameters for <b>c5.1</b> , <b>c5.2</b> , <b>c5.3</b> , <b>c5.4</b> , <b>c5.5</b> , <b>c5.6</b> , and <b>c5.7</b> . ....	29
TABLE 6.1	Crystallographic data and refinement parameters for <b>c6.1</b> , <b>c6.2</b> , <b>c6.3</b> , <b>c6.4</b> , <b>c6.5</b> , <b>c6.6</b> , <b>c6.7</b> , and <b>c6.8</b> . ....	37
TABLE 6.2	Crystallographic data and refinement parameters for <b>c6.9</b> , <b>c6.10</b> , <b>c6.11</b> , <b>c6.12</b> , <b>c6.13</b> , <b>c6.14</b> , <b>c6.15</b> , and <b>c6.16</b> . ....	38
TABLE 6.3	Experimental details of the isothermal evaporation syntheses of novel uranyl selenates and selenite-selenates (temperature: 23°C; time: 72 hours). ....	38
TABLE 7.1	Crystallographic data and refinement parameters for Fe <sub>2</sub> (SeO <sub>3</sub> ) <sub>3</sub> ( <b>c7.1</b> ) and Fe <sub>2</sub> (HPO <sub>3</sub> ) <sub>3</sub> ( <b>c7.2</b> ). ....	45
TABLE 7.2	Calculated partial charges for featured selected compounds. ....	46

# CONTENTS

ABSTRACT .....	iii
ACKNOWLEDGEMENTS.....	viii
LIST OF FIGURES.....	x
LIST OF TABLES.....	xiii
CONTENTS .....	xiv
LIST OF INCLUDED ARTICLES .....	xvi
OTHER COMMUNICATIONS .....	xvii
LIST OF NEW COMPOUNDS.....	xix
<b>1 INTRODUCTION .....</b>	<b>1</b>
<b>2 BRIEF DESCRIPTION OF RESULTS.....</b>	<b>5</b>
2.1 Objects and methods.....	5
2.2 Crystal chemical studies of copper selenites .....	8
2.2.1 Synthetic procedures .....	8
2.2.2 Structural description of eight novel phases .....	9
2.2.3 Linkage of selenite groups with [OCu <sub>4</sub> ] <sup>6+</sup> dimers .....	14
2.3 Crystal chemical studies of nickel and cobalt selenites.....	16
2.3.1 Crystal growth in the PbO–NiO–SeO <sub>2</sub> –H <sub>2</sub> O system .....	16
2.3.2 Structural description of three novel structural forms.....	18
2.4 Crystal chemical studies of vanadate selenites.....	22
2.4.1 Pathways for synthesis of lead vanadate selenites.....	22
2.4.2 Structural description of three novel phases .....	23
2.5 Crystal chemical studies of selenium compounds with manganese and bismuth .....	29
2.5.1 Synthetic procedures .....	29
2.5.2 Structural description of seven novel phases.....	30
2.6 Crystal chemical studies of uranyl selenates and selenite-selenates.....	37
2.6.1 Synthetic procedures .....	38
2.6.2 Structural description of sixteen novel phases .....	39

2.6.3	Dimensional reduction .....	42
2.7	Analogy between electron lone pairs of selenites and hydrogen-in-phosphites .....	44
2.7.1	Synthesis and structural characterization of iron selenite and phosphite .....	44
2.7.2	Calculation of partial charges.....	46
<b>3</b>	<b>CONCLUSION AND PERSPECTIVES .....</b>	<b>47</b>
	REFERENCES.....	49
	INCLUDED ARTICLES .....	55
A-I	Unprecedented layer topology in the crystal structure of a new organically templated uranyl selenite-selenate .....	55
A-II	Structural topology and dimensional reduction in uranyl oxysalts: eight novel phases in the methylamine-(UO <sub>2</sub> )(NO <sub>3</sub> ) <sub>2</sub> -H <sub>2</sub> SeO <sub>4</sub> -H <sub>2</sub> O system .....	59
A-III	Revised bismuth chloroselenite system: evidence of a noncentrosymmetric structure with a giant unit cell .....	77
A-IV	pH-Controlled pathway and systematic hydrothermal phase diagram for elaboration of synthetic lead nickel selenites.....	111
A-V	Oxocentered Cu(II) lead selenite honeycomb lattices hosting Cu(I)Cl <sub>2</sub> groups obtained by chemical vapor transport reactions.....	149
A-VI	Topologically and geometrically flexible structural units in seven new organically templated uranyl selenates and selenite-selenates.....	165
A-VII	Emulating exhalative chemistry: synthesis and structural characterization of ilinskite, Na[Cu <sub>5</sub> O <sub>2</sub> ](SeO <sub>3</sub> ) <sub>2</sub> Cl <sub>3</sub> , and its K-analogue.....	181
A-VIII	[NaCl][Cu(HSeO <sub>3</sub> ) <sub>2</sub> ], NaCl-intercalated Cu(HSeO <sub>3</sub> ) <sub>2</sub> : synthesis, crystal structure and comparison with related compounds.....	193
A-IX	Dimers of oxocentered [OCu <sub>4</sub> ] <sup>6+</sup> tetrahedra in two novel copper selenite chlorides, K[Cu <sub>3</sub> O](SeO <sub>3</sub> ) <sub>2</sub> Cl and Na <sub>2</sub> [Cu <sub>7</sub> O <sub>2</sub> ](SeO <sub>3</sub> ) <sub>4</sub> Cl <sub>4</sub> , and related minerals and inorganic compounds.....	201

## LIST OF INCLUDED ARTICLES

- A-I** Kovrugin V.M., Gurzhiy V.V., Krivovichev S.V., Tananaev I.G., Myasoedov B.F. Unprecedented layer topology in the crystal structure of a new organically templated uranyl selenite-selenate. *Mendeleev Communications*. 2012, 22 (1), 11–12.
- A-II** Kovrugin V.M., Gurzhiy V.V., Krivovichev S.V. Structural topology and dimensional reduction in uranyl oxysalts: eight novel phases in the methylamine–(UO<sub>2</sub>)(NO<sub>3</sub>)<sub>2</sub>–H<sub>2</sub>SeO<sub>4</sub>–H<sub>2</sub>O system. *Structural Chemistry*. 2012, 23 (6), 2003–2017.
- A-III** Aliev A., Kovrugin V.M., Colmont M., Terryn C., Huvé M., Siidra O.I., Krivovichev S.V., Mentré O. Revised bismuth chloroselenite system: evidence of a noncentrosymmetric structure with a giant unit cell. *Crystal Growth & Design*. 2014, 14 (6), 3026–3034.
- A-IV** Kovrugin V.M., Colmont M., Colis S., Terryn C., Siidra O.I., Krivovichev S.V., Mentré O. pH controlled pathway and systematic hydrothermal phase diagram for elaboration of synthetic lead nickel selenites. *Inorganic Chemistry*. 2015, 54 (5), 2425–2434.
- A-V** Kovrugin V.M., Colmont M., Siidra O.I., Mentré O, Al-Shuray A., Gurzhiy V.V., Krivovichev S.V. Oxocentered Cu(II) lead selenite honeycomb lattices hosting Cu(I)Cl<sub>2</sub> groups obtained by chemical vapor transport reactions. *Chemical Communications*. 2015, 51 (46), 9563–9566.
- A-VI** Gurzhiy V.V., Kovrugin V.M., Tyumentseva O.S., Mikhaylenko P.A., Krivovichev S.V. Tananaev I.G. Topologically and geometrically flexible structural units in seven new organically templated uranyl selenates and selenite-selenates. *Journal of Solid State Chemistry*. 2015, 229, 32–40.
- A-VII** Kovrugin V.M., Siidra O.I., Colmont M., Mentré O, Krivovichev S.V. Emulating exhalative chemistry: synthesis and structural characterization of ilinskite, Na[Cu<sub>5</sub>O<sub>2</sub>](SeO<sub>3</sub>)<sub>2</sub>Cl<sub>3</sub>, and its K-analogue. *Mineralogy and Petrology*. 2015, 109, 421–430.
- A-VIII** Kovrugin V.M., Krivovichev S.V., Mentré O, Colmont M. [NaCl][Cu(HSeO<sub>3</sub>)<sub>2</sub>], NaCl-intercalated Cu(HSeO<sub>3</sub>)<sub>2</sub>: synthesis, crystal structure and comparison with related compounds. *Zeitschrift für Kristallographie*. 2015, 230, 573–577.
- A-IX** Kovrugin V.M., Colmont M., Mentré O, Siidra O.I., Krivovichev S.V. Dimers of oxocentered [OCu<sub>4</sub>]<sup>6+</sup> tetrahedra in two novel copper selenite chlorides, K[Cu<sub>3</sub>O](SeO<sub>3</sub>)<sub>2</sub>Cl and Na<sub>2</sub>[Cu<sub>7</sub>O<sub>2</sub>](SeO<sub>3</sub>)<sub>4</sub>Cl<sub>4</sub>, and related minerals and inorganic compounds. *Mineralogical Magazine*. 2015, in press, *accepted*.



## OTHER COMMUNICATIONS

- P-I** Kovrugin V.M., Gurzhiy V.V., Krivovichev S.V. Synthesis and crystal structure of new uranyl selenate. Volume of Abstracts of the Young Scientific Conference of St Petersburg State University “Geology is our Future”. Russia, St. Petersburg, 29–30 Apr. 2009, p. 27–28. [in Russian]
- P-II** Gurzhiy V.V., Kovrugin V.M., Krivovichev S.V., Tananaev I.G., Myasoedov B.F. Synthesis and crystal structure of  $(\text{CH}_3\text{NH}_3)_4(\text{H}_3\text{O})_2[(\text{UO}_2)_5(\text{SeO}_4)_8(\text{H}_2\text{O})](\text{H}_2\text{O})_4$ . Volume of Abstracts of the XXIV International Chugaev Conference on Coordination Chemistry. Russia, Repino, 15–19 Jun. 2009, p. 256–257. [in Russian]
- P-III** Kovrugin V.M., Gurzhiy V.V., Krivovichev S.V. Geometrical isomerism in layered uranyl selenates: synthesis and crystal structure of  $(\text{CH}_3\text{NH}_3)_4(\text{H}_3\text{O})_2[(\text{UO}_2)_5(\text{SeO}_4)_8(\text{H}_2\text{O})](\text{H}_2\text{O})_4$ . Volume of Abstracts of the International Scientific Conference “Clays, clay minerals, and layered materials 2009”. Russia, Zvenigorod, 21–25 Sept. 2009, p. 89.
- P-IV** Gurzhiy V.V., Kovrugin V.M., Krivovichev S.V., Tananaev I.G., Myasoedov B.F. Inorganic uranyl selenates: synthesis and structure of new compounds in the  $(\text{UO}_2)(\text{NO}_3)_2\text{-H}_2\text{SeO}_4\text{-H}_2\text{O-CH}_3\text{NH}_2$  (methylamine) system. Volume of Abstracts of the III Russian Meeting on Organic Mineralogy with International Participation “Organic Mineralogy 2009”. Russia, Syktyvkar, 10–12 Nov. 2009, p. 21–24. [in Russian]
- P-V** Kovrugin V.M., Gurzhiy V.V., Krivovichev S.V. Synthesis, structural studies and topological analysis of new uranyl selenates with methylamine. Volume of Abstracts of the IV Russian School on Radiochemistry and Nuclear Technologies. Russia, Ozersk, 6–10 Sept. 2010, p. 57–58. [in Russian]
- P-VI** Kovrugin V.M., Gurzhiy V.V., Krivovichev S.V. Geometrical isomerism in new uranyl selenates. Volume of Abstracts of the International Scientific Conference “Fedorov Session 2010”. Russia, St-Petersburg, 12–15 Oct. 2010, p. 36–37. [in Russian]
- P-VII** Kovrugin V.M., Gurzhiy V.V., Krivovichev S.V., Tananaev I.G. Synthesis and crystal structures of new uranyl selenite-selenate  $[\text{C}_2\text{H}_8\text{N}][(\text{H}_5\text{O}_2)(\text{H}_2\text{O})][(\text{UO}_2)_2(\text{SeO}_4)_3(\text{H}_2\text{SeO}_3)](\text{H}_2\text{O})$  with novel type of inorganic layer. Volume of Abstracts of the 6th National Crystal Chemical Conference. Russia, Suzdal, 1–4 Jun. 2011, p. 114–116. [in Russian]
- P-VIII** Kovrugin V.M., Gurzhiy V.V., Krivovichev S.V., Tananaev I.G. Geometrical isomerism in layered uranyl selenite-selenates: synthesis and crystal structure of  $(\text{C}_2\text{H}_8\text{N})_3(\text{C}_2\text{H}_7\text{N})[(\text{UO}_2)_3(\text{SeO}_4)_4(\text{HSeO}_3)(\text{H}_2\text{O})]$ . Volume of Abstracts of the XVII International Conference on Crystal Chemistry, X-ray Diffraction and Spectroscopic Studies of Minerals. Russia, St-Petersburg, 20–24 Jun. 2011, p. 96–97.

- P-IX** Kovrugin V.M., Gurzhiy V.V., Krivovichev S.V., Tananaev I.G. Dimensional reduction in uranyl oxysalts with general formula  $A_n(\text{UO}_2)_p(\text{TO}_4)_q(\text{H}_2\text{O})_r$  ( $A$  = monovalent cation,  $T$  = S, Se, Cr, Mo). Volume of Abstracts of the Joint meeting DGK, DMG, ÖMG. Austria, Salzburg, 20–24 Sept. 2011, p. 96.
- P-X** Kovrugin V.M., Gurzhiy V.V., Krivovichev S.V. Geometrical features of two novel layered uranium selenite-selenates. Volume of Abstracts of the European Mineralogical Conference. Germany, Frankfurt-am-Main, 6–8 Sept 2012, p. 564.
- P-XI** Kovrugin V.M., Gurzhiy V.V., Krivovichev S.V. Dimensional reduction in uranyl oxysalts with monovalent cations. Volume of Abstracts of the International Scientific Conference “Fedorov Session 2012”. Russia, Saint-Petersburg, 9–11 Oct. 2012, p. 423–424. [in Russian]
- P-XII** Kovrugin V., Gurzhiy V., Krivovichev S. Application of the principle of dimensional reduction to uranyl oxysalts with monovalent cations. Volume of Abstracts of the GACMAC 2013 Joint Annual Meeting. Canada, MB, Winnipeg, 22–24 May 2013, p. 123.
- P-XIII** Kovrugin V., Colmont M., Mentré O., Krivovichev S. Crystal structures of two novel compounds in the PbO–NiO–SeO<sub>2</sub> system. Volume of Abstracts of the GACMAC 2013 Joint Annual Meeting. Canada, MB, Winnipeg, 22–24 May 2013, p. 123–124.
- P-XIV** Kovrugin V.M., Colmont M., Mentré O., Siidra O.I., Krivovichev S.V. Crystal structures of two novel polymorphic modifications of PbNi(SeO<sub>3</sub>)<sub>2</sub> Volume of Abstracts of the 7th National Crystal Chemical Conference. Russia, Suzdal, 17–21 Jun. 2013, p. 115. [in Russian]
- P-XV** Kovrugin V.M., Siidra O.I., Mentré O., Krivovichev S.V. Structural variety of novel Pb and Bi selenites. Abstract book of the 28th European Crystallographic Meeting. UK, Warwick. 25–29 Aug 2013. Acta Crystallographica, 2013, A69, p. s136.
- P-XVI** Kovrugin V.M., Colmont M., Mentré O., Siidra O.I., Krivovichev S.V. Synthesis and Crystal Structure of Pb<sub>4</sub>(V<sub>3</sub>O<sub>8</sub>)<sub>2</sub>(SeO<sub>3</sub>)<sub>3</sub>. Abstract book of the 28th European Crystallographic Meeting. UK, Warwick. 25–29 Aug 2013. Acta Crystallographica, 2013, A69, p. s465.
- P-XVII** Kovrugin V.M., Colmont M., Mentré O., Siidra O.I., Krivovichev S.V. Synthesis and Crystal Structure of Pb<sub>2</sub>(VO<sub>2</sub>)(SeO<sub>3</sub>)<sub>2</sub>Cl. Volume of Abstracts of the International Scientific Conference “Crystallogenesis and Mineralogy – III”. Russia, Novosibirsk, 27 Sept–01 Oct 2013, p. 91.
- P-XVIII** Kovrugin V.M., Colmont M., Siidra O.I., Krivovichev S.V., Mentré O. Chemical vapor transport method as a pathway to novel copper selenites. Volume of Abstracts of the National Scientific Conference “CRISTECH 2014”. France, Autrans, 6–8 Oct 2014, p. 27.

## LIST OF NEW COMPOUNDS

- c2.1** –  $\text{K}[\text{Cu}_5\text{O}_2](\text{SeO}_3)_2\text{Cl}_3$   
**c2.2** –  $\text{Na}[\text{Cu}_5\text{O}_2](\text{SeO}_3)_2\text{Cl}_3$   
**c2.3** –  $\text{K}[\text{Cu}_3\text{O}](\text{SeO}_3)_2\text{Cl}$   
**c2.4** –  $\text{Na}_2[\text{Cu}_7\text{O}_2](\text{SeO}_3)_4\text{Cl}_4$   
**c2.5** –  $[\text{NaCl}][\text{Cu}(\text{HSeO}_3)_2]$   
**c2.6** –  $[\text{Cu}^+\text{Cl}_2][\text{Pb}_2\text{Cu}^{2+}_9\text{O}_4](\text{SeO}_3)_4\text{Cl}_5$   
**c2.7** –  $[\text{Cu}^+\text{Cl}_2][\text{PbCu}^{2+}_5\text{O}_2](\text{SeO}_3)_2\text{Cl}_3$   
**c2.8** –  $\text{K}_{(1-x)}[\text{Cu}^+\text{Cl}_2][\text{Pb}_x\text{Cu}^{2+}_{(6-x)}\text{O}_2](\text{SeO}_3)_2\text{Cl}_{(4-x)}$ ,  $x = 0.20$   
**c3.1** –  $\alpha\text{-PbNi}(\text{SeO}_3)_2$   
**c3.2** –  $\beta\text{-PbNi}(\text{SeO}_3)_2$   
**c3.3** –  $\text{PbNi}_2(\text{SeO}_2\text{OH})_2(\text{SeO}_3)_2$   
**c3.4** –  $\alpha\text{-PbCo}(\text{SeO}_3)_2$   
**c4.1** –  $\beta\text{-(V}^{5+}_2\text{O}_3)(\text{SeO}_3)_2$   
**c4.2** –  $\text{Pb}_2(\text{V}^{4+}\text{O})(\text{SeO}_3)_3$   
**c4.3** –  $\beta\text{-Pb}_4(\text{V}^{5+}_3\text{O}_8)_2(\text{SeO}_3)_3(\text{H}_2\text{O})$   
**c5.1** –  $\text{Mn}(\text{SeO}_4)(\text{H}_2\text{O})_2$   
**c5.2** –  $\text{Mn}_2[\text{Bi}_2\text{O}](\text{SeO}_3)_4$   
**c5.3** –  $\text{MnBi}(\text{SeO}_3)_2\text{Cl}$   
**c5.4** –  $\text{Mn}_4(\text{Mn}_5\text{Bi})(\text{SeO}_3)_8\text{Cl}_5$   
**c5.5** –  $\text{Bi}_6(\text{SeO}_3)_4\text{Cl}_{10}$   
**c5.6** –  $\beta\text{-Bi}(\text{SeO}_3)\text{Cl}$   
**c5.7** –  $\text{PbBi}_{10}(\text{SeO}_3)_{12}\text{Cl}_8$   
**c6.1** –  $[\text{CH}_6\text{N}]_2[(\text{UO}_2)(\text{SeO}_4)_2(\text{H}_2\text{O})](\text{H}_2\text{O})$   
**c6.2** –  $[\text{CH}_6\text{N}]_2[(\text{UO}_2)(\text{SeO}_4)_2(\text{H}_2\text{O})]$   
**c6.3** –  $[\text{CH}_6\text{N}]_2[(\text{UO}_2)_2(\text{SeO}_4)_3]$   
**c6.4** –  $[\text{CH}_6\text{N}](\text{H}_3\text{O})[(\text{UO}_2)_2(\text{SeO}_4)_3(\text{H}_2\text{O})](\text{H}_2\text{O})$   
**c6.5** –  $[\text{CH}_6\text{N}]_4[(\text{UO}_2)_3(\text{SeO}_4)_5](\text{H}_2\text{O})_4$   
**c6.6** –  $[\text{CH}_6\text{N}](\text{H}_5\text{O}_2)(\text{H}_3\text{O})_2[(\text{UO}_2)_3(\text{SeO}_4)_5](\text{H}_2\text{O})_4$   
**c6.7** –  $[\text{CH}_6\text{N}]_4(\text{H}_3\text{O})_2[(\text{UO}_2)_5(\text{SeO}_4)_8(\text{H}_2\text{O})](\text{H}_2\text{O})_4$   
**c6.8** –  $[\text{CH}_6\text{N}]_{1.5}(\text{H}_5\text{O}_2)_{1.5}(\text{H}_3\text{O})_3[(\text{UO}_2)_5(\text{SeO}_4)_8(\text{H}_2\text{O})](\text{H}_2\text{SeO}_4)_{2.6}(\text{H}_2\text{O})_3$   
**c6.9** –  $[\text{C}_2\text{H}_8\text{N}]_2[(\text{UO}_2)(\text{SeO}_4)_2(\text{H}_2\text{O})]$   
**c6.10** –  $[\text{C}_2\text{H}_8\text{N}]_2[(\text{UO}_2)_2(\text{SeO}_4)_3(\text{H}_2\text{O})]$   
**c6.11** –  $[\text{C}_4\text{H}_{15}\text{N}_3][\text{H}_3\text{O}]_{0.5}[(\text{UO}_2)_2(\text{SeO}_4)_{2.93}(\text{SeO}_3)_{0.07}(\text{H}_2\text{O})](\text{NO}_3)_{0.5}$   
**c6.12** –  $[\text{C}_2\text{H}_8\text{N}]_3[\text{H}_5\text{O}_2][(\text{UO}_2)_2(\text{SeO}_4)_3(\text{H}_2\text{O})_2]_2(\text{H}_2\text{O})_5$   
**c6.13** –  $[\text{C}_2\text{H}_8\text{N}]_2[\text{H}_3\text{O}][(\text{UO}_2)_3(\text{SeO}_4)_4(\text{HSeO}_3)(\text{H}_2\text{O})](\text{H}_2\text{SeO}_3)_{0.2}$   
**c6.14** –  $[\text{C}_4\text{H}_{12}\text{N}]_3[\text{H}_3\text{O}][(\text{UO}_2)_3(\text{SeO}_4)_5(\text{H}_2\text{O})]$   
**c6.15** –  $[\text{C}_2\text{H}_8\text{N}]_3(\text{C}_2\text{H}_7\text{N})[(\text{UO}_2)_3(\text{SeO}_4)_4(\text{HSeO}_3)(\text{H}_2\text{O})]$   
**c6.16** –  $[\text{C}_2\text{H}_8\text{N}][(\text{H}_5\text{O}_2)(\text{H}_2\text{O})][(\text{UO}_2)_2(\text{SeO}_4)_3(\text{H}_2\text{SeO}_3)](\text{H}_2\text{O})$   
**c7.1** –  $\text{Fe}_2(\text{SeO}_3)_3$



# 1 INTRODUCTION

Nowadays, in the domain of the fundamental studies and elaboration of novel crystalline materials investigations have been slowed down. Actual researchers' activity focuses on more lucrative projects dedicated to specific materials suitable for particular applications in electronics, nuclear, energy, space industries *etc.*... In most of the cases, the following research scenario is based on the modifications and re-investigations of already well-known compounds in order to optimize their physical and chemical properties by doping, coating, shaping *etc.*... the so-called "material science". The current situation leads to deficiencies of new atomic-scale architectures for the needs of a whole range of various material sciences with their increasing demands for novel materials based on specific crystal structures determining different innovating properties.

On the other hand, Nature has not yet revealed all its own secrets concerning the origin and physical conditions of the crystal growth of all mineral species on the Earth. The structural architectures found in known crystalline compounds designed by Nature's hand cover a whole range from *0D* to *3D* frameworks, and offer unexploited potentialities in terms of study of their innovating physical properties. The ways of natural formation of many mineral groups remains undiscovered. At the same time, researchers use a wide variety of synthetic methods in attempts to perceive the Nature and to emulate the natural techniques in laboratory. For example, the *chemical vapour transport reactions method* provides a unique opportunity to model physical and chemical conditions existing in fumarolic environments and may be used not only to model exhalative processes, but also to predict possible mineral phases that may form in fumaroles. In particular, the K-analogue of ilinskite, a rare mineral sublimate from the fumaroles of the Tolbachik volcano (Kamchatka peninsula, Russia), synthesized under the framework of the present study, is not known in Nature, whereas it may well form from volcanic gases in a K-rich local geochemical environment. This is just an isolated example among so many others.

This thesis is clearly dedicated to a work at the interface between solid-state chemistry and mineralogy. To our knowledge, it is one of the first dedicated to the synthesis of various series of novel metal-oxide compounds using innovative so-called "geo-inspired" approach. Here we assume the emulation and modelling of natural crystal growth processes in order to obtain complex functional materials with a potential in terms of specific physical properties.

Over the past two decades chemistry of selenium-containing compounds has been developed intensively by many researchers, generating a large amount of experimental knowledge in various

fundamental and applied research areas: in medicine (Rayman 2000), biochemistry (Tapiero et al. 2003), organic chemistry (Pyrzynska 1996), physics (Qu and Peng 2002; Hsu et al. 2008), nuclear technology (Puranen et al. 2010), Earth sciences (Mandarino 1994; Séby et al. 2001), and structural chemistry (Choudhury et al. 2002; Krivovichev et al. 2005a).

Selenium has been shown to be a versatile chemical element in terms of crystal chemistry. Depending on the growth conditions, selenium occurs in several oxidation states and is, therefore, redox sensitive, at the interface between anionic ( $\text{Se}^{2-}$ ) and cationic ( $\text{Se}^{4+}$ ,  $\text{Se}^{6+}$ ) functions. The present work focuses on the Se oxide compounds in the oxidation states of +4 (selenites) and +6 (selenates) with broad structural diversifications. The field of selenides ( $\text{Se}^{2-}$  ions) essentially insoluble in water is out of the scope of this work. However, it should be noted that they are more prevalent in Nature (85 IMA approved minerals) than Se oxysalts.

In geochemical environments, selenites and selenates are relatively rare oxo-anion groups. By the end of the XX<sup>th</sup> century, only 16 selenium oxysalts were known to occur naturally. Last twenty years have witnessed an impressive progress in the chemistry of natural selenium based phases resulted in discovery of another 17 new minerals. It gives a total of 33 different mineral species approved by the International Mineralogical Association to date. Natural selenites notably dominate selenates among known minerals, as probable result of the easy reduction processes of selenates to selenites and elemental selenium in aqueous environments.

The study of selenites and selenates has occupied scientists for over a century and a half. The first Se compound, so-called mineral “kerstenite” (discredited in 2006 by IMA and referred to molybdenite or olsacherite), was sketchily described by C. Kersten in (Kersten 1839). Nevertheless, although much chemical information about Se compounds has been reported in details so far, only a few reviews have been published. In 1994 J. Mandarino summarized geochemical characteristics of natural and synthetic selenites (Mandarino 1994). Five years later V. Verma presented a complete review of synthetic, thermoanalytical, IR, Raman and X-ray studies on metal selenites (Verma 1999). The absence of actual reviews on selenites and selenates prompted the present work as well. Here, we also tried to rationalize structural features and principles of crystal growth, an important task for the implementation and design of novel functional oxide materials.

Selenium atom has the electron configuration  $[\text{Ar}] 3d^{10} 4s^2 4p^4$ , and, therefore, six valence electrons in the outermost shell. In the crystal structures of selenates,  $\text{Se}^{6+}$  are tetrahedrally coordinated by four  $\text{O}^{2-}$  resulted in  $(\text{Se}^{6+}\text{O}_4)^{2-}$  anionic groups commonly described with two Se–O single and two Se=O double bonds. In selenites,  $\text{Se}^{4+}$  cation form a  $(\text{Se}^{4+}\text{O}_3)^{2-}$  triangular pyramid with Se located at its apical corner, given as two Se–O single and one Se=O double bond. A lone electron pair is stereochemically active and acts as a complementary external ligand forming  $(E\text{Se}^{4+}\text{O}_3)^{2-}$  tetrahedra (*E*: lone electron pair). Note curious exceptions in which lone electron pair directly bond to metals observed e.g. in  $\text{BaCoAs}_2\text{O}_5$  (David et al. 2014). The co-presence of such lone pairs combined with the electronic properties of other metals (transition, heavy, and actinide) in the structures of compounds leads to engaging inorganic chemistry. Furthermore, the interest to selenium oxide compounds has also been stimulated by the attempts to understand purely fundamental reasons for such structural diversity and its underlying crystal chemical mechanisms.

Inorganic copper oxoselenites attract considerable attention due to their fascinating structural and physical properties as well as mineralogical and geochemical importance. Of special interest are mixed-valence  $\text{Cu}^+-\text{Cu}^{2+}$  systems with separate symmetrically independent monovalent and divalent copper sites due to their contrasted coordinations combined in one crystal structure. The specific feature of many copper oxoselenites is the presence in their crystal structures of oxocentered  $(\mu_4-\text{O})\text{Cu}_4$  tetrahedral units that polymerize to form extended structural complexes (Krivovichev et al. 2013b). In [Chapter 2.2](#), we report on the structural characterization of eight novel copper oxoselenites inspired by mineralogical discoveries in such unusual geological conditions as volcanic fumaroles.

The research on ternary oxoselenite systems with lead and nickel/cobalt as transition metals constituents was not yet carried out. In [Chapter 2.3](#), we present a scrupulous investigation of the crystal growth in the  $\text{PbO}-\text{NiO}-\text{SeO}_2$  system in hydrothermal conditions. It led to the synthesis of four novel lead nickel/cobalt selenites.

The crystal chemistry of selenium-containing vanadates possesses specific structural features due to the structural peculiar features of  $\text{VO}_4$ ,  $\text{VO}_5$  and  $\text{VO}_6$  groups. In addition, this richness of coordination number is increased by the various valence states offered in the crystal structures (Evans and Hughes 1990; Schindler et al. 2000; Boudin et al. 2000). The incorporation of asymmetric selenite groups and heavy cations, such as  $\text{Pb}^{2+}$ , with stereochemically active lone electron pairs into the structures of vanadates could result in a formation of structural cavities leading to materials with open architectures. In [Chapter 2.4](#), we describe the pathways for synthesis of lead vanadate selenites, report on crystal structures of three novel phases, and discuss the phenomenon of polymorphism in vanadate selenites.

[Chapter 2.5](#) contains a structural characterization of seven new compounds: one manganese selenate, three bismuth selenites, and three manganese bismuth selenites. The last three phases are the first examples of oxide compounds containing both bismuth and manganese cations.

Sixteen novel uranyl selenates and mixed valence selenite-selenates discussed in [Chapter 2.6](#) demonstrate an exceptional structural diversity, which is studied using a graph theory. The diversity of polyhedral units found in uranyl selenates and selenite-selenates formed by polymerization of U and Se coordination polyhedra is unique: starting from isolated complexes to nanotubules (Krivovichev et al. 2005b; Krivovichev et al. 2005a; Alekseev et al. 2008). The topology and geometry of these units is controlled by a number of factors governing interactions between organic and inorganic substructures, *i.e.* hydrophilic-hydrophobic interactions, charge-density matching and weak hydrogen bonding. Composition-structure relationships in uranyl selenates and selenite-selenates is rationalized using the principle of dimensional reduction previously proposed by *J. Long et al.* (Long et al. 1996; Tulsky and Long 2001; Alekseev et al. 2007; Krivovichev 2009).

In [Chapter 2.7](#), the analogy between lone electron pairs of selenite groups and H-P bonds of the phosphite anions is discussed through two isotypic compounds,  $\text{Fe}_2(\text{SeO}_3)_3$  and  $\text{Fe}_2(\text{HPO}_3)_3$ . It demonstrates that in solids containing  $(\text{HPO}_3)^{2-}$  and  $(\text{ESeO}_3)^{2-}$  anions, the H atom is negatively charged and possesses a partial hydridic character in the phosphites.

The present work was carried out under the framework of the international co-tutorial thesis project between St. Petersburg State University (Russia) and University of Lille 1 (France). It contains the results of syntheses, and crystal chemical characterization of 39 novel oxide compounds containing selenium in the oxidation states of +4 and +6.

Brief overview is provided in [Chapter 2](#) of the thesis. It is subdivided into seven parts:

1. Objects and methods
2. Crystal chemical studies of copper selenites
3. Crystal chemical studies of nickel and cobalt selenites
4. Crystal chemical studies of vanadium selenites
5. Crystal chemical studies of selenium compounds with manganese and bismuth
6. Crystal chemical studies of uranyl selenates and selenite-selenates
7. Analogy between electron lone pairs of selenites and hydrogen-in-phosphites

Detailed description of the theoretical and experimental results can be found in 9 original papers appended at the end of the present thesis.



## 2 BRIEF DESCRIPTION OF RESULTS

This work presents the results of synthetic, and crystal chemical characterization of a large variety of novel oxide crystalline compounds containing selenium in the oxidation states of +4 and +6. These two states are characterized by different oxo-anions, namely  $(\text{SeO}_3)^{2-}$  and  $(\text{SeO}_4)^{2-}$ . Within the framework of this thesis, an innovative so-called “geo-inspired” approach assumed emulation and modelling of natural crystal growth processes was applied. For the crystal chemical studies we used either a traditional descriptive procedure based on consideration of the crystal structures in terms of coordinations of cations, or the modern theory of anion-centered tetrahedra (Krivovichev et al. 2013b) developed by the St. Petersburg school of crystallography and the UCCS group of solid-state chemistry in Lille, in cases when the traditional structural interpretation does not reflect basic principles of structural architecture. Experimental details for all studied phases are discussed in relevant chapters.

### 2.1 Objects and methods

Crystalline samples studied in the present work were synthesized and characterized in between the University of Lille 1, Unité de catalyse et chimie du solide (France), and the St. Petersburg State University, Department of crystallography (Russia).

In the present work, we used several methods to synthesize the crystalline products. Most of them were selected due to their analogy with crystallogenic chemical processes occurring in Nature. In particular, the *chemical vapour transport reactions (CVT)* (Binnewies et al. 2013) were used for synthesis of a series of copper oxoselenites, bismuth selenite oxochlorides, and one vanadate selenite. This method can be considered as modelling of the natural environments, *e.g.* where copper oxoselenites are formed from the condensation of volcanic gases emanating from cooling magmatic chambers deep under the Earth’s surface long after the period of eruptive activities. Likely, during these volcanic CVT reactions the selenites and metal halides play the role of transport agents as it was originally suggested by *Filatov et al.* (Filatov et al. 1992).

The crystalline samples of lead nickel/cobalt selenites, lead vanadate selenites, and one manganese bismuth selenite were prepared by using the *hydrothermal techniques*. The aqueous reactions were performed in 23 ml Teflon-lined autoclaves that were heated in mechanical convection ovens. Although

the thermal treatment varied from one phase to another, in general, the autoclaves were held static for several days, followed by controlled slow cooling to room temperature. This kind of process is regarded as similar to that known from the oxidation zones of mineral deposits at small depths or subsurface zones, where most of known natural metal selenium oxysalts are formed.

For synthesis of a large series of uranyl selenates and selenite-selenates the *isothermal evaporation* from aqueous solutions under ambient conditions was applied. Analogous process of oxidation of high-level radioactive liquid waste (created by the reprocessing of spent nuclear fuel) accompanying the decay of unstable uranium isotopes results in their release into the environment and formation of various crystalline uranyl compounds containing different elements formed in thermal fission. Although  $^{79}\text{Se}$  isotope exists in spent nuclear fuel as a fission product in small amount ( $<0.05\%$  (Choppin et al. 2001)), its long half-life of  $3.27 \cdot 10^5$  years (Jörg et al. 2010) combined with its high mobility leads to wide geochemical and mineralogical abundance of selenium-containing uranyl complexes in the oxidation zones of uranium deposits and the areas of deep geological repositories for disposal of radioactive wastes.

Single-crystal X-ray diffraction data for novel phases were collected using a Stoe IPDS II Image-Plate X-ray diffractometer (University of St. Petersburg, Russia), a Bruker DUO APEX II CCD four-circle diffractometer with a Mo- $I\mu\text{S}$  micro-focus tube (University of St. Petersburg, Russia; University of Lille 1, France), and a Bruker X8 APEX II CCD diffractometer with a fine-focus X-ray tube (University of Lille 1, France). More than a hemisphere of 3D data were collected for each crystal using monochromatic  $\text{MoK}\alpha$  X-radiation,  $\lambda = 0.71073 \text{ \AA}$ .

The crystal structures were solved by direct methods and refined by means of the SHELX program package (Sheldrick 2008). The final structural models were checked for missing symmetry operations using the PLATON program (Spek 2009). For convenience, sometimes JANA 2006 (Petříček et al. 2006) and the charge filling method implemented in SUPERFLIP (Palatinus and Chapuis 2007) was also used. The final models included all atomic positional parameters and anisotropic-displacement parameters for atoms in all studied crystal structures.

Powder X-ray diffraction analyses of the powder samples were performed at room temperature using a D8 Advance Bruker AXS diffractometer,  $\text{CuK}\alpha$  X-radiation,  $\lambda = 1.5418 \text{ \AA}$  (University of Lille 1, France).

Infra-red absorption spectra were measured between  $4000$  and  $400 \text{ cm}^{-1}$  with a Perkin–Elmer Spectrum Two spectrometer equipped with a diamond attenuated total reflectance (ATR) accessory (University of Lille 1, France).

Scanning electron microscope and energy-dispersive X-ray (SEM/EDS) analyses were performed on a HITACHI S4700 microscope at  $20 \text{ kV}$  acceleration voltage and a current of  $15 \mu\text{A}$  at different magnifications (University of Lille 1, France). The ratios were determined using a semi-quantitative routine deconvolution.

The magnetic properties of the samples were analysed in collaboration with Dr. Silviu Colis at the Institut de Physique et Chimie des Matériaux de Strasbourg (IPCMS, France) using a MPMS SQUID-VSM (Quantum Design) magnetometer in a temperature and field range of  $1.8\text{--}300 \text{ K}$  and  $0\text{--}7 \text{ T}$ . The susceptibility versus temperature was measured under  $0.02 \text{ T}$  after the sample was cooled in a field of  $0.1 \text{ T}$  (FC) or in zero field (ZFC). In some cases, the powders were previously magnetically “aligned” at  $7 \text{ T}$  in a polymeric gel that freezes the particle orientation below  $\sim 303 \text{ K}$ .

Multiphoton SHG microscopy measurements on single crystals have been carried out in collaboration with Dr. Christine Terryn at the Plateforme Imagerie Cellulaire et Tissulaire, Université de Reims (France). A laser-scanning microscope LSM 710 NLO Zeiss was used for the measurements with the excitation provided by a CHAMELEON femtosecond Titanium-Sapphire laser set at 860 nm, tuning the power until SHG was detected on selected single crystal samples deposited on a glass plate. Samples were imaged with a 20x, 0.8 NA objective lens. Emitted signal of SHG was collected with a band-pass filter (420 to 440 nm).

## 2.2 Crystal chemical studies of copper selenites

Crystallographic data and experimental parameters for the crystal structures of eight novel compounds listed below are summarized in [Table 2.1](#).

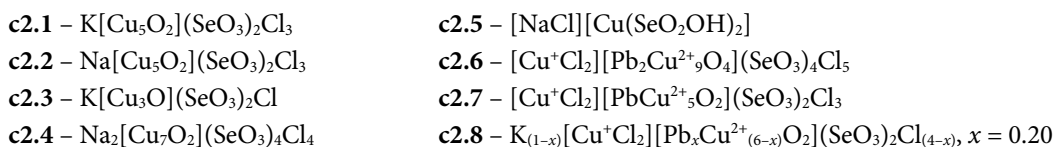


TABLE 2.1 Crystallographic data and refinement parameters for c2.1, c2.2, c2.3, c2.4, c2.5, c2.6, c2.7, and c2.8.

	<b>c2.1</b>	<b>c2.2</b>	<b>c2.3</b>	<b>c2.4</b>	<b>c2.5</b>	<b>c2.6</b>	<b>c2.7</b>	<b>c2.8</b>
Mr (g mol <sup>-1</sup> )	749.07	732.96	535.09	1172.40	755.83	1869.77	2103.20	1992.64
sp. gr.	<i>Pnma</i>	<i>Pnma</i>	<i>P</i> -1	<i>P</i> -1	<i>C2/c</i>	<i>C2/m</i>	<i>C2/m</i>	<i>C2/m</i>
<i>a</i> (Å)	18.1691(6)	17.749(2)	7.6821(5)	7.4362(6)	13.9874(7)	18.605(17)	18.4956(4)	15.116(1)
<i>b</i> (Å)	6.4483(2)	6.4412(6)	8.1179(5)	8.3361(7)	7.2594(4)	6.204(6)	6.1454(1)	6.1853(4)
<i>c</i> (Å)	10.5684(4)	10.488(1)	8.7836(6)	9.134(1)	9.0421(5)	12.673(11)	15.2985(4)	9.2672(9)
$\alpha$ (°)	90	90	113.19(1)	110.28(1)	90	90	90	90
$\beta$ (°)	90	90	108.73(1)	106.21(1)	127.04(1)	109.87(2)	119.31(1)	95.965(5)
$\gamma$ (°)	90	90	98.245(4)	105.16(1)	90	90	90	90
<i>V</i> (Å <sup>3</sup> )	1238.19(7)	1199.0(2)	453.32(5)	467.94(8)	732.81(7)	1376(2)	1516.3(1)	861.7(1)
<i>Z</i>	4	4	2	1	2	2	2	1
$\rho$ (g/cm <sup>3</sup> )	4.018	4.060	3.920	4.160	3.425	4.514	4.607	3.840
$\mu$ (mm <sup>-1</sup> )	15.333	15.523	15.757	16.263	13.313	25.78	25.02	15.52
$\lambda$ (MoK $\alpha$ ) (Å)	0.71073	0.71073	0.71073	0.71073	0.71073	0.71073	0.71073	0.71073
total rflns	9584	7946	5607	11190	3926	12055	8423	5430
indep rflns	2233	2042	1749	2842	1170	3370	2841	1479
Rint	0.027	0.098	0.050	0.047	0.026	0.093	0.025	0.030
<i>R</i> <sub>1</sub> [ <i>I</i> > 2 $\sigma$ ( <i>I</i> )]	0.018	0.049	0.048	0.027	0.021	0.035	0.028	0.045
<i>wR</i> <sub>2</sub> [ <i>I</i> > 2 $\sigma$ ( <i>I</i> )]	0.040	0.065	0.117	0.060	0.051	0.040	0.077	0.116
<i>R</i> <sub>1</sub> [all data]	0.023	0.099	0.080	0.032	0.030	0.095	0.029	0.061
<i>wR</i> <sub>2</sub> [all data]	0.041	0.077	0.133	0.062	0.053	0.048	0.078	0.125
GOF	1.035	0.991	1.014	1.070	1.081	0.716	1.126	1.070
$\Delta\rho_{\text{max}}$ , $\Delta\rho_{\text{min}}$ , (e Å <sup>-3</sup> )	0.74, -0.77	1.62, -1.67	1.62, -1.62	0.85, -0.95	0.70, -0.65	1.75, -1.86	4.19, -3.39	4.25, -1.99

### 2.2.1 Synthetic procedures

Single crystals of all novel copper selenites were prepared by the chemical vapour transport (CVT) reactions. In the course of the CVT reactions, a precursor is partially transported by a gaseous agent from a source zone to a deposition zone under the action of a temperature gradient. The general scheme of the CVT method is shown in [Figure 2.1a](#). Mixtures of initial reagents in a various molar ratios ([Table 2.2](#)) were ground and loaded into silica tubes (*ca.* 15 cm), which were further evacuated to 10<sup>-2</sup> mbar and sealed. The tubes were placed horizontally into a tubular two-zone furnace, heated to 500–550 °C for 3–4 days and subsequently slowly cooled to room temperature. The temperature gradient between the source (hot) and

deposition (cold) zones of the tube in the furnace was about 50 °C. Crystals of novel phases were observed in the different zones of the tubes in association with already known compounds are shown in Figure 2.1d.

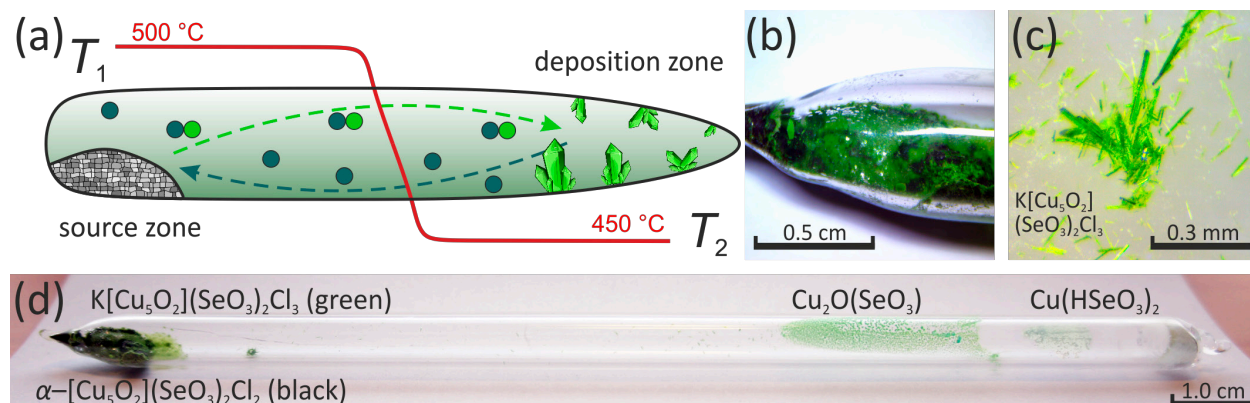


FIGURE 2.1 General scheme of the CVT method – (a), the source zone of the tube – (b), the crystals of  $K[Cu_5O_2](SeO_3)_2Cl_3$  (c2.1) picked out from the source zone – (c), and a common view of the sealed silica tube after the CVT synthesis – (d).

TABLE 2.2 Experimental details of the CVT syntheses of c2.1, c2.2, c2.3, c2.4, c2.5, c2.6, c2.7, and c2.8.

	c2.1	c2.2	c2.3	c2.4	c2.5	c2.6	c2.7	c2.8
<b>molar ratios:</b>								
SeO <sub>2</sub>	2	2	2	2	2	1	1	1
CuO	4	4	4	4	4	0	2	2
CuCl <sub>2</sub>	1	1	1	1	1	2.25	1.50	1.50
CuCl	0	0	0	0	0	1.25	0	0
KCl	1	0	3	0	0	0	0	1
NaCl	0	1	0	3	3	0.50	1	0
PbO	0	0	0	0	0	0.75	0.50	0.50
<b>conditions:</b>								
temp. (°C)	500	500	500	500	500	500	550	550
time (h)	72	72	72	72	72	96	72	72
cooling (h)	24	24	24	24	24	12	6	6

## 2.2.2 Structural description of eight novel phases

### $A[Cu_5O_2](SeO_3)_2Cl_3$ ( $A = K^+, Na^+$ )

$K[Cu_5O_2](SeO_3)_2Cl_3$  (c2.1) and  $Na[Cu_5O_2](SeO_3)_2Cl_3$  (c2.2), are isotypic and represent synthetic analogues of natural Na-ilinskite (Vergasova et al. 1997; Krivovichev et al. 2013a). They come from the frame of the fascinating study of inorganic topologies based on oxocentered tetrahedra recently reviewed by Krivovichev and co-workers (Krivovichev et al. 2013b). The crystal structures of c2.1 (K) and c2.2 (Na) contain four symmetrically independent copper sites with different mixed-ligand coordination environments. The Cu(1) site is coordinated by five ligands to form  $\{Cu[(4O)+Cl]\}$  square pyramids. The Cu(3) site has a distorted  $[3O+Cl]$  square coordination. The coordinations of the Cu(2) and Cu(4) sites in c2.1 (K) and c2.2 (Na) are different as due to the shift of the Cl(3) site induced by the greater size of the  $K^+$  cations compared to  $Na^+$ . Thus, the Cu(2) site has a distorted square pyramidal  $[(3O+Cl)+Cl]$  coordination in c2.2 (Na), and a distorted  $[(3O+Cl)+2Cl]$  octahedral environment in the crystal structure of c2.1 (K). The Cu(4) atom

possesses an octahedral [(4O)+2Cl] coordination in **c2.2** (Na), whereas the shift of the Cl(3) atoms is influenced by larger size of K<sup>+</sup> cations in **c2.1** (K) results in the change of a coordination polyhedron of Cu(4) to a five-fold square {Cu[(4O+Cl)]} pyramid with one axial Cu(4)–Cl(3) bond, analogous to the environment of the Cu(1) sites in both structures. There are two symmetrically independent selenium sites in the crystal structures of **c2.1** (K) and **c2.2** (Na), which have typical oxygen coordination of triangular pyramid with a stereochemically active lone pair of electrons as a complementary ligand. The arrangement of coordinating ligands of Na<sup>+</sup> in **c2.2** (Na) consists of one oxygen and four chlorine atoms, forming a distorted {Na[(O+2Cl)+2Cl]} trigonal bipyramid. K<sup>+</sup> cations in **c2.1** (K) are surrounded by five oxygen and four chlorine atoms each.

Interestingly, the crystal structures of **c2.1** (K) and **c2.2** (Na) contain “additional” oxygen atoms, which are coordinated solely by Cu<sup>2+</sup> cations, resulting in the formation of oxocentered (OCu<sub>4</sub>)<sup>6+</sup> tetrahedra. The (OCu<sub>4</sub>)<sup>6+</sup> tetrahedra share common corners to form the [Cu<sub>5</sub>O<sub>2</sub>]<sup>6+</sup> sheets parallel to (100) (Figure 2.2). The [Cu<sub>5</sub>O<sub>2</sub>]<sup>6+</sup> sheets in the crystal structures of **c2.1** (K) and **c2.2** (Na) are surrounded by selenite triangular pyramids and chlorine anions to produce a microporous framework. The pores are filled by alkali metal cations and lone pairs of electrons of the selenite groups. Detailed description of the crystal structures of **c2.1** (K) and **c2.2** (Na) can be found in the article A-VII (see Included Articles).

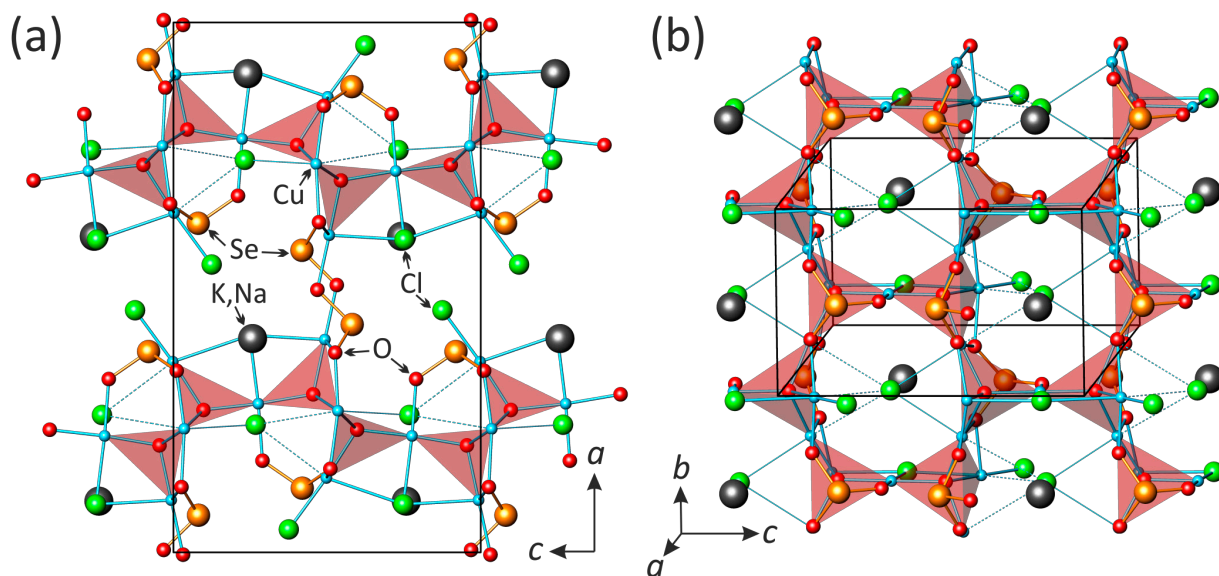


FIGURE 2.2 The crystal structures of  $A[\text{Cu}_5\text{O}_2](\text{SeO}_3)_2\text{Cl}_3$  ( $A^+ = \text{K}^+$  (c2.1),  $\text{Na}^+$  (c2.2)) in two different projections featuring side and top view of the  $[\text{O}_2\text{Cu}_5]^{6+}$  sheet of oxocentered  $(\text{OCu}_4)^{6+}$  tetrahedra highlighted by red colour.

### **K[Cu<sub>3</sub>O](SeO<sub>3</sub>)<sub>2</sub>Cl and Na<sub>2</sub>[Cu<sub>7</sub>O<sub>2</sub>](SeO<sub>3</sub>)<sub>4</sub>Cl<sub>4</sub>**

The structure of  $\text{K}[\text{Cu}_3\text{O}](\text{SeO}_3)_2\text{Cl}$  (**c2.3**) contains three symmetrically independent Cu<sup>2+</sup> sites. The Cu(1) site is surrounded by four O and one Cl atoms to form an unusual distorted trigonal bipyramid in a {Cu[(2O+Cl)+2O]} coordination. The Cu(2) atom has a typical planar-square [(4O)] coordination. The coordination polyhedron of Cu(3) can be described as a distorted {Cu[(4O)+(O+Cl)]} octahedron. All these various Cu coordination polyhedra are combined into sheets parallel to (001). The structure of **c2.3** contains

two symmetrically independent  $\text{Se}^{4+}$  cations that form typical  $(\text{SeO}_3)^{2-}$  triangular pyramids. The  $\text{K}^+$  cation is coordinated by seven  $\text{O}^{2-}$  and two  $\text{Cl}^-$  anions in a distorted arrangement.

In the crystal structure of  $\text{Na}_2[\text{Cu}_7\text{O}_2](\text{SeO}_3)_4\text{Cl}_4$  (**c2.4**), there are four symmetrically independent Cu sites. The Cu(1) site forms a  $\{\text{Cu}[(4\text{O})]\}$  square, similar to the Cu(2) site in the structure of **c2.3**. The Cu(2) and Cu(4) sites are coordinated by three O and one Cl to form  $\{\text{Cu}[(3\text{O}+\text{Cl})]\}$  planar squares. The same  $[(3\text{O}+\text{Cl})]$  coordination has been also observed in the crystal structures of **c2.1** and **c2.2**. The Cu(3) site in the crystal structure of **c2.4** has a triangular bipyramidal  $[(2\text{O}+\text{Cl})+2\text{O}]$  coordination. Two symmetrically independent Se sites form typical  $(\text{SeO}_3)^{2-}$  trigonal pyramids. The symmetrically unique  $\text{Na}^+$  cation is surrounded by six  $\text{O}^{2-}$  and one  $\text{Cl}^-$  anion to form an approximately triangular prismatic oxygen environment.

In the crystal structure of **c2.3**, two  $(\text{OCu}_4)^{6+}$  tetrahedra share a common Cu...Cu edge to form the  $[\text{O}_2\text{Cu}_6]^{8+}$  dimer, while in **c2.4**  $[\text{O}_2\text{Cu}_7]^{10+}$  dimeric units are formed by two  $(\text{OCu}_4)^{6+}$  tetrahedra sharing a common Cu atom. The selenite groups and Cl atoms surround these dimers to form the  $\{[\text{O}_2\text{Cu}_6](\text{SeO}_3)_4\text{Cl}_2\}^{2-}$  and  $\{[\text{O}_2\text{Cu}_7](\text{SeO}_3)_4\text{Cl}_4\}^{2-}$  structural units in **c2.3** and **c2.4**, respectively, which are further interconnected into sheets (Figure 2.3). The interlayer space is occupied by the alkali cations. A comparison of the mode of linkage of  $(\text{SeO}_3)^{2-}$  with the oxo-centered dimers in known copper oxoselenites is given in the Section 2.2.3. Detailed description of the crystal structures of **c2.3** and **c2.4** (Na) can be found in the article **A-IX** (see Included Articles).

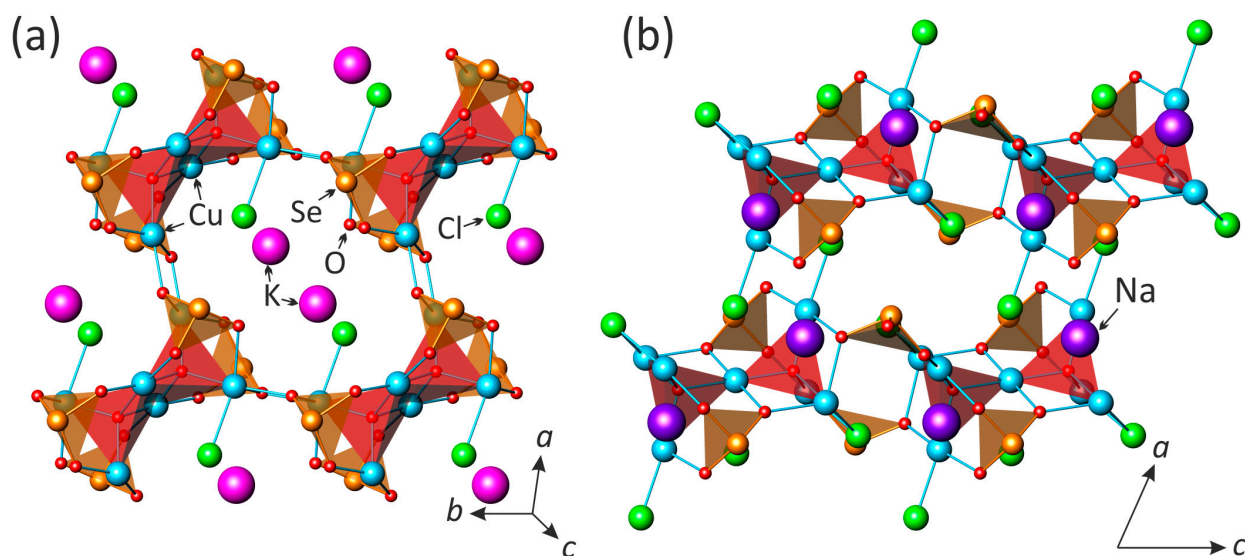


FIGURE 2.3 The crystal structures of  $\text{K}[\text{Cu}_5\text{O}](\text{SeO}_3)_2\text{Cl}$  (**c2.3**) and  $\text{Na}_2[\text{Cu}_7\text{O}_2](\text{SeO}_3)_4\text{Cl}_4$  (**c2.4**). The  $(\text{OCu}_4)^{6+}$  tetrahedra are highlighted by red colour.

### **[NaCl][Cu(SeO<sub>2</sub>OH)<sub>2</sub>]**

The crystal structure of  $[\text{NaCl}][\text{Cu}(\text{SeO}_2\text{OH})_2]$  (**c2.5**) contains one symmetrically independent Cu site octahedrally coordinated by four O and two Cl atoms. The Cu site forms a  $(\text{CuO}_4)$  square complemented by two long Cu–Cl bonds resulting in a  $[(4\text{O})+(2\text{Cl})]$  coordination observed for Cu(4) in the structure of **c2.2**. There is one Se site coordinated by three O atoms to form a trigonal  $(\text{SeO}_3)$  pyramid typical for selenites. One of the three Se–O bonds is elongated compared to two other bonds owing to the protonation of the  $\text{O}_h(1)$  site. The  $(\text{CuO}_4)$  squares and  $(\text{SeO}_2\text{OH})$  groups share common oxygen atoms to form

electroneutral  $[\text{Cu}(\text{SeO}_2\text{OH})_2]$  sheets parallel to the (100) plane (Figure 2.4). Between two  $(\text{SeO}_2\text{OH})^-$  group the  $\text{O}_h(1)\cdots\text{O}(2)$  hydrogen bond creates a  $[(\text{SeO}_2\text{OH})_2]^{2-}$  dimer that provides additional stabilization of the copper diselenite sheet.

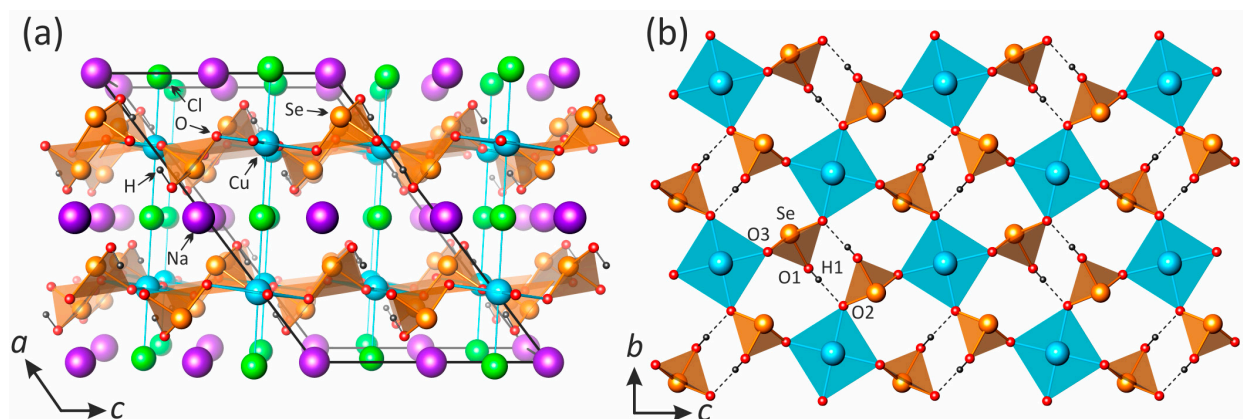


FIGURE 2.4 Projections of the  $[\text{Cu}(\text{HSeO}_3)_2]^0$  sheet (a) and the crystal structure of  $[\text{NaCl}][\text{Cu}(\text{HSeO}_3)_2]$  (**c2.5**) featuring two-dimensional  $[\text{Cu}(\text{HSeO}_3)_2]^0$  sheets with intercalated  $\dots\text{Na}\text{--Cl}\dots$  chains.

In the crystal structure of **c2.5**, the  $[\text{Cu}(\text{HSeO}_3)_2]$  sheets alternate with the sheets consisting of zigzag  $\text{--Na--Cl--Na--Cl--}$  chains formed by Cl atoms and disordered Na sites. The chains are parallel to the  $c$ -axis. The linkage between the alternating electroneutral  $[\text{Cu}(\text{HSeO}_3)_2]^0$  and  $[\text{NaCl}]^0$  sheets is provided by the  $\text{Cu--Cl}$  and  $\text{Na--O}$  bonds. The coordination of Na is fivefold and consists of three O and two Cl atoms.<sup>o</sup>

The **c2.5** compound can be considered as a member of the series of compounds based upon the  $M(\text{SeO}_2\text{OH})_2$  sheets ( $M = \text{Cu}^{2+}, \text{Co}^{2+}, \text{Cd}^{2+}$ ). The prototype structure for this group is  $[\text{Cu}(\text{SeO}_2\text{OH})_2]$  (Effenberger 1985) that does not have any chemical species separating the copper hydroselenite sheets. In other compounds, the interlayer space between the  $[\text{Cu}(\text{SeO}_2\text{OH})_2]^0$  sheets is occupied by structural units of different complexity. In all the compounds, the  $[\text{Cu}(\text{SeO}_2\text{OH})_2]^0$  sheets have approximately the same planar dimensions (measured as distances between a couple of atoms related by symmetry operations), except for  $[\text{Cu}(\text{SeO}_2\text{OH})_2](\text{H}_2\text{O})_2$  (Lafont and Trombe 1995), where the sheets are strongly corrugated. Detailed description of **c2.5** can be found in the article **A-VIII** (see Included Articles).

**$[\text{Cu}^+\text{Cl}_2][\text{Pb}_2\text{Cu}^{2+}_9\text{O}_4](\text{SeO}_3)_4\text{Cl}_5$ ,  $[\text{Cu}^+\text{Cl}_2][\text{PbCu}^{2+}_5\text{O}_2](\text{SeO}_3)_2\text{Cl}_3$ ,  
and  $\text{K}_{(1-x)}[\text{Cu}^+\text{Cl}_2][\text{Pb}_x\text{Cu}_{(6-x)}\text{O}_2](\text{SeO}_3)_2\text{Cl}_{(4-x)}$ ,  $x = 0.20$**

The crystal structures of these three compounds are very unusual owing to the incorporation of linear  $(\text{Cu}^+\text{Cl}_2)^-$  units in the voids of a pseudo honeycomb sheets made of oxo-centred  $(\text{O}(\text{Cu}/\text{Pb})_4)^{6+}$  tetrahedra and  $(\text{SeO}_3)^{2-}$  groups. In  $[\text{Cu}^+\text{Cl}_2][\text{Pb}_2\text{Cu}_9\text{O}_4](\text{SeO}_3)_4\text{Cl}_5$  (**c2.6**),  $[\text{Cu}^+\text{Cl}_2][\text{PbCu}_5\text{O}_2](\text{SeO}_3)_2\text{Cl}_3$  (**c2.7**), and  $\text{K}_{(1-x)}[\text{Cu}^+\text{Cl}_2][\text{Pb}_x\text{Cu}_{(6-x)}\text{O}_2](\text{SeO}_3)_2\text{Cl}_{(4-x)}$ ,  $x = 0.20$  (**c2.8**),  $\text{Cu}^+$  cations form two relatively short  $\text{Cu}^+\text{--Cl}$  bonds, which result in the formation of tightly bonded  $(\text{Cu}^+\text{Cl}_2)^-$  anionic groups that can be considered as separate structural entities. The  $\text{Cu}^{2+}$  cations have mixed oxochloride coordinations with typical trends of Jahn-Teller  $d^9$  ions. The Cu(1) and Cu(2) sites in **c2.6**, the Cu(4) site in **c2.7**, and Cu(3) site in **c2.8** form distorted  $\{\text{Cu}[(4\text{O})+(2\text{Cl})]\}$  octahedra similar to those found for Cu(4) and Cu(1) in the structures of **c2.2** and **c2.5**, respectively. The Cu(3) site in **c2.6**, the Cu(2) and Cu(3) sites in **c2.7**, and the Cu(1) site in **c2.8** are octahedrally  $[(3\text{O}+\text{Cl})+2\text{Cl}]$  coordinated with  $(\text{CuO}_3\text{Cl})$  squares complemented by two long  $\text{Cu--Cl}$  bonds.



The same coordination was observed for Cu(2) in the structure of **c2.1**. The Cu(4) site in **c2.6** forms a trigonal  $\{\text{Cu}[(3\text{O})+(\text{O}+\text{Cl})]\}$  bipyramids, whereas the Cu(1) site in **c2.7** and the Cu(4) site in **c2.8** are  $[(2\text{O}+\text{Cl})+(\text{O}+\text{Cl})]$  coordinated. The Pb atoms have asymmetrical coordinations consisting of three strong Pb–O bonds located in one coordination hemisphere and four long Pb–Cl in another. This coordination of  $\text{Pb}^{2+}$  cations is consistent with the presence of stereoactive lone electron pairs.  $\text{Se}^{4+}$  cations form standard  $(\text{SeO}_3)^{2-}$  selenite triangular pyramidal oxoanions. The structure of **c2.8** has one symmetrically independent K site with the site-occupation factor (s.o.f.) equal to 0.8. Its coordination polyhedron can be described as a distorted hexagonal bipyramid.

In the crystal structure of **c2.6** there are two additional O atoms, that form  $(\text{OCu}^{2+}_3\text{Pb})$  and  $(\text{OCu}^{2+}_4)$  tetrahedra, respectively. The oxocentered tetrahedra share common corners to form  $[\text{O}_4\text{Pb}_2\text{Cu}^{2+}_9]^{14+}$  double chains. These chains are growing parallel to the  $b$ -axis, and its common value for the three compounds ( $b \approx 6.2$  Å) denotes similar arrangement between the oxocentered building units in the full series. These types of chains of anion-centered tetrahedra are original and have not been observed in inorganic compounds previously. The  $\text{SeO}_3$  groups are attached to the triangular bases of oxo-centered tetrahedra that results in formation of 1D  $\{[\text{O}_4\text{Pb}_2\text{Cu}^{2+}_9](\text{SeO}_3)_4\}^{6+}$  complex interconnected *via* Pb–O bonds into 2D metal-oxide double sheets (Figure 2.5a). The projection of the sheets in the  $(b,c)$  plane leads to a honeycomb-like lattice of tetrahedra (Figure 2.5b). In contrast, monometallic  $[\text{O}_2\text{Cu}_5]$  honeycomb-sheets are reported in several compounds based upon anion-centered tetrahedra (Krivovichev et al. 2013b). The sheets are surrounded by  $\text{Cl}^-$  anions in the interleaves and accommodate both linear  $[\text{Cu}^+\text{Cl}_2]^-$  anions and  $\text{Cl}^-$  ions in the larger and smaller honeycomb windows, respectively. Taking into account the relative strength of the  $\text{Cu}^+\text{--Cl}$  bonds and weak interactions between them and the rest of the structure, these units may be considered as guest anions embedded in the complex metal oxochloride matrix based upon anion-centered tetrahedra.

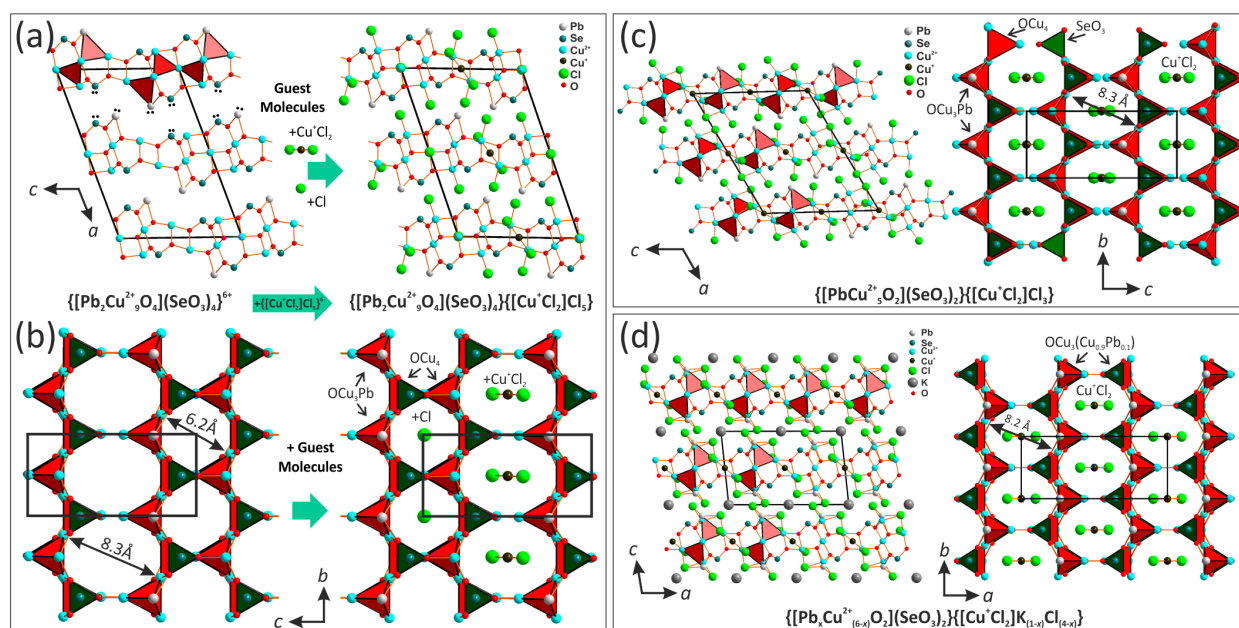


FIGURE 2.5 Projections of the structures of  $[\text{Cu}^+\text{Cl}_2][\text{Pb}_2\text{Cu}_9\text{O}_4](\text{SeO}_3)_4\text{Cl}_5$  (**c2.6**) – (a) and (b),  $[\text{Cu}^+\text{Cl}_2][\text{PbCu}_5\text{O}_2](\text{SeO}_3)_2\text{Cl}_3$  (**c2.7**) – (c), and  $\text{K}_{(1-x)}[\text{Cu}^+\text{Cl}_2][\text{Pb}_x\text{Cu}^{2+}_{(6-x)}\text{O}_2](\text{SeO}_3)_2\text{Cl}_{(4-x)}$ ,  $x = 0.20$  (**c2.8**) – (d).

A very similar 'host-guest' principle is at work in the structures of **c2.7** and **c2.8** as well. Here the (OCu<sup>2+</sup><sub>3</sub>Pb) and (OCu<sup>2+</sup><sub>4</sub>) tetrahedra share corners to produce single chains extending along the common *b* parameter that have the [O<sub>2</sub>PbCu<sub>5</sub>]<sup>8+</sup> and [O<sub>2</sub>Pb<sub>*x*</sub>Cu<sup>2+</sup><sub>(6-*x*)</sub>]<sup>8+</sup> compositions, respectively. The experimental partial Pb<sup>2+</sup> for Cu<sup>2+</sup> substitution is allowed by the oxo-centered framework in this particular topology. Together with SeO<sub>3</sub> groups, these chains form 1D {[O<sub>2</sub>M<sub>6</sub>](SeO<sub>3</sub>)<sub>2</sub>]<sup>4+</sup> metal-oxide (*M* = Cu<sup>2+</sup>, Pb<sup>2+</sup>) backbones of the structures that are arranged to form pseudo honeycomb sheets (Figure 2.5c, d). Due to the elementary single-chains, only large honeycomb windows are created that accommodate the (Cu<sup>+</sup>Cl<sub>2</sub>)<sup>-</sup> guest anions as observed in **c2.6**. The structure of **c2.8** contains additional K<sup>+</sup> cations located in the interlayer space between the metal oxoselenite chloride sheets. In all three structures, lone electron pairs on the Pb<sup>2+</sup> and Se<sup>4+</sup> cations are oriented toward the interlayer space, thus conforming the 'chemical scissor' principle of structural organization in compounds with lone electron pair cations. Detailed description of the crystal structures of **c2.6**, **c2.7**, and **c2.8** can be found in the article **A-V** (see Included Articles).

### 2.2.3 Linkage of selenite groups with [OCu<sub>4</sub>]<sup>6+</sup> dimers

The novel compounds **c2.3** and **c2.4** are the new members of a structural family of minerals and synthetic compounds (Table 2.3) characterized by dimers composed of edge-sharing (O(Cu/Pb)<sub>4</sub>)<sup>6+</sup> tetrahedra polymerized into [O<sub>2</sub>(Cu/Pb)<sub>6</sub>]<sup>8+</sup> units or corner-sharing (OCu<sub>4</sub>)<sup>6+</sup> tetrahedra into [O<sub>2</sub>Cu<sub>7</sub>]<sup>10+</sup> units. Figure 2.6 provides an overview of the observed coordination environments of the dimers of oxocentered tetrahedra in the crystal structures of related copper minerals and synthetic compounds. Existence and frequent occurrence of such oxocentered units in different structures provides an indirect evidence for the importance of such units as pre-nucleation building blocks existing in gaseous media as it occurs in volcanic fumaroles or evacuated silica ampoules used in the CVT method.

TABLE 2.3 Crystallographic data for minerals and inorganic copper compounds based upon dimers composed of oxo-centered tetrahedra.

Cu:O	Fig.	Chemical formula	Mineral name	Space group	<i>a</i> (Å); <i>α</i> (°)	<i>b</i> (Å); <i>β</i> (°)	<i>c</i> (Å); <i>γ</i> (°)	<i>V</i> (Å <sup>3</sup> )	Ref.
6:2	2.6a	K[Cu <sub>3</sub> O](SeO <sub>3</sub> ) <sub>2</sub> Cl		<i>P</i> -1	7.682; 113.2	8.118; 108.7	8.784; 98.2	453	<b>c2.3</b>
6:2	2.6a	Cu[Cu <sub>3</sub> O](SeO <sub>3</sub> ) <sub>3</sub> -I		<i>P2</i> <sub>1</sub> / <i>a</i>	15.990	13.518; 90.5	17.745	3836	[1]
6:2	2.6b	Cu[Cu <sub>3</sub> O](SeO <sub>3</sub> ) <sub>3</sub> -II		<i>P</i> -1	7.992; 77.3	8.141; 66.6	8.391; 81.4	484	[1]
6:2	2.6c	KPb <sub>0.5</sub> Cu[PbCu <sub>5</sub> O <sub>2</sub> ]Zn(SeO <sub>3</sub> ) <sub>2</sub> Cl <sub>10</sub>	prewittite	<i>Pnmm</i>	9.132	19.415	13.213	2343	[2]
6:2	2.6d	NaK[Cu <sub>3</sub> O](SO <sub>4</sub> ) <sub>3</sub>	euchlorine	<i>C2</i> / <i>c</i>	18.41	9.43; 113.7	14.21	2259	[3]
6:2	2.6d	K <sub>2</sub> [Cu <sub>3</sub> O](SO <sub>4</sub> ) <sub>3</sub>	fedotovite	<i>C2</i> / <i>c</i>	19.037	9.479; 111.0	14.231	2397	[4]
6:2	2.6e	(NMe <sub>2</sub> H <sub>2</sub> ) <sub>4</sub> [Cu <sub>6</sub> O <sub>2</sub> ](SO <sub>4</sub> ) <sub>6</sub> (DMF) <sub>4</sub>		<i>P2</i> <sub>1</sub> / <i>n</i>	13.105	10.514; 103.2	18.753	2516	[5]
6:2	2.6f	(NMe <sub>2</sub> H <sub>2</sub> ) <sub>4</sub> [Cu <sub>6</sub> O <sub>2</sub> ](SO <sub>4</sub> ) <sub>6</sub> (DMF) <sub>2</sub>		<i>P</i> -1	8.588; 106.5	10.684; 104.6	12.817; 105.9	1012	[5]
7:2	2.6h	KCd[Cu <sub>7</sub> O <sub>2</sub> ](SeO <sub>3</sub> ) <sub>2</sub> Cl <sub>9</sub>	burnsite	<i>P6</i> <sub>3</sub> / <i>mmc</i>	8.781	8.781	15.521	1036	[6]
7:2	2.6g	Na <sub>2</sub> [Cu <sub>7</sub> O <sub>2</sub> ](SeO <sub>3</sub> ) <sub>4</sub> Cl <sub>4</sub>		<i>P</i> -1	7.436; 110.3	8.336; 106.2	9.134; 105.2	468	<b>c2.4</b>

References: 1 – (Effenberger and Pertlik 1986); 2 – (Shuvalov et al. 2013); 3 – (Scordari and Stasi 1990); 4 – (Starova et al. 1991); 5 – (Burrows et al. 2012); 6 – (Krivovichev et al. 2002; Burns et al. 2002).

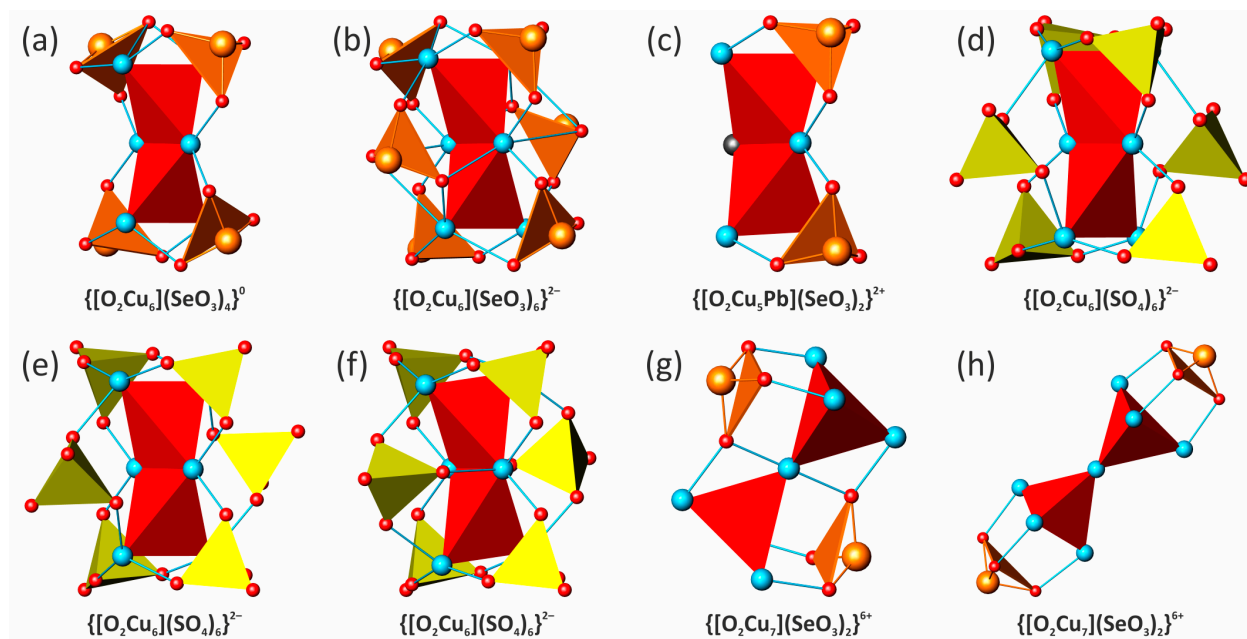


FIGURE 2.6 Coordination environment of the dimers composed of oxo-centered tetrahedra in the crystal structures of different minerals and synthetic compounds listed in Table 2.3.

## 2.3 Crystal chemical studies of nickel and cobalt selenites

Here we continue to consider divalent transition metals in which the Jahn-Teller effect characteristic for metallic cation is more or less pronounced depending on its coordination. One of the goals is to explore topologies of selenite compounds in which the transition metal adopts an octahedral coordination. Crystallographic data and experimental parameters for the crystal structures of the compounds studied in this chapter are summarized in Table 3.1. Detailed description of the solid phases produced in the studied system and analysis of the magnetic properties can be found in the article A-IV (see Included Articles).

TABLE 3.1 Crystallographic data and refinement parameters for  $\alpha$ -PbNi(SeO<sub>3</sub>)<sub>2</sub> (c3.1),  $\beta$ -PbNi(SeO<sub>3</sub>)<sub>2</sub> (c3.2), PbNi<sub>2</sub>(SeO<sub>2</sub>OH)<sub>2</sub>(SeO<sub>3</sub>)<sub>2</sub> (c3.3), and  $\alpha$ -PbCo(SeO<sub>3</sub>)<sub>2</sub> (c3.4).

	c3.1	c3.2	c3.3	c3.4
$M_r$ (g mol <sup>-1</sup> )	519.82	519.82	834.47	520.04
space group	<i>Pnma</i>	<i>Cmc2<sub>1</sub></i>	<i>P2/c</i>	<i>Pnma</i>
$a$ (Å)	12.7476(4)	5.4715(4)	13.6824(10)	12.8208(4)
$b$ (Å)	5.4562(2)	9.1963(6)	5.2692(5)	5.4902(2)
$c$ (Å)	7.8332(2)	11.4436(9)	19.3476(13)	7.9085(2)
$\beta$ (°)	90	90	129.524(4)	90
$V$ (Å <sup>3</sup> )	544.83(3)	575.81(7)	1075.94(16)	556.67(3)
$Z$	4	4	4	4
$\rho$ (g/cm <sup>3</sup> )	6.337	5.996	5.151	6.205
$\mu$ (mm <sup>-1</sup> )	47.637	45.074	32.668	46.221
$\lambda$ (MoK $\alpha$ ) (Å)	0.71073	0.71073	0.71073	0.71073
total rflns	10212	2345	5454	3226
indep rflns	823	686	2083	742
$R_{int}$	0.0336	0.0260	0.0459	0.0260
$R_1$ [ $I > 2\sigma(I)$ ]	0.0139	0.0141	0.0496	0.0186
$wR_2$ [ $I > 2\sigma(I)$ ]	0.0360	0.0346	0.0992	0.0429
$R_1$ [all data]	0.0165	0.0142	0.0783	0.0203
$wR_2$ [all data]	0.0387	0.0346	0.1104	0.0439
GOF	1.090	1.109	1.187	1.142
$\Delta\rho_{max}, \Delta\rho_{min}$ ( $e \text{ \AA}^{-3}$ )	1.573, -1.110	1.310, -1.073	2.916, -2.912	0.971, -1.887
ICSD	428905	428906	428907	428904

### 2.3.1 Crystal growth in the PbO–NiO–SeO<sub>2</sub>–H<sub>2</sub>O system

#### Synthetic procedures

In this system we present a systematic exploration of the phase diagram in hydrothermal conditions, a rare methodology dealing with solvothermal methods, where most of the reported phases are obtained fortuitously. Our exploration of the crystal growth in the PbO–NiO–SeO<sub>2</sub>–H<sub>2</sub>O system consisted of examination of 36 possible combinations of molar ratios of the solid precursors within the Gibbs triangle (Figure 3.1). In all syntheses the  $m\text{PbO} + n\text{NiO} + (k/5)\text{SeO}_2$  ( $m, n, k = 1, 2, \dots, 8$ ) molar sum was fixed as constant equaled to 10 mmol, and the mixture was completed with 6 ml of distilled water. It has been experimentally established that only acidic conditions favor the crystallization of structural varieties. Thus, a large stoichiometric excess of SeO<sub>2</sub> was necessary to achieve successful reactions, and the amount of

selenium dioxide was multiplied by five. The pH values increase from ~1 to ~5.5–6.0 on decreasing the SeO<sub>2</sub> content in studied experimental range. The solid products were systematically analyzed by powder XRD analysis, while representative crystals of each of the present phases were also selected by morphology and colors and tested by single-crystal XRD analysis. It led to the single crystal phase distribution given in Figure 3.1a, where the crystallization domains of phases are illustrated by different colors.

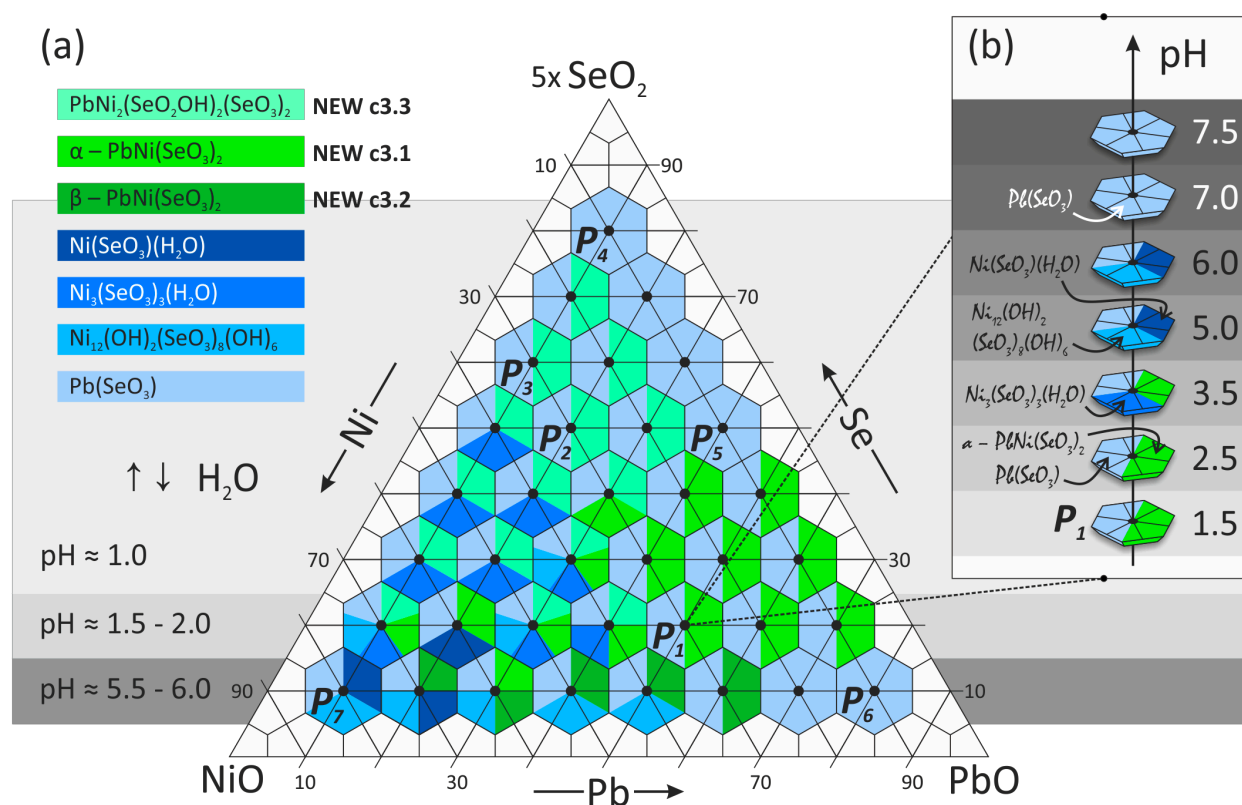


FIGURE 3.1 Experimental crystallization diagram of the PbO–NiO–SeO<sub>2</sub>–H<sub>2</sub>O system at 200 °C with the pH zones shown in background by grey colors – (a); series of the experiments with a PbO / NiO / SeO<sub>2</sub> molar ratio of 5 : 3 : 10 corresponding to the  $P_1$  point with various pH values – (b).

The hydrothermal chemical reactions were performed during 36 hours in 23 mL Teflon-lined vessels heated in an oven at 200 °C. At the end of the experiment time, the vessels were cooled during 48 hours. The precipitate was filtered through filter paper. Single crystals of three novel lead nickel selenites,  $\alpha$ -PbNi(SeO<sub>3</sub>)<sub>2</sub> (**c3.1**),  $\beta$ -PbNi(SeO<sub>3</sub>)<sub>2</sub> (**c3.2**), and PbNi<sub>2</sub>(SeO<sub>2</sub>OH)<sub>2</sub>(SeO<sub>3</sub>)<sub>2</sub> (**c3.3**), have been observed in the mixtures with already reported compounds: Ni(SeO<sub>3</sub>)(H<sub>2</sub>O) (Engelen et al. 1996), Ni<sub>3</sub>(SeO<sub>3</sub>)<sub>3</sub>(H<sub>2</sub>O) (Wildner 1991; Mcmanus et al. 1991), Ni<sub>12</sub>(OH)<sub>6</sub>(SeO<sub>3</sub>)<sub>8</sub>(OH)<sub>2</sub> (Amorós et al. 1996), and Pb(SeO<sub>3</sub>) (Popovkin et al. 1963; Fischer 1972; Koskenlinna and Valkonen 1977). Single crystals of the cobalt selenite,  $\alpha$ -PbCo(SeO<sub>3</sub>)<sub>2</sub> (**c3.4**), were obtained by the reaction analogous to that used to obtain compound **c3.1**. Attempts to synthesize the Co-analogue of compounds **c3.2** and **c3.3** using similar techniques proved unsuccessful. The novel lead selenites crystals occur as yellow needles (**c3.1**), yellow prisms (**c3.2**), green plates (**c3.3**), and purple needles (**c3.4**) up to 300  $\mu$ m in maximal dimension.

### **Brief analysis of the synthesized phases**

The analysis of the different produced solid phases allows a rough rationalization on the basis of the starting stoichiometry and pH value. The  $\text{Pb}(\text{SeO}_3)$  compound is the most frequent phase in the system, and it has been observed as a solid product with variable degree of crystallinity in each hydrothermal experiment, sometimes found as a predominant white powder. This proves a preferred complexation of  $\text{Pb}^{2+}$  by  $(\text{SeO}_3)^{2-}$  and enhanced precipitation independently of the pH. Also we note that rich lead compounds appear in the right zone of the diagram while lead-free nickel selenites have been obtained at the left side with low Pb concentrations. This result, even though expected, demonstrates formation mechanisms controlled by the solution concentrations of each species. Finally, occulting the systematic presence of  $\text{Pb}(\text{SeO}_3)$ , low pH values favor reactivity of  $(\text{SeO}_2\text{OH})^-$  groups (e.g. in **c3.3**), while selenite groups dominate at higher pH values (e.g. in **c3.1** and **c3.2** polymorphs).

### **Role of pH**

To gain more information about the reaction processes in the  $\text{PbO-NiO-SeO}_2\text{-H}_2\text{O}$  phase diagram, an in-depth investigation was carried out for the particular  $P_1$  ( $\text{PbO} / \text{NiO} / \text{SeO}_2$  molar ratio of 5 : 3 : 10) stoichiometric mixture at various pH values up to 7.5 (in order to prevent the reduction of  $\text{SeO}_2$  to  $\gamma$ -Se metal (Pourbaix 1974; Takeno 2005)). The reagents were mixed with 1.75 M aqueous NaOH solution until the required pH values. Then, the hydrothermal treatment was applied. The resulted products of these series as a function of the pH values are shown in [Figure 3.1b](#). The results obtained in the course of the hydrothermal experiments demonstrate an essential role of the pH values, especially dealing with the influence of the degree of condensation of the ionic species. Once more at all pH the  $\text{Pb}(\text{SeO}_3)$  is revealed as very stable. For the other products, we observe that water molecules and, subsequently, hydroxide anions are progressively incorporated into the compound structures on increasing the pH. In particular, at low pH of 1.5–2.5 only condensed compounds,  $\alpha\text{-PbNi}(\text{SeO}_3)_2$  (**c3.1**) and  $\text{Pb}(\text{SeO}_3)$  are formed. The reaction occurring with pH value of 3.5 leads to reported compound  $\text{Ni}_3(\text{SeO}_3)_3(\text{H}_2\text{O})$  with one-third of  $\text{Ni}^{2+}$  coordinated by water molecules. Increasing the pH to 5.0–6.0 markedly increases the incorporation of water molecules and/or hydroxyl groups leading to  $\text{Ni}_{12}(\text{OH})_6(\text{SeO}_3)_8(\text{OH})_2$  and  $\text{Ni}(\text{SeO}_3)(\text{H}_2\text{O})$ . The crystal structure of the latter is only composed of  $\text{NiO}_5(\text{H}_2\text{O})$  polyhedra, while the tubular crystal structure of  $\text{Ni}_{12}(\text{OH})_2(\text{SeO}_3)_8(\text{OH})_6$  contains half of the protonated  $(\text{NiO}_5(\text{OH}))^{9-}$  octahedra. With pH values greater than 7.0, only the very stable solid products  $\text{Pb}(\text{SeO}_3)$  phase is observed.

### **2.3.2 Structural description of three novel structural forms**

#### **$\alpha\text{-PbM}(\text{SeO}_3)_2$ ( $M = \text{Ni}^{2+}, \text{Co}^{2+}$ )**

The isotopic compounds **c3.1** and **c3.4** are built up from a 3D framework composed of anionic  $(\text{SeO}_3)^{2-}$  and  $(\text{MO}_6)^{10-}$  building units sharing common corners ([Figure 3.2](#)). We find one symmetrically independent  $M^{2+}$  position with rather regular  $(\text{MO}_6)^{10-}$  octahedral coordination. There are two independent Se atoms per formula unit, where  $\text{Se}^{4+}$  cations form typical  $(\text{SeO}_3)^{2-}$  triangular pyramids. The unique  $\text{Pb}^{2+}$  site is surrounded by O anions shared by  $(\text{SeO}_3)^{2-}$  and  $(\text{MO}_6)^{10-}$  groups. It forms asymmetric  $\text{Pb}^{2+}$  coordination with a stereochemically active lone pair directed toward the empty space. In [Figure 3.2b](#), a 3D metal cationic framework of the crystal structures of **c3.1** and **c3.4** is represented as a black-and-white graph with black

and white nodes symbolizing coordination polyhedra of  $M^{2+}$  and  $Se^{4+}$ , respectively. It highlights the topological connectivity of the  $SeO_3$  and  $MO_6$  polyhedra in complex 3D framework with stretched rectangular channels extending along [010] direction occupied by the lead cations and the  $Se^{4+}$  lone pairs. In the (010) plane, their sections are arranged in a crossed manner with alternate of the two orientations [201] and the [20-1] with respect to the  $Pnma$  symmetry. The channels are bordered by six  $MO_6$  and six  $SeO_3$  polyhedra (Figure 3.2a). Divalent lead cations reside in the cavities and balance the charge of the framework of the compounds **c3.1** and **c3.4**. Detailed description of the crystal structures of **c3.1** and **c3.4** can be found in article A-IV (see Included Articles).

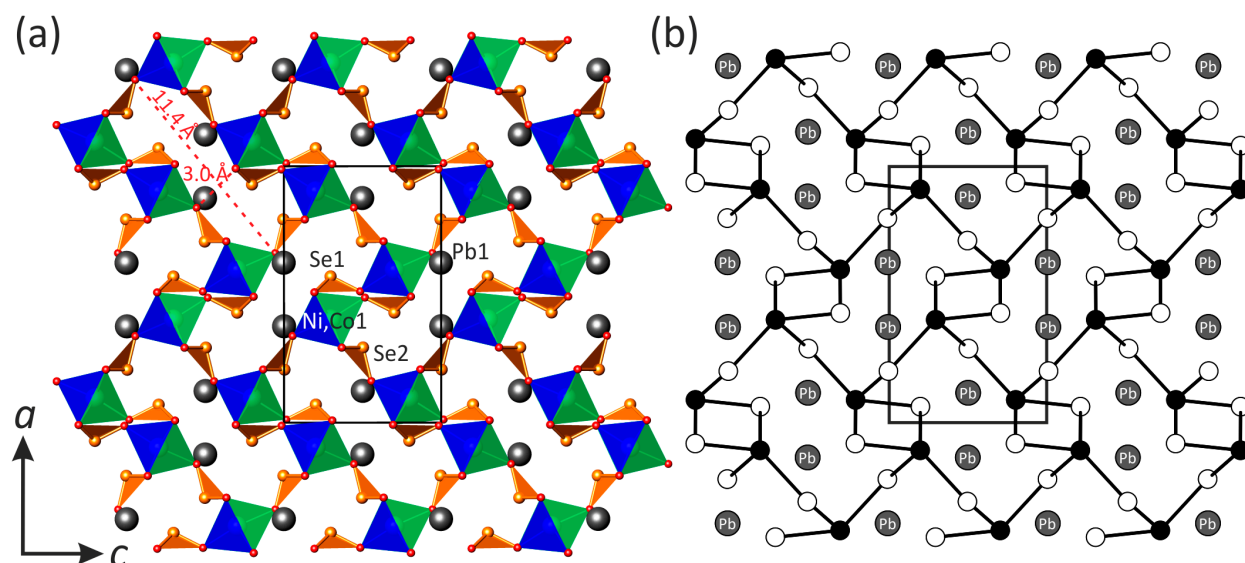


FIGURE 3.2 General projection of the crystal structures of  $\alpha$ - $PbM(SeO_3)_2$  ( $M = Ni^{2+}$  (**c3.1**),  $Co^{2+}$  (**c3.4**)) along the  $b$ -axis – (a), and the corresponding black-and-white graph – (b),  $M^{2+}$   $Se^{4+}$  are black and white circles, respectively.

### **$\beta$ -PbNi(SeO<sub>3</sub>)<sub>2</sub>**

The crystal structure of **c3.2** contains one symmetrically independent  $Ni^{2+}$  cation that forms a slightly distorted  $NiO_6$  octahedron. Two independent  $Se^{4+}$  sites have a trigonal pyramidal coordination. In the crystal structure of **c3.2** a coordination polyhedron of a unique  $Pb^{2+}$  ion is asymmetric and obviously indicates that the  $6s^2$  lone pair is stereochemically active. Similarly to what found in the  $\alpha$ - $PbNi(SeO_3)_2$  form (**c3.1**), the  $\beta$ -form is built up from isolated  $NiO_6$  octahedra interlinked by  $SeO_3$  groups via common oxygen corners. However, the linkage modes differ in both structures. The crystal structure of **c3.2** (Figure 3.3) is essentially two dimensional (2D) and is based upon  $[Ni(SeO_3)_2]^{2-}$  sheets, which lay parallel to (001). The lone pairs of electrons of  $Se^{4+}$  cations are oriented in the [001] direction toward the vacant part of the interlayer space. Cavities are filled by the  $Pb^{2+}$  cations, which serve to balance charge and achieve the cohesion between the sheets. The shortest interlayer O...O contacts across the interlayer is about 3.36 Å, much greater than the sum of van der Waals radii and involves a true 2D-character. The black-and-white graph corresponding to the layered nickel selenite structural units is shown in Figure 3.3c. This kind of layered topology is one of the most common in inorganic oxysalts (Krivovichev 2004; Krivovichev 2009). The noncentrosymmetric character of **c3.2** is well evidenced on Figure 3.3a where only “up”  $SeO_3$  orientations are found in the crystal structure. Detailed description of the crystal structure of **c3.2** can be found in the article A-IV (see Included Articles).

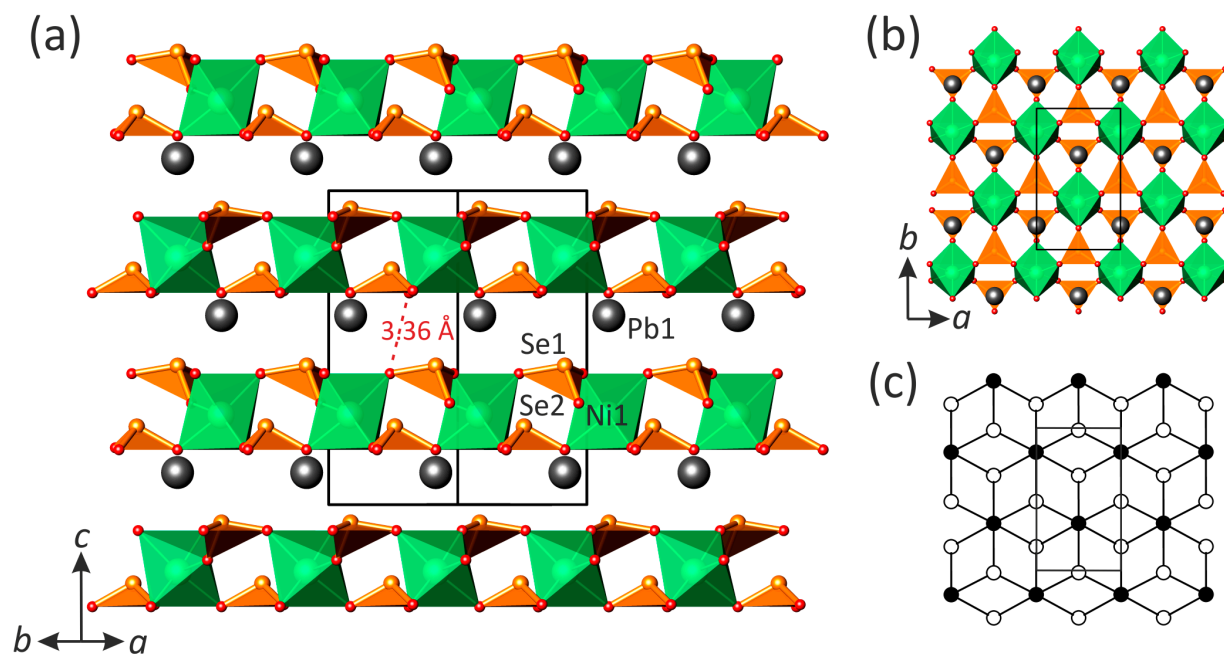


FIGURE 3.3 The crystal structure of  $\beta$ - $\text{PbNi}(\text{SeO}_3)_2$  (c3.2) in two different projections – (a) and (b), and the black-and-white graph corresponding to the Ni–Se sheet in the structure– (c).

### **$\text{PbNi}_2(\text{SeO}_2\text{OH})_2(\text{SeO}_3)_2$**

In the crystal structure of **c3.3** there are two symmetrically independent  $\text{Ni}^{2+}$  sites with rather regular octahedral coordination. The four crystallographically inequivalent  $\text{Se}^{4+}$  atoms are asymmetrically coordinated by three oxygen atoms in a trigonal pyramidal geometry. However, two of them are protonated leading to strongly distorted  $(\text{Se}(3)\text{O}_2\text{OH})^-$  and  $(\text{Se}(4)\text{O}_2\text{OH})^-$  trigonal pyramids with one long Se–O bond, and two shorter Se–O bonds. The two independent  $\text{Pb}^{2+}$  cations are eight-fold oxygen coordinated. They both show a distorted square antiprismatic arrangement with lone pairs of electrons oriented toward the longest oxygen neighbors.

In the crystal structure of **c3.3**, the  $\text{NiO}_6$  octahedra are sharing their vertices with  $\text{SeO}_3$  groups, forming a 3D framework encapsulating channels propagating along the [010] direction (Figure 3.4a). Four independent channels are occupied alternately by divalent lead cations and lone pairs of electrons of the  $\text{Se}^{4+}$  cations. It is striking that in the  $(a,b)$  projection the similitude between Pb1 and Pb2 channels suggests a  $V/2$  sub-cell. In fact the projection in the  $(a,b)$  plane evidences channels growing along the  $c$ -axis with a clear distinction between Pb1 and Pb2 sites (Figure 3.4b).

Figure 3.4c shows the black-and-white graph corresponding to a 3D metal cationic framework of **c3.3**. Its structural architecture is closely related to that observed in the crystal structure of  $\text{PbFe}_2(\text{SeO}_3)_4$  (Johnston and Harrison 2004) and represents an interesting topological variation of the primitive cubic (**pcu**) network (Krivovichev 2014). Detailed description of the crystal structure of **c3.3** can be found in the article **A-IV** (see Included Articles).



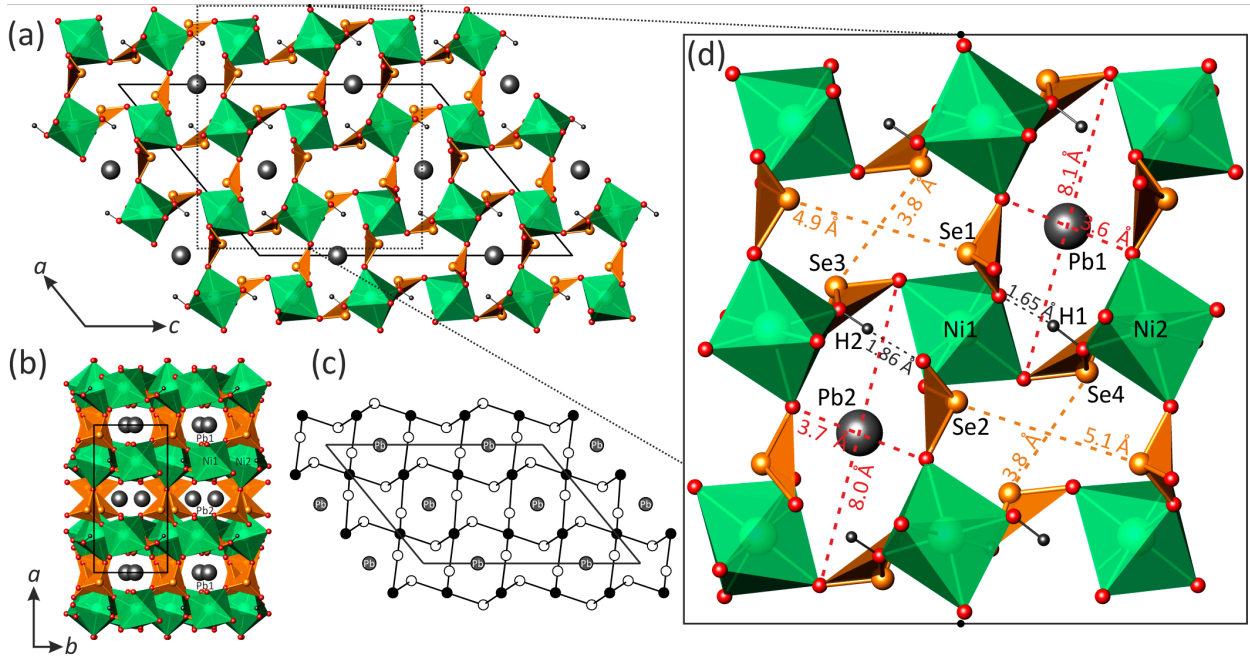


FIGURE 3.4 General projection of the crystal structure of  $\text{PbNi}_2(\text{SeO}_2\text{OH})_2(\text{SeO}_3)_2$  (c3.3) along the  $b$  and  $c$ -axis – (a) and (b), respectively; its black-and-white graph – (c); and more detailed fragment of the structure – (d).

## 2.4 Crystal chemical studies of vanadate selenites

Crystallographic data and experimental parameters for the crystal structures of the compounds studied in this chapter are summarized in [Table 4.1](#).

TABLE 4.1 Crystallographic data and refinement parameters for  $\beta$ -(V<sub>2</sub>O<sub>3</sub>)(SeO<sub>3</sub>)<sub>2</sub> (c4.1), Pb<sub>2</sub>(VO)(SeO<sub>3</sub>)<sub>3</sub> (c4.2), and  $\beta$ -Pb<sub>4</sub>(V<sub>3</sub>O<sub>8</sub>)<sub>2</sub>(SeO<sub>3</sub>)<sub>3</sub>(H<sub>2</sub>O) (c4.3).

	<b>c4.1</b>	<b>c4.2</b>	<b>c4.3</b>
<i>M<sub>r</sub></i> (g mol <sup>-1</sup> )	403.80	862.20	1789.30
space group	<i>P</i> 2 <sub>1</sub> / <i>c</i>	<i>P</i> 2 <sub>1</sub> / <i>n</i>	<i>P</i> -1
<i>a</i> (Å)	7.1812(3)	5.1938(3)	7.1425(2)
<i>b</i> (Å)	7.0753(2)	16.1141(9)	7.1933(2)
<i>c</i> (Å)	14.0486(5)	11.2533(6)	21.5261(7)
$\alpha$ (°)	90	90	90.0190(10)
$\beta$ (°)	101.5462(15)	90.527(2)	98.1800(10)
$\gamma$ (°)	90	90	94.5980(10)
<i>V</i> (Å <sup>3</sup> )	699.35(4)	941.79(9)	1091.12(6)
<i>Z</i>	4	4	2
$\rho$ (g/cm <sup>3</sup> )	3.835	6.081	5.446
$\mu$ (mm <sup>-1</sup> )	13.105	48.272	38.305
$\lambda$ (MoK $\alpha$ ) (Å)	0.71073	0.71073	0.71073
total rflns	7488	9381	21653
indep rflns	2126	3062	6579
<i>R</i> <sub>int</sub>	0.0252	0.0305	0.0272
<i>R</i> <sub>1</sub> [ <i>I</i> > 2 $\sigma$ ( <i>I</i> )]	0.0232	0.0236	0.0260
<i>wR</i> <sub>2</sub> [ <i>I</i> > 2 $\sigma$ ( <i>I</i> )]	0.0503	0.0411	0.0535
<i>R</i> <sub>1</sub> [all data]	0.0298	0.0322	0.0302
<i>wR</i> <sub>2</sub> [all data]	0.0527	0.0429	0.0549
GOF	1.065	1.059	1.042
$\Delta\rho_{\max}, \Delta\rho_{\min}$ (e Å <sup>-3</sup> )	1.03, -0.49	1.40, -1.34	5.06, -2.96

### 2.4.1 Pathways for synthesis of lead vanadate selenites

The PbO–VO<sub>x</sub>–SeO<sub>2</sub> ternary system has not been widely explored so far, and it counts only six known phases, namely, Pb<sub>2</sub>(V<sup>5+</sup><sub>2</sub>O<sub>5</sub>)(SeO<sub>3</sub>)<sub>2</sub> (Li et al. 2010), Pb<sub>2</sub>(V<sup>4+</sup>O)<sub>3</sub>(SeO<sub>3</sub>)<sub>5</sub> (Li et al. 2010), Pb<sub>4</sub>(V<sup>5+</sup>O<sub>2</sub>)<sub>2</sub>(SeO<sub>3</sub>)<sub>4</sub>(Se<sub>2</sub>O<sub>5</sub>) (Yeon et al. 2012),  $\alpha$ -Pb<sub>4</sub>(V<sup>5+</sup><sub>3</sub>O<sub>8</sub>)<sub>2</sub>(SeO<sub>3</sub>)<sub>3</sub>(H<sub>2</sub>O) (Cao et al. 2014), Pb<sub>2</sub>(V<sup>5+</sup>O<sub>2</sub>)(SeO<sub>3</sub>)<sub>2</sub>Cl (Cao et al. 2014), and Pb(V<sup>5+</sup>O<sub>2</sub>)(SeO<sub>3</sub>)F (Cao et al. 2014). Further investigation was motivation for us in this part of the present study. Most of the reported compounds have been prepared by the hydrothermal techniques at 200–230 °C, which is expected owing to good solubility and reactivity of (Se<sup>4+</sup>O<sub>3</sub>)<sup>2-</sup> anions in solution, while Pb<sup>2+</sup> oxysalts are prone to the phase formation in aqueous solutions as demonstrated by our previous results. Only two of the compounds, Pb<sub>4</sub>(V<sup>5+</sup>O<sub>2</sub>)<sub>2</sub>(SeO<sub>3</sub>)<sub>4</sub>(Se<sub>2</sub>O<sub>5</sub>) (Yeon et al. 2012) and Pb<sub>2</sub>(V<sup>5+</sup>O<sub>2</sub>)(SeO<sub>3</sub>)<sub>2</sub>Cl (Cao et al. 2014), were synthesized using the CVT method. Interestingly, the latter can be also obtained by the hydrothermal method (Cao et al. 2014).

In the context of the present work, single crystals of the new  $\beta$ -(V<sup>5+</sup><sub>2</sub>O<sub>3</sub>)(SeO<sub>3</sub>)<sub>2</sub> (**c4.1**) have been grown by the chemical vapor transport (CVT) method described in general form in the [Section 2.1](#), while new Pb-containing phases, Pb<sub>2</sub>(V<sup>4+</sup>O)(SeO<sub>3</sub>)<sub>3</sub> (**c4.2**)  $\beta$ -Pb<sub>4</sub>(V<sup>5+</sup><sub>3</sub>O<sub>8</sub>)<sub>2</sub>(SeO<sub>3</sub>)<sub>3</sub>(H<sub>2</sub>O) (**c4.3**), were obtained by

using the hydrothermal techniques in the course of the phase diagram exploration. Due to time restrictions, “hydrothermal” phase diagrams using both PbO and PbCl<sub>2</sub> precursor have not been studied systematically, in contrast with the Ni-containing system developed in the Section 2.1. At least our investigation of the systems included an examination of several combinations of molar ratios of the solid precursors within the Gibbs’ triangle (Figure 4.1) in a similar way as described in the Section 2.3.1.

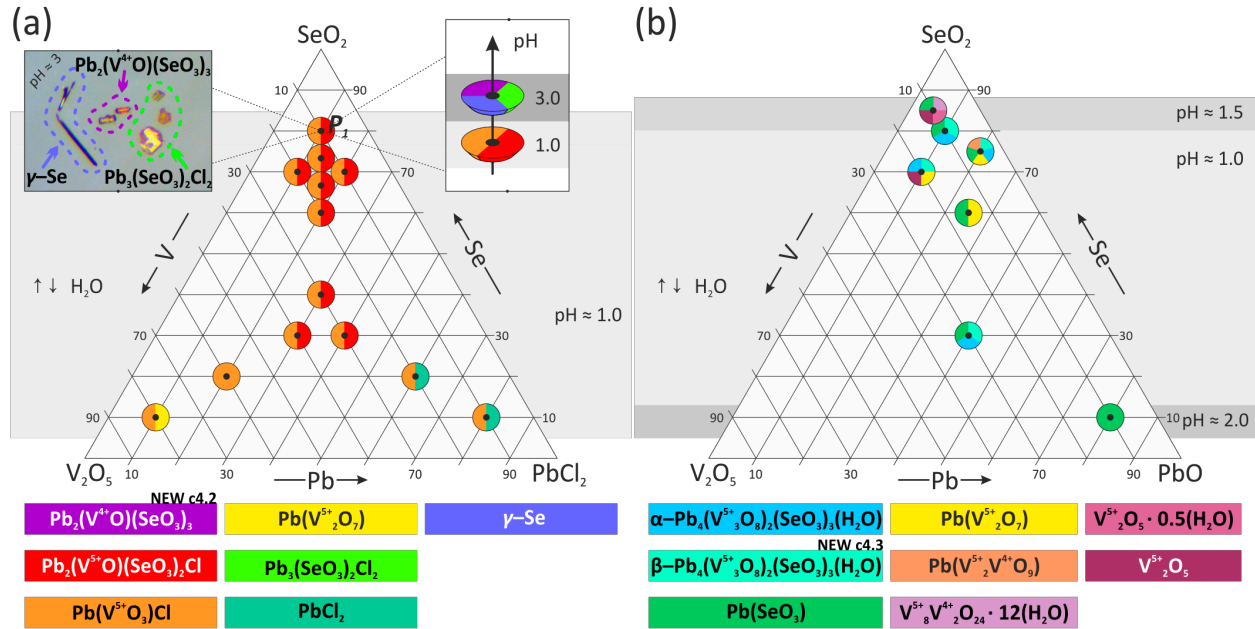
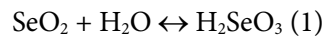


FIGURE 4.1 Experimental crystallization diagram of the PbCl<sub>2</sub>-V<sub>2</sub>O<sub>5</sub>-SeO<sub>2</sub>-H<sub>2</sub>O (a) and PbO-V<sub>2</sub>O<sub>5</sub>-SeO<sub>2</sub>-H<sub>2</sub>O (b) systems at 200 °C with the pH zones shown in the background by gray colors.

The reaction products have been identified by means of single crystal (for both systems) and powder (only for the PbO-V<sub>2</sub>O<sub>5</sub>-SeO<sub>2</sub>-H<sub>2</sub>O system) X-ray diffraction methods. As in the case of the Ni-system, self-acidification was achieved owing to the SeO<sub>2</sub> reaction with water according to the following reactions:



In the PbCl<sub>2</sub>-V<sub>2</sub>O<sub>5</sub>-SeO<sub>2</sub>-H<sub>2</sub>O system, the Pb<sub>2</sub>(VO<sub>2</sub>)(SeO<sub>3</sub>)<sub>2</sub>Cl (Cao et al. 2014) and Pb(VO<sub>3</sub>)Cl (Jo et al. 2009) phases dominate, while PbCl<sub>2</sub> and Pb(V<sub>2</sub>O<sub>7</sub>) occur in the PbCl<sub>2</sub>-rich and V<sub>2</sub>O<sub>5</sub>-rich regions of the diagram, respectively. Using the PbO precursor, more contrasted phases have been identified depending on the zone of the crystallization diagram. Our study allowed to identify one new phase in each system, namely, Pb<sub>2</sub>(V<sup>4+</sup>O)(SeO<sub>3</sub>)<sub>3</sub> (**c4.2**), and β-Pb<sub>4</sub>(V<sup>5+</sup><sub>3</sub>O<sub>8</sub>)<sub>2</sub>(SeO<sub>3</sub>)<sub>3</sub>(H<sub>2</sub>O) (**c4.3**), described below.

## 2.4.2 Structural description of three novel phases

### β-(V<sub>2</sub>O<sub>3</sub>)(SeO<sub>3</sub>)<sub>2</sub>

The crystal structure of the new β-polymorph of (V<sub>2</sub>O<sub>3</sub>)(SeO<sub>3</sub>)<sub>2</sub> (monoclinic symmetry, *P*<sub>2</sub><sub>1</sub>/*c*) (**c4.1**) contains two V<sup>5+</sup> atoms and two Se<sup>4+</sup> atoms. The V(1) site is coordinated by six oxygen atoms to form an irregular [1<sub>s</sub>+4+1<sub>r</sub>]-octahedron with one short (V(1)-O(4) = 1.586 Å) and one elongated bond (V(1)-O(3) = 2.385 Å). The V(2) site forms a square [1<sub>s</sub>+4]-pyramid with one short V(2)-O(9) = 1.570 Å bond.

This kind of five-fold coordination has been observed e.g. in the crystal structures of  $A_4\text{Cd}(\text{VO})(\text{V}_2\text{O}_7)_2\text{Cl}$  ( $A = \text{Rb}, \text{Tl}$ ) (Mertens and Müller-Buschbaum 1997).  $\text{Se}^{4+}$  cations form the typical  $(\text{SeO}_3)^{2-}$  triangular pyramids with a stereoactive lone pair acting as a complementary ligand.

In the structure of **c4.1**, a pair of edge-sharing vanadate octahedra shares their common oxygen corners with two vanadate square pyramids to form a  $(\text{V}_4\text{O}_{18})^{16-}$  tetramer. The selenite anions play different structural roles. The  $\text{Se}(2)\text{O}_3$  triangular pyramids are attached to the tetramer in such a way that selenite triangular  $\text{O}_3$  bases are relatively parallel to the V–V–V–V plane of the tetramer. The  $\text{Se}(1)\text{O}_3$  groups are located in between the vanadate tetramers and provide their linkage into the metal-oxide sheets through the formation of the Se–O–V bridges (Figure 4.2a). The 2D vanadate selenite complexes with an interlayer spacing of about 3.3 Å are oriented parallel to (-201) plane. The structural feature of this type of sheets in addition to their electro-neutrality is the presence of large lengthy channels of size  $3 \times 10$  Å running along [100].

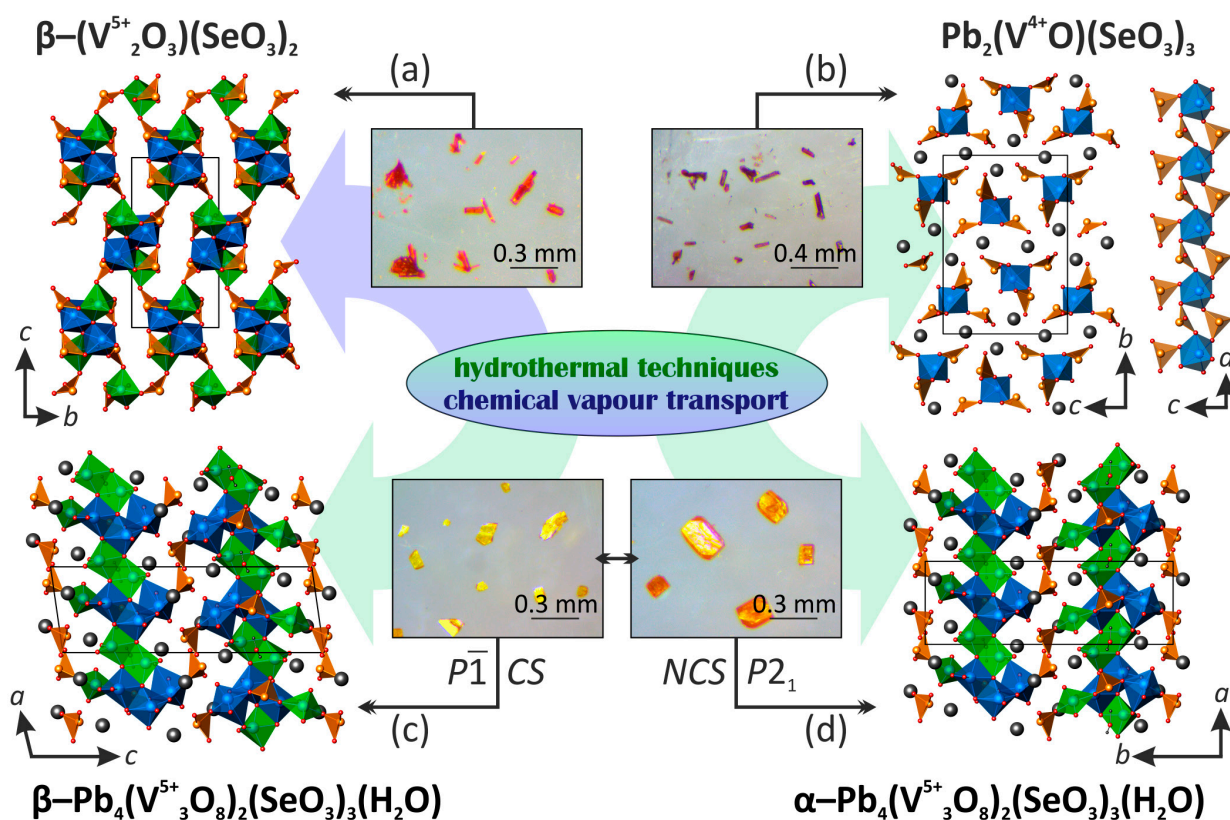


FIGURE 4.2 Projections of the structures and optical images of the crystals of c4.1, c4.2, c4.3, and  $\alpha\text{-Pb}_4(\text{V}_3\text{O}_8)_2(\text{SeO}_3)_3(\text{H}_2\text{O})$ .  $\text{VO}_6$  octahedra,  $\text{VO}_5$  square pyramids,  $\text{SeO}_3$  triangular pyramids, and  $\text{Pb}^{2+}$  cations are blue, green, orange, and grey, respectively.

### Polymorphism of $(\text{V}_2\text{O}_3)(\text{SeO}_3)_2$

The crystal structures of the two polymorphs,  $\alpha\text{-(V}_2\text{O}_3)(\text{SeO}_3)_2$  (Lee and Kwon 1996) and  $\beta\text{-(V}_2\text{O}_3)(\text{SeO}_3)_2$  (**c4.1**), both consist of vanadate tetrameric structural units with different geometry. The crystal structure of  $\alpha$ -modification is based upon chains extended along the  $a$ -axis, and composed of  $(\text{SeO}_3)^{2-}$  pyramids and square-like octahedral  $(\text{V}_4\text{O}_{18})^{16-}$  tetramers shown in Figure 4.3a. The tetramer is built up from two pairs of edge-shared  $\text{V}^{5+}$  octahedra linked through common oxygen equatorial corners. Its  $\text{V}^{5+}$  centers have rather

regular square planar geometry with the V(1)···V(2) lengths of 3.41, 3.53 Å and the V–V–V angles between 88.7° and 91.3°. In contrast, in the structure of  $\beta$ -form (**c4.1**), the tetramer is cruciform (Figure 4.3b). The two mutually perpendicular V(1)···V(1)' and V(2)···V(2)' distances across the tetramer are 3.20 Å and 6.28 Å, respectively. The distribution of short and long V–O distances is highlighted in the Figure 4.3b.

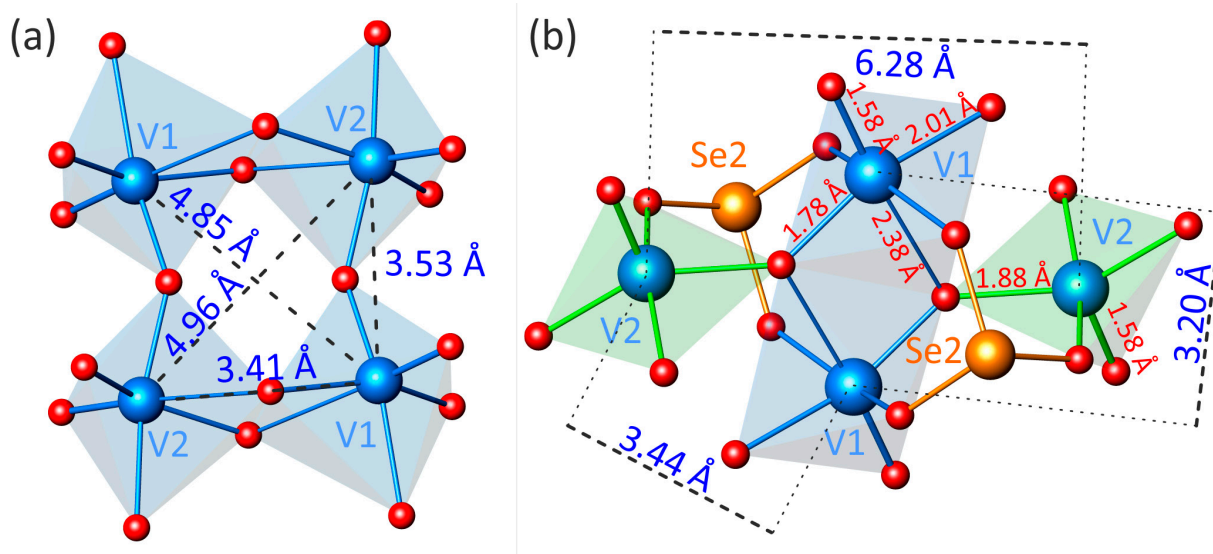


FIGURE 4.3 Vanadate tetrameric structural units in the structures of  $\alpha$ -(V<sub>2</sub>O<sub>3</sub>)(SeO<sub>3</sub>)<sub>2</sub> and  $\beta$ -(V<sub>2</sub>O<sub>3</sub>)(SeO<sub>3</sub>)<sub>2</sub> (**c4.1**) – (a) and (b), respectively.

It is noteworthy that the crystal structures of both polymorphic compounds are related with those of chemically similar (V<sub>2</sub>O<sub>3</sub>)(TeO<sub>3</sub>)<sub>2</sub> (Darriet and Galy 1973; Millet et al. 1999) and (V<sub>2</sub>O<sub>3</sub>)(XO<sub>4</sub>)<sub>2</sub> (X = S, Se) (Tudo et al. 1969; Richter and Mattes 1992; Tyutyunnik et al. 2010). Such a wide variety of the crystal structures of similar chemical compositions can be caused by the presence of chemically different strong short, equatorial and weak long bonds in VO<sub>n</sub> polyhedra, which give rise to a large diversity of different geometries of structural units. Also contributing is the fact that the asymmetric selenite groups with stereochemically active lone electron pair could form structural cavities leading to materials with open architectures.

### **Pb<sub>2</sub>(V<sup>4+</sup>O)(SeO<sub>3</sub>)<sub>3</sub>**

This phase is fundamentally different from the other ones since it contains so-called *vanadyl* (V=O)<sup>2+</sup> ions. In the crystal structure of Pb<sub>2</sub>(V<sup>4+</sup>O)(SeO<sub>3</sub>)<sub>3</sub> (**c4.2**), there is a unique V<sup>4+</sup> position octahedrally coordinated by six O atoms and isolated in the cell. The (VO<sub>6</sub>)<sup>8-</sup> octahedron contains one short *vanadyl* bond (V(1)–O(7) = 1.615 Å), four equatorial bonds with the average bond length of 2.035 Å, and one shortened *trans* bond (V(1)–O(5) = 2.096 Å). Occurrence of such short *trans* bond length is rather rare for the compounds with octahedrally coordinated V<sup>4+</sup> sites (Schindler et al. 2000), and is commonly more closed to 2.2 Å. Nevertheless, it has been observed *e.g.* in the crystal structures of A<sub>2</sub>(VO)<sub>3</sub>(P<sub>2</sub>O<sub>7</sub>)<sub>2</sub> (A = Rb, K) (Leclaire et al. 1988; Lii et al. 1990). In both cases, the valence bond of this “long” oxygen corner is completed by bonding to an oxo-anion (SeO<sub>3</sub> or P<sub>2</sub>O<sub>7</sub>), while the V=O oxygen atom it is not further bonded. Three symmetrically independent Se sites form typical (SeO<sub>3</sub>)<sup>2-</sup> triangular pyramids. The structure of **c4.2** contains two symmetrically independent Pb<sup>2+</sup> sites. Both lead cations are surrounded by ten common O atoms with vanadate and selenite groups. Generally, all Pb<sup>2+</sup> cations demonstrate short and strong Pb–O bonds in one coordination hemisphere and long weaker Pb–O bonds in another.

The structure of **c4.2** can be considered as formed from *1D* vanadate selenite chains with divalent lead cations located in between providing *3D* cohesion of the structure (Figure 4.2b). Single vanadate octahedra share five their oxygen corners with adjacent selenite triangular pyramids to form  $[(VO_2)(SeO_3)_3]^{4-}$  chains running along the *a*-axis. Both bidentate  $Se(2)O_3$  and  $Se(3)O_3$  groups bridge between two adjacent  $V(1)O_6$  octahedra, whereas  $Se(1)O_3$  triangular pyramid is monodentate and shares only one corner with the *trans*-one of the vanadate octahedron. Orientation of the *1D* structural units can be considered as planar and parallel to (010) with divalent lead cations providing their linkage (Figure 4.2b).

### **$\beta$ -Pb<sub>4</sub>(V<sub>3</sub>O<sub>8</sub>)<sub>2</sub>(SeO<sub>3</sub>)<sub>3</sub>(H<sub>2</sub>O)**

New  $\beta$ -polymorphic modification of  $Pb_4(V_3O_8)_2(SeO_3)_3(H_2O)$  (**c4.3**) contains six  $V^{5+}$ , three  $Se^{4+}$ , and four  $Pb^{2+}$  cations per one unit cell. Pentavalent vanadium cations occupy six-fold and five-fold sites.  $V(1)$ ,  $V(2)$ , and  $V(4)$  sites are octahedrally  $[1_s+4+1_t]$  coordinated by six O atoms with each one short bond.  $V(3)$ ,  $V(5)$ , and  $V(6)$  have a distorted square  $[1_s+(1_s+3)]$ -pyramidal environment with two short bonds ( $\langle V-O_s \rangle$  equals 1.643 Å, 1.651 Å, and 1.652 Å for  $V(3)$ ,  $V(5)$ , and  $V(6)$ , respectively) and three equatorial bonds. In the structure of **c4.3**, there are three symmetrically independent  $Se^{4+}$  cations that have typical oxygen coordination of triangular pyramid. The coordination polyhedra of four unique  $Pb^{2+}$  cations are strongly distorted because of the stereoactivity of their  $6s^2$  lone electron pairs.  $Pb(1)$  and  $Pb(2)$  cations are surrounded by eight O atoms with six and seven relatively short strong  $Pb-O$  bonds. The O(26) atom located at a distance of 2.616 Å from  $Pb(1)$  belongs to a water molecule. It links via hydrogen bonding with non-bonded oxygen vertex of the  $Se(3)O$  group ( $O(26)-O(20) = 2.644$  Å), and it forms a long hydrogen contact ( $O(26)-O(17) = 3.269$  Å) with the oxygen atom bridged between  $Se(3)O$  and  $V(3)O_5$  groups.  $Pb(3)$  and  $Pb(4)$  sites are coordinated by nine O atoms. Six of them are located at relatively short distances.

The crystal structure of **c4.3** is built up from vanadate selenite *1D* structural units (Figure 4.4) further bridged by divalent lead cations into a *3D* framework (Figure 4.5). It will be discussed in the next section by analogy to the  $\alpha$ -form. An interesting feature of the crystal structure of **c4.3** is a presence of two chiral vanadate selenite arch-like ribbons related to each other by the inversion centre (Figure 4.2c). Adjacent chiral ribbons bridged via strong metal oxide linkages form *2D* structural units parallel to (010) (Figure 4.5b).  $Pb(1)$  and  $Pb(2)$  cations provide additional interconnection of the layers into a *3D* framework. Water molecules filled the remaining void space in the structure and hydrogen bonding does not participate in the connection of adjacent structural units.

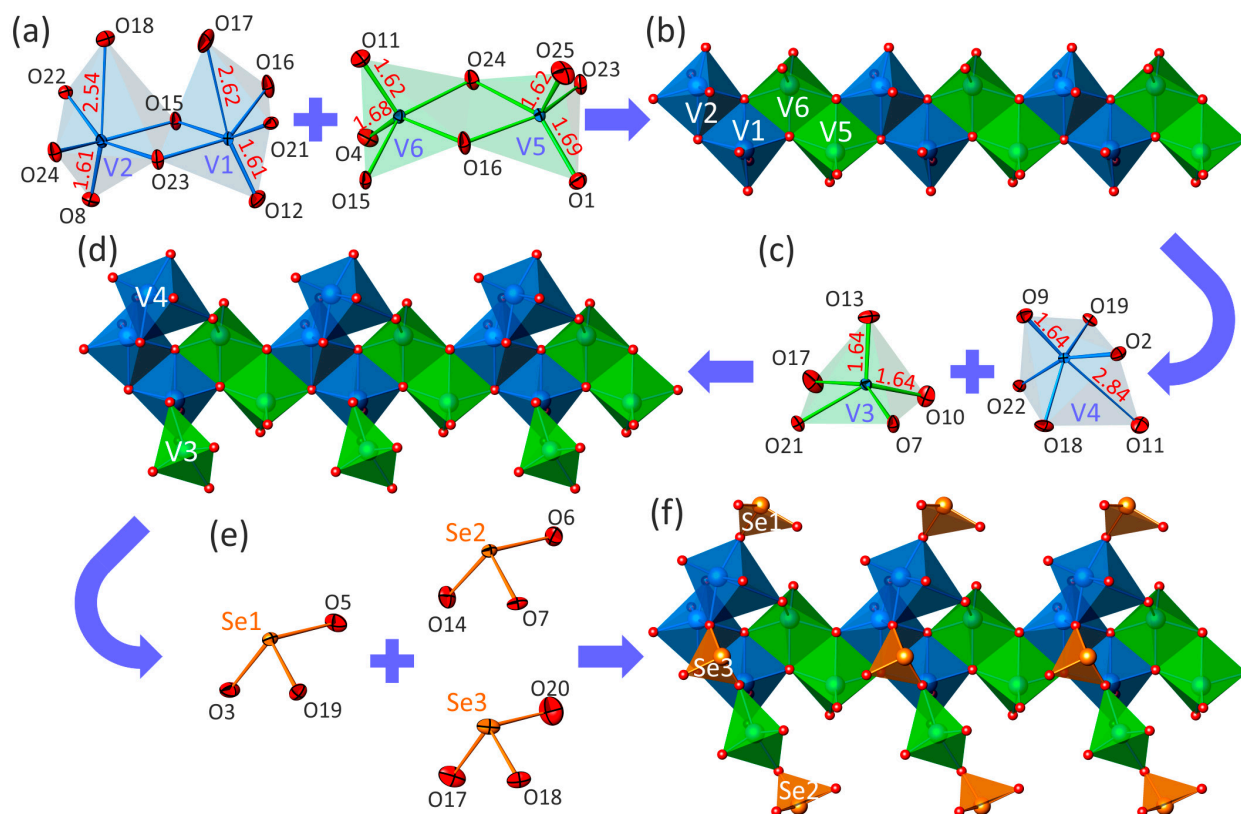


FIGURE 4.4 Structural units in the crystal structure of  $\beta$ - $\text{Pb}_4(\text{V}^{5+}_3\text{O}_8)_2(\text{SeO}_3)_3(\text{H}_2\text{O})$  (c4.3).

### Polymorphism of $\text{Pb}_4(\text{V}_3\text{O}_8)_2(\text{SeO}_3)_3(\text{H}_2\text{O})$

Both  $\alpha$ - and  $\beta$ -polymorphic compounds have been synthesized within the framework of the present study. But the  $\alpha$ -form of  $\text{Pb}_4(\text{V}_3\text{O}_8)_2(\text{SeO}_3)_3(\text{H}_2\text{O})$  has been very recently described in (Cao et al. 2014). It crystallizes in the monoclinic noncentrosymmetric  $P2_1$  space group, while the  $\beta$ -form (c4.3) has triclinic symmetry, space group  $P-1$ . Crystal structures of both polymorphs based upon the same 1D vanadate selenite units are very similar and have very close unit-cell parameters with approximately equal volumes (Figure 4.2c, d).

Significant differences between them are that the structure of  $\alpha$ - $\text{Pb}_4(\text{V}_3\text{O}_8)_2(\text{SeO}_3)_3(\text{H}_2\text{O})$  consists of two rotated vanadate selenite ribbons (designated as  $\mathbf{A}$  and  $\mathbf{A}^{21}$ ) as a result of operation of the  $2_1$  screw axis, whereas the structure of  $\beta$ -modification (c4.3) contains two chiral inverted vanadate selenite ribbons (designated as  $\mathbf{A}$  and  $\mathbf{A}^{-1}$ ) related to each other by the inversion centre (Figure 4.5). The mode of packing of the vanadate selenite ribbons along the  $b$ - and  $c$ -axis respectively for the two forms remains the same in both polymorphic modifications, and this is achieved by  $\text{SeO}_3$  groups common in the two structures, which is very rare to the best of our knowledge. In the structure of the  $\alpha$ -polymorph, the ribbon  $\mathbf{A}$  is connected to adjacent rotated ribbon  $\mathbf{A}^{21}$  forming a layer composed of alternating ribbons in a  $\dots\mathbf{A}\text{-}\mathbf{A}^{21}\text{-}\mathbf{A}\text{-}\mathbf{A}^{21}\text{-}\mathbf{A}\dots$  sequence (Figure 4.5a). The structure of  $\beta$ -phase (c4.3) has a  $\dots\mathbf{A}\text{-}\mathbf{A}^{-1}\text{-}\mathbf{A}\text{-}\mathbf{A}^{-1}\text{-}\mathbf{A}\dots$  packing sequence of the vanadate selenite ribbons (Figure 4.5b). Adjacent layers of the same sequences in both structures are placed directly under each other.

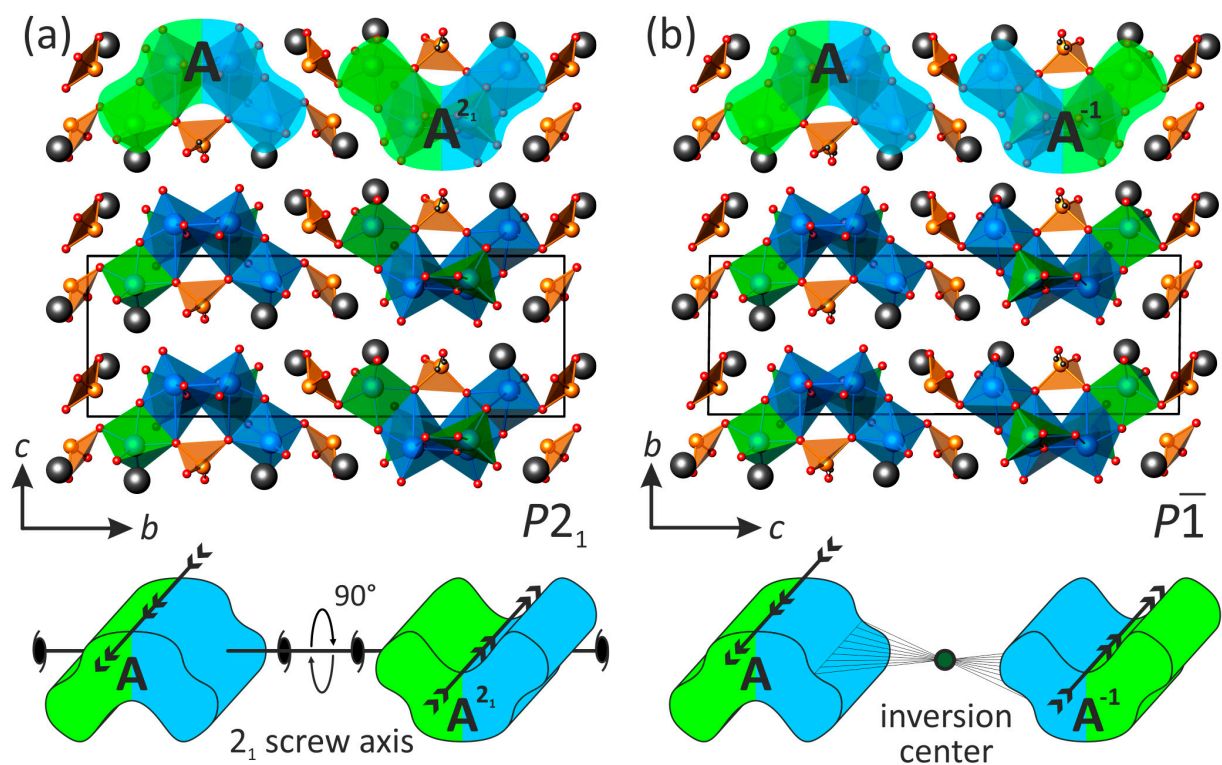


FIGURE 4.5 Mode of stacking of the vanadate selenite ribbons in the crystal structures of  $\alpha$ - $\text{Pb}_4(\text{V}_3\text{O}_8)_2(\text{SeO}_3)_3(\text{H}_2\text{O})$ - (a) and  $\beta$ - $\text{Pb}_4(\text{V}_3\text{O}_8)_2(\text{SeO}_3)_3(\text{H}_2\text{O})$  (c4.3) (b).



## 2.5 Crystal chemical studies of selenium compounds with manganese and bismuth

$\text{Bi}^{3+}$  ion has strong affinity to oxo-centered topologies (Huvé et al. 2006; Colmont et al. 2008; Aliev et al. 2012; Kozin et al. 2013; Colmont et al. 2013; Aliev et al. 2013; Lü et al. 2014), and, therefore, its combination with  $\text{SeO}_3$  groups promises to appear very unusual phases. In addition, the substitution of  $\text{Bi}^{3+}$  for  $\text{Mn}^{2+}$  ion in several oxo-centered phases (Abraham et al. 2002; Aliev et al. 2014) encouraged us to work with manganese phases as well. Although our results showed only one oxo-centered new phase (**c5.2**), seven novel compounds have been identified. Crystallographic data and experimental parameters for the crystal structures of the compounds studied in this chapter and listed below are summarized in [Table 5.1](#).

<b>c5.1</b> – $\text{Mn}(\text{SeO}_4)(\text{H}_2\text{O})_2$	<b>c5.5</b> – $\text{Bi}_6(\text{SeO}_3)_4\text{Cl}_{10}$
<b>c5.2</b> – $\text{Mn}_2[\text{Bi}_2\text{O}](\text{SeO}_3)_4$	<b>c5.6</b> – $\beta\text{-Bi}(\text{SeO}_3)\text{Cl}$
<b>c5.3</b> – $\text{MnBi}(\text{SeO}_3)_2\text{Cl}$	<b>c5.7</b> – $\text{PbBi}_{10}(\text{SeO}_3)_{12}\text{Cl}_8$
<b>c5.4</b> – $\text{Mn}_4(\text{Mn}_5\text{Bi})(\text{SeO}_3)_8\text{Cl}_5$	

TABLE 5.1 Crystallographic data and refinement parameters for **c5.1**, **c5.2**, **c5.3**, **c5.4**, **c5.5**, **c5.6**, and **c5.7**.

	<b>c5.1</b>	<b>c5.2</b>	<b>c5.3</b>	<b>c5.4</b>	<b>c5.5</b>	<b>c5.6</b>	<b>c5.7</b>
$M_r$ (g mol <sup>-1</sup> )	233.93	1051.68	553.29	1896.37	2116.22	371.4	4104.1
space group	<i>Pbca</i>	<i>Pccn</i>	<i>P-1</i>	<i>Pbcm</i>	<i>P2_1/c</i>	<i>Cc</i>	<i>Ccca</i>
<i>a</i> (Å)	10.4353(5)	10.8771(3)	7.0926(8)	10.7914(2)	21.460(2)	22.7052(3)	15.819(6)
<i>b</i> (Å)	9.2420(5)	19.9770(5)	7.2695(6)	15.9782(3)	8.4012(9)	76.785(4)	17.871(7)
<i>c</i> (Å)	10.5349(6)	5.5058(1)	8.0160(8)	17.5682(3)	15.3370(18)	16.0550(3)	15.857(6)
$\alpha$ (°)	90	90	88.226(4)	90	90	90	90
$\beta$ (°)	90	90	72.005(3)	90	110.639(5)	135.000(2)	90
$\gamma$ (°)	90	90	64.560(4)	90	90	90	90
<i>V</i> (Å <sup>3</sup> )	1016.02(9)	1196.37(5)	352.47(6)	3029.23(10)	2587.7(5)	19792.4(12)	4483(3)
<i>Z</i>	8	4	2	4	4	192	4
$\rho$ (g/cm <sup>3</sup> )	3.059	5.839	5.213	4.158	5.432	5.981	6.079
$\mu$ (mm <sup>-1</sup> )	9.71	43.63	37.40	19.55	47.37	52.08	53.17
$\lambda$ (MoK $\alpha$ ) (Å)	0.71073	0.71073	0.71073	0.71073	0.71073	0.71073	0.71073
total rflns	6089	8112	7238	32242	25390	242854	10469
indep rflns	1808	1895	2194	4767	4534	35097	2253
$R_{\text{int}}$	0.0295	0.0247	0.0198	0.0310	0.0421	0.0962	0.0496
$R_1$ [ $I > 2\sigma(I)$ ]	0.0227	0.0285	0.0208	0.0220	0.0291	0.0612	0.0667
$wR_2$ [ $I > 2\sigma(I)$ ]	0.0467	0.0620	0.0436	0.0529	0.0711	0.0645	0.0639
$R_1$ [all data]	0.0302	0.0325	0.0219	0.0317	0.0333	0.1124	0.1057
$wR_2$ [all data]	0.0489	0.0637	0.0441	0.0565	0.0767	0.0694	0.0859
GOF	1.030	1.143	1.056	1.021	1.088	1.32	0.92
$\Delta\rho_{\text{max}}, \Delta\rho_{\text{min}}$ (e Å <sup>-3</sup> )	0.70, -0.93	2.54, -1.47	1.90, -1.67	0.73, -1.16	3.42, -2.95	5.39, -4.51	5.38, -7.01

### 2.5.1 Synthetic procedures

Novel compounds studied in this chapter have been synthesized by different techniques.

Evaporation method from aqueous solution of hydrated manganese(II) chloride (2.4 mmol), 40% selenic acid  $\text{H}_2\text{SeO}_4$  (4.7 mmol) and distilled water (10 ml) was used for synthesis of  $\text{Mn}(\text{SeO}_4)(\text{H}_2\text{O})_2$  (**c5.1**). The solution was stirred with a magnetic stirrer at 80 °C for 3 hours until it became fully homogeneous, then was poured onto a watch glass and left in a fume hood at room temperature. It should be noted that

on heating above 160 °C the selenic acid  $\text{H}_2\text{Se}^{6+}\text{O}_4$  can be easily decomposed with the formation of selenious acid  $\text{H}_2\text{Se}^{4+}\text{O}_3$  and oxygen (De 2003). Single crystals of **c5.1** suitable for X-ray analysis were grown after two days.

Single crystals of  $\text{Mn}_2[\text{Bi}_2\text{O}](\text{SeO}_3)_4$  (**c5.2**), have been obtained from the hydrothermal reaction of  $\text{SeO}_2$  (2.5 mmol),  $\text{MnO}_2$  (2.0 mmol),  $\text{Mn}_2\text{O}_3$  (0.25 mmol), and  $\text{BiOCl}$  (3.0 mmol). The reaction was run in the 23-mL autoclave for two days at 200 °C and then cooled at a rate of 3.7 °C/h to 22 °C.

The other compounds have been prepared using the CVT method. The  $\text{MnBi}(\text{SeO}_3)_2\text{Cl}$  (**c5.3**) and  $\text{Bi}_6(\text{SeO}_3)_4\text{Cl}_{10}$  (**c5.5**) compounds were grown together as a result of the same chemical vapour transport reaction of  $\text{SeO}_2$  (4 mmol),  $\text{Mn}_2\text{O}_3$  (1.0 mmol),  $\text{Bi}_2\text{O}_3$  (1.0 mmol) and  $\text{BiCl}_3$  (2.0 mmol) performed in a sealed evacuated silica tube over a temperature gradient of 400 °C to 350 °C during 100 hours. The  $\text{Mn}_4(\text{Mn}_5\text{Bi})(\text{SeO}_3)_8\text{Cl}_5$  (**c5.4**) phase was synthesized by the CVT reaction of the same stoichiometric mixture that used for two previous compounds. The temperature gradient was 450 °C to 400 °C for 240 hours of thermal treatment. Concurrently, in the UCCS research group, other two new compounds,  $\beta\text{-Bi}(\text{SeO}_3)\text{Cl}$  (**c5.6**) and  $\text{PbBi}_{10}(\text{SeO}_3)_{12}\text{Cl}_8$  (**c5.7**), have been synthesized by Dr. Almaz Aliev. The crystals of **c5.6** were grown by the CVT reaction of the mixture of  $\text{SeO}_2$  (1.0 mmol),  $\text{MnO}_2$  (1.0 mmol),  $\text{BiOCl}$  (1.0 mmol), and a drop of concentrated solution of  $\text{HCl}$ , while the mixture of  $\text{SeO}_2$  (1.0 mmol),  $\text{PbO}$  (1.0 mmol),  $\text{BiOCl}$  (1.0 mmol), and a drop of concentrated solution of  $\text{HCl}$  was used for preparation of the compound **c5.7**. The drops of hydrochloric acid were considered and used as a transport agent in these cases.

## 2.5.2 Structural description of seven novel phases

### **$\text{Mn}(\text{Se}^{6+}\text{O}_4)(\text{H}_2\text{O})_2$**

The crystal structure of  $\text{Mn}(\text{SeO}_4)(\text{H}_2\text{O})_2$  (**c5.1**) contains one symmetrically inequivalent octahedrally coordinated  $\text{Mn}^{2+}$  cation. Four of six of its oxygen ligands are interacting with adjacent  $\text{Se}^{6+}$  cations, while two others belong to water molecules arranged in *cis*-position relative to each other. A unique crystallographically independent  $\text{Se}^{6+}$  site has tetrahedral coordination and linked by sharing of all its four vertices with adjacent  $\text{MnO}_4(\text{H}_2\text{O})_2$  octahedra into a 3D framework (Figure 5.1a).

The framework of the crystal structure of **c5.1** can be regarded as composed of interlinked heteropolyhedral sheets (Figure 5.1b). The structural topology of analogous framework was described by S.V. Krivovichev at the example of  $\text{Zn}(\text{SeO}_4)(\text{H}_2\text{O})_2$  using a graphical approach (Krivovichev 2007). The representation of the sheet as a black-and-white graph is shown in Figure 5.1c. It is based upon hexagonal non-planar rings. The orientations of black ( $\text{Mn}^{2+}$ ) and white ( $\text{Se}^{6+}$ ) vertices relative to the graph plane are depicted by symbols U (up) and D (down). The symbols also designate the direction of links between adjacent sheets within the 3D framework of the crystal structure.

The structure of **c5.1** belongs to the variscite structural type  $M(\text{TO}_4)(\text{H}_2\text{O})_2$ , where  $M = \text{Fe}^{3+}$ ,  $\text{Al}^{3+}$ ,  $\text{Ga}^{3+}$ ,  $\text{In}^{3+}$  or  $\text{Zn}^{2+}$ , and  $T = \text{P}^{5+}$ ,  $\text{As}^{5+}$  or  $\text{Se}^{6+}$ . This type includes such minerals as mansfieldite, scorodite, strengite, yanomaite, and variscite itself. It should be noted, that  $\text{Mn}(\text{SeO}_4)(\text{H}_2\text{O})_2$  is the second example of the variscite-type compound containing metal cations in the oxidation state of +2 and Se cations in tetrahedral coordination.

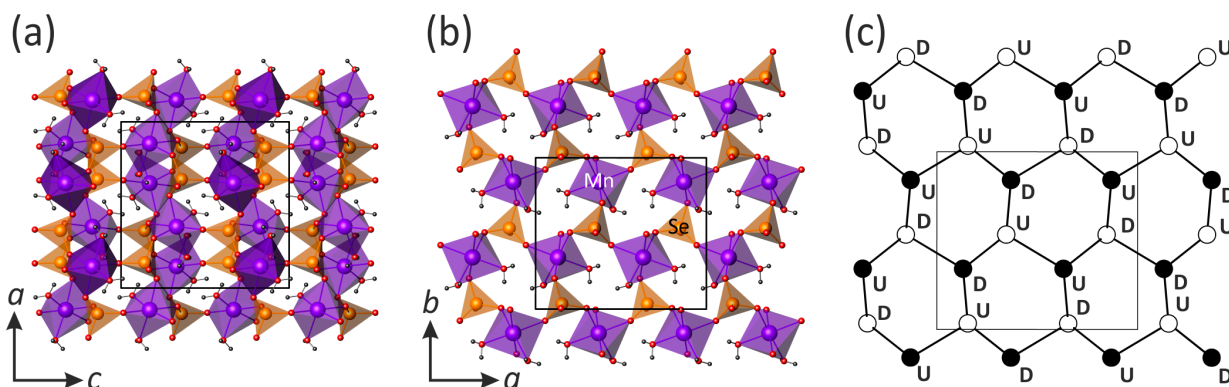


FIGURE 5.1 View of the crystal structure of  $\text{Mn}(\text{SeO}_4)(\text{H}_2\text{O})_2$  (c5.1) projected along the  $a$ -axis – (a); heteropolyhedral sheet parallel to the (001) plane – (b) and its black-and-white graph with symbols designating the direction of bonds to adjacent sheets – (c).

### $\text{Mn}_2[\text{Bi}_2\text{O}](\text{SeO}_3)_4$

The structure of  $\text{Mn}_2[\text{Bi}_2\text{O}](\text{SeO}_3)_4$  (c5.2) contains only a single crystallographic Bi site coordinated by 8 oxygen atoms. The coordination polyhedron of  $\text{Bi}^{3+}$  can be described as a distorted square anti-prism. The unique  $\text{Mn}^{2+}$  cation site has a distorted octahedral coordination. Each  $\text{MnO}_6$  octahedron shares two edges with adjacent octahedra to form  $[\text{MnO}_4]^{6-}$  zigzag chains running along the  $c$ -axis (Figure 5.2a). Two crystallographically independent  $\text{Se}^{4+}$  sites form typical selenite pyramids. The crystal structure of c5.2 contains an “additional” oxygen atom, which is coordinated solely by four  $\text{Bi}^{3+}$  cations forming oxo-centered ( $\text{OBi}_4$ )<sup>10+</sup> tetrahedra. They share *trans*-oriented edges to form infinite  $[\text{Bi}_2\text{O}]^{4+}$  chains along the  $c$ -axis (Figure 5.2c). These chains are rather common in the crystal chemistry of oxo-centred bismuth phases, e.g. in  $[\text{Bi}_2\text{O}]\text{AuO}_4$  (Krivovichev et al. 2013b). The chains are further linked through  $\text{SeO}_3$  groups and  $[\text{MnO}_4]^{6-}$  structural units into a 3D framework with pseudo-tetragonal empty channels occupied by lone electron pairs of  $\text{Se}^{4+}$  cations (Figure 5.2b).

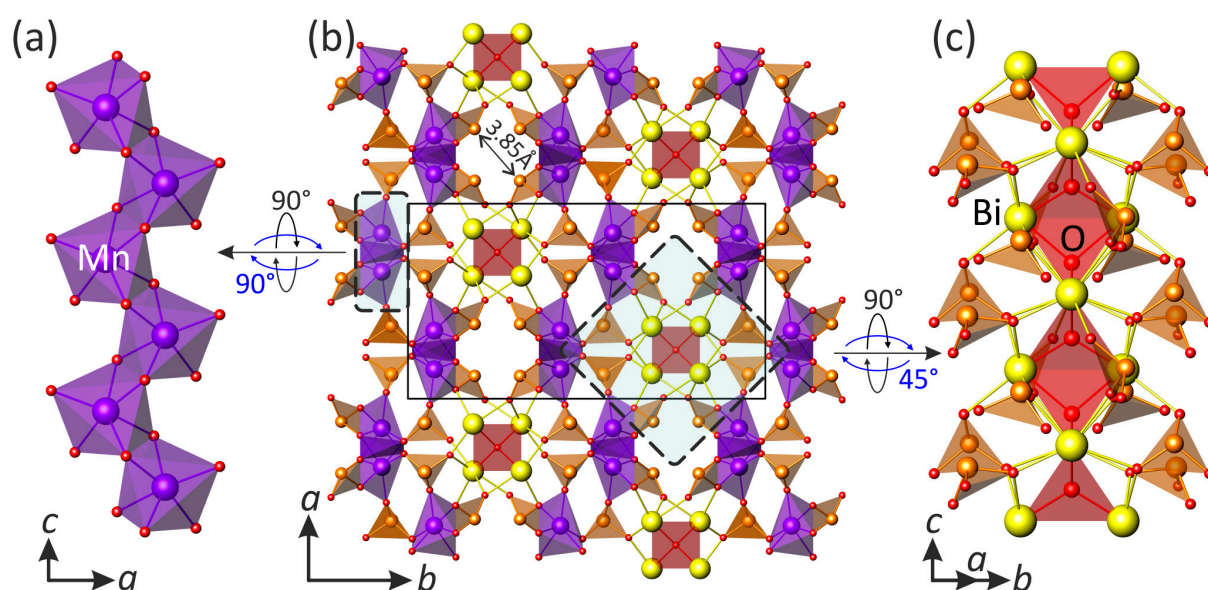


FIGURE 5.2 Projection of the crystal structure of  $\text{Mn}_2[\text{Bi}_2\text{O}](\text{SeO}_3)_4$  (c5.2) (b) composed of  $[\text{MnO}_4]^{6-}$  (a) and  $[\text{Bi}_2\text{O}]^{4+}$  chains (c).

The structural architecture of **c5.2** is closely related to that observed in the crystal structures of  $\text{Tb}_2\text{O}[\text{SeO}_3]_2$  (Wontcheu and Schleid 2002) and  $M_3\text{O}_2\text{Cl}[\text{SeO}_3]_2$  ( $M^{3+} = \text{Tb}$  (Wontcheu and Schleid 2005) and  $\text{Y}$  (Zitzer et al. 2011)). In their structures the lone electron pairs of  $\text{Se}^{4+}$  cations form similar empty channels running between four cationic  $[\text{Tb}_2\text{O}]^{4+}$  chains in  $\text{Tb}_2\text{O}[\text{SeO}_3]_2$  and  $[\text{M}_3\text{O}_2]^{5+}$  double chains in  $M_3\text{O}_2\text{Cl}[\text{SeO}_3]_2$  ( $M^{3+} = \text{Tb}$  and  $\text{Y}$ ).

### **MnBi(SeO<sub>3</sub>)<sub>2</sub>Cl**

In the crystal structure of  $\text{MnBi}(\text{SeO}_3)_2\text{Cl}$  (**c5.3**), there is one symmetrically inequivalent Mn site. The  $\text{Mn}^{2+}$  cations form  $(\text{MnO}_4\text{Cl}_2)^{8-}$  octahedra, which are interconnected *via* common Cl–Cl and O–O edges to infinite zigzag chains running along the *a*-axis (Figure 5.3). The chains are further linked by typical selenite  $\text{SeO}_3$  groups into sheets parallel to (001).

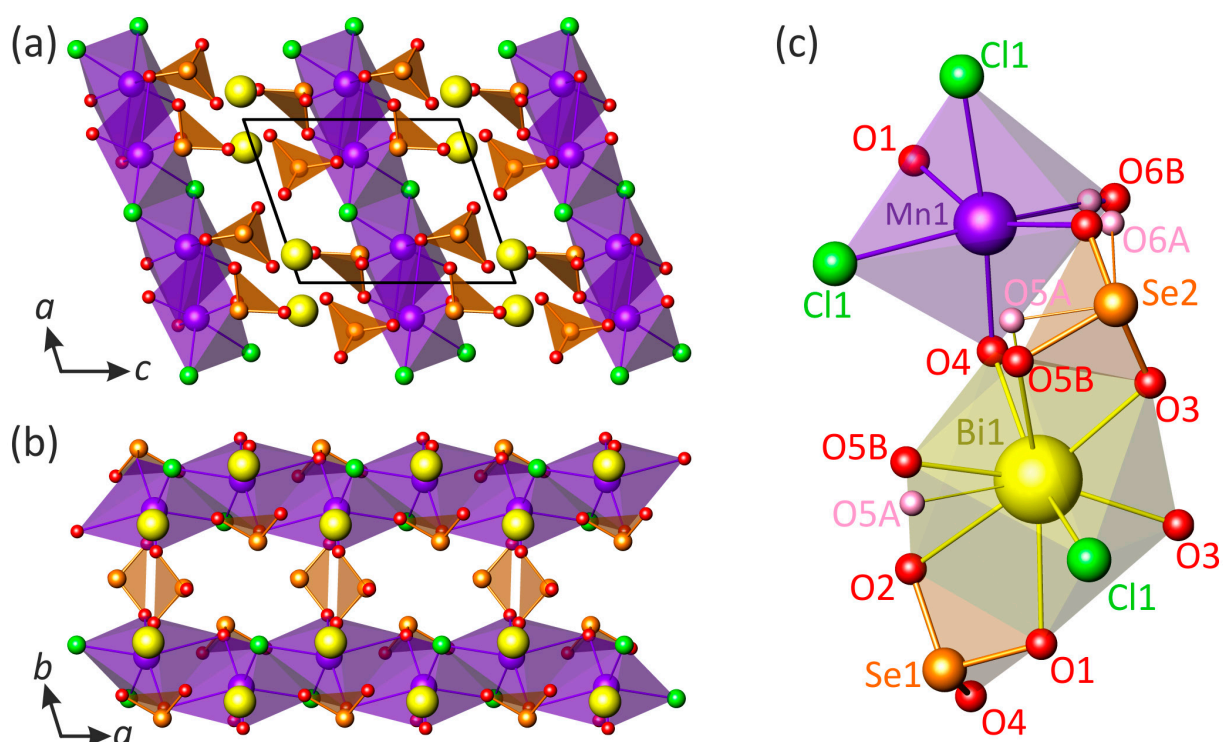


FIGURE 5.3 General projections of the crystal structure of  $\text{MnBi}(\text{SeO}_3)_2\text{Cl}$  (**c5.3**) along [010] – (a) and [001] – (b) (disordered O sites are omitted for clarity); anionic arrangement of metal cations in the structure – (c).

During the structure solution and refinement process, two possible conformations of one of two symmetrically inequivalent selenite anions were observed due to disorder of two O sites. A refinement of the occupancies of the disordered O atoms gave ratios of 0.50/0.50 and 0.67/0.33 for O(5)a/O(5)b and O(6)a/O(6)b, respectively. A refinement of the anisotropic thermal parameters of the O(3) site placed at the third corner of the  $\text{Se}(2)\text{O}_3$  group resulted in normal thermal values, while the  $\text{Se}(2)$  showed the high thermal parameters. The two conformations of the  $\text{Se}(2)\text{O}_3$  selenite group (Figure 5.3c) may denote partial Bi/Mn disorder that was not taken into account at this stage. In the structure of **c5.3**, a symmetrically unique  $\text{Bi}^{3+}$  cation is in nine-fold distorted coordination of eight oxygen and single chlorine atoms (Figure 5.3c). The  $\text{Bi}^{3+}$  cations separate the sheets composed of selenite and manganese polyhedra from one another and serve to balance charge.

The structure of **c5.3** is isotypic with previously studied  $\text{MnSm}(\text{SeO}_3)_2\text{Cl}$ ,  $\text{CoSm}(\text{SeO}_3)_2\text{Cl}$ , and  $\text{CuGd}(\text{SeO}_3)_2\text{Cl}$  (Wickleder and Hamida 2003).

### $\text{Mn}^{2+}_4(\text{Mn}^{2+}_5, \text{Bi}^{3+})(\text{SeO}_3)_8\text{Cl}_5$

The compound  $\text{Mn}_4(\text{Mn}_5, \text{Bi})(\text{SeO}_3)_8\text{Cl}_5$  (**c5.4**) is an example of a partially Bi/Mn disordered structure, in the sense that several subunits assembled in the crystal structure show statistic cationic distribution over mixed sites. The crystal structure of **c5.4** is based upon 2D structural units composed of distorted square antiprisms of four crystallographically inequivalent mixed sites statistically occupied by mainly  $\text{Mn}^{2+}$  and  $\text{Bi}^{3+}$  cations. The edge-sharing antiprisms are arranged in check-wise fashion (Figure 5.4a). A refinement of the mixed sites gave the following cationic distributions:  $0.97\text{Mn}^{2+}/0.03\text{Bi}^{3+}$ ,  $0.92\text{Mn}^{2+}/0.08\text{Bi}^{3+}$ ,  $0.87\text{Mn}^{2+}/0.13\text{Bi}^{3+}$ , and  $0.37\text{Mn}^{2+}/0.63\text{Bi}^{3+}$  for Mn(3), Mn(4), Mn(5), and Bi(6), respectively, under restraints of neutral charge.

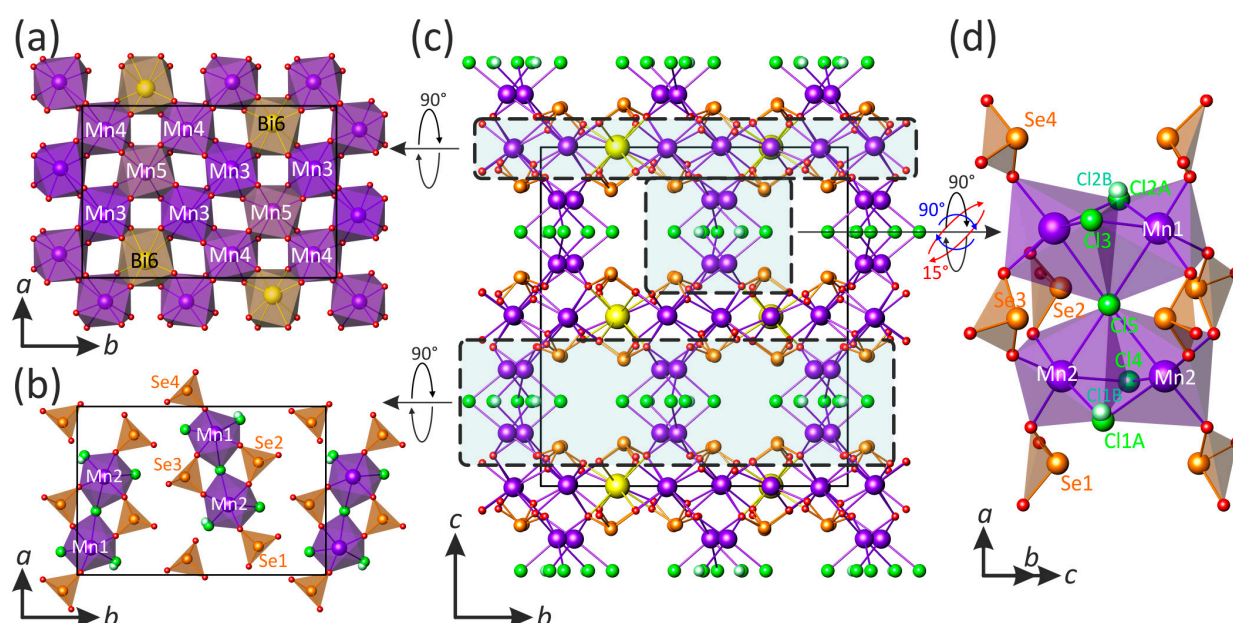


FIGURE 5.4 Projection of the crystal structure of  $\text{Mn}_4(\text{Mn}_5, \text{Bi})(\text{SeO}_3)_8\text{Cl}_5$  (**c5.4**) along [100] – (c), the sheet of square antiprisms – (a), the tetrameric unit – (d), and their arrangement in the structure – (b).

In the structure of **c5.4**, there are two fully ordered  $\text{Mn}^{2+}$  sites, which are octahedrally surrounded by three oxygen and three chlorine atoms each. A couple of the octahedra share their common  $\text{Cl}_3$  face to form a dimer, which is further linked through one of the Cl corners with adjacent dimer into a square-like tetrameric unit. Four symmetrically inequivalent  $\text{Se}^{4+}$  triangular pyramids are connected to the O corners of the tetrameric unit as shown in Figure 5.4d. An inspection of a Fourier difference electron-density map showed that two of five crystallographically independent  $\text{Cl}^-$  sites are disordered. A refinement of their occupancies indicated the same 0.58/0.42 ratio for both Cl(1)a/Cl(1)b and Cl(2)a/Cl(2)b sites. The arrangement of the tetrameric units in the structure of **c5.4** is shown in Figure 5.4b.

The tetrameric units are connected to the 2D sheets *via* sharing of O–O edges of octahedra and selenite pyramids with the square antiprisms resulting in a complex 3D framework with large pseudo-tetragonal empty channels occupied by lone electron pairs of  $\text{Se}^{4+}$  cations along the *a*-axis (Figure 5.4c).

**Bi<sub>6</sub>(SeO<sub>3</sub>)<sub>4</sub>Cl<sub>10</sub>**

The crystal structure of Bi<sub>6</sub>(SeO<sub>3</sub>)<sub>4</sub>Cl<sub>10</sub> (**c5.5**) is formed by six distorted oxochloride polyhedra of bismuth, Bi(1)O<sub>3</sub>Cl<sub>4</sub>, Bi(2)O<sub>5</sub>Cl<sub>4</sub>, Bi(3)O<sub>3</sub>Cl<sub>5</sub>, Bi(4)O<sub>5</sub>Cl<sub>4</sub>, Bi(5)O<sub>5</sub>Cl<sub>4</sub>, and Bi(6)O<sub>5</sub>Cl<sub>4</sub>, linked to four crystallographically inequivalent Se<sup>4+</sup> cations resulting in a 3D framework. The stereoactive behaviour of the lone electron pairs on the Bi<sup>3+</sup> cations is manifested by the particularly asymmetric coordination environments around these cations. Coordination polyhedra of Bi share their edges and corners to build Bi<sub>6</sub>(SeO<sub>3</sub>)<sub>4</sub>Cl<sub>10</sub> blocks linked together in such a way as to create an open structure with some kind of empty channels bordered by the anions (essentially Cl<sup>-</sup>) and parallel to the *b*-axis (Figure 5.5).

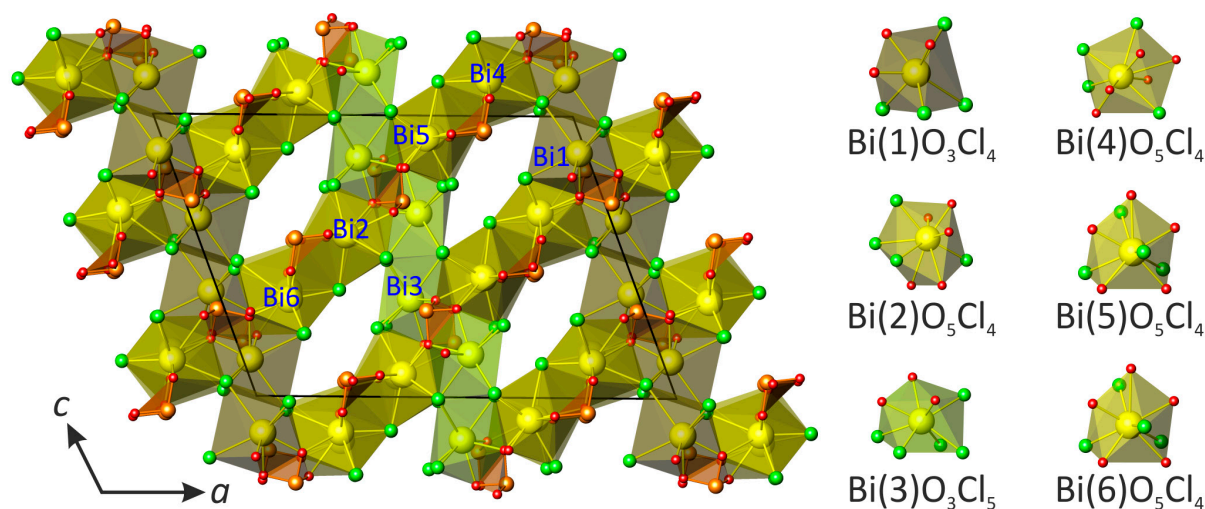


FIGURE 5.5 Projection of the crystal structure of Bi<sub>6</sub>(SeO<sub>3</sub>)<sub>4</sub>Cl<sub>10</sub> (**c5.5**) on the (010) plane, showing BiO<sub>*x*</sub>Cl<sub>*x*</sub> polyhedra (yellow) and SeO<sub>3</sub> groups (orange) sharing their edges and corners.

In the structure of **c5.5**, the cavities are around 9.7 Å long and 3.8 Å wide. The close inspection of a Fourier difference electron-density map showed a high residual peak (8.71 *e*/Å<sup>3</sup>) at a distance of 0.86 Å from the Se(3) site indicating its possible splitting into two satellite positions. The coupled refinement of the occupancies of the Se(3)/Se(3)' sites resulted in the 0.95/0.05 ratio. While the Se–O distances for Se(3) are plausible (1.71–1.74 Å), those for the Se(3)' site are too long (2.09–2.41 Å), which suggested its occupation by Bi<sup>3+</sup>. The final Bi(3)a/Bi(3)b and Se(3)a/Se(3)b occupancies were refined to the ratio of 0.96/0.04. Detailed description of the crystal structure of **c5.5** can be found in the article **A-III** (see Included Articles).

**β-Bi(SeO<sub>3</sub>)Cl with giant unit cell**

The crystal structure of β-Bi(SeO<sub>3</sub>)Cl (**c5.6**) is very unusual and complex. Noteworthy, beyond its NCS character, the volume cell is strikingly large (19792 Å<sup>3</sup>). A total of 48 bismuth, 48 selenium, and 48 chlorine crystallographically independent atoms have been localized. The structure of **c5.6** can be described as built from two blocks, [Bi<sub>8</sub>Cl<sub>16</sub>]<sup>8+</sup> (Figure 5.6c) and [Bi<sub>12</sub>Cl<sub>32</sub>]<sup>4+</sup> (Figure 5.6d), regularly sandwiched between [Bi<sub>14</sub>(SeO<sub>3</sub>)<sub>24</sub>]<sup>6-</sup> sheets (Figure 5.6d). In Figure 5.6a, the BiO<sub>*x*</sub> polyhedra are shown by yellow color, whereas, for the sake of clarity, the [Bi<sub>8</sub>Cl<sub>16</sub>]<sup>8+</sup> and [Bi<sub>12</sub>Cl<sub>32</sub>]<sup>4+</sup> sheets are represented as an arrangement of Bi (yellow) and Cl (green) atoms (Figure 5.6b). It should be noted that similar halide layers with the composition [Bi<sub>8</sub>Cl<sub>16</sub>]<sup>8+</sup> have also been found in the new compound PbBi<sub>10</sub>(SeO<sub>3</sub>)<sub>12</sub>Cl<sub>8</sub> (**c5.7**) described below. The

$[\text{Bi}_{14}(\text{SeO}_3)_{24}]^{6-}$  structural unit is built by the association of  $\text{Bi}^{3+}$  cations and  $\text{SeO}_3$  pyramids. In  $\text{BiO}_x$  units with  $x$  in between 8 and 10, all the Bi-centered polyhedra are asymmetric, which is typical of the bismuth coordination due to the stereoactive behaviour of the  $6s^2$  lone pairs on  $\text{Bi}^{3+}$  cations.

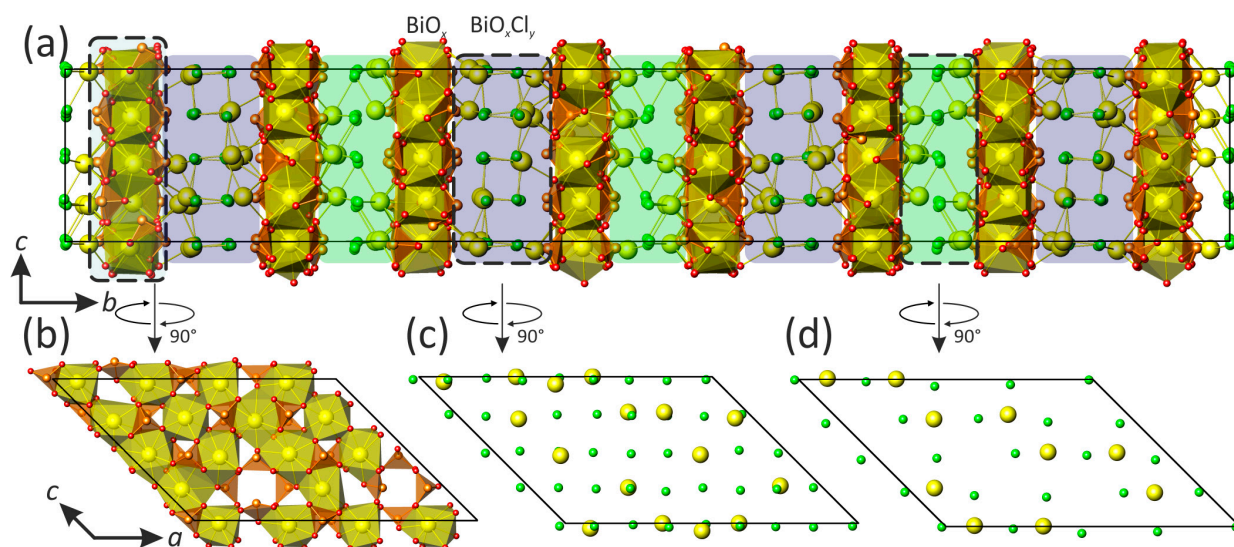


FIGURE 5.6 Projection of the crystal structure of  $\beta\text{-Bi}(\text{SeO}_3)\text{Cl}$  (c5.6) along  $[100]$  – (a). An alternation of three different parallel layers:  $[\text{Bi}_{14}(\text{SeO}_3)_{24}]^{6-}$  – (b),  $[\text{Bi}_{12}\text{Cl}_{32}]^{4+}$  – (c), and  $[\text{Bi}_8\text{Cl}_{16}]^{8+}$  – (d).

The large value of the  $b$ -parameter ( $\sim 76$  Å) can be explained by the variety of different modules stacked along the  $b$ -axis. In other words, the ordering between the  $[\text{Bi}_8\text{Cl}_{16}]^{8+}$  and  $[\text{Bi}_{12}\text{Cl}_{32}]^{4+}$  cationic units sandwiched between the  $[\text{Bi}_{14}(\text{SeO}_3)_{24}]^{6-}$  anionic sheets is the key factor for the formation of a giant cell and responsible for the doubling of  $b$ -parameter (Figure 5.6f). Detailed examination of the crystal structure of c5.6 and the analysis of the  $\alpha \rightarrow \beta \rightarrow \gamma$  phase transitions associated with a dramatic fluctuation of structural complexity together with the transitional character of the  $\beta$  phase can be found in the article A-III (see Included Articles).

### **PbBi<sub>10</sub>(SeO<sub>3</sub>)<sub>12</sub>Cl<sub>8</sub>**

The crystal structure of  $\text{PbBi}_{10}(\text{SeO}_3)_{12}\text{Cl}_8$  (c5.7) contains five independent sites occupied by heavy cations. One of them, Bi(1), is fully occupied by  $\text{Bi}^{3+}$ , while a refinement of the four others indicated the same mixed  $\text{Bi}^{3+}/\text{Pb}^{2+}$  occupancy of 0.9/0.1. Taking into account Bi/Pb–O and Bi–Cl bond lengths smaller than 3.10 Å, the following irregular coordination polyhedra of heavy cations can be observed: Bi(1)O<sub>8</sub>, Bi(2)O<sub>10</sub>, Bi(3)O<sub>10</sub>, Bi(4)O<sub>10</sub>, and Bi(5)O<sub>4</sub>Cl<sub>4</sub>. Three crystallographically inequivalent triangular pyramidal selenite groups are connected to the 2D structural units composed of Bi(1)O<sub>8</sub>, Bi(2)O<sub>10</sub>, Bi(3)O<sub>10</sub> and Bi(4)O<sub>10</sub> polyhedra by sharing of common O–O edges (Figure 5.7). Generally, the structure of c5.7 can be described as a 2D network, with the  $[(\text{Pb},\text{Bi})_{14}(\text{SeO}_3)_{24}]^{n-}$  sheet (Figure 5.7b) sandwiched between the  $[(\text{Pb},\text{Bi})_8\text{Cl}_{16}]^{n+}$  layers (Figure 5.7c) laying parallel to the (010) plane. The structural architecture of c5.7 is closely related to that observed in the crystal structure of  $\text{CaNd}_{10}(\text{SeO}_3)_{12}\text{Cl}_{18}$  (Berdonosov et al. 2007). Detailed description of the crystal structure of c5.7 can be found in the article A-III (see Included Articles).

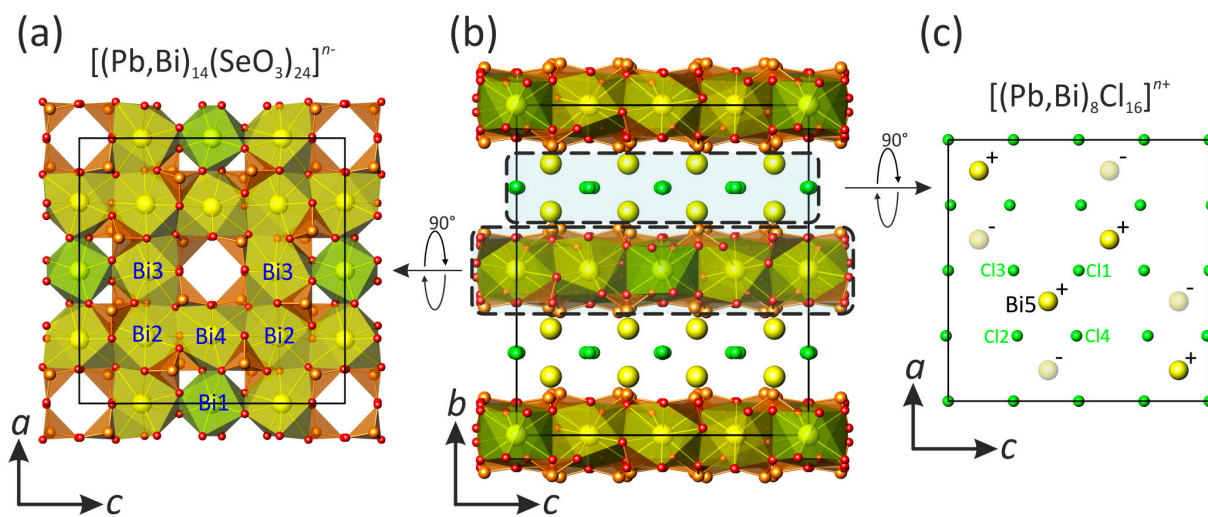


FIGURE 5.7 Projection of the crystal structure of  $\text{PbBi}_{10}(\text{SeO}_3)_{12}\text{Cl}_8$  (c5.7) along the  $a$  axis – (b), two parallel cationic and anionic layers:  $[(\text{Pb,Bi})_{14}(\text{SeO}_3)_{24}]^{n-}$  – (a) and  $[(\text{Pb,Bi})_8\text{Cl}_{16}]^{n+}$  – (c).



## 2.6 Crystal chemical studies of uranyl selenates and selenite-selenates

Crystallographic data and experimental parameters for the crystal structures of 16 novel compounds listed below are summarized in Table 6.1 and 6.2.

<b>c6.1</b> –	$[\text{CH}_6\text{N}]_2$ $[(\text{UO}_2)(\text{SeO}_4)_2(\text{H}_2\text{O})](\text{H}_2\text{O})$	<b>c6.9</b> –	$[\text{C}_2\text{H}_8\text{N}]_2$ $[(\text{UO}_2)(\text{SeO}_4)_2(\text{H}_2\text{O})]$
<b>c6.2</b> –	$[\text{CH}_6\text{N}]_2$ $[(\text{UO}_2)(\text{SeO}_4)_2(\text{H}_2\text{O})]$	<b>c6.10</b> –	$[\text{C}_2\text{H}_8\text{N}]_2$ $[(\text{UO}_2)_2(\text{SeO}_4)_3(\text{H}_2\text{O})]$
<b>c6.3</b> –	$[\text{CH}_6\text{N}]_2$ $[(\text{UO}_2)_2(\text{SeO}_4)_3]$	<b>c6.11</b> –	$[\text{C}_4\text{H}_{15}\text{N}_3][\text{H}_3\text{O}]_{0.5}$ $[(\text{UO}_2)_2(\text{SeO}_4)_{2.93}(\text{SeO}_3)_{0.07}(\text{H}_2\text{O})](\text{NO}_3)_{0.5}$
<b>c6.4</b> –	$[\text{CH}_6\text{N}](\text{H}_3\text{O})$ $[(\text{UO}_2)_2(\text{SeO}_4)_3(\text{H}_2\text{O})](\text{H}_2\text{O})$	<b>c6.12</b> –	$[\text{C}_2\text{H}_8\text{N}]_3[\text{H}_5\text{O}_2]$ $[(\text{UO}_2)_2(\text{SeO}_4)_3(\text{H}_2\text{O})_2](\text{H}_2\text{O})_5$
<b>c6.5</b> –	$[\text{CH}_6\text{N}]_4$ $[(\text{UO}_2)_3(\text{SeO}_4)_5](\text{H}_2\text{O})_4$	<b>c6.13</b> –	$[\text{C}_2\text{H}_8\text{N}]_2[\text{H}_3\text{O}]$ $[(\text{UO}_2)_3(\text{SeO}_4)_4(\text{HSeO}_3)(\text{H}_2\text{O})](\text{H}_2\text{SeO}_3)_{0.2}$
<b>c6.6</b> –	$[\text{CH}_6\text{N}](\text{H}_5\text{O}_2)(\text{H}_3\text{O})_2$ $[(\text{UO}_2)_3(\text{SeO}_4)_5](\text{H}_2\text{O})_4$	<b>c6.14</b> –	$[\text{C}_4\text{H}_{12}\text{N}]_3[\text{H}_3\text{O}]$ $[(\text{UO}_2)_3(\text{SeO}_4)_5(\text{H}_2\text{O})]$
<b>c6.7</b> –	$[\text{CH}_6\text{N}]_4(\text{H}_3\text{O})_2$ $[(\text{UO}_2)_5(\text{SeO}_4)_8(\text{H}_2\text{O})](\text{H}_2\text{O})_4$	<b>c6.15</b> –	$[\text{C}_2\text{H}_8\text{N}]_3(\text{C}_2\text{H}_7\text{N})$ $[(\text{UO}_2)_3(\text{SeO}_4)_4(\text{HSeO}_3)(\text{H}_2\text{O})]$
<b>c6.8</b> –	$[\text{CH}_6\text{N}]_{1.5}(\text{H}_5\text{O}_2)_{1.5}(\text{H}_3\text{O})_3$ $[(\text{UO}_2)_5(\text{SeO}_4)_8(\text{H}_2\text{O})](\text{H}_2\text{SeO}_4)_{2.6}(\text{H}_2\text{O})_3$	<b>c6.16</b> –	$[\text{C}_2\text{H}_8\text{N}][(\text{H}_5\text{O}_2)(\text{H}_2\text{O})]$ $[(\text{UO}_2)_2(\text{SeO}_4)_3(\text{H}_2\text{SeO}_3)](\text{H}_2\text{O})$

TABLE 6.1 Crystallographic data and refinement parameters for c6.1, c6.2, c6.3, c6.4, c6.5, c6.6, c6.7, and c6.8.

	<b>c6.1</b>	<b>c6.2</b>	<b>c6.3</b>	<b>c6.4</b>	<b>c6.5</b>	<b>c6.6</b>	<b>c6.7</b>	<b>c6.8</b>
$M_r$ , (g mol <sup>-1</sup> )	639.99	623.99	1020.98	1042.96	1692.97	1678.91	2709.91	2946.25
sp. gr.	<i>Pnma</i>	<i>P2<sub>1</sub>/c</i>	<i>P2<sub>1</sub></i>	<i>P2<sub>1</sub>/c</i>	<i>Pnna</i>	<i>Ibca</i>	<i>Pca2<sub>1</sub></i>	<i>Pnma</i>
$a$ (Å)	7.5496(7)	8.2366(10)	8.583(1)	8.4842(10)	16.422(1)	20.956(2)	31.505(2)	30.973(2)
$b$ (Å)	12.014(1)	7.5888(6)	10.073(1)	10.2368(8)	18.4773(9)	34.767(8)	10.369(1)	37.022(2)
$c$ (Å)	15.836(1)	22.260(2)	10.095(1)	24.228(2)	10.3602(5)	18.663(2)	16.242(1)	10.417(1)
$\beta$ (°)	90	104.566(9)	95.98(1)	102.803(9)	90	90	90	90
$V$ (Å <sup>3</sup> )	1436.3(2)	1346.7(2)	867.7(2)	2051.9(3)	3143.7(3)	13597(4)	5305.9(6)	11945(1)
$Z$	4	4	2	4	4	16	4	8
$\rho$ (g/cm <sup>3</sup> )	2.960	3.078	3.908	3.376	3.577	3.280	3.392	3.277
$\mu$ (mm <sup>-1</sup> )	16.423	17.507	25.012	21.166	21.319	19.720	20.814	20.086
$\lambda$ (MoK $\alpha$ ) (Å)	0.71073	0.71073	0.71073	0.71073	0.71073	0.71073	0.71073	0.71073
total rflns	10099	12119	5477	12326	18468	32094	27846	61466
indep rflns	1605	3656	2931	3602	2774	4913	8463	10116
$R_{\text{int}}$	0.0875	0.0828	0.1271	0.1698	0.1191	0.3280	0.2070	0.2139
$R_1$ [ $I > 2\sigma(I)$ ]	0.0467	0.0466	0.1072	0.0674	0.0541	0.1040	0.0852	0.0858
$wR_2$ [ $I > 2\sigma(I)$ ]	0.0860	0.0637	0.2712	0.1551	0.1119	0.1867	0.1901	0.1736
$R_1$ [all data]	0.0566	0.0785	0.1126	0.0957	0.0790	0.2138	0.1305	0.1556
$wR_2$ [all data]	0.0882	0.0688	0.2766	0.1693	0.1216	0.2287	0.2150	0.2083
GOF	1.334	0.996	1.083	1.049	1.104	0.968	0.997	1.055
$\Delta\rho_{\text{max}}$ , $\Delta\rho_{\text{min}}$ , $e \text{ \AA}^{-3}$	1.44, -3.13	1.59, -2.21	8.61, -3.16	2.84, -1.99	2.23, -1.82	2.58, -1.43	2.44, -1.84	2.90, -1.49
CCDC #	866552	866549	866547	866553	866546	866551	866548	866550

TABLE 6.2 Crystallographic data and refinement parameters for c6.9, c6.10, c6.11, c6.12, c6.13, c6.14, c6.15, and c6.16.

	c6.9	c6.10	c6.11	c6.12	c6.13	c6.14	c6.15	c6.16
$M_r$ , (g mol <sup>-1</sup> )	666.15	1079.14	2256.03	2267.28	1685.05	1770.70	1685.07	1217.08
sp. gr.	$P2_12_12_1$	$P2_12_12_1$	$P2_1/c$	$P2_1/c$	$P2_1/m$	$P2_1/m$	$Pnma$	$P2_1/n$
$a$ (Å)	7.5363(7)	11.2154(5)	11.1679(4)	12.451(5)	8.3116(4)	8.941(2)	11.659(1)	14.7979(8)
$b$ (Å)	12.202(1)	11.2263(5)	10.9040(4)	31.126(5)	18.6363(8)	19.300(4)	14.956(2)	10.0238(6)
$c$ (Å)	16.760(2)	16.9138(8)	17.9913(6)	14.197(4)	11.5623(5)	11.377(3)	22.194(2)	16.4176(9)
$\beta$ (°)	90.00	90.00	98.019(1)	120.39(2)	97.582(1)	97.510(4)	90.00	111.628(1)
$V$ (Å <sup>3</sup> )	1541.2(2)	2129.6(2)	2169.6(2)	4746(2)	1775.3(1)	1946.5(7)	3870.0(7)	2263.8(2)
$Z$	4	4	2	4	2	2	4	4
$\rho$ (g/cm <sup>3</sup> )	2.871	3.366	3.457	3.173	3.152	3.021	2.892	3.571
$\mu$ (mm <sup>-1</sup> )	15.306	20.394	20.036	18.323	19.286	17.217	17.310	20.822
$\lambda$ (MoK $\alpha$ ) (Å)	0.71073	0.71073	0.71073	0.71073	0.71073	0.71073	0.71073	0.71073
total rflns	13644	17184	23671	34682	23753	18435	10911	25431
indep rflns	4492	6112	4988	10896	5323	4597	1680	5476
$R_{int}$	0.056	0.065	0.072	0.096	0.076	0.120	0.112	0.073
$R_1$ [ $I > 2\sigma(I)$ ]	0.031	0.029	0.033	0.048	0.036	0.040	0.060	0.027
$wR_2$ [ $I > 2\sigma(I)$ ]	0.063	0.048	0.074	0.106	0.097	0.058	0.096	0.052
$R_1$ [all data]	0.035	0.038	0.049	0.104	0.055	0.099	0.095	0.041
$wR_2$ [all data]	0.064	0.050	0.077	0.122	0.102	0.066	0.105	0.054
GOF	0.940	0.934	0.964	0.875	0.979	0.737	1.127	0.928
$\Delta\rho_{max}$ , $\Delta\rho_{min}$ , $e$ Å <sup>-3</sup>	2.34, -1.45	1.10, -1.20	2.82, -2.00	4.61, -4.34	2.79, -2.23	1.65, -1.38	1.05, -1.21	2.39, -1.81
CCDC #	901940	901941	901942	901943	901944	901945	901946	824406

## 2.6.1 Synthetic procedures

Single crystals of all novel uranyl selenates and selenite-selenates were prepared by isothermal evaporation under ambient conditions from aqueous solutions of uranyl nitrate hexahydrate, 40%–solution of selenic acid, the respective amine, and deionized distilled water. Yellow-green homogeneous liquid solutions in the vials were left open to the air in a fume hood at the room temperature for several days, after which they were capped and left standing at room temperature. Experimental details containing various molar ratios of initial reagents for syntheses of 16 novel phases are summarized in Table 6.3.

TABLE 6.3 Experimental details of the isothermal evaporation syntheses of novel uranyl selenates and selenite-selenates (temperature: 23°C; time: 72 hours).

c.:	6.1	6.2	6.3	6.4	6.5	6.6	6.7	6.8	6.9	6.10	6.11	6.12	6.13	6.14	6.15	6.16
<b>molar ratios:</b>																
SeO <sub>2</sub>	0.5	0.4	0.7	0.4	0.8	0.7	0.4	0.7	4.1	4.1	0.7	0.7	0.7	4.7	0.5	0.8
UO <sub>2</sub> (NO <sub>3</sub> ) <sub>2</sub> ·6H <sub>2</sub> O <sup>1</sup>	0.1	0.1	0.1	0.1	0.1	0.2	0.1	0.2	0.4	0.4	0.2	0.1	0.1	0.1	0.1	0.1
CH <sub>5</sub> N <sup>2</sup>	0.4	0.5	0.2	0.5	0.1	0.1	0.5	0.1								
C <sub>2</sub> H <sub>7</sub> N <sup>3</sup>												0.2	0.2		0.4	0.1
C <sub>4</sub> H <sub>11</sub> N <sup>4</sup>														0.1		
C <sub>4</sub> H <sub>13</sub> N <sub>3</sub> <sup>5</sup>											0.1					
C <sub>3</sub> H <sub>7</sub> NO <sup>6</sup>									1.3	1.3						
H <sub>2</sub> O (ml)	2	2	2	2	2	2	2	2	2	2	2	2	2	2	2	2

<sup>1</sup> uranium materials used in these experiments were depleted; <sup>2</sup> methylamine (MA); <sup>3</sup> dimethylamine (DMA); <sup>4</sup> diethylamine (DEA); <sup>5</sup> diethylenetriamine (DETA); <sup>6</sup> *N,N*-dimethylformamide (DMF).

## 2.6.2 Structural description of sixteen novel phases

All novel phases of organically templated uranyl selenates and selenite-selenates presented in this work can be diversified as belonging to several groups according to different  $U^{6+}:Se^{6+/4+}$  ratios of inorganic structural units: 1:2 – **c6.1**, **c6.2**, **c6.9**, **c6.16**; 2:3 – **c6.3**, **c6.4**, **c6.10-c6.12**; 3:5 – **c6.5**, **c6.6**, **c6.13-c6.15**; and 5:8 – **c6.7**, **c6.8**. The crystal structures of all phases contain uranyl  $(UO_7)^{8-}$  pentagonal bipyramids, selenate  $(Se^{6+}O_4)^{2-}$  tetrahedra, or/and selenite  $(Se^{4+}O_3)^{2-}$  triangular pyramids with a stereochemically active lone pair of electrons as a complementary ligand. The polyhedra are linked into inorganic structural units with relatively open architectures (those where corner-linkage of polyhedra dominates over edge-linkage). In the crystal structures,  $U^{6+}$  cations form approximately linear uranyl ions,  $[UO_2]^{2+}$ , with the average  $\langle U=O \rangle$  bond length of 1.756 Å among all the structures presented in this study. These basic uranyl entities are coordinated in their equatorial planes by five oxygen atoms (or four O and one  $H_2O$  molecule) to form  $UO_7$  (or  $UO_6(H_2O)$ ) pentagonal bipyramids with the average  $\langle U-O_{eq} \rangle$  bond length equal to 2.390 Å. Generally, the  $U-O_{eq}H_2$  bond lengths are longer and lie in range of 2.42–2.54 Å. The average  $\langle Se-O \rangle$  bond distance in selenate and selenite groups equals to 1.628 Å. In the structures, the 1D and 2D inorganic structural units are separated and templated by organic species and water molecules. Detailed description of all the crystal structures of novel synthesized uranyl selenates and selenite-selenates can be found in the articles **A-I** (**c6.16**), **A-II** (**c6.1-c6.8**), and **A-VI** (**c6.9-c6.15**) (see Included Articles). Only topological features of the structures are discussed below in this chapter.

Topology of uranyl selenate and selenite-selenate units in the structures under consideration can be visualized using the nodal representation. Within this approach (Krivovichev 2004; Krivovichev 2009; Krivovichev 2010), the  $U^{6+}$  and  $Se^{6+/4+}$  coordination polyhedra are symbolized by black and white nodes, respectively. The vertices are linked by an edge if two respective polyhedra share a common oxygen atom. The resulting graph is used to investigate topological relations between similar structures. **Figure 6.1** shows a whole topological diversity of inorganic structural units in the crystal structures of novel compounds **c6.1-c6.16**.

### **Compounds with U:Se = 1:2**

Crystal structures of  $[CH_6N]_2[(UO_2)(SeO_4)_2(H_2O)](H_2O)$  (**c6.1**),  $[CH_6N]_2[(UO_2)(SeO_4)_2(H_2O)]$  (**c6.2**), and  $[C_2H_8N]_2[(UO_2)(SeO_4)_2(H_2O)]$  (**c6.9**), are based upon structural units with composition  $[(UO_2)(SeO_4)_2(H_2O)]^{2-}$ . In the structures of **c6.1** and **c6.9** the  $(UO_6(H_2O))^{6-}$  pentagonal bipyramids share corners with two adjacent  $(SeO_4)^{2-}$  tetrahedra to form  $[(UO_2)(SeO_4)_2(H_2O)]^{2-}$  1D chains arranged into the pseudo sheets parallel (**Figure 6.1a, b**), while the structure of **c6.2** is based upon 2D sheets of the same composition (**Figure 6.1c, d**). The chains have been observed first in the structure of  $Mn[(UO_2)(SO_4)_2(H_2O)](H_2O)_5$  (Tabachenko et al. 1975) and later in a number of amine-templated uranyl oxysalts. The layered topology of **c6.2** is common for a large number of sheet topologies with the composition  $[A_nO_2(SO_4)_2(H_2O)]$  (Krivovichev 2009).

The crystal structure of  $[C_2H_8N][(H_5O_2)(H_2O)][(UO_2)_2(SeO_4)_3(H_2SeO_3)](H_2O)$  (**c6.16**) is based upon  $[(UO_2)_2(SeO_4)_3(H_2SeO_3)]^{2-}$  sheets formed as a result of condensation of the  $(UO_7)^{8-}$ ,  $(Se^{6+}O_4)^{2-}$ , and  $(Se^{4+}O(OH)_2)^0$  coordination units by sharing common oxygen atoms. In topological structure of the sheet (**Figure 6.1e, f**), the selenate group coordinates three uranyl ions, whereas diprotonated selenite groups coordinate one uranyl ion each. This topology has never been observed in any other inorganic oxysalts.

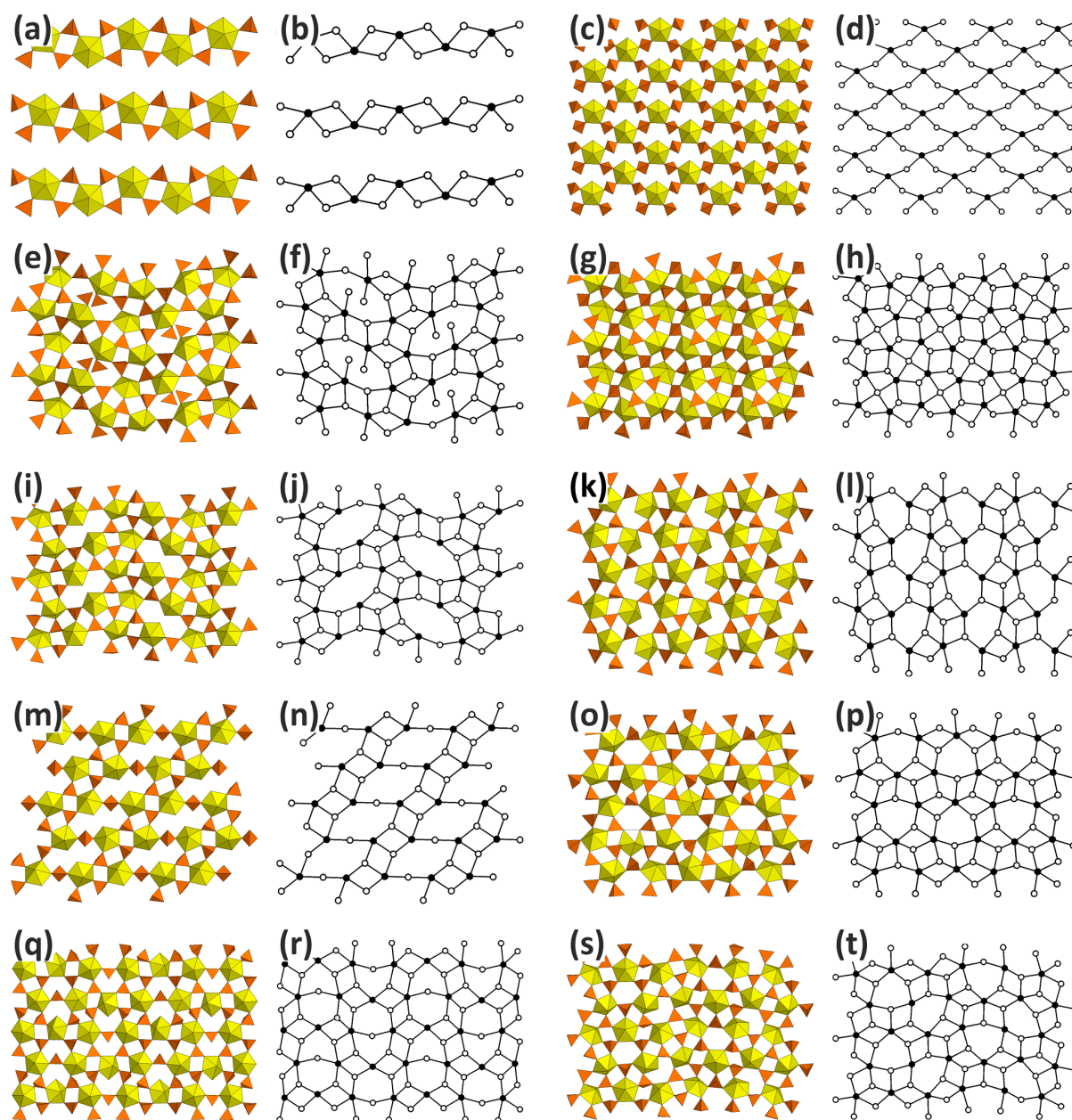


FIGURE 6.1 Topological diversity of inorganic structural units in the crystal structures of novel compounds. Uranyl pentagonal bipyramids and selenate/selenite groups are shown by yellow and orange in polyhedral representation and by black and white vertices in graphs.

### **Compounds with U:Se = 2:3**

In the crystal structures with a U:Se ratio of 2:3,  $[\text{CH}_6\text{N}]_2[(\text{UO}_2)_2(\text{SeO}_4)_3]$  (**c6.3**),  $[\text{CH}_6\text{N}](\text{H}_3\text{O})[(\text{UO}_2)_2(\text{SeO}_4)_3(\text{H}_2\text{O})](\text{H}_2\text{O})$  (**c6.4**),  $[\text{C}_2\text{H}_8\text{N}]_2[(\text{UO}_2)_2(\text{SeO}_4)_3(\text{H}_2\text{O})]$  (**c6.10**),  $[\text{C}_4\text{H}_{15}\text{N}_3][\text{H}_3\text{O}]_{0.5}[(\text{UO}_2)_2(\text{SeO}_4)_{2.93}(\text{SeO}_3)_{0.07}(\text{H}_2\text{O})](\text{NO}_3)_{0.5}$  (**c6.11**), and  $[\text{C}_2\text{H}_8\text{N}]_3[\text{H}_5\text{O}_2][(\text{UO}_2)_2(\text{SeO}_4)_3(\text{H}_2\text{O})_2]_2(\text{H}_2\text{O})_5$  (**c6.12**), coordination polyhedra of  $\text{U}^{6+}$  and  $\text{Se}^{6+/4+}$  share common ligands to produce 2D sheets with the chemical compositions  $[(\text{UO}_2)_2(\text{SeO}_4)_{3-x}(\text{SeO}_3)_x(\text{H}_2\text{O})_n]^{2-}$  ( $n = 0, 1, 2; x = 0, 0.07$ ). Topology of the sheet with  $n = 0$  observed in **c6.3** is based only upon 4-membered rings of alternating uranyl and selenate polyhedra (Figure 6.1g, h). It was already reported *e.g.* in  $[\text{CH}_6\text{N}_3]_2[(\text{UO}_2)_2(\text{SeO}_4)_3]$  (Krivovichev et al. 2009).

Crystal structures of **c6.4**, **c6.10**, and **c6.11** with  $n = 1$  are based upon structural units with same composition  $[(\text{UO}_2)_2(\text{SeO}_4)_3(\text{H}_2\text{O})]^{2-}$ , but with different topologies of linkage of U and Se polyhedra. The structure of **c6.4** contains 2D sheets (Figure 6.1i, j) similar to those found in the structure of **c6.16**. The important difference between these two topologies is related to the presence of additional selenite polyhedra coordinated uranyl group and located in large 8-membered rings of the sheet in the crystal structure of **c6.16**. The topology of the sheet in **c6.4** is rare and has been observed in unique uranyl selenate  $\text{K}(\text{H}_3\text{O})[(\text{UO}_2)_2(\text{SeO}_4)_3(\text{H}_2\text{O})](\text{H}_2\text{O})_6$  (Ling et al. 2010).

In the sheets of **c6.10** and **c6.11** (Figure 6.1k, l), 6-membered rings share edges to form chains separated by complex chains of dense 4-membered rings. This type of structural unit was observed in half dozen organically templated crystal structures with protonated molecules as counter ions (Krivovichev 2009).

The analysis of the topology of the sheets of **c6.10** and **c6.11** indicates that non-shared corners of selenate groups may have either up-, down- or disordered (up-or-down) orientations relative to the plane of the sheet. This ambiguity gives rise to geometric isomers with various orientations of the selenium polyhedra. To identify and classify the isomers of this type, *Krivovichev and Burns* proposed a geometrical approach based on orientation matrices of the isomers (Krivovichev and Burns 2003). According to this approach, as applied to the structures in hand, the symbols **u** (up), **d** (down), **m** (orientation up-down topologically equivalent) or  $\square$  (white vertex is missing in the graph) are assigned to each white vertex. Interestingly, the orientation matrices of the sheets in the crystal structures of **c6.10** and **c6.11** are equivalent and can be written in row as (**u** $\square$ **dd**)(**uu** $\square$ **d**). Thus, the uranyl selenate sheets observed in these crystal structures correspond to the same geometrical isomers.

The topology of the  $[(\text{UO}_2)_2(\text{SeO}_4)_3(\text{H}_2\text{O})_n]^{2-}$  sheet with  $n = 2$  in **c6.12** contains columns of edge-shared large hollow 8-membered rings and dense 4-membered rings (Figure 6.1m, n). This topology has never been observed in uranyl selenates.

### **Compounds with U:Se = 3:5**

The crystal structures of  $[\text{CH}_6\text{N}]_4[(\text{UO}_2)_3(\text{SeO}_4)_5](\text{H}_2\text{O})_4$  (**c6.5**) and  $[\text{CH}_6\text{N}](\text{H}_5\text{O}_2)(\text{H}_3\text{O})_2[(\text{UO}_2)_3(\text{SeO}_4)_5](\text{H}_2\text{O})_4$  (**c6.6**) are based upon topologically similar inorganic sheets with the composition  $[(\text{UO}_2)_3(\text{SeO}_4)_5]^{4-}$  (Figure 6.1o, p). The sheets are built from 4- and 6-membered rings. This topology of uranyl was observed in some uranyl selenate and chromate compounds (Krivovichev 2009).

Using the geometrical approach based on determination of the orientation of non-shared vertices of selenate tetrahedra, the orientation rows for the sheets in **c6.5** and **c6.6** may be written as ( $\square$ **uu** $\square$ **dd**)(**mddmuu**) and ( $\square$ **ud** $\square$ **ud**)(**duuddd**)( $\square$ **du** $\square$ **du**)(**ddddud**), respectively. Thus, the uranyl selenate and selenite-selenate sheets observed in these crystal structures correspond to different geometrical isomers.

The crystal structures of  $[\text{C}_2\text{H}_8\text{N}]_2[\text{H}_3\text{O}][(\text{UO}_2)_3(\text{SeO}_4)_4(\text{HSeO}_3)(\text{H}_2\text{O})](\text{H}_2\text{SeO}_3)_{0.2}$  (**c6.13**),  $[\text{C}_4\text{H}_{12}\text{N}]_3[\text{H}_3\text{O}][(\text{UO}_2)_3(\text{SeO}_4)_5(\text{H}_2\text{O})]$  (**c6.14**) and  $[\text{C}_2\text{H}_8\text{N}]_3(\text{C}_2\text{H}_7\text{N})[(\text{UO}_2)_3(\text{SeO}_4)_4(\text{HSeO}_3)(\text{H}_2\text{O})]$  (**c6.15**) have the same topology of inorganic sheets (Figure 6.1q, r) built up from 4- and 6-membered rings. This topology of inorganic complexes is typical for uranyl selenite-selenates, and it was observed e.g. in  $[\text{C}_5\text{H}_{14}\text{N}]_4[(\text{UO}_2)_3(\text{SeO}_4)_4(\text{HSeO}_3)(\text{H}_2\text{O})](\text{H}_2\text{SeO}_3)(\text{HSeO}_4)$  (Krivovichev et al. 2006).

The orientation matrices for **c6.13**, **c6.14** and **c6.15** have dimensions  $6 \times 2$ . The series of symbols written in row (**duuudd**)(**ud**□**du**□), (**dumudm**)(**ud**□**du**□) and (**ududud**)(**ud**□**du**□) for their inorganic sheets completely characterizes the topological structure of the geometric isomers **c6.13**, **c6.14** and **c6.15**.

### **Compounds with U:Se = 5:8**

The crystal structures of  $[\text{CH}_6\text{N}]_4(\text{H}_3\text{O})_2[(\text{UO}_2)_5(\text{SeO}_4)_8(\text{H}_2\text{O})](\text{H}_2\text{O})_4$  (**c6.7**) and  $[\text{CH}_6\text{N}]_{1.5}(\text{H}_5\text{O}_2)_{1.5}(\text{H}_3\text{O})_3[(\text{UO}_2)_5(\text{SeO}_4)_8(\text{H}_2\text{O})](\text{H}_2\text{SeO}_4)_{2.6}(\text{H}_2\text{O})_3$  (**c6.8**) are based upon sheets with the chemical composition  $[(\text{UO}_2)_5(\text{SeO}_4)_8(\text{H}_2\text{O})]^{6-}$  (Figure 6.1s, t). They contain 4- and 6-membered rings: 6-membered rings share vertices to form corner-sharing pairs separated by chains of edge-sharing 4-membered rings. The pairs are stretched alternatively along mutual perpendicular directions. The compounds **c6.7** and **c6.8** are the first examples of this topology for uranyl selenates.

Using the geometrical approach based on determination of the orientation of non-shared vertices of selenate tetrahedra, the orientation rows for the sheets in **c6.7** and **c6.8** may be written as (**uu**□**uu**)(**ddud**□), (**dd**□**dd**)(**duuu**□), and (**du**□**dd**)(**dudu**□), respectively. Thus, the uranyl selenate and selenite-selenate sheets observed in these crystal structures correspond to different geometrical isomers.

### **2.6.3 Dimensional reduction**

In order to investigate the chemistry-structure relationships, we employed the dimensional reduction principle (Long et al. 1996; Tulsy and Long 2001). Here, the whole range of the compounds with the general formula  $A_n(\text{UO}_2)_p(\text{TO}_4)_q(\text{H}_2\text{O})_r$  ( $A^+$  = monovalent cation, and  $T^{6+}$  = Se, S, Cr, Mo) has been analysed. It was supposed that the basic highly-polymerized 3D parent structure is that of  $(\text{UO}_2)(\text{TO}_4)$ , whereas the role of reducing agents is played by  $A_2(\text{TO}_4)$  and  $\text{H}_2\text{O}$ . As a consequence, the relationships between different compositions and structures may be visualized using the  $\text{UO}_2\text{TO}_4 - A_2\text{TO}_4 - \text{H}_2\text{O}$  compositional diagram (Figure 6.2). List of all relevant compounds and dimensional characteristics of their structures can be found in the article **A-II** (see Included Articles).

The diagram shown in Figure 6.2 may be divided into regions, where structures have the same dimensionality values (0 = finite clusters, 1 = chains, 2 = sheets, 3 = frameworks). Definition of the borders between the fields is not unambiguous and is rather tentative in character. For instance, due to the presence of only one point (**36**) corresponding to the 0D phases, the borders between the 0D and 1D fields are hypothetical. We suppose these borders are subparallel to the borders between 1D-and-2D, 2D-and-3D fields, and are in agreement with the principle of dimensional reduction for inorganic oxysalts. However, some deviations are observed. The points **21** and **23** are located within the 2D field, but correspond to the 3D framework structures with the  $A_6(\text{UO}_2)_2(\text{TO}_4)_3(\text{H}_2\text{O})_6$  and  $A_6(\text{UO}_2)_2(\text{TO}_4)_3(\text{H}_2\text{O})_{7.5}$  compositions, respectively. We attribute these deviations to the double role of  $\text{H}_2\text{O}$ : in most cases, it acts as reducing agent, whereas, in the cases of **21** and **23**, it simply fills cavities of the uranyl-based framework.

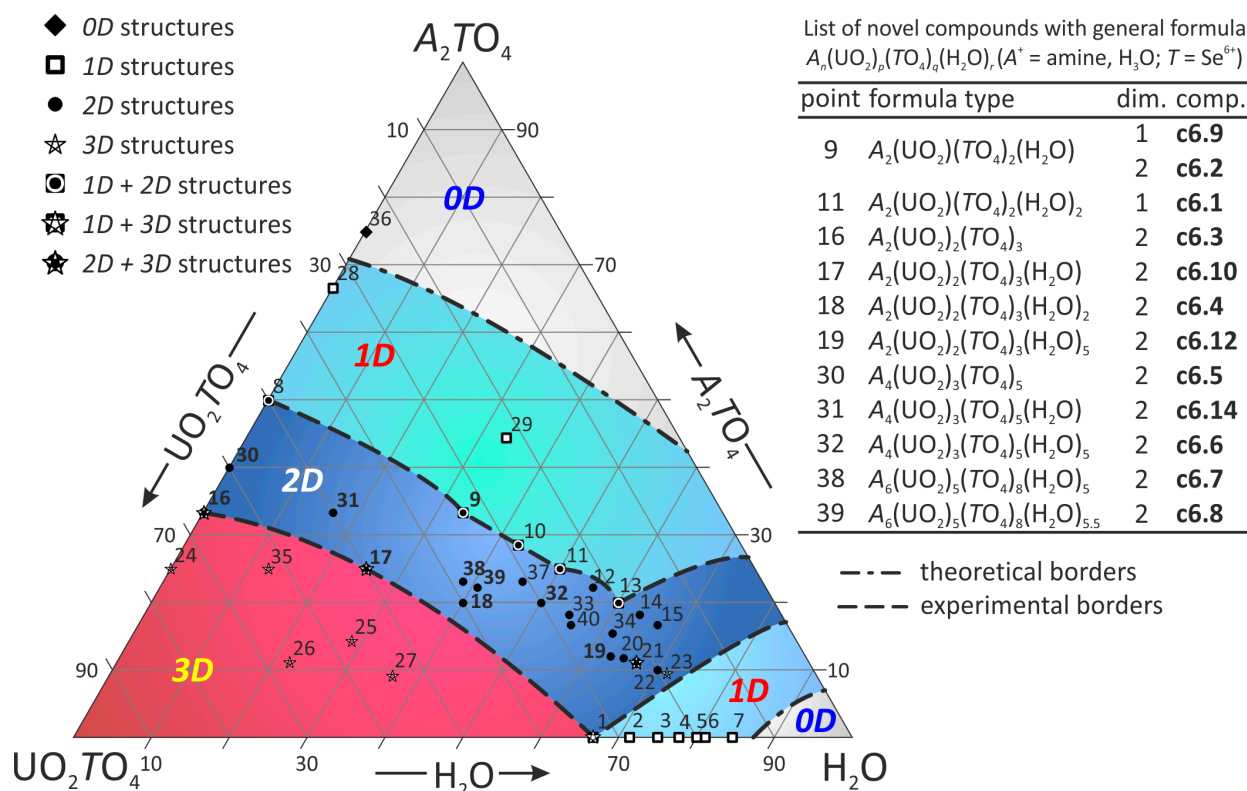


FIGURE 6.2 Dimensional fields on the compositional diagram of the  $\text{UO}_2\text{TO}_4 - \text{A}_2\text{TO}_4 - \text{H}_2\text{O}$  ( $A$  = monovalent cation,  $T = \text{S, Se, Cr, Mo}$ ) system.

For more detailed demonstration of the principle of dimensional reduction in the system, one may consider the line originating from the left and ending at the top corner of the diagram. The line describes compounds with the composition  $A_n(\text{UO}_2)_p(\text{TO}_4)_q$ . The points 24, 30, 28, and 36 correspond to the structures with dimensionalities equal to 3, 2, 1, and 0, respectively. The points 16 and 8 are located on the borders between 2D- and 3D, 1D- and 2D fields, respectively. Thus, the dimensionality of the structural unit is decreasing from the points 24 to 36, which is in agreement with the principle of dimensional reduction.

## 2.7 Analogy between electron lone pairs of selenites and hydrogen-in-phosphites

In this section we present the fascinating results obtained at the end of this co-tutorial thesis project, with original evidence of negatively charged hydrogen in phosphites. These  $(\text{HPO}_3)^{2-}$  anions, which result from phosphonic acid  $\text{HPO}(\text{OH})_2$  upon deprotonation, are commonly encountered as a tridentate or more tetrahedral ligand in solids. The H–P bond of  $(\text{HPO}_3)^{2-}$  is commonly viewed as resulting from protonation of the phosphorus lone pair. Although the phosphite groups in solution have been subject of spectroscopic studies (Loub 1991), there has been no clear characterization of the H–P bond of phosphite anions in crystalline solids.

In the context of the present studies, we have synthesized two isotypic compounds,  $\text{Fe}_2(\text{SeO}_3)_3$  and  $\text{Fe}_2(\text{HPO}_3)_3$ . The tunnel crystal structures of those clearly show an analogy between lone electron pairs of selenite groups and H–P bonds of phosphite anions. It demonstrates that in solids containing  $(\text{HPO}_3)^{2-}$  and  $(\text{ESeO}_3)^{2-}$  anions, the H–P bond in phosphites has the same role as does the lone pair *E* of selenites (Figure 7.1), suggesting that the H atom is negatively charged and the H–P bond possesses some hydridic character in  $(\text{HPO}_3)^{2-}$  anions.

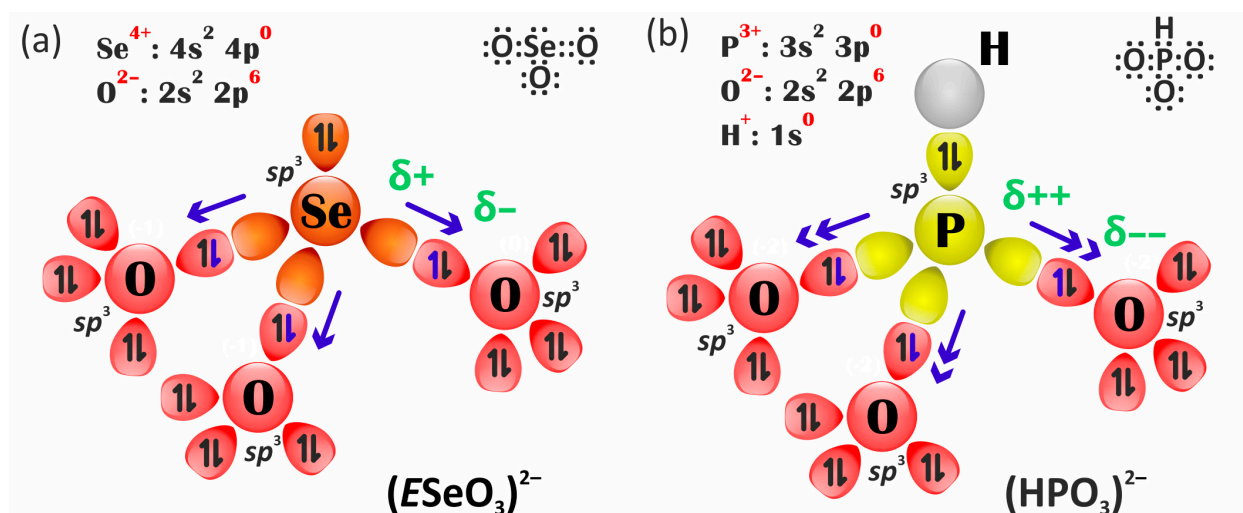


FIGURE 7.1 Lewis structures and simplified artistic representation of orbital models of  $(\text{ESeO}_3)^{2-}$  (a) and  $(\text{HPO}_3)^{2-}$  (b) anions, which highlight the similar role of  $\text{H}_{\text{HPO}_3}$  and  $\text{E}_{\text{SeO}_3}$  from the geometrical point of view.

### 2.7.1 Synthesis and structural characterization of iron selenite and phosphite

Single crystals of  $\text{Fe}_2(\text{SeO}_3)_3$  (c7.1) and  $\text{Fe}_2(\text{HPO}_3)_3$  (c7.2) have been prepared by hydrothermal techniques. The reagents  $\text{FeCl}_3 \cdot 6\text{H}_2\text{O}$ ,  $\text{Li}_2\text{CO}_3$  and  $\text{SeO}_2/\text{H}_3\text{PO}_3$  were mixed in a molar ratio of 1 : 1.5 : 2.5, and then dissolved the mixture in 6 ml of distilled water. The hydrothermal reactions were performed in 23 ml Teflon-lined autoclaves that were heated to 160 °C in ovens. The temperature of autoclaves was held constant for two days, followed by cooling to room temperature during 48 hours. It should be note that another way for synthesis of  $\text{Fe}_2(\text{HPO}_3)_3$  was reported in (Sghyar et al. 1991), where the crystalline compound was obtained by an isothermal slow evaporation from the aqueous solution containing 20% of



$\text{Fe}_2\text{O}_3$ , 30% of  $\text{H}_3\text{PO}_3$ , and 50% of water at 90 °C. Crystallographic data and experimental parameters for the crystal structures of the compounds are summarized in Table 7.1.

TABLE 7.1 Crystallographic data and refinement parameters for  $\text{Fe}_2(\text{SeO}_3)_3$  (c7.1) and  $\text{Fe}_2(\text{HPO}_3)_3$  (c7.2).

	c7.1	c7.2
$M_r$ (g mol <sup>-1</sup> )	492.58	351.63
space group	$P6_3/m$	$P6_3/m$
$a$ (Å)	7.8720(9)	8.0195(2)
$c$ (Å)	7.3258(10)	7.3700(2)
$V$ (Å <sup>3</sup> )	393.15(10)	410.48(2)
$Z$	2	2
$\rho$ (g/cm <sup>3</sup> )	4.161	2.845
$\mu$ (mm <sup>-1</sup> )	17.603	4.144
$\lambda$ (MoK $\alpha$ ) (Å)	0.71073	0.71073
total rflns	3894	8590
indep rflns	472	475
$R_{\text{int}}$	0.0303	0.0325
$R_1$ [ $I > 2\sigma(I)$ ]	0.0141	0.0133
$wR_2$ [ $I > 2\sigma(I)$ ]	0.0308	0.0413
$R_1$ [all data]	0.0157	0.0154
$wR_2$ [all data]	0.0311	0.0433
GOF	1.098	1.249
$\Delta\rho_{\text{max}}\Delta\rho_{\text{min}}$ (e Å <sup>-3</sup> )	0.451, -0.426	0.423, -0.309

The crystal structures of  $\text{Fe}_2(\text{SeO}_3)_3$  (c7.1) and  $\text{Fe}_2(\text{HPO}_3)_3$  (c7.2) contain  $[\text{Fe}_2\text{O}_9]^{12-}$  dimers of face-sharing  $\text{Fe}^{3+}\text{O}_6$  octahedra. The average Fe–O bond lengths of  $\text{Fe}_2(\text{SeO}_3)_3$  and  $\text{Fe}_2(\text{HPO}_3)_3$  are nearly the same, and so are their Fe–Fe distances (2.987 Å and 2.980 Å, respectively). The  $[\text{Fe}_2\text{O}_9]^{12-}$  dimers share all their six vertices with  $(\text{ESeO}_3)^{2-}$  or  $(\text{HPO}_3)^{2-}$  tetrahedra, forming hexagonal channels along the  $c$ -axis (Figure 7.2). The H–P bonds are pointed toward the axis of each tunnel as do the lone pairs of  $(\text{ESeO}_3)^{2-}$ . The Se–O bonds (1.676–1.722 Å) are longer than the P–O bonds (1.513–1.540 Å), but the tunnel is larger in diameter for  $\text{Fe}_2(\text{HPO}_3)_3$  than for  $\text{Fe}_2(\text{SeO}_3)_3$ . The H–P bond is 1.310 Å, whereas the center of each lone pair of selenite anion is at a distance of  $\approx 0.260$  Å from the Se (calculated using the program HYBRIDE based on a theory developed by Verbaere and co-workers. (Verbaere et al. 1978)).

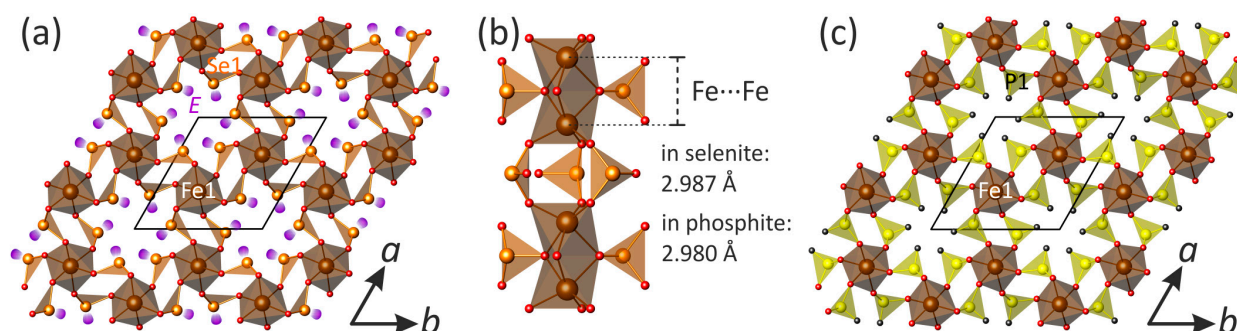


FIGURE 7.2 View of the crystal structures of  $\text{Fe}_2(\text{SeO}_3)_3$  (c7.1) and  $\text{Fe}_2(\text{HPO}_3)_3$  (c7.2) along the  $c$ -axis – (a) and (c), respectively; mode of linkage of iron (brown) and selenite (orange) polyhedra in c7.1 – (b).

## 2.7.2 Calculation of partial charges

For a number of phases of already reported phosphite phases with various crystal structures of different dimensionalities, the partial charges on P and H were calculated using the Henry's method (Henry 2002; Henry 2008) in order to find systematic residual partial negative charges on the H atoms (Table 7.2). The latter indicates a weak but significant hydride character, e.g. the weakly negative charge of  $-0.024$  electron units (*e.u.*) found for the H atoms in  $\text{Fe}_2(\text{HPO}_3)_3$ , and  $-0.108$  *e.u.* and  $-0.099$  *e.u.* for the H atoms of two inequivalent phosphite groups in  $\text{Sr}(\text{H}_2\text{O})_2[(\text{UO}_2)(\text{HPO}_3)_2]$  (Villa et al. 2013).

TABLE 7.2 Calculated partial charges for featured selected compounds.

	partial charges, $\pm q$			ref.
	H	P / Se / As	O / Cl	
$\text{Fe}_2(\text{HPO}_3)_3$	$-0.024$	$+0.170$	$-0.382$ ( $\times 2$ ), $-0.293$	[1], <b>c7.2</b>
$\text{Sc}_2(\text{HPO}_3)_3$	$-0.068$	$+0.304$	$-0.602$ ( $\times 2$ ), $-0.695$	[2]
$\text{Al}_2(\text{HPO}_3)_3$	$-0.042$	$+0.454$	$-0.504$ ( $\times 2$ ), $-0.573$	[3]
$\text{Ga}_2(\text{HPO}_3)_3$	$-0.032$	$+0.479$	$-0.437$ ( $\times 2$ ), $-0.483$	[3]
$\text{Fe}_2(\text{HPO}_3)\text{F}_2$	$-0.048$	$+0.401$	$-0.453$ ( $\times 2$ ), $-0.452$	[4]
$\text{Sr}(\text{H}_2\text{O})_2[(\text{UO}_2)(\text{HPO}_3)_2]$	$-0.108$	$+0.170$	$-0.539$ , $-0.707$ , $-0.695$	[5]
	$-0.099$	$+0.199$	$-0.666$ , $-0.585$ , $-0.676$	
$\text{Ni}_{11}(\text{HPO}_3)_2(\text{OH})_6$	$-0.045$	$+0.478$	$-0.420$ ( $\times 3$ )	[6]
	$-0.048$	$+0.459$	$-0.432$ ( $\times 3$ )	
$\text{PCl}_3$		$+0.340$	$-0.114$ ( $\times 2$ ), $-0.113$	[7]
$\text{Fe}_2(\text{SeO}_3)_3$		$+0.056$	$-0.353$ ( $\times 2$ ), $-0.280$	<b>c7.1</b>
$\text{Sc}_2(\text{SeO}_3)_3$		$+0.088$	$-0.558$ ( $\times 2$ ), $-0.661$	[8]
		$+0.231$	$-0.468$ ( $\times 2$ ), $-0.467$	
$\text{Zn}_3(\text{AsO}_3)_2$		$+0.206$	$-0.469$ ( $\times 2$ ), $-0.470$	[9]

[1] – (Sghyar et al. 1991); [2] – (Ewald et al. 2003); [3] – (Morris et al. 1994); [4] – (Liu et al. 2009); [5] – (Villa et al. 2013); [6] – (Marcos et al. 1993); [7] – (Enjalbert et al. 1980); [8] – (Wontcheu and Schleid 2003); [9] – (Ghose et al. 1977).

In  $\text{Fe}_2(\text{HPO}_3)_3$ , the calculated partial charges for O and P atoms are  $\delta_{\text{O}} \approx -0.34$  *e.u.* and  $\delta_{\text{P}} \approx +0.17$  *e.u.*, respectively. Dealing with bigger ligands, e.g. chlorides in  $\text{PCl}_3$ , the bond  $\text{P}^{3+}\text{-Cl}^-$  polarization is displaced in favor of high partial positive charge on the phosphorus atom ( $\delta_{\text{Cl}} = -0.11$  and  $\delta_{\text{P}} = +0.34$ ), which is not suitable for the formation of a H–P bond. Similar effects can be expected in arsenites by lowering the metal electronegativity ( $\chi_{\text{P}} > \chi_{\text{As}}$ ), which play in favor of stereoactive “free” lone pairs in  $\text{AsO}_3$  groups. A more electronegative selenium cation ( $\chi_{\text{Se}} \gg \chi_{\text{P}}$ ) generates less polarized Se–O bonds, as in  $\text{Fe}_2(\text{SeO}_3)_3$ , leading to  $\delta_{\text{Se}} \approx +0.056$  *e.u.*, which is also not suitable for the formation of H–Se bonds and is responsible for  $(\text{ESeO}_3)^{2-}$  ions in solids.

In fact, complementary *ab-initio* molecular calculations performed in collaboration with the group of Prof. Dr. M. Whangbo have validated the partial negative charge of the H atom due to the almost zero participation of p-states and strong contribution of H in the HOMO molecular orbital. We have also proved that due to its geometry and charge the  $\text{HPO}_3$  groups are very weak magnetic connectors between two magnetic centres, e.g.  $\text{PO}_4$ ,  $\text{SeO}_3$ ... This work is still in preparation.

### 3 CONCLUSION AND PERSPECTIVES

The exploration of several metal-oxide chemical systems containing selenium with various metals ( $\text{Cu}^{+2+}$ ,  $\text{Ni}^{2+}$ ,  $\text{Co}^{2+}$ ,  $\text{V}^{4+/5+}$ ,  $\text{Mn}^{2+/3+}$ ,  $\text{Fe}^{3+}$ ,  $\text{Pb}^{2+}$ ,  $\text{Bi}^{3+}$ ,  $\text{U}^{6+}$ ) were presented in this work. Crystal chemistry of a large group of novel oxide compounds of  $\text{Se}^{4+}$  and  $\text{Se}^{6+}$  was mainly investigated by means of X-ray single crystal structural analysis. Further characterizations have not been detailed in this manuscript but can be found in the appended articles, accepted during my work. From the crystallographic viewpoint, most of the phases present a very well ordered assembly between distinct units leading to very good quality crystals. Only compounds described on the basis of oxo-centered  $\text{O}(\text{Bi}/\text{Mn})_4$  units show a tendency for disorder. This is a general situation favoured in the  $\text{Bi}^{3+}$  case, because O–Bi bonds based on the sums of ionic radii give a contribution of 0.596 valence unit, greater than the 0.5 needed and leading to distortion or Bi substitution, which is the case here.

This thesis is one of the first dedicated to the synthesis of the series of novel metal-oxide compounds using the “geo-inspired” approach assumed emulation of natural crystal growth processes in order to obtain complex functional materials with a potential in terms of specific physical properties. A large variety of resulted novel compounds clearly shows the appropriateness of using this approach for prospecting of new functional materials. The good results obtained from the CVT and in solution validates that selenite and selenate groups are very suitable structural templating agents for the crystal growth of minerals in various geochemical environments.

In the context of this work, eight novel copper oxoselenites were obtained by the chemical vapour transport reactions. This result proves the efficiency of the CVT method for the synthesis of unique mixed  $\text{Cu}^+ - \text{Cu}^{2+}$  oxyhalide compounds. The compounds described herein are based upon oxocentered  $(\mu_4\text{-O})\text{Cu}_4$  tetrahedral units that polymerize to form structural complexes of different dimensionality.

The  $\text{PbO-NiO-SeO}_2$  ternary system was scrupulously investigated in hydrothermal conditions. Three novel lead nickel selenites and one novel lead cobalt selenite were synthesized and characterized. According to the experimental results, the pH values of the solution play the essential role in hydrolysis and condensation processes by hydrothermal reactions in the studied system, and determine structural architectures of resulted products of the syntheses.

Three novel compounds were prepared in the course of the investigation of the ternary systems with lead, vanadium, and selenium. Two of them are new polymorphic modifications of already known compounds. Discussion of polymorphism demonstrated a large diversity of geometries of structural units

in the crystal structures of vanadate selenites, which can be caused in part by the presence of chemically differ bonds in ( $V^{5+}O_n$ ) polyhedra. Also contributing is the fact that the asymmetric selenite groups with stereochemically active lone electron pairs could form structural cavities leading to materials with open architectures.

Seven novel Se compounds containing manganese and bismuth were synthesized by using various techniques: evaporation from aqueous solution, hydrothermal reactions, and chemical vapour transport reactions. Three phases of them represent the first examples of oxoselenites containing both bismuth and manganese cations.

Sixteen novel selenium-containing uranyl oxysalts templated by organic amines were reported. The observed topologies of the structural units of new compounds have been investigated using a graph theory, and a special approach based upon construction of orientation matrices has been applied to distinguish different geometrical isomers of uranyl selenates and selenite-selenates with the same structural topologies. Analysis of known  $A_n(UO_2)_p(TO_4)_q(H_2O)_r$  compounds ( $A^+$  = monovalent cation, and  $T^{6+}$  = Se, S, Cr, Mo) using the principle of dimensional reduction combined with the composition-structure diagram allowed to separate on it specific fields corresponding to the formation of uranyl structures with specific dimensionalities of their structural units.

The given analogy between lone electron pairs of selenite groups and H–P bonds of phosphite anions at the examples of isotypic selenite and phosphite compounds supported by calculations of partial charges, suggests that the H atom is negatively charged and the H–P bond possesses some hydridic character in  $(HPO_3)^{2-}$ . It offers promising potentialities for synthesis of open structures decorated by polarized P–H or Se–E units, *i.e.* cationic intercalation materials, molecular sieves, catalysis *etc.*...

Overall results of the present study contribute to the fundamental knowledge of the crystal chemistry of synthetic and natural oxide compounds of selenium in the oxidation states of +4 and +6. The “geo-inspired” approach used for the synthesis of novel metal-oxide compounds is innovative and can be used within the framework of renewal of modern inorganic chemistry and purposeful design of novel complex functional materials with a potential in terms of specific physical properties. The number of discovered Se oxo-compounds allows to predict possible mineral phases that may form in various geochemical environments. Observed open architectures in most of the new compounds give an opportunity to use their cavities for the intercalation/extraction of mobile organic ions into/out of them for catalysis and ion exchange chemistry in perspective. Further elaboration of more condensed Se structures with transition metals can lead to interesting magnetic properties. The only limitation is synthetic methods due to high volatility of selenium oxysalts.

## REFERENCES

- Abraham F., Cousin O., Mentré O., Ketatni E. M. Crystal Structure Approach of the Disordered New Compounds  $\text{Bi}_{\sim 1.2}\text{M}_{\sim 1.2}\text{PO}_{5.5}$  (M=Mn, Co, Zn): The Role of Oxygen-Centered Tetrahedra Linkage in the Structure of Bismuth-Transition Metal Oxy-phosphates // *J. Solid State Chem.* 2002. Vol. 167. P. 168–181.
- Alekseev E. V., Krivovichev S. V., Armbruster T., Depmeier W., Suleimanov E. V., Chuprunov E. V., Golubev A. V. Dimensional Reduction in Alkali Metal Uranyl Molybdates: Synthesis and Structure of  $\text{Cs}_2[(\text{UO}_2)\text{O}(\text{MoO}_4)]$  // *Z. Anorg. Allg. Chem.* 2007. Vol. 633. P. 1979–1984.
- Alekseev E. V., Krivovichev S. V., Depmeier W. A crown ether as template for microporous and nanostructured uranium compounds // *Angew. Chem. Int. Ed. Engl.* 2008. Vol. 47. P. 549–51.
- Aliev A., Endara D., Huvé M., Colmont M., Roussel P., Delevoye L., Tran T. T., Halasyamani P. S., Mentré O. Labile degree of disorder in bismuth-oxophosphate compounds: Illustration through three new structural types // *Inorg. Chem.* 2014. Vol. 53. P. 861–871.
- Aliev A., Huvé M., Colis S., Colmont M., Dinia A., Mentré O. Two-Dimensional Antiferromagnetism in the  $[\text{Mn}_{3+x}\text{O}_7][\text{Bi}_4\text{O}_{4.5-y}]$  Compound with a Maple-Leaf Lattice // *Angew. Chemie Int. Ed.* 2012. Vol. 51. P. 9393–9397.
- Aliev A., Olchowka J., Colmont M., Capoen E., Wickleder C., Mentré O. New  $[\text{PbBi}_2\text{O}_4][\text{Bi}_2\text{O}_2]\text{Cl}_2$  and  $[\text{Pb}_n\text{Bi}_{10-n}\text{O}_{13}][\text{Bi}_2\text{O}_2]_n\text{Cl}_{4+n}$  series by association of sizable subunits: relationship with Arppe's compound  $\text{Bi}_{24}\text{O}_{31}\text{Cl}_{10}$  and luminescence properties. // *Inorg. Chem.* 2013. Vol. 52. P. 8427–8435.
- Amorós P., Marcos M. D., Roca M., Beltrán-Porter A., Beltrán-Porter D. Synthetic Pathways for New Tubular Transition Metal Hydroxo- and Fluoro-Selenites: Crystal Structures of  $\text{M}_{12}(\text{X})_2(\text{SeO}_3)_8(\text{OH})_6$  (M= $\text{Co}^{2+}$ ,  $\text{Ni}^{2+}$ ; X= $\text{OH}^-$ ,  $\text{F}^-$ ) // *J. Solid State Chem.* 1996. Vol. 126. P. 169–176.
- Berdonosov P. S., Olenev A. V., Dolgikh V. A., Lightfoot P. The synthesis and crystal structures of the first rare-earth alkaline-earth selenite chlorides  $\text{MNd}_{10}(\text{SeO}_3)_{12}\text{Cl}_8$  (M=Ca and Sr) // *J. Solid State Chem.* 2007. Vol. 180. P. 3019–3025.
- Binnewies M., Glaum R., Schmidt M., Schmidt P. Chemical Vapor Transport Reactions - A Historical Review // *Z. Anorg. Allg. Chem.* 2013. Vol. 639. P. 219–229.
- Boudin S., Guesdon A., Leclaire A., Borel M.-M. Review on vanadium phosphates with mono and divalent metallic cations: syntheses, structural relationships and classification, properties // *Int. J. Inorg. Mater.* 2000. Vol. 2. P. 561–579.
- Burns P. C., Krivovichev S. V., Filatov S. K. New  $\text{Cu}^{2+}$  Coordination Polyhedra in the Crystal Structure of Burnsite,  $\text{KCdCu}_7\text{O}_2(\text{SeO}_3)_2\text{Cl}_9$  // *Can. Mineral.* 2002. Vol. 40. P. 1587–1595.
- Burrows A. D., Mahon M. F., Sebestyen V. M., Lan Y., Powell A. K. Synthesis, structures, and magnetic behavior of new anionic copper(II) sulfate aggregates and chains. // *Inorg. Chem.* 2012. Vol. 51. P. 10983–9.

- Cao X.-L., Kong F., Hu C.-L., Xu X., Mao J.-G.  $\text{Pb}_4\text{V}_6\text{O}_{16}(\text{SeO}_3)_3(\text{H}_2\text{O})$ ,  $\text{Pb}_2\text{VO}_2(\text{SeO}_3)_2\text{Cl}$ , and  $\text{PbVO}_2(\text{SeO}_3)\text{F}$ : New Lead(II)-Vanadium(V) Mixed-Metal Selenites Featuring Novel Anionic Skeletons. // *Inorg. Chem.* 2014. Vol. 53. P. 8816–8824.
- Choppin G., Rydberg J., Liljenzin J.-O. *Radiochemistry and Nuclear Chemistry*, 3rd edn. Butterworth-Heinemann, Woburn, MA
- Choudhury A., Kumar U., Rao C. N. R. Three-dimensional organically templated open-framework transition metal selenites // *Angew. Chemie - Int. Ed.* 2002. Vol. 41. P. 158–161.
- Colmont M., Endara D., Aliev A., Terryn C., Huvé M., Mentré O.  $\text{Bi}_2\text{O}_3\text{--CuO--P}_2\text{O}_5$  system: Two novel compounds built from the intergrowths oxocentered polycationic 1D-ribbons // *J. Solid State Chem.* 2013. Vol. 203. P. 266–272.
- Colmont M., Huvé M., Ketatni E. M., Mentré O. Polymorphism and anionic vacancies in the  $\text{Bi}_6(\text{M,Bi})_1\text{P}_2(\text{O,F})_{16-x}$  Aurivillius derivatives // *Solid State Sci.* 2008. Vol. 10. P. 533–543.
- Darriet J., Galy J. Tellurium (IV) Vanadium (V) Oxide,  $\text{Te}_2\text{V}_2\text{O}_9$  // *Cryst. Struct. Commun* 1973. Vol. 2. P. 237–238.
- David R., Kabbour H., Pautrat A., Touati N., Whangbo M.-H., Mentré O. Two-orbital three-electron stabilizing interaction for direct  $\text{Co}^{2+}\text{--As}^{3+}$  bonds involving square-planar  $\text{CoO}_4$  in  $\text{BaCoAs}_2\text{O}_5$  // *Angew. Chem. Int. Ed. Engl.* 2014. Vol. 53. P. 3111–3114.
- De A. K. *A text book of inorganic chemistry*. New Age International, New Delhi
- Effenberger H.  $\text{Cu}(\text{SeO}_2\text{OH})_2$ : Synthesis and crystal structure // *Zeitschrift für Krist. - Cryst. Mater.* 1985. Vol. 173. P. 267–272.
- Effenberger H., Pertlik F. Die Kristallstrukturen der Kupfer(II)-oxo-selenite  $\text{Cu}_2\text{O}(\text{SeO}_3)$  (kubisch und monoklin) und  $\text{Cu}_4\text{O}(\text{SeO}_3)_3$  (monoklin und triklin) // *Monatshefte für Chemie Chem. Mon.* 1986. Vol. 117. P. 887–896.
- Engelen B., Baumer U., Hermann B., Muller H., Unterderweide K., Bäumer U., Hermann B., Müller H., Unterderweide K. Zur Polymorphie und Pseudosymmetrie der Hydrate  $\text{MSeO}_3\cdot\text{H}_2\text{O}$  ( $\text{M}=\text{Mn, Co, Ni, Zn, Cd}$ ) // *Z. Anorg. Allg. Chem.* 1996. Vol. 622. P. 1886–1892.
- Enjalbert R., Savariault J. M., Legros J. P. Etude structurale a 123 K du trichlorure de phosphore  $\text{PCl}_3$  // *Comptes Rendus l'Académie des Sci. - Ser. C* 1980. Vol. C290. P. 239–241.
- Evans H. T. J., Hughes J. M. Crystal chemistry of the natural vanadium bronzes // *Am. Mineral.* 1990. Vol. 75. P. 508–521.
- Ewald B., Prots Y., Kniep R. Crystal structure of discandium tris-monohydrogenphosphate (III),  $\text{Sc}_2(\text{HPO}_3)_3$  // *Z. Kristallogr.* 2003. Vol. 218. P. 377–378.
- Filatov S. K., Semenova T. F., Vergasova L. P. Types of polymerization of  $[\text{OCu}_4]^{6+}$  in inorganic compounds with “additional” oxygen atoms // *Dokl. Akad. Nauk (in Russ.)* 1992. Vol. 322. P. 539–539.
- Fischer R. Die Kristallstruktur von Molybdomenit,  $\text{PbSeO}_3$  // *TMPM Tschermarks Mineral. und Petrogr. Mitteilungen* 1972. Vol. 17. P. 196–207.
- Ghose S., Boving P., La Chapelle W. A., Wan C. Reinerite,  $\text{Zn}_3(\text{AsO}_3)_2$ : an arsenite with a novel type of Zn-tetrahedral double chain // *Am. Mineral.* 1977. Vol. 62. P. 1129–1134.
- Henry M. Nonempirical Quantification of Molecular Interactions in Supramolecular Assemblies // *ChemPhysChem* 2002. Vol. 3. P. 561–569.
- Henry M. Non-covalent interactions in solid-state molecular tectonics // In: Putz M V. (ed) *Advances in quantum chemical bonding structures*. Transworld Research Network, Kerala, India, pp 153–211
- Hsu F.-C., Luo J.-Y., Yeh K.-W., Chen T.-K., Huang T.-W., Wu P. M., Lee Y.-C., Huang Y.-L., Chu Y.-Y., Yan D.-C., Wu M.-K. Superconductivity in the PbO-type structure  $\alpha\text{-FeSe}$  // *Proc. Natl. Acad. Sci.* 2008. Vol. 105. P. 14262–14264.

- Huvé M., Colmont M., Mentré O. Bi<sup>3+</sup>/M<sup>2+</sup> oxyphosphate: a continuous series of polycationic species from the 1D single chain to the 2D planes. Part 1: From HREM images to crystal-structure deduction. // *Inorg. Chem.* 2006. Vol. 45. P. 6604–11.
- Jo V., Kim M. K., Shim I.-W., Ok K. M. Synthesis, Structure, and Characterization of a Layered Mixed Metal Oxychloride, PbVO<sub>3</sub>Cl // *Bull. Korean Chem. Soc.* 2009. Vol. 30. P. 2145–2148.
- Johnston M. G., Harrison W. T. A. Two new octahedral/pyramidal frameworks containing both cation channels and lone-pair channels: syntheses and structures of Ba<sub>2</sub>Mn<sup>II</sup>Mn<sup>III</sup>(SeO<sub>3</sub>)<sub>6</sub> and PbFe<sub>2</sub>(SeO<sub>3</sub>)<sub>4</sub> // *J. Solid State Chem.* 2004. Vol. 177. P. 4680–4686.
- Jörg G., Bühnenmann R., Hollas S., Kivel N., Kossert K., Van Winckel S., Gostomski C. L. V. Preparation of radiochemically pure <sup>79</sup>Se and highly precise determination of its half-life // *Appl. Radiat. Isot.* 2010. Vol. 68. P. 2339–2351.
- Kersten C. Ueber mehrere neue Vorkommnisse des Selens // *Ann. der Phys. und Chemie* 1839. Vol. 122. P. 265–280.
- Koskenlinna M., Valkonen J. Lead selenite, PbSeO<sub>3</sub> // *Cryst. Struct. Commun.* 1977. Vol. 6. P. p813–816.
- Kozin M. S., Aliev A., Colmont M., Mentré O., Siidra O. I., Krivovichev S. V. Novel bismuth oxophosphate halides [Bi<sub>8</sub>O<sub>8</sub>][BiO<sub>2</sub>](PO<sub>4</sub>)<sub>2</sub>X (X=Cl, Br) based on oxocentered 2D blocks and their relationships to the Aurivillius phases // *J. Solid State Chem.* 2013. Vol. 199. P. 56–61.
- Krivovichev S. V. On the algorithmic complexity of crystals // *Mineral. Mag.* 2014. Vol. 78. P. 415–435.
- Krivovichev S. V. Crystal chemistry of selenates with mineral-like structures. IV. Crystal structure of Zn(SeO<sub>4</sub>)(H<sub>2</sub>O)<sub>2</sub>, a new compound with a mixed framework of the variscite type // *Geol. Ore Depos.* 2007. Vol. 49. P. 542–546.
- Krivovichev S. V. *Structural Crystallography of Inorganic Oxysalts.* Oxford University Press, Oxford
- Krivovichev S. V. Combinatorial topology of salts of inorganic oxoacids: zero-, one- and two-dimensional units with corner-sharing between coordination polyhedra // *Crystallogr. Rev.* 2004. Vol. 10. P. 185–232.
- Krivovichev S. V. Actinyl compounds with hexavalent elements (S, Cr, Se, Mo) - Structural diversity, nanoscale chemistry, and cellular automata modeling // *Eur. J. Inorg. Chem.* 2010. Vol. 2010. P. 2594–2603.
- Krivovichev S. V., Burns P. C. Geometrical isomerism in uranyl chromates II. Crystal structures of Mg<sub>2</sub>[(UO<sub>2</sub>)<sub>3</sub>(CrO<sub>4</sub>)<sub>3</sub>](H<sub>2</sub>O)<sub>17</sub> and Ca<sub>2</sub>[(UO<sub>2</sub>)<sub>3</sub>(CrO<sub>4</sub>)<sub>5</sub>](H<sub>2</sub>O)<sub>19</sub> // *Z. Kristallogr.* 2003. Vol. 218. P. 683–690.
- Krivovichev S. V., Filatov S. K., Vergasova L. P. The crystal structure of ilinskite, NaCu<sub>5</sub>O<sub>2</sub>(SeO<sub>3</sub>)<sub>2</sub>Cl<sub>3</sub>, and review of mixed-ligand CuO<sub>m</sub>Cl<sub>n</sub> coordination geometries in minerals and inorganic compounds // *Mineral. Petrol.* 2013a. Vol. 107. P. 235–242.
- Krivovichev S. V., Gurzhiy V. V., Tananaev I. G., Myasoedov B. F. Uranyl selenates with organic templates: Principles of structure and characteristics of self-organization // *Russ. J. Gen. Chem.* 2009. Vol. 79. P. 2723–2730.
- Krivovichev S. V., Kahlenberg V., Kaindl R., Mersdorf E., Tananaev I. G., Myasoedov B. F. Nanoscale tubules in uranyl selenates // *Angew. Chem. Int. Ed. Engl.* 2005a. Vol. 44. P. 1134–1136.
- Krivovichev S. V., Kahlenberg V., Tananaev I. G., Kaindl R., Mersdorf E., Myasoedov B. F. Highly porous uranyl selenate nanotubules // *J. Am. Chem. Soc.* 2005b. Vol. 127. P. 1072–3.
- Krivovichev S. V., Mentré O., Siidra O. I., Colmont M., Filatov S. K. Anion-Centered Tetrahedra in Inorganic Compounds // *Chem. Rev.* 2013b. Vol. 113. P. 6459–6535.
- Krivovichev S. V., Tananaev I. G., Kahlenberg V., Myasoedov B. F. Synthesis and crystal structure of a new uranyl selenite(IV)-selenate(VI), [C<sub>5</sub>H<sub>14</sub>N]<sub>4</sub>[(UO<sub>2</sub>)<sub>3</sub>(SeO<sub>4</sub>)<sub>4</sub>(HSeO<sub>3</sub>)(H<sub>2</sub>O)](H<sub>2</sub>SeO<sub>3</sub>)(HSeO<sub>4</sub>) // *Radiochemistry* 2006. Vol. 48. P. 217–222.

- Krivovichev S. V., Vergasova L. P., Starova G. L., Filatov S. K., Britvin S. N., Roberts A. C., Steele I. M. Burns site,  $\text{KCaCu}_7\text{O}_2(\text{SeO}_3)_2\text{Cl}_9$ , a New Mineral Species from the Tolbachik Volcano, Kamchatka Peninsula, Russia // *Can. Mineral.* 2002. Vol. 40. P. 1171–1175.
- Lafont A.-M., Trombe J.-C. “Layered hydrogenselenite” I. Synthesis, structure redetermination of  $[\text{Cu}(\text{HSeO}_3)_2(\text{H}_2\text{O})_2]$  and determination of  $[\text{Cu}(\text{HSeO}_3)_2(\text{NO}_3)_2]^{2-} \cdot 2\text{NH}_4^+, \text{NH}_4\text{NO}_3$ . Structural relationships of these complexes with  $[\text{Cu}(\text{HSeO}_3)_2]$  // *Inorganica Chim. Acta* 1995. Vol. 234. P. 19–25.
- Leclaire A., Chahboun H., Groult D., Raveau B. Concerning the intersecting tunnel structure of a novel vanadyl diphosphate  $\text{K}_2(\text{VO})_3(\text{P}_2\text{O}_7)_2$  and its structural relationships with other V(V) and V(IV) phosphates and relatives // *J. Solid State Chem.* 77:170–179.
- Lee K.-S., Kwon Y.-U. Crystal structure of  $\text{V}_2\text{Se}_2\text{O}_9$  and phase relations in the  $\text{V}_2\text{O}_5$ - $\text{SeO}_2$  system // *J. Korean Chem. Soc.* 1996. Vol. 40. P. 379–383.
- Li P.-X., Kong F., Hu C.-L., Zhao N., Mao J.-G. A Series of New Phases Containing Three Different Asymmetric Building Units // *Inorg. Chem.* 2010. Vol. 49. P. 5943–5952.
- Lii K.-H., Wang Y.-P., Chng C.-Y., Wang S.-L., Ku H.-C. Crystal Structure and Magnetic Properties of a Vanadium (IV) Pyrophosphate:  $\text{Rb}_2\text{V}_3\text{P}_4\text{O}_{17}$  // *J. Chinese Chem. Soc.* 1990. Vol. 37. P. 141–149.
- Ling J., Sigmon G. E., Ward M., Roback N., Carman Burns P. Syntheses, structures, and IR spectroscopic characterization of new uranyl sulfate/selenate 1D-chain, 2D-sheet and 3D-framework // *Z. Kristallogr.* 2010. Vol. 225. P. 230–239.
- Liu L., Wang X., Xu L., Liu X., Liu L., Bi B., Pang W. Synthesis, characterization and magnetic properties of a novel fluorinated iron phosphite  $\text{Fe}_2(\text{HPO}_3)\text{F}_2$  with infinite  $-\text{Fe}-\text{F}-\text{Fe}-\text{O}-\text{Fe}-$  linkage and  $-\text{Fe}-\text{F}-\text{Fe}-$  layer // *Inorganica Chim. Acta* 2009. Vol. 362. P. 3881–3884.
- Long J. R., McCarty L. S., Holm R. H. A Solid-State Route to Molecular Clusters: Access to the Solution Chemistry of  $[\text{Re}_6\text{Q}_8]^{2+}$  (Q = S, Se) Core-Containing Clusters via Dimensional Reduction // *J. Am. Chem. Soc.* 1996. Vol. 118. P. 4603–4616.
- Loub J. Crystal chemistry of inorganic phosphites // *Acta Crystallogr.* 1991. Vol. B47. P. 468–473.
- Lü M., Aliev A., Olchowka J., Colmont M., Huvé M., Wickleder C., Mentré O. Multidimensional open-frameworks: combinations of one-dimensional channels and two-dimensional layers in novel Bi/M oxo-chlorides. // *Inorg. Chem.* 2014. Vol. 53. P. 528–36.
- Mandarino J. A. Natural and synthetic selenites and selenates and their Gladstone-Dale compatibility // *Eur. J. Mineral.* 1994. Vol. 6. P. 337–349.
- Marcos M. D., Amorós P., Beltrán-Porter A., Martínez-Manez R., Attfield J. P. Novel crystalline microporous transition-metal phosphites  $\text{M}_{11}(\text{HPO}_3)_8(\text{OH})_6$  (M=Zn, Co, Ni). X-ray powder diffraction structure determination of the cobalt and nickel derivatives // *Chem. Mater.* 1993. Vol. 5. P. 121–128.
- Mcmanus A. V. P., Harrison W. T. A., Cheetham A. K. The synthesis and crystal structure of a new nickel selenite hydrate,  $\text{Ni}_3(\text{SeO}_3)_3 \cdot \text{H}_2\text{O}$  // *J. Solid State Chem.* 1991. Vol. 92. P. 253–260.
- Mertens B., Müller-Buschbaum H. Synthese und röntgen-strukturuntersuchung von  $\text{Rb}_4\text{Cd}(\text{VO})(\text{V}_2\text{O}_7)_2\text{Cl}$  und  $\text{Tl}_4\text{Cd}(\text{VO})(\text{V}_2\text{O}_7)_2\text{Cl}$  // *Z. Naturforsch.* 1997. Vol. 52. P. 453–456.
- Millet P., Galy J., Johnsson M. Crystal growth and structure of  $\text{V}_2\text{Se}_2\text{O}_9$ ; comparison with  $\text{V}_2\text{Te}_2\text{O}_9$  // *Solid State Sci.* 1999. Vol. 1. P. 279–286.
- Morris R. E., Attfield M. P., Cheetham A. K. Synthesis and structures of two isostructural phosphites,  $\text{Al}_2(\text{HPO}_3)_3$  and  $\text{Ga}_2(\text{HPO}_3)_3$  // *Acta Crystallogr.* 1994. Vol. C50. P. 473–476.
- Palatinus L., Chapuis G. SUPERFLIP – a computer program for the solution of crystal structures by charge flipping in arbitrary dimensions // *J. Appl. Crystallogr.* 2007. Vol. 40. P. 786–790.
- Petříček V., Dušek M., Palatinus L. Jana2006. The crystallographic computing system. Institute of Physics of the ASCR, Prague, Czech Republic



- Popovkin B. A., Cheremisinov V. P., Simanov Y. P. Study of the crystal structure and vibration spectrum of lead selenite // *J. Struct. Chem.* 1963. Vol. 4. P. 38–43.
- Pourbaix M. Atlas of electrochemical equilibria in aqueous solutions. National Association of Corrosion Engineers, Houston, Tex
- Puranen A., Johnsson M., Dähn R., Cui D. Reduction of selenite and selenate on anoxically corroded iron and the synergistic effect of uranyl reduction // *J. Nucl. Mater.* 2010. Vol. 406. P. 230–237.
- Pyrzynska K. Speciation analysis of some organic selenium compounds. A review // *Analyst* 1996. Vol. 121. P. 77R–83R.
- Qu L., Peng X. Control of Photoluminescence Properties of CdSe Nanocrystals in Growth // *J. Am. Chem. Soc.* 2002. Vol. 124. P. 2049–2055.
- Rayman M. P. The importance of selenium to human health // *Lancet* 2000. Vol. 356. P. 233–241.
- Richter K. L., Mattes R. Preparation, raman-spectra, and crystal structures of  $V_2O_3(SO_4)_2$ ,  $K[VO(SO_4)_2]$ , and  $NH_4[VO(SO_4)_2]$  // *Z. Anorg. Allg. Chem.* 1992. Vol. 611. P. 158–164.
- Schindler M., Hawthorne F. C., Baur W. H. Crystal chemical aspects of vanadium: Polyhedral geometries, characteristic bond valences, and polymerization of  $(VO_n)$  polyhedra // *Chem. Mater.* 2000. Vol. 12. P. 1248–1259.
- Scordari F., Stasi F. The crystal structure of euchlorine,  $NaKCu_3O(SO_4)_3$  // *Neues Jahrb. für Mineral. Abhandlungen* 1990. Vol. 161. P. 241–253.
- Séby F., Potin-Gautier M., Giffaut E., Borge G., Donard O. F. . A critical review of thermodynamic data for selenium species at 25°C // *Chem. Geol.* 2001. Vol. 171. P. 173–194.
- Sghyar M., Durand J., Cot L., Rafiq M. Structure du phosphite de fer:  $Fe_2(PO_3H)_3$  // *Acta Crystallogr.* 1991. Vol. C47. P. 2515–2517.
- Sheldrick G. M. A short history of SHELX. // *Acta Crystallogr.* 2008. Vol. A64. P. 112–22.
- Shuvalov R. R., Vergasova L. P., Semenova T. F., Filatov S. K., Krivovichev S. V., Siidra O. I., Rudashevsky N. S. Prewittite,  $KPb_{1.5}Cu_6Zn(SeO_3)_2O_2Cl_{10}$ , a new mineral from Tolbachik fumaroles, Kamchatka peninsula, Russia: Description and crystal structure // *Am. Mineral.* 2013. Vol. 98. P. 463–469.
- Spek A. L. Structure validation in chemical crystallography // *Acta Crystallogr. Sect. D Biol. Crystallogr.* 2009. Vol. 65. P. 148–155.
- Starova G. L., Filatov S. K., Vergasova L. P. The Crystal Structure of Fedotovite,  $K_2Cu_3O(SO_4)_3$  // *Mineral. Mag.* 1991. Vol. 55. P. 613–616.
- Tabachenko V. V., Serezhkin V. N., Serezhkina L. B., Kovba L. M. Crystal structure of manganese sulfatouranylate  $MnUO_2(SO_4)_2 \cdot 5H_2O$  // *Koord. Khim.* 1975. Vol. 5. P. 1563–1568.
- Takeno N. Atlas of Eh-pH diagrams. Geological Survey of Japan Open File Report No.419. National Institute of Advanced Industrial Science and Technology, Research Center for Deep Geological Environments
- Tapiero H., Townsend D., Tew K. . The antioxidant role of selenium and seleno-compounds // *Biomed. Pharmacother.* 2003. Vol. 57. P. 134–144.
- Tudo J., Jolibois B., Laplace G. Préparation et étude des sulfates de vanadium V:  $V_2O_5 \cdot 2SO_3$  et  $V_2O_5 \cdot 4SO_3 \cdot 3H_2O$  // *Comptes Rendus l'Académie des Sci. - Ser. C* 1969. Vol. 269. P. 978–980.
- Tulsky E. G., Long J. R. Dimensional Reduction: A Practical Formalism for Manipulating Solid Structures // *Chem. Mater.* 2001. Vol. 13. P. 1149–1166.
- Tyutyunnik A. P., Krasil'nikov V. N., Zubkov V. G., Perelyaeva L. A., Baklanova I. V. Synthesis, structure, and properties of  $V_2O_3(XO_4)_2$  (X=S, Se) // *Russ. J. Inorg. Chem.* 2010. Vol. 55. P. 501–507.
- Verbaere A., Marchand R., Tournoux M. Localisation du doublet solitaire dans les composés oxygénés cristallisés du thallium I // *J. Solid State Chem.* 1978. Vol. 23. P. 383–390.
- Vergasova L. P., Semenova T. F., Shuvalov R. R., Filatov S. K., Ananiev V. V. Ilinskite  $NaCu_5O_2(SeO_3)_2Cl_3$  - a new mineral of volcanic exhalations // *Dokl. Akad. Nauk (in Russ.)* 1997. Vol. 353. P. 641–644.

- Verma V. P. A review of synthetic, thermoanalytical, IR, Raman and X-ray studies on metal selenites // *Thermochim. Acta* 1999. Vol. 327. P. 63–102.
- Villa E. M., Diwu J., Alekseev E. V., Depmeier W., Albrecht-Schmitt T. E. Structural changes within the alkaline earth uranyl phosphites // *Dalton Trans.* 2013. Vol. 42. P. 9637–9644.
- Wickleder M. S., Hamida M. Ben CoSm(SeO<sub>3</sub>)<sub>2</sub>Cl, CuGd(SeO<sub>3</sub>)<sub>2</sub>Cl, MnSm(SeO<sub>3</sub>)<sub>2</sub>Cl, CuGd<sub>2</sub>(SeO<sub>3</sub>)<sub>4</sub> und CuSm<sub>2</sub>(SeO<sub>3</sub>)<sub>4</sub>: Übergangsmetallhaltige Selenite von Samarium und Gadolinium // *Z. Anorg. Allg. Chem.* 2003. Vol. 629. P. 556–562.
- Wildner M. Crystal structures of Co<sub>3</sub>(SeO<sub>3</sub>)<sub>3</sub>·H<sub>2</sub>O and Ni<sub>3</sub>(SeO<sub>3</sub>)<sub>3</sub>·H<sub>2</sub>O, two new isotypic compounds // *Monatshefte für Chemie Chem. Mon.* 1991. Vol. 122. P. 585–594.
- Wontcheu J., Schleid T. Tb<sub>2</sub>Se<sub>2</sub>O<sub>7</sub>: Terbium(III) Oxide Oxoselenate(IV) according to Tb<sub>2</sub>O[SeO<sub>3</sub>]<sub>2</sub> with a “Lone—Pair” Channel Structure // *Z. Anorg. Allg. Chem.* 2002. Vol. 628. P. 1941–1945.
- Wontcheu J., Schleid T. Tb<sub>3</sub>O<sub>2</sub>Cl[SeO<sub>3</sub>]<sub>2</sub> and Tb<sub>5</sub>O<sub>4</sub>Cl<sub>3</sub>[SeO<sub>3</sub>]<sub>2</sub>: Oxide Chloride Oxoselenates(IV) of Trivalent Terbium with “Lone-Pair” Channel or Layer Structures // *Z. Anorg. Allg. Chem.* 2005. Vol. 631. P. 309–315.
- Wontcheu J., Schleid T. Sc<sub>2</sub>Se<sub>3</sub>O<sub>9</sub>: Scandium(III) Oxoselenate(IV) According to Sc<sub>2</sub>[SeO<sub>3</sub>]<sub>3</sub> with a Hexagonal “Lone-Pair” Channel Structure // *Z. Anorg. Allg. Chem.* 2003. Vol. 629. P. 1463–1465.
- Yeon J., Kim S., Nguyen S. D., Lee H., Halasyamani P. S. New Vanadium Selenites: Centrosymmetric Ca<sub>2</sub>(VO<sub>2</sub>)<sub>2</sub>(SeO<sub>3</sub>)<sub>3</sub>(H<sub>2</sub>O)<sub>2</sub>, Sr<sub>2</sub>(VO<sub>2</sub>)<sub>2</sub>(SeO<sub>3</sub>)<sub>3</sub>, and Ba(V<sub>2</sub>O<sub>5</sub>)(SeO<sub>3</sub>), and Noncentrosymmetric and Polar A<sub>4</sub>(VO<sub>2</sub>)<sub>2</sub>(SeO<sub>3</sub>)<sub>4</sub>(Se<sub>2</sub>O<sub>5</sub>) (A=Sr<sup>2+</sup> or Pb<sup>2+</sup>) // *Inorg. Chem.* 2012. Vol. 51. P. 609–619.
- Zitzer S., Schleifenbaum F., Schleid T. Synthesis, crystal structure and spectroscopic properties of Y<sub>3</sub>O<sub>2</sub>Cl[SeO<sub>3</sub>]<sub>2</sub>: Eu<sup>3+</sup> // *Z. Kristallogr.* 2011. Vol. 226. P. 651–656.

## INCLUDED ARTICLES

**A-I**

### **Unprecedented layer topology in the crystal structure of a new organically templated uranyl selenite-selenate**

Vadim M. Kovrugin, Vladislav V. Gurzhiy, Sergey V. Krivovichev, Ivan G. Tananaev, and  
Boris F. Myasoedov

Published in: *Mendeleev Communications*, 2012, Vol. 22 (1), p. 11–12.

DOI: 10.1016/j.mencom.2012.01.003

Reprinted with kind permission from Elsevier B. V.



## Unprecedented layer topology in the crystal structure of a new organically templated uranyl selenite-selenate

Vadim M. Kovrugin,<sup>\*a</sup> Vladislav V. Gurzhiy,<sup>a,b</sup> Sergey V. Krivovichev,<sup>a</sup>  
Ivan G. Tananaev<sup>c</sup> and Boris F. Myasoedov<sup>c</sup>

<sup>a</sup> Department of Geology, St. Petersburg State University, 199034 St. Petersburg, Russian Federation.  
Fax: +7 812 328 9647; e-mail: kovrugin\_vm@hotmail.com

<sup>b</sup> Department of Chemistry, St. Petersburg State University, 198504 St. Petersburg, Russian Federation

<sup>c</sup> A. N. Frumkin Institute of Physical Chemistry and Electrochemistry, Russian Academy of Sciences, 119991 Moscow, Russian Federation

DOI: 10.1016/j.mencom.2012.01.003

The crystal structure of the new organically templated uranyl selenite-selenate  $[\text{C}_2\text{H}_8\text{N}][(\text{H}_5\text{O}_2)(\text{H}_2\text{O})][(\text{UO}_2)_2(\text{SeO}_4)_3(\text{H}_2\text{SeO}_3)](\text{H}_2\text{O})$  is based upon complex layers with a unique topology, which was not observed previously in inorganic compounds.

The oxo salt compounds of uranyl have been intensively studied owing to their importance in radioactive waste management, uranium mineralogy, catalysis, ion-exchange, *etc.*<sup>1</sup> Special attention was attracted to organically templated uranyl compounds as promising materials for separation and extraction technologies. A variety of compounds of this class, including organically templated uranium sulfates,<sup>2–6</sup> selenites,<sup>7</sup> molybdates,<sup>8–12</sup> vanadates<sup>13,14</sup> and silicates,<sup>15</sup> have been prepared recently. Uranyl selenates,<sup>16–21</sup> which can form nanotubular structures<sup>22–24</sup> that have no analogues among well-known inorganic oxo salts, are of special interest. Here, we report on the synthesis<sup>†</sup> and structural characterization of a new uranyl selenite-selenate,  $[\text{C}_2\text{H}_8\text{N}][(\text{H}_5\text{O}_2)(\text{H}_2\text{O})][(\text{UO}_2)_2(\text{SeO}_4)_3(\text{H}_2\text{SeO}_3)](\text{H}_2\text{O})$  **1**, with an unprecedented layer topology.

The crystal structure of **1**<sup>‡</sup> contains two independent U atoms that form the linear uranyl cation  $[\text{O}=\text{U}=\text{O}]^{2+}$ . The U=O bond lengths are 1.751(5)–1.765(4) Å. Both uranyl cations formed by the U(1) and U(2) atoms are surrounded in the equatorial plane

by five  $\text{O}_{\text{eq}}$  atoms to form the pentagonal bipyramids  $[\text{UO}_7]^{8-}$ . In the crystal structure of **1**, the U– $\text{O}_{\text{eq}}$  bond lengths vary from 2.378(4) to 2.414(5) Å. In the structure of **1**, three sites [Se(1), Se(2) and Se(3)] of four independent Se positions correspond to  $\text{Se}^{\text{VI}}$ , whereas the Se(4) site is occupied by  $\text{Se}^{\text{IV}}$ . The  $\text{Se}^{\text{VI}}$  positions are surrounded by four O atoms each with the average  $\langle \text{Se}–\text{O} \rangle$  bond lengths of 1.638, 1.636 and 1.642 Å for Se(1), Se(2) and Se(3), respectively. The Se(4) site has a trigonal pyramidal coordination with an apex occupied by the  $\text{Se}^{\text{IV}}$  atom. This coordination is typical of the  $\text{Se}^{\text{IV}}$  atom with a stereoactive lone electron pair. The  $\text{Se}(4)\text{O}_3$  trigonal pyramid is strongly distorted with one short Se(4)–O(17) bond [1.661(4) Å], and the Se(4)–O(18) and Se(4)–O(19) bonds being appreciably longer [1.713(5) and 1.735(5) Å, respectively]. Such a distorted coordination geometry is typical of biprotonated selenite groups ( $\text{H}_2\text{SeO}_3$ ); in particular, it was observed in the structure of  $[\text{C}_3\text{H}_{14}\text{N}]_4(\text{UO}_2)_3(\text{SeO}_4)_4(\text{HSeO}_3)(\text{H}_2\text{O})(\text{H}_2\text{SeO}_3)(\text{HSeO}_4)$ .<sup>27</sup>

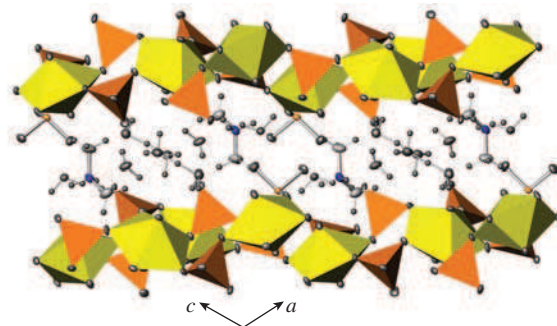
The crystal structure of **1** is based upon  $[(\text{UO}_2)_2(\text{SeO}_4)_3(\text{H}_2\text{SeO}_3)]^{2-}$  layers formed as a result of the condensation of  $[\text{UO}_7]^{8-}$ ,  $[\text{SeO}_4]^{2-}$  and  $(\text{H}_2\text{SeO}_3)$  coordination units by sharing common oxygen atoms. The  $[(\text{UO}_2)_2(\text{SeO}_4)_3(\text{H}_2\text{SeO}_3)]^{2-}$  layers are parallel to (101) (Figure 1). Protonated dimethylamine molecules,  $[\text{C}_2\text{H}_8\text{N}]^+$ , and  $[\text{H}_5\text{O}_2]^+$  hydroxonium complexes are located in the interlayer space and form hydrogen bonds to the O atoms of uranyl groups and selenium oxo complexes.

Figure 2(a) shows the structure of the  $[(\text{UO}_2)_2(\text{SeO}_4)_3(\text{H}_2\text{SeO}_3)]^{2-}$  layer in more detail. The selenate tetrahedra and  $(\text{H}_2\text{SeO}_3)$  trigonal pyramids coordinate uranyl ions in a mono-

<sup>†</sup> The yellowish green transparent plates of **1** were prepared by evaporation from aqueous solutions. A mixture of 0.0503 g (0.1 mmol) of  $\text{UO}_2(\text{NO}_3)_2 \cdot 6\text{H}_2\text{O}$ , 0.0045 g (0.1 mmol) of dimethylamine, 0.1160 g (0.8 mmol) of 40%  $\text{H}_2\text{SeO}_4$ , and 2 ml of distilled water was stirred until complete homogenization, poured onto a watch glass, and kept in a fume hood at room temperature. The crystals of **1** crystallized on the bottom of the vessel after three days.

<sup>‡</sup> *Crystallographic data.* Crystals of **1** ( $\text{C}_2\text{H}_{19}\text{N}_2\text{O}_{23}\text{Se}_4\text{U}_2$ ,  $M = 1217.08$ ) are monoclinic, space group  $P2_1/n$ , at 293 K:  $a = 14.7979(8)$ ,  $b = 10.0238(6)$  and  $c = 16.4176(9)$  Å,  $\beta = 111.628(1)^\circ$ ,  $V = 2263.8(2)$  Å<sup>3</sup>,  $Z = 4$ ,  $d_{\text{calc}} = 3.571$  g cm<sup>-3</sup>,  $\mu(\text{MoK}\alpha) = 20.822$  cm<sup>-1</sup>,  $F(000) = 2168$ . Intensities of 25431 reflections were measured with a Bruker SMART APEX II CCD diffractometer [ $\lambda(\text{MoK}\alpha) = 0.71073$  Å,  $2\theta_{\text{max}} = 58^\circ$ ] and 5476 independent reflections ( $R_{\text{int}} = 0.0734$ ) were used in further refinement. The structure was solved by direct method and refined by the full-matrix least-squares technique against  $F^2$  in the anisotropic-isotropic approximation. Hydrogen atoms of  $\text{H}_2\text{O}$  groups were located from the Fourier synthesis of the electron density. The H(C,N) atom positions were calculated. The refinement converged to  $wR_2 = 0.0538$  and GOF = 0.928 for all independent reflections [ $R_1 = 0.0265$  was calculated against  $F$  for 4285 observed reflections with  $I > 2\sigma(I)$ ]. All calculations were performed using SHELXTL PLUS 5.0.16.

CCDC 824406 contains the supplementary crystallographic data for this paper. These data can be obtained free of charge from The Cambridge Crystallographic Data Centre via www.ccdc.cam.ac.uk/data\_request/cif. For details, see ‘Notice to Authors’, *Mendeleev Commun.*, Issue 1, 2012.



**Figure 1** Crystal structure of **1** projected along the  $b$  axis. Displacement ellipsoids are drawn at a 50% probability level.

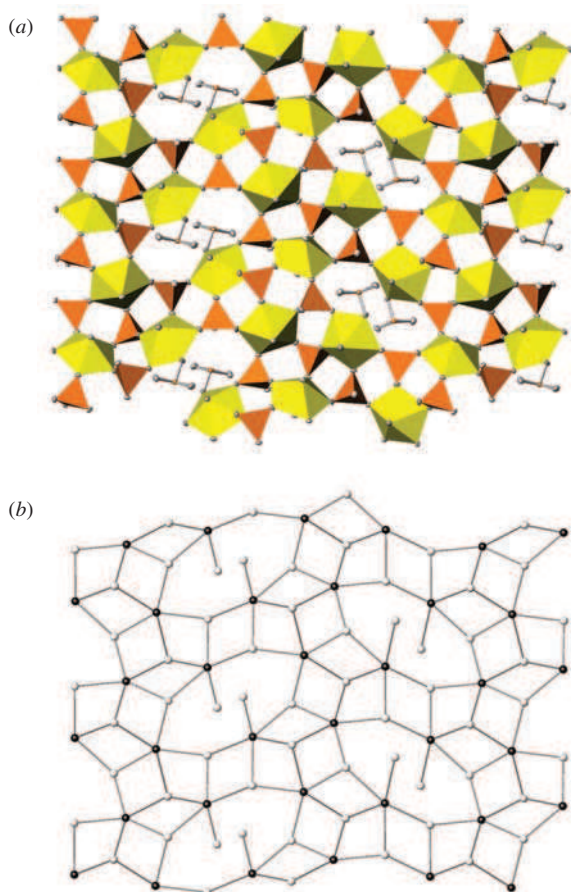


**Figure 2** (a) Projection of the uranyl selenite-selenate layer in the crystal structure of **1** (displacement ellipsoids at 50% probability level) and (b) its topology shown as a graph (U and Se polyhedra are symbolized by black and white nodes, respectively).

dentate fashion; however, their topological roles are remarkably distinct. The selenate group coordinates three uranyl ions, whereas protonated selenite groups coordinate one uranyl ion each. This is in agreement with the empirical rule formulated previously that, in uranyl selenite-selenate complexes, the connectivity of selenite is lower than that of selenate anions.<sup>28</sup> The linkage topology of the U and Se polyhedra can be described in terms of the graph theory<sup>29</sup> if U and Se atoms are symbolized by black and white nodes. The nodes are linked by a line if the corresponding atoms are bonded to the same bridging O atom. An idealized version of the black-and-white graph for the uranyl selenite-selenate complex in **1** is shown in Figure 2(b). This topology is unprecedented for both the chemistry of uranium and the structural chemistry of uranyl oxo salts in general. The topology is remarkable due to the presence of 1-connected branches inside eight-membered rings; this feature has been observed in just two other organically templated uranyl oxo salt compounds<sup>21,30</sup> and has never been observed in other inorganic oxo salts.

This work was supported by the Federal Target Programme ‘Scientific and Scientific-Pedagogical Personnel of the Innovative Russia’ (contract no. 02.740.11.0326) and the St. Petersburg State University (grant no. 3.37.84.2011).

## References

- 1 T. E. Albrecht-Schmitt, P. C. Burns and S. V. Krivovichev, in *The Chemistry of the Actinide and Transactinide Elements*, eds. L. R. Morss, N. M. Edelstein and J. Fuger, Springer, Dordrecht, 2010, vol. 6, pp. 4157–4191.
- 2 A. J. Norquist, M. B. Doran, P. M. Thomas and D. O’Hare, *Inorg. Chem.*, 2003, **42**, 5949.
- 3 A. J. Norquist, M. B. Doran, P. M. Thomas and D. O’Hare, *Dalton Trans.*, 2003, 1168.
- 4 M. B. Doran, B. E. Cockbain, A. J. Norquist and D. O’Hare, *Dalton Trans.*, 2004, 3810.
- 5 M. B. Doran, B. E. Cockbain and D. O’Hare, *Dalton Trans.*, 2005, 1774.
- 6 M. S. Bharara and E. V. Gorden, *Dalton Trans.*, 2010, **39**, 3557.
- 7 P. M. Almond and T. E. Albrecht-Schmitt, *Inorg. Chem.*, 2003, **42**, 5693.
- 8 P. S. Halasyamani, R. J. Francis, S. M. Walker and D. O’Hare, *Inorg. Chem.*, 1999, **38**, 271.
- 9 S. V. Krivovichev and P. C. Burns, *J. Solid State Chem.*, 2003, **170**, 106.
- 10 S. V. Krivovichev, T. Armbruster, D. Yu. Chernyshov, P. C. Burns, E. V. Nazarchuk and W. Depmeier, *Micropor. Mesopor. Mater.*, 2005, **78**, 225.
- 11 S. V. Krivovichev, P. C. Burns, T. Armbruster, E. V. Nazarchuk and W. Depmeier, *Micropor. Mesopor. Mater.*, 2005, **78**, 217.
- 12 S. V. Krivovichev, C. L. Cahill, E. V. Nazarchuk, P. C. Burns and T. Armbruster, W. Depmeier, *Micropor. Mesopor. Mater.*, 2005, **78**, 209.
- 13 L. Jouffret, Z. Shao, M. Rivenet and F. Abraham, *J. Solid State Chem.*, 2010, **183**, 2290.
- 14 L. Jouffret, M. Rivenet and F. Abraham, *J. Solid State Chem.*, 2010, **183**, 84.
- 15 X. Wang, J. Huang and A. J. Jacobson, *J. Am. Chem. Soc.*, 2002, **124**, 15190.
- 16 S. V. Krivovichev, V. V. Gurzhiy, I. G. Tananaev and B. F. Myasoedov, *Russ. J. Gen. Chem.*, 2009, **79**, 2723.
- 17 S. V. Krivovichev, V. V. Gurzhiy, I. G. Tananaev and B. F. Myasoedov, *Z. Kristallogr.*, 2009, **224**, 316.
- 18 J. Ling, G. E. Sigmon and P. C. Burns, *J. Solid State Chem.*, 2009, **182**, 402.
- 19 J. Ling, G. E. Sigmon, M. Ward, N. Roback and P. C. Burns, *Z. Kristallogr.*, 2010, **225**, 230.
- 20 V. V. Gurzhiy, S. V. Krivovichev, P. C. Burns, I. G. Tananaev and B. F. Myasoedov, *Radiokhimiya*, 2010, **52**, 3 [*Radiochem. (Engl. Transl.)*, 2010, **52**, 1].
- 21 S. V. Krivovichev, V. V. Gurzhiy, I. G. Tananaev and B. F. Myasoedov, *Radiokhimiya*, 2010, **52**, 8 [*Radiochem. (Engl. Transl.)*, 2010, **52**, 7].
- 22 S. V. Krivovichev, V. Kahlenberg, R. Kaindl, E. Mersdorf, I. G. Tananaev and B. F. Myasoedov, *Angew. Chem. Int. Ed.*, 2005, **44**, 1134.
- 23 S. V. Krivovichev, V. Kahlenberg, I. G. Tananaev, R. Kaindl, E. Mersdorf and B. F. Myasoedov, *J. Am. Chem. Soc.*, 2005, **127**, 1072.
- 24 E. V. Alekseev, S. V. Krivovichev and W. Depmeier, *Angew. Chem. Int. Ed.*, 2008, **47**, 549.
- 25 A. Altomare, G. Cascarano, C. Giacovazzo, A. Guagliardi, M. C. Burla, G. Polidori and M. Camalli, *J. Appl. Crystallogr.*, 1994, **27**, 435.
- 26 G. M. Sheldrick, *Acta Crystallogr.*, 2008, **A64**, 112.
- 27 S. V. Krivovichev, I. G. Tananaev, V. Kahlenberg and B. F. Myasoedov, *Radiokhimiya*, 2006, **48**, 197 [*Radiochem. (Engl. Transl.)*, 2006, **48**, 217].
- 28 S. V. Krivovichev, I. G. Tananaev, V. Kahlenberg and B. F. Myasoedov, *Dokl. Akad. Nauk*, 2005, **403**, 349 [*Dokl. Phys. Chem. (Engl. Transl.)*, 2005, **403**, 124].
- 29 S. V. Krivovichev, *Structural Crystallography of Inorganic Oxysalts*, Oxford University Press, Oxford, 2008.
- 30 E. V. Alekseev, S. V. Krivovichev and W. Depmeier, *Radiokhimiya*, 2008, **50**, 385 [*Radiochem. (Engl. Transl.)*, 2008, **50**, 445].

Received: 13th May 2011; Com. 11/3725

## A-II

# **Structural topology and dimensional reduction in uranyl oxysalts: eight novel phases in the methylamine-(UO<sub>2</sub>)(NO<sub>3</sub>)<sub>2</sub>-H<sub>2</sub>SeO<sub>4</sub>-H<sub>2</sub>O system**

Vadim M. Kovrugin, Vladislav V. Gurzhiy, and Sergey V. Krivovichev

Published in: *Structural Chemistry*, 2012, Vol. 23 (6), p. 2003–2017.

DOI: 10.1007/s11224-012-0001-7

Reprinted with kind permission from Springer Science+Business Media, LLC.





# Structural topology and dimensional reduction in uranyl oxysalts: eight novel phases in the *methylamine*– $(\text{UO}_2)(\text{NO}_3)_2\text{–H}_2\text{SeO}_4\text{–H}_2\text{O}$ system

Vadim M. Kovrugin · Vladislav V. Gurzhiy ·  
Sergey V. Krivovichev

Received: 19 February 2012 / Accepted: 21 March 2012 / Published online: 6 May 2012  
© Springer Science+Business Media, LLC 2012

**Abstract** Single crystals of eight novel uranyl selenates,  $(\text{CH}_3\text{NH}_3)_2[(\text{UO}_2)(\text{SeO}_4)_2(\text{H}_2\text{O})](\text{H}_2\text{O})$  (**I**) and  $(\text{CH}_3\text{NH}_3)_2[(\text{UO}_2)(\text{SeO}_4)_2(\text{H}_2\text{O})]$  (**II**),  $(\text{CH}_3\text{NH}_3)_2[(\text{UO}_2)_2(\text{SeO}_4)_3]$  (**III**) and  $(\text{CH}_3\text{NH}_3)(\text{H}_3\text{O})[(\text{UO}_2)_2(\text{SeO}_4)_3(\text{H}_2\text{O})](\text{H}_2\text{O})$  (**IV**),  $(\text{CH}_3\text{NH}_3)_4[(\text{UO}_2)_3(\text{SeO}_4)_5](\text{H}_2\text{O})_4$  (**V**) and  $(\text{CH}_3\text{NH}_3)(\text{H}_5\text{O}_2)(\text{H}_3\text{O})_2[(\text{UO}_2)_3(\text{SeO}_4)_5](\text{H}_2\text{O})_4$  (**VI**),  $(\text{CH}_3\text{NH}_3)_4(\text{H}_3\text{O})_2[(\text{UO}_2)_5(\text{SeO}_4)_8(\text{H}_2\text{O})](\text{H}_2\text{O})_4$  (**VII**), and  $(\text{CH}_3\text{NH}_3)_{1.5}(\text{H}_5\text{O}_2)_{1.5}(\text{H}_3\text{O})_3[(\text{UO}_2)_5(\text{SeO}_4)_8(\text{H}_2\text{O})](\text{H}_2\text{SeO}_4)_{2.6}(\text{H}_2\text{O})_3$  (**VIII**), have been prepared by isothermal evaporation from aqueous solutions and structurally characterized. The observed structural topologies of uranyl selenate units have been investigated using graph theory. The principle of dimensional reduction has been used for analysis of the uranyl oxysalts with general chemical formula  $A_n(\text{UO}_2)_p(\text{TO}_4)_q(\text{H}_2\text{O})_r$  ( $A$  = monovalent cation, and  $T = \text{S, Se, Cr, Mo}$ ), which allowed to construct three-component composition–structure diagram with separate dimensionality fields for different chemical compositions.

**Keywords** Uranium · Selenium · Methylamine · Uranyl oxysalts · Crystal structure · Single crystal X-ray diffraction · Topology · Dimensional reduction

## Introduction

Mathematical and topological models of inorganic chemical structures are of particular importance for understanding relations between their chemical composition and structural geometry and topology [1]. Simple topological models allowed to establish some important regularities, relationships and hierarchy among known simple and complex structure types [2–5]. In this paper, we report on structural topologies of eight novel uranium selenates and structure–composition relationships in complex uranyl compounds in general. It should be noted that structural chemistry of inorganic uranium compounds has had many important advances over the last 15 years partially summarized in [6–9]. In particular, introduction of two-dimensional tilings (so-called anion topologies [10]) and graphs [11, 12] led to deeper understanding of topological organization in uranium-based systems, including nanoscale structures such as uranium peroxide nanospheres [13–15] and uranyl selenate nanotubules [16–18]. The use of novel synthesis techniques allowed to prepare whole series of novel uranium compounds, e.g., mixed-valent uranium silicates [19–21] and uranyl borates [22–24]. Owing to their environmental and technological importance, uranyl oxysalts containing tetrahedral oxyanions of VIth group of the Periodic Table received particular attention [25]. Alekseev et al. [26] rationalized “composition–structure” relationships in uranyl molybdates using the principle of dimensional reduction proposed by Long et al. [27] for the description of decreasing dimensionality of chalcogenide structural units in Re sulfides and selenides. This principle was applied to various materials, including a wide class of ternary compounds [28], organic–inorganic composites [29], and some inorganic-oxysalt-based systems [12]. The principle of dimensional reduction states that incorporation of an ionic reagent and water into parent salts results in derivative compounds with decreasing

V. M. Kovrugin · V. V. Gurzhiy · S. V. Krivovichev (✉)  
Department of Crystallography, Faculty of Geology,  
St. Petersburg State University, University Emb. 7/9,  
Saint Petersburg, Russia 199034  
e-mail: skrivovi@mail.ru

S. V. Krivovichev  
Institute of Silicate Chemistry, Russian Academy of Sciences,  
Makarova Emb. 6, Saint Petersburg, Russia 199034

dimensionality of the structural unit. In addition to new experimental data on uranyl selenates, the present paper reports further extension of the dimensional reduction principle onto wide class of uranyl oxysalts containing monovalent organic and inorganic cations that play the role of reduction agents in complex systems.

## Experimental

### Caution

Although all uranium materials used in these experiments are depleted, extra care should always be used when handling uranium-containing materials.

### Materials

Methylamine (40 wt% in H<sub>2</sub>O, Sigma-Aldrich), selenic acid (40 wt% in H<sub>2</sub>O, 99.95 %, Aldrich), and UO<sub>2</sub>(NO<sub>3</sub>)<sub>2</sub>·6H<sub>2</sub>O (Vekton) were used as received. Deionized distilled water was also used in these syntheses.

### Synthesis

Crystals of new eight organic–inorganic compounds (CH<sub>3</sub>NH<sub>3</sub>)<sub>2</sub>[(UO<sub>2</sub>)(SeO<sub>4</sub>)<sub>2</sub>(H<sub>2</sub>O)](H<sub>2</sub>O) (**I**), (CH<sub>3</sub>NH<sub>3</sub>)<sub>2</sub>[(UO<sub>2</sub>)(SeO<sub>4</sub>)<sub>2</sub>(H<sub>2</sub>O)] (**II**), (CH<sub>3</sub>NH<sub>3</sub>)<sub>2</sub>[(UO<sub>2</sub>)<sub>2</sub>(SeO<sub>4</sub>)<sub>3</sub>] (**III**), (CH<sub>3</sub>NH<sub>3</sub>)(H<sub>3</sub>O)[(UO<sub>2</sub>)<sub>2</sub>(SeO<sub>4</sub>)<sub>3</sub>(H<sub>2</sub>O)](H<sub>2</sub>O) (**IV**), (CH<sub>3</sub>NH<sub>3</sub>)<sub>4</sub>[(UO<sub>2</sub>)<sub>3</sub>(SeO<sub>4</sub>)<sub>5</sub>](H<sub>2</sub>O)<sub>4</sub> (**V**), (CH<sub>3</sub>NH<sub>3</sub>)(H<sub>5</sub>O<sub>2</sub>)(H<sub>3</sub>O)<sub>2</sub>[(UO<sub>2</sub>)<sub>3</sub>(SeO<sub>4</sub>)<sub>5</sub>](H<sub>2</sub>O)<sub>4</sub> (**VI**), (CH<sub>3</sub>NH<sub>3</sub>)<sub>4</sub>(H<sub>3</sub>O)<sub>2</sub>[(UO<sub>2</sub>)<sub>5</sub>(SeO<sub>4</sub>)<sub>8</sub>(H<sub>2</sub>O)](H<sub>2</sub>O)<sub>4</sub> (**VII**) and (CH<sub>3</sub>NH<sub>3</sub>)<sub>1.5</sub>(H<sub>5</sub>O<sub>2</sub>)<sub>1.5</sub>(H<sub>3</sub>O)<sub>3</sub>[(UO<sub>2</sub>)<sub>5</sub>(SeO<sub>4</sub>)<sub>8</sub>(H<sub>2</sub>O)](H<sub>2</sub>SeO<sub>4</sub>)<sub>2.6</sub>(H<sub>2</sub>O)<sub>3</sub> (**VIII**) have been prepared by evaporation from aqueous solutions of uranyl nitrate, 40 %—solution of selenic acid, 40 %—solution of methylamine, and deionized distilled water. Yellow–green homogeneous liquid solutions were left in a fume hood at room temperature. The crystals of compound **I** were synthesized through the reaction of 0.0502 g (0.1 mmol) of uranyl nitrate, 0.0124 g (0.4 mmol) of methylamine, 0.0725 g (0.5 mmol) of selenic acid, and 2.0031 g (111.3 mmol) of deionized distilled water. The solid products were formed after 2 days in small amount. The crystals of compounds **II**, **IV**, and **VII** were synthesized through the reaction of 0.0504 g (0.1 mmol) of uranyl nitrate, 0.0155 g (0.5 mmol) of methylamine, 0.0580 g (0.4 mmol) of selenic acid, and 2.0067 g (111.5 mmol) of deionized distilled water. The solid products were formed after 3 days in small amount. The crystals of compound **III** were synthesized through the reaction of 0.0498 g (0.1 mmol) of uranyl nitrate, 0.0061 g (0.2 mmol) of methylamine, 0.1015 g (0.7 mmol) of selenic acid, and 1.9954 g (110.9 mmol) of deionized distilled water. The solid products were formed after 2 days in small amount.

The crystals of compound **V** were synthesized through the reaction of 0.0505 g (0.1 mmol) of uranyl nitrate, 0.0031 g (0.1 mmol) of methylamine, 0.1160 g (0.8 mmol) of selenic acid, and 1.9986 g (111.0 mmol) of deionized distilled water. The solid products were formed after 2 days in small amount. The compounds **VI** and **VIII** were synthesized through the reaction of 0.1004 g (0.2 mmol) of uranyl nitrate, 0.0030 g (0.1 mmol) of methylamine, 0.1014 g (0.7 mmol) of selenic acid, and 2.0023 g (111.2 mmol) of deionized distilled water. The solid products were formed after 3 days in small amount.

### X-ray crystallographic analysis

Single crystals selected for data collection were examined under an optical microscope, encased in epoxy and mounted on a glass fiber. Data were collected by means of a STOE IPDS II diffractometer using monochromated MoK<sub>α</sub> radiation and frame widths of 2° in  $\omega$ . The unit-cell parameters were refined by least-squares techniques. The data were corrected for Lorentz, polarization, and background effects. An analytical absorption correction based on the indexed faces was applied. The structures were solved by direct methods and refined by means of the programs SHELXL-97 [30] and SIR-92 [31]. Attempts to refine anisotropic parameters of several oxygen atoms positions and positions of atoms in organic methylamine molecules resulted in physically unrealistic values. Due to the low quality of crystals of most phases, their metastability and sensitivity to air, only relatively rough structural models could be obtained. As a consequence, crystallographic agreement index ( $R_1$ ) values for some crystals are not of the same order as those obtained from perfect crystals. Due to these reasons, we were unable to localize the positions of H atoms as well, and the details of the hydrogen bonding system remain unclear. However, some approximate schemes can be derived from O–O contacts involving sites occupied by the H<sub>2</sub>O molecules and hydronium cations. Relevant crystallographic data are listed in Tables 1 and 2. Selected interatomic distances are given in Table 3. CCDC files 866553, 866549, 866547, 866553, 866546, 866551, 866548, and 866550 contain the supplementary crystallographic data for the compounds **I**, **II**, **III**, **IV**, **V**, **VI**, **VII**, and **VIII** reported in this paper. These data can be obtained free of charge from The Cambridge Crystallographic Data Centre via [www.ccdc.cam.ac.uk/data\\_request/cif](http://www.ccdc.cam.ac.uk/data_request/cif).

## Results

Compounds with U:Se = 1:2

Compounds with U:Se = 1:2 can be described by the general formula (CH<sub>3</sub>NH<sub>3</sub>)[(UO<sub>2</sub>)(SeO<sub>4</sub>)<sub>2</sub>(H<sub>2</sub>O)](H<sub>2</sub>O)<sub>*n*</sub>,

**Table 1** Crystallographic Data for **I–V** in the system  $\text{UO}_2(\text{NO}_3)_2\text{--H}_2\text{SeO}_4\text{--methylamine--H}_2\text{O}$ 

Compound	<b>I</b>	<b>II</b>	<b>III</b>	<b>IV</b>
Empirical formula	$(\text{CH}_3\text{NH}_3)_2[(\text{UO}_2)(\text{SeO}_4)_2(\text{H}_2\text{O})](\text{H}_2\text{O})$	$(\text{CH}_3\text{NH}_3)_2[(\text{UO}_2)(\text{SeO}_4)_2(\text{H}_2\text{O})]$	$(\text{CH}_3\text{NH}_3)_2[(\text{UO}_2)_2(\text{SeO}_4)_3]$	$(\text{CH}_3\text{NH}_3)(\text{H}_3\text{O})[(\text{UO}_2)_2(\text{SeO}_4)_3(\text{H}_2\text{O})](\text{H}_2\text{O})$
fw	639.99	623.99	1020.98	1042.96
Crystal system	Orthorhombic	Monoclinic	Monoclinic	Monoclinic
Space group	<i>Pnma</i>	<i>P2<sub>1</sub>/c</i>	<i>P2<sub>1</sub></i>	<i>P2<sub>1</sub>/c</i>
<i>a</i> (Å)	7.5496(7)	8.2366(10)	8.5827(13)	8.4842(10)
<i>b</i> (Å)	12.0135(9)	7.5888(6)	10.0730(15)	10.2368(8)
<i>c</i> (Å)	15.8362(13)	22.260(2)	10.0915(14)	24.228(2)
$\alpha$ (deg)	90.00	90.00	90.00	90.00
$\beta$ (deg)	90.00	104.566(9)	95.980(12)	102.803(9)
$\gamma$ (deg)	90.00	90.00	90.00	90.00
<i>V</i> (Å <sup>3</sup> )	1436.3(2)	1346.7(2)	867.7(2)	2051.9(3)
<i>Z</i>	4	4	2	4
<i>D<sub>c</sub></i> (g cm <sup>-3</sup> )	2.960	3.078	3.908	3.376
$\mu$ (mm <sup>-1</sup> )	16.423	17.507	25.012	21.166
2 $\theta$ range (deg)	4.26–53.66	3.78–58.64	4.06–50.00	3.44–50.00
Reflections collected	10099	12119	5477	12326
Independent reflections	1605 [ <i>R</i> (int) = 0.0875]	3656 [ <i>R</i> (int) = 0.0828]	2931 [ <i>R</i> (int) = 0.1271]	3602 [ <i>R</i> (int) = 0.1698]
gof <sup>a</sup>	1.334	0.996	1.083	1.049
<i>R</i> <sub>1</sub> , <i>wR</i> <sub>2</sub> [ <i>I</i> > 2 $\sigma$ ( <i>I</i> )] <sup>a</sup>	0.0467, 0.0860	0.0466, 0.0637	0.1072, 0.2712	0.0674, 0.1551
<i>R</i> <sub>1</sub> , <i>wR</i> <sub>2</sub> [all data]	0.0566, 0.0882	0.0785, 0.0688	0.1126, 0.2766	0.0957, 0.1693

$$wR_2 = [\Sigma[w(F_o^2 - F_c^2)^2] / \Sigma w(F_o^2)]^{1/2}$$

$$^a \text{gof} = [\Sigma w(F_o^2 - F_c^2)^2 / (n_{\text{obs}} - n_{\text{param}})]^{1/2}$$

$$^b R_1 = \Sigma(|F_o| - |F_c|) / \Sigma |F_o|$$

where  $n = 1$  (**I**) and 0 (**II**). These compounds are probably the most stable in the system, which is manifested by their frequent occurrence in the experiments and relatively high quality of their crystals. The crystal structures of **I** and **II** contain one symmetrically independent  $\text{U}^{6+}$  cation each that forms two short  $\text{U}^{6+}\text{--O}^{2-}$  bonds [1.755(10)–1.775(6) Å] resulting in formation of nearly linear uranyl cations,  $[\text{UO}_2]^{2+}$ . This basic uranyl entity is coordinated in the equatorial plane by four oxygen atoms and one  $\text{H}_2\text{O}$  molecule, which forms pentagonal bipyramids with the  $\text{U}^{6+}\text{--O}_{\text{eq}}$  bond lengths in range of 2.331(9)–2.360(7) Å. There are two independent Se atoms per formula unit in each structure. The  $\text{Se}^{6+}$  cations in the structures are tetrahedrally coordinated by four O atoms, forming  $[\text{SeO}_4]^{2-}$  tetrahedra. The interpolyhedral  $\text{Se--O}_{\text{br}}$  bonds are longer (1.628(9)–1.656(6) Å;  $\text{O}_{\text{br}}$  = O atom bridging between U and Se polyhedra) than the  $\text{Se--O}_{\text{t}}$  bonds (1.593(10)–1.624(7) Å;  $\text{O}_{\text{t}}$  = terminal O atom in selenate group).

Crystal structures of **I** and **II** are based upon complex units with composition  $[(\text{UO}_2)(\text{SeO}_4)_2(\text{H}_2\text{O})]^{2-}$ , but with different topologies of linkage of U and Se polyhedra for different values of  $n$ . For  $n = 1$ , the structure contains 1D chains, for  $n = 0$  the structure is based upon 2D sheets (Fig. 1). The  $[\text{UO}_6(\text{H}_2\text{O})]^{6-}$  pentagonal bipyramids share

corners with two  $[\text{SeO}_4]^{2-}$  tetrahedra to form  $[(\text{UO}_2)(\text{SeO}_4)_2(\text{H}_2\text{O})]^{2-}$  chains running parallel to the *c* axis in the structure of **I**, and  $[(\text{UO}_2)(\text{SeO}_4)_2(\text{H}_2\text{O})]^{2-}$  sheets which are parallel to  $(10\bar{1})$  in the structure of **II**. The chains of **I** are arranged into sheets parallel to  $(010)$  plane.

In both structures, protonated  $[\text{CH}_3\text{NH}_3]^+$  methylamine cations and water molecules are arranged between the chains and the sheets and provide their linkage into a three-dimensional structures.

#### Compounds with U:Se = 2:3

In the crystal structures of **III** and **IV**, there are two symmetrically independent U positions. They have typical pentagonal bipyramidal coordination. The uranyl bond lengths are in the range of 1.746(9)–1.771(10) Å. In the equatorial plane, both uranyl cations are coordinated by five  $\text{O}^{2-}$  anions of the selenate groups in the crystal structure of **III**, whereas, in the structure of **IV**, the U(2) site is coordinated by four  $\text{O}^{2-}$  anions and one  $\text{H}_2\text{O}$ (17) group. The average  $\langle \text{U--O}_{\text{eq}} \rangle$  bond length is 2.34 Å in **III**. In the crystal structure of **IV**, the  $\text{U--O}_{\text{eq}}$  bond lengths are in the range of 2.32(1)–2.41(1) Å, and the  $\text{U--H}_2\text{O}$ (17) bond length is 2.494(16) Å. Each structure contains three

**Table 2** Crystallographic Data for **VI–IX** in the system  $\text{UO}_2(\text{NO}_3)_2\text{--H}_2\text{SeO}_4\text{--methylamine--H}_2\text{O}$ 

Compound	<b>V</b>	<b>VI</b>	<b>VII</b>	<b>VIII</b>
Empirical formula	$(\text{CH}_3\text{NH}_3)_4[(\text{UO}_2)_3(\text{SeO}_4)_5](\text{H}_2\text{O})_4$	$(\text{CH}_3\text{NH}_3)(\text{H}_5\text{O}_2)(\text{H}_3\text{O})_2[(\text{UO}_2)_3(\text{SeO}_4)_5](\text{H}_2\text{O})_4$	$(\text{CH}_3\text{NH}_3)_4(\text{H}_3\text{O})_2[(\text{UO}_2)_5(\text{SeO}_4)_8(\text{H}_2\text{O})](\text{H}_2\text{O})_4$	$(\text{CH}_3\text{NH}_3)_{1.5}(\text{H}_5\text{O}_2)_{1.5}(\text{H}_3\text{O})_3[(\text{UO}_2)_5(\text{SeO}_4)_8(\text{H}_2\text{O})](\text{H}_2\text{SeO}_4)_{2.6}(\text{H}_2\text{O})_3$
fw	1692.97	1678.91	2709.91	2946.25
Crystal system	Orthorhombic	Orthorhombic	Orthorhombic	Orthorhombic
Space group	<i>Pnna</i>	<i>Ibca</i>	<i>Pca2</i> <sub>1</sub>	<i>Pnma</i>
<i>a</i> (Å)	16.4221(14)	20.956(2)	31.505(2)	30.9728(19)
<i>b</i> (Å)	18.4773(9)	34.767(8)	10.3688(6)	37.022(2)
<i>c</i> (Å)	10.3602(5)	18.663(2)	16.2424(11)	10.4171(5)
$\alpha$ (deg)	90.00	90.00	90.00	90.00
$\beta$ (deg)	90.00	90.00	90.00	90.00
$\gamma$ (deg)	90.00	90.00	90.00	90.00
<i>V</i> (Å <sup>3</sup> )	3143.7(3)	13597(4)	5305.9(6)	11945.0(11)
<i>Z</i>	4	16	4	8
<i>D</i> <sub>c</sub> (g cm <sup>-3</sup> )	3.577	3.280	3.392	3.277
$\mu$ (mm <sup>-1</sup> )	21.319	19.720	20.814	20.086
2 $\theta$ range (deg)	4.40–50.00	2.34–47.00	2.58–49.00	2.20–49.00
Reflections collected	18,468	32,094	27,846	61,466
Independent reflections	2774 [ <i>R</i> (int) = 0.1191]	4913 [ <i>R</i> (int) = 0.3280]	8463 [ <i>R</i> (int) = 0.2070]	10116 [ <i>R</i> (int) = 0.2139]
gof <sup>a</sup>	1.104	0.968	0.997	1.055
<i>R</i> <sub>1</sub> , <i>wR</i> <sub>2</sub> [ <i>I</i> > 2 $\sigma$ ( <i>I</i> )] <sup>b</sup>	0.0541, 0.1119	0.1040, 0.1867	0.0852, 0.1901	0.0858, 0.1736
<i>R</i> <sub>1</sub> , <i>wR</i> <sub>2</sub> [all data]	0.0790, 0.1216	0.2138, 0.2287	0.1305, 0.2150	0.1556, 0.2083

$$wR_2 = [\sum(w(F_o^2 - F_c^2)^2) / \sum w(F_o^2)]^{1/2}$$

$$^a \text{gof} = [\sum w(F_o^2 - F_c^2)^2 / (n_{\text{obs}} - n_{\text{param}})]^{1/2}$$

$$^b R_1 = \sum(|F_o| - |F_c|) / \sum |F_o|$$

symmetrically independent  $[\text{SeO}_4]^{2-}$  tetrahedra. The  $\langle\text{Se–O}\rangle$  bond lengths are 1.66 and 1.62 Å for **III**, and the compound **IV**, respectively.

In both structures, the  $[\text{UO}_7]^{8-}$ ,  $[\text{UO}_6(\text{H}_2\text{O})]^{6-}$  and  $[\text{SeO}_4]^{2-}$  coordination polyhedra share common ligands to produce 2D sheets with the chemical compositions  $[(\text{UO}_2)_2(\text{SeO}_4)_3]^{2-}$  in **III** and  $[(\text{UO}_2)_2(\text{SeO}_4)_3(\text{H}_2\text{O})]^{2-}$  in **IV**. The sheets are parallel to (100) and (10 $\bar{1}$ ) in the compounds **III** and **IV**, respectively (Fig. 2). The interpolyhedral Se–O<sub>br</sub>–U angles are in the range of 136(2)–146(3)°, with the average value of 140° in **III**, and 133.9(8)–144.8(9)°, with the average value of 138.5° in **IV**, which is in general agreement with the average value of 136.8° reported in [32].

The structure of **III** contains two protonated linear methylamine molecules  $[\text{CH}_3\text{NH}_3]^+$  as interlayer species. In the interlayer space of **IV**, there are two protonated  $[\text{CH}_3\text{NH}_3]^+$  cations and one  $\text{H}_2\text{O}$  molecule.

#### Compounds with U:Se = 3:5

The crystal structures of **V** and **VI** contain three crystallographically independent U atoms each. All the  $\text{U}^{6+}$  sites

adopt the pentagonal bipyramidal coordination geometry with two short uranyl bonds ( $\langle\text{U–O}_{\text{Ur}}\rangle = 1.75$  Å in both **V** and **VI**). In the equatorial plane, the uranyl cations are surrounded by five O atoms ( $\langle\text{U–O}_{\text{eq}}\rangle = 2.40$  Å). There are five tetrahedrally coordinated Se sites in each structure ( $\langle\text{Se–O}\rangle = 1.64$  and 1.62 Å in **V** and **VI**, respectively). In the structure of **VI**, one of the tetrahedra is disordered in terms of the O(13) and O(14) sites, which have 50 % occupancy each.

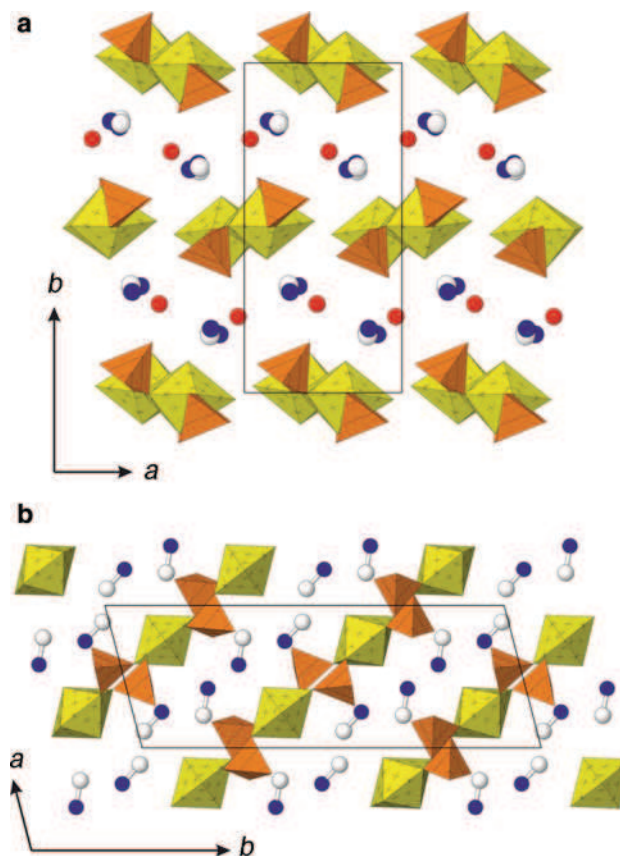
In both structures, the  $[\text{UO}_7]^{8-}$  pentagonal bipyramids and  $[\text{SeO}_4]^{2-}$  tetrahedra are linked through common vertices to form sheets with the composition  $[(\text{UO}_2)_3(\text{SeO}_4)_5]^{4-}$ . In the structure of **V**, the uranyl selenate sheets are corrugated and oriented parallel to (100). In the structure of **VI**, the inorganic two-dimensional complexes are more or less planar and run parallel to (010) (Fig. 3).

Both structures contain protonated methylamine molecules  $[\text{CH}_3\text{NH}_3]^+$  and water molecules that provide three-dimensional linkage of the uranyl selenate sheets via hydrogen bonding. In the interlayer space of the crystal structure of **VI** there is one independent  $[\text{H}_5\text{O}_2]^+$  cation (the respective O(33)–O(34) interatomic distance is 2.30(12) Å) and two hydronium cations  $[\text{H}_3\text{O}]^+$ .

**Table 3** Selected bond distances (Å) and angles (deg) in the structures of **I–VIII**

	U–O <sub>ur</sub>	U–O <sub>eq</sub>	U–H <sub>2</sub> O <sub>eq</sub>	Se–O <sub>br</sub>	Se–O <sub>t</sub>	U–O <sub>ur</sub> –Se
<b>I</b>	(1.762) 1.755(10)–1.769(12) (1.767) 1.759(6)–1.775(6) (1.770) 1.769(10)–1.771(10) (1.751) 1.746(9)–1.758(9) (1.753) 1.740(14)–1.759(15) (1.75) 1.67(3)–1.81(3) (1.758) 1.751(10)–1.764(10) (1.72) 1.69(2)–1.77(2)	(2.336) 2.331(9)–2.340(9) (2.347) 2.335(6)–2.360(7) (2.34) 2.22(5)–2.44(6) (2.375) 2.316(14)–2.407(14) (2.403) 2.369(11)–2.43(2) (2.40) 2.33(4)–2.45(3) (2.39) 2.31(2)–2.48(3) (2.396) 2.364(18)–2.421(19)	2.482(13) 2.513(6) – 2.494(16) – – – 2.54(3) 2.51(2)	(1.630) 1.628(9)–1.632(8) (1.646) 1.638(7)–1.656(6) (1.66) 1.59(3)–1.74(6) (1.628) 1.608(15)–1.654(14) (1.643) 1.44(2)–1.657(14) (1.62) 1.55(3)–1.68(3) (1.61) 1.55(4)–1.66(3) (1.619) 1.575(19)–1.652(17)	(1.602) 1.593(10)–1.610(8) (1.614) 1.610(6)–1.624(7) (1.65) 1.65(3)–1.65(4) (1.597) 1.583(16)–1.605(19) (1.609) 1.608(13)–1.95(3) (1.60) 1.54(4)–1.66(4) (1.55) 1.50(5)–1.62(3) (1.587) 1.56(2)–1.61(2)	(139.8) 138.2(5)–141.3(5) (140.4) 132.5(4)–147.7(4) (140) 136(2)–146(3) (138.5) 133.9(8)–144.8(9) (135.2) 127.0(6)–145.1(13) (136.8) 129.6(19)–146.2(19) (136.8) 129(2)–152.9(13) (137.6) 126.3(13)–150.2(14)

In brackets given are average value in the crystal structures

**Fig. 1** The crystal structures of **I** and **II** projected along the *c* (**a**), and *b* (**b**) axes, respectively. Legend: U polyhedra = yellow; Se polyhedra = orange; C and N atoms are white and blue, respectively; red circles = H<sub>2</sub>O groups (Color figure online)

## Compounds with U:Se = 5:8

Five symmetrically independent uranium positions were observed in the crystal structures of **VII** and **VIII**. All U sites have typical seven-coordinate pentagonal bipyramidal coordination geometries with the average  $\langle \text{U}^{6+}\text{--O}_{\text{Ur}} \rangle$  uranyl bond lengths equal to 1.76 and 1.73 Å for **VII** and **VIII**, respectively. The uranyl cations are equatorially coordinated by five O atoms, which leads to the formation of pentagonal bipyramids with the  $\text{U}^{6+}\text{--O}_{\text{eq}}$  bond lengths in the range of 2.31(2)–2.48(3) Å for **VII** and 2.36(2)–2.42(2) Å for **VIII**. In both structures, four out of the five equatorial oxide ligands of  $[\text{U}(\text{O})_2]^{2+}$  cations belong to the  $[\text{SeO}_4]^{2-}$  groups; the fifth is an H<sub>2</sub>O molecule. The U(1)–H<sub>2</sub>O bond length is 2.54(3) and 2.51(2) Å in **VII** and **VIII**, respectively. The Se atoms in both structures are tetrahedrally coordinated by four O atoms each, forming  $[\text{SeO}_4]^{2-}$  tetrahedra. The  $\langle \text{Se--O} \rangle$  bond lengths of tetrahedra are 1.61 and 1.62 Å for **VII** and **VIII**, respectively.

The structures of **VII** and **VIII** are based upon sheets with the chemical composition  $[(\text{UO}_2)_5(\text{SeO}_4)_8(\text{H}_2\text{O})]^{6-}$ . The sheets are formed by corner sharing between  $[\text{U}\phi_7]^{n-}$

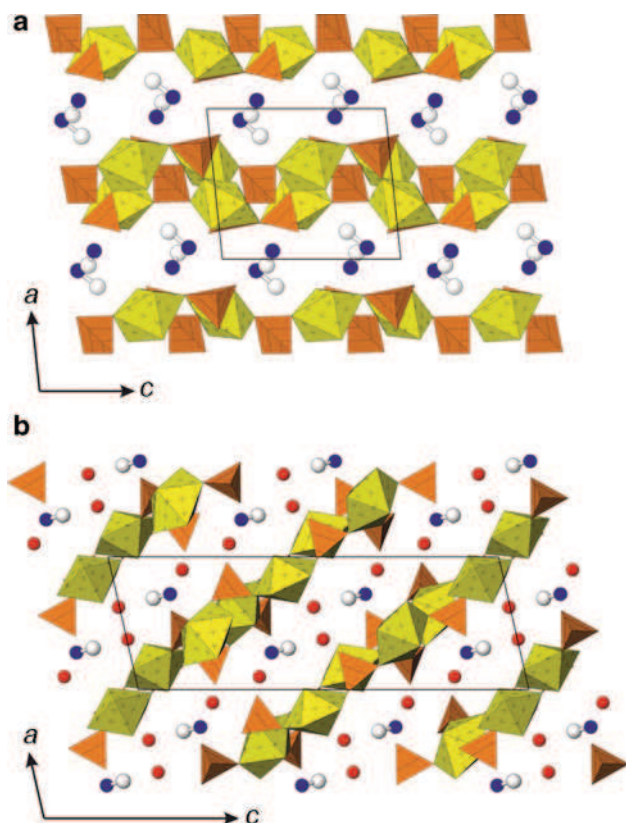


**Fig. 2** The crystal structures of **III** and **IV** projected along the *b* axes (**a**, **b**, respectively). Legend is as in Fig. 1

( $\varphi = \text{O}, \text{H}_2\text{O}$ ;  $n = 6, 8$ ) pentagonal bipyramids and  $[\text{SeO}_4]^{2-}$  tetrahedra. In the structure of **VII**, the uranyl selenate sheets are slightly corrugated and arranged in parallel with the (001) plane (Fig. 4a). In the structure of **VIII**, the uranyl selenate sheets are planar and run parallel to (010) (Fig. 4b). The interpolyhedral Se–O<sub>br</sub>–U angles in **VII** and **VIII** have the average values of 136.8° and 137.6°, respectively, which are in general agreement with the average value of 136.8° reported in [32].

The compounds **VII** and **VIII** contain as interlayer species protonated methylamine  $[\text{CH}_3\text{NH}_3]^+$  cations, hydronium  $[\text{H}_3\text{O}]^+$  and  $[\text{H}_5\text{O}_2]^+$  cations and water molecules as interlayer species. Assignment of the interlayer sites to the  $[\text{H}_3\text{O}]^+$  cations was based upon the presence of three  $\text{H}_3\text{O}^+\cdots\text{O}$  contacts in the range of 2.6–2.9 Å. The  $[\text{H}_5\text{O}_2]^+$  cations are characterized by the presence of a strong hydrogen bond within the cation and two additional  $\text{O}\cdots\text{O}$  contacts in the range of 2.3–2.4 Å corresponding to a strong hydrogen bond within the cation and two additional  $\text{O}\cdots\text{O}$  contacts in the range of 2.7–2.9 Å for each O atom of the  $[\text{H}_5\text{O}_2]^+$  cation. In contrast,  $\text{H}_2\text{O}$  groups form from two to three weak hydrogen bonds to adjacent O atoms with the  $\text{O}\cdots\text{O}$  interatomic distances longer than 2.9 Å. In the interlayer space of **VIII**, there are also three disordered electroneutral ( $\text{H}_2\text{SeO}_4$ ) groups.

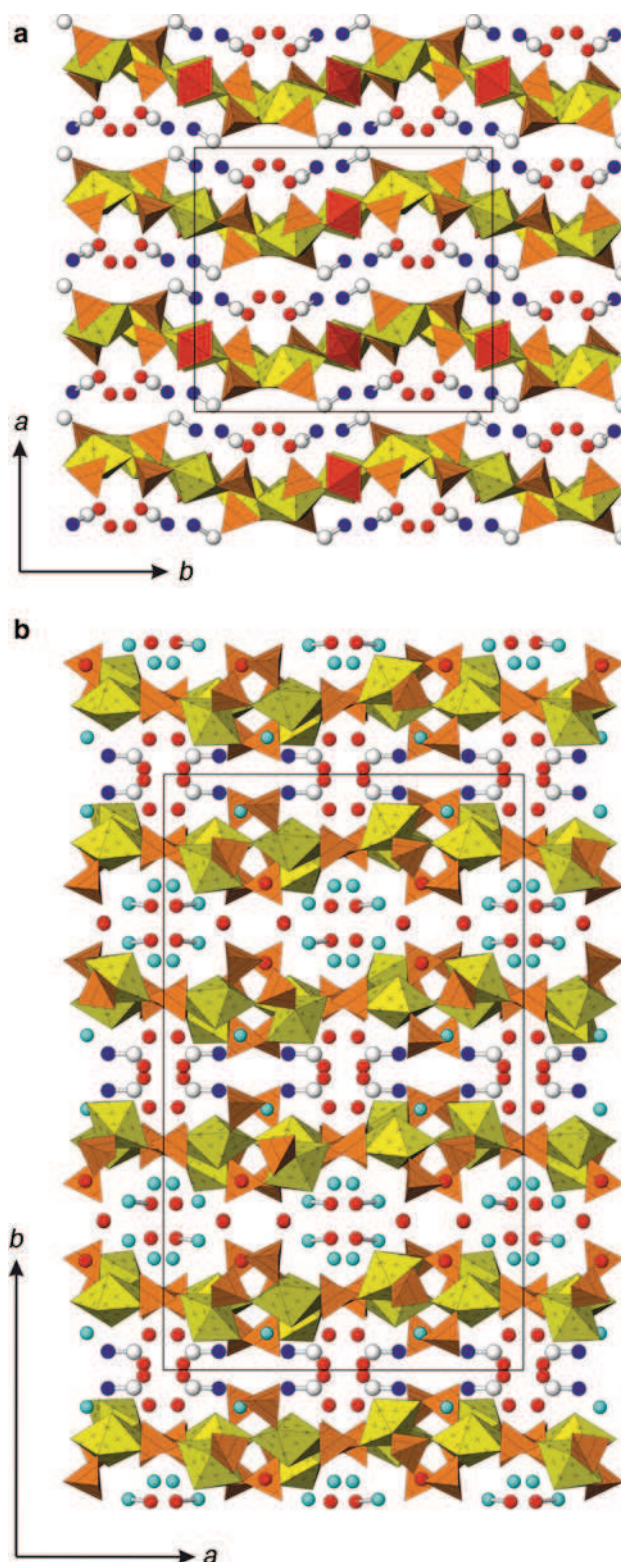


**Fig. 3** The crystal structures of **V** and **VI** projected along the *c* axes (**a**, **b**, respectively). Legend is as in Fig. 1; the selenate tetrahedra in **V** with disordered orientations are shown in red; cyan circles =  $[\text{H}_3\text{O}]^+$  groups (Color figure online)

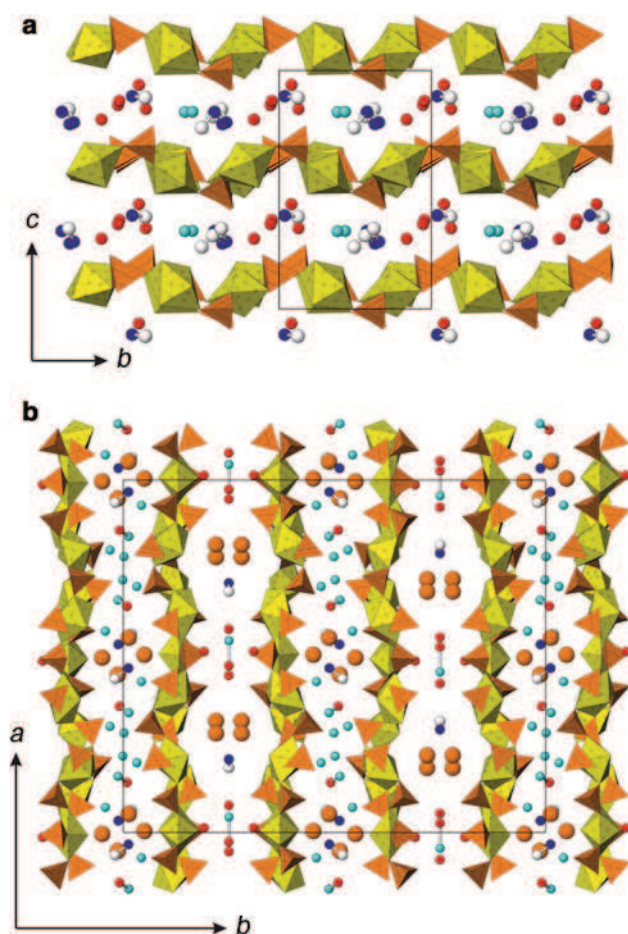


**Fig. 4** The crystal structures of **VII** and **VIII** projected along the *a* (**a**) and *c* (**b**) axes, respectively. Legend is as in Fig. 1; cyan circles =  $[\text{H}_3\text{O}]^+$  groups; orange circles indicate positions of disordered Se atoms in the interlayer space (Color figure online)

## Discussion

### Topological analysis

Topological structure of uranyl selenate units in the structures under consideration here can be visualized using the nodal representation. Within this approach [11, 12, 25], the U and Se coordination polyhedra are symbolized by black and white nodes, respectively. The vertices are linked by an edge if two respective polyhedra share a common oxygen atom. The resulting graph is used to investigate topological relations between similar structures.

Figure 5c and d show black-and-white graphs corresponding to the topological structures of the 1D- and 2D-units of **I** and **II**. The  $[(\text{UO}_2)(\text{SeO}_4)_2(\text{H}_2\text{O})]^{2-}$  chain observed in the structure of **I** corresponds to the simple 1D graph. Chains of this type are quite common for uranyl compounds with  $[\text{TO}_4]^{n-}$  tetrahedra (T = S, Se, P, As). They have been observed first in the structure of

$\text{Mn}[(\text{UO}_2)(\text{SO}_4)_2(\text{H}_2\text{O})](\text{H}_2\text{O})_5$  [33] and later in a number of amine-templated uranyl sulfates [34–39] and other compounds, including  $[(\text{UO}_2)(\text{H}_2\text{PO}_4)_2(\text{H}_2\text{O})](\text{H}_2\text{O})_2$  [40],  $[(\text{UO}_2)(\text{H}_2\text{AsO}_4)_2(\text{H}_2\text{O})]$  [41],  $M[(\text{UO}_2)(\text{SeO}_4)_2(\text{H}_2\text{O})](\text{H}_2\text{O})_4$  ( $M = \text{Mg}, \text{Zn}$ ) [42],  $[\text{C}_5\text{H}_{16}\text{N}_2]_2[(\text{UO}_2)(\text{SeO}_4)_2(\text{H}_2\text{O})](\text{NO}_3)_2$  [43]. The black-and-white graph of the sheet observed in the structure of **II** (Fig. 5d) consists of four-connected black and two-connected white vertices. This graph corresponds to the topology observed in a number of layered uranyl selenates:  $[\text{C}_5\text{H}_{14}\text{N}_2]_2[(\text{UO}_2)(\text{SeO}_4)_2(\text{H}_2\text{O})]_2(\text{H}_2\text{O})$ ,  $[\text{C}_4\text{H}_{12}\text{N}]_2[(\text{UO}_2)(\text{SeO}_4)_2(\text{H}_2\text{O})]$  [9],  $(\text{H}_3\text{O})_2[(\text{UO}_2)(\text{SeO}_4)_2(\text{H}_2\text{O})](\text{H}_2\text{O})$  [44], and  $\text{K}_2(\text{H}_5\text{O}_2)(\text{H}_3\text{O})[(\text{UO}_2)_2(\text{SeO}_4)_4(\text{H}_2\text{O})_2](\text{H}_2\text{O})_4$  [45]. The graph contains tight four-membered rings and extended voids of about  $3 \times 15 \text{ \AA}^2$  in dimensions.

Figure 6a, b show uranyl selenate sheets in the structures of **III**, and **IV**, respectively. The corresponding black-and-white graphs are depicted in Fig. 6c, d, respectively. The topology of **III** is based only upon four-membered rings of alternating black and white nodes. The graph has been observed in uranyl selenates  $(\text{H}_3\text{O})[\text{C}_3\text{H}_5\text{N}_2]_2[(\text{UO}_2)_2(\text{SeO}_4)_3]$  [9] and  $[\text{CH}_6\text{N}_3]_2[(\text{UO}_2)_2(\text{SeO}_4)_3]$  [46]. Topology of the  $[(\text{UO}_2)_3(\text{SeO}_4)_5]^{2-}$  sheet in **IV** contains four- and eight-membered rings. This topology is relatively rare and has previously been observed in  $\text{K}(\text{H}_3\text{O})[(\text{UO}_2)_2(\text{SeO}_4)_3(\text{H}_2\text{O})](\text{H}_2\text{O})_6$  [47] and  $[\text{N}_8\text{C}_{26}\text{H}_4]_{0.5}[(\text{UO}_2)_2(\text{SO}_4)_3(\text{H}_2\text{O})](\text{H}_2\text{O})_2$  [48].

The crystal structures of **V** and **VI** are based upon topologically similar inorganic sheets with the composition  $[(\text{UO}_2)_3(\text{SeO}_4)_5]^{4-}$  (Fig. 7a, b). Their graphs (Fig. 7c, d) are built from four- and six-membered rings. This topology of uranyl was observed in some selenate and chromate compounds, e.g., in  $\text{Mg}_2[(\text{UO}_2)_3(\text{SeO}_4)_5](\text{H}_2\text{O})_{16}$  [49] and  $\text{Mg}_2[(\text{UO}_2)_3(\text{CrO}_4)_5](\text{H}_2\text{O})_{17}$  [50].

The black-and-white graphs corresponding to the topological structures of the  $[(\text{UO}_2)_5(\text{SeO}_4)_8(\text{H}_2\text{O})]^{6-}$  sheet in **VII** and **VIII** are shown in Fig. 8a, b. They contain both four- and six-membered rings. Six-membered rings share vertices to form corner-sharing pairs separated by chains of edge-sharing four-membered rings. The pairs are stretched alternatively along  $[120]$  and  $[\bar{1}20]$ . All white vertices are three-connected, whereas black vertices are either four- or five-connected, which correspond to the  $[\text{UO}_6(\text{H}_2\text{O})]^{6-}$  and  $[\text{UO}_7]^{8-}$  pentagonal bipyramids, respectively. This topology has previously been observed in  $[\text{N}_3\text{C}_6\text{H}_{18}]_2[(\text{UO}_2)_5(\text{SO}_4)_8(\text{H}_2\text{O})]$  [51], but **VII** and **VIII** are the first examples of this topology for uranyl selenates.

### Geometrical isomerism

To define topology of a structure by means of its nodal representation is not always enough to define its complete

**Fig. 5** The  $[(\text{UO}_2)(\text{SeO}_4)_2(\text{H}_2\text{O})]^{2-}$  chains in the crystal structure of **I** (a) and  $[(\text{UO}_2)(\text{SeO}_4)_2(\text{H}_2\text{O})]^{2-}$  sheets in the crystal structure of **II** in polyhedral representations (legend as in Fig. 1), and their graphs (c, d, respectively). See text for details

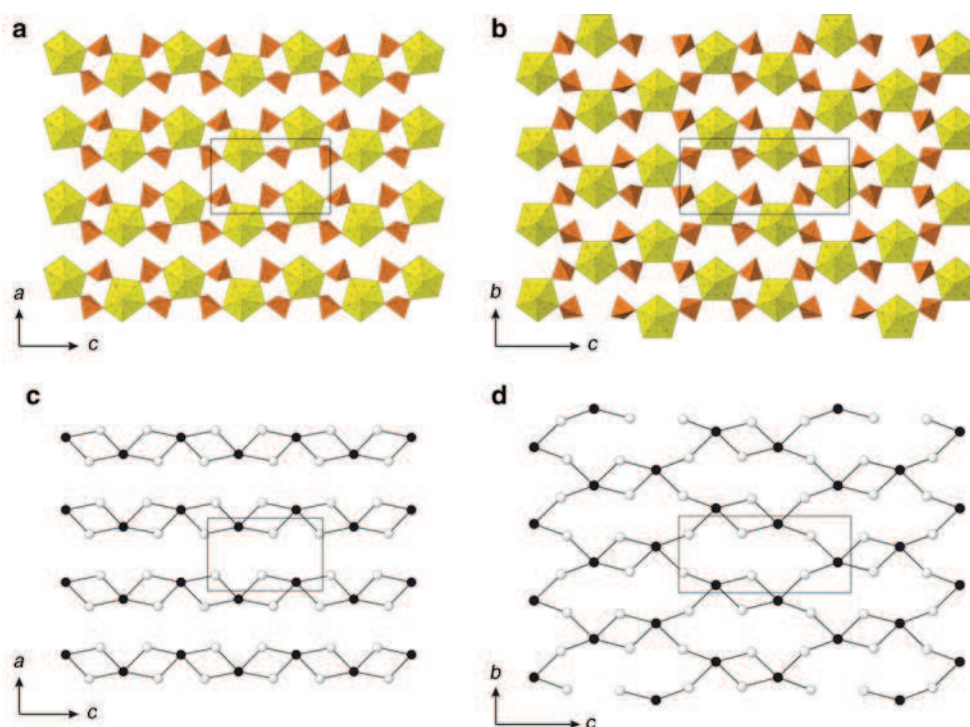


**Fig. 6** The two-dimensional uranyl selenate sheets in the crystal structures of **III** (a) and **IV** (b) and their *black-and-white* graphs (c, d, respectively) (Color figure online)

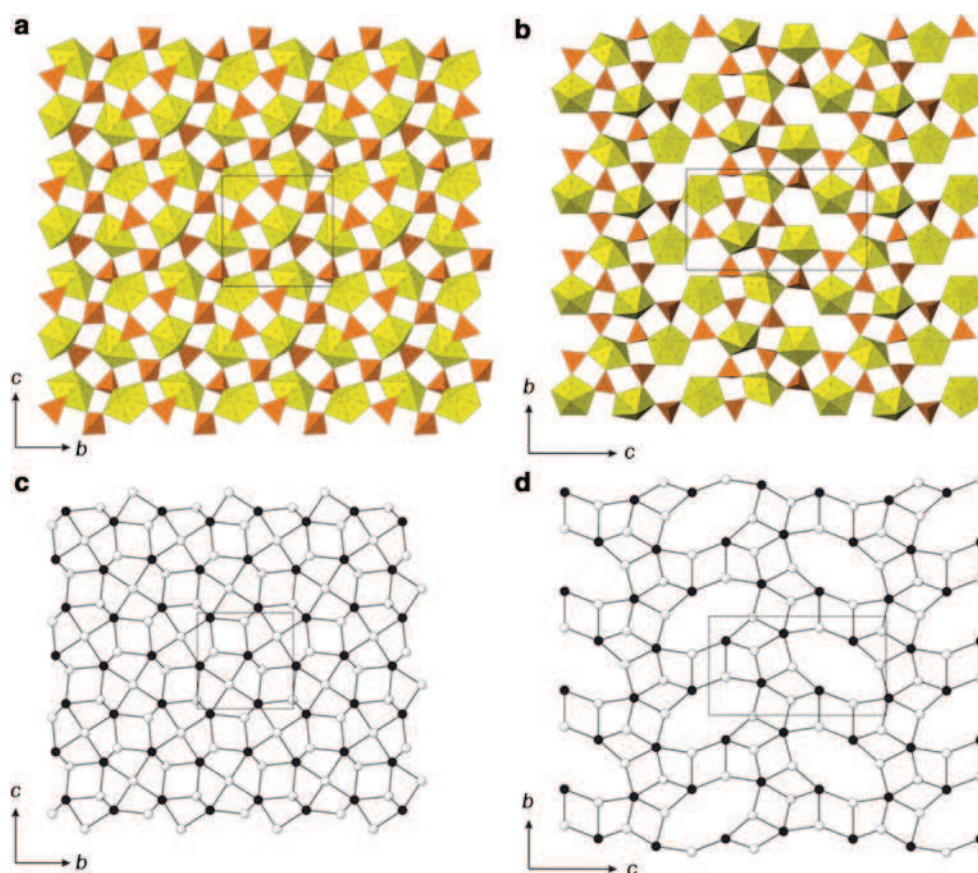
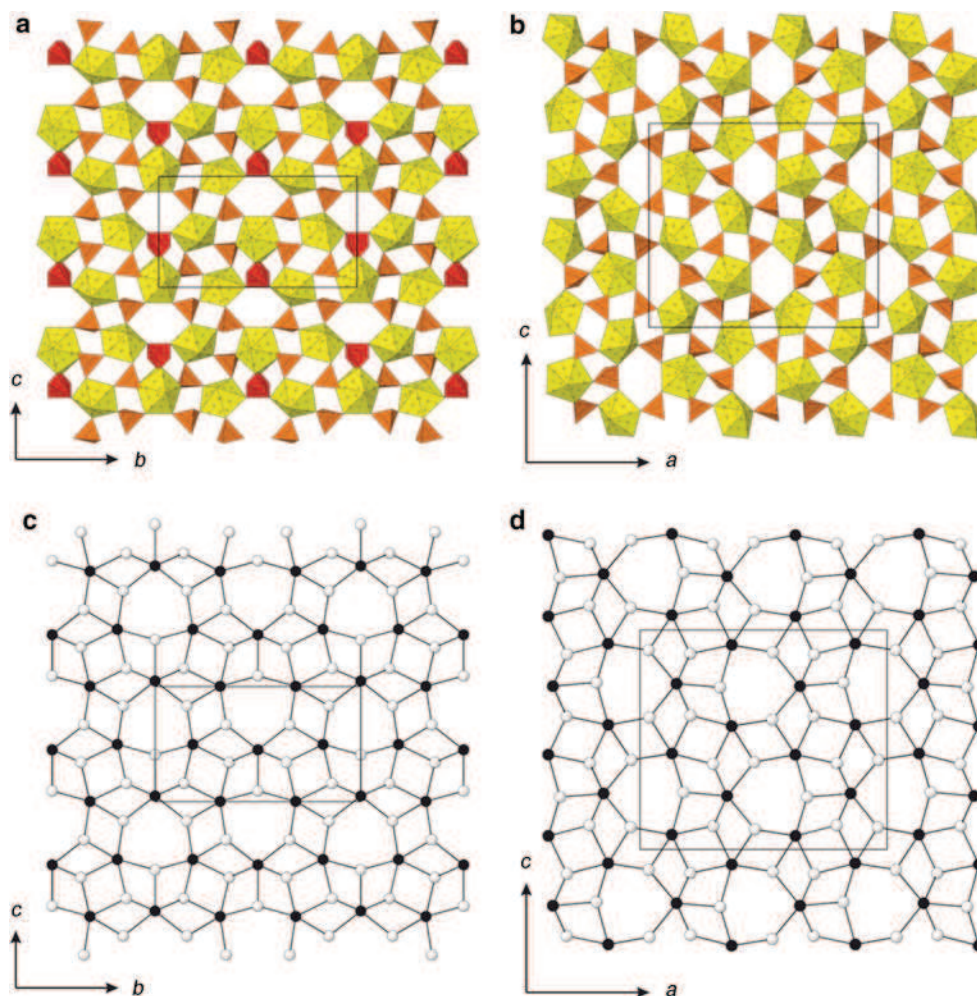




**Fig. 7** The  $[(\text{UO}_2)_3(\text{SeO}_4)_5(\text{H}_2\text{O})]^{2-}$  sheets in the crystal structure of **V** (a) and **VI** (b) and their black-and-white graphs (c, d, respectively). The selenate tetrahedra in **V** with disordered orientations are shown in red (Color figure online)



topological structure. This is particularly true for compounds, which contain tetrahedra with terminal O atoms not involved in an interpolyhedral bonding. In this case, detailed examination of orientations of tetrahedra may reveal geometrical difference between the sheets with the same black-and-white graph, which led Krivovichev and Burns [50] to the definition of geometrical isomerism. It is important to note that geometrical isomers cannot be transformed into each other by simple rotations of tetrahedra and such a transformation is impossible without breaking of chemical bonds. To distinguish between the  $[(\text{UO}_2)_3(\text{SeO}_4)_5]^{2-}$  sheets with the same graph observed in the structures of **IV**,  $\text{K}(\text{H}_3\text{O})[(\text{UO}_2)_2(\text{SeO}_4)_3(\text{H}_2\text{O})](\text{H}_2\text{O})_6$  [47], and  $[\text{N}_8\text{C}_{26}\text{H}_4]_{0.5}[(\text{UO}_2)_2(\text{SO}_4)_3(\text{H}_2\text{O})](\text{H}_2\text{O})_2$  [48], one has to analyze orientations of tetrahedra relative to the plane of the sheet. As can be seen in the black-and-white graph of the topology (Fig. 6d), each  $[\text{TO}_4]^{2-}$  ( $T = \text{Se}, \text{S}$ ) tetrahedron in the sheet is three-connected, i.e., it shares three of its corners with adjacent either four- or five-connected  $[\text{UO}_6(\text{H}_2\text{O})]^{6-}$  and  $[\text{UO}_7]^{8-}$  pentagonal bipyramids. The fourth corner is non-shared and may have either up-,

down- or disordered (up-or-down) orientation relative to the plane of the sheet. This ambiguity gives rise to geometric isomers with various orientations of the tetrahedra. To identify and classify the isomers of this type, we use their orientation matrices [50]. According to this approach, as applied to the structures in hand, symbols **u** (up), **d** (down), **m** (disordered up-or-down orientation), or  $\square$  (white vertex is missing in the graph) are assigned to each white vertex.

The graphs shown in Fig. 9 have the **u** and **d** symbols written near white vertices. It can be seen that the systems of the **u** and **d** symbols are different for the sheets, which therefore should be considered as different geometrical isomers. The isomers can be distinguished by their orientation matrices that provide short notations of the translationally independent rectangular system of the **u**, **d**, and  $\square$  symbols. The orientation matrix for the sheet of the crystal structure of **IV** shown in Fig. 9c has  $8 \times 2$  dimensions and can be written in row as (**uududd** $\square\square$ )(**dd** $\square\square$ **uudu**). It is noteworthy that the crystal structure of  $\text{K}(\text{H}_3\text{O})[(\text{UO}_2)_2(\text{SeO}_4)_3(\text{H}_2\text{O})](\text{H}_2\text{O})_6$  [47] has the same orientation matrix

**Fig. 8** Two-dimensional sheets in the crystal structures of **VII** (a) and **VIII** (b) and their *black-and-white* graphs (c, d, respectively) (Color figure online)

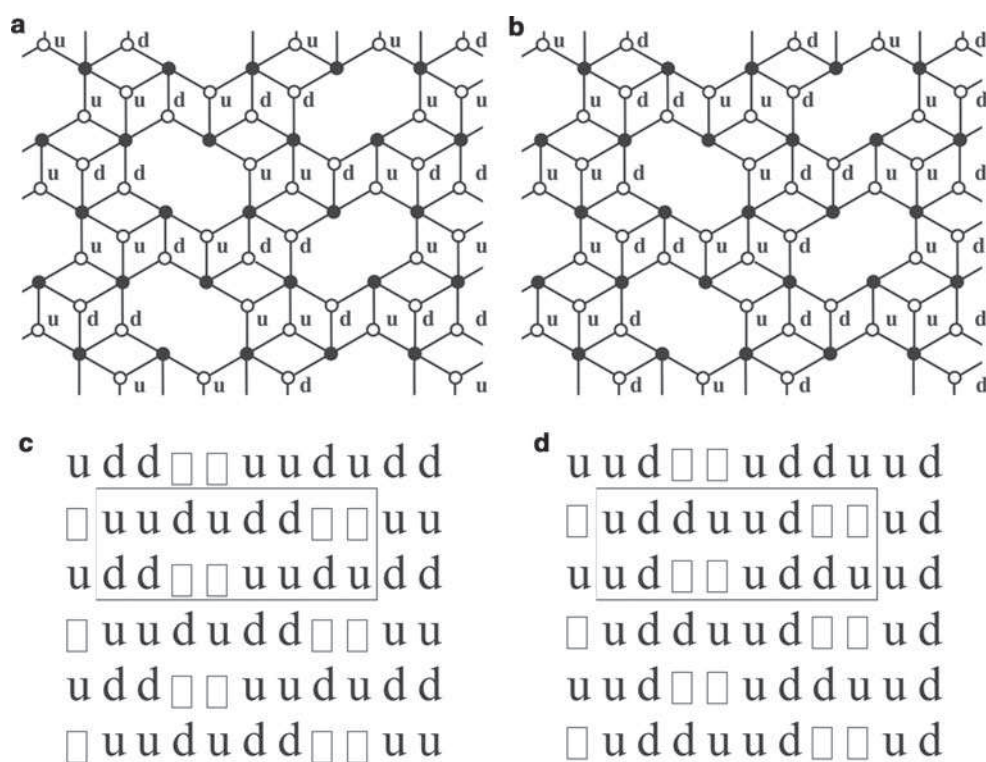
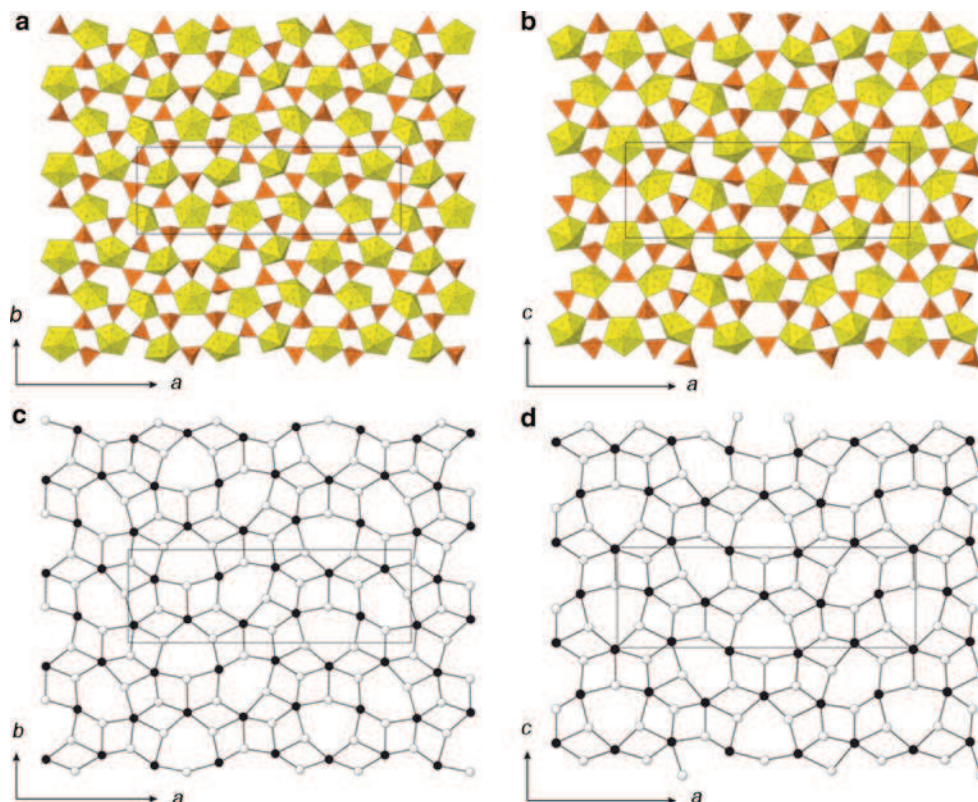


**Fig. 9** *Black-and-white* graphs of the uranyl selenate sheets in the structures of **IV** and  $\text{K}(\text{H}_3\text{O})[(\text{UO}_2)_2(\text{SeO}_4)_3(\text{H}_2\text{O})](\text{H}_2\text{O})_6$  (a) and in the structure of  $[\text{N}_8\text{C}_{26}\text{H}_4]_{0.5}[(\text{UO}_2)_2(\text{SO}_4)_3(\text{H}_2\text{O})](\text{H}_2\text{O})_2$  (b) with the orientation symbols of tetrahedra; extended tables of orientation symbols

(c, d, respectively). Translationally independent orientation matrices of tetrahedra are selected in (c) and (d) by *rectangular* areas (Color figure online)

**Fig. 10** Black-and-white graphs of uranyl selenate sheets in the structures of **V** (a) and **VI** (b) with the orientation symbols of tetrahedra; extended tables of orientation symbols (c, d, respectively). Translationally independent orientation matrices of tetrahedra are selected in (c) and (d) by rectangular areas (Color figure online)

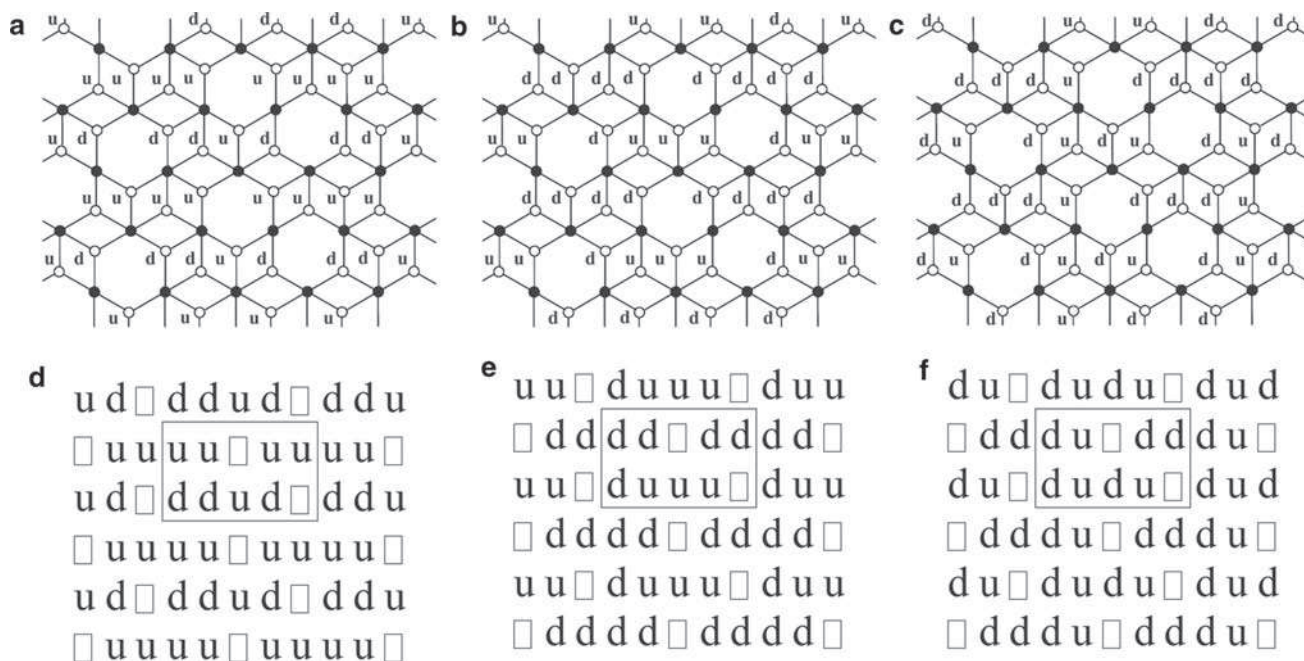
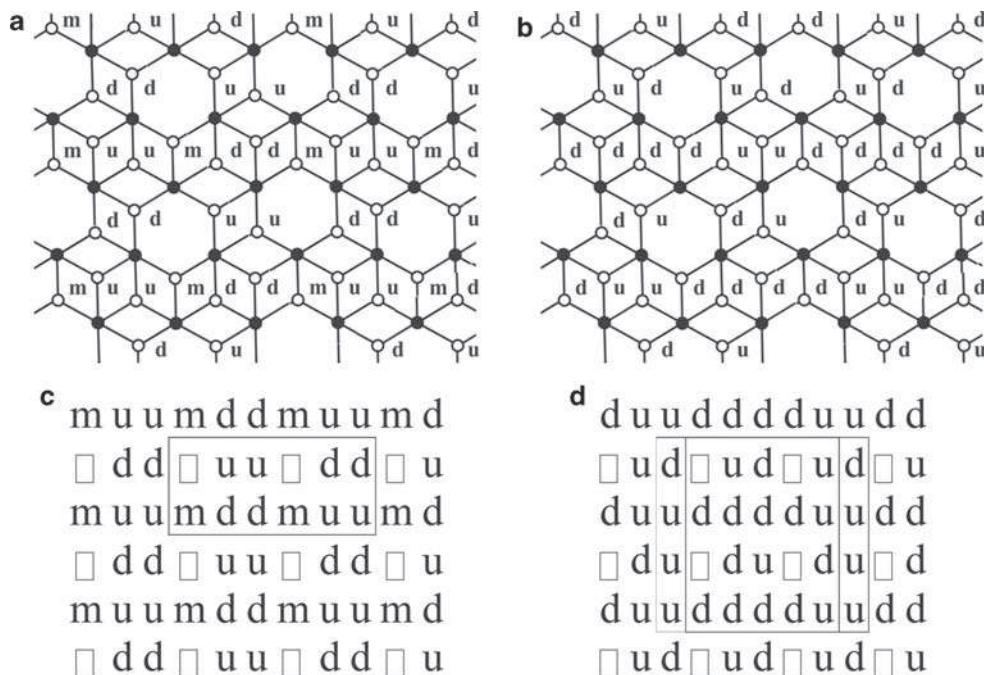


**Fig. 11** Black-and-white graphs of uranyl selenate sheets in the structures of **VII** (a), **VIII** (b), and  $[N_3C_6H_{18}]_2[(UO_2)_5(SO_4)_8(H_2O)]$  (c) with the orientation symbols of tetrahedra; extended tables of

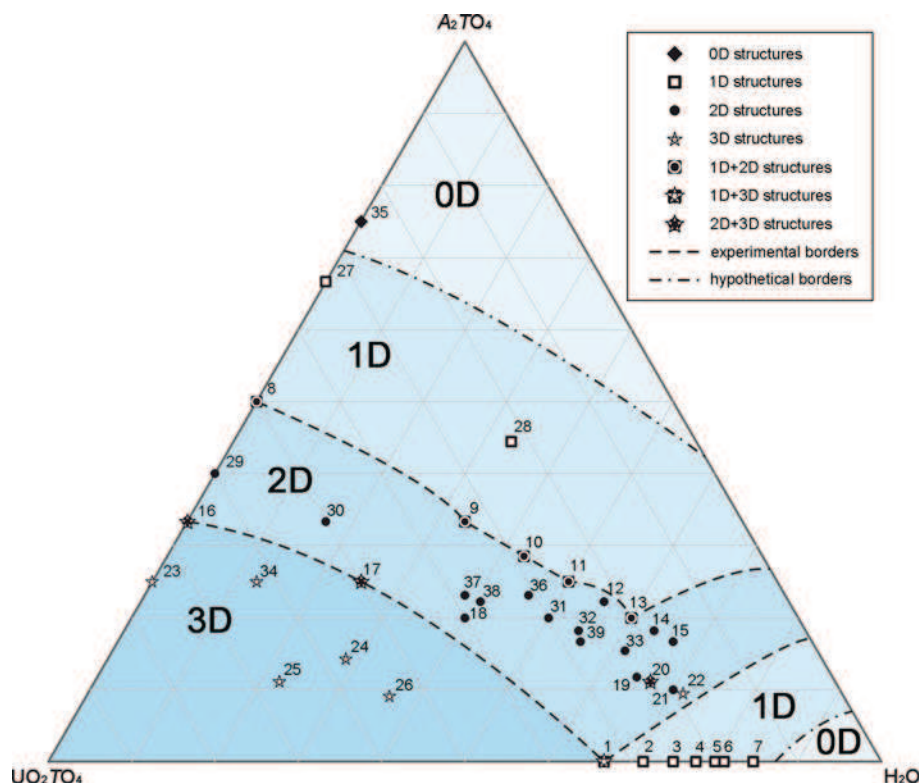
orientation symbols (d–f, respectively). Translationally independent orientation matrices of tetrahedra are selected in (d–f) by rectangular areas (Color figure online)

of the inorganic sheet. The orientation matrix of the sheet of the crystal structure of  $[N_8C_{26}H_{41}O_{0.5}[(UO_2)_2(SO_4)_3(H_2O)](H_2O)_2]$  [48] shown in Fig. 9d can be written as (udduud□□)(ud□□uddu).

The black-and-white graph corresponding to the inorganic  $[(UO_2)_3(SeO_4)_5]^{4-}$  sheets in **V**, and **VI** are shown in Fig. 10a, b, respectively, with the orientation symbol

indicated at each white vertex. The orientation matrices (Fig. 10c, d) have dimensions  $6 \times 2$  and  $6 \times 4$  for **V** and **VI**, respectively. The series of symbols written in row (□uu□dd)(mddmuu) and (□ud□ud)(duuddd) (□du□du)(ddddud) for the inorganic sheets completely characterizes the topological structure of the geometric isomers **V** and **VI**. It should be noted that the matrix of **VI**

**Fig. 12** Dimensional fields on the compositional diagram of the  $\text{UO}_2\text{TO}_4\text{-A}_2\text{TO}_4\text{-H}_2\text{O}$  ( $A$  = monovalent cation,  $T$  = S, Se, Cr, Mo) system. See Table 4 for the list of compounds and references



contain the **m** symbol, which symbolizes selenate tetrahedron that has no preferred orientation due to its disordered arrangement.

The black-and-white graphs for the  $[(\text{UO}_2)_5(\text{H}_2\text{O})(\text{SO}_4)_8]^{6-}$  sheets in **VII**, **VIII**, and  $[\text{N}_3\text{C}_6\text{H}_{18}][(\text{UO}_2)_5(\text{SO}_4)_8(\text{H}_2\text{O})]$  with the **u**, **d** and  $\square$  symbols written near the white vertices are shown in Fig. 11. Orientation matrices for these sheets may be written as  $(\mathbf{uu}\square\mathbf{uu})(\mathbf{ddud}\square)$ ,  $(\mathbf{dd}\square\mathbf{dd})(\mathbf{duuu}\square)$ , and  $(\mathbf{du}\square\mathbf{dd})(\mathbf{dudu}\square)$ , respectively (Fig. 11a–c).

Dimensional reduction in uranyl oxysalts with general formula  $A_n(\text{UO}_2)_p(\text{TO}_4)_q(\text{H}_2\text{O})_r$

The eight novel compounds reported herein can be described by the general formula  $[\text{CH}_3\text{NH}_3]_n(\text{UO}_2)_p(\text{TO}_4)_q(\text{H}_2\text{O})_r$ . In order to investigate the chemistry–structure relationships, we employ the dimensional reduction principle [26–29]. In order to put the study in more general context, the whole range of the compounds with the general formula  $A_n(\text{UO}_2)_p(\text{TO}_4)_q(\text{H}_2\text{O})_r$  ( $A$  = monovalent cation, and  $T$  = S, Se, Cr, Mo) has been analyzed. It was supposed that the basic highly-polymerized three-dimensional parent structure is that of  $(\text{UO}_2)(\text{TO}_4)$ , whereas the role of reducing agents is played by  $A_2(\text{TO}_4)$  and  $\text{H}_2\text{O}$ . As a consequence, the relationships between different compositions and structures may be visualized using the

$\text{UO}_2\text{TO}_4\text{-A}_2\text{TO}_4\text{-H}_2\text{O}$  compositional diagram (Fig. 12). Table 4 summarizes formulas and dimensional characteristics of the structures of respective compounds.

The diagram shown in Fig. 12 may be divided into regions, where structures have the same dimensionality values (0 = finite clusters, 1 = chains, 2 = sheets, 3 = frameworks). Definition of the borders between the fields is not unambiguous and is rather tentative in character. For instance, due to the presence of only one point (35) corresponding to the 0D phases, the borders between the 0D and 1D fields are hypothetical. We suppose these borders are subparallel to the borders between 1D-and-2D, 2D-and-3D fields, and are in agreement with the principle of dimensional reduction for inorganic oxysalts. However, some deviations are observed. The points 20 and 22 are located within the 2D field, but correspond to the 3D framework structures with the  $A_6(\text{UO}_2)_2(\text{TO}_4)_3(\text{H}_2\text{O})_6$  and  $A_6(\text{UO}_2)_2(\text{TO}_4)_3(\text{H}_2\text{O})_{7.5}$  compositions, respectively. We attribute these deviations to the double role of  $\text{H}_2\text{O}$ : in most cases, it acts as reducing agent, whereas, in the cases of 20 and 22, it simply fills cavities of the uranyl-based framework.

For more detailed demonstration of the principle of dimensional reduction in the system, one may consider the line originating from the left and ending at the top corner of the diagram. The line describes compounds with the composition  $A_n(\text{UO}_2)_p(\text{TO}_4)_q$ . The points 23, 29, 27, and 35 correspond to the structures with dimensionalities equal to

**Table 4** Phases of inorganic oxysalts with general formula  $A_n(\text{UO}_2)_p(\text{TO}_4)_q(\text{H}_2\text{O})_r$  in the  $\text{UO}_2\text{TO}_4\text{--A}_2\text{TO}_4\text{--H}_2\text{O}$  system

Point	Formula type	$n$	$p$	$q$	$r$	$D^a$	$T$	$A$	References
1	$(\text{UO}_2)(\text{TO}_4)(\text{H}_2\text{O})_2$	0	1	1	2	1	Se, Cr	–	[52, 53]
						3	Mo	–	[54]
2	$(\text{UO}_2)(\text{TO}_4)(\text{H}_2\text{O})_{2,5}$	0	2	2	5	1	S	–	[55]
3	$(\text{UO}_2)(\text{TO}_4)(\text{H}_2\text{O})_3$	0	1	1	3	1	Cr	–	[52]
4	$(\text{UO}_2)(\text{TO}_4)(\text{H}_2\text{O})_{3,5}$	0	2	2	7	1	S	–	[56, 57]
5	$(\text{UO}_2)(\text{TO}_4)(\text{H}_2\text{O})_4$	0	1	1	4	1	Se	–	[58]
6	$(\text{UO}_2)(\text{TO}_4)(\text{H}_2\text{O})_{4,3}$	0	1	1	4.3	1	Cr	–	[52]
7	$(\text{UO}_2)(\text{TO}_4)(\text{H}_2\text{O})_{5,5}$	0	2	2	11	1	Cr	–	[59]
8	$\text{A}_2(\text{UO}_2)(\text{TO}_4)_2$	2	1	2	0	1	Mo	Li	[60]
						2	Mo	Na, K, Rb, Cs	[61–64]
						2	Cr, Mo	Tl	[65]
9	$\text{A}_2(\text{UO}_2)(\text{TO}_4)_2(\text{H}_2\text{O})$	2	1	2	1	1	Se	Amine, $\text{H}_3\text{O}$	[66]
						2	S, Se	Amine, $\text{H}_3\text{O}$	[67], <b>II</b>
						2	Mo	K, Rb, Cs, $\text{NH}_4$	[63, 64, 68–70]
10	$\text{A}_2(\text{UO}_2)(\text{TO}_4)_2(\text{H}_2\text{O})_{1,5}$	4	2	4	3	1-2	Se	Amine	[25]
11	$\text{A}_2(\text{UO}_2)(\text{TO}_4)_2(\text{H}_2\text{O})_2$	2	1	2	2	1	S, Se	Amine	[47]
						2	S, Se	K, Rb, Cs, $\text{NH}_4$	[71–76]
						2	Se	Amine, $\text{H}_3\text{O}$	[77–79], <b>I</b>
12	$\text{A}_2(\text{UO}_2)(\text{TO}_4)_2(\text{H}_2\text{O})_{2,5}$	4	2	4	5	2	Se	Amine	[80]
13	$\text{A}_2(\text{UO}_2)(\text{TO}_4)_2(\text{H}_2\text{O})_3$	2	1	2	3	1	Se	Amine	[66]
						2	S, Se	Amine, $\text{H}_3\text{O}$	[81]
14	$\text{A}_2(\text{UO}_2)(\text{TO}_4)_2(\text{H}_2\text{O})_{3,5}$	4	2	4	7	2	Se	K, $\text{H}_3\text{O}$	[82]
15	$\text{A}_2(\text{UO}_2)(\text{TO}_4)_2(\text{H}_2\text{O})_4$	2	1	2	4	2	Se, Mo	Na	[83, 84]
16	$\text{A}_2(\text{UO}_2)_2(\text{TO}_4)_3$	2	2	3	0	2	S, Se	Amine, $\text{H}_3\text{O}$	[9, 66, 85], <b>III</b>
						2	S, Mo	Cs	[86, 87]
						3	Mo	Rb, Cs	[87]
						3	Mo	Tl	[88]
17	$\text{A}_2(\text{UO}_2)_2(\text{TO}_4)_3(\text{H}_2\text{O})$	2	2	3	1	2	Se	Amine	[9, 75, 89]
						3	Se	$\text{H}_3\text{O}$	[77]
18	$\text{A}_2(\text{UO}_2)_2(\text{TO}_4)_3(\text{H}_2\text{O})_2$	2	2	3	2	2	Se	K, $\text{H}_3\text{O}$	[45]
						2	Se	Amine, $\text{H}_3\text{O}$	[66, 89], <b>IV</b>
19	$\text{A}_2(\text{UO}_2)_2(\text{TO}_4)_3(\text{H}_2\text{O})_{5,5}$	4	2	6	11	2	Se	$\text{H}_3\text{O}$	[90]
20	$\text{A}_2(\text{UO}_2)_2(\text{TO}_4)_3(\text{H}_2\text{O})_6$	2	2	3	6	2	Se, Cr	K, Rb, $\text{NH}_4$	[73, 91, 92]
						3	Se	Rb, $\text{H}_3\text{O}$	[93, 94]
21	$\text{A}_2(\text{UO}_2)_2(\text{TO}_4)_3(\text{H}_2\text{O})_7$	2	2	3	7	2	Se	K, $\text{H}_3\text{O}$	[47]
22	$\text{A}_2(\text{UO}_2)_2(\text{TO}_4)_3(\text{H}_2\text{O})_{7,5}$	4	4	6	15	3	Se	Na	[95]
23	$\text{A}_2(\text{UO}_2)_3(\text{TO}_4)_4$	2	3	4	0	3	Mo	Na, K	[9]
24	$\text{A}_2(\text{UO}_2)_4(\text{TO}_4)_5(\text{H}_2\text{O})_2$	2	4	5	2	3	Mo	Amine	[96]
25	$\text{A}_2(\text{UO}_2)_6(\text{TO}_4)_7(\text{H}_2\text{O})_2$	2	6	7	2	3	S	Amine	[97]
						3	Mo	Rb, Cs, $\text{NH}_4$	[63, 98]
26	$\text{A}_2(\text{UO}_2)_6(\text{TO}_4)_7(\text{H}_2\text{O})_4$	2	6	7	4	3	Mo	Amine	[99]
27	$\text{A}_4(\text{UO}_2)(\text{TO}_4)_3$	4	1	3	0	1	Cr	Na	[100]
28	$\text{A}_4(\text{UO}_2)(\text{TO}_4)_3(\text{H}_2\text{O})_{1,5}$	8	2	6	3	1	Mo	Na, Tl	[83]
29	$\text{A}_4(\text{UO}_2)_3(\text{TO}_4)_5$	4	3	5	0	2	Se	Amine, $\text{H}_3\text{O}$	<b>V</b>
30	$\text{A}_4(\text{UO}_2)_3(\text{TO}_4)_5(\text{H}_2\text{O})$	4	3	5	1	2	Se	Rb	[73]
31	$\text{A}_4(\text{UO}_2)_3(\text{TO}_4)_5(\text{H}_2\text{O})_5$	4	3	5	5	2	Se	Amine, $\text{H}_3\text{O}$	<b>VI</b>
32	$\text{A}_4(\text{UO}_2)_3(\text{TO}_4)_5(\text{H}_2\text{O})_6$	4	3	5	6	2	Se	Amine, $\text{H}_3\text{O}$	[66]
33	$\text{A}_4(\text{UO}_2)_3(\text{TO}_4)_5(\text{H}_2\text{O})_8$	4	3	5	8	2	Cr	K	[91]

**Table 4** continued

Point	Formula type	<i>n</i>	<i>p</i>	<i>q</i>	<i>r</i>	<i>D</i> <sup>a</sup>	<i>T</i>	<i>A</i>	References
34	A <sub>4</sub> (UO <sub>2</sub> ) <sub>5</sub> (TO <sub>4</sub> ) <sub>7</sub> (H <sub>2</sub> O)	4	5	7	1	3	Mo	NH <sub>4</sub>	[101]
35	A <sub>6</sub> (UO <sub>2</sub> )(TO <sub>4</sub> ) <sub>4</sub>	6	1	4	0	0	Mo	Na, Rb, Cs, Tl	[63, 83, 102, 103]
36	A <sub>6</sub> (UO <sub>2</sub> ) <sub>4</sub> (TO <sub>4</sub> ) <sub>7</sub> (H <sub>2</sub> O) <sub>6</sub>	6	4	7	6	2	Cr	K	[104]
37	A <sub>6</sub> (UO <sub>2</sub> ) <sub>5</sub> (TO <sub>4</sub> ) <sub>8</sub> (H <sub>2</sub> O) <sub>5</sub>	6	5	8	5	2	Se	Amine, H <sub>3</sub> O	VII
38	A <sub>6</sub> (UO <sub>2</sub> ) <sub>5</sub> (TO <sub>4</sub> ) <sub>8</sub> (H <sub>2</sub> O) <sub>5,5</sub>	12	10	16	11	2	Se	Amine, H <sub>3</sub> O	VIII
39	A <sub>6</sub> (UO <sub>2</sub> ) <sub>5</sub> (TO <sub>4</sub> ) <sub>8</sub> (H <sub>2</sub> O) <sub>10</sub>	6	5	8	10	2	Se	H <sub>3</sub> O	[105]

*T* = S, Se, Cr, Mo; *A* = monovalent cation

<sup>a</sup> *D* dimensionality of structural unit

3, 2, 1, and 0, respectively. The points **16** and **8** are located on the borders between 2D-and-3D, 1D-and-2D fields, respectively. Thus, the dimensionality of the structural unit is decreasing from the points **23** to **35**, which is in agreement with the principle of dimensional reduction.

## Conclusions

In this study, we have reported eight novel phases in the methylamine–(UO<sub>2</sub>)(NO<sub>3</sub>)<sub>2</sub>–H<sub>2</sub>SeO<sub>4</sub>–H<sub>2</sub>O system. Structural topologies of these phases are conveniently described using nodal representation, which provides essential tools for topological description and classification of complex inorganic structures. However, some structural complications such as the presence of 3-connected tetrahedra may lead to loss of information about precise topological arrangement. In this case, additional techniques have to be applied to distinguish different geometrical isomers, e.g., the approach based upon construction of orientation matrices. The structures of the eight new phases are thus completely characterized by combination of graph and orientation matrices. Analysis of the A<sub>*n*</sub>(UO<sub>2</sub>)<sub>*p*</sub>(TO<sub>4</sub>)<sub>*q*</sub>(H<sub>2</sub>O)<sub>*r*</sub> compounds (*A* = monovalent cation, and *T* = S, Se, Cr, Mo) using the principle of dimensional reduction and composition-structure diagram allowed to separate specific fields corresponding to the formation of structures with specific dimensionalities of their structural units.

**Acknowledgments** This study was supported by RFBR (Grant 12-03-90711 to VVG) and St. Petersburg State University through the internal grant 3.37.84.2011 and the X-Ray Diffraction Resource Center.

## References

- Hyde BG, Andersson S (1989) Inorganic crystal structures. Wiley, New York
- Hansen S, Andersson S, Fälth L (1982) Z Kristallogr 160:9
- Andersson S, Hyde BG (1982) Z Kristallogr 158:119
- Andersson S (1983) Angew Chem Int Ed 22:69
- Nyman H, Hyde BG, Andersson S (1984) Acta Crystallogr B40:441
- Burns PC, Miller ML, Ewing RC (1996) Can Miner 34:845
- Burns PC (1999) Rev Miner 38:23
- Burns PC (2005) Can Miner 43:1839
- Krivovichev SV, Burns PC, Tananaev IG (eds) (2007) Structural chemistry of inorganic compounds. Elsevier, Amsterdam
- Miller ML, Finch RJ, Burns PC, Ewing RC (1996) J Mater Res 11:3048
- Krivovichev SV (2004) Crystallogr Rev 10:185
- Krivovichev SV (2008) Structural crystallography of inorganic oxysalts. Oxford University Press, Oxford
- Burns PC, Hughes Kubatko KA, Sigmon G, Fryer BJ, Gagnon JE, Antonio MR, Soderholm L (2005) Angew Chem Int Ed 44:2135
- Sigmon G, Unruh DK, Ling J, Weaver B, Ward M, Pressprich L, Simonetti A, Burns PC (2009) Angew Chem Int Ed 48:2737
- Burns PC (2010) C R Chim 13:737
- Krivovichev SV, Kahlenberg V, Kaindl R, Mersdorf E, Tananaev IG, Myasoedov BF (2005) Angew Chem Int Ed 44:1134
- Krivovichev SV, Kahlenberg V, Tananaev IG, Kaindl R, Mersdorf E, Myasoedov BF (2005) J Am Chem Soc 127:1072
- Alekseev EV, Krivovichev SV, Depmeier W (2008) Angew Chem Int Ed 47:549
- Chen CS, Lee SF, Lii KH (2005) J Am Chem Soc 127:12208
- Lin C, Chen C, Shiryaev AA, Zubavichus YV, Lii KH (2008) Inorg Chem 47:4445
- Lee CS, Wang SL, Lii KH (2009) J Am Chem Soc 131:15116
- Wang S, Alekseev EV, Miller HM, Depmeier W, Albrecht-Schmitt TE (2010) Inorg Chem 49:9755
- Wang S, Alekseev EV, Stritzinger JT, Depmeier W, Albrecht-Schmitt TE (2010) Inorg Chem 49:6690
- Wang S, Alekseev EV, Stritzinger JT, Depmeier W, Albrecht-Schmitt TE (2010) Inorg Chem 49:2948
- Krivovichev SV (2010) Eur J Inorg Chem 2010:2594
- Alekseev EV, Krivovichev SV, Armbruster T, Depmeier W, Suleimanov EV, Chuprunov EV, Golubev AV (2007) Z Anorg Allg Chem 633:1979
- Long JR, McCarty LS, Holm RH (1996) J Am Chem Soc 118:4603
- Tulsky EG, Long JR (2001) Chem Mater 13:1149
- Haddad S, Awwadi F, Willet RD (2003) Cryst Growth Des 3:501
- Sheldrick GM (2008) Acta Crystallogr A64:112
- Altomare A, Cascarano G, Giacovazzo C, Guagliardi A, Burla MC, Polidori G, Camalli M (1994) J Appl Crystallogr 27:435
- Krivovichev SV (2004) Radiochemistry 46:434
- Tabachenko VV, Serezhkin VN, Serezhkina LB, Kovba LM (1979) Koord Khim 5:1563

34. Mikhailov YUN, Gorbunova YUE, Demchenko EA, Serezhkina LB, Serezhkin VN (2000) *Zh Neorg Khim* 45:1711
35. Norquist AJ, Thomas PM, Doran MB, O'Hare D (2002) *Chem Mater* 14:5179
36. Norquist AJ, Doran MB, Thomas PM, O'Hare D (2003) *Dalton Trans* 2003:1168
37. Norquist AJ, Doran MB (2003) *Solid State Sci* 5:1149
38. Thomas PM, Norquist AJ, Doran MB (2003) *J Mater Chem* 13:88
39. Stuart CL, Doran MB, Norquist AJ, O'Hare D (2003) *Acta Crystallogr E* 59:m446
40. Mercier R, Pham TM, Colomban P (1985) *Solid State Ion* 15:113
41. Gesing TM, Rüscher CH (2000) *Z Anorg Chem* 626:1414
42. Krivovichev SV, Kahlenberg V (2005) *Z Naturforsch* 60b:538
43. Krivovichev SV, Kahlenberg V (2005) *Z Anorg Allg Chem* 631:2352
44. Krivovichev SV (2008) *Zap Vseross Miner Ova* 137(1):54
45. Gurzhiy VV, Tyumentseva OS, Krivovichev SV, Tananaev IG, Myasoedov BF (2011) *Radiochemistry* 53:569
46. Krivovichev SV, Gurzhiy VV, Tananaev IG, Myasoedov BF (2009) *Russ J Gen Chem* 79:2723
47. Ling J, Sigmon GE, Ward M, Roback N, Burns PC (2010) *Z Kristallogr* 225:230
48. Doran MB, Norquist AJ, Stuart CL, O'Hare D (2004) *Acta Crystallogr E* 60:m996
49. Krivovichev SV, Kahlenberg V (2004) *Z Anorg Allg Chem* 630:2736
50. Krivovichev SV, Burns PC (2003) *Z Kristallogr* 218:683
51. Norquist AJ, Doran MB, Thomas PM, O'Hare D (2003) *Inorg Chem* 42:5949
52. Krivovichev SV, Burns PC (2003) *Z Kristallogr* 218:568
53. Marukhnov AV, Serezhkin VN, Pushkin DV, Smirnov OP, Plakhtii VP (2008) *Russ J Inorg Chem* 53:1283
54. Serezhkin VN, Efremov VA, Trunov VK (1980) *Crystallogr Rep* 25:494
55. Van den Putten N, Loopstra BO (1974) *Cryst Struct Commun* 3:377
56. Zalkin A, Ruben H, Templeton DH (1978) *Inorg Chem* 17:3701
57. Brandenburg NP, Loopstra BO (1973) *Cryst Struct Commun* 2:243
58. Serezhkin VN, Soldatkina MA, Efremov VA (1981) *Zh Strukt Khim* 22:171
59. Serezhkin VN, Trunov VK (1981) *Crystallogr Rep* 26:301
60. Krivovichev SV, Burns PC (2003) *Solid State Sci* 5:481
61. Sadikov GG, Krasovskaya TI, YuA Polyakov, Nikolaev VP (1998) *Izv Akad Nauk SSSR Neorg Mater* 24:109
62. Krivovichev SV, Burns PC (2002) *J Solid State Chem* 168:245
63. Krivovichev SV, Burns PC (2005) *Can Miner* 43:713
64. Krivovichev SV, Finch R, Burns PC (2002) *Can Miner* 40:193
65. Krivovichev SV, Locock AJ, Burns PC (2005) *Z Kristallogr* 220:10
66. Gurzhiy VV, Krivovichev SV, Tananaev IG (2012) *Radiochemistry* (in prep)
67. Medrish IV, Vologzhanina AV, Starikova ZA, Antipin MYU, Serezhkina LB, Serezhkin VN (2005) *Russ J Inorg Chem* 50:360
68. Rastsvetaeva RK, Barinova AV, Fedoseev AM, Budantseva NA, Nikolaev YUV (1999) *Dokl Ross Akad Nauk* 365:68
69. Andreev GB, MYu Antipin, Fedoseev AM, Budantseva NA (2001) *Russ J Coord Chem* 27:208
70. Khrustalev VN, Andreev GB, Antipin MYU, Fedoseev AM, Budantseva NA, Shirokova IB (2000) *Russ J Inorg Chem* 45:1845
71. Niinisto L, Toivonen J, Valkonen J (1979) *Acta Chem Scand* A33:621
72. Mikhailov YUN, Gorbunova YUE, Shishkina OV, Serezhkina LB, Serezhkin VN (2001) *Russ J Inorg Chem* 46:1661
73. Krivovichev SV, Kahlenberg V (2005) *Z Anorg Allg Chem* 631:739
74. Mikhailov YUN, Gorbunova YUE, Serezhkina LB, Demchenko EA, Serezhkin VN (1997) *Zh Neorg Khim* 42:1413
75. Serezhkin VN, Verevkin AG, Smirnov OP, Plahtii VP (2010) *Russ J Inorg Chem* 55:1600
76. Niinisto L, Toivonen J, Valkonen J (1978) *Acta Chem Scand* A32:647
77. Ling J, Sigmon GE, Burns PC (2009) *J Solid State Chem* 182:402
78. Krivovichev SV (2008) *Geol Ore Depos* 50:789
79. Krivovichev SV (2008) *Geol Ore Depos* 50:795
80. Krivovichev SV, Kahlenberg V (2005) *Z Anorg Allg Chem* 631:2358
81. Baggio RF, de Benyacar MAR, Perazzo BO, de Perazzo PK (1977) *Acta Crystallogr B* 33:3495
82. Gurzhiy VV, Tyumentseva OS, Krivovichev SV, Tananaev IG, Myasoedov BF (2012) *Radiochemistry* 54:43
83. Krivovichev SV, Burns PC (2003) *Can Miner* 41:707
84. Mikhailov YUN, Gorbunova YUE, Baeva EE, Serezhkina LB, Serezhkin VN (2001) *Russ J Inorg Chem* 46:2017
85. Norquist AJ, Doran MB, Thomas PM, O'Hare D (2003) *Dalton Trans* 2003:1168
86. Ross M, Evans HT Jr (1960) *J Inorg Nucl Chem* 15:338
87. Krivovichev SV, Cahill CL, Burns PC (2002) *Inorg Chem* 41:34
88. Nazarchuk EV, Krivovichev SV, Burns PC (2005) *Radiochemistry* 47:447
89. Krivovichev SV, Gurzhiy VV, Tananaev IG, Myasoedov BF (2006) *Dokl Phys Chem* 409:228
90. Krivovichev SV, Kahlenberg V (2005) *Radiochemistry* 47:452
91. Krivovichev SV, Burns PC (2003) *Z Kristallogr* 218:725
92. YuN Mikhailov, YuE Gorbunova, Serezhkina LB, Serezhkin VN (1997) *Zh Neorg Khim* 42:734
93. Blatov VA, Serezhkina LB, Serezhkin VN, Trunov VK (1988) *Russ J Coord Chem* 14:1705
94. Kuchumova NV, Shtokova IP, Serezhkina LB, Serezhkin VN (1989) *Zh Neorg Khim* 34:1029
95. Baeva EE, Virovets AV, Peresyphkina EV, Serezhkina LB (2006) *Russ J Inorg Chem* 51:210
96. Krivovichev SV, Cahill CL, Nazarchuk EV, Burns PC, Armbruster T, Depmeier W (2005) *Micropor Mesopor Mater* 78:225
97. Doran M, Norquist AJ, O'Hare D (2002) *Chem Commun* 2002:2946
98. Krivovichev SV, Burns PC (2001) *Can Miner* 39:207
99. Krivovichev SV, Armbruster T, DYu Chernyshov, Burns PC, Nazarchuk EV, Depmeier W (2005) *Micropor Mesopor Mater* 78:225
100. Krivovichev SV, Burns PC (2003) *Z Anorg Allg Chem* 629:1965
101. Krivovichev SV, Cahill CL, Burns PC (2003) *Inorg Chem* 42:2459
102. Krivovichev SV, Burns PC (2002) *Can Miner* 40:210
103. Krivovichev SV, Burns PC (2001) *Can Miner* 39:197
104. Sykora RE, McDaniel SM, Albrecht-Schmitt TE (2004) *J Solid State Chem* 177:1431
105. Krivovichev SV, Kahlenberg V (2005) *Radiochemistry* 47:415





### **A-III**

## **Revised bismuth chloroselenite system: evidence of a noncentrosymmetric structure with a giant unit cell**

Almaz Aliev, Vadim M. Kovrugin, Marie Colmont, Christine Terryn, Marrielle Huvé, Oleg I. Siidra,  
Sergey V. Krivovichev, and Olivier Mentré

Published in: *Crystal Growth & Design*, 2014, Vol. 14 (6), p. 3026–3034.

DOI: 10.1021/cg500293w

Reprinted with kind permission from American Chemical Society.



# Revised Bismuth Chloroselenite System: Evidence of a Noncentrosymmetric Structure with a Giant Unit Cell

Almaz Aliev,<sup>†</sup> V. M. Kovrugin,<sup>†,§</sup> Marie Colmont,<sup>\*,†</sup> Christine Terryn,<sup>‡</sup> Marielle Huvé,<sup>†</sup> O. I. Siidra,<sup>§</sup> S. V. Krivovichev,<sup>§</sup> and Olivier Mentré<sup>†</sup>

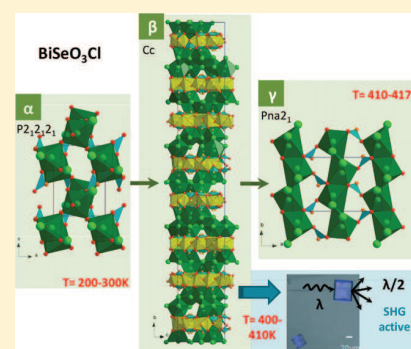
<sup>†</sup>Université Lille 1, Université Lille Nord France, ENSCL, CNRS, UCCS, UMR 8181, F-59652 Villeneuve d'Ascq, France

<sup>‡</sup>Plateforme Imagerie Cellulaire et Tissulaire, 51 rue Cognacq-Jay, 51100 Reims, France

<sup>§</sup>St. Petersburg State University, Department of Crystallography, University Emb. 7/9, 199034 St. Petersburg, Russia

## S Supporting Information

**ABSTRACT:** The reactions between PbO, Bi<sub>2</sub>O<sub>3</sub> (or BiOCl), and SeO<sub>2</sub> by the chemical vapor transport method using HCl as a transporting agent afforded three novel bismuth/lead chloroselenites, namely,  $\beta$ -BiSeO<sub>3</sub>Cl (**1**), Bi<sub>6</sub>(SeO<sub>3</sub>)<sub>4</sub>Cl<sub>10</sub> (**2**), and PbBi<sub>10</sub>(SeO<sub>3</sub>)<sub>12</sub>Cl<sub>8</sub> (**3**). Compound **1** is noncentrosymmetric (space group Cc, SHG active) and has a giant unit cell ( $V = 19792(2) \text{ \AA}^3$ ). In the context of the complex BiSeO<sub>3</sub>Cl phase diagram reported by Oppermann et al., it was assigned to the undescribed  $\beta$ -form on the basis of its IR spectra and powder X-ray diffraction pattern. The comparison between the  $\alpha$ -,  $\beta$ -, and  $\gamma$ -forms suggests their formation via the condensation of volatile Bi(SeO<sub>3</sub>)Cl molecules. Analysis of the structures of the  $\alpha$ -,  $\beta$ -, and  $\gamma$ -forms indicates that the  $\alpha \rightarrow \beta \rightarrow \gamma$  phase transitions are associated with a dramatic fluctuation of structural complexity together with the transitional character of the  $\beta$  phase. Compounds **1** and **3** are layered compounds with identical  $[\text{M}_8\text{Cl}_{16}]^{8+}$  and  $[\text{M}_{14}(\text{SeO}_3)_{24}]^{6-}$  layers, where M stands for Bi in **1** and Pb/Bi in **3**. There are additional  $[\text{Bi}_{12}\text{Cl}_{32}]^{4+}$  layered subunits in **1**. The crystal structure of **2** consists of the  $[\text{Bi}_6(\text{SeO}_3)_4\text{Cl}_{10}]$  building blocks forming an open framework with six-membered-ring channels. These three compounds complete the poorly known bismuth selenium oxochloride panorama.



## INTRODUCTION

The search for noncentrosymmetric (NCS) compounds is an important field for solid state chemists due to their promising properties for nonlinear optics (NLO) including second harmonic generation (SHG) and dielectrics including piezoelectricity, pyroelectricity, and ferroelectricity.<sup>1,2</sup> In particular, NLO materials have become tremendously important and are drawing more and more attention owing to their promising applications in laser science and technology. However, the search for the new compounds with NLO coefficients remains a chemical challenge. It can be resolved using a rational “design” approach but appears rather limited to particular chemical systems together with the controlled association of well-defined building units such as OBi<sub>4</sub> oxocentered tetrahedra<sup>3,4</sup> or oxo-fluoride metal units.<sup>5</sup> The lone-pair (LP) polyanions, such as EO<sub>3</sub> where E stand for the external s<sup>2</sup> electrons, also favorably arrange in NCS crystal structures, as for instance, in the compound BiO(IO<sub>3</sub>) with efficient SHG,<sup>6</sup> E allowing asymmetric or one-side coordination around the polyanion. In this context, selenite oxides are also promising materials with complex crystal structures.<sup>7,8</sup> As poorly involved in the creation of chemical bonds, the terminal LP could form voids in the structure, up to their segregation into cavities, channels, or layered interleaves. The use of halide ions as additional anions enhances this tendency, as recently shown in several examples

of bismuth oxochloride structures, i.e., Arppe's compound derivatives<sup>9</sup> or multidimensional open frameworks.<sup>10</sup> Combining both NCS and low-dimensional specificities appear as a challenge for multifunctional materials.

The BiOCl–SeO<sub>2</sub> binary system studied here was poorly explored and consists of one single chemical composition, Bi(SeO<sub>3</sub>)Cl, that crystallizes in three polymorphs.<sup>11,12</sup> As already discussed in other papers,<sup>9</sup> the combined use of bismuth, halide, and selenium may lead to the formation of materials related to the Sillen phases.

Here we used chemical vapor transport to evidence novel bismuth–selenium oxochlorides. This method is particularly well suited to the system because of the high volatility of SeO<sub>2</sub> and BiCl<sub>3</sub> at low temperatures. As a transport agent, HCl is used, though SeO<sub>2</sub> can be considered as playing the same role.<sup>13</sup>

In this paper, we report on the synthesis of three new bismuth selenite halides, 1-  $\beta$ -BiSeO<sub>3</sub>Cl, 2- Bi<sub>6</sub>(SeO<sub>3</sub>)<sub>4</sub>Cl<sub>10</sub>, and 3- PbBi<sub>10</sub>(SeO<sub>3</sub>)<sub>12</sub>Cl<sub>8</sub> and describe their structural peculiarities. For the layered  $\beta$ -BiSeO<sub>3</sub>Cl that has a noncentrosymmetric

**Received:** February 27, 2014

**Revised:** April 18, 2014

**Published:** April 23, 2014

**Table 1.** Crystal Data, Measurement and Structural Refinement Parameters for  $\beta$ -BiSeO<sub>3</sub>Cl, Bi<sub>6</sub>(SeO<sub>3</sub>)<sub>4</sub>Cl<sub>10</sub>, and PbBi<sub>10</sub>(SeO<sub>3</sub>)<sub>12</sub>Cl<sub>8</sub>

	$\beta$ -BiSeO <sub>3</sub> Cl	Bi <sub>6</sub> (SeO <sub>3</sub> ) <sub>4</sub> Cl <sub>10</sub>	PbBi <sub>10</sub> (SeO <sub>3</sub> ) <sub>12</sub> Cl <sub>8</sub>
Crystal Data			
crystal symmetry	monoclinic	monoclinic	orthorhombic
space group	Cc	P2 <sub>1</sub> /c	Ccca
<i>a</i> (Å)	22.7052(3)	21.460(2)	15.819(6)
<i>b</i> (Å)	76.785(4)	8.4012(9)	17.871(7)
<i>c</i> (Å)	16.0550(3)	15.3370(18)	15.857(6)
$\beta$ (deg)	135.000(2)	110.639(5)	
<i>V</i> (Å <sup>3</sup> )	19792(2)	2587.7 (5)	4483 (3)
<i>Z</i>	192	4	4
<i>D<sub>x</sub></i> (g/cm <sup>3</sup> )	5.470	5.432	6.079
$\mu$ (mm <sup>-1</sup> ) (for $\lambda$ K $\alpha$ = 0.71073 Å)	52.04	47.37	53.17
appearance	colorless platelet	colorless needle	colorless platelet
crystal size (mm <sup>3</sup> )	0.13 × 0.09 × 0.05	0.81 × 0.37 × 0.13	0.16 × 0.15 × 0.06
Data Collection			
$\lambda$ (Mo K $\alpha$ ) (Å)	0.71073	0.71073	0.71073
scan mode	$\omega$ and $\varphi$	$\omega$ and $\varphi$	$\omega$ and $\varphi$
$\theta$ (min–max) (deg)	1.1–26.5	2.0–30.5	2.2–26.4
R(int) (%)	0.096	0.045	0.050
recording reciprocal space	–28 ≤ <i>h</i> ≤ 28 –96 ≤ <i>k</i> ≤ 96 –20 ≤ <i>l</i> ≤ 20	–30 ≤ <i>h</i> ≤ 30 –11 ≤ <i>k</i> ≤ 7 –20 ≤ <i>l</i> ≤ 21	–15 ≤ <i>h</i> ≤ 19 –22 ≤ <i>k</i> ≤ 21 –19 ≤ <i>l</i> ≤ 19
Refinement			
measured, independent obs <sup>a</sup> refl	242854, 35097, 20 337	34697, 7843, 6363	10469, 2253, 1504
no. of refined parameters	1637	298	115
refinement method	<i>F</i> <sup>2</sup>	<i>F</i> <sup>2</sup>	<i>F</i> <sup>2</sup>
<i>R</i> <sub>1</sub> ( <i>F</i> <sup>2</sup> )(obs)/ <i>R</i> <sub>1</sub> ( <i>F</i> <sup>2</sup> )(all)	0.0612/0.1124	0.0299/0.0427	0.0667/0.1057
<i>wR</i> <sub>2</sub> ( <i>F</i> <sup>2</sup> )(obs)/ <i>wR</i> <sub>2</sub> ( <i>F</i> <sup>2</sup> )(all)	0.0645/0.0694	0.0330/0.0442	0.0639/0.0859
GOF(obs)/GOF(all)	1.32/1.63	1.46/1.76	0.84/0.92
$\Delta\rho_{\max}/\Delta\rho_{\min}$ (e·Å <sup>-3</sup> )	5.39/–4.51	3.42/–2.97	5.38/–7.01
extinction coefficient		0.0070(13)	0.0022(13)

<sup>a</sup>obs = [*I* > 3 $\sigma$ (*I*)].

crystal structure and a giant unit cell (*V* = 19783 Å<sup>3</sup>), the SHG properties have been quantified.

## EXPERIMENTAL SECTION

**Syntheses.** The crystals of the three compounds reported here were obtained by the chemical vapor transport (CVT) method. The precursors were ground together and loaded into a quartz tube (ca. 20 cm). The evacuated and sealed ampules were placed into tubular furnace with precursors' side of the ampules being in the center and other side being close to the edge of the furnace. The central part of the furnace was heated at 450 °C for 14 days. The temperature difference between the hot and cold ends of the ampule is about 50 °C.

**1-  $\beta$ -BiSeO<sub>3</sub>Cl.** Transparent colorless square platelet crystals of **1** were found on the walls of the cold side of the quartz ampule with the precursor mixture 1BiOCl + 1SeO<sub>2</sub> + 1MnO<sub>2</sub> and a drop of concentrated solution of HCl. An energy-dispersive spectroscopy (EDS) analysis indicated the absence of manganese in the obtained crystals.

**2- Bi<sub>6</sub>(SeO<sub>3</sub>)<sub>4</sub>Cl<sub>10</sub>.** The transparent colorless needles of **2** were found on the walls of the cold side of the quartz ampule with the mixture of 2BiCl<sub>3</sub> + 1 Bi<sub>2</sub>O<sub>3</sub> + 4SeO<sub>2</sub> + 1Mn<sub>2</sub>O<sub>3</sub> in the absence of HCl. An EDS analysis showed no Mn in the obtained crystals.

For **1** and **2**, attempts to incorporate manganese was tested in order to induce transport/magnetic properties. However, using chemical transport it is clear that Mn species are poorly mobile.

**3- PbBi<sub>10</sub>(SeO<sub>3</sub>)<sub>12</sub>Cl<sub>8</sub>.** The crystals of **3** are the transparent colorless platelets which were picked out from the walls of the cold side of the quartz ampule with the mixture of 1PbO + 1BiOCl + 1SeO<sub>2</sub> and a

drop of concentrated solution of HCl. The presence of lead was evidenced by an electron probe microanalyzer (EPMA) analysis, and the ratio Pb/Bi was found to be 0.8:15.5.

The synthesis of the corresponding polycrystalline samples by a solid state route for the three compounds failed, due to the rather low temperature at which selenium oxide becomes volatile (close to 350 °C).

**Single crystal X-ray Diffraction.** Crystals of **1** (colorless platelet), **2** (colorless needle), and **3** (colorless platelet) were mounted on glass fibers and studied on a Bruker X8 APEX II diffractometer equipped with a microfocus X-ray tube with the Mo K $\alpha$  radiation at 50 kV and 40 mA. The collected data were integrated using the Bruker program Saint Plus 6.025.<sup>14</sup> The unit-cell parameters were refined from the full data set. Multiscan absorption correction was performed for the three compounds using SADABS.<sup>15</sup> The structures were solved by Superflip method.<sup>16</sup> Jana 2006 program was used for structure refinements.<sup>17</sup> All relevant details of the data collection and evaluation for the three new structures are listed in Table 1. Atomic coordinates and anisotropic displacement parameters as well as the results of bond-valence calculations<sup>18,19</sup> are given in Supporting Information.

**Transmission Electron Microscopy TEM.** EDS studies were performed on a FEI Tecnai G220 transmission electron microscope. The material was crushed and dropped in the form of alcohol suspensions on carbon-supported copper grids followed by evaporation under ambient conditions. The EDS analysis was performed in order to validate the refined stoichiometry of the obtained single crystals.

**Infrared Spectroscopy.** Infrared spectra of **1** were measured between 4000 and 400 cm<sup>-1</sup> with a Perkin–Elmer Spectrum Two spectrometer equipped with a diamond attenuated total reflectance

(ATR) accessory. It was compared to the IR spectra reported for previously known  $\text{BiSeO}_3\text{Cl}$  forms.

**Multiphoton SHG Microscopy.** In this study, a laser scanning microscope LSM 710 NLO Zeiss (Iena, Germany) was used as implemented at the Plateforme d'Imagerie Cellulaire et Tissulaire, Reims, France. Excitation was provided by a CHAMELEON femtosecond Titanium-Sapphire laser (Coherent, Santa Clara, USA) set at 860 nm, tuning the power until SHG was detected ( $\rightarrow$  16% maximal power,  $\sim$ 0.55 mW) on selected single crystal of **1** deposited on a glass plate. Samples were imaged with a 20 $\times$ , 0.8 NA objective lens. Emitted signal of SHG was collected with a bandpass filter (420–440 nm) and compared to emission for KDP crystals collected in the same conditions.

**$\text{BiSeO}_3\text{Cl}$  Phase Diagram.** The compounds with the  $\text{BiSeO}_3\text{Cl}$  composition have already been reported in the literature as three different polymorphic modifications,  $\alpha$ ,  $\beta$ , and  $\gamma$  (Figure 1). The  $\gamma$ -

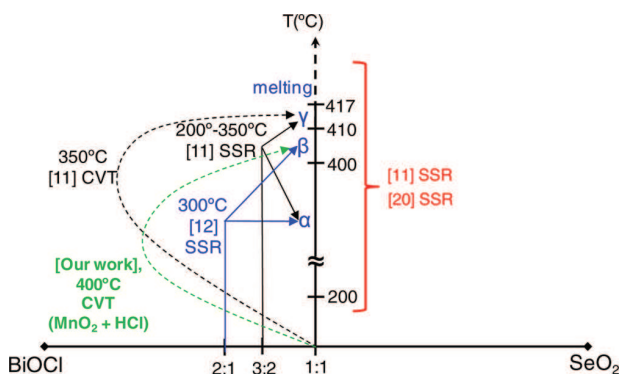


**Figure 1.** Phase relationships for  $\text{BiSeO}_3\text{Cl}$  depending on temperature and stoichiometric amounts of  $\text{BiOCl}$  and  $\text{SeO}_2$ . Figure is built on information's taken from our work and refs 11, 12, and 20. SSR stands for solid state reaction and CVT is for chemical vapor transport.

form (space group  $Pna2_1$ ,  $a = 11.707(2)$ ,  $b = 7.047(1)$ ,  $c = 5.315(1)$  Å) was prepared in evacuated ( $10^{-2}$  Pa) silica tubes from the 3:2 mixtures of  $\text{BiOCl}$  and  $\text{SeO}_2$  by Ibragimov et al.<sup>11</sup> The mixtures were placed in the tubes in a dry chamber under a nitrogen atmosphere. The phase composition of the reaction products was determined by X-ray diffraction. Solid-state reactions were run at 200 °C, 250 °C, 300 °C, and 350 °C for 240 h, followed by a furnace-cooling or quenching in ice water. Using a starting mixture enriched in  $\text{BiOCl}$ , the product was systematically the  $\gamma$ -form. Single crystals of the  $\alpha$ - $\text{BiSeO}_3\text{Cl}$  (space group  $P2_12_12_1$ ,  $a = 6.353(2)$ ,  $b = 7.978(3)$ ,  $c = 8.651(4)$  Å) was obtained by Berdonosov et al.<sup>12</sup> by heating of the evacuated quartz tube with  $\text{BiOCl}$  and  $\text{SeO}_2$  in 2:1 ratio at 300 °C for 240 h. According to them, if the starting mixture was enriched in  $\text{BiOCl}$ , the reaction products occasionally contained yellow  $\text{BiOCl}$  platelets and colorless parallelepipedal crystals of  $\gamma$ - $\text{BiSeO}_3\text{Cl}$ . Oppermann et al.<sup>20</sup> reported the sequence of phase transitions occurring with temperature starting from the  $\alpha$ -form as follows:  $\alpha \rightarrow \beta$  at 400 °C/2 °C and  $\beta \rightarrow \gamma$  at 410 °C/2 °C and going until melting point at 417 °C/2 °C. This was deduced from differential thermal analysis performed by Oppermann et al.<sup>20</sup>

The crystal structure of the  $\alpha$ - and  $\gamma$ -forms are shown in Figure 2 according to the crystallographic data reported in refs 11 and 12. Optical properties as well as dielectric properties of the NCS  $\gamma$ -form have been investigated.<sup>11</sup> Optical conclusions are that dielectric relaxation due to ions jumping over the defect vacancies in the crystal lattice occurs. The  $\beta$ - $\text{BiSeO}_3\text{Cl}$  polymorph was announced as stable in a very narrow thermal domain from the high temperature transformation of  $\alpha$ - $\text{BiSeO}_3\text{Cl}$  between 400 and 410 °C.<sup>20</sup> However, the crystal structure of the  $\beta$  phase was not solved at this temperature from the powder XRD data. Thus, there are only very few data available (XRD powder pattern and IR spectra) for the  $\beta$ -form.<sup>20</sup> Therefore, the

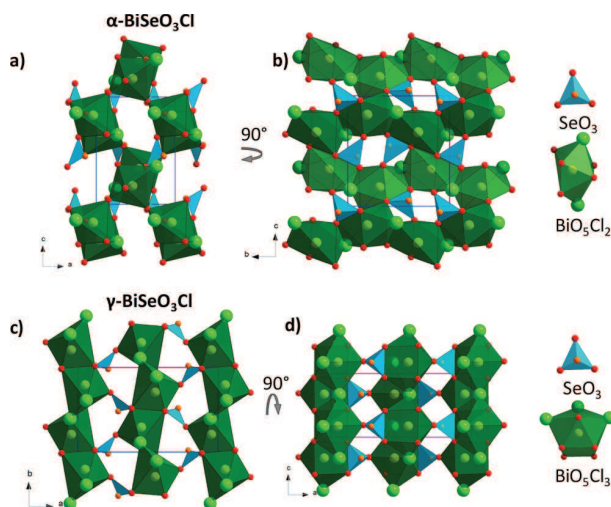


**Figure 2.** Crystal structure of  $\alpha$ - $\text{BiSeO}_3\text{Cl}$ : (a) projection along the  $b$ -axis, (b) along the  $a$ -axis. The crystal structure of  $\gamma$ - $\text{BiSeO}_3\text{Cl}$ : (c) projection along the  $c$ -axis, (d) along the  $b$ -axis.

formal identification of the phase is rather difficult. Here we report on the synthesis and crystal structure of this phase.

**Crystal Structure of  $\beta$ - $\text{BiSeO}_3\text{Cl}$ .** Colorless platelet single crystals have been isolated from the CVT products. An EDS analysis performed on single crystals shows evidence of Bi, Se, and Cl with a ratio of the elements 1.0/1.1/0.9. The majority of the tested crystals correspond to the phase with the lattice parameters,  $a = 22.7052(3)$  Å,  $b = 76.785(4)$  Å,  $c = 16.0550(3)$  Å, and  $\beta = 135.000(2)^\circ$ , space group Cc. Beyond its NCS character, the volume cell is strikingly large, and the structure is very complex. A total of 48 bismuth, 48 selenium, and 48 chlorine independent atoms have been located. The positions of the oxygen atoms were derived by the inspection of the local Fourier-difference electron-density maps. Because of the high number of refined parameters, anisotropic thermal parameters were refined for the Bi and Se atoms only. The final cycles of least-squares refinement including atomic coordinates and anisotropic thermal parameters for all cations and isotropic thermal parameters of anions converged to  $R_1 = 0.0612$ ,  $wR_2 = 0.0645$  (racemic twinning domains 91%, 9%). The crystal data and selected bond lengths are given in Tables S1–S8 of Supporting Information, respectively. The crystal-structure data for  $\beta$ - $\text{BiSeO}_3\text{Cl}$  phase were deposited with the depository number CSD-426283. It is noteworthy that residual electronic density remains quite high ( $5.39 \text{ e } \text{Å}^{-3}$ ) at the end of the refinement. This is not surprising in the case of giant cell in the presence of heavy elements. For example, other referenced bismuth selenites show similar electronic density; see refs 11 and 12. The same phenomenon was also observed for crystals 2 and 3.

The crystal structures of the  $\alpha$ - and  $\gamma$ - $\text{BiSeO}_3\text{Cl}$  structures are shown in Figure 2. The  $\text{BiO}_5\text{Cl}_2$  polyhedra in the former and the  $\text{BiO}_5\text{Cl}_2$  polyhedra in the latter are interconnected via  $\text{SeO}_3$  triangular pyramids by sharing respective edges and corners. The  $\text{Bi}^{3+}$  cations can be considered as interstitial ions in the  $[\text{ClSeO}_3]^{3-}$  anionic sublattice, so that both compounds can be considered as three-dimensional (3D).

The  $\beta$ - $\text{BiSeO}_3\text{Cl}$  crystal structure can be described as 2D (Figure 3a,b), which is of interest from the viewpoint of the reported  $\alpha \rightarrow \beta \rightarrow \gamma$  sequence of transitions. The crystal structure is built from two blocks,  $[\text{Bi}_8\text{Cl}_{16}]^{8+}$  (Figure 3c) and  $[\text{Bi}_{12}\text{Cl}_{32}]^{4+}$  (Figure 3d), regularly sandwiched between  $[\text{Bi}_{14}(\text{SeO}_3)_{24}]^{6-}$  layers (Figure 3d). In Figure 3a, the  $\text{BiO}_5\text{Cl}_2$  polyhedra are shown in green, whereas, for the sake of clarity, the  $[\text{Bi}_8\text{Cl}_{16}]^{8+}$  and  $[\text{Bi}_{12}\text{Cl}_{32}]^{4+}$  layers are represented as an arrangement of Bi (yellow) and Cl (green) atoms (Figure 3b). Similar halide layers with the composition  $[\text{Bi}_8\text{Cl}_{16}]^{8+}$  have been already observed in the structure  $\text{Bi}_8(\text{SeO}_3)_3\text{Br}_6$ <sup>21</sup> and have also been found in the new compound  $\text{PbBi}_{10}(\text{SeO}_3)_{12}\text{Cl}_8$  described below.

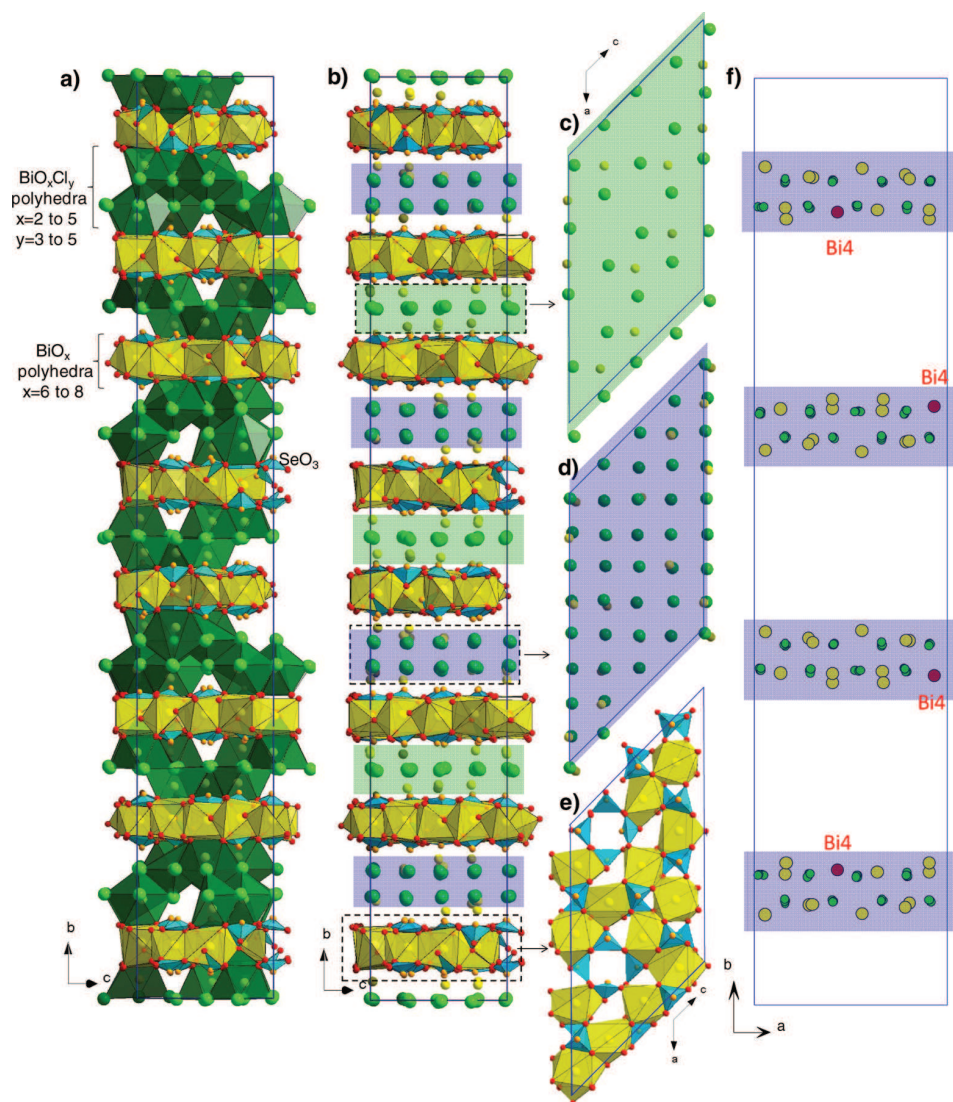


**Figure 3.** (a) The crystal of  $\beta$ -BiSeO<sub>3</sub>Cl projected along the  $a$  axis. BiO <sub>$x$</sub>  polyhedra are shown in yellow and BiO <sub>$x$</sub> Cl <sub>$y$</sub>  in green; (b) the same projection without the interlayer BiO <sub>$x$</sub> Cl <sub>$y$</sub>  polyhedra. It shows an alternation of three different parallel layers: (c) [Bi<sub>8</sub>Cl<sub>16</sub>]<sup>8+</sup> (green), (d) [Bi<sub>12</sub>Cl<sub>32</sub>]<sup>4+</sup> (blue), and (e) [Bi<sub>14</sub>(SeO<sub>3</sub>)<sub>24</sub>]<sup>6-</sup> presented as an association of distorted Bi–O <sub>$x$</sub>  polyhedra and SeO<sub>3</sub> by sharing edges and corners. (f) Focus on [Bi<sub>12</sub>Cl<sub>32</sub>]<sup>4+</sup> layers enhances the complex stacking along  $b \sim 76$  Å, through the Bi<sub>4</sub> atom position.

The Se<sup>4+</sup> cations form SeO<sub>3</sub> triangular pyramids with the lone electron pairs pointing externally. The Se–O bond lengths and the O–Se–O bond angles are in the typical range from 1.65 to 1.75 Å and from 92.8° to 106.4, respectively (see Tables S7 and S8, Supporting Information). The [Bi<sub>14</sub>(SeO<sub>3</sub>)<sub>24</sub>]<sup>6-</sup> layer is built by the association of Bi<sup>3+</sup> cations and the SeO<sub>3</sub> triangles. In BiO <sub>$x$</sub>  units (shown in yellow in Figure 3d) with  $x$  in between 8 and 10, all the bi-centered polyhedra are asymmetric, which is typical of the bismuth coordination due to the stereoactive behavior of the 6s<sup>2</sup> lone pairs on Bi<sup>3+</sup> cations. The BVS for the 48 independent Bi atoms is in the 2.7–3.6 range (see Table S9, Supporting Information).

The large value of the  $b$ -parameter ( $\sim 76$  Å) can be explained by the variety of different modules stacked along the  $b$ -axis. In other words, the ordering between the [Bi<sub>12</sub>Cl<sub>32</sub>]<sup>4+</sup> and [Bi<sub>8</sub>Cl<sub>16</sub>]<sup>8+</sup> cationic units sandwiched between the [Bi<sub>14</sub>(SeO<sub>3</sub>)<sub>24</sub>]<sup>6-</sup> anionic layers is the key factor for the formation of a giant cell and responsible for the doubling of  $b$ -parameter (Figure 3f).

Structural complexity of the BiSeO<sub>3</sub>Cl polymorphs may be quantified using Shannon information theory.<sup>22–24</sup> According to this theory, structural complexity may be quantitatively evaluated from the

Shannon information encoded in the atomic arrangement of the unit cell. The structural information amounts,  $I_{G,\text{total}}$  for the  $\alpha$ - and  $\gamma$ -forms are identical and equal to 62.039 bits per unit cell (bits/u.c.),<sup>25</sup> which allows classification of their structures as simple.<sup>24</sup> In contrast, the structure of the  $\beta$ -form is very complex, as its structural information equals 4705.880 bits/u.c. This value is quite high, and, on average, only 0.02% of inorganic structures are classified as very complex as detailed in ref 25. The reason for such an explosive increase in structural complexity can be seen in the transitional character of the  $\beta$ -phase. In order to understand structural reconstructions during the  $\alpha \rightarrow \beta \rightarrow \gamma$  transition, one may consider the arrangements (packing) of the heavy Bi atoms in the three structures. As it can be seen from Figure 4a that the arrangement of Bi atoms in the structure of the  $\alpha$ -phase is three-dimensional and is of the diamond type with the coordination number of each Bi atom equal to four (only Bi–Bi contacts  $< 5.5$  Å are considered; Figure 4d). The average  $\langle \text{Bi–Bi} \rangle$  interatomic distance is 4.344 Å. The arrangement of the Bi atoms in the  $\gamma$ -form is 2D (Figure 4c) and corresponds to the simple planar hexagonal net with each Bi atom surrounded by six neighbors (Figure 4e). The average  $\langle \text{Bi–Bi} \rangle$  interatomic distance is 4.823 Å. The arrangement of the Bi atoms in

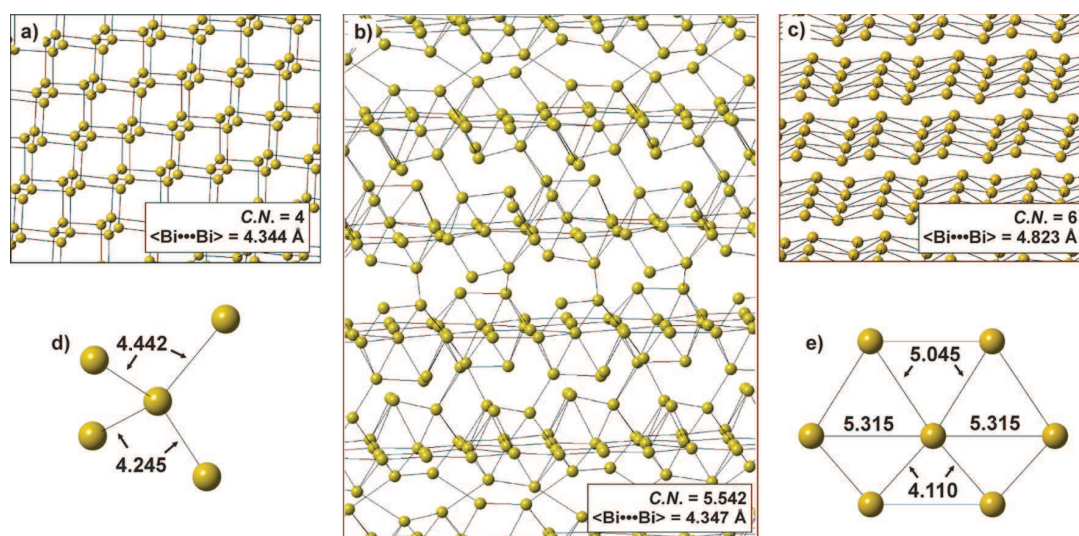


**Figure 4.** Arrangement of the Bi atoms in the structures of the  $\alpha$ -,  $\beta$ -, and  $\gamma$ -polymorphs of  $\text{BiSeO}_3\text{Cl}$  (a, b, and c, respectively) and the local coordination environments of Bi atoms in the structures of the  $\alpha$ - and  $\gamma$ -phases (d and e, respectively). Only Bi–Bi contacts shorter than 5.5 Å are taken into account. The boxes in a, b, and c contain average Bi coordination numbers (CN) and the average <Bi–Bi> interatomic distances.

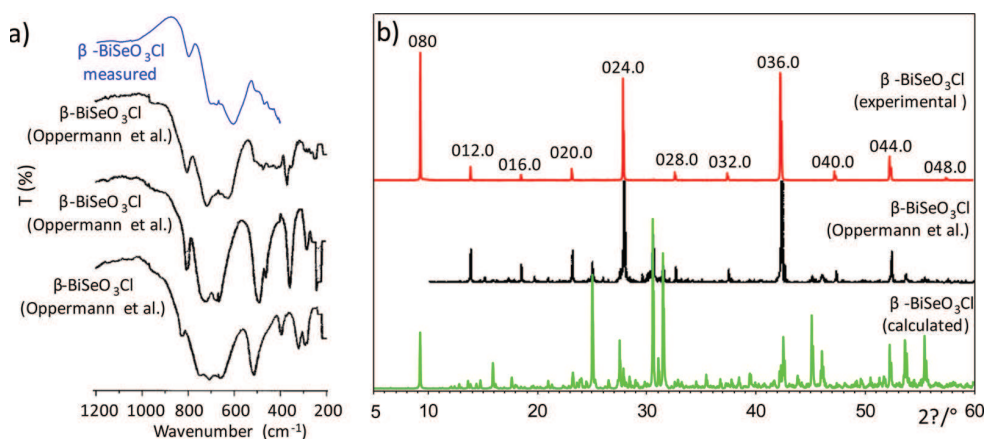


**Figure 5.** (a) Infrared red spectrum of the prepared  $\beta'$ - $\text{BiSeO}_3\text{Cl}$  (in blue) compared to the spectrum of  $\beta$ - $\text{BiSeO}_3\text{Cl}$ ,  $\alpha$ - $\text{BiSeO}_3\text{Cl}$  and  $\gamma$ - $\text{BiSeO}_3\text{Cl}$  (in black) (from Oppermann et al.<sup>20</sup>). (b) XRD patterns of experimental  $\beta$ - $\text{BiSeO}_3\text{Cl}$  (red),  $\beta$ - $\text{BiSeO}_3\text{Cl}$  from Oppermann's work (black) and of XRDP calculated from data of the crystal structure (green). Our  $\beta$ - $\text{BiSeO}_3\text{Cl}$  reassembles the  $\beta$ -form mentioned by Oppermann et al.<sup>20</sup> Differences between simulated and experimental XRD powder patterns for  $\beta$ - $\text{BiSeO}_3\text{Cl}$  imply preferred orientation (along  $(0n0)$ ) as the X-ray diagram was measured using single crystals on a silicon sample holder.

the structure of transitional  $\beta$ -phase is intermediate between three- and two-dimensional with Bi atoms segregated into planes perpendicular to the  $b$  axis (Figure 4b). The average coordination number of Bi atoms is 5.542, i.e., intermediate between 4 (as in  $\alpha$ -phase) and 6 (as in  $\gamma$ -phase). The <Bi–Bi> distance is 4.347 Å. The  $\alpha \rightarrow \beta \rightarrow \gamma$  transition is therefore associated with the regrouping of the Bi atoms from a three-dimensional (diamond-like) to two-dimensional (simple hexagonal) arrangement with the surprising narrow-range stabilization of the intermediate highly complex structure. This complexity-generating mechanism seems to be relatively abundant in inorganic compounds. Perhaps, the most simple example is the temperature-driven phase transition from the high-temperature  $\text{SiO}_2$  with the cristobalite structure ( $I_{G,\text{total}} = 5.510$  bits/u.c.) to the room-temperature quartz structure (8.265 bits/u.c.) through the transitional tridymite topology with the higher complexity (17.510 bits/u.c.) compared to cristobalite and quartz polymorphs. The unusually high complexity of  $\beta$ - $\text{BiSeO}_3\text{Cl}$  can thus be assigned to its existence as an intermediate phase between the structurally simple  $\alpha$ - and  $\gamma$ -forms.

In order to check whether the phase under study is indeed the  $\beta$ -phase reported previously, the infrared (IR) spectra of  $\beta$ - $\text{BiSeO}_3\text{Cl}$  were measured between 4000 and 400  $\text{cm}^{-1}$  using crushed crystals. On Figure 5a, the IR spectrum is compared to those reported for the  $\alpha$ -,  $\beta$ -, and  $\gamma$ -forms in ref 20. At first glance, the IR spectrum matches rather well. However, on this basis only, it remains rather difficult to make a definite conclusion, since the vibrational spectra for all the polymorphs include the Se–O, Bi–O, and Bi–Cl bands that are not expected to be drastically shifted (cf. strong similarities between the IR spectra of the  $\alpha$ -,  $\beta$ -, and  $\gamma$ -forms). In Figure 5b, the theoretical X-ray diffraction pattern is compared to the experimental patterns reported for the  $\beta$ -form<sup>20</sup> and for the phase presented above. Taking into account significant preferred orientation effects along the  $\beta$ -[010] directions, a good compatibility is confirmed. Finally, we presume that our refined model indeed corresponds to the mysterious  $\beta$ -form. This assessment involves first order  $\alpha \rightarrow \beta$  and  $\beta \rightarrow \gamma$  reconstructive transitions through a complex intermediate  $\beta$ -phase with extraordinary complexity and the giant unit cell ( $V = 19792 \text{ \AA}^3$ ).

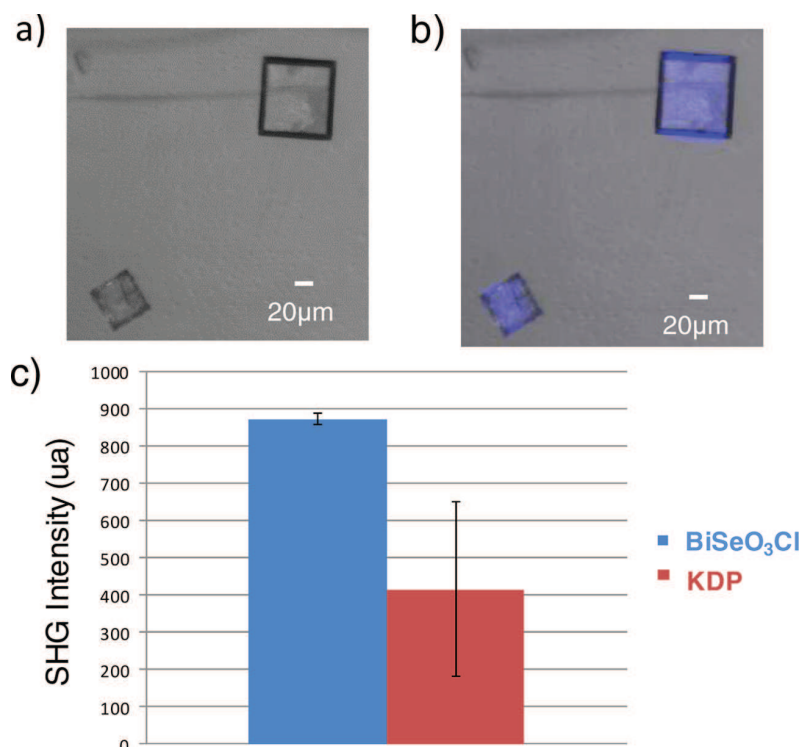


**Figure 6.** (a) Transmission image of a crystal of BiSeO<sub>3</sub>Cl, (b) color: emitting surface ( $\lambda_{em} = 420\text{--}440$  nm,  $\lambda_{em} = 860$  nm), (c) SHG intensity of BiSeO<sub>3</sub>Cl single crystals compared to KDP with experimental error bars.

For  $\beta$ -BiSeO<sub>3</sub>Cl, only the noncentrosymmetric structure model with the space group *Cc* leads to an acceptable convergence of the least-squares refinement. This noncentrosymmetric behavior arises from the fact that no inversion centers have been found in any of the three distinct layered subunits, probably the result of the stereoactive behavior of the LP on Bi<sup>3+</sup> cations. The second harmonic generation effect was therefore tested for the single crystals of **1** by means of a laser scanning microscope (selected  $\lambda = 860$  nm). Figure 6 shows the crystal of **1** in the absence and in the presence of emission. The color at the surface of the single crystals shows an intrinsic homogeneous distribution of the emitted doubled frequency light collected with a band-pass filter (420–440 nm). Recent quantitative data collected on single crystal of compound **1** give an efficiency doubled from KDP (KH<sub>2</sub>PO<sub>4</sub>) (wavelength: 860 nm, frequency 80 MHz) as presented on Figure 6c). It is noteworthy that errors on measurement of KDP efficiency are quite large, although it was registered on three different samples. It is due to the large thickness of the crystals.

Oppermann et al. have concluded that volatile BiSeO<sub>3</sub>Cl molecules are formed during the CVT process.<sup>20</sup> We have tried to figure out the configurations of these imaginary molecules by analyzing the structures of the  $\alpha$ -,  $\beta$ -, and  $\gamma$ -forms of BiSeO<sub>3</sub>Cl. With that purpose in mind, for each Bi atom the closest Cl atom and SeO<sub>3</sub> group was selected, leading to the individual BiSeO<sub>3</sub>Cl molecules shown in the Figure 7a for the  $\alpha$ -form and Figure 7b for the  $\gamma$ -form. Selection of this kind is more complicated in  $\beta$ -BiSeO<sub>3</sub>Cl due to the high number of independent atomic positions: Bi (48), Se (48), and Cl (48), that all display versatile coordination environments. In fact, the full structure can be divided into individual BiSeO<sub>3</sub>Cl groups, in agreement with the proposed real existence of such molecules and their reorganization across phase transitions observed upon heating.<sup>20</sup> Only two extreme geometries with the shortest (Figure 7c) and longest (Figure 7d) Bi–Cl bonds are shown in this paper.

**The Crystal Structure of Bi<sub>6</sub>(SeO<sub>3</sub>)<sub>4</sub>Cl<sub>10</sub>.** Colorless needle-like single crystals of Bi<sub>6</sub>(SeO<sub>3</sub>)<sub>4</sub>Cl<sub>10</sub> have been isolated after another CVT synthesis involving the initial composition 2BiCl<sub>3</sub> + 1 Bi<sub>2</sub>O<sub>3</sub> + 4SeO<sub>2</sub> + 1Mn<sub>2</sub>O<sub>3</sub> as detailed above. The pertinent data of the diffraction-data

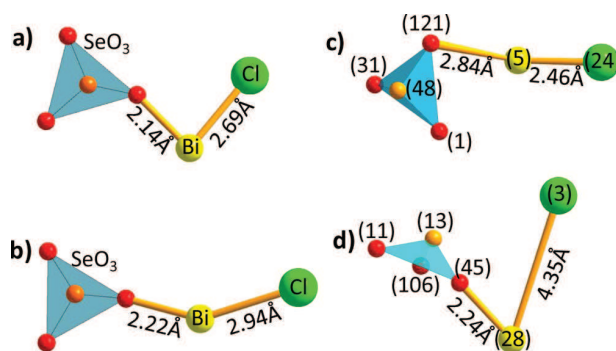


**Figure 7.** BiSeO<sub>3</sub>Cl "molecules" in the structures of (a)  $\alpha$ -BiSeO<sub>3</sub>Cl and (b)  $\gamma$ -BiSeO<sub>3</sub>Cl. BiSeO<sub>3</sub>Cl "molecules" with (c) shortest and (d) longest Bi–Cl bonds which are the two extreme representatives of 48 Bi atoms in  $\beta$ -BiSeO<sub>3</sub>Cl.

collection and structural solution and refinement are summarized in Table 1. Ten Bi atoms were localized using the charge-flipping method, whereas the remaining atoms (4 Se, 10 Cl, and 12 O) were deduced from the inspection of the difference Fourier maps. The structure refinement rapidly converged to a reasonable reliability factor.

The crystal structure is shown in Figure 8a,b. It can be considered as formed from six distorted bicentered oxochloride polyhedra: Bi(1)-O<sub>3</sub>Cl<sub>4</sub>, Bi(2)O<sub>3</sub>Cl<sub>5</sub>, Bi(3)O<sub>3</sub>Cl<sub>4</sub>, Bi(4)O<sub>3</sub>Cl<sub>4</sub>, Bi(5)O<sub>4</sub>Cl<sub>4</sub>, and Bi(6)-O<sub>4</sub>Cl<sub>4</sub>, linked to four Se atoms with the Bi–O, Bi–Cl, and Se–O distances in the same range as those observed for the compound **1**, leading to a 3D network. The BVS values for the Bi atoms are in the range of 2.9–3.1. The stereoactive behavior of the lone electron pairs on the Bi<sup>3+</sup> and Se<sup>4+</sup> cations is manifested by the particularly asymmetric coordination environments around these cations. Bi coordination polyhedra share edges and corners to build Bi<sub>6</sub>(SeO<sub>3</sub>)<sub>4</sub>Cl<sub>10</sub> blocks linked together in such a way as to create an



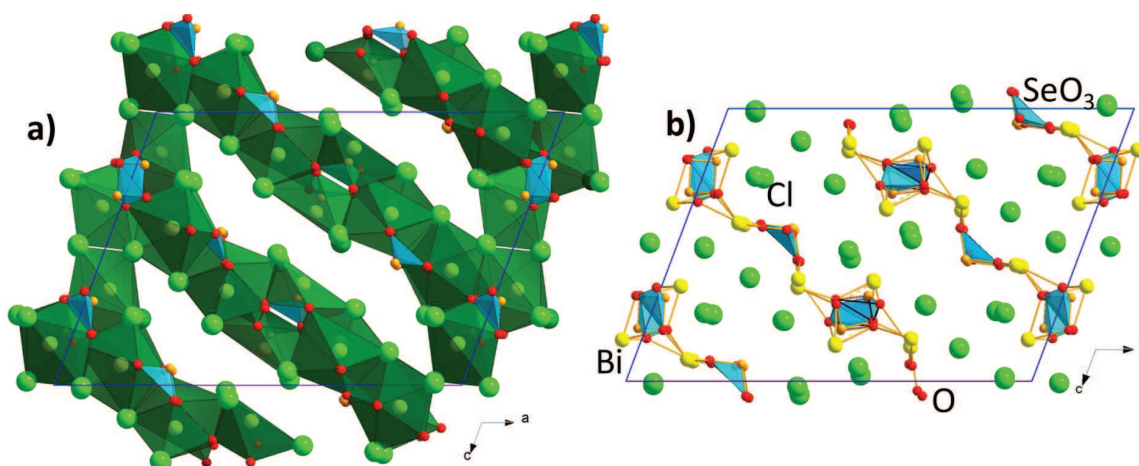


**Figure 8.** (a) The crystal structure of  $\text{Bi}_6(\text{SeO}_3)_4\text{Cl}_{10}$  projected along the  $b$  axis, showing  $\text{BiO}_x\text{Cl}_y$  polyhedra (dark green) and  $\text{SeO}_3$  groups (blue) sharing edges and corners. (b) The same projection with omission of the  $\text{BiO}_x\text{Cl}_y$  polyhedra for clarity.

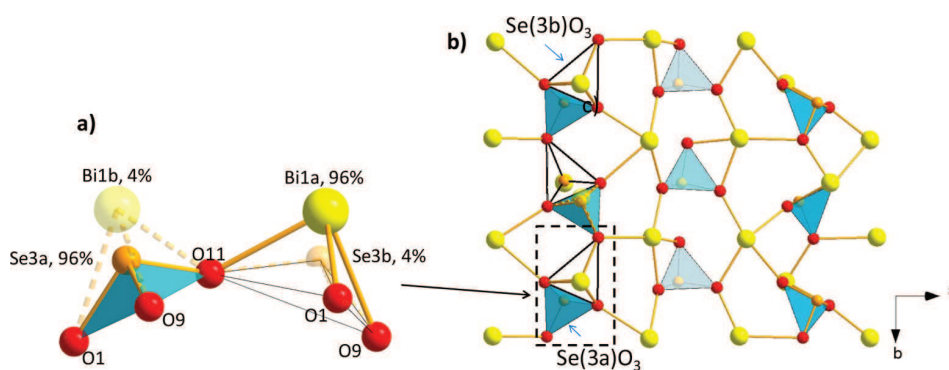


**Figure 9.** (a) Oxygen coordination of the Bi1a and Se3a atoms, (b) part of the structure of  $\text{Bi}_6(\text{SeO}_3)_4\text{Cl}_{10}$  projected along the  $c$  axis.

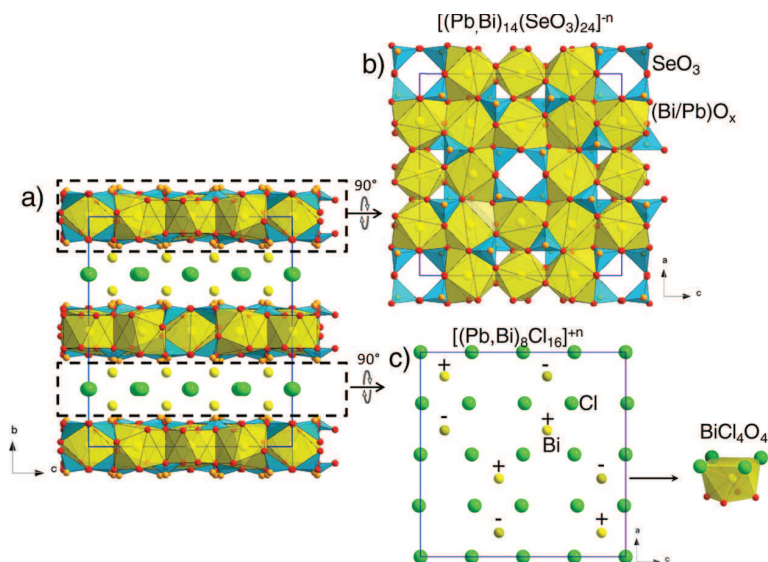


**Figure 10.** (a) The crystal structure of  $\text{PbBi}_{10}(\text{SeO}_3)_{12}\text{Cl}_8$  projected along the  $a$  axis with two parallel cationic and anionic layers: (b)  $[(\text{Pb,Bi})_{14}(\text{SeO}_3)_{24}]^{n-}$  built on association of distorted  $\text{BiO}_x$  polyhedra (yellow) and  $\text{SeO}_3$  groups (blue) (c)  $[(\text{Pb,Bi})_8\text{Cl}_{16}]^{n+}$  layers parallel to the  $ac$  plane. The labels  $\pm$  stand for Bi  $y$  coordinate above or below the chloride planes.

open structure with some kind of empty cavities bordered by the anions (essentially  $\text{Cl}^-$ ) and parallel to the  $b$  axis. These cavities are delimited by 12 edges (1- edges:  $\text{Cl}-\text{Cl}$  and  $\text{Cl}-\text{O}$  and faces:  $\text{Cl}-\text{Cl}-$

$\text{Cl}$ ) as shown on Figure 8a. The cavities are around 9.7 Å long and 3.8 Å wide. The presence of such tunnels with  $n$ -membered rings (MRs; here  $n = 12$ ) was already observed in other selenites and especially in

the structure of  $\text{Bi}_2(\text{V}^{\text{O}}\text{O}_2)_2(\text{SeO}_3)_4$  (8-MR).<sup>26</sup> Focusing on the chloride arrangement, it reveals a 2D character of the structure with  $\text{Cl}^-$  crenel-layered (Figure 8b).

The close inspection of a Fourier difference electron-density map showed a high residual peak ( $8.71 \text{ e}/\text{\AA}^3$ )  $0.86 \text{ \AA}$  away from the Se3 site indicating its possible splitting into two satellite positions. The coupled refinement of the occupancies of the Se3/Se3' sites resulted in the 0.95/0.05 ratio. While the Se–O distances for Se3 are plausible ( $1.71$ – $1.74 \text{ \AA}$ ), those for the Se3' site are too long ( $2.09$ – $2.41 \text{ \AA}$ ), which suggested its occupation by Bi. The final Bi1a/Bi1b and Se3a/Se3b occupancies were refined to the ratio of 0.96/0.04 (Figure 9a). The weak statistical Bi/Se disorder occurs within the chains formed by edge-sharing  $-\text{OSeO}_2\text{BiO}-$  dimers running along the  $b$ -axis (Figure 9b).

The atomic positions, isotropic and anisotropic displacement parameters, and principal distances are given in Tables S9–S11 of Supporting Information. The crystal-structure data for  $\text{Bi}_6(\text{SeO}_3)_4\text{Cl}_{10}$  phase were deposited with the depository number CSD-426286.

**The Crystal Structure of  $\text{PbBi}_{10}(\text{SeO}_3)_{12}\text{Cl}_8$ .** Colorless platelet crystals of **3** were mounted on a glass fiber for the X-ray diffraction analysis. The unit-cell parameters and systematic absences were consistent with the orthorhombic space group  $Ccca$ . Seven independent Bi sites were found from charge flipping, while other sites have been deduced from the inspection of difference electron-density maps. At this stage, the formula was established as  $\text{Bi}_{11}(\text{SeO}_3)_{12}\text{Cl}_8$ , which is not electroneutral. Taking into account the presence of Pb during the synthesis, an elemental analysis was performed. The EPMA microprobe analysis provided the ratio Pb/Bi of 0.8:1.5, which is reasonably close to the expected 1:10 ratio for an electroneutral structure. The mixed Bi/Pb occupancy of 1/9 has been considered for the Bi2, Bi3, Bi4, and Bi5, since their bond-valence sum values are 2.77, 2.59, 2.52, 2.47 v.u., respectively. The resulting electroneutral formula is  $\text{PbBi}_{10}(\text{SeO}_3)_{12}\text{Cl}_8$ , and the structure is shown on Figure 10a. If all Bi/Pb–O and Bi–Cl bond lengths smaller than  $3.10 \text{ \AA}$  are taken into account, the following irregular coordination polyhedra can be observed: Bi(1) $\text{O}_8$ , Bi(2) $\text{O}_{10}$ , Bi(3) $\text{O}_{10}$ , Bi(4) $\text{O}_{10}$ , and Bi(5) $\text{O}_4\text{Cl}_4$ . The Bi–O bond lengths vary from 2.37 to  $2.75 \text{ \AA}$ , whereas the Bi–Cl bond lengths are in the range from 2.96 to  $3.10 \text{ \AA}$ .

In the  $\text{SeO}_3$  groups,  $\text{Se}^{4+}$ –O bond lengths and  $\text{O}=\text{Se}^{4+}$ –O bond angles are between 1.65 and  $1.75 \text{ \AA}$ , and  $92.8$  and  $106.4^\circ$ , respectively, as expected. The structure can be described as a 2D network, with the  $[(\text{Pb,Bi})_{14}(\text{SeO}_3)_{24}]^{n-}$  layer (Figure 10b) sandwiched between the  $[(\text{Pb,Bi})_8\text{Cl}_{16}]^{n+}$  (Figure 10c) layers parallel to the  $ac$  plane. This structure is polystructural with  $\text{CaNd}_{10}(\text{SeO}_3)_{12}\text{Cl}_{18}$  crystal structure published by Berdonosov et al. in 2007.<sup>27</sup>

Technical details of the data acquisition and refinement parameters are gathered in Table 1. The crystal-structure data for  $\text{PbBi}_{10}(\text{SeO}_3)_{12}\text{Cl}_8$  are deposited with the depository number CSD-426285. The atomic coordinates, displacement parameters, and selected bond-lengths are gathered in Tables S12–S14 of Supporting Information.

## CONCLUSIONS

The discovery of new bismuth selenite halides (Cl, Br, or I) remains occasional, while our study sheds light on three new architectures with structural similarities arising from the asymmetric coordinations of the  $\text{Bi}^{3+}$ ,  $\text{Se}^{4+}$ , and/or  $\text{Pb}^{2+}$  lone pair cations. As expected from the likely interleave role of halogen anions, two of the three obtained structures are layered. These compounds were obtained as small single crystals only. Up to now, our attempts to scale the preparation into larger amounts of material were unsuccessful. This is a common limitation regarding the works previously reported for several selenites, which remains problematic for further characterization of such complex structural architectures. This blank gap could be filled by using soft chemistry processes, such solvothermal routes currently tested by our research group in the selenite chemical systems. In summary, even if CVT is

shown here as a powerful tool to access complex (i.e., giant) crystal structures, alternative synthesis routes must be developed. At least in the case of  $\text{BiSeO}_3\text{Cl}$ , the role of preformed molecules could be the key parameter for the stabilization of particular polymorphs forms using high temperature methods. Finally, it is worth concluding that, in this work, we have prepared and characterized the mysterious  $\beta$ - $\text{BiSeO}_3\text{Cl}$  phase shown reported previously as stable only in a narrow thermal range ( $\Delta T = 7^\circ\text{C}$ ). The structure of this phase can be described as very complex, and the complexity-generating mechanism can be assigned to its role as a transitional phase between structurally simple  $\alpha$ - and  $\gamma$ -polymorphs.

## ASSOCIATED CONTENT

### Supporting Information

Tables of fractional atomic coordinates and isotropic or equivalent isotropic displacement parameters, atomic displacement parameters, selected bond distances and angles and interatomic distances, and bond sum valence values. This material is available free of charge via the Internet at <http://pubs.acs.org>.

## AUTHOR INFORMATION

### Corresponding Author

\*Email: [marie.colmont@ensc-lille.fr](mailto:marie.colmont@ensc-lille.fr). Fax: (+) 33 3 20 43 64 34.

### Notes

The authors declare no competing financial interest.

## ACKNOWLEDGMENTS

The Fonds Européen de Développement Régional (FEDER), CNRS, Région Nord Pas-de-Calais, and Ministère de l'Éducation Nationale de l'Enseignement Supérieur et de la Recherche are acknowledged for funding the X-ray diffractometers. Laurence Burylo and Nora Djellal are thanked for their precious technical help. This work was carried out under the framework of the Multi-InMaDe project supported by the ANR (Grant ANR 2011-JS-08 003 01). S.V.K. acknowledges financial support from St. Petersburg State University (Internal Grant 3.38.136.2014).

## REFERENCES

- (1) Ok, K. M.; Chi, E. O.; Halasyamani, P. S. *Chem. Soc. Rev.* **2006**, *35*, 710–717.
- (2) Halasyamani, P. S. In *Functional Oxides*; Bruce, D. W.; O'Hare, D.; Walton, R. I., Eds.; John Wiley & Sons, Ltd: New York, 2010; pp 1–39.
- (3) Endara, D.; Colmont, M.; Huvé, M.; Capet, F.; Lejay, J.; Aschehoug, P.; Mentré, O. *Inorg. Chem.* **2012**, *51*, 9557–9562.
- (4) Colmont, M.; Endara, D.; Aliev, A.; Terryn, C.; Huvé, M.; Mentré, O. *J. Solid State Chem.*
- (5) Lu, H.; Gautier, R.; Donakowski, M. D.; Tran, T. T.; Edwards, B. W.; Nino, J. C.; Halasyamani, P. S.; Liu, Z.; Poeppelmeier, K. R. *J. Am. Chem. Soc.* **2013**, *135*, 11942–11950.
- (6) Nguyen, S. D.; Yeon, J.; Kim, S.-H.; Halasyamani, P. S. *J. Am. Chem. Soc.* **2011**, *133*, 12422–12425.
- (7) Krivovichev, S. V.; Filatov, S. K.; Vergasova, L. P. *Mineral. Petrol.* **2013**, *107*, 235–242.
- (8) Zhang, S.-Y.; Hu, C.-L.; Li, P.-X.; Jiang, H.-L.; Mao, J.-G. *Dalton Trans. Camb. Engl.* **2003** **2012**, *41*, 9532–9542.
- (9) Aliev, A.; Olchowka, J.; Colmont, M.; Capoen, E.; Wickleder, C.; Mentré, O. *Inorg. Chem.* **2013**.
- (10) Lü, M.; Aliev, A.; Olchowka, J.; Colmont, M.; Huvé, M.; Wickleder, C.; Mentré, O. *Inorg. Chem.* **2014**, *53*, 528–536.

- (11) Ibragimov, S. A.; Berdonosov, P. S.; Dolgikh, V. A.; Huong, D. Q.; Oppermann, H. *Inorg. Mater.* **2002**, *38*, 1291–1296.
- (12) Berdonosov, P. S.; Stefanovitch, S. Y.; Dolgikh, V. A. *J. Solid State Chem.* **2000**, *149*, 236–241.
- (13) Schmidt, P.; Binnewies, M.; Glaum, R.; Schmidt, M. In *Advanced Topics on Crystal Growth*; Ferreira, S., Ed.; InTech: Rijeka, Croatia, 2013.
- (14) SAINT: *Area-Detector Integration Software*; Siemens Industrial Automation, Inc.: Madison, 1996.
- (15) SADABS: *Area-Detector Absorption Correction*; Siemens Industrial Automation, Inc.: Madison, 1995.
- (16) Palatinus, L.; Chapuis, G. *J. Appl. Crystallogr.* **2007**, *40*, 786–790.
- (17) Petricek, V.; Dusek, M.; Palatinus, L. *Jana2006. The Crystallographic Computing System*; Institute of Physics: Praha, Czech Republic, 2006.
- (18) Brese, N. E.; O’Keeffe, M. *Acta Crystallogr.* **1991**, *B47*, 192–197.
- (19) Krivovichev, S. V. *Z. Kristallogr.* **2012**, *227*, 575–579.
- (20) Oppermann, H.; Huong, D. Q.; Zhang, M.; Schmidt, P.; Popovkin, B. A.; Ibragimov, S. A.; Berdonosov, P. S.; Dolgikh, V. A. *Z. Anorg. Allg. Chem.* **2001**, *627*, 1347–1356.
- (21) Ruck, M.; Schmidt, P. *Z. Anorg. Allg. Chem.* **2003**, *629*, 2133–2143.
- (22) Krivovichev, S. V. *Acta Crystallogr.* **2012**, *A68*, 393–398.
- (23) Krivovichev, S. V. *Mineral. Mag.* **2013**, *77*, 275–326.
- (24) Krivovichev, S. V. *Angew. Chem., Int. Ed.* **2014**, *53*, 654–661.
- (25) The structural complexity is measured as an amount of information encoded in the atomic arrangement of the unit cell using formula

$$I_{G,\text{total}} = -v \sum_{i=1}^k p_i \log_2 p_i$$

where  $I_{G,\text{total}}$  is the amount of structural information per unit cell (in bits/u.c. = unit-cell),  $k$  is the number of different crystallographic orbits, and  $p_i$  is the random choice probability for an atom from the  $i$ th crystallographic orbit; that is,  $p_i = m_i/v$ , where  $m_i$  is a multiplicity of a crystallographic orbit relative to the reduced unit cell, and  $v$  is the number of atoms in the reduced unit cell.<sup>22–24</sup>

- (26) Li, P.-X.; Kong, F.; Hu, C.-L.; Zhao, N.; Mao, J.-G. *Inorg. Chem.* **2010**, *49*, 5943–5952.
- (27) Berdonosov, P. S.; Olenev, A. V.; Dolgikh, V. A.; Lightfoot, P. *J. SSC* **2007**, *180*, 3019–3025.

## **Revised Bismuth Chloroselenite System: Evidence of a Noncentrosymmetric Structure with a Giant Unit Cell**

Almaz Aliev,<sup>†</sup> Vadim M. Kovrugin,<sup>†,§</sup> Marie Colmont,<sup>\*,†</sup> Christine Terryn,<sup>‡</sup> Marielle Huvé,<sup>†</sup>  
Oleg I. Siidra,<sup>§</sup> Sergey V. Krivovichev,<sup>§</sup> and Olivier Mentré<sup>†</sup>

<sup>†</sup> *Université Lille 1, Université Lille Nord France, ENSCL, CNRS, UCCS, UMR 8181, F-59652 Villeneuve d'Ascq, France*

<sup>‡</sup> *Plateforme Imagerie Cellulaire et Tissulaire, 51 rue Cognacq-Jay, 51100 Reims, France*

<sup>§</sup> *St. Petersburg State University, Department of Crystallography, University Emb. 7/9, 199034 St. Petersburg, Russia*

*Table S 1. Fractional atomic coordinates and isotropic or equivalent isotropic displacement parameters ( $\text{\AA}^2$ ) of  $\beta$ '-BiSeO<sub>3</sub>Cl*

	<i>x</i>	<i>y</i>	<i>z</i>	$U_{\text{iso}}^*/U_{\text{eq}}$
Bi1	0.83058 (11)	0.94300 (3)	0.73001 (15)	0.0177 (4)
Bi2	1.07566 (13)	0.94440 (3)	0.46808 (18)	0.0264 (5)
Bi3	0.70037 (11)	0.97961 (3)	0.20999 (16)	0.0220 (4)
Bi4	1.06773 (11)	0.64526 (3)	-0.03419 (15)	0.0228 (4)
Bi5	1.33606 (11)	0.64057 (2)	0.24423 (15)	0.0212 (4)
Bi6	0.20161 (11)	0.97967 (3)	0.98544 (15)	0.0225 (4)
Bi7	1.07824 (11)	0.93894 (3)	0.97991 (15)	0.0193 (4)
Bi8	1.46187 (12)	0.69444 (2)	0.24901 (16)	0.0203 (4)
Bi9	0.81348 (12)	0.94041 (2)	0.97290 (16)	0.0195 (4)
Bi10	1.32491 (11)	0.72959 (3)	0.23065 (16)	0.0230 (4)
Bi11	0.56859 (11)	0.94315 (3)	0.70624 (16)	0.0226 (5)
Bi12	0.60026 (12)	0.72966 (3)	0.00583 (16)	0.0227 (4)
Bi13	1.71596 (11)	0.69307 (3)	0.49162 (16)	0.0189 (4)
Bi14	0.57719 (11)	0.93881 (3)	0.96639 (15)	0.0182 (4)
Bi15	0.46336 (12)	0.69460 (2)	-0.25002 (17)	0.0205 (4)
Bi16	0.71410 (11)	0.89270 (2)	0.96130 (15)	0.0214 (4)
Bi17	0.19496 (12)	0.89061 (2)	0.96828 (16)	0.0227 (4)
Bi18	0.93629 (11)	0.98330 (2)	0.21303 (15)	0.0208 (4)
Bi19	0.57328 (14)	0.94379 (3)	0.47180 (18)	0.0284 (5)
Bi20	0.33122 (11)	0.94270 (3)	0.72515 (15)	0.0175 (4)
Bi21	0.59311 (11)	0.64301 (3)	0.00160 (16)	0.0228 (4)
Bi22	0.47572 (12)	0.69188 (2)	-0.48591 (16)	0.0200 (4)
Bi23	1.44964 (12)	0.69202 (2)	-0.01131 (16)	0.0202 (4)
Bi24	0.94820 (12)	0.69029 (2)	0.24077 (16)	0.0205 (4)
Bi25	1.43687 (11)	0.98320 (2)	0.45218 (15)	0.0216 (4)
Bi26	0.56673 (11)	0.94148 (2)	0.22464 (16)	0.0194 (4)
Bi27	1.06752 (11)	0.94354 (2)	0.22051 (16)	0.0209 (4)
Bi28	0.31955 (12)	0.94413 (3)	0.96752 (17)	0.0217 (4)
Bi29	0.06782 (11)	0.94169 (3)	0.70155 (16)	0.0192 (4)
Bi30	1.20987 (12)	0.69290 (3)	0.48564 (16)	0.0198 (5)
Bi31	0.86148 (11)	0.64257 (2)	0.25664 (15)	0.0216 (4)
Bi32	0.81983 (12)	0.94446 (3)	0.46690 (17)	0.0223 (4)
Bi33	0.59420 (12)	0.65299 (2)	-0.23989 (16)	0.0236 (4)
Bi34	1.21683 (11)	0.89518 (3)	0.25882 (16)	0.0233 (4)
Bi35	0.71694 (13)	0.69409 (3)	-0.24904 (18)	0.0272 (5)
Bi36	1.31605 (12)	0.94072 (3)	0.44967 (17)	0.0220 (4)
Bi37	0.83292 (11)	0.73328 (2)	0.00286 (15)	0.0213 (4)
Bi38	0.97632 (12)	0.69085 (2)	-0.23281 (16)	0.0215 (4)
Bi39	0.95534 (13)	0.69348 (2)	-0.00543 (16)	0.0220 (4)
Bi40	1.33195 (11)	0.65284 (2)	0.00054 (15)	0.0230 (4)
Bi41	1.97117 (13)	0.69324 (3)	0.50905 (17)	0.0234 (5)
Bi42	0.43823 (11)	0.90224 (2)	1.21751 (15)	0.0244 (4)
Bi43	0.94066 (11)	0.90340 (2)	0.44939 (15)	0.0210 (4)
Bi44	1.71996 (11)	0.68922 (3)	0.24888 (16)	0.0206 (4)
Bi45	0.09225 (11)	0.73326 (2)	-0.23850 (15)	0.0208 (4)
Bi46	0.69651 (11)	0.89252 (2)	0.21257 (15)	0.0226 (4)
Bi47	0.20934 (13)	0.69421 (3)	-0.25626 (18)	0.0279 (5)
Bi48	1.20802 (11)	0.68897 (3)	0.23673 (15)	0.0208 (5)
Se1	0.6006 (3)	0.71982 (6)	-0.2450 (4)	0.0175 (9)
Se2	1.4514 (3)	0.96971 (6)	0.2349 (4)	0.0178 (10)
Se3	0.3584 (3)	0.72290 (6)	-0.2470 (4)	0.0178 (10)
Se4	0.3243 (3)	0.71976 (6)	-0.0211 (4)	0.0159 (9)
Se5	0.6831 (3)	0.97129 (6)	0.7010 (4)	0.0178 (10)
Se6	1.5675 (3)	0.72283 (6)	0.4630 (4)	0.0162 (10)
Se7	1.4418 (3)	0.91766 (6)	0.4442 (4)	0.0152 (9)

Se8	1.1859 (3)	0.97145 (6)	0.4595 (4)	0.0162 (10)
Se9	0.6850 (3)	0.91496 (6)	0.4568 (4)	0.0179 (10)
Se10	1.5892 (3)	0.66495 (6)	0.5095 (4)	0.0162 (9)
Se11	0.1035 (3)	0.71812 (6)	-0.0159 (3)	0.0164 (9)
Se12	0.8577 (3)	0.66381 (6)	-0.2466 (4)	0.0154 (9)
Se13	0.1849 (3)	0.91498 (6)	0.7046 (4)	0.0160 (9)
Se14	0.7102 (3)	0.91368 (6)	0.7519 (4)	0.0193 (10)
Se15	0.0905 (3)	0.72137 (6)	-0.4878 (3)	0.0145 (9)
Se16	0.2123 (3)	0.97271 (6)	0.7549 (4)	0.0161 (10)
Se17	1.0629 (3)	0.72135 (6)	0.2128 (4)	0.0155 (9)
Se18	1.2106 (3)	0.91382 (6)	0.4604 (4)	0.0158 (9)
Se19	0.9402 (3)	0.91799 (6)	0.2301 (4)	0.0188 (9)
Se20	0.9522 (3)	0.96977 (6)	0.4615 (4)	0.0194 (10)
Se21	1.0679 (3)	0.66369 (6)	0.4640 (4)	0.0182 (10)
Se22	1.3324 (3)	0.72079 (6)	0.4516 (4)	0.0182 (10)
Se23	0.7109 (3)	0.97280 (6)	0.4615 (4)	0.0160 (10)
Se24	0.4860 (2)	0.97070 (6)	1.0009 (3)	0.0128 (9)
Se25	1.2252 (3)	0.96822 (6)	0.2314 (3)	0.0164 (9)
Se26	0.8337 (3)	0.72145 (6)	-0.2452 (4)	0.0138 (9)
Se27	0.3371 (3)	0.66498 (6)	-0.2430 (4)	0.0161 (10)
Se28	0.9573 (3)	0.97157 (6)	1.0029 (3)	0.0169 (10)
Se29	1.5631 (3)	0.66412 (6)	0.2150 (4)	0.0156 (9)
Se30	1.0847 (3)	0.66319 (6)	0.2089 (4)	0.0154 (9)
Se31	0.1068 (3)	0.66777 (5)	-0.2272 (4)	0.0166 (9)
Se32	0.4823 (3)	0.91309 (6)	0.7490 (4)	0.0169 (10)
Se33	0.8188 (3)	0.66766 (6)	-0.0164 (4)	0.0224 (11)
Se34	1.8634 (3)	0.72154 (6)	0.5122 (3)	0.0150 (9)
Se35	0.9542 (3)	0.91420 (6)	0.7006 (4)	0.0163 (9)
Se36	0.8230 (3)	0.71815 (6)	0.2031 (4)	0.0178 (10)
Se37	1.5939 (3)	0.72089 (6)	0.2138 (4)	0.0184 (10)
Se38	0.3624 (3)	0.66400 (6)	-0.4850 (4)	0.0152 (9)
Se39	0.4572 (3)	0.97135 (6)	0.7028 (4)	0.0190 (10)
Se40	0.7812 (2)	0.93444 (5)	0.2323 (3)	0.0150 (8)
Se41	1.8414 (3)	0.66332 (6)	0.4651 (4)	0.0172 (9)
Se42	0.7250 (3)	0.96818 (6)	0.0116 (4)	0.0175 (10)
Se43	0.9863 (3)	0.97088 (6)	0.7640 (3)	0.0150 (9)
Se44	0.4531 (3)	0.91378 (6)	0.9988 (4)	0.0182 (10)
Se45	0.2812 (3)	0.93386 (6)	1.1231 (4)	0.0199 (9)
Se46	0.6584 (3)	0.68454 (5)	-0.0166 (3)	0.0179 (9)
Se47	0.9832 (3)	0.91322 (6)	1.0068 (4)	0.0171 (10)
Se48	1.2675 (3)	0.68405 (6)	0.0926 (3)	0.0181 (9)
Cl1	1.2203 (7)	0.63687 (15)	-0.0152 (9)	0.022 (2)*
Cl2	1.2218 (8)	0.74843 (17)	0.2307 (11)	0.035 (3)*
Cl3	0.3422 (7)	0.88815 (15)	0.9989 (10)	0.022 (3)*
Cl4	0.9444 (8)	0.75008 (16)	0.2008 (11)	0.035 (3)*
Cl5	0.8350 (8)	0.88790 (16)	0.9798 (11)	0.028 (3)*
Cl6	0.2023 (8)	0.75092 (17)	-0.0340 (11)	0.034 (3)*
Cl7	0.0885 (8)	0.88932 (17)	0.7398 (11)	0.033 (3)*
Cl8	0.9708 (8)	0.63797 (16)	-0.2603 (10)	0.027 (3)*
Cl9	0.5978 (7)	0.88771 (13)	0.7417 (9)	0.019 (2)*
Cl10	-0.0219 (8)	0.74981 (17)	-0.2656 (11)	0.034 (3)*
Cl11	0.7055 (9)	0.74831 (18)	0.2136 (12)	0.039 (3)*
Cl12	0.7230 (8)	0.75087 (16)	-0.0132 (10)	0.031 (3)*
Cl13	0.4782 (7)	0.63944 (14)	-0.2578 (9)	0.020 (2)*
Cl14	1.4385 (8)	0.74860 (16)	0.4523 (11)	0.035 (3)*
Cl15	0.7021 (7)	0.63785 (16)	-0.0263 (10)	0.026 (3)*
Cl16	0.9658 (7)	0.63849 (15)	-0.0243 (10)	0.027 (2)*
Cl17	0.7048 (7)	0.85959 (16)	0.2259 (10)	0.026 (3)*
Cl18	0.4714 (8)	0.63940 (17)	-0.0122 (11)	0.032 (3)*
Cl19	0.3378 (6)	0.88694 (13)	1.2263 (8)	0.016 (2)*

CI20	0.9616 (9)	0.63774 (18)	0.2365 (12)	0.038 (3)*
CI21	0.0855 (7)	0.88734 (15)	0.9730 (10)	0.024 (2)*
CI22	0.4835 (8)	0.74876 (16)	-0.0040 (10)	0.032 (3)*
CI23	0.2040 (8)	0.85810 (17)	0.9732 (11)	0.030 (3)*
CI24	1.3371 (8)	0.60863 (17)	0.2333 (11)	0.029 (3)*
CI25	0.8356 (7)	0.61035 (16)	0.2289 (10)	0.026 (3)*
CI26	0.7153 (8)	0.85961 (19)	0.9856 (12)	0.038 (3)*
CI27	0.5891 (7)	0.88808 (16)	-0.0097 (10)	0.025 (3)*
CI28	1.4476 (7)	0.63901 (15)	0.2133 (9)	0.022 (2)*
CI29	0.7059 (8)	0.63807 (18)	0.2208 (11)	0.035 (3)*
CI30	0.5973 (8)	0.99811 (17)	0.0039 (11)	0.034 (3)*
CI31	0.5946 (8)	0.49836 (15)	0.7640 (10)	0.030 (3)*
CI32	1.4547 (7)	0.63925 (15)	0.4691 (10)	0.027 (2)*
CI33	1.2171 (7)	0.63797 (15)	0.2297 (10)	0.025 (2)*
CI34	1.2091 (7)	0.86071 (16)	0.2284 (10)	0.025 (3)*
CI35	1.3300 (7)	0.88723 (14)	0.4703 (10)	0.023 (2)*
CI36	0.5847 (7)	0.61036 (15)	-0.0220 (9)	0.022 (2)*
CI37	0.5921 (8)	0.99879 (17)	0.2158 (11)	0.039 (3)*
CI38	0.8420 (6)	0.88698 (14)	0.2402 (9)	0.018 (2)*
CI39	0.8435 (9)	1.00126 (19)	0.2294 (12)	0.040 (3)*
CI40	0.9596 (8)	0.63859 (16)	0.4735 (10)	0.029 (3)*
CI41	1.3414 (9)	1.00095 (19)	0.2497 (12)	0.041 (3)*
CI42	0.8491 (7)	1.00016 (15)	0.0147 (10)	0.030 (3)*
CI43	0.8391 (7)	0.88829 (14)	0.4706 (9)	0.023 (2)*
CI44	0.5927 (7)	0.89013 (14)	0.2269 (9)	0.023 (2)*
CI45	1.0885 (6)	0.61103 (14)	-0.0217 (9)	0.018 (2)*
CI46	1.3521 (8)	1.00044 (17)	0.4807 (11)	0.038 (3)*
CI47	1.0932 (6)	0.88796 (13)	0.2324 (8)	0.016 (2)*
CI48	0.1005 (9)	0.9987 (2)	0.9883 (12)	0.043 (4)*
O1	1.3423 (16)	0.6703 (3)	0.118 (2)	0.012 (6)*
O2	0.0907 (19)	0.7161 (4)	-0.137 (3)	0.030 (8)*
O3	0.589 (2)	0.6707 (4)	-0.137 (3)	0.027 (8)*
O4	1.8401 (18)	0.6696 (4)	0.364 (3)	0.024 (7)*
O5	0.8377 (18)	0.7166 (4)	0.110 (3)	0.027 (7)*
O6	1.3358 (18)	0.7141 (4)	0.350 (3)	0.024 (7)*
O7	0.2172 (16)	0.7164 (3)	-0.137 (2)	0.016 (6)*
O8	0.7183 (16)	0.7136 (3)	0.116 (2)	0.012 (6)*
O9	0.837 (2)	0.6764 (4)	-0.352 (3)	0.030 (8)*
O10	1.0826 (18)	0.9196 (4)	1.099 (2)	0.022 (6)*
O11	0.0791 (19)	0.9221 (4)	0.599 (3)	0.023 (7)*
O12	0.7136 (19)	0.6708 (4)	-0.133 (3)	0.025 (7)*
O13	0.5801 (16)	0.9218 (3)	0.347 (2)	0.015 (6)*
O14	0.8359 (18)	0.9220 (4)	0.106 (2)	0.022 (7)*
O15	0.4597 (17)	0.7164 (4)	-0.148 (2)	0.019 (6)*
O16	0.4585 (18)	0.9566 (4)	0.896 (2)	0.024 (6)*
O17	0.9566 (17)	0.7156 (3)	0.101 (2)	0.015 (6)*
O18	1.6735 (15)	0.7079 (3)	0.322 (2)	0.010 (5)*
O19	0.9599 (18)	0.9591 (4)	0.652 (2)	0.026 (7)*
O20	0.5825 (18)	0.9195 (4)	0.853 (2)	0.019 (7)*
O21	1.0950 (18)	0.6692 (4)	0.117 (3)	0.026 (7)*
O22	1.0897 (15)	0.7081 (3)	0.156 (2)	0.009 (5)*
O23	0.7102 (16)	0.9586 (4)	0.643 (2)	0.019 (6)*
O24	0.5401 (18)	0.9252 (4)	1.054 (2)	0.023 (6)*
O25	0.9571 (17)	0.9259 (3)	0.896 (2)	0.016 (6)*
O26	0.3346 (16)	0.7098 (3)	-0.356 (2)	0.014 (6)*
O27	1.5960 (18)	0.7100 (4)	0.408 (3)	0.017 (7)*
O28	0.827 (2)	0.9203 (5)	0.348 (3)	0.033 (9)*
O29	1.0407 (17)	0.9586 (3)	1.059 (2)	0.014 (6)*
O30	1.090 (2)	0.9634 (5)	0.863 (3)	0.039 (9)*
O31	1.3469 (17)	0.6947 (3)	0.227 (2)	0.015 (6)*

O32	0.7032 (18)	0.7170 (4)	-0.154 (3)	0.022 (7)*
O33	0.9194 (15)	0.7096 (3)	-0.184 (2)	0.009 (5)*
O34	1.2119 (17)	0.9197 (4)	0.359 (2)	0.012 (6)*
O35	1.4608 (19)	0.6713 (4)	0.105 (3)	0.021 (6)*
O36	1.4620 (17)	0.7158 (3)	0.356 (2)	0.020 (6)*
O37	0.3322 (17)	0.6751 (4)	-0.600 (2)	0.020 (6)*
O38	0.073 (2)	0.6961 (4)	-0.023 (3)	0.037 (8)*
O39	0.6279 (16)	0.9263 (3)	0.643 (2)	0.016 (6)*
O40	0.9538 (17)	0.9214 (4)	0.350 (2)	0.018 (6)*
O41	0.3408 (18)	0.7178 (4)	0.098 (3)	0.025 (7)*
O42	0.7195 (17)	0.9665 (4)	0.369 (2)	0.019 (7)*
O43	1.5947 (18)	0.7135 (4)	0.111 (3)	0.025 (7)*
O44	1.5043 (18)	0.6777 (4)	0.400 (2)	0.019 (6)*
O45	0.2150 (17)	0.9275 (4)	0.817 (2)	0.022 (6)*
O46	1.2095 (19)	0.9592 (4)	0.400 (3)	0.025 (7)*
O47	0.963 (2)	0.6699 (4)	0.357 (3)	0.030 (8)*
O48	0.3262 (18)	0.9204 (4)	1.091 (2)	0.022 (7)*
O49	1.4524 (19)	0.9207 (4)	0.350 (3)	0.018 (7)*
O50	0.2935 (17)	0.9599 (3)	0.808 (2)	0.013 (6)*
O51	0.6835 (19)	0.6709 (4)	0.084 (3)	0.020 (7)*
O52	0.5749 (17)	0.6986 (4)	-0.294 (2)	0.020 (6)*
O53	1.0927 (15)	0.6767 (3)	0.402 (2)	0.011 (5)*
O54	0.2042 (15)	0.7144 (3)	0.100 (2)	0.008 (5)*
O55	0.9637 (15)	0.9212 (3)	0.609 (2)	0.008 (5)*
O56	0.4623 (18)	0.9211 (3)	1.112 (3)	0.023 (6)*
O57	0.7089 (17)	0.9212 (4)	0.129 (2)	0.018 (6)*
O58	0.4648 (16)	0.6717 (3)	-0.390 (2)	0.010 (5)*
O59	0.5909 (18)	0.7176 (4)	-0.157 (2)	0.026 (7)*
O60	1.1684 (18)	0.6750 (4)	0.317 (3)	0.025 (7)*
O61	0.9642 (17)	0.9667 (3)	0.370 (2)	0.018 (6)*
O62	1.9244 (17)	0.6742 (4)	0.577 (2)	0.021 (6)*
O63	0.9523 (17)	0.9248 (3)	1.060 (2)	0.020 (6)*
O64	1.0818 (17)	0.9647 (4)	0.354 (2)	0.019 (6)*
O65	1.9659 (17)	0.7155 (3)	0.612 (2)	0.016 (6)*
O66	0.5792 (17)	0.9639 (4)	0.592 (2)	0.018 (6)*
O67	0.712 (2)	0.9593 (4)	0.816 (3)	0.024 (8)*
O68	0.4602 (18)	0.9655 (4)	0.602 (3)	0.023 (7)*
O69	1.2096 (16)	0.9588 (3)	0.568 (2)	0.017 (6)*
O70	0.7275 (18)	0.9457 (4)	0.255 (2)	0.018 (7)*
O71	1.2015 (19)	0.9471 (4)	0.240 (3)	0.025 (7)*
O72	1.4633 (17)	0.9657 (4)	0.355 (2)	0.021 (6)*
O73	0.6267 (18)	0.9610 (4)	0.402 (2)	0.023 (7)*
O74	0.8617 (17)	0.6971 (3)	0.265 (2)	0.014 (6)*
O75	0.7949 (16)	0.9263 (3)	0.813 (2)	0.012 (6)*
O76	0.8719 (16)	0.9596 (3)	0.891 (2)	0.015 (6)*
O77	1.5868 (17)	0.6724 (3)	0.609 (2)	0.018 (6)*
O78	0.005 (2)	0.7092 (4)	-0.600 (3)	0.043 (8)*
O79	0.2553 (18)	0.6766 (4)	-0.351 (2)	0.022 (7)*
O80	0.4542 (16)	0.9255 (3)	0.806 (2)	0.013 (6)*
O81	0.2157 (18)	0.9654 (4)	0.864 (3)	0.026 (7)*
O82	0.2018 (16)	0.9207 (3)	1.078 (2)	0.014 (6)*
O83	1.349 (2)	0.9676 (4)	0.114 (3)	0.033 (8)*
O84	1.4797 (19)	0.9487 (4)	0.238 (3)	0.029 (7)*
O85	1.5113 (17)	0.7096 (4)	0.159 (2)	0.022 (6)*
O86	1.5934 (16)	0.7112 (3)	0.573 (2)	0.016 (6)*
O87	0.7086 (16)	0.9270 (3)	0.563 (2)	0.015 (6)*
O88	0.8356 (17)	0.6755 (4)	-0.183 (2)	0.017 (6)*
O89	0.0932 (17)	0.6717 (4)	-0.141 (2)	0.020 (6)*
O90	0.0921 (15)	0.6761 (3)	-0.425 (2)	0.010 (5)*
O91	0.7062 (16)	0.9641 (4)	0.098 (2)	0.015 (6)*



O92	1.336 (2)	0.9202 (4)	0.352 (3)	0.023 (7)*
O93	0.5385 (17)	0.9583 (3)	0.810 (2)	0.012 (6)*
O94	0.1773 (17)	0.7097 (4)	-0.427 (2)	0.021 (6)*
O95	1.2923 (17)	0.9254 (3)	0.562 (2)	0.018 (6)*
O96	0.7923 (17)	0.9602 (3)	0.565 (2)	0.017 (6)*
O97	0.2104 (19)	0.6709 (4)	-0.136 (3)	0.026 (7)*
O98	0.4562 (17)	0.9592 (3)	1.057 (2)	0.016 (6)*
O99	1.8351 (15)	0.7087 (3)	0.402 (2)	0.009 (5)*
O100	1.0408 (16)	0.9252 (3)	0.817 (2)	0.012 (6)*
O101	1.5912 (16)	0.6771 (3)	0.325 (2)	0.014 (6)*
O102	0.4555 (19)	0.9252 (4)	0.638 (3)	0.019 (7)*
O103	1.1288 (15)	0.9264 (3)	0.405 (2)	0.007 (5)*
O104	1.4187 (16)	0.7102 (3)	0.568 (2)	0.015 (6)*
O105	1.6697 (16)	0.6772 (3)	0.566 (2)	0.014 (6)*
O106	0.2114 (15)	0.9275 (3)	0.649 (2)	0.011 (6)*
O107	0.7100 (15)	0.9275 (3)	0.396 (2)	0.012 (6)*
O108	1.2102 (16)	0.9633 (4)	0.114 (2)	0.014 (6)*
O109	0.9627 (19)	0.9651 (4)	1.113 (3)	0.021 (6)*
O110	1.5970 (18)	0.6751 (4)	0.162 (3)	0.021 (7)*
O111	0.0828 (18)	0.6889 (4)	-0.289 (2)	0.021 (7)*
O112	0.8480 (16)	0.6887 (3)	-0.020 (2)	0.011 (6)*
O113	1.8368 (18)	0.7101 (4)	0.570 (2)	0.025 (7)*
O114	0.3729 (14)	0.9270 (3)	0.8940 (18)	0.001 (5)*
O115	0.7536 (16)	0.7094 (3)	-0.353 (2)	0.017 (6)*
O116	0.7094 (17)	0.9199 (4)	0.860 (2)	0.021 (6)*
O117	1.0032 (19)	0.6745 (4)	0.158 (3)	0.030 (8)*
O118	0.8382 (17)	0.7143 (4)	-0.139 (2)	0.016 (6)*
O119	0.699 (2)	0.9476 (4)	-0.053 (3)	0.021 (8)*
O120	0.8750 (17)	0.9266 (3)	0.648 (2)	0.018 (6)*
O121	1.2356 (16)	0.6709 (3)	0.136 (2)	0.010 (5)*
O122	0.9617 (17)	0.6697 (3)	-0.145 (2)	0.016 (6)*
O123	0.0931 (15)	0.7146 (3)	-0.385 (2)	0.009 (5)*
O124	0.9804 (18)	0.9383 (4)	0.240 (3)	0.024 (7)*
O125	1.2492 (15)	0.7075 (3)	0.397 (2)	0.008 (5)*
O126	0.8390 (17)	0.6711 (4)	0.104 (2)	0.018 (6)*
O127	0.9749 (15)	0.9487 (3)	0.510 (2)	0.007 (5)*
O128	0.3414 (16)	0.6719 (3)	-0.136 (2)	0.013 (6)*
O129	1.0905 (15)	0.7101 (3)	0.323 (2)	0.015 (6)*
O130	1.7569 (15)	0.6756 (3)	0.409 (2)	0.012 (5)*
O131	0.4248 (15)	0.6773 (3)	-0.181 (2)	0.008 (5)*
O132	0.9588 (18)	0.9583 (4)	0.820 (2)	0.021 (6)*
O133	0.3424 (17)	0.6765 (3)	-0.422 (2)	0.020 (6)*
O134	0.8502 (18)	0.9674 (4)	0.371 (2)	0.020 (6)*
O135	0.1282 (16)	0.9608 (3)	0.644 (2)	0.016 (6)*
O136	0.832 (2)	0.9660 (5)	0.100 (3)	0.036 (9)*
O137	0.3342 (17)	0.7110 (3)	-0.186 (2)	0.020 (6)*
O138	1.3313 (18)	0.9657 (4)	0.348 (2)	0.022 (7)*
O139	0.3482 (17)	0.6976 (4)	-0.023 (2)	0.020 (6)*
O140	1.4721 (17)	0.9383 (3)	0.495 (2)	0.016 (6)*
O141	0.3758 (16)	0.9591 (3)	0.646 (2)	0.017 (6)*
O142	0.585 (2)	0.6946 (4)	-0.036 (3)	0.032 (8)*
O143	0.5877 (18)	0.9629 (4)	1.104 (2)	0.024 (7)*
O144	0.2230 (18)	0.9445 (4)	0.990 (2)	0.022 (7)*

*Table S 2. Atomic displacement parameters ( $\text{\AA}^2$ ) of  $\beta'$ -BiSeO<sub>3</sub>Cl*

	$U^{11}$	$U^{22}$	$U^{33}$	$U^{12}$	$U^{13}$	$U^{23}$
Bi1	0.0089 (9)	0.0283 (12)	0.0123 (10)	0.0010 (8)	0.0062 (9)	0.0014 (8)
Bi2	0.0247 (12)	0.0304 (13)	0.0290 (12)	-0.0001 (9)	0.0207 (11)	-0.0009 (9)
Bi3	0.0124 (9)	0.0321 (11)	0.0163 (9)	-0.0045 (8)	0.0082 (8)	-0.0034 (8)
Bi4	0.0140 (9)	0.0317 (12)	0.0202 (9)	-0.0020 (8)	0.0112 (8)	-0.0020 (8)
Bi5	0.0179 (10)	0.0263 (11)	0.0185 (9)	0.0022 (8)	0.0125 (9)	0.0014 (8)
Bi6	0.0136 (9)	0.0325 (12)	0.0203 (9)	-0.0023 (8)	0.0116 (9)	-0.0007 (8)
Bi7	0.0141 (10)	0.0264 (11)	0.0178 (10)	-0.0006 (7)	0.0114 (9)	-0.0003 (7)
Bi8	0.0178 (10)	0.0246 (10)	0.0171 (10)	-0.0014 (8)	0.0118 (9)	-0.0006 (8)
Bi9	0.0114 (10)	0.0255 (10)	0.0170 (10)	0.0002 (7)	0.0084 (9)	0.0000 (7)
Bi10	0.0179 (10)	0.0324 (12)	0.0226 (10)	-0.0016 (8)	0.0157 (9)	0.0014 (8)
Bi11	0.0135 (10)	0.0303 (12)	0.0207 (11)	-0.0039 (8)	0.0109 (10)	-0.0050 (8)
Bi12	0.0191 (10)	0.0277 (11)	0.0181 (9)	0.0028 (8)	0.0120 (9)	0.0039 (8)
Bi13	0.0157 (11)	0.0237 (11)	0.0176 (11)	0.0001 (7)	0.0118 (10)	0.0002 (7)
Bi14	0.0172 (10)	0.0233 (11)	0.0150 (9)	-0.0005 (7)	0.0117 (9)	0.0001 (7)
Bi15	0.0192 (10)	0.0247 (10)	0.0194 (10)	0.0017 (8)	0.0142 (10)	0.0022 (8)
Bi16	0.0182 (10)	0.0298 (11)	0.0187 (9)	-0.0009 (8)	0.0139 (9)	-0.0003 (7)
Bi17	0.0181 (10)	0.0239 (11)	0.0206 (10)	-0.0009 (8)	0.0117 (9)	-0.0020 (8)
Bi18	0.0188 (10)	0.0266 (10)	0.0197 (9)	-0.0006 (8)	0.0146 (9)	-0.0020 (7)
Bi19	0.0287 (12)	0.0275 (13)	0.0259 (12)	0.0029 (9)	0.0182 (11)	0.0021 (8)
Bi20	0.0109 (10)	0.0292 (12)	0.0119 (10)	-0.0003 (8)	0.0078 (9)	-0.0015 (7)
Bi21	0.0182 (10)	0.0262 (11)	0.0238 (9)	-0.0022 (8)	0.0148 (9)	-0.0001 (8)
Bi22	0.0185 (11)	0.0261 (11)	0.0157 (10)	0.0003 (8)	0.0122 (10)	-0.0015 (8)
Bi23	0.0177 (10)	0.0262 (10)	0.0171 (10)	-0.0003 (8)	0.0124 (9)	-0.0011 (7)
Bi24	0.0191 (11)	0.0264 (11)	0.0182 (10)	0.0020 (8)	0.0140 (10)	0.0008 (7)
Bi25	0.0157 (10)	0.0261 (10)	0.0218 (10)	0.0001 (8)	0.0128 (9)	0.0003 (8)
Bi26	0.0112 (10)	0.0298 (11)	0.0173 (9)	0.0001 (7)	0.0101 (9)	0.0014 (7)
Bi27	0.0136 (10)	0.0270 (11)	0.0186 (10)	-0.0023 (8)	0.0102 (9)	0.0007 (8)
Bi28	0.0145 (10)	0.0315 (11)	0.0184 (10)	-0.0023 (8)	0.0113 (9)	-0.0009 (8)
Bi29	0.0126 (10)	0.0269 (11)	0.0155 (10)	-0.0003 (7)	0.0089 (9)	-0.0021 (8)
Bi30	0.0178 (11)	0.0221 (12)	0.0207 (11)	0.0001 (8)	0.0141 (10)	-0.0011 (7)
Bi31	0.0134 (9)	0.0298 (11)	0.0196 (9)	0.0001 (8)	0.0109 (9)	0.0002 (8)
Bi32	0.0142 (10)	0.0329 (12)	0.0193 (10)	-0.0014 (9)	0.0117 (9)	-0.0031 (9)
Bi33	0.0209 (10)	0.0293 (11)	0.0208 (10)	-0.0008 (8)	0.0148 (9)	-0.0005 (8)
Bi34	0.0195 (10)	0.0296 (11)	0.0233 (9)	-0.0011 (8)	0.0160 (9)	-0.0010 (8)
Bi35	0.0240 (12)	0.0234 (12)	0.0284 (12)	-0.0002 (8)	0.0164 (11)	-0.0021 (8)
Bi36	0.0136 (10)	0.0280 (11)	0.0213 (10)	0.0015 (8)	0.0112 (9)	0.0018 (8)
Bi37	0.0206 (10)	0.0243 (10)	0.0212 (9)	0.0002 (8)	0.0155 (9)	0.0010 (7)
Bi38	0.0173 (11)	0.0282 (11)	0.0175 (10)	-0.0021 (8)	0.0117 (10)	-0.0022 (8)
Bi39	0.0235 (11)	0.0245 (11)	0.0177 (10)	-0.0019 (8)	0.0144 (10)	-0.0020 (7)
Bi40	0.0211 (10)	0.0262 (11)	0.0224 (10)	0.0000 (8)	0.0156 (9)	-0.0016 (8)
Bi41	0.0250 (12)	0.0247 (11)	0.0259 (11)	0.0028 (8)	0.0199 (11)	0.0028 (8)
Bi42	0.0149 (10)	0.0346 (11)	0.0200 (9)	-0.0002 (8)	0.0110 (9)	0.0007 (8)
Bi43	0.0133 (9)	0.0303 (11)	0.0152 (9)	0.0011 (8)	0.0085 (8)	0.0010 (7)
Bi44	0.0133 (10)	0.0276 (12)	0.0168 (10)	0.0002 (8)	0.0092 (9)	-0.0004 (8)
Bi45	0.0192 (10)	0.0248 (10)	0.0222 (9)	0.0013 (8)	0.0160 (9)	0.0016 (7)
Bi46	0.0196 (10)	0.0247 (11)	0.0196 (9)	-0.0006 (8)	0.0124 (9)	0.0024 (8)
Bi47	0.0262 (12)	0.0218 (12)	0.0265 (12)	-0.0007 (8)	0.0154 (11)	-0.0034 (8)
Bi48	0.0148 (10)	0.0291 (12)	0.0183 (10)	0.0010 (8)	0.0116 (10)	0.0006 (7)
Se1	0.015 (2)	0.018 (2)	0.019 (2)	0.0055 (19)	0.012 (2)	0.0058 (19)
Se2	0.015 (2)	0.028 (3)	0.010 (2)	-0.002 (2)	0.009 (2)	-0.0045 (19)
Se3	0.016 (3)	0.020 (3)	0.014 (2)	0.000 (2)	0.009 (2)	0.0012 (18)
Se4	0.010 (2)	0.020 (2)	0.013 (2)	0.0002 (19)	0.006 (2)	0.0015 (18)
Se5	0.014 (3)	0.025 (3)	0.020 (2)	-0.002 (2)	0.014 (2)	-0.002 (2)
Se6	0.011 (2)	0.018 (3)	0.018 (2)	-0.0006 (19)	0.010 (2)	0.0013 (19)
Se7	0.012 (2)	0.024 (2)	0.014 (2)	-0.0016 (18)	0.011 (2)	0.0009 (18)
Se8	0.015 (2)	0.022 (3)	0.014 (2)	-0.0028 (19)	0.011 (2)	-0.0036 (18)
Se9	0.009 (2)	0.027 (3)	0.008 (2)	0.0023 (19)	0.003 (2)	0.0015 (18)

Se10	0.013 (2)	0.016 (2)	0.017 (2)	-0.0013 (18)	0.010 (2)	-0.0023 (18)
Se11	0.010 (2)	0.023 (3)	0.009 (2)	0.0055 (18)	0.005 (2)	0.0021 (17)
Se12	0.012 (2)	0.024 (3)	0.016 (2)	0.0013 (19)	0.012 (2)	0.0004 (18)
Se13	0.011 (2)	0.024 (3)	0.013 (2)	0.0041 (19)	0.009 (2)	0.0025 (18)
Se14	0.017 (3)	0.015 (3)	0.023 (3)	0.0015 (19)	0.014 (2)	-0.001 (2)
Se15	0.011 (2)	0.025 (3)	0.009 (2)	-0.0004 (18)	0.008 (2)	-0.0001 (18)
Se16	0.011 (2)	0.025 (3)	0.006 (2)	0.0009 (19)	0.004 (2)	-0.0014 (18)
Se17	0.006 (2)	0.029 (3)	0.017 (2)	0.0026 (18)	0.010 (2)	0.0035 (19)
Se18	0.017 (2)	0.022 (3)	0.012 (2)	0.0003 (19)	0.012 (2)	0.0018 (18)
Se19	0.012 (2)	0.020 (2)	0.013 (2)	0.0016 (18)	0.005 (2)	0.0017 (18)
Se20	0.012 (2)	0.023 (3)	0.025 (3)	0.000 (2)	0.014 (2)	-0.001 (2)
Se21	0.020 (3)	0.015 (3)	0.014 (2)	0.003 (2)	0.010 (2)	0.0024 (18)
Se22	0.016 (3)	0.019 (2)	0.017 (2)	0.0013 (19)	0.011 (2)	-0.0009 (18)
Se23	0.009 (2)	0.021 (3)	0.018 (2)	-0.0021 (18)	0.009 (2)	-0.0038 (19)
Se24	0.002 (2)	0.022 (2)	0.007 (2)	0.0018 (17)	0.0004 (19)	0.0026 (17)
Se25	0.005 (2)	0.030 (3)	0.007 (2)	0.0027 (18)	0.002 (2)	-0.0002 (18)
Se26	0.007 (2)	0.024 (3)	0.014 (2)	0.0004 (18)	0.009 (2)	0.0006 (18)
Se27	0.012 (2)	0.020 (3)	0.015 (2)	-0.0010 (18)	0.009 (2)	0.0011 (18)
Se28	0.009 (2)	0.034 (3)	0.0015 (19)	0.000 (2)	0.0015 (19)	-0.0013 (18)
Se29	0.017 (2)	0.016 (2)	0.015 (2)	0.0001 (19)	0.012 (2)	-0.0005 (17)
Se30	0.014 (2)	0.021 (2)	0.014 (2)	0.0017 (18)	0.011 (2)	0.0019 (17)
Se31	0.020 (3)	0.014 (2)	0.023 (2)	0.0003 (18)	0.017 (2)	0.0026 (18)
Se32	0.014 (2)	0.019 (2)	0.020 (2)	0.0000 (18)	0.013 (2)	-0.0009 (18)
Se33	0.022 (3)	0.021 (3)	0.014 (2)	-0.001 (2)	0.009 (2)	-0.0004 (18)
Se34	0.010 (2)	0.022 (2)	0.007 (2)	0.0003 (19)	0.005 (2)	0.0013 (17)
Se35	0.014 (2)	0.028 (3)	0.015 (2)	-0.0008 (19)	0.013 (2)	0.0019 (18)
Se36	0.009 (2)	0.027 (3)	0.016 (2)	-0.0010 (19)	0.009 (2)	-0.0026 (19)
Se37	0.021 (3)	0.018 (2)	0.020 (2)	0.0027 (19)	0.016 (2)	-0.0004 (18)
Se38	0.010 (2)	0.022 (2)	0.017 (2)	-0.0001 (18)	0.010 (2)	0.0000 (19)
Se39	0.016 (2)	0.028 (3)	0.020 (2)	0.001 (2)	0.015 (2)	-0.001 (2)
Se40	0.004 (2)	0.024 (2)	0.012 (2)	0.0027 (17)	0.0039 (19)	-0.0003 (17)
Se41	0.018 (2)	0.016 (2)	0.019 (2)	0.0010 (18)	0.013 (2)	0.0008 (18)
Se42	0.013 (2)	0.026 (3)	0.011 (2)	0.0029 (19)	0.007 (2)	0.0010 (18)
Se43	0.010 (2)	0.022 (2)	0.009 (2)	0.0014 (18)	0.006 (2)	0.0006 (17)
Se44	0.015 (2)	0.023 (3)	0.016 (2)	-0.001 (2)	0.011 (2)	-0.0011 (19)
Se45	0.015 (2)	0.029 (3)	0.019 (2)	0.0016 (19)	0.013 (2)	0.0002 (18)
Se46	0.014 (2)	0.026 (2)	0.011 (2)	0.0014 (19)	0.008 (2)	-0.0002 (17)
Se47	0.009 (2)	0.024 (3)	0.019 (2)	-0.0023 (18)	0.010 (2)	-0.0025 (19)
Se48	0.012 (2)	0.028 (3)	0.016 (2)	0.0032 (18)	0.010 (2)	0.0019 (18)

**Table S 3. Selected Bi-O distances ( $\text{\AA}$ ) in  $\beta$ '-BiSeO<sub>3</sub>Cl ( $d_{\text{max}}=3\text{\AA}$ )**

Atom1	Atom2	d, $\text{\AA}$	Atom1	Atom2	d, $\text{\AA}$	Atom1	Atom2	d, $\text{\AA}$	
Bi1	O23	2.336(33)	Bi9	O14	2.299(44)	Bi15	O131	2.264(39)	
	O75	2.366(40)		O116	2.301(35)		O15	2.383(21)	
	O76	2.399(32)		O67	2.356(27)		O26	2.402(45)	
	O87	2.423(21)		O119	2.387(33)		O142	2.453(40)	
	O132	2.448(36)		O75	2.531(44)		O133	2.525(38)	
	O120	2.492(42)		O136	2.643(24)		O104	2.609(32)	
	O25	2.501(22)		O63	2.663(28)		O3	2.734(25)	
	O96	2.502(33)		O76	2.849(36)		O59	2.760(38)	
Bi2	O103	2.472(39)	Bi10	O6	2.115(28)	Bi16	O116	2.602(38)	
	O69	2.479(31)		O54	2.268(29)		O20	2.973(38)	
	O64	2.482(39)		O36	2.450(53)	Bi17	O82	2.842(29)	
	O61	2.486(28)		O41	2.562(37)		Bi18	O136	2.142(30)
	O135	2.494(31)	Bi11	O31	2.733(47)	O61		2.473(21)	
	O40	2.636(30)		O102	2.390(35)	O109	2.500(33)		
	O106	2.639(20)		O140	2.436(41)	O64	2.739(34)		
	O124	2.666(40)		O68	2.445(49)	Bi19	O66	2.399(35)	
O11	2.668(48)		O93	2.490(23)	O72		2.441(36)		
Bi3	O127	2.822(43)		O39	2.539(29)		O39	2.465(10)	
	O143	2.220(31)		O66	2.565(55)		O73	2.528(15)	
	O91	2.236(40)		O67	2.670(25)		O23	2.536(22)	
	O42	2.480(39)		O119	2.765(21)		O140	2.607(35)	
	O134	2.588(28)		O20	2.809(40)		O87	2.623(14)	
Bi4	O70	2.655(31)		O116	2.888(25)		O49	2.629(20)	
	O122	2.535(13)	Bi12	O43	2.169(31)		O13	2.706(14)	
	O21	2.743(20)		O8	2.265(42)		O84	2.733(30)	
O89	2.965(25)	O15		2.485(41)	Bi20	O106	2.356(34)		
Bi5	O121	2.836(12)		O59		2.636(40)	O69	2.381(35)	
	Bi6	O30	2.192(14)		O142	2.736(39)	O16	2.410(53)	
O108		2.303(44)	Bi13	O115	2.347(32)	O50	2.419(13)		
O81		2.446(14)		O27	2.395(38)	O141	2.457(23)		
O83		2.559(20)		O9	2.396(28)	O114	2.463(29)		
O144		2.735(11)		O105	2.404(50)	O80	2.469(38)		
Bi7		O25	2.267(24)		O18	2.435(27)		O95	2.476(29)
		O100	2.352(33)		O113	2.436(26)	Bi21	O51	2.590(30)
		O10	2.366(38)		O101	2.443(41)		Bi22	O52
	O82	2.462(54)		O130	2.482(32)	O58	2.317(23)		
	O29	2.478(36)	Bi14	O80	2.304(14)	O77	2.342(46)		
	O132	2.512(32)		O24	2.334(32)	O104	2.446(32)		
	O30	2.797(23)		O20	2.415(37)	O44	2.576(44)		
	O108	2.826(12)		O16	2.469(28)	O86	2.580(36)		
Bi8	O44	2.270(34)		O93	2.489(41)	O37	2.682(41)		
	O31	2.372(34)		O57	2.559(32)	O6	2.848(31)		
	O36	2.373(39)		O143	2.759(37)	O36	2.965(21)		
	O27	2.495(29)		O91	2.840(21)				
	O101	2.610(40)							
	O85	2.644(25)							
	O1	2.675(51)							
	O41	2.689(28)							
O35	2.902(34)								

*Table S 4. Continued*

Atom1	Atom2	d, Å	Atom1	Atom2	d, Å	Atom1	Atom2	d, Å			
Bi23	O139	2.215(24)	Bi29	O127	2.242(42)	Bi36	O34	2.334(24)			
	O35	2.326(41)		O55	2.303(55)		O46	2.402(41)			
	O128	2.340(41)		O11	2.373(31)		O71	2.441(51)			
	O85	2.418(30)		O19	2.380(21)		O92	2.479(50)			
	O137	2.543(32)		O135	2.583(36)		O95	2.509(33)			
	O131	2.616(33)		O100	2.649(37)		O102	2.656(23)			
	O110	2.732(13)		O45	2.651(29)		O138	2.694(18)			
	O43	2.877(12)		O30	2.811(27)		O141	2.779(12)			
	Bi24	O47		2.271(32)	Bi30		O53	2.318(54)	Bi37	O68	2.999(37)
		O74		2.314(22)			O94	2.375(40)		O5	2.084(11)
O126		2.333(21)	O79	2.384(24)		O17	2.440(37)				
O78		2.376(23)	O125	2.423(30)		O32	2.468(16)				
O53		2.558(36)	O129	2.430(48)		O118	2.776(13)				
O117		2.671(29)	O26	2.447(36)		Bi38	O122	2.322(36)			
O5		2.708(40)	O60	2.550(37)			O33	2.405(27)			
O129		2.576(44)	O133	2.555(35)		O89	2.417(47)				
Bi25		O138	2.163(34)	Bi31		O47	2.657(38)	O38		2.424(31)	
		O72	2.433(33)			O4	2.948(44)	O9		2.518(37)	
	O68	2.472(28)	Bi32	O107	2.279(27)	O2	2.687(20)				
	O66	2.724(44)		O42	2.337(24)	O62	2.694(41)				
Bi26	O84	2.202(46)	Bi33	O96	2.391(26)	Bi39	O113	2.840(47)			
	O56	2.297(23)		O70	2.428(50)		O112	2.306(21)			
	O13	2.321(31)		O120	2.599(39)		O17	2.394(33)			
	O98	2.417(21)		O19	2.617(40)		O22	2.471(25)			
	O107	2.579(36)		O134	2.728(40)		O117	2.481(42)			
	O73	2.593(27)		O28	2.747(33)		O118	2.483(31)			
	O24	2.662(33)		O55	2.920(24)		O88	2.543(43)			
	O143	2.825(46)		O3	2.206(30)		O33	2.666(32)			
	Bi27	O124		2.245(46)	Bi34		O12	2.363(42)	Bi40	O38	2.883(51)
		O109		2.361(26)			O58	2.548(34)		O21	2.929(41)
O63		2.454(40)	O77	2.749(40)		O122	2.971(26)				
O29		2.489(22)	O34	2.529(20)		O1	2.186(39)				
O64		2.520(56)	O92	2.743(21)		O97	2.406(31)				
O103		2.572(29)	O10	2.886(45)		O35	2.538(48)				
O46		2.647(30)	Bi35	O32		2.488(33)	O128	2.766(31)			
O71		2.841(42)		O118		2.496(13)	Bi41	O111		2.330(27)	
O10		2.871(48)	O88	2.525(13)		O65		2.438(12)			
Bi28		O34	2.955(21)	O86		2.535(26)	O62	2.467(20)			
	O45	2.235(15)	O115	2.611(32)	O90	2.505(40)					
	O81	2.334(29)	O12	2.621(30)	O99	2.529(36)					
	O144	2.459(56)	O112	2.661(30)	O123	2.567(38)					
	O50	2.496(26)	O105	2.673(41)	O78	2.655(33)					
	O114	2.570(34)	O77	2.679(26)	O4	2.788(37)					
	O98	2.593(21)	O52	2.782(31)	O74	2.802(36)					
	O48	2.617(21)			O47	2.926(34)					
	O83	2.646(32)			Bi42	O48	2.288(34)				
	O56	2.895(38)				O49	2.381(24)				
				O56		2.563(42)					
						O13	2.736(34)				

*Table S 5. Continued*

Atom1	Atom2	d, Å
Bi43	O28	2.248(21)
	O40	2.284(43)
	O55	2.610(27)
	O11	2.652(24)
Bi44	O130	2.314(34)
	O110	2.325(58)
	O4	2.449(35)
	O99	2.455(29)
	O18	2.509(35)
	O51	2.563(10)
	O43	2.750(18)
	O8	2.818(38)
	Bi45	O2
O7		2.417(35)
O65		2.473(42)
O123		2.765(32)
Bi46	O57	2.694(29)
	O28	2.991(26)
Bi47	O123	2.444(56)
	O7	2.473(29)
	O90	2.483(26)
	O137	2.539(28)
	O111	2.560(48)
	O94	2.576(50)
	O97	2.620(16)
	O139	2.709(13)
	O128	2.732(27)
Bi48	O79	2.733(37)
	O60	2.292(40)
	O37	2.346(35)
	O21	2.368(29)
	O125	2.473(11)
	O22	2.476(19)
	O121	2.522(33)
	O6	2.826(37)
	O54	2.892(31)
	O99	2.455(21)
	O18	2.509(38)
	O51	2.563(46)
O43	2.750(29)	
O8	2.818(35)	

**Table S 6. Selected Bi-Cl distances ( $\text{\AA}$ ) in  $\beta'$ -BiSeO<sub>3</sub>Cl ( $d_{\max}=4\text{\AA}$ )**

Atom1	Atom2	d, $\text{\AA}$	Atom1	Atom2	d, $\text{\AA}$	Atom1	Atom2	d, $\text{\AA}$
Bi1	Cl24	3.966(14)	Bi25	Cl46	2.628(21)	Bi48	Cl33	3.927(12)
Bi3	Cl30	2.738(13)		Cl41	2.676(15)			
	Cl37	2.922(21)		Cl37	3.341(12)			
	Cl39	3.461(23)		Cl30	3.425(20)			
Bi4	Cl42	3.794(12)	Bi26	Cl44	3.983(12)			
	Cl16	2.483(20)	Bi31	Cl40	2.493(13)			
	Cl45	2.652(12)		Cl25	2.509(13)			
	Cl8	2.653(14)		Cl20	2.538(26)			
	Cl33	3.075(11)		Cl29	3.169(22)			
	Cl1	3.317(19)		Cl15	3.259(11)			
Bi5	Cl24	2.460(14)	Bi33	Cl13	2.650(18)			
	Cl33	2.548(20)		Cl15	2.690(12)			
	Cl32	2.560(11)		Cl34	3.168(20)			
	Cl28	2.905(20)		Cl47	3.173(11)			
	Cl1	2.977(12)		Cl32	3.472(12)			
Bi6	Cl48	2.747(23)	Bi34	Cl35	2.484(11)			
	Cl31	2.897(12)		Cl47	2.584(16)			
	Cl41	3.422(14)		Cl34	2.674(13)			
	Cl46	3.790(22)		Cl19	3.199(17)			
Bi7	Cl21	3.970(12)		Cl21	3.312(13)			
Bi10	Cl2	2.751(21)	Bi37	Cl4	2.607(12)			
	Cl14	2.910(13)		Cl12	2.684(20)			
	Cl6	3.430(14)		Cl14	3.329(22)			
	Cl10	3.780(21)		Cl2	3.442(15)			
Bi12	Cl11	2.760(14)	Bi40	Cl28	2.648(10)			
	Cl22	2.933(20)		Cl1	2.661(18)			
	Cl12	3.421(21)		Cl43	3.215(12)			
	Cl4	3.798(13)		Cl17	3.270(13)			
Bi13	Cl23	3.935(14)		Cl18	3.469(22)			
Bi14	Cl27	3.904(13)	Bi42	Cl19	2.655(16)			
Bi16	Cl9	2.528(10)		Cl3	2.725(13)			
	Cl26	2.568(15)		Cl8	3.136(13)			
	Cl5	2.569(22)		Cl45	3.165(10)			
	Cl27	3.202(21)		Cl44	3.525(19)			
	Cl38	3.208(12)	Bi43	Cl38	2.693(11)			
Bi17	Cl23	2.501(14)		Cl43	2.807(19)			
	Cl21	2.550(20)		Cl36	3.144(18)			
	Cl7	2.603(14)		Cl18	3.325(14)			
	Cl19	2.961(90)		Cl17	3.471(13)			
	Cl3	3.020(19)	Bi44	Cl29	3.940(14)			
Bi18	Cl42	2.612(13)	Bi45	Cl10	2.631(20)			
	Cl39	2.680(23)		Cl6	2.695(13)			
	Cl31	3.377(19)		Cl22	3.360(14)			
	Cl48	3.471(13)		Cl11	3.462(25)			
Bi21	Cl29	2.519(13)	Bi46	Cl44	2.530(20)			
	Cl36	2.522(12)		Cl17	2.533(13)			
	Cl18	2.624(22)		Cl27	2.549(12)			
	Cl15	2.835(21)		Cl43	2.965(10)			
	Cl13	2.977(12)		Cl38	3.034(17)			

*Table S 7. Selected Se-O distances (Å) in  $\beta'$ -BiSeO<sub>3</sub>Cl*

Atom1	Atom2	d, Å	Atom1	Atom2	d, Å	Atom1	Atom2	d, Å
Se1	O59	1.585(46)	Se17	O129	1.643(32)	Se33	O126	1.662(39)
	O32	1.672(33)		O22	1.737(39)		O12	1.716(28)
	O52	1.722(31)		O17	1.765(27)		O112	1.762(28)
Se2	O83	1.679(28)	Se18	O95	1.617(23)	Se34	O113	1.670(44)
	O84	1.724(35)		O103	1.684(30)		O99	1.705(31)
	O72	1.774(41)		O34	1.709(43)		O65	1.710(29)
Se3	O137	1.689(42)	Se19	O14	1.733(25)	Se35	O120	1.645(33)
	O15	1.702(29)		O40	1.740(41)		O100	1.696(21)
	O26	1.740(33)		O124	1.756(36)		O55	1.716(41)
Se4	O41	1.675(54)	Se20	O134	1.658(33)	Se36	O8	1.740(31)
	O7	1.745(24)		O61	1.688(45)		O5	1.750(59)
	O139	1.793(33)		O127	1.709(24)		O74	1.771(23)
Se5	O67	1.724(46)	Se21	O90	1.732(33)	Se37	O85	1.646(36)
	O23	1.733(42)		O47	1.751(32)		O18	1.685(21)
	O66	1.764(27)		O53	1.759(39)		O43	1.757(55)
Se6	O86	1.671(33)	Se22	O104	1.678(21)	Se38	O133	1.673(41)
	O27	1.725(52)		O125	1.742(30)		O37	1.678(35)
	O36	1.778(27)		O6	1.762(56)		O58	1.751(28)
Se7	O140	1.690(24)	Se23	O96	1.665(23)	Se39	O141	1.658(31)
	O49	1.706(59)		O73	1.675(36)		O93	1.698(22)
	O92	1.724(37)		O42	1.699(44)		O68	1.726(56)
Se8	O46	1.675(53)	Se24	O98	1.705(42)	Se40	O57	1.622(25)
	O69	1.715(33)		O16	1.706(34)		O28	1.726(41)
	O64	1.750(28)		O143	1.740(29)		O70	1.730(45)
Se9	O87	1.660(33)	Se25	O108	1.704(39)	Se41	O62	1.640(24)
	O107	1.727(39)		O138	1.723(27)		O4	1.673(55)
	O13	1.766(25)		O71	1.744(36)		O130	1.714(31)
Se10	O105	1.644(31)	Se26	O115	1.646(21)	Se42	O91	1.743(44)
	O44	1.724(26)		O33	1.696(30)		O119	1.748(34)
	O77	1.733(42)		O118	1.724(42)		O136	1.752(39)
Se11	O54	1.660(22)	Se27	O79	1.643(25)	Se43	O19	1.699(36)
	O2	1.757(55)		O128	1.733(40)		O132	1.709(44)
	O38	1.800(35)		O131	1.745(30)		O30	1.763(35)
Se12	O88	1.680(43)	Se28	O76	1.705(21)	Se44	O114	1.687(20)
	O9	1.701(47)		O29	1.725(33)		O24	1.726(38)
	O122	1.730(28)		O109	1.754(55)		O56	1.767(53)
Se13	O106	1.685(39)	Se29	O101	1.710(32)	Se45	O82	1.717(33)
	O45	1.704(34)		O110	1.718(54)		O144	1.729(28)
	O11	1.785(31)		O35	1.737(29)		O48	1.766(44)
Se14	O39	1.694(21)	Se30	O117	1.645(41)	Se46	O51	1.652(44)
	O75	1.712(31)		O60	1.668(27)		O142	1.654(50)
	O116	1.812(43)		O21	1.712(57)		O3	1.744(30)
Se15	O123	1.691(39)	Se31	O89	1.644(45)	Se47	O10	1.673(32)
	O94	1.708(35)		O97	1.692(35)		O63	1.690(42)
	O78	1.715(28)		O111	1.774(31)		O25	1.724(33)
Se16	O135	1.687(21)	Se32	O20	1.684(29)	Se48	O121	1.656(39)
	O50	1.694(33)		O102	1.696(46)		O31	1.754(21)
	O81	1.788(55)		O80	1.725(40)		O1	1.784(36)



Table S 8. Selected Se-O angles in  $\beta'$ -BiSeO<sub>3</sub>Cl

A1	A2	A3	^ (°)	A1	A2	A3	^ (°)	A1	A2	A3	^ (°)
			A2-A1-A3				A2-A1-A3				A2-A1-A3
Se1	O59	O32	105.2	Se17	O129	O22	105.0	Se33	O12	O126	104.9
	O59	O52	94.8		O129	O17	99.1		O12	O112	94.6
	O32	O52	94.1		O22	O17	92.1		O126	O112	95.2
Se2	O72	O84	93.0	Se18	O95	O103	105.3	Se34	O99	O113	102.8
	O72	O83	105.4		O95	O34	92.4		O99	O65	93.8
	O84	O83	99.3		O103	O34	97.3		O113	O65	98.2
Se3	O15	O137	94.4	Se19	O40	O14	108.5	Se35	O120	O100	105.0
	O15	O26	91.3		O40	O124	93.7		O120	O55	97.5
	O137	O26	104.9		O14	O124	99.6		O100	O55	94.2
Se4	O41	O7	103.8	Se20	O127	O134	93.0	Se36	O8	O5	104.5
	O41	O139	96.2		O127	O61	96.1		O8	O74	96.5
	O7	O139	91.2		O134	O61	101.6		O5	O74	94.6
Se5	O67	O23	105.2	Se21	O90	O47	94.5	Se37	O85	O18	105.0
	O67	O66	97.9		O90	O53	107.1		O85	O43	93.2
	O23	O66	91.9		O47	O53	92.5		O18	O43	94.8
Se6	O86	O27	104.7	Se22	O104	O125	104.8	Se38	O37	O133	105.7
	O86	O36	97.1		O104	O6	96.9		O37	O58	90.1
	O27	O36	94.1		O125	O6	94.7		O133	O58	93.5
Se7	O140	O92	98.2	Se23	O73	O96	104.2	Se39	O141	O93	104.8
	O140	O49	93.0		O73	O42	98.2		O141	O68	95.7
	O92	O49	105.2		O96	O42	89.0		O93	O68	94.3
Se8	O69	O46	106.5	Se24	O16	O98	102.6	Se40	O57	O70	102.1
	O69	O64	94.0		O16	O143	90.4		O57	O28	94.6
	O46	O64	93.6		O98	O143	92.4		O70	O28	93.3
Se9	O87	O107	106.7	Se25	O71	O138	96.5	Se41	O62	O4	97.7
	O87	O13	95.3		O71	O108	93.5		O62	O130	108.7
	O107	O13	92.7		O138	O108	103.1		O4	O130	94.6
Se10	O105	O44	105.8	Se26	O115	O33	107.7	Se42	O119	O136	95.8
	O105	O77	95.1		O115	O118	94.3		O119	O91	97.0
	O44	O77	90.4		O33	O118	93.0		O136	O91	107.4
Se11	O54	O2	106.4	Se27	O79	O128	98.9	Se43	O132	O19	107.5
	O54	O38	97.7		O79	O131	105.9		O132	O30	91.8
	O2	O38	93.5		O128	O131	90.4		O19	O30	92.1
Se12	O88	O9	107.2	Se28	O76	O29	105.6	Se44	O114	O24	104.1
	O88	O122	95.1		O76	O109	94.4		O114	O56	95.8
	O9	O122	92.2		O29	O109	93.8		O24	O56	91.2
Se13	O106	O45	102.2	Se29	O110	O101	105.4	Se45	O144	O82	94.6
	O106	O11	95.3		O110	O35	93.8		O144	O48	92.4
	O45	O11	93.7		O101	O35	94.9		O82	O48	99.0
Se14	O75	O39	105.0	Se30	O60	O117	108.1	Se46	O51	O3	95.6
	O75	O116	92.7		O60	O21	88.9		O51	O142	97.6
	O39	O116	94.1		O117	O21	101.4		O3	O142	93.9
Se15	O78	O123	96.3	Se31	O89	O97	101.0	Se47	O63	O25	103.0
	O78	O94	107.0		O89	O111	98.2		O63	O10	101.1
	O123	O94	94.5		O97	O111	91.8		O25	O10	92.6
Se16	O135	O81	95.7	Se32	O102	O20	97.4	Se48	O121	O31	97.7
	O135	O50	104.4		O102	O80	104.2		O121	O1	98.8
	O81	O50	90.5		O20	O80	93.4		O31	O1	92.5

*Table S 9. Bond sum valence values of selected atoms in  $\beta'$ -BiSeO<sub>3</sub>Cl*

<b>Atom</b>	<b>BVS</b>	<b>Atom</b>	<b>BVS</b>	<b>Atom</b>	<b>BVS</b>	<b>Atom</b>	<b>BVS</b>
<b>Bi1</b>	3.31(19)	<b>Bi25</b>	3.20(17)	<b>Se1</b>	4.7(5)	<b>Se25</b>	4.0(4)
<b>Bi2</b>	2.69(15)	<b>Bi26</b>	3.2(2)	<b>Se2</b>	3.2(3)	<b>Se26</b>	3.8(4)
<b>Bi3</b>	3.04(17)	<b>Bi27</b>	2.80(16)	<b>Se3</b>	4.2(4)	<b>Se27</b>	3.6(3)
<b>Bi4</b>	3.28(13)	<b>Bi28</b>	2.90(19)	<b>Se4</b>	3.4(4)	<b>Se28</b>	3.4(3)
<b>Bi5</b>	3.55(12)	<b>Bi29</b>	3.06(19)	<b>Se5</b>	3.7(4)	<b>Se29</b>	3.8(4)
<b>Bi6</b>	3.3(2)	<b>Bi30</b>	3.4(2)	<b>Se6</b>	3.9(4)	<b>Se30</b>	4.1(4)
<b>Bi7</b>	3.1(2)	<b>Bi31</b>	3.26(13)	<b>Se7</b>	3.5(4)	<b>Se31</b>	3.9(5)
<b>Bi8</b>	3.08(18)	<b>Bi32</b>	2.99(17)	<b>Se8</b>	3.4(3)	<b>Se32</b>	4.3(4)
<b>Bi9</b>	2.89(17)	<b>Bi33</b>	3.17(16)	<b>Se9</b>	3.7(4)	<b>Se33</b>	3.8(3)
<b>Bi10</b>	3.2(2)	<b>Bi34</b>	3.04(11)	<b>Se10</b>	3.9(4)	<b>Se34</b>	4.2(5)
<b>Bi11</b>	2.86(17)	<b>Bi35</b>	2.70(14)	<b>Se11</b>	3.7(3)	<b>Se35</b>	3.9(3)
<b>Bi12</b>	3.1(2)	<b>Bi36</b>	2.74(17)	<b>Se12</b>	4.1(5)	<b>Se36</b>	3.5(5)
<b>Bi13</b>	3.18(19)	<b>Bi37</b>	3.4(3)	<b>Se13</b>	3.7(4)	<b>Se37</b>	4.0(4)
<b>Bi14</b>	3.0(2)	<b>Bi38</b>	2.9(2)	<b>Se14</b>	4.0(3)	<b>Se38</b>	4.1(4)
<b>Bi15</b>	3.00(17)	<b>Bi39</b>	2.82(18)	<b>Se15</b>	4.4(4)	<b>Se39</b>	3.7(3)
<b>Bi16</b>	3.06(10)	<b>Bi40</b>	3.24(16)	<b>Se16</b>	3.8(4)	<b>Se40</b>	4.2(4)
<b>Bi17</b>	3.16(11)	<b>Bi41</b>	2.98(17)	<b>Se17</b>	4.1(4)	<b>Se41</b>	3.6(3)
<b>Bi18</b>	3.6(2)	<b>Bi42</b>	3.16(17)	<b>Se18</b>	3.9(4)	<b>Se42</b>	3.5(3)
<b>Bi19</b>	2.89(15)	<b>Bi43</b>	3.09(16)	<b>Se19</b>	3.3(3)	<b>Se43</b>	4.1(5)
<b>Bi20</b>	3.33(18)	<b>Bi44</b>	3.03(19)	<b>Se20</b>	3.8(4)	<b>Se44</b>	3.5(3)
<b>Bi21</b>	3.26(11)	<b>Bi45</b>	3.3(2)	<b>Se21</b>	3.7(3)	<b>Se45</b>	3.4(4)
<b>Bi22</b>	3.05(18)	<b>Bi46</b>	3.33(11)	<b>Se22</b>	3.9(4)	<b>Se46</b>	4.0(3)
<b>Bi23</b>	3.4(3)	<b>Bi47</b>	2.79(17)	<b>Se23</b>	4.3(4)	<b>Se47</b>	4.3(5)
<b>Bi24</b>	3.05(19)	<b>Bi48</b>	2.92(18)	<b>Se24</b>	4.0(4)	<b>Se48</b>	3.9(3)

**Table S 10. Fractional atomic coordinates and isotropic or equivalent isotropic displacement parameters ( $\text{\AA}^2$ ) of  $\text{Bi}_6(\text{SeO}_3)_4\text{Cl}_{10}$**

	<i>x</i>	<i>y</i>	<i>z</i>	$U_{\text{iso}}^*/U_{\text{eq}}$	Occ. (<1)
Bi1a	0.48273 (2)	0.34082 (5)	0.36920 (3)	0.01344 (12)	0.960 (2)
Bi1b	0.5189 (5)	0.4141 (18)	0.1366 (8)	0.025 (4)	0.040 (2)
Se3a	0.51770 (5)	0.43441 (13)	0.19264 (8)	0.01236 (19)*	0.9604
Se3b	0.4825 (11)	0.331 (3)	0.3145 (16)	0.005 (4)*	0.0396
Bi2	0.853973 (19)	1.11560 (5)	0.57426 (3)	0.01572 (12)	
Bi3	0.95274 (2)	0.83971 (5)	0.84829 (3)	0.01647 (12)	
Bi4	0.66931 (2)	0.61536 (6)	0.37377 (3)	0.02098 (13)	
Bi5	0.86877 (2)	0.62396 (5)	0.58018 (3)	0.01797 (12)	
Bi6	0.66324 (2)	1.12862 (5)	0.34402 (3)	0.01840 (12)	
Se1	0.73099 (5)	1.34197 (12)	0.56176 (7)	0.0113 (3)	
Se2	1.01931 (5)	0.93685 (12)	0.69363 (7)	0.0109 (3)	
Se4	0.72380 (5)	0.84150 (12)	0.55349 (7)	0.0124 (3)	
Cl1	0.84786 (13)	0.6432 (3)	0.74343 (18)	0.0175 (7)	
Cl2	1.06902 (13)	0.8894 (4)	1.00701 (18)	0.0180 (7)	
Cl3	0.55971 (17)	0.6180 (4)	0.4501 (2)	0.0263 (10)	
Cl4	0.86972 (16)	1.1267 (4)	0.75028 (19)	0.0233 (9)	
Cl5	0.92933 (14)	0.6500 (3)	0.98585 (18)	0.0186 (8)	
Cl6	0.79082 (14)	0.6136 (4)	0.38048 (19)	0.0221 (8)	
Cl7	0.79039 (13)	1.1190 (4)	0.37837 (19)	0.0211 (8)	
Cl8	0.57275 (15)	0.1470 (4)	0.4788 (2)	0.0259 (9)	
Cl9	0.66974 (17)	0.3475 (5)	0.2228 (2)	0.0324 (11)	
Cl10	0.66601 (15)	0.8907 (5)	0.2209 (2)	0.0313 (11)	
O1	0.5591 (4)	0.3434 (10)	0.2993 (6)	0.017 (2)	
O2	0.7435 (4)	1.1414 (9)	0.5547 (6)	0.016 (3)	
O3	0.8129 (4)	1.3825 (9)	0.5756 (6)	0.017 (2)	
O4	0.7267 (5)	0.6416 (10)	0.5358 (6)	0.020 (3)	
O5	0.8063 (4)	0.8702 (9)	0.5658 (6)	0.016 (2)	
O6	1.0442 (4)	0.9601 (10)	0.8133 (5)	0.015 (2)	
O7	0.9458 (4)	0.8439 (10)	0.6870 (5)	0.016 (2)	
O8	0.6905 (4)	0.3686 (9)	0.4441 (5)	0.014 (2)	
O9	0.4469 (4)	0.4603 (12)	0.2189 (6)	0.021 (3)	
O10	0.9888 (4)	1.1233 (10)	0.6566 (5)	0.015 (2)	
O11	0.4453 (4)	0.1178 (10)	0.2828 (6)	0.020 (2)	
O12	0.6821 (4)	0.8812 (11)	0.4383 (6)	0.018 (2)	

**Table S 9. Atomic displacement parameters ( $\text{Å}^2$ ) of  $\text{Bi}_6(\text{SeO}_3)_4\text{Cl}_{10}$**

	$U^{11}$	$U^{22}$	$U^{33}$	$U^{12}$	$U^{13}$	$U^{23}$
Bi1a	0.01377 (18)	0.01563 (19)	0.01177 (19)	-0.00004 (13)	0.00556 (13)	-0.00031 (13)
Bi1b	0.004 (4)	0.047 (8)	0.025 (6)	0.006 (4)	0.005 (4)	0.003 (5)
Bi2	0.01209 (16)	0.01578 (18)	0.01791 (18)	-0.00019 (13)	0.00359 (13)	-0.00043 (14)
Bi3	0.01887 (18)	0.01502 (18)	0.01827 (18)	0.00109 (14)	0.00996 (14)	-0.00113 (14)
Bi4	0.01430 (18)	0.0215 (2)	0.0221 (2)	-0.00059 (15)	0.00018 (15)	0.00140 (16)
Bi5	0.02051 (19)	0.01522 (18)	0.01863 (18)	0.00105 (15)	0.00744 (15)	0.00117 (14)
Bi6	0.01736 (18)	0.01718 (19)	0.01796 (18)	-0.00022 (14)	0.00287 (14)	0.00045 (15)
Se1	0.0126 (4)	0.0113 (4)	0.0120 (4)	-0.0002 (3)	0.0069 (3)	-0.0006 (3)
Se2	0.0122 (4)	0.0127 (4)	0.0082 (4)	-0.0001 (3)	0.0041 (3)	0.0006 (3)
Se4	0.0139 (4)	0.0118 (4)	0.0123 (4)	0.0012 (3)	0.0058 (3)	-0.0004 (3)
Cl1	0.0170 (11)	0.0231 (12)	0.0134 (10)	-0.0039 (9)	0.0064 (9)	-0.0034 (9)
Cl2	0.0158 (11)	0.0257 (13)	0.0116 (10)	-0.0023 (10)	0.0036 (8)	0.0000 (9)
Cl3	0.0315 (15)	0.0270 (15)	0.0253 (14)	-0.0046 (12)	0.0162 (12)	-0.0074 (11)
Cl4	0.0295 (14)	0.0265 (14)	0.0145 (11)	0.0063 (11)	0.0086 (10)	0.0026 (10)
Cl5	0.0221 (12)	0.0229 (13)	0.0148 (11)	0.0014 (10)	0.0116 (9)	0.0031 (9)
Cl6	0.0156 (11)	0.0343 (15)	0.0168 (11)	-0.0004 (11)	0.0063 (9)	0.0013 (11)
Cl7	0.0140 (11)	0.0334 (15)	0.0157 (11)	0.0009 (10)	0.0049 (9)	-0.0010 (10)
Cl8	0.0228 (13)	0.0334 (16)	0.0182 (12)	0.0072 (12)	0.0032 (10)	0.0061 (11)
Cl9	0.0288 (15)	0.048 (2)	0.0249 (14)	0.0100 (14)	0.0148 (12)	0.0150 (14)
Cl10	0.0196 (13)	0.048 (2)	0.0287 (15)	-0.0069 (13)	0.0113 (11)	-0.0183 (14)
O1	0.013 (3)	0.018 (4)	0.020 (4)	0.005 (3)	0.005 (3)	0.007 (3)
O2	0.015 (3)	0.007 (3)	0.032 (4)	0.002 (3)	0.014 (3)	0.001 (3)
O3	0.008 (3)	0.010 (3)	0.026 (4)	0.000 (3)	0.000 (3)	0.001 (3)
O4	0.032 (5)	0.008 (3)	0.022 (4)	-0.002 (3)	0.013 (3)	-0.004 (3)
O5	0.010 (3)	0.009 (3)	0.025 (4)	-0.001 (3)	0.001 (3)	-0.001 (3)
O6	0.018 (4)	0.017 (4)	0.011 (3)	-0.009 (3)	0.008 (3)	0.000 (3)
O7	0.015 (3)	0.019 (4)	0.016 (3)	-0.006 (3)	0.006 (3)	-0.001 (3)
O8	0.018 (3)	0.013 (3)	0.012 (3)	0.002 (3)	0.006 (3)	-0.006 (3)
O9	0.014 (4)	0.035 (5)	0.017 (4)	0.004 (3)	0.007 (3)	0.011 (3)
O10	0.012 (3)	0.014 (3)	0.015 (3)	-0.003 (3)	0.001 (3)	-0.001 (3)
O11	0.013 (3)	0.015 (4)	0.021 (4)	0.000 (3)	-0.007 (3)	-0.004 (3)
O12	0.013 (3)	0.022 (4)	0.016 (4)	-0.002 (3)	0.001 (3)	-0.001 (3)

*Table S 102. Selected interatomic distances (Å) in Bi<sub>6</sub>(SeO<sub>3</sub>)<sub>4</sub>Cl<sub>10</sub>*

Atom1	Atom2	d	Atom1	Atom2	d
<b>Bi1a</b>	O1	2.252(11)	Se1	O2	1.7157(77)
	O11	2.2718(82)		O8	1.7193(69)
	O9	2.3797(90)	O3	1.7285(88)	
	Cl8	2.6305(29)	Se2	O10	1.7154(82)
	Cl3	2.8716(32)		O7	1.7308(88)
	Cl10	3.0273(30)		O6	1.7323(74)
	<b>Bi1b</b>	Cl3	3.2263(37)	Se4	O4
O11		2.092(16)	O12		1.7084(82)
O9		2.347(17)	O5	1.7299(89)	
O1		2.410(15)	Se3a	O11	1.7133(83)
Cl8		2.894(13)		O9	1.7174(99)
Cl3		3.037(14)	O1	1.7394(81)	
Cl8		3.071(14)	Se3b	O1	1.7429(278)
Cl9	3.086(11)	O9		1.7674(246)	
<b>Bi2</b>	O5	2.2848(78)	O11	1.9515(258)	
	O2	2.2926(88)			
	O3	2.4120(78)			
	Cl4	2.6015(31)			
	Cl7	2.8282(27)			
	Cl5	3.3134(31)			
	Cl2	3.3208(33)			
	<b>Bi3</b>	O10	2.2252(87)		
		O7	2.4255(81)		
		O6	2.4302(92)		
Cl1		2.7975(24)			
Cl5		2.8268(30)			
Cl2		2.8363(23)			
Cl4		3.0592(31)			
Cl2		3.3246(33)			
<b>Bi4</b>	O8	2.3070(75)			
	O4	2.3629(82)			
	O12	2.4189(92)			
	Cl6	2.5732(32)			
	O11	2.7663(72)			
	Cl3	2.9739(40)			
	Cl9	3.2312(38)			
	Cl10	3.2766(38)			
<b>Bi5</b>	O3	2.3448(80)			
	O6	2.4293(73)			
	O5	2.4325(79)			
	O7	2.6309(75)			
	Cl1	2.6997(31)			
	O4	2.884(11)			
	Cl6	2.9283(26)			
	Cl2	2.9516(33)			
	Cl5	2.9519(31)			
<b>Bi6</b>	O8	2.4759(74)			
	O12	2.4825(91)			
	Cl7	2.5916(28)			
	O9	2.6286(86)			
	Cl9	2.6533(38)			
	O1	2.7641(83)			
	Cl10	2.7647(38)			
	Cl8	3.3012(37)			

*Table S 13. Bond sum valence values of selected atoms in  $\text{PbBi}_{10}(\text{SeO}_3)_{12}\text{Cl}_8$*

<b>Atom</b>	<b>BVS</b>
<b>Bi1</b>	3.45(9)
<b>Bi2</b>	2.77(7)
<b>Pb2</b>	2.90(7)
<b>Bi3</b>	2.59(7)
<b>Pb3</b>	2.72(7)
<b>Bi4</b>	2.86(8)
<b>Pb4</b>	3.00(8)
<b>Bi5</b>	2.47(7)
<b>Pb5</b>	2.67(7)
<b>Se1</b>	4.28(19)
<b>Se2</b>	3.76(17)
<b>Se3</b>	3.84(16)

**Table S 11. Fractional atomic coordinates and isotropic or equivalent isotropic displacement parameters ( $\text{\AA}^2$ ) in  $\text{PbBi}_{10}(\text{SeO}_3)_{12}\text{Cl}_8$**

	<i>x</i>	<i>y</i>	<i>z</i>	$U_{\text{iso}}^*/U_{\text{eq}}$	Occ. (<1)
Bi1	0.5	0	0	0.0157 (10)	
Bi2	0.25	0	0.25	0.0390 (10)	0.9
Pb2	0.25	0	0.25	0.0390 (10)	0.1
Bi3	0.5	0	0.26397 (19)	0.0359 (11)	0.9
Pb3	0.5	0	0.26397 (19)	0.0359 (11)	0.1
Bi4	0.2407 (2)	0	0	0.0279 (9)	0.9
Pb4	0.2407 (2)	0	0	0.0279 (9)	0.1
Bi5	0.61813 (12)	-0.17735 (7)	0.38264 (13)	0.0278 (5)	0.9
Pb5	0.61813 (12)	-0.17735 (7)	0.38264 (13)	0.0278 (5)	0.1
Se1	0.3767 (2)	0.12635 (19)	0.1494 (2)	0.0090 (9)	
Se2	0.6504 (3)	0.1232 (2)	0.1218 (2)	0.0197 (11)	
Se3	0.3905 (3)	-0.11306 (18)	0.3900 (2)	0.0184 (11)	
Cl1	0.5	-0.2528 (7)	0.5	0.041 (6)	
Cl2	0.75	0.25	0.2359 (9)	0.046 (7)	
Cl3	0	0.25	0.25	0.072 (11)	
Cl4	0.75	0.25	0.0086 (11)	0.044 (7)	
O1	0.7551 (18)	0.0913 (16)	0.1223 (17)	0.017 (5)*	
O2	0.2930 (17)	0.0761 (14)	0.1235 (16)	0.013 (5)*	
O3	0.4605 (19)	0.0742 (17)	0.1230 (18)	0.021 (6)*	
O4	0.6216 (17)	0.0715 (16)	0.2073 (17)	0.016 (6)*	
O5	0.371 (2)	-0.098 (2)	0.4956 (19)	0.026 (9)*	
O6	0.6236 (17)	0.0679 (15)	0.0364 (17)	0.014 (5)*	
O7	0.4953 (16)	-0.099 (2)	0.3767 (18)	0.013 (6)*	
O8	0.3779 (17)	0.1014 (16)	0.2539 (19)	0.021 (6)*	
O9	0.3631 (18)	-0.0214 (12)	0.3627 (18)	0.018 (5)*	

**Table S 15. Atomic displacement parameters ( $\text{\AA}^2$ ) in  $\text{PbBi}_{10}(\text{SeO}_3)_{12}\text{Cl}_8$**

	$U^{11}$	$U^{22}$	$U^{33}$	$U^{12}$	$U^{13}$	$U^{23}$
Bi1	0.025 (2)	0.0130 (10)	0.0091 (16)	0	0	0
Bi2	0.065 (2)	0.0204 (9)	0.0315 (15)	0.0145 (12)	0.0253 (11)	0.0127 (10)
Pb2	0.065 (2)	0.0204 (9)	0.0315 (15)	0.0145 (12)	0.0253 (11)	0.0127 (10)
Bi3	0.057 (2)	0.0246 (15)	0.0259 (16)	-0.0132 (12)	0	0
Pb3	0.057 (2)	0.0246 (15)	0.0259 (16)	-0.0132 (12)	0	0
Bi4	0.0326 (19)	0.0227 (14)	0.0283 (13)	0	0	-0.0011 (9)
Pb4	0.0326 (19)	0.0227 (14)	0.0283 (13)	0	0	-0.0011 (9)
Bi5	0.0300 (10)	0.0128 (6)	0.0408 (11)	-0.0002 (7)	0.0060 (6)	-0.0006 (7)
Pb5	0.0300 (10)	0.0128 (6)	0.0408 (11)	-0.0002 (7)	0.0060 (6)	-0.0006 (7)
Se1	0.0087 (16)	0.0137 (16)	0.0045 (14)	-0.0002 (12)	-0.0052 (12)	0.0030 (12)
Se2	0.033 (2)	0.0054 (15)	0.0203 (19)	-0.0021 (15)	-0.0042 (17)	0.0022 (13)
Se3	0.038 (2)	0.0120 (14)	0.0057 (17)	-0.0012 (17)	0.0059 (13)	-0.0012 (13)
Cl1	0.082 (16)	0.014 (5)	0.028 (9)	0	-0.010 (8)	0
Cl2	0.099 (18)	0.025 (6)	0.012 (7)	-0.023 (9)	0	0
Cl3	0.12 (3)	0.018 (10)	0.080 (17)	0.009 (11)	0.051 (16)	-0.001 (13)
Cl4	0.083 (17)	0.021 (9)	0.027 (9)	-0.003 (12)	0	0

**Table S 126. Selected interatomic distances ( $\text{\AA}$ ) in  $\text{PbBi}_{10}(\text{SeO}_3)_{12}\text{Cl}_8$**

atom1	atom2	d, $\text{\AA}$	atom1	atom2	d, $\text{\AA}$
Bi1	4xO6	2.372(27)	Se1	1xO2	1.650(27)
	4xO3	2.440(30)		1xO3	1.670(31)
Bi2 Pb2	2xO4	2.490(28)	Se2	1xO8	1.720(31)
	2xO2	2.520(26)		1xO4	1.700(28)
	2xO9	2.560(29)		1xO6	1.730(28)
	2xO1	2.600(28)		1xO1	1.750(29)
Bi3 Pb3	2xO8	2.720(28)	Se3	1xO7	1.690(27)
	2xO4	2.480(28)		1xO5	1.720(31)
	2xO7	2.520(33)		1xO9	1.750(23)
	2xO8	2.650(28)		1xO2	2.980(28)
	2xO3	2.670(30)		1xO4	3.000(28)
Bi4 Pb4	2xO9	2.700(29)	Bi5 Pb5	1xCl1	2.962(6)
	2xO5	2.490(34)		1xCl4	3.002(2)
	2xO2	2.520(26)		1xCl2	3.094(9)
	2xO6	2.530(27)		1xCl3	3.099(2)
	2xO1	2.540(28)			
Bi5 Pb5	2xO9	2.750(29)			
	1xO7	2.400(30)			
	1xO5	2.400(33)			
	1xO8	2.450(30)			
	1xO1	2.530(29)			

**Table S 17. Bond sum valence values of selected atoms in  $\text{Bi}_6(\text{SeO}_3)_4\text{Cl}_{10}$**

Atom	BVS
<b>Bi1a</b>	3.10(3)
<b>Bi1b</b>	2.88(5)
<b>Bi2</b>	3.17(2)
<b>Bi3</b>	3.06(2)
<b>Bi4</b>	2.96(2)
<b>Bi5</b>	3.072(18)
<b>Bi6</b>	3.113(17)
<b>Se1</b>	3.83(5)
<b>Se2</b>	3.77(5)
<b>Se3a</b>	3.81(5)



---

<b>Se3b</b>	3.01(12)
<b>Se4</b>	3.89(5)

---



**A-IV**  
**pH-Controlled pathway and systematic hydrothermal phase  
diagram for elaboration of synthetic lead nickel selenites**

Vadim M. Kovrugin, Marie Colmont, Christine Terryn, Silviu Colis, Oleg I. Siidra, Sergey V. Krivovichev,  
and Olivier Mentré

Published in: *Inorganic Chemistry*, 2015, Vol. 54 (5), p. 2425–2434.

DOI: 10.1021/ic503055v

Reprinted with kind permission from American Chemical Society.



# pH Controlled Pathway and Systematic Hydrothermal Phase Diagram for Elaboration of Synthetic Lead Nickel Selenites

Vadim M. Kovrugin,<sup>†,‡</sup> Marie Colmont,<sup>†</sup> Christine Terryn,<sup>§</sup> Silviu Colis,<sup>||</sup> Oleg I. Siidra,<sup>‡</sup> Sergey V. Krivovichev,<sup>‡</sup> and Olivier Mentré<sup>\*,†</sup>

<sup>†</sup>Université Lille Nord de France, UMR 8181 CNRS, Unité de Catalyse et de Chimie du Solide (UCCS USTL), 59655 Villeneuve d'ASCQ, France

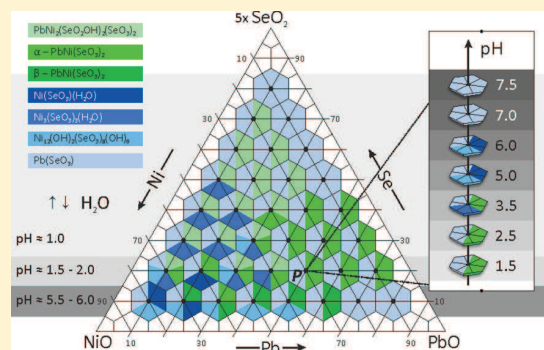
<sup>‡</sup>Department of Crystallography, Saint-Petersburg State University, Universitetskaya nab. 7/9, 199034 St. Petersburg, Russia

<sup>§</sup>Plateforme Imagerie Cellulaire et Tissulaire, 51 rue Cognacq-Jay, 51100 Reims, France

<sup>||</sup>Institut de Physique et Chimie des Matériaux de Strasbourg (IPCMS), UMR 7504 CNRS and Université de Strasbourg (UDS-ECPM), F-67034 Cedex 2 Strasbourg, France

## Supporting Information

**ABSTRACT:** The PbO–NiO–SeO<sub>2</sub> ternary system was fully studied using constant hydrothermal conditions at 473 K. It yields the establishment of the corresponding phase diagram using a systematic assignment of reaction products by both powder and single-crystal X-ray diffraction. It leads to the preparation of three novel lead nickel selenites,  $\alpha$ -PbNi(SeO<sub>3</sub>)<sub>2</sub> (I),  $\beta$ -PbNi(SeO<sub>3</sub>)<sub>2</sub> (II), and PbNi<sub>2</sub>(SeO<sub>2</sub>OH)<sub>2</sub>(SeO<sub>3</sub>)<sub>2</sub> (III), and one novel lead cobalt selenite,  $\alpha$ -PbCo(SeO<sub>3</sub>)<sub>2</sub> (IV), which have been structurally characterized. The crystal structures of the  $\alpha$ -forms I, IV, and III are based on a 3D complex nickel selenite frameworks, whereas the  $\beta$ -PbNi(SeO<sub>3</sub>)<sub>2</sub> modification (II) consists of nickel selenite sheets stacked in a noncentrosymmetric structure, second-harmonic generation active. The pH value of the starting solution was shown to play an essential role in the reactive processes. Magnetic measurements of I, III, and IV are discussed.



## INTRODUCTION

The demand for specific noncentrosymmetric (NCS) crystal structures is very strong because interesting physical properties, such as second-harmonic generation (SHG),<sup>1</sup> piezoelectricity,<sup>2</sup> ferroelectricity,<sup>3</sup> and pyroelectricity,<sup>4</sup> can be expected. In particular, nonlinear optic materials have become tremendously important and are drawing more and more attention owing to their promising applications in laser science and technology. The NCS compounds are commonly observed when dealing with (Ti<sup>4+</sup>, V<sup>5+</sup>, Mo<sup>6+</sup>) octahedrally coordinated *d*<sup>0</sup> transition metals susceptible to second-order Jahn–Teller (SOJT) effects. Typical SOJT asymmetric coordination environments are also favored for cations with a stereoactive lone pair of electrons (As<sup>3+</sup>, Se<sup>4+</sup>, Sb<sup>3+</sup>, Pb<sup>2+</sup>, and Bi<sup>3+</sup>, etc.) in more drastic manner leading to a diversity of unusual polyhedral coordination. The crystal chemistry of metal selenites is very rich as first reviewed by Verma.<sup>5</sup> The incorporation of heavy lone pair cations such as Pb<sup>2+</sup>/Bi<sup>3+</sup> with selenite groups increases the chance to achieve asymmetric building units or NCS crystal structures as demonstrated in several earlier works dedicated to the exploration of PbO/Bi<sub>2</sub>O<sub>3</sub>–MO<sub>x</sub>–SeO<sub>2</sub> (M = Cu<sup>2+</sup>, V<sup>3+</sup>, Ge<sup>4+</sup>, Nb<sup>5+</sup>, V<sup>5+</sup>, Mo<sup>6+</sup>, W<sup>6+</sup>; *x* = 1, 2; *y* = 1, 2, 3, 5) ternary systems.<sup>6–11</sup> From the experimental viewpoint, due to the low and close

melting and sublimation temperatures (340 and 350 °C, respectively), the crystal growth of selenites is generally achieved using either chemical transport routes,<sup>12,13</sup> recently leading to original bismuth selenites, including giant cell compounds,<sup>14</sup> or hydrothermal methods due to the good solubility and reactivity of (SeO<sub>3</sub>)<sup>2–</sup> anions. However, as recently demonstrated by the evidence of a number of phases in competition in the CoSeO<sub>3</sub>–SeO<sub>2</sub>–H<sub>2</sub>O phase diagram<sup>15</sup> and other hybrid inorganic–organic systems,<sup>16,17</sup> a systematic approach may be preferred for exhaustive search of novel crystal structures. Thus, research was not yet carried out on ternary systems with lead and nickel/cobalt as transition metals constituents. Herein, we present a scrupulous investigation of the PbO–NiO–SeO<sub>2</sub> system in hydrothermal conditions. It leads to the synthesis of four novel lead selenites,  $\alpha$ -PbNi(SeO<sub>3</sub>)<sub>2</sub> (I),  $\beta$ -PbNi(SeO<sub>3</sub>)<sub>2</sub> (II), PbNi<sub>2</sub>(SeO<sub>2</sub>OH)<sub>2</sub>(SeO<sub>3</sub>)<sub>2</sub> (III), and  $\alpha$ -PbCo(SeO<sub>3</sub>)<sub>2</sub> (IV), that have been structurally characterized by single-crystal X-ray diffraction (XRD). Their magnetic properties will be also discussed in this Article.

**Received:** December 22, 2014

**Published:** February 17, 2015

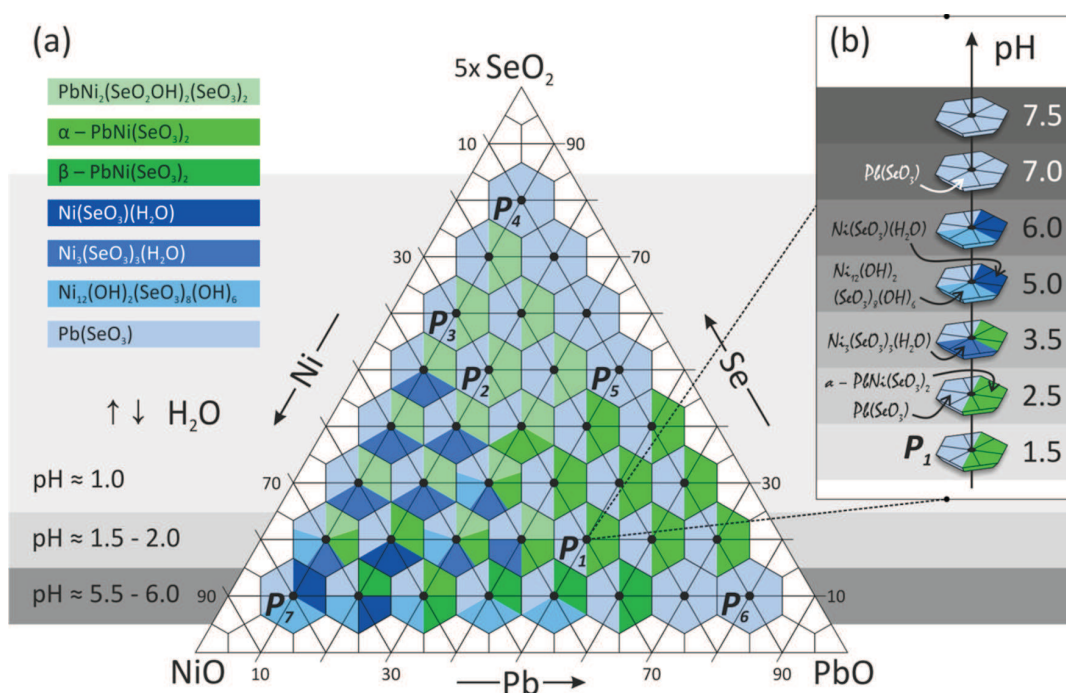


**Figure 1.** Experimental crystallization diagram of the PbO–NiO–SeO<sub>2</sub>–H<sub>2</sub>O system at 423 K with the pH zones shown in the background by gray colors (a), and the series of experiments with a PbO:NiO:SeO<sub>2</sub> molar ratio of 5:3:10 corresponding to the P<sub>1</sub> point with various pH values (b). The black points indicate the experimental combinations of the molar ratios of precursors. The compositions of various phases synthesized in each experimental point are shown by hexagons of different colors.

**Table 1.** Crystallographic Data for the compounds  $\alpha$ -PbNi(SeO<sub>3</sub>)<sub>2</sub> (I),  $\beta$ -PbNi(SeO<sub>3</sub>)<sub>2</sub> (II), PbNi<sub>2</sub>(SeO<sub>2</sub>OH)<sub>2</sub>(SeO<sub>3</sub>)<sub>2</sub> (III), and  $\alpha$ -PbCo(SeO<sub>3</sub>)<sub>2</sub> (IV)

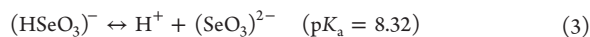
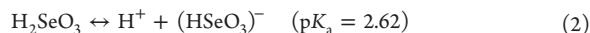
	I	II	III	IV
$M_r$ (g mol <sup>-1</sup> )	519.82	519.82	834.47	520.04
cryst syst	orthorhombic	orthorhombic	monoclinic	orthorhombic
space group	<i>Pnma</i>	<i>Cmc2<sub>1</sub></i>	<i>P2/c</i>	<i>Pnma</i>
<i>a</i> (Å)	12.7476(4)	5.4715(4)	13.6824(10)	12.8208(4)
<i>b</i> (Å)	5.4562(2)	9.1963(6)	5.2692(5)	5.4902(2)
<i>c</i> (Å)	7.8332(2)	11.4436(9)	19.3476(13)	7.9085(2)
$\alpha$ (deg)	90	90	90	90
$\beta$ (deg)	90	90	129.524(4)	90
$\gamma$ (deg)	90	90	90	90
<i>V</i> (Å <sup>3</sup> )	544.83(3)	575.81(7)	1075.94 (16)	556.67(3)
<i>Z</i>	4	4	4	4
$\rho$ (g/cm <sup>3</sup> )	6.337	5.996	5.151	6.205
$\mu$ (mm <sup>-1</sup> )	47.637	45.074	32.668	46.221
$\lambda$ (Mo K $\alpha$ ) (Å)	0.71073	0.71073	0.71073	0.71073
$\theta_{\text{min-max}}$ (deg)	3.1–29.6	3.6–28.0	1.9–28.0	3.0–28.0
reflns collected	10212	2345	5454	3226
indep reflns ( $R_{\text{int}}$ )	823 (0.0336)	686 (0.0260)	2083 (0.0459)	742 (0.0260)
$R_1$ ( $I > 2\sigma(I)$ )	0.0139	0.0141	0.0496	0.0186
w $R_2$ ( $I > 2\sigma(I)$ )	0.0360	0.0346	0.0992	0.0429
$R_1$ (all data)	0.0165	0.0142	0.0783	0.0203
w $R_2$ (all data)	0.0387	0.0346	0.1104	0.0439
GOF	1.090	1.109	1.187	1.142
$\Delta\rho_{\text{max}}/\Delta\rho_{\text{min}}$ (e Å <sup>-3</sup> )	1.573/–1.110	1.310/–1.073	2.916/–2.912	0.971/–1.887

## EXPERIMENTAL SECTION

**Syntheses.** Commercial PbO (99,999%, Aldrich), SeO<sub>2</sub> (99%, Alfa Aesar), NiO (99%, Sigma-Aldrich), and CoO (95%, Alfa Aesar) were used as received. After weighing and grinding, the reagents were mixed in 6 mL of distilled water. When necessary, sodium hydroxide solution

was used to adjust the pH to its desired value. Our exploration of the crystal growth in the PbO–NiO–SeO<sub>2</sub>–H<sub>2</sub>O system consisted of examination of 36 possible combinations of molar ratios of the solid precursors within the Gibbs's triangle (Figure 1a). In all syntheses the  $m\text{PbO} + n\text{NiO} + (k/5)\text{SeO}_2$  ( $m, n, k = 1, 2, \dots, 8$ ) molar sum was fixed as constant equal to 10 mmol, and the mixture was completed with 6 mL of

distilled water. It has been experimentally established that only acidic conditions favor the crystallization of structural varieties. In our study, the reactive medium self-acidifies by solubilization of  $\text{SeO}_2$  into selenous acid according to the following reactions:



Then a large stoichiometric excess of  $\text{SeO}_2$  was necessary to achieve reactions as shown in Figure 1a, where the amount of selenium dioxide is multiplied by five. The pH values increase from ~1 to ~5.5–6.0 on decreasing the  $\text{SeO}_2$  content in our experimental range. The solid products were systematically analyzed by powder XRD (PXRD) analysis (after grinding), while representative crystals of each of the present phases were also selected by morphology and colors and tested by single-crystal XRD analysis. It leads to the phase distribution given in Figure 1a, where the crystallization domains of phases are illustrated by different colors.

The chemical reactions were performed during 36 h in 23 mL Teflon-lined Parr reaction vessels heated in an oven at 473 K. At the end of the experiment time, the vessels were cooled during 48 h. The precipitate was filtered through filter paper. Single crystals of three novel lead selenites with nickel,  $\alpha$ - $\text{PbNi}(\text{SeO}_3)_2$  (I),  $\beta$ - $\text{PbNi}(\text{SeO}_3)_2$  (II), and  $\text{PbNi}_2(\text{SeO}_2\text{OH})_2(\text{SeO}_3)_2$  (III), have been prepared by the hydrothermal techniques. They have been observed in the mixtures already reported:  $\text{Ni}(\text{SeO}_3)(\text{H}_2\text{O})$ ,<sup>18</sup>  $\text{Ni}_3(\text{SeO}_2)_3(\text{H}_2\text{O})$ ,<sup>19,20</sup>  $\text{Ni}_{12}(\text{OH})_6(\text{SeO}_3)_8(\text{OH})_2$ ,<sup>21</sup> and  $\text{Pb}(\text{SeO}_3)$ .<sup>22–25</sup> Single crystals of the cobalt selenite,  $\alpha$ - $\text{PbCo}(\text{SeO}_3)_2$  (IV) were obtained by the reaction analogous to that used to obtain compound I. Attempts to synthesize the Co analogue of compounds II and III using similar techniques proved unsuccessful. In general, out of IV our hydrothermal conditions using cobalt precursors rarely lead to crystal growth, which is one motivation of our study. The novel lead selenite crystals occur as yellow needles (I), yellow prisms (II), green plates (III), and purple needles (IV) up to 300  $\mu\text{m}$  in maximal dimension.

**X-ray Diffraction.** Powder X-ray diffraction analyses of all of the powder samples were performed at room temperature in a  $2\theta$  range of  $10$ – $60^\circ$  with a scan step width of  $0.02^\circ$  using a D8 Advance Bruker AXS diffractometer ( $\text{Cu K}\alpha$  radiation,  $\lambda = 1.5418 \text{ \AA}$ ). Single crystals selected for data collection were examined under an optical microscope and mounted on a glass fiber. Data were collected by means of a Bruker DUO four-circle diffractometer equipped with an APEX II CCD detector and monochromated  $\text{Mo K}\alpha$  radiation. Unit-cell parameters were refined by the least-squares techniques using the full recorded data set. The data were integrated and corrected for absorption using a multiscan type model implemented in the Bruker programs APEX<sup>26</sup> and SADABS.<sup>27</sup> The structures were solved by direct methods and refined by means of the program SHELXL-2013.<sup>28</sup> Crystallographic data are summarized in Table 1. The visible difference in the quality of the crystallographic data of compound III is a result of the relatively poor quality and small size of the collected crystal. Fractional atomic coordinates, atomic displacement parameters, and selected bond distances are listed in Tables S1–S12 of the Supporting Information. The crystal structure data for  $\alpha$ - $\text{PbCo}(\text{SeO}_3)_2$ ,  $\alpha$ - $\text{PbNi}(\text{SeO}_3)_2$ ,  $\beta$ - $\text{PbNi}(\text{SeO}_3)_2$ , and  $\text{PbNi}_2(\text{SeO}_2\text{OH})_2(\text{SeO}_3)_2$  were deposited with the depository numbers CSD-428904, CSD-428905, CSD-428906, and CSD-428907, respectively.

**SQUID.** The magnetic properties of the samples were analyzed using a MPMS SQUID-VSM (Quantum Design) magnetometer in a temperature and field range of 1.8–300 K and 0–7 T, respectively. The temperature dependence variation of the magnetization was carried out under a magnetic field of 0.1 T after cooling the sample in a field of 0.1 T (FC, field cooling) or in zero field (ZFC, zero-field cooling). Using these variations,  $\chi$  and  $\chi^{-1}$  vs  $T$  could be obtained that could inform on the magnetic interactions. All measurements were carried out on nonaligned samples (random crystallites orientation).

**Multiphoton SHG Microscopy.** For compound II, a laser scanning microscope LSM 710 NLO Zeiss (Jena, Germany) was used as

implemented at the Plateforme d'Imagerie Cellulaire et Tissulaire, Reims, France. Excitation was provided by a CHAMELEON femto-second titanium–sapphire laser (Coherent, Santa Clara, CA, USA) set at 860 nm, tuning the power until SHG was detected. Samples were imaged with a  $20\times$ , 0.8 NA objective lens. The emitted signal of SHG was collected with a bandpass filter (420–440 nm). The analyzed zone is performed by pixels of  $0.55 \times 0.55 \mu\text{m}^2$ .

**Partial Charge and Dipole Moment Calculations.** We have chosen to follow Henry's model for determination of partial charges using scales of atomic nonempirical electronegativity and hardness (to measure the resistance the atom can oppose to the flow of electronic density) implemented in the program PACHA. This software uses a nonempirical method to determine partial charges using crystal structure data and two parameters per chemical element: configuration energy and the radius of the most diffuse valence orbital to avoid any unphysical aspects.<sup>29</sup>

## RESULTS AND DISCUSSION

**Phases in Competition.** The analysis of the different solid phases in competition allows a rough rationalization on the basis of the starting stoichiometry and pH value. First, we note that the  $\text{Pb}(\text{SeO}_3)$  compound is the most frequent phase in the system, and it has been observed as a solid product with variable degree of

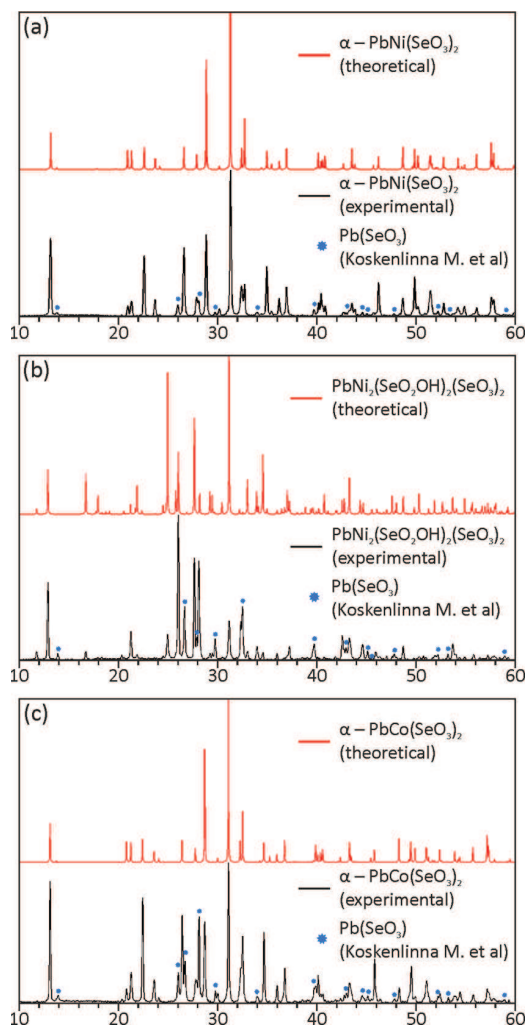


**Figure 2.** Theoretical (red) and experimental (black) PXRD patterns for the crystal structures of  $\alpha$ - $\text{PbNi}(\text{SeO}_3)_2$  (a),  $\text{PbNi}_2(\text{SeO}_2\text{OH})_2(\text{SeO}_3)_2$  (b), and  $\alpha$ - $\text{PbCo}(\text{SeO}_3)_2$  (c).

Table 2. Solid Products of the Experiments with a PbO/NiO/SeO<sub>2</sub> Molar Ratio of 5:3:10 (Point P<sub>1</sub> in Figure 1a)

no.	pH		solid products
	before reaction	after reaction	
P <sub>1</sub>	1.0	1.5	Pb(SeO <sub>3</sub> ); α-PbNi(SeO <sub>3</sub> ) <sub>2</sub> (I)
1	1.5	2.5	Pb(SeO <sub>3</sub> ); α-PbNi(SeO <sub>3</sub> ) <sub>2</sub> (I)
2	2.0	3.5	Pb(SeO <sub>3</sub> ); α-PbNi(SeO <sub>3</sub> ) <sub>2</sub> (I); Ni <sub>3</sub> (SeO <sub>3</sub> ) <sub>3</sub> (H <sub>2</sub> O)
3	3.0	5.0	Pb(SeO <sub>3</sub> ); Ni(SeO <sub>3</sub> )(H <sub>2</sub> O); Ni <sub>12</sub> (OH) <sub>6</sub> (SeO <sub>3</sub> ) <sub>8</sub> (OH) <sub>2</sub>
4	4.0	6.0	Pb(SeO <sub>3</sub> ); Ni(SeO <sub>3</sub> )(H <sub>2</sub> O); Ni <sub>12</sub> (OH) <sub>6</sub> (SeO <sub>3</sub> ) <sub>8</sub> (OH) <sub>2</sub>
5	5.0	7.0	Pb(SeO <sub>3</sub> )
6	6.0	7.5	Pb(SeO <sub>3</sub> )

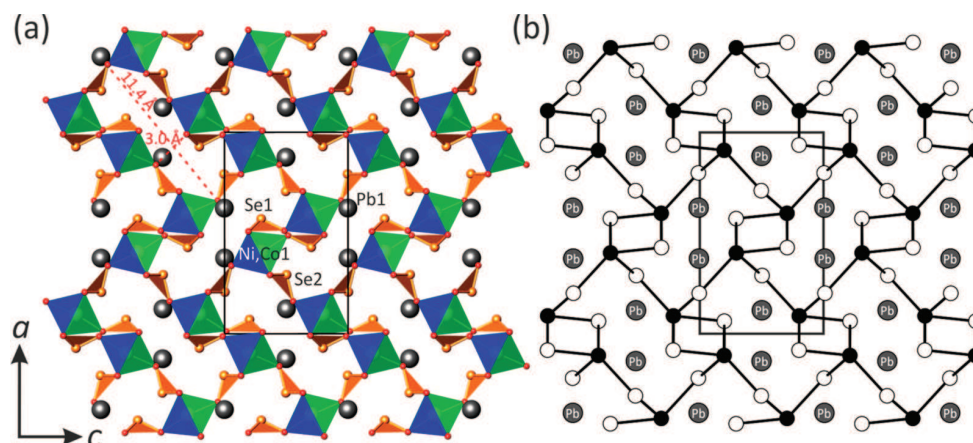


Figure 3. General projection of the crystal structures of  $\alpha$ -PbM(SeO<sub>3</sub>)<sub>2</sub> (M = Ni<sup>2+</sup> (I), Co<sup>2+</sup> (IV)) along the *b* axis (a) and the corresponding black-and-white graph (b). Legend, panel a: MO<sub>6</sub> octahedra, blue-green; SeO<sub>3</sub> trigonal pyramids, orange; Pb<sup>2+</sup>, gray balls. Legend panel b: M<sup>2+</sup>, black circles; Se<sup>4+</sup>, white circles.

crystallinity in each hydrothermal experiment, sometimes found as a predominant white powder. This proves a preferred complexation of Pb<sup>2+</sup> by (SeO<sub>3</sub>)<sup>2-</sup> and enhanced precipitation independently of the pH. Second, about the cationic stoichiometry, rich lead compounds appear in the right zone of the diagram while lead-free nickel selenites (Ni(SeO<sub>3</sub>)(H<sub>2</sub>O))<sup>18</sup> and Ni<sub>3</sub>(SeO<sub>2</sub>)<sub>3</sub>(H<sub>2</sub>O))<sup>19,20</sup> have been obtained at the left side with low Pb concentrations. This result, even though expected, demonstrates formation mechanisms controlled by the solution concentrations of each species. Finally, occulting the systematic presence of Pb(SeO<sub>3</sub>)<sub>2</sub>,<sup>22–25</sup> low pH values favor reactivity of (HSeO<sub>3</sub>)<sup>-</sup> groups (e.g., in PbNi<sub>2</sub>(SeO<sub>2</sub>OH)<sub>2</sub>(SeO<sub>3</sub>)<sub>2</sub>), while selenite groups predominate at higher pH values (e.g., PbNi(SeO<sub>3</sub>) polymorphs) in good agreement with the acidic reactions and pK<sub>s</sub> given earlier (eqs 2 and 3).

Experimental (black) and theoretical (red) PXRD patterns for new phases described later,  $\alpha$ -PbNi(SeO<sub>3</sub>)<sub>2</sub> (I), PbNi<sub>2</sub>(SeO<sub>2</sub>OH)<sub>2</sub>(SeO<sub>3</sub>)<sub>2</sub> (III), and  $\alpha$ -PbCo(SeO<sub>3</sub>)<sub>2</sub> (IV), are represented in Figure 2, leading to a mixture with diamagnetic Pb(SeO<sub>3</sub>). It enables the measurement of their magnetic properties. Intensities of the reflections in the PXRD patterns are affected by relatively strong preferred orientation, due to anisotropic crystallite shape related to the crystal structures. Theoretical patterns were generated with PowderCell 2.4 from the single-crystal data without taking into account the preferred orientation. The PXRD patterns of I and III correspond to the samples performed for the P<sub>1</sub> point (PbO:NiO:SeO<sub>2</sub> = 5:3:10) and P<sub>2</sub> point (PbO:NiO:SeO<sub>2</sub> = 2:3:25) of Figure 1a, respectively. The solid products of IV for the powder X-ray diffraction analysis have been obtained with stoichiometry to analogous I by replacing NiO by CoO. For other stoichiometries,

PXRD patterns corresponding to the P<sub>3</sub>, P<sub>4</sub>, P<sub>5</sub>, P<sub>6</sub>, and P<sub>7</sub> points in Figure 1a are provided as examples in the Supporting Information (Figures S1–S5).

**Influence of the pH.** To gain more information about the reaction processes in the PbO–NiO–SeO<sub>2</sub>–H<sub>2</sub>O phase diagram, an in-depth investigation was carried out for the particular P<sub>1</sub> (PbO:NiO:SeO<sub>2</sub> molar ratio of 5:3:10) stoichiometric mixture at various pH values up to 7.5 (in order to prevent the reduction of SeO<sub>2</sub> to  $\gamma$ -Se metal<sup>30,31</sup>). The reagents were mixed with 1.75 M aqueous NaOH solution until the required pH values. Then, the hydrothermal treatment was applied. The resulted products of these series as a function of the pH values are listed in Table 2 and shown in Figure 1b. Experimental PXRD patterns are provided in the Supporting Information (Figures S6–S11).

The results obtained in the course of the hydrothermal experiments demonstrated an essential role of the pH values, especially dealing with the influence of the degree of condensation of the ionic species. Once more at all pH the Pb(SeO<sub>3</sub>) is revealed as very stable. For the other products, we observe that water molecules and, subsequently, hydroxide anions are progressively incorporated into the compound structures on increasing the pH. In particular, at low pH of 1.5–2.5 only condensed compounds,  $\alpha$ -PbNi(SeO<sub>3</sub>)<sub>2</sub> (I) and Pb(SeO<sub>3</sub>)<sub>2</sub>,<sup>22–25</sup> are formed. The reaction occurring with pH value of 3.5 leads to reported compound Ni<sub>3</sub>(SeO<sub>3</sub>)<sub>3</sub>(H<sub>2</sub>O))<sup>20</sup> with one-third of Ni<sup>2+</sup> coordinated by water molecules. Increasing the pH to 5.0–6.0 markedly increases the incorporation of water molecules and/or hydroxyl groups leading to Ni<sub>12</sub>(OH)<sub>2</sub>(SeO<sub>3</sub>)<sub>8</sub>(OH)<sub>6</sub><sup>21</sup> and Ni(SeO<sub>3</sub>)<sub>3</sub>(H<sub>2</sub>O))<sup>18</sup>. The crystal structure of the latter is only composed of



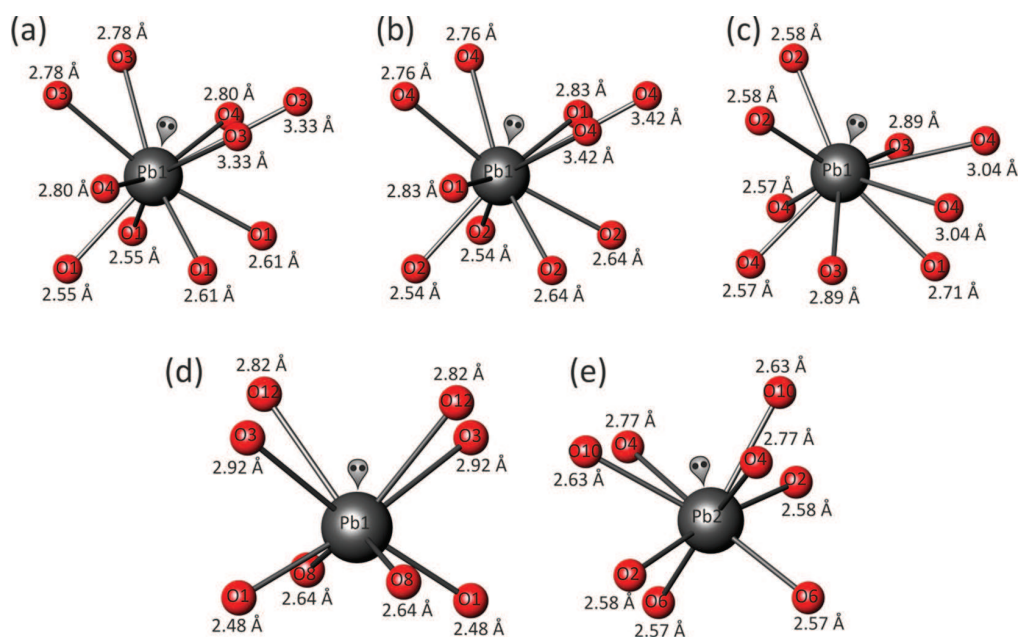


Figure 4. Coordination environment of Pb<sup>2+</sup> cations in the crystal structures of I (a), IV (b), II (c), and III (d and e).

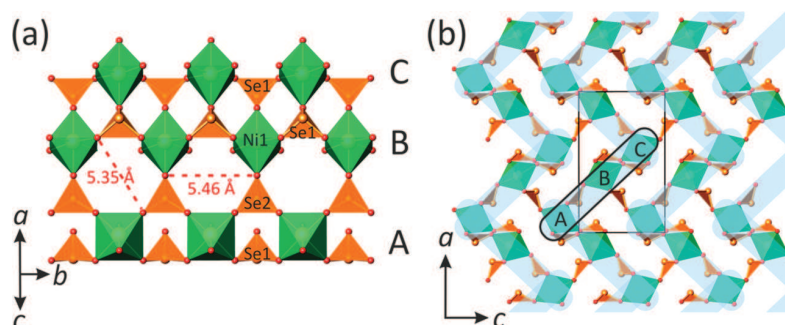


Figure 5. Polyhedral representation of the channel walls in  $\alpha$ -PbNi(SeO<sub>3</sub>)<sub>2</sub> (a) and its projection along the *b* axis as a combination of the pseudoribbons cross-linked into a 3D framework (Pb<sup>2+</sup> cations are omitted for clarity) (b). Legend: NiO<sub>6</sub> octahedra, green; SeO<sub>3</sub> trigonal pyramids, orange.

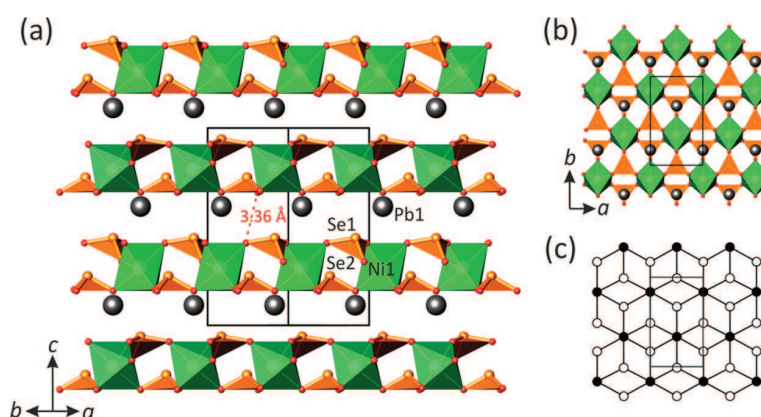


Figure 6. Crystal structure of  $\beta$ -PbNi(SeO<sub>3</sub>)<sub>2</sub> in two different projections (a and b), and the black-and-white graph corresponding to the Ni–Se sheet in the structure (Pb<sup>2+</sup> cations are omitted for clarity) (c). Designations as in Figure 4.

NiO<sub>5</sub>(H<sub>2</sub>O) polyhedra, while the tubular crystal structure of Ni<sub>12</sub>(OH)<sub>2</sub>(SeO<sub>3</sub>)<sub>8</sub>(OH)<sub>6</sub><sup>21</sup> contains half of the protonated (NiO<sub>5</sub>(OH))<sup>9-</sup> octahedra. With pH values greater than 7.0, only the very stable solid products Pb(SeO<sub>3</sub>)<sup>22–25</sup> phase is observed.

## STRUCTURAL DESCRIPTION

$\alpha$ -PbM(SeO<sub>3</sub>)<sub>2</sub> (M = Ni<sup>2+</sup>, Co<sup>2+</sup>). The isotypic compounds I and IV crystallize in orthorhombic symmetry (space group *Pnma*). They are built up from a 3D framework composed of

**Table 3.** Calculated Partial Charges for I ( $\alpha$ -PbNi( $\text{SeO}_3$ )<sub>2</sub>), II ( $\beta$ -PbNi( $\text{SeO}_3$ )<sub>2</sub>), III (PbNi<sub>2</sub>( $\text{SeO}_2\text{OH}$ )<sub>2</sub>( $\text{SeO}_3$ )<sub>2</sub>), and IV ( $\alpha$ -PbCo( $\text{SeO}_3$ )<sub>2</sub>)

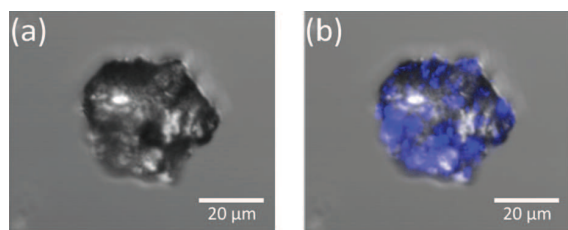
$\alpha$ -PbNi( $\text{SeO}_3$ ) <sub>2</sub>		PbNi <sub>2</sub> ( $\text{SeO}_2\text{OH}$ ) <sub>2</sub> ( $\text{SeO}_3$ ) <sub>2</sub>	
atom	charge $\pm q$	atom	charge $\pm q$
Pb1	+0.74952	Pb1	+0.81193
Se1	+0.24784	Pb2	+0.82647
Se2	+0.24417	Se1	+0.27735
Ni1	+0.93022	Se2	+0.27396
O1	-0.37204	Se3	+0.28956
O2	-0.33946	Se4	+0.28127
O3	-0.36119	Ni1	+0.99233
O4	-0.36583	Ni2	+0.96340
		O1	-0.36194
		O2	-0.35874
		O3	-0.35630
		O4	-0.35919
		O5	-0.33540
		O6	-0.35710
		O7	-0.33391
		O8	-0.35640
		O9	-0.38723
		O10	-0.35713
		O11	-0.38634
		O12	-0.35635
		H1	+0.20398
		H2	+0.20493

$\beta$ -PbNi( $\text{SeO}_3$ ) <sub>2</sub>	
atom	charge $\pm q$
Pb1	+0.77033
Se1	+0.25253
Se2	+0.22790
Ni1	+0.90996
O1	-0.35484
O2	-0.35920
O3	-0.35784
O4	-0.36482

$\alpha$ -PbCo( $\text{SeO}_3$ ) <sub>2</sub>	
atom	charge $\pm q$
Pb1	+0.73096
Se1	+0.23494
Se2	+0.23527
Co1	+1.00606
O1	-0.37077
O2	-0.37602
O3	-0.35183
O4	-0.36630



**Figure 7.** Transmission image of a crystal of  $\beta$ -PbNi( $\text{SeO}_3$ )<sub>2</sub> (a); emitting surface ( $\lambda_{\text{em}} = 420\text{--}440$  nm,  $\lambda_{\text{exc}} = 860$  nm), blue color (b).

anionic ( $\text{SeO}_3$ )<sup>2-</sup> and ( $\text{MO}_6$ )<sup>10-</sup> building units sharing common corners (Figure 3). We find one symmetrically independent  $\text{M}^{2+}$  position with rather regular ( $\text{MO}_6$ )<sup>10-</sup> octahedral coordination. The average bonding  $\langle \text{M}-\text{O} \rangle$  distances are 2.077 Å for I and 2.113 Å for IV. There are two independent Se atoms per formula unit where  $\text{Se}^{4+}$  cations form typical ( $\text{SeO}_3$ )<sup>2-</sup> triangular pyramids with Se located at its apical corner and a stereoactive lone pair acting as a complementary external ligand. The average  $\langle \text{Se}-\text{O} \rangle$  distance is 1.704 Å for both compounds,  $\text{M} = \text{Ni}^{2+}$  (I) and  $\text{Co}^{2+}$  (IV). The unique  $\text{Pb}^{2+}$  site is surrounded by O anions shared by ( $\text{SeO}_3$ )<sup>2-</sup> and ( $\text{MO}_6$ )<sup>10-</sup> groups, forming asymmetric polyhedra. In both compounds the  $\text{Pb}^{2+}$  cations demonstrate eight short strong  $\text{Pb}-\text{O}$  bonds (2.552–2.802 and 2.539–2.827 Å in I and IV, respectively) in one coordination hemisphere, and

two longer weaker bonds (3.332 and 3.418 Å in I and IV, respectively) in the other hemisphere (Figure 4a,b) with a clear location of the stereochemically active lone pair. In Figure 3b a 3D metal cationic framework of the crystal structures of I and IV is represented as a black-and-white graph with black-and-white nodes symbolizing coordination polyhedra of  $\text{M}^{2+}$  and  $\text{Se}^{4+}$ , respectively. It highlights the topological connectivity of the  $\text{SeO}_3$  and  $\text{MO}_6$  polyhedra in complex 3D framework with stretched rectangular channels extending along the [010] direction occupied by the lead cations and the  $\text{Se}^{4+}$  lone pairs with a dimension of  $3.1 \times 11.4$  Å<sup>2</sup>, measured as the shortest and longest O...O distances across the channels (Figure 3b). In the (010) plane, their sections are arranged in a crossed manner with alternate of the two orientations [201] and the [20 $\bar{1}$ ] with respect to the  $Pnma$  symmetry. The channels are bordered by six  $\text{MO}_6$  and six  $\text{SeO}_3$  polyhedra (Figure 3a). The projection of the channel walls is given in the figure resulting in a three  $\text{M}$ -octahedra-wide pseudoribbons (Figure 5a). Within the pseudoribbon, there are void spaces that are bounded by six-membered rings with a dimension of  $5.35 \times 5.46$  Å<sup>2</sup>. The pseudoribbons are further cross-linked into a 3D  $[\text{M}(\text{SeO}_3)_2]^{2-}$  framework through common  $\text{SeO}_3$  trigonal pyramids (Figure 5b). Divalent lead cations reside in the cavities and balance the charge of the framework of compounds I and IV. In general, it is typical for heteropolyhedral frameworks in inorganic oxysalts to be based upon interconnecting chains oriented parallel to each other.<sup>32</sup> The framework topology found out for  $\alpha$ -PbM( $\text{SeO}_3$ )<sub>2</sub> ( $\text{M} = \text{Ni}^{2+}$  and  $\text{Co}^{2+}$ ) has been observed previously, e.g., in the structures of  $(\text{H}_3\text{O})[\text{Fe}(\text{HPO}_4)_2]$ ,<sup>33</sup>  $\text{Na}_3[\text{In}(\text{PO}_4)_2]$ ,<sup>34</sup> and  $\text{Pb}[\text{Fe}(\text{AsO}_4)(\text{AsO}_3\text{OH})]$ .<sup>35</sup>

**$\beta$ -PbNi( $\text{SeO}_3$ )<sub>2</sub>.** The crystal structure of II adopts an orthorhombic symmetry (noncentrosymmetric space group,  $Cmc2_1$ ). It contains one symmetrically independent  $\text{Ni}^{2+}$  cation that forms a slightly distorted  $\text{NiO}_6$  octahedron: the trans O–Ni–O bond angles fall in the range of 155.82–172.69°, whereas the cis angles range from 80.91° to 102.94°. The Ni–O bond lengths are 2.045(5)–2.148(6) Å. Two independent  $\text{Se}^{4+}$  sites have a trigonal pyramidal coordination with an apex occupied by the selenium cation as already mentioned previously. The average  $\langle \text{Se}-\text{O} \rangle$  bond lengths of the trigonal pyramids are 1.698 and 1.707 Å for Se1 and Se2 sites, respectively. In the crystal structure of II a unique  $\text{Pb}^{2+}$  ion has seven short  $\text{Pb}-\text{O}$  bonds (2.569–2.885 Å) in the first coordination hemisphere, whereas the second hemisphere is occupied by two longer bonds (3.035 Å) (Figure 4c). Once again, the coordination polyhedra of the lead cation is asymmetric and obviously indicates that the  $6s^2$  lone pair is stereochemically active. In contrast, we have recently described the crystal structure of  $\text{PbBi}_4\text{O}_6\text{Cl}_2$  in which the  $\text{Pb}^{2+}$  lone pair activity is fully quenched.<sup>36</sup>

Similarly to what was found in the  $\alpha$ -PbNi( $\text{SeO}_3$ )<sub>2</sub> form (I), the  $\beta$ -form is built up from isolated  $\text{NiO}_6$  octahedra interlinked by  $\text{SeO}_3$  groups via common oxygen corners. However, the linkage modes differ in both structures. The crystal structure of II (Figure 6a) is essentially two-dimensional (2D) and is based upon  $[\text{Ni}(\text{SeO}_3)_2]^{2-}$  sheets. They are shown in Figure 6b and lay parallel to (001). The lone pairs of electrons of  $\text{Se}^{4+}$  cations are shifted in the [001] direction toward the vacant part of the interlayer space. The sheets in II are very similar to 2D pseudoribbons delimiting the channels of I and IV. Same cavities are filled by the  $\text{Pb}^{2+}$  cations, which serve to balance charge and achieve the cohesion between the sheets. The shortest interlayer O...O contacts across the interlayer is about 3.36 Å, much greater than the sum of van der Waals radii and involves a true 2D-

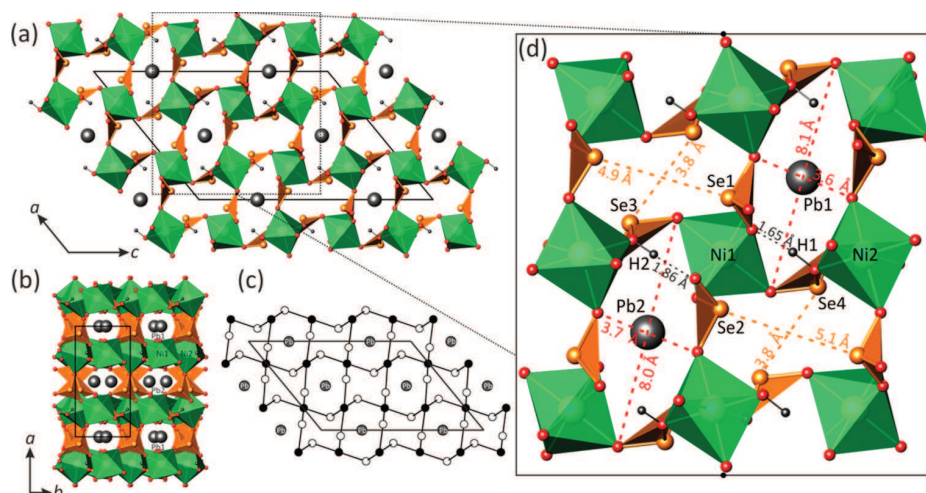


**Figure 8.** General projection of the crystal structure of  $\text{PbNi}_2(\text{SeO}_2\text{OH})_2(\text{SeO}_3)_2$  along the  $b$  and  $c$  axes (a and b), respectively; its black-and-white graph (c); and more detailed fragment of the structure (d). Legend as in Figure 4.

character. The black-and-white graph corresponding to the layered nickel selenite structural units is shown in Figure 6c. This kind of layer topology is one of the most common in inorganic oxysalts<sup>32,37</sup> and has been recently observed, for instance, in the crystal structure of steklite,  $\text{K}[\text{Al}(\text{SO}_4)_2]$ ,<sup>38</sup> where  $(\text{AlO}_6)$  octahedra are linked by  $(\text{SO}_4)$  tetrahedra. In selenites, it has been reported for the crystal structures of  $\text{K}_2[\text{M}(\text{SeO}_3)_2]$  ( $\text{M} = \text{Mn}$  and  $\text{Co}$ ).<sup>39,40</sup> The NCS character of **II** is well evidenced on Figure 6a where only “up”  $\text{SeO}_3$  orientations are found in the crystal structure. Dipole moments were calculated for **II** due to its noncentrosymmetry. In this calculation performed using Pacha,<sup>29</sup> local charges given in Table 3 have been used. In general, it is noteworthy that the charge distribution is very similar in the four new selenites, due to similar concomitant groups.  $\text{Ni}^{2+}$  and  $\text{Co}^{2+}$  show a similar degree of covalence leading to a residual covalence charge close to  $\sim +1$ . As expected the Se–O bonds are very strong leading to a residual charge around  $+0.25$ . Finally, the shortest Pb–O distances also bring a strong degree of covalence leading to Pb partial charge close to  $+1$ . For **II**, all  $\text{SeO}_3$  groups stand in to bring local dipole moments that do not cancel each other. The moments are mainly oriented along the  $[001]$  direction with values of 1.87 and 2.07 Debyes for  $\text{Se}(1)\text{O}_3$  and  $\text{Se}(2)\text{O}_3$ , respectively. Other local dipoles arise from distorted  $\text{NiO}_6$  octahedra and  $\text{Pb}^{2+}$  complex coordination polyhedra that also lead to a net nonzero polarization due to the  $Cmc2_1$  symmetry. Finally each individual layer shown on Figure 6a brings its own total dipole, mainly parallel to  $c$  but with different  $(a, b)$  components. Our calculations performed on the  $[\text{Pb}_4\text{Ni}_4(\text{SeO}_3)_8]$  unit-cell content containing two layers lead to  $M = 21.51$  Debyes almost parallel to  $c$  (negative charge barycenter (1.157,  $-0.111$ , 2.197), positive charge barycenter ( $-1.189$ ,  $-0.256$ ,  $-1.617$ )). This important value is expected to lead to strong SHG effects. Our analysis was performed on three different crystals of **II** as detailed in the Experimental Section. Dealing with a rather thick crystal, only some areas of the crystal surface show a significant SHG signal as shown in blue color in Figure 7. This feature is rather common and was observed recently in  $[\text{Bi}_{12}\text{O}_{15}][\text{Li}_2(\text{SO}_4)_4]$ .<sup>41</sup> It is noteworthy that in the experimental setting the detected SHG signal is maximal in the horizontal plane (below the crystal), which reduces the detection for thick and irregular absorbing samples. In addition the refinement of racemic twinned domains (ratio  $\sim 60:40$ ) suggests

the possibility for local SHG quenching at the antiphase boundary.

**Polymorphism in  $\text{PbNi}(\text{SeO}_3)_2$ .** In our experiments, we have observed two modifications of  $\text{PbNi}(\text{SeO}_3)_2$  that differ in both crystallographic parameters and structural topology. The  $\alpha$ -phase has a notably smaller unit-cell volume ( $544.83 \text{ \AA}^3$ ) than the  $\beta$ -phase ( $575.81 \text{ \AA}^3$ ) and, as a consequence, a remarkably higher density ( $6.337$  versus  $5.996 \text{ g/cm}^3$ , respectively). In terms of structural complexity expressed as a Shannon information amount per unit cell,<sup>42,43</sup> the  $\beta$ -phase is considerably more simple ( $58.439$  bits per unit cell) than the  $\alpha$ -phase ( $116.877$  bits per unit cell). It is a general observation that a high-temperature polymorph is structurally simpler than its low-temperature counterpart (due to the increase in both vibrational and configurational entropies),<sup>44</sup> which, together with the data on density and unit-cell volumes, strongly suggest that the  $\alpha$ - and  $\beta$ -modifications of  $\text{PbNi}(\text{SeO}_3)_2$  are low- and high-temperature polymorphs, respectively. This conclusion agrees well with the 3D and 2D characters of their structures, respectively, which is frequently observed in inorganic compounds (that is, structural dimensionality of a low-temperature polymorph is higher than that of its high-temperature counterpart<sup>45</sup>).

**$\text{PbNi}_2(\text{SeO}_2\text{OH})_2(\text{SeO}_3)_2$ .** The crystal structure of **III** adopts a monoclinic symmetry (space group,  $P2_1/c$ ). There are two symmetrically independent  $\text{Ni}^{2+}$  sites with rather regular octahedral coordination with the average  $\langle \text{Ni}-\text{O} \rangle$  bond lengths equal to 2.064 and 2.077  $\text{\AA}$  for  $\text{Ni}1$  and  $\text{Ni}2$  sites, respectively. The four crystallographically inequivalent  $\text{Se}^{4+}$  atoms are asymmetrically coordinated by three oxygen atoms in a trigonal pyramidal geometry. However, two of them are protonated leading to strongly distorted  $(\text{Se}(3)\text{O}_2\text{OH})^-$  and  $(\text{Se}(4)\text{O}_2\text{OH})^-$  trigonal pyramids with one long Se–O bond (1.810 and 1.785  $\text{\AA}$  for  $\text{Se}(3)$  and  $\text{Se}(4)$ , respectively) and two shorter Se–O bonds (1.659–1.676 and 1.649–1.675  $\text{\AA}$  for  $\text{Se}3$  and  $\text{Se}4$ , respectively). Similarly distorted coordination geometry is typical of hydroxide ligands, as reported for instance in the crystal structure of  $\text{Ni}(\text{HSeO}_3) \cdot 4\text{H}_2\text{O}$ .<sup>46</sup> The average  $\langle \text{Se}-\text{O} \rangle$  bond lengths are equal to 1.695, 1.693, 1.715, and 1.703  $\text{\AA}$  for  $\text{Se}(1)\text{O}_3$ ,  $\text{Se}(2)\text{O}_3$ ,  $\text{Se}(3)\text{O}_2\text{OH}$ , and  $\text{Se}(4)\text{O}_2\text{OH}$ , respectively. The two independent  $\text{Pb}^{2+}$  cations are 8-fold oxygen coordinated (Figure 3d,e) with Pb–O distances in the ranges of 2.481–2.916 and 2.567–2.765  $\text{\AA}$  for  $\text{Pb}1$  and  $\text{Pb}2$ , respectively. They both

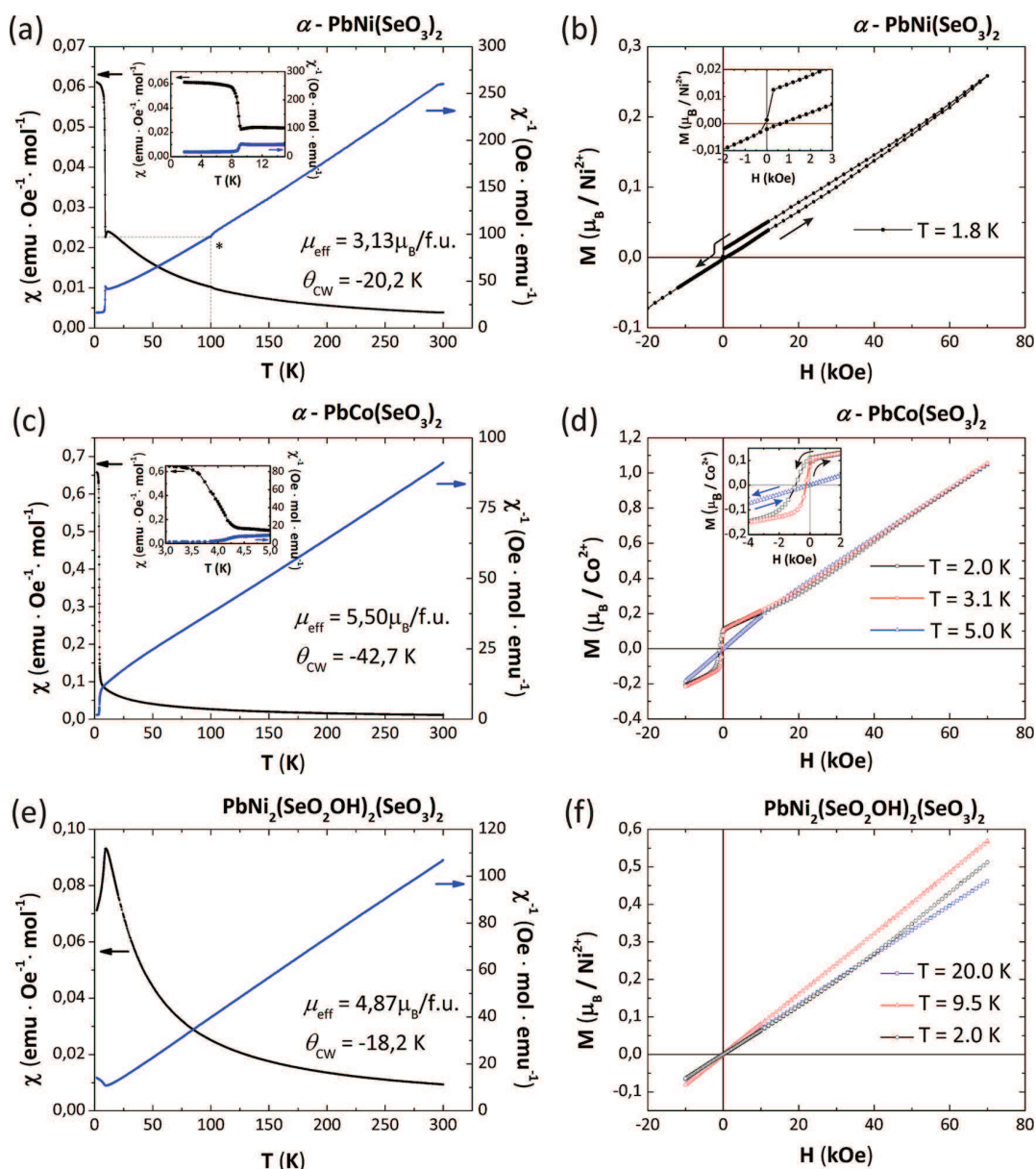


**Figure 9.** Thermal evolution of the magnetic susceptibility for I (a), IV (c), and III (e). Magnetization as a function of applied field for I (b), IV (d), and III (f).

show a distorted square antiprismatic arrangement with lone pairs of electrons oriented toward the longest oxygen neighbors, similarly to lead coordination in  $\text{PbMo}_2\text{O}_5(\text{SeO}_3)_2$ .<sup>10</sup>

In the crystal structure of III, the  $\text{NiO}_6$  octahedra are sharing their vertices with  $\text{SeO}_3$  groups, forming a 3D framework encapsulating channels propagating along the [010] direction (Figure 8a). Four independent channels are occupied alternately by divalent lead cations and lone pairs of electrons of the  $\text{Se}^{4+}$  cations. The channels containing  $\text{Pb}^{2+}$  are bordered by  $\text{O}^{2-}$  ions and have a cross-section of maximum of  $\sim 3.6 \times 8.1 \text{ \AA}^2$  taking into account the shortest  $\text{O} \cdots \text{O}$  separations. Those bordered by  $\text{Se}^{4+}$  ions  $\text{Se} \cdots \text{Se}$  are  $\sim 3.8 \times 5.1 \text{ \AA}^2$  large on the basis of the  $\text{Se} \cdots \text{Se}$  distances (Figure 8d). It is striking that in the  $(a,b)$  projection the similitude between Pb1 and Pb2 channels suggests a  $V/2$  subcell. In fact the projection in the  $(a,b)$  plane evidences channels

growing along the  $c$ -axis with a clear distinction between Pb2 and Pb1 sites (Figure 8b).

Figure 8c shows the black-and-white graph corresponding to a 3D metal cationic framework of III. Its structural architecture is closely related to that observed in the crystal structure of  $\text{PbFe}_2(\text{SeO}_3)_4$ <sup>47</sup> and represents an interesting topological variation of the primitive cubic (pcu) network.<sup>48</sup>

## MAGNETIC PROPERTIES

The powder samples selected for magnetic measurements have been prepared from stoichiometries corresponding to the  $P_1$  (I and IV (replacing NiO by CoO)) and  $P_2$  (III) points in Figure 1a. After Rietveld refinement though strong preferred orientation effects, the refined phase weight fractions of impurity (diamagnetic  $\text{Pb}(\text{SeO}_3)$ ) are 0.17, 0.42, and 0.15 for the powder samples of I, III, and IV, respectively. Magnetic data were

normalized taking into account the massic contribution of the second phase. PXRD patterns are shown in Figure 2.

The FC magnetic susceptibility  $\chi$  and  $\chi^{-1}$  versus temperature are plotted in Figure 9a,c for  $\alpha$ -PbNi(SeO<sub>3</sub>)<sub>2</sub> (I) and  $\alpha$ -PbCo(SeO<sub>3</sub>)<sub>2</sub> (IV). In the high-temperature range,  $\chi^{-1}(T)$  could be fitted using a Curie–Weiss law  $\chi = C/(T - \theta_{CW})$ . Both compounds show very similar behavior dominated by anti-ferromagnetic exchanges as given by the negative Curie–Weiss temperatures,  $\theta_{CW} = -20.2$  and  $-42.7$  K, respectively. The deduced effective moments are  $3.13 \mu_B$  and  $5.50 \mu_B$  per formula unit, respectively. It indicates significant spin–orbit couplings (SOC) compared to calculated spin-only values, i.e.,  $2.83 \mu_B/\text{Ni}^{2+}$  and  $3.87 \mu_B/\text{Co}^{2+}$ . One should also note that the exaggerated value measured in the cobalt compound compared to the commonly observed  $\mu_{\text{eff}} \sim 4.5 \mu_B$  probably denote an approximate determination of the IV compound's weight fraction in the biphasic sample, due to preferred orientation effects mentioned previously.

For I the broad peak below 100 K and the upturn of the susceptibility below 9 K suggests the setting of short-range antiferromagnetic correlations but is immediately masked by the appearing of a magnetic moment. In IV a similar, but even more abrupt, phenomenon occurs below 4.5 K. In both compounds, it is accompanied by a ZFC/FC divergence at low temperature, as shown in Supporting Information Figure S12. It is ascribed to intrinsic spin-canting due to favored antisymmetric exchanges (Dzyaloshinski–Moriya interactions) in this crystal structure with strong SOC ions. As expected from the strongest SOC for Co<sup>2+</sup>, the M(H) magnetization plot indicates a largest remanent moment for IV compared to I, i.e.,  $0.1 \mu_B/\text{Co}^{2+}$  against  $0.01 \mu_B/\text{Ni}^{2+}$  as shown on the Figures 9b,d. In the mean-field approximation, the Curie–Weiss temperature is given as  $\theta_{CW} = 2zJS(S+1)/3k_B$ , where the z-number of neighbors interact with the same J force with a central M<sup>2+</sup> ion. Theoretically, this approximation is available in the Heisenberg case but could lead to an approximated value for Co<sup>2+</sup> and Ni<sup>2+</sup> ions where spin–orbit coupling should favor anisotropic spins (XY or Ising).

Dealing with similar crystal structures of I and IV, one can derive  $J_{(I)}/J_{(IV)} = \theta_{CW(I)}(S_{\text{Co}^{2+}})(S_{\text{Co}^{2+}} + 1)/\theta_{CW(IV)}(S_{\text{Ni}^{2+}})(S_{\text{Ni}^{2+}} + 1) = 0.89$ . This involves very similar J coupling values. Taking into account that each metal center is surrounded by z = 8 other metals with plausible M–O–O–M superexchange paths ( $4.8 \text{ \AA} < \text{M–M} < 6.2 \text{ \AA}$  and O–O distance smaller than the sum of their ionic radii), one can also estimate the mean J value to  $J/k_B \sim -1.9$  and  $-2.1$  K, respectively.

$\chi(T)$  and  $\chi^{-1}(T)$  of compound III are shown on Figure 9e. It shows a paramagnetic regime above the setting of an antiferromagnetic transition at  $T_N = 10$  K. The Curie–Weiss law above  $T_N$  yields  $\mu_{\text{eff}} = 4.87 \mu_B/(\text{formula unit (f.u.)})$ . ( $3.44 \mu_B/\text{Ni}^{2+}$ ) and  $\theta_{CW} = -18.2$  K in good agreement with predominant antiferromagnetic exchanges between Ni<sup>2+</sup> ions with strong SOC. Once more, in a mean-field approximation we deduce a mean  $J_{\text{Ni–Ni}}/k_B$  of  $-1.71$  K from the  $\theta_{CW}$  value, taking into account z equals eight Ni neighbors around each Ni<sup>2+</sup> with efficient geometrical SSE paths under conditions given previously. This low value is nearly similar to the one found for compound I and gives an indication for weak but comparable Ni–O–O–Ni negative exchanges mediated by SeO<sub>3</sub> corners in both compounds.

## CONCLUSION

In this work, the PbO–NiO–SeO<sub>2</sub> ternary system in hydrothermal conditions at 473 K was investigated. Three novel lead

nickel selenites and one novel lead cobalt selenite were synthesized and characterized. The PbNi(SeO<sub>3</sub>)<sub>2</sub> compound crystallizes in two polymorphic orthorhombic modifications,  $\alpha$  (I) and  $\beta$  (II). The PbCo(SeO<sub>3</sub>)<sub>2</sub> phase (IV) is isotypic with I. According to the experimental results, the pH values of the solution play the essential role in hydrolysis and condensation processes by hydrothermal reactions in the studied system and determine structural architectures of resulted products of the syntheses. The observed dependence of the structural variety and the structural units upon the pH values is remarkable and can be used for preparation of new transition metal oxoselenites and similar groups of heavy-element compounds with novel structural architectures.

## ASSOCIATED CONTENT

### Supporting Information

Tables listing fractional atomic coordinates, atomic displacement parameters, and selected bond distances, figures showing experimental XRD patterns and temperature dependences of magnetization, and crystallographic information files. This material is available free of charge via the Internet at <http://pubs.acs.org>.

## AUTHOR INFORMATION

### Corresponding Author

\*E-mail: [olivier.mentre@ensc-lille.fr](mailto:olivier.mentre@ensc-lille.fr).

### Notes

The authors declare no competing financial interest.

## ACKNOWLEDGMENTS

This work was carried out under the framework of the Multi-InMaDe project supported by the ANR (Grant ANR 2011-JS-08 00301). The Fonds Européen de Développement Régional (FEDER), CNRS, Région Nord Pas-de-Calais, and Ministère de l'Éducation Nationale de l'Enseignement Supérieur et de la Recherche are acknowledged for funding the X-ray diffractometers. V.M.K. thanks l'Ambassade de France en Russie and l'Agence Campus France (Contract Nos. 768231K, 779116K, 794852B, 808399A, and 808400J) for the partial support of this work. S.V.K. and O.I.S. acknowledge financial support from St. Petersburg State University (Internal Grant 3.38.136.2014).

## REFERENCES

- (1) Dadap, J. I.; Shan, J.; Heinz, T. F. *J. Opt. Soc. Am. B* **2004**, *21*, 1328–1347.
- (2) Cady, W. G. *Piezoelectricity: An Introduction to the Theory and Applications of Electromechanical Phenomena in Crystals*; Dover Publications: New York, 1964; p 822.
- (3) Jona, F.; Shirane, G. *Ferroelectric Crystals*; Pergamon Press: Oxford, U.K., 1962; p 402.
- (4) Lang, S. B. *Sourcebook of Pyroelectricity*; Gordon and Breach Science: London, New York, 1974; p 562.
- (5) Verma, V. P. *Thermochim. Acta* **1999**, *327*, 63–102.
- (6) Effenberger, H. *J. Solid State Chem.* **1988**, *73*, 118–126.
- (7) Li, P.-X.; Kong, F.; Hu, C.-L.; Zhao, N.; Mao, J.-G. *Inorg. Chem.* **2010**, *49*, 5943–5952.
- (8) Yeon, J.; Kim, S.; Nguyen, S. D.; Lee, H.; Halasyamani, P. S. *Inorg. Chem.* **2012**, *51*, 609–619.
- (9) Zhang, S.-Y.; Hu, C.-L.; Li, P.-X.; Jiang, H.-L.; Mao, J.-G. *Dalton Trans.* **2012**, *41*, 9532–9542.
- (10) Oh, S.; Lee, D. W.; Ok, K. M. *Inorg. Chem.* **2012**, *51*, 5393–5399.
- (11) Oh, S.-J.; Lee, D. W.; Ok, K. M. *Dalton Trans.* **2012**, *41*, 2995–3000.

- (12) Kovrugin, V. M.; Colmont, M.; Mentré, O.; Siidra, O. I.; Krivovichev, S. V. *Mineral. Mag.* **2015**, submitted for publication.
- (13) Kovrugin, V. M.; Siidra, O. I.; Colmont, M.; Mentré, O.; Krivovichev, S. V. *Mineral. Petrol.* **2015**, submitted for publication.
- (14) Aliev, A.; Kovrugin, V. M.; Colmont, M.; Terryn, C.; Huvé, M.; Siidra, O. I.; Krivovichev, S. V.; Mentré, O. *Cryst. Growth Des.* **2014**, *14*, 3026–3034.
- (15) Vlaev, L. T.; Genieva, S. D.; Gospodinov, G. G. *J. Therm. Anal. Calorim.* **2005**, *81*, 469–475.
- (16) Forster, P. M.; Stock, N.; Cheetham, A. K. *Angew. Chem., Int. Ed.* **2005**, *44*, 7608–7611.
- (17) Sonnauer, A.; Stock, N. *Eur. J. Inorg. Chem.* **2008**, 2008, 5038–5045.
- (18) Engelen, B.; Bäumer, U.; Hermann, B.; Müller, H.; Unterderweide, K. Z. *Anorg. Allg. Chem.* **1996**, *622*, 1886–1892.
- (19) Wildner, M. *Monatsh. Chem.* **1991**, *122*, 585–594.
- (20) Mcmanus, A. V. P.; Harrison, W. T. A.; Cheetham, A. K. *J. Solid State Chem.* **1991**, *92*, 253–260.
- (21) Amorós, P.; Marcos, M. D.; Roca, M.; Beltrán-Porter, A.; Beltrán-Porter, D. J. *Solid State Chem.* **1996**, *126*, 169–176.
- (22) Popovkin, B. A.; Cheremisinov, V. P.; Simanov, Y. P. *J. Struct. Chem.* **1963**, *4*, 38–43.
- (23) Fischer, R. *Tschermaks Mineral. Petrogr. Mitt.* **1972**, *17*, 196–207.
- (24) Koskenlinna, M.; Valkonen, J. *Cryst. Struct. Commun.* **1977**, *6*, 813–816.
- (25) Pasero, M.; Rotiroti, N. *Neues Jahrb. für Mineral., Monatsh.* **2003**, *2003*, 145–152.
- (26) APEX; Bruker AXS: Madison, WI, USA, 2007.
- (27) SADABS; Bruker AXS: Madison, WI, USA, 2001.
- (28) Sheldrick, G. M. *Acta Crystallogr.* **2008**, *A64*, 112–122.
- (29) Henry, M. *ChemPhysChem* **2002**, *3*, 561–569.
- (30) Pourbaix, M. *Atlas of electrochemical equilibria in aqueous solutions*; National Association of Corrosion Engineers: Houston, TX, USA, 1974; p 644.
- (31) Takeno, N. *Atlas of Eh-pH diagrams*, Geological Survey of Japan Open File Report No.419; National Institute of Advanced Industrial Science and Technology, Research Center for Deep Geological Environments: Tsukuba, Japan, 2005; p 287.
- (32) Krivovichev, S. V. *Structural Crystallography of Inorganic Oxysalts*; Oxford University Press: Oxford, U.K., 2009.
- (33) Vencato, I.; Mattievich, E.; Moreira, L. F.; Mascarenhas, Y. P. *Acta Crystallogr.* **1989**, *C45*, 367–371.
- (34) Liü, K.-H. *Eur. J. Solid State Inorg. Chem.* **1996**, *33*, 519–526.
- (35) Effenberger, H.; Hejny, C.; Pertlik, F. *Monatsh. Chem.* **1996**, *127*, 127–133.
- (36) Aliev, A.; Olchowka, J.; Colmont, M.; Capoen, E.; Wickleder, C.; Mentré, O. *Inorg. Chem.* **2013**, *52*, 8427–8435.
- (37) Krivovichev, S. V. *Crystallogr. Rev.* **2004**, *10*, 185–232.
- (38) Murashko, M. N.; Pekov, I. V.; Krivovichev, S. V.; Chernyatyeva, A. P.; Yapaskurt, V. O.; Zadov, A. E.; Zelensky, M. E. *Geol. Ore Deposits (Transl. of Geol. Rudn. Mestorozhd.)* **2013**, *55*, 594–600.
- (39) Wildner, M. *Acta Crystallogr.* **1992**, *C48*, 595–595.
- (40) Wildner, M. *Acta Crystallogr.* **1992**, *C48*, 410–412.
- (41) Lü, M.; Colmont, M.; Huvé, M.; De Waele, I.; Terryn, C.; Aliev, A.; Mentré, O. *Inorg. Chem.* **2014**, *53*, 12058–12065.
- (42) Krivovichev, S. V. *Acta Crystallogr.* **2012**, *A68*, 393–398.
- (43) Krivovichev, S. V. *Angew. Chem., Int. Ed.* **2014**, *53*, 654–661.
- (44) Krivovichev, S. V. *Mineral. Mag.* **2013**, *77*, 275–326.
- (45) Krivovichev, S. V.; Cahill, C. L.; Burns, P. C. *Inorg. Chem.* **2002**, *41*, 34–39.
- (46) Engelen, B.; Boldt, K.; Unterderweide, K.; Bäumer, U. *Z. Anorg. Allg. Chem.* **1995**, *621*, 331–339.
- (47) Johnston, M. G.; Harrison, W. T. A. *J. Solid State Chem.* **2004**, *177*, 4680–4686.
- (48) Krivovichev, S. V. *Mineral. Mag.* **2014**, *78*, 415–435.

# **pH controlled pathway and systematic hydrothermal phase diagram for elaboration of synthetic lead nickel selenites**

## **SUPPLEMENTARY INFORMATION**

*Vadim M. Kovrugin*<sup>†,‡</sup>, *Marie Colmont*<sup>†</sup>, *Christine Terryn*<sup>§</sup>, *Silviu Colis*<sup>||</sup>, *Oleg I. Siidra*<sup>‡</sup>,  
*Sergey V. Krivovichev*<sup>‡</sup>, *Olivier Mentré*<sup>†\*</sup>

<sup>†</sup> Université Lille Nord de France, UMR 8181 CNRS, Unité de Catalyse et de Chimie du Solide (UCCS USTL), 59655 Villeneuve d'ASCQ, France

<sup>‡</sup> Department of Crystallography, Saint-Petersburg State University, Universitetskaya nab. 7/9, 199034 St. Petersburg, Russia

<sup>§</sup> Plateforme Imagerie Cellulaire et Tissulaire, 51 rue Cognacq-Jay, 51100 Reims, France

<sup>||</sup> Institut de Physique et Chimie des Matériaux de Strasbourg (IPCMS), UMR 7504 CNRS and Université de Strasbourg (UDS-ECPM), F-67034 Strasbourg Cedex 2, France

## SUPPLEMENTARY INFORMATION

Experimental XRD patterns of the samples corresponding to the  $P_3$ – $P_7$  points (Figure 1a) are shown in Figures S1–S5. Experimental XRD patterns of the samples corresponding to the series of the experiments with the same  $\text{PbO} : \text{NiO} : \text{SeO}_2 = 5 : 3 : 10$  and various pH are shown in Figures S6–S11. Taking into account impossibility to observe crystals corresponding to other phases in the samples and small intensities of “undefined peaks” observed in the XRD patterns, we do not consider them as representative phases and not indicate them on the triangle crystallization diagram in Figure 1a.

Temperature dependences of magnetization measured at 200 Oe for  $\alpha$  –  $\text{PbNi}(\text{SeO}_3)_2$  (**I**), and  $\alpha$  –  $\text{PbCo}(\text{SeO}_3)_2$  (**IV**) are shown in Figure S12.

Fractional atomic coordinates, atomic displacement parameters, and selected bond distances are listed in Tables S1–S3 for  $\alpha$  –  $\text{PbNi}(\text{SeO}_3)_2$  (**I**), Tables S4–S6 for  $\beta$  –  $\text{PbNi}(\text{SeO}_3)_2$  (**II**), Tables S7–S9 for  $\text{PbNi}_2(\text{SeO}_2\text{OH})_2(\text{SeO}_3)_2$  (**III**), and Tables S10–S12 for  $\alpha$  –  $\text{PbCo}(\text{SeO}_3)_2$  (**IV**).



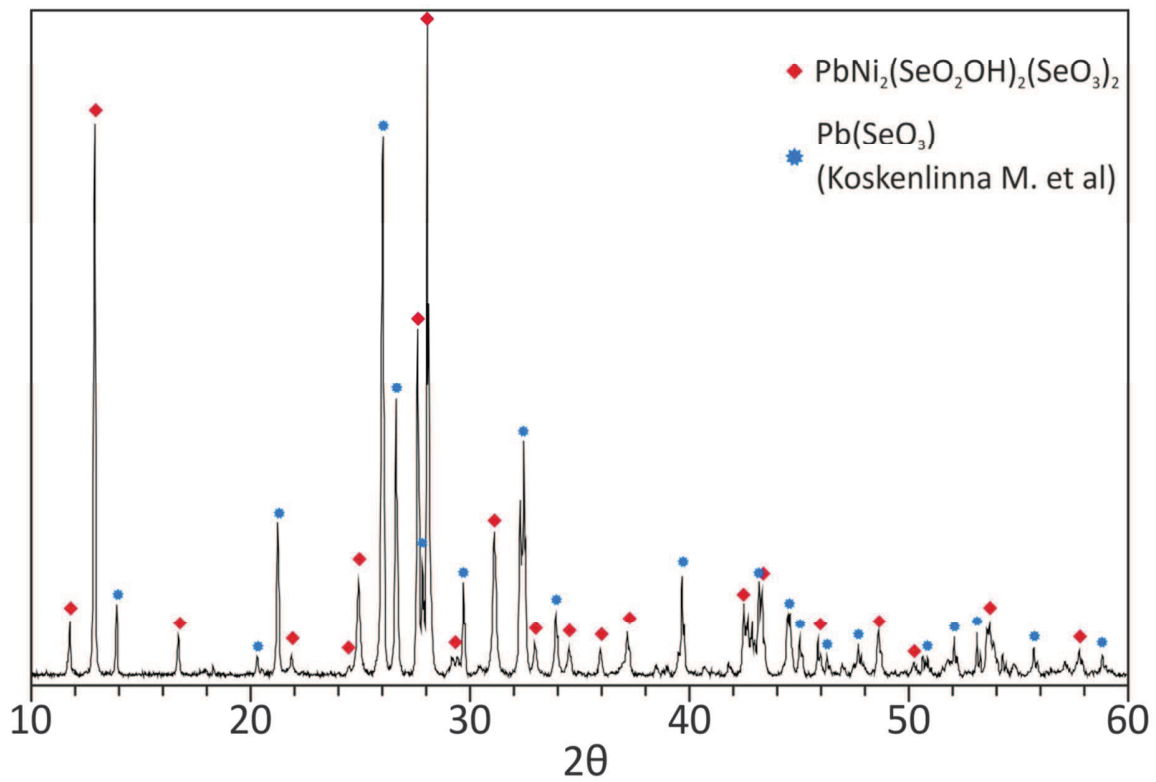


**Figure S1.** Experimental XRD pattern for the  $P_3$  experimental point with  $\text{PbO} : \text{NiO} : \text{SeO}_2 = 1 : 3 : 30$ .

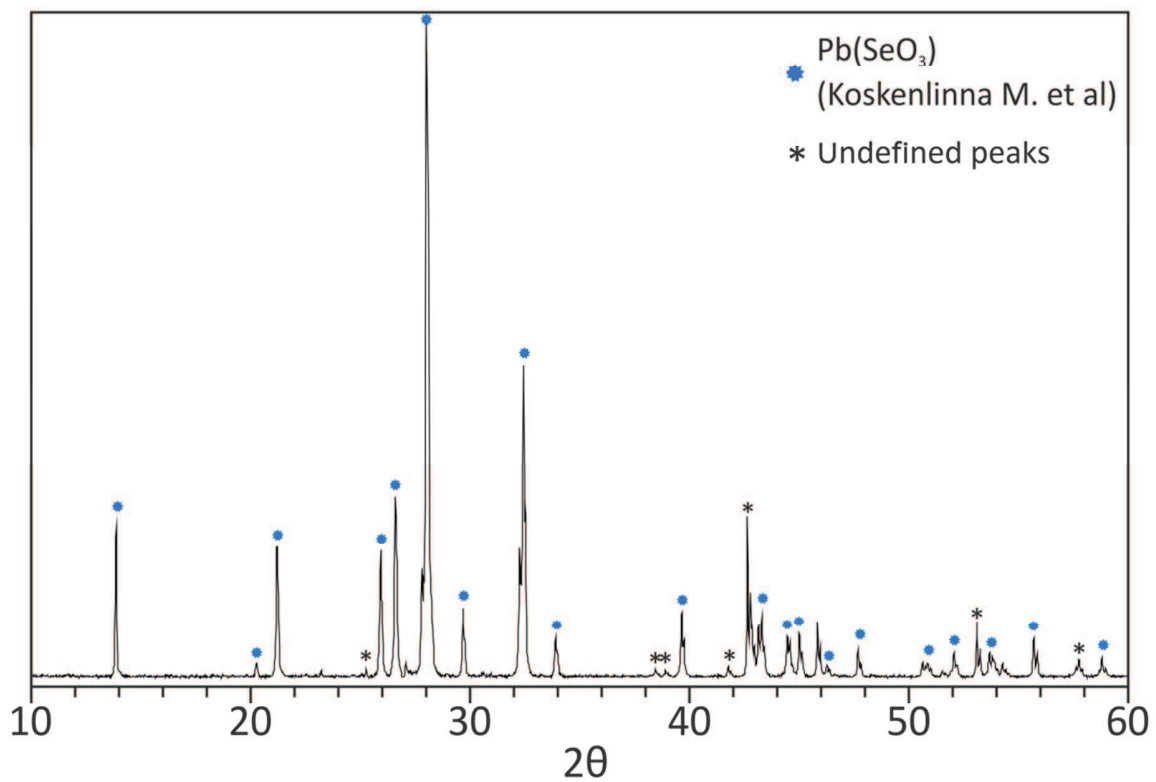


**Figure S2.** Experimental XRD pattern for the  $P_4$  experimental point with  $\text{PbO} : \text{NiO} : \text{SeO}_2 = 1 : 1 : 40$ .

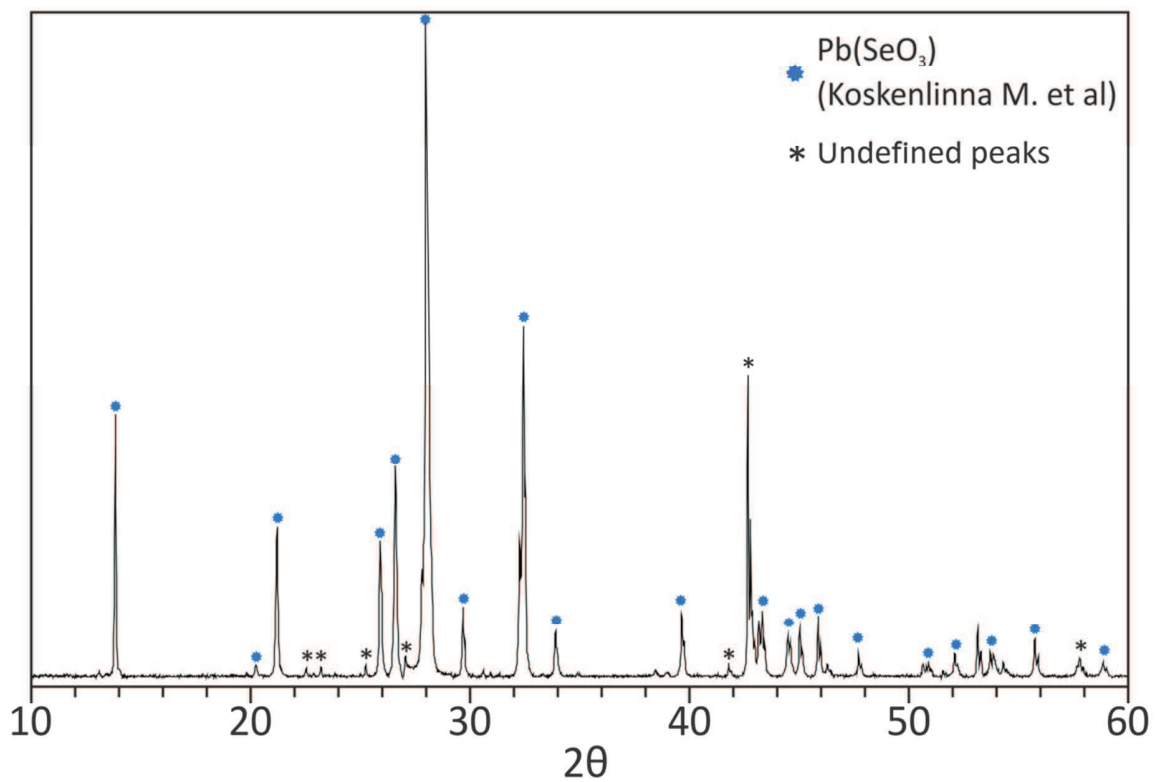


**Figure S3.** Experimental XRD pattern for the  $P_5$  experimental point with  $\text{PbO} : \text{NiO} : \text{SeO}_2 = 4 : 1 : 25$ .

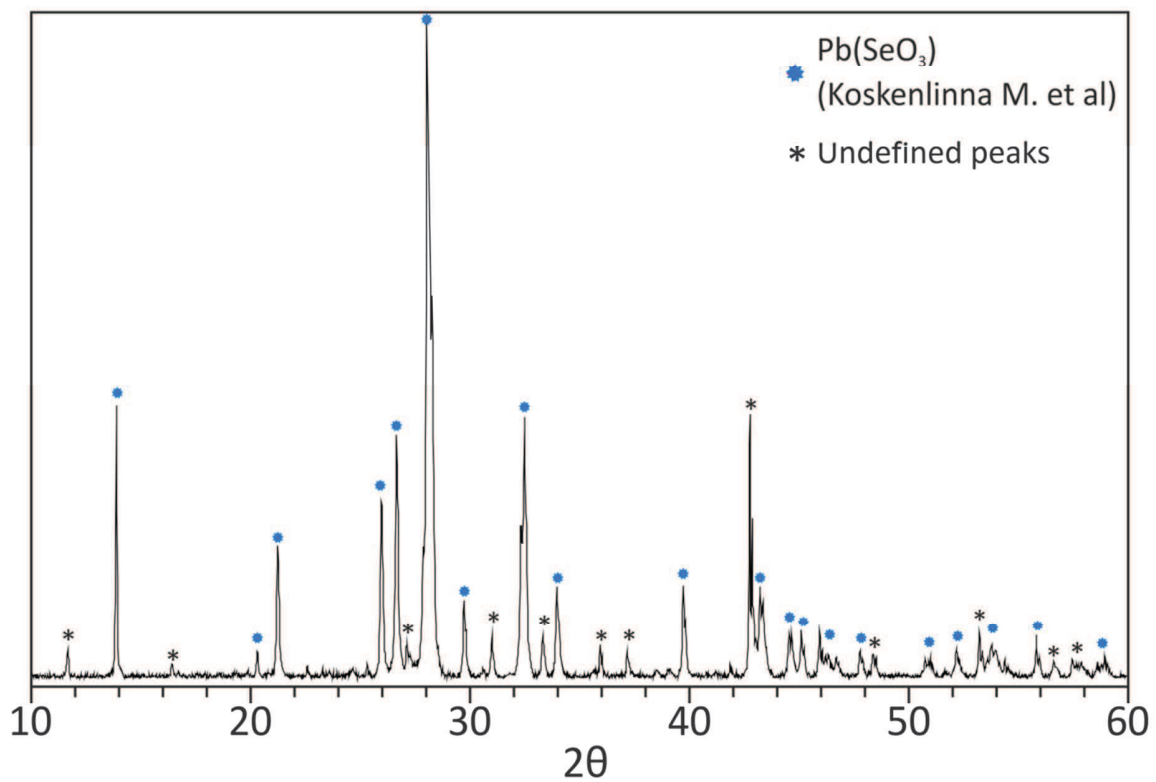


**Figure S4.** Experimental XRD pattern for the  $P_6$  experimental point with  $\text{PbO} : \text{NiO} : \text{SeO}_2 = 8 : 1 : 5$ .

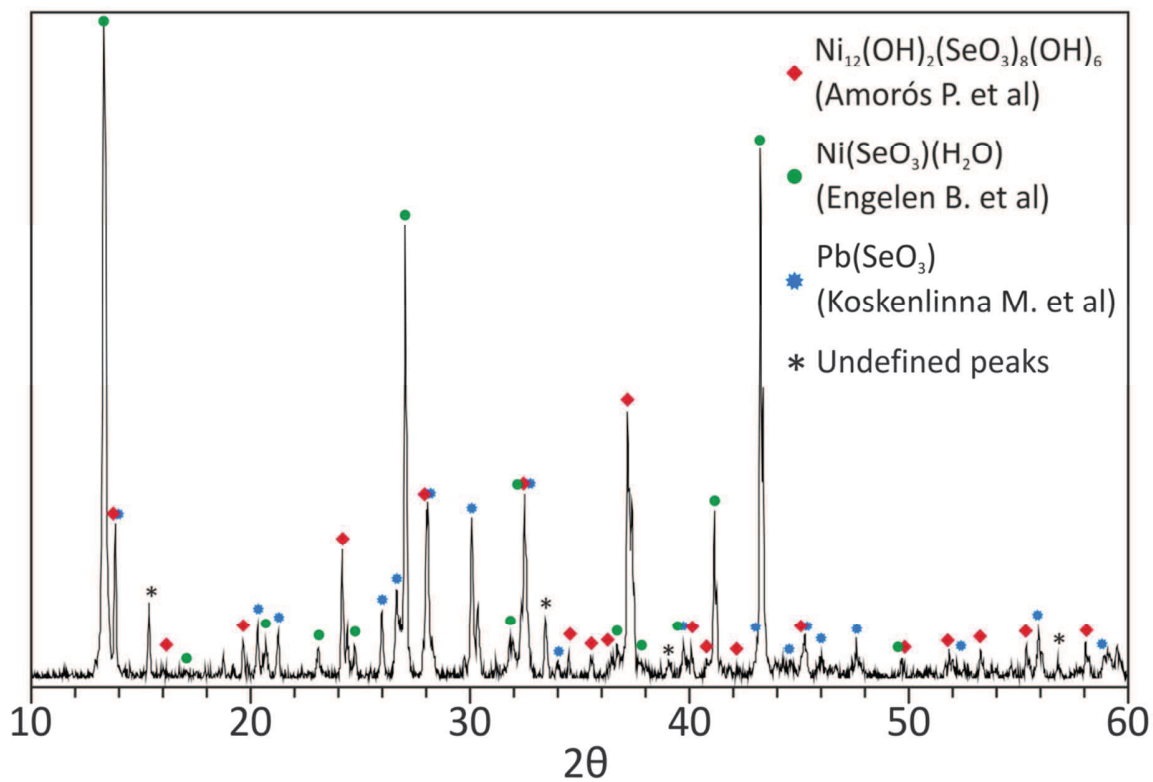


**Figure S5.** Experimental XRD pattern for the  $P_7$  experimental point with  $\text{PbO} : \text{NiO} : \text{SeO}_2 = 1 : 8 : 5$ .

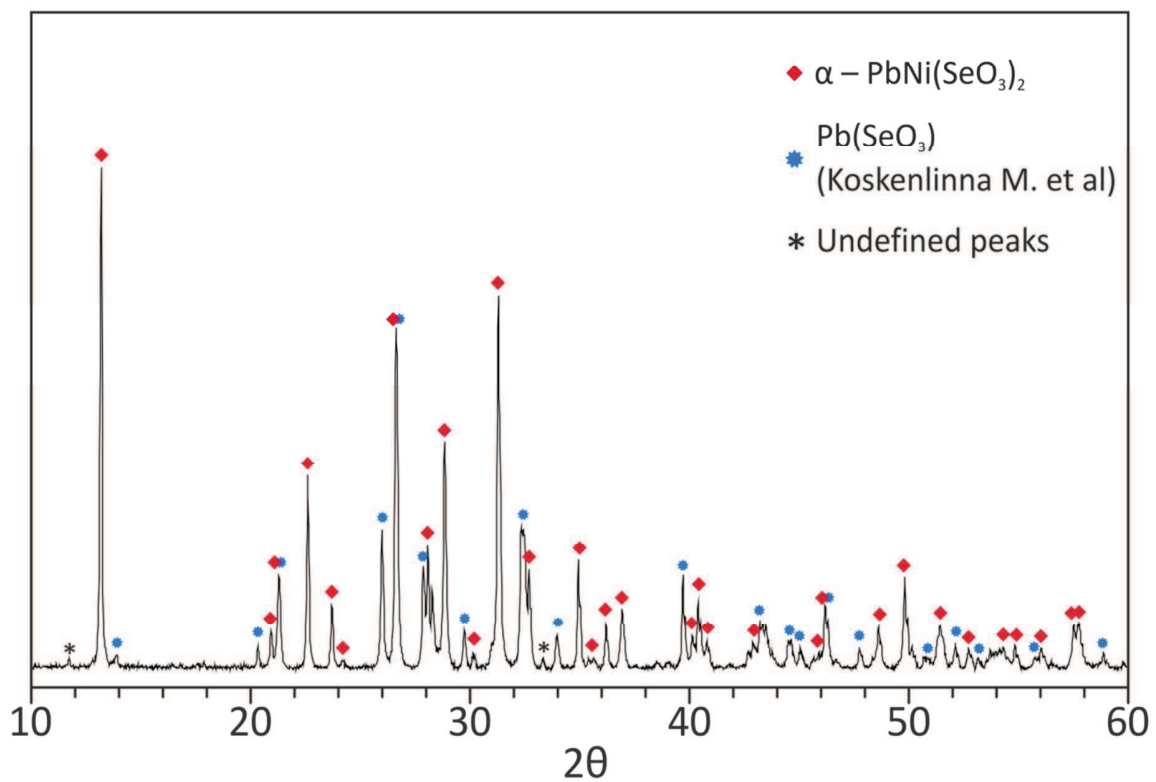


**Figure S6.** Experimental XRD pattern for the experiment of the pH series #1.

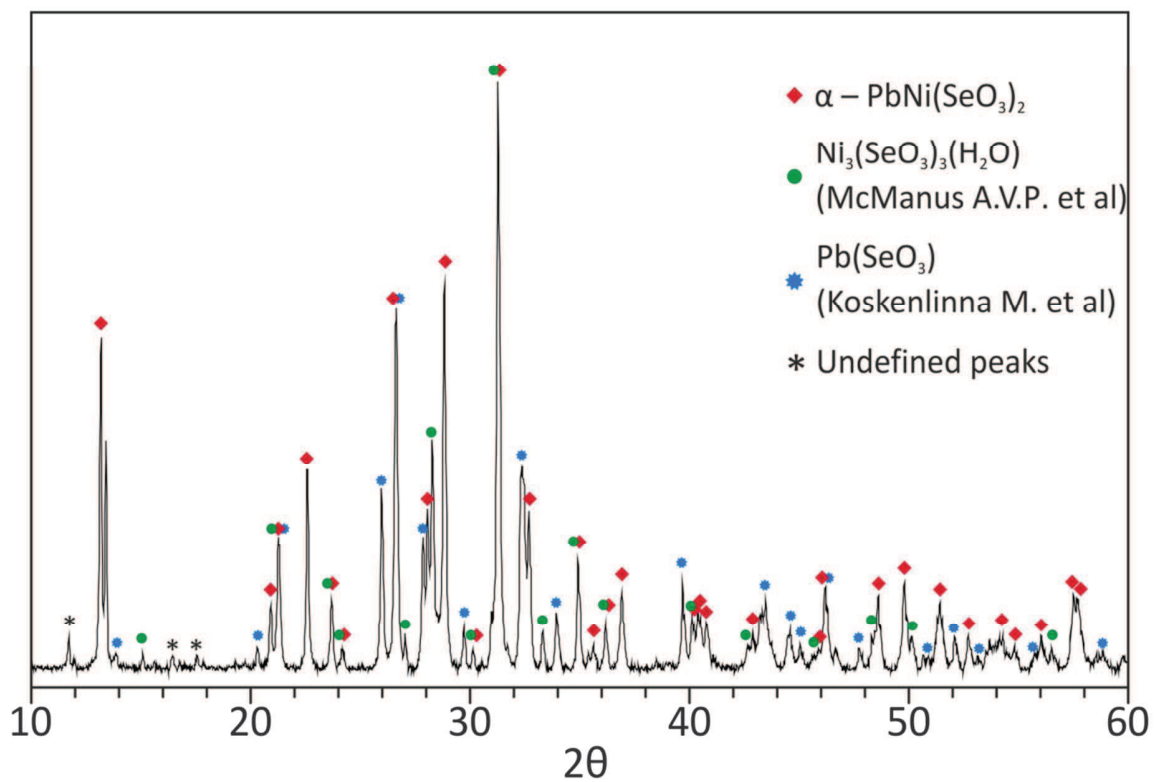


**Figure S7.** Experimental XRD pattern for the experiment of the pH series #2.

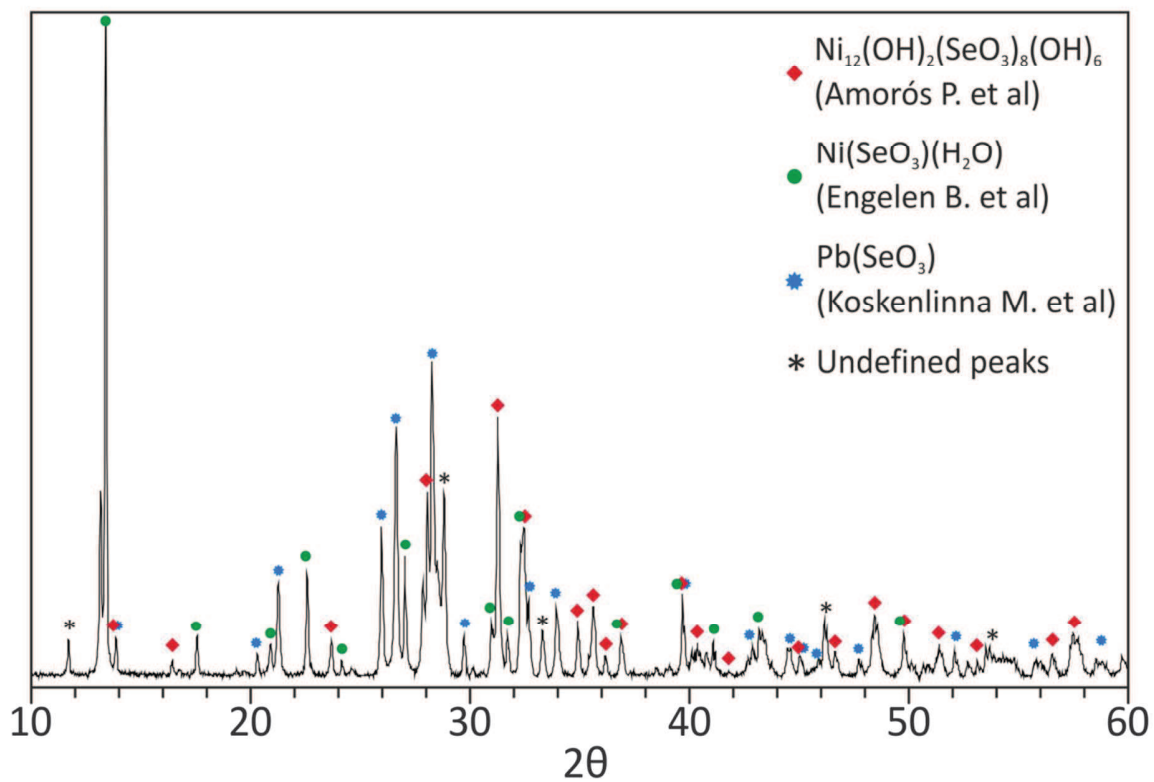


**Figure S8.** Experimental XRD pattern for the experiment of the pH series #3.



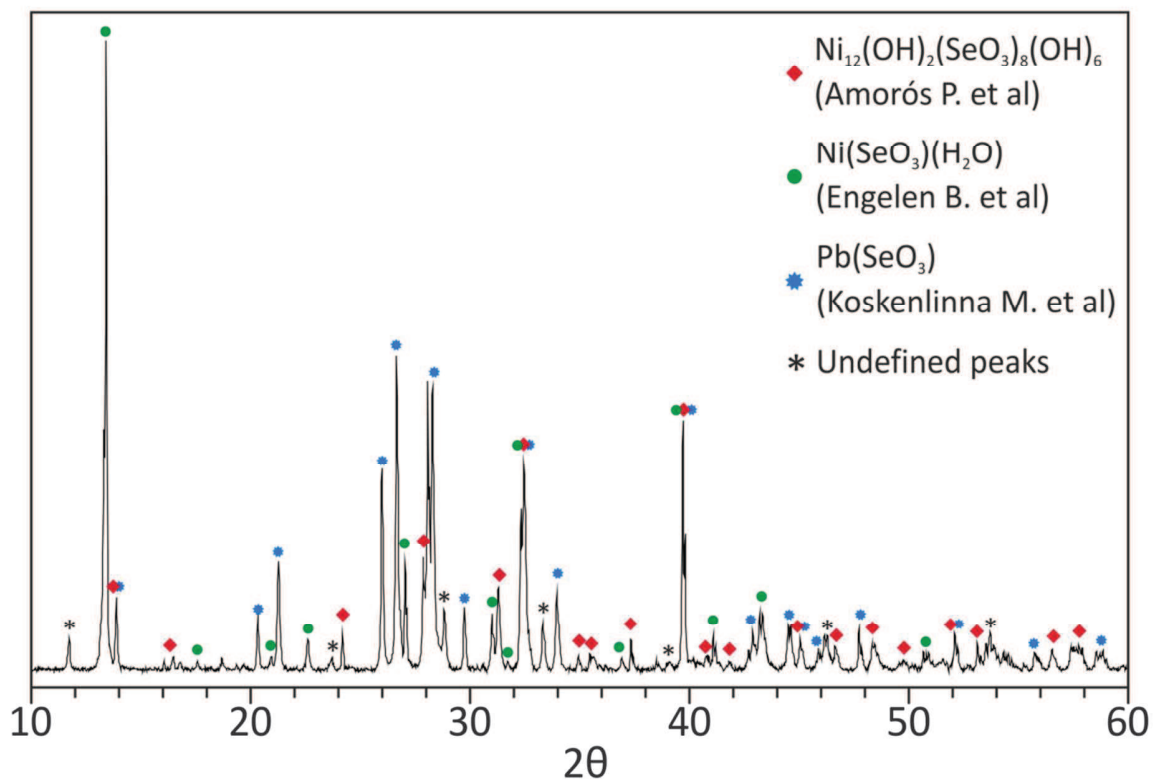


**Figure S9.** Experimental XRD pattern for the experiment of the pH series #4.

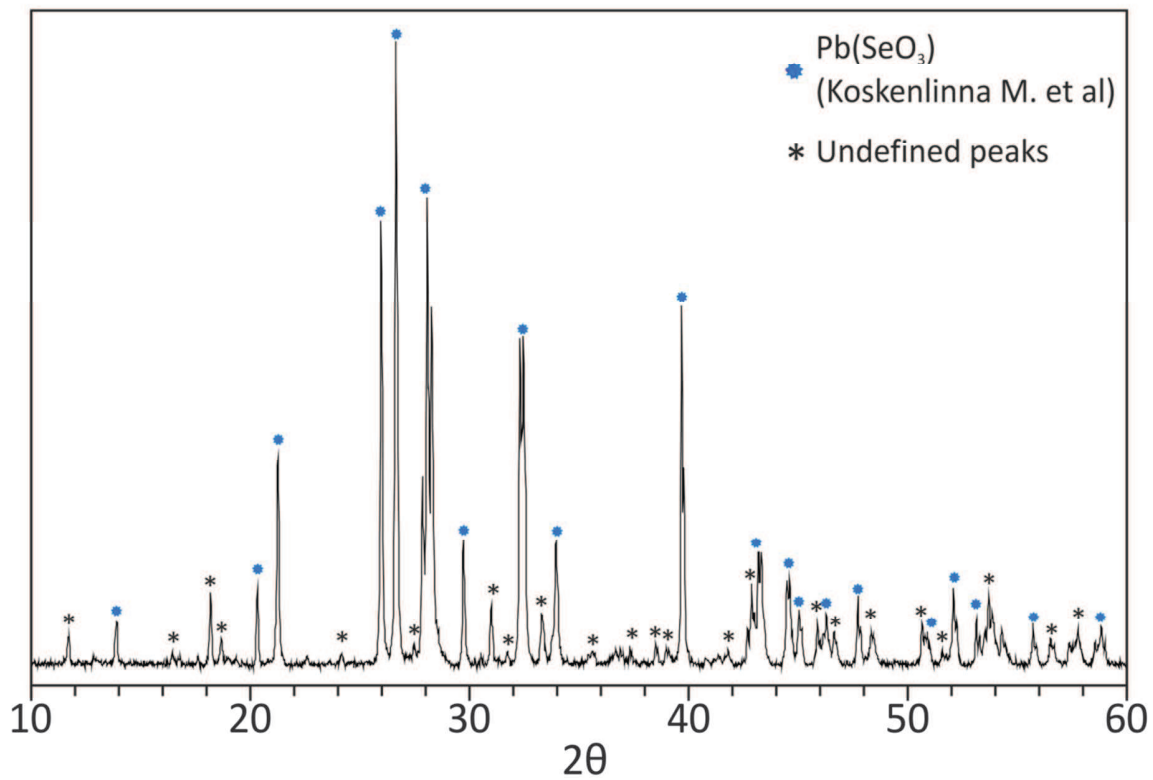


**Figure S10.** Experimental XRD pattern for the experiment of the pH series #5.

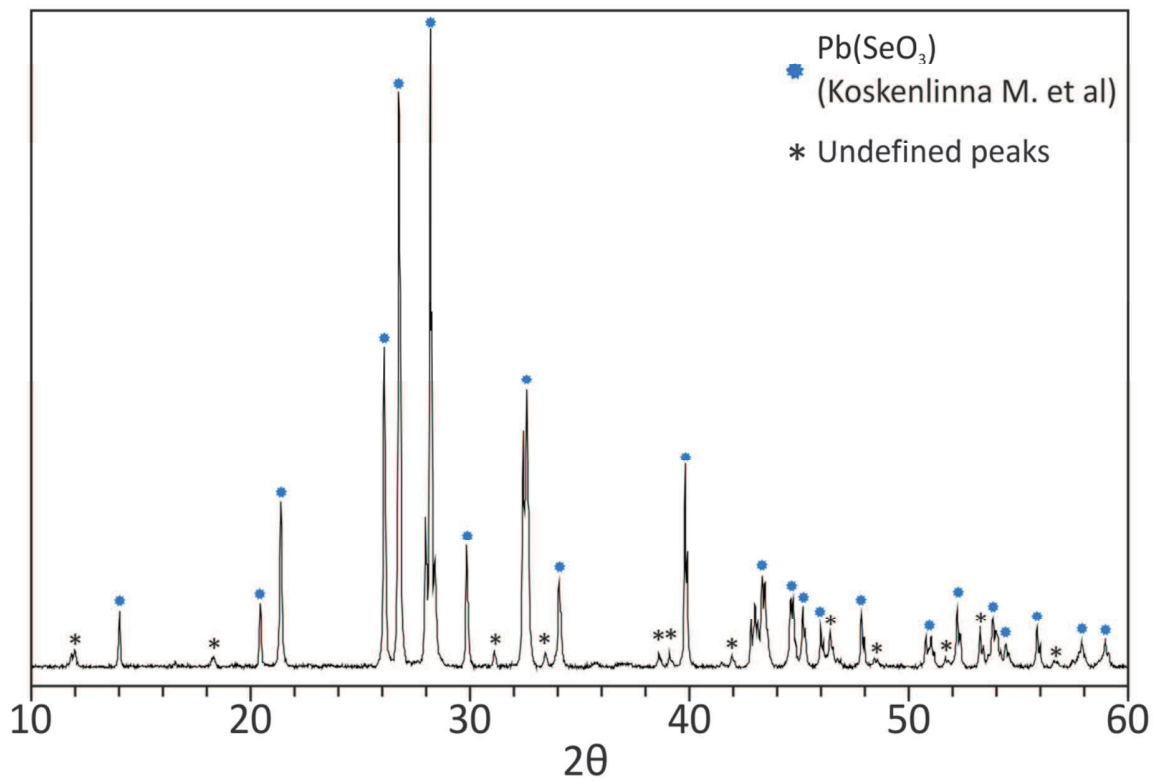


**Figure S11.** Experimental XRD pattern for the experiment of the pH series #6.

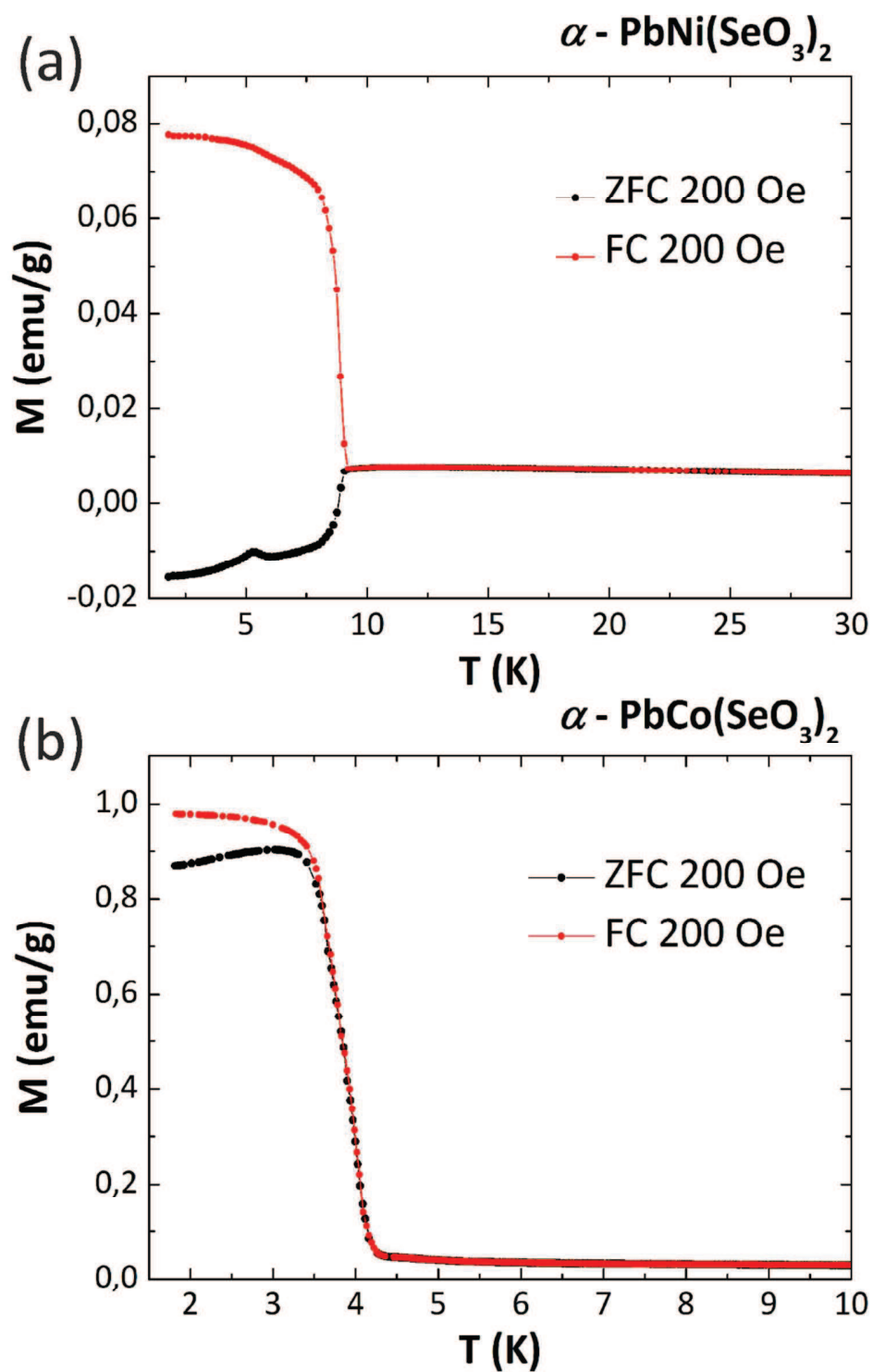


Figure S12. Temperature dependence of magnetization for the compounds I (a), and IV (b) at applied field of 200 Oe.

**Table S1. Fractional atomic coordinates and isotropic or equivalent isotropic displacement parameters ( $\text{\AA}^2$ ) for  $\alpha$  –  $\text{PbNi}(\text{SeO}_3)_2$  (I)**

	<i>x</i>	<i>y</i>	<i>z</i>	$U_{iso}^*/U_{eq}$
Pb1	0.12387(2)	0.7500	0.49878(2)	0.01338(7)
Se1	-0.07061(3)	0.7500	0.20286(5)	0.00755(9)
Se2	0.29315(3)	0.2500	0.49668(5)	0.00834(10)
Ni1	0.09654(4)	0.2500	0.20165(7)	0.00737(11)
O1	-0.00843(14)	0.9895(3)	0.3065(3)	0.0104(4)
O2	-0.0121(3)	0.7500	0.0156(3)	0.0116(6)
O3	0.29270(15)	0.0080(4)	0.6327(3)	0.0161(4)
O4	0.1617(2)	0.2500	0.4453(4)	0.0109(6)

**Table S2. Atomic displacement parameters ( $\text{\AA}^2$ ) for  $\alpha - \text{PbNi}(\text{SeO}_3)_2$  (I)**

	$U^{11}$	$U^{22}$	$U^{33}$	$U^{12}$	$U^{13}$	$U^{23}$
Pb1	0.01252(10)	0.01413(12)	0.01349(10)	0.000	-0.00148(5)	0.000
Se1	0.00788(17)	0.00646(19)	0.00830(19)	0.000	-0.00098(13)	0.000
Se2	0.00752(19)	0.0070(2)	0.0105(2)	0.000	-0.00006(12)	0.000
Ni1	0.0086(2)	0.0061(3)	0.0074(2)	0.000	0.00042(18)	0.000
O1	0.0142(9)	0.0071(10)	0.0098(10)	-0.0032(9)	0.0003(7)	-0.0017(7)
O2	0.0159(16)	0.0131(16)	0.0058(14)	0.000	0.0006(10)	0.000
O3	0.0117(9)	0.0110(10)	0.0255(12)	0.0023(8)	-0.0023(8)	0.0085(9)
O4	0.0087(13)	0.0145(15)	0.0096(13)	0.000	-0.0016(11)	0.000

**Table S3. Selected bond distances (Å) for  $\alpha$  – PbNi(SeO<sub>3</sub>)<sub>2</sub> (I)**

<b>Distance</b>			<b>Distance</b>		
Pb1–O1	2.5517(19)	2x	Se2–O3	1.696(2)	2x
Pb1–O1	2.6117(19)	2x	Se2–O4	1.723(3)	
Pb1–O3	2.777(2)	2x	<Se2–O>	1.705	
Pb1–O4	2.8020(7)	2x	Ni1–O2	2.013(3)	
Pb1–O3	3.332(2)	2x	Ni1–O3	2.066(2)	2x
<Pb1–O>	2.686/2.815		Ni1–O	2.082(3)	
Se1–O2	1.646(3)		Ni1–O1	2.1177(19)	2x
Se1–O1	1.7308(19)	2x	<Ni1–O>	2.077	
<Se1–O>	1.703				

**Table S4. Fractional atomic coordinates and isotropic or equivalent isotropic displacement parameters ( $\text{\AA}^2$ ) for  $\beta$  –  $\text{PbNi}(\text{SeO}_3)_2$  (II)**

	<i>x</i>	<i>y</i>	<i>z</i>	$U_{iso}^*/U_{eq}$
Pb1	0.0000	0.17035(3)	0.39771(4)	0.01406(13)
Se1	0.0000	0.17011(8)	0.05752(16)	0.0095(3)
Se2	0.5000	-0.01334(9)	0.25160(9)	0.0089(2)
Ni1	0.0000	-0.16633(11)	0.21430(16)	0.0095(4)
O1	0.0000	0.0626(7)	0.1770(7)	0.0182(16)
O2	0.2457(10)	0.2795(7)	0.0827(4)	0.0161(12)
O3	0.5000	0.1516(8)	0.3192(7)	0.0160(17)
O4	0.7272(10)	-0.1025(5)	0.3252(4)	0.0110(11)



**Table S5. Atomic displacement parameters ( $\text{\AA}^2$ ) for  $\beta$  –  $\text{PbNi}(\text{SeO}_3)_2$  (II)**

	$U^{11}$	$U^{22}$	$U^{33}$	$U^{12}$	$U^{13}$	$U^{23}$
Pb1	0.0183(2)	0.01208(17)	0.0118(2)	0.000	0.000	0.00092(15)
Se1	0.0092(6)	0.0117(4)	0.0076(5)	0.000	0.000	-0.0010(3)
Se2	0.0109(6)	0.0074(4)	0.0085(5)	0.000	0.000	0.0000(3)
Ni1	0.0098(8)	0.0092(6)	0.0095(11)	0.000	0.000	-0.0003(4)
O1	0.028(5)	0.013(3)	0.013(3)	0.000	0.000	0.004(3)
O2	0.010(3)	0.020(2)	0.018(3)	-0.005(2)	0.0006(19)	0.0002(16)
O3	0.023(4)	0.009(3)	0.016(4)	0.000	0.000	-0.001(2)
O4	0.006(3)	0.013(2)	0.014(3)	0.002(2)	-0.0001(16)	0.0046(15)

**Table S6. Selected bond distances (Å) for  $\beta$  – PbNi(SeO<sub>3</sub>)<sub>2</sub> (II)**

<b>Distance</b>			<b>Distance</b>		
Pb1–O4	2.569(5)	2x	Se2–O3	1.703(7)	
Pb1–O2	2.575(5)	2x	Se2–O4	1.710(5)	2x
Pb1–O1	2.713(8)		<Se2–O>	1.707	
Pb1–O3	2.885(2)	2x			
Pb1–O4	3.035(5)	2x	Ni1–O4	2.045(5)	2x
<Pb1–O>	2.760		Ni1–O3	2.061(8)	
			Ni1–O2	2.110(5)	2x
Se1–O1	1.688(7)		Ni1–O1	2.148(6)	
Se1–O2	1.703(5)	2x	<Ni1–O>	2.087	
<Se1–O>	1.698				

**Table S7. Fractional atomic coordinates and isotropic or equivalent isotropic displacement parameters ( $\text{\AA}^2$ ) for  $\text{PbNi}_2(\text{SeO}_2\text{OH})_2(\text{SeO}_3)_2$  (III)**

	<i>x</i>	<i>y</i>	<i>z</i>	$U_{iso}^*/U_{eq}$
Pb1	0.5000	0.0603(2)	0.7500	0.0137(2)
Pb2	0.0000	0.1543(2)	0.2500	0.0112(2)
Se1	0.43392(12)	0.5742(3)	0.58937(8)	0.0078(3)
Se2	0.07522(12)	0.5929(3)	0.41204(8)	0.0073(3)
Se3	0.35251(13)	0.9681(4)	0.37783(8)	0.0096(4)
Se4	0.85218(13)	0.0679(4)	0.88268(9)	0.0103(4)
Ni1	0.25061(17)	0.0850(5)	0.49646(11)	0.0081(5)
Ni2	0.75040(17)	0.5483(5)	0.75378(11)	0.0106(5)
O1	0.3956(10)	0.289(3)	0.6065(7)	0.021(3)*
O2	0.2215(9)	0.123(3)	0.2939(6)	0.016(3)
O3	0.3316(9)	0.773(3)	0.5839(6)	0.013(3)
O4	0.1738(9)	0.394(2)	0.4129(6)	0.012(3)
O5	0.3689(9)	0.035(3)	0.4685(6)	0.014(3)
O6	0.1121(9)	0.864(3)	0.3877(6)	0.014(2)*
O7	0.8690(9)	0.131(2)	0.9732(6)	0.011(3)
O8	0.7190(9)	0.215(3)	0.7980(6)	0.013(2)*
O9	0.7980(9)	0.747(3)	0.8630(6)	0.012(2)*
H1	0.738(10)	0.70(4)	0.874(9)	0.018*
O10	0.9370(9)	0.513(3)	0.3101(6)	0.012(2)*
O11	0.2977(9)	0.643(2)	0.3568(6)	0.012(2)*
H2	0.252(12)	0.56(3)	0.375(9)	0.018*
O12	0.5668 (9)	0.650(3)	0.6938(6)	0.014(2)*

**Table S8. Atomic displacement parameters ( $\text{\AA}^2$ ) for  $\text{PbNi}_2(\text{SeO}_2\text{OH})_2(\text{SeO}_3)_2$  (III)**

	$U^{11}$	$U^{22}$	$U^{33}$	$U^{12}$	$U^{13}$	$U^{23}$
Pb1	0.0119(4)	0.0132(7)	0.0111(4)	0.000	0.0050(3)	0.000
Pb2	0.0114(4)	0.0081(6)	0.0110(4)	0.000	0.0057(3)	0.000
Se1	0.0088(7)	0.0046(10)	0.0089(6)	0.0006(6)	0.0052(6)	0.0006(5)
Se2	0.0098(7)	0.0028(10)	0.0099(7)	-0.0002(6)	0.0066(6)	-0.0005(5)
Se3	0.0088(7)	0.0089(12)	0.0086(7)	0.0017(7)	0.0044(6)	0.0009(6)
Se4	0.0094(7)	0.0112(12)	0.0089(7)	-0.0005(6)	0.0052(6)	0.0006(6)
Ni1	0.0095(8)	0.0042(15)	0.0077(8)	-0.0003(8)	0.0041(7)	-0.0001(7)
Ni2	0.0104(9)	0.0104(15)	0.0083(8)	0.0019(8)	0.0048(7)	0.0015(7)
O2	0.011(5)	0.020(10)	0.012(5)	0.005(5)	0.005(4)	0.002(4)
O3	0.013(5)	0.021(9)	0.011(5)	0.006(5)	0.009(4)	0.002(5)
O4	0.010(5)	0.014(9)	0.006(4)	0.007(5)	0.002(4)	-0.002(4)
O5	0.015(5)	0.014(9)	0.013(5)	-0.004(5)	0.009(4)	-0.002(4)
O7	0.015(5)	0.006(9)	0.017(5)	0.000(5)	0.012(5)	-0.001(4)

**Table S9. Selected bond distances (Å) for PbNi<sub>2</sub>(SeO<sub>2</sub>OH)<sub>2</sub>(SeO<sub>3</sub>)<sub>2</sub> (III)**

<b>Distance</b>			<b>Distance</b>	
Pb1–O1	2.481(12)	2x	Se4–O7	1.649(10)
Pb1–O8	2.639(10)	2x	Se4–O8	1.675(10)
Pb1–O12	2.821(12)	2x	Se4–O9	1.785(14)
Pb1–O3	2.916(11)	2x	<Se4–O>	1.703
<Pb1–O>	2.714			
			Ni1–O5	2.024(10)
Pb2–O6	2.567(11)	2x	Ni1–O4	2.051(12)
Pb2–O2	2.580(10)	2x	Ni1–O1	2.062(12)
Pb2–O10	2.634(12)	2x	Ni1–O6	2.075(11)
Pb2–O4	2.765(10)	2x	Ni1–O7	2.075(10)
<Pb2–O>	2.637		Ni1–O3	2.098(12)
			<Ni1–O>	2.064
Se1–O1	1.692(15)			
Se1–O12	1.695(10)		Ni2–O12	2.058(10)
Se1–O3	1.698(11)		Ni2–O11	2.058(10)
<Se1–O>	1.695		Ni2–O9	2.058(11)
			Ni2–O10	2.066(10)
Se2–O6	1.678(13)		Ni2–O	2.110(13)
Se2–O4	1.699(11)		Ni2–O8	2.113(13)
Se2–O10	1.703(9)		<Ni2–O>	2.077
<Se2–O>	1.693			
			H1–O9	1.001
Se3–O5	1.659(10)		H1–O3	1.645
Se3–O2	1.676(10)		H2–O11	0.993
Se3–O11	1.810(13)		H2–O4	1.856
<Se3–O>	1.715			

**Table S10. Fractional atomic coordinates and isotropic or equivalent isotropic displacement parameters ( $\text{\AA}^2$ ) for  $\alpha$  –  $\text{PbCo}(\text{SeO}_3)_2$  (IV)**

	<i>x</i>	<i>y</i>	<i>z</i>	$U_{iso}^*/U_{eq}$
Pb1	0.37668(2)	0.7500	0.49989(2)	0.01509(11)
Se1	0.20857(4)	0.2500	0.50674(6)	0.01019(14)
Se2	0.57180(4)	0.7500	0.79491(7)	0.00867(14)
Co1	0.40394(5)	0.2500	0.80269(9)	0.00906(16)
O1	0.3388(3)	0.2500	0.5591(5)	0.0137(7)
O2	0.51074(18)	0.9890(4)	0.6923(4)	0.0118(6)
O3	0.5121(3)	0.7500	0.9805(4)	0.0139(8)
O4	0.20969(19)	0.0089(5)	0.3730(4)	0.0196(6)

**Table S11. Atomic displacement parameters ( $\text{\AA}^2$ ) for  $\alpha$  –  $\text{PbCo}(\text{SeO}_3)_2$  (IV)**

	$U^{11}$	$U^{22}$	$U^{33}$	$U^{12}$	$U^{13}$	$U^{23}$
Pb1	0.01398(15)	0.01643(16)	0.01487(16)	0.000	−0.00100(7)	0.000
Se1	0.0090(3)	0.0083(3)	0.0132(3)	0.000	−0.00016(17)	0.000
Se2	0.0094(2)	0.0071(2)	0.0095(3)	0.000	−0.00132(18)	0.000
Co1	0.0093(3)	0.0089(4)	0.0090(4)	0.000	0.0004(3)	0.000
O1	0.0081(16)	0.0190(19)	0.0142(19)	0.000	−0.0032(15)	0.000
O2	0.0147(12)	0.0084(13)	0.0123(14)	0.0033(10)	0.0019(9)	0.0028(10)
O3	0.018(2)	0.015(2)	0.0088(19)	0.000	0.0000 (14)	0.000
O4	0.0144(12)	0.0122(13)	0.0321(17)	−0.0016(10)	−0.0025(12)	−0.0092(12)

**Table S12. Selected bond distances (Å) for  $\alpha$  – PbCo(SeO<sub>3</sub>)<sub>2</sub> (IV)**

<b>Distance</b>			<b>Distance</b>		
Pb1–O2	2.539(2)	2x	Se2–O3	1.656(4)	
Pb1–O2	2.644(3)	2x	Se2–O2	1.730(2)	2x
Pb1–O4	2.759(3)	2x	<Se2–O>	1.705	
Pb1–O1	2.8269(9)	2x			
Pb1–O4	3.418(3)	2x	Co1–O3	2.024(4)	
<Pb1–O>	2.838/2.692		Co1–O1	2.100(4)	
			Co1–O4	2.110(3)	2x
Se1–O4	1.694(3)	2x	Co1–O2	2.166(2)	2x
Se1–O1	1.720(4)		<Co1–O>	2.113	
<Se1–O>	1.703				



**A-V**

**Oxocentered Cu(II) lead selenite honeycomb lattices hosting Cu(I)Cl<sub>2</sub> groups obtained by chemical vapor transport reactions**

Vadim M. Kovrugin, Marie Colmont, Oleg I. Siidra, Olivier Mentré, Alexandr Al-Shuray,  
Vladislav V. Gurzhiy, and Sergey V. Krivovichev

Published in: *Chemical Communications*, 2015, Vol. 51 (46), p. 9563–9566.

DOI: 10.1039/c5cc01426c

Reprinted with kind permission from Royal Society of Chemistry.





Cite this: *Chem. Commun.*, 2015, 51, 9563

Received 15th February 2015,  
Accepted 30th April 2015

DOI: 10.1039/c5cc01426c

www.rsc.org/chemcomm

## Oxocentered Cu(II) lead selenite honeycomb lattices hosting Cu(I)Cl<sub>2</sub> groups obtained by chemical vapor transport reactions†

Vadim M. Kovrugin,<sup>ab</sup> Marie Colmont,<sup>b</sup> Oleg I. Siidra,<sup>a</sup> Olivier Mentré,<sup>b</sup> Alexander Al-Shuray,<sup>a</sup> Vladislav V. Gurzhiy<sup>a</sup> and Sergey V. Krivovichev<sup>\*a</sup>

Chemical vapor transport (CVT) reactions were used to prepare three modular mixed-valent Cu(I)–Cu(II) compounds, (Pb<sub>2</sub>Cu<sup>2+</sup><sub>9</sub>O<sub>4</sub>)(SeO<sub>3</sub>)<sub>4</sub>–(Cu<sup>+</sup>Cl<sub>2</sub>)Cl<sub>5</sub> (**1**), (PbCu<sup>2+</sup><sub>5</sub>O<sub>2</sub>)(SeO<sub>3</sub>)<sub>2</sub>(Cu<sup>+</sup>Cl<sub>2</sub>)Cl<sub>3</sub> (**2**), and (Pb<sub>x</sub>Cu<sup>2+</sup><sub>(6-x)</sub>O<sub>2</sub>)(SeO<sub>3</sub>)<sub>2</sub>(Cu<sup>+</sup>Cl<sub>2</sub>)K<sub>(1-x)</sub>Cl<sub>(4-x)</sub> ( $x = 0.20$ ) (**3**). In their crystal structures chains of anion-centered (OCu<sup>2+</sup><sub>4</sub>) and (OCu<sup>2+</sup><sub>3</sub>Pb) tetrahedra form honeycomb-like double layers with cavities occupied by linear [Cu<sup>+</sup>Cl<sub>2</sub>]<sup>–</sup> groups.

Inorganic copper oxocompounds attract considerable attention due to their interesting structural and physical properties<sup>1</sup> as well as mineralogical and geochemical importance.<sup>2</sup> Of special interest are mixed-valent Cu(I)–Cu(II) systems with separate symmetrically independent monovalent and divalent copper sites due to their contrasted coordinations combined in one crystal structure. Herein we report on the synthesis and characterization of three novel Cu(I)–Cu(II) lead oxoselenite chlorides inspired by mineralogical discoveries in such unusual geological conditions as volcanic fumaroles.<sup>2g,3</sup> Here copper oxoselenites form from volcanic gases emanating from cooling magmatic chambers deep under the Earth's surface long after the period of eruptive activities. The formation of such Cu compounds in fumaroles provides a useful hint for their synthesis under laboratory conditions, in particular, the chemical vapor transport (CVT) method.<sup>4</sup> The specific feature of many Cu oxoselenites is the presence in their crystal structures of oxocentered (μ<sub>4</sub>–O)Cu<sub>4</sub> tetrahedral units that polymerize to form extended structural complexes.<sup>2g,3</sup> Likely, during these reactions the selenites and metal halides play the role of transport agents.<sup>5</sup> In order to reproduce natural exhalative chemistry, in this work, we investigate the formation of phases in the PbO–Cu<sup>2+</sup>Cl<sub>2</sub>–Cu<sup>+</sup>Cl–Cu<sup>2+</sup>O–SeO<sub>2</sub> system containing Pb<sup>2+</sup> cations that possess stereochemically

active 6s<sup>2</sup> lone electron pairs favouring formation segregation of structural compartments occupied by these pairs.<sup>6</sup> In addition, the preference of Pb<sup>2+</sup> ions for similar OPb<sub>4</sub> tetrahedral units is an asset for creation of more complex edifices.

Crystallographic information for three novel compounds synthesized by the CVT reaction method (Fig. 1a) is summarized in Table 1. Schematic representations of coordination environments of cations in the crystal structures of 1–3 are shown in

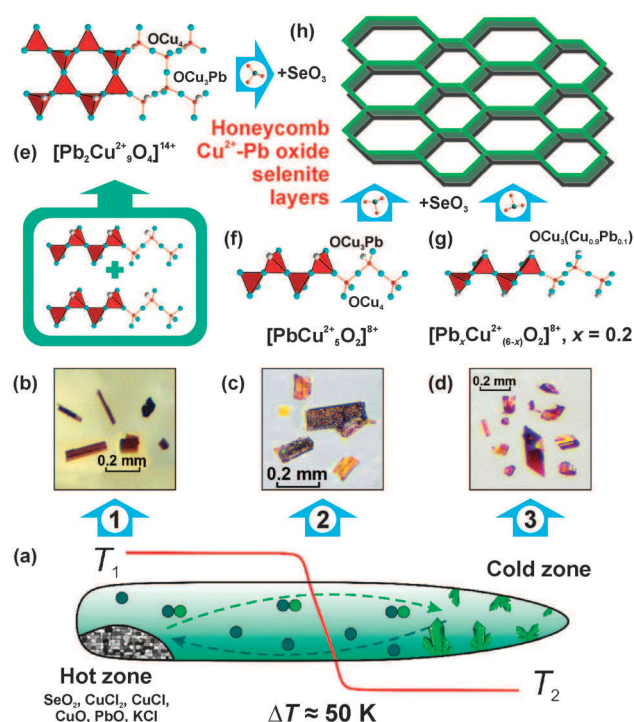


Fig. 1 General scheme of syntheses by the method of CVT reactions (a), the crystals of **1**, **2** and **3** (b–d), and the scheme of formation of honeycomb Cu<sup>2+</sup>–Pb selenite layers (e–h). The types of oxo-centered 1-dimensional units (shown in red) formed by corner-sharing OCu<sub>4</sub> and OCu<sub>3</sub>Pb tetrahedra in the structures of **1**, **2** and **3** are shown. (legend: Cu = cyan balls; Pb = grey balls). See text for details.

<sup>a</sup> Department of Crystallography, St. Petersburg State University, University Emb. 7/9, 199034 St. Petersburg, Russia. E-mail: s.krivovichev@spbu.ru

<sup>b</sup> UCCS, UMR 8181, Université Lille Nord de France, USTL, F-59655 Villeneuve d'Ascq, France

† Electronic supplementary information (ESI) available: CIF files, experimental section, IR spectra, and tables with bond-valence analysis for 1–3. See DOI: 10.1039/c5cc01426c

Fig. S1, ESI† In all the compounds, Cu<sup>+</sup> cations form two relatively short Cu<sup>+</sup>–Cl bonds (2.058–2.118 Å), which result in the formation of tightly bonded [CuCl<sub>2</sub>]<sup>–</sup> anionic groups that can be considered as separate structural entities. The Cu<sup>2+</sup> cations have mixed oxochloride coordinations that have previously been observed in Cu oxochloride compounds,<sup>2a</sup> with typical trends of Jahn–Teller d<sup>9</sup> ions. The Cu(1) and Cu(2) sites in **1**, the Cu(4) site in **2**, and Cu(3) site in **3** form [CuO<sub>4</sub>Cl<sub>2</sub>] distorted octahedra with four short equatorial Cu–O and two long apical Cu–Cl bonds. The Cu(3) site in **1**, the Cu(2) and Cu(3) sites in **2**, and the Cu(1) site in **3** are octahedrally coordinated with [CuO<sub>3</sub>Cl] squares complemented by two long Cu–Cl bonds. The Cu(4) site in **1** forms a [CuO<sub>4</sub>Cl] trigonal bipyramid, whereas the Cu(1) site in **2** and the Cu(4) site in **3** form [CuO<sub>3</sub>Cl<sub>2</sub>] trigonal bipyramids. The Pb atoms have asymmetrical coordinations consisting of three strong Pb–O bonds (2.356–2.420 Å) located in one coordination hemisphere and four long Pb–Cl in another. This coordination of Pb<sup>2+</sup> cations is typical for lead oxohalide compounds<sup>7</sup> and is consistent with the presence of stereoactive lone electron pairs. In all the compounds under consideration, Se<sup>4+</sup> cations form standard (SeO<sub>3</sub>)<sup>2–</sup> selenite triangular pyramidal oxo-anions (Se–O = 1.688–1.726 Å). The structure of **3** has one symmetrically independent K site with the site-occupation factor (s.o.f.) equal to 0.8. Its coordination polyhedron can be described as a distorted hexagonal bipyramid. Bond-valence sums<sup>8</sup> calculated for all the sites in the crystal structures of **1–3** are in full agreement with their expected oxidation states (in valence units): Cu<sup>+</sup> sites – 1.00–1.16, Cu<sup>2+</sup> sites – 1.96–2.14, Pb<sup>2+</sup> sites – 1.95–1.96, Se<sup>4+</sup> sites – 4.03–4.16, and K<sup>+</sup> site – 0.80.

The high variability of cation coordinations in the structures of **1–3** makes their uniform description in terms of cation coordination polyhedra a difficult task. It is therefore more reasonable to look for more mundane consideration, e.g. in terms of cation arrays or coordination of anions.<sup>9</sup> In addition to the O atoms associated with the SeO<sub>3</sub> groups, all three

compounds contain additional O<sub>a</sub> atoms (oxo-anions) not bonded to Se<sup>4+</sup> cations and tetrahedrally coordinated by four metal atoms (Cu and Pb). In the crystal structure of **1** there are two additional O atoms, O(2) and O(4), that form (OCu<sup>2+</sup><sub>3</sub>Pb) and (OCu<sup>2+</sup><sub>4</sub>) tetrahedra, respectively. The oxo-centered tetrahedra share common corners to form [O<sub>4</sub>Pb<sub>2</sub>Cu<sup>2+</sup><sub>9</sub>]<sup>14+</sup> double chains depicted in Fig. 1e. These chains are growing parallel to the *b*-axis, and its common value for the three compounds (*b* ~ 6.2 Å) denotes similar arrangement between the oxo-centered building units in the full series. These types of chains of anion-centered tetrahedra are original and have not been observed in inorganic compounds previously. The SeO<sub>3</sub> groups are attached to the triangular bases of oxo-centered tetrahedra that results in the formation of complex 1-dimensional {[O<sub>4</sub>Pb<sub>2</sub>Cu<sup>2+</sup><sub>9</sub>](SeO<sub>3</sub>)<sub>4</sub>]<sup>6+</sup> interconnected *via* Pb–O bonds in 2-dimensional metal-oxide double layers (Fig. 2b). The projection of the layers in the (*bc*) plane leads to a honeycomb-like lattice of tetrahedra, even though this idealized vision neglects the disconnections occurring at the oxocentered-oxoanion contacts. In contrast, monometallic [O<sub>2</sub>Cu<sub>5</sub>] honeycomb-layers are reported in several compounds based upon anion-centered tetrahedra.<sup>9</sup> The layers are surrounded by Cl<sup>–</sup> anions in the interleaves and accommodate both linear [Cu<sup>+</sup>Cl<sub>2</sub>]<sup>–</sup> anions and Cl<sup>–</sup> ions in the larger and smaller honeycomb-windows, respectively. The interactions between the Cl<sup>–</sup> ions of the [Cu<sup>+</sup>Cl<sub>2</sub>]<sup>–</sup> groups and host cationic networks are restricted to rather weak Cu<sup>2+</sup>–Cl<sup>–</sup> (>2.975 Å), Pb<sup>2+</sup>–Cl<sup>–</sup> (>3.396 Å) and K<sup>+</sup>–Cl<sup>–</sup> (>3.478 Å) bonds with bond-valences not exceeding 0.08 valence units (Tables S1–S3, ESI†). Taking into account the relative strength of the Cu<sup>+</sup>–Cl bonds and weak interactions between them and the rest of the structure, these units may be considered as guest anions embedded in the complex metal oxochloride matrix based upon anion-centered tetrahedra.

A very similar ‘host–guest’ principle is at work in the structures of **2** and **3** as well. Here the (OCu<sup>2+</sup><sub>3</sub>Pb) and (OCu<sup>2+</sup><sub>4</sub>) tetrahedra share corners to produce single chains extending along the common *b*-parameter that have [O<sub>2</sub>Pb<sub>x</sub>Cu<sup>2+</sup><sub>(6–x)</sub>]<sup>8+</sup>

Table 1 Crystallographic data for **1**, **2**, and **3**

	<b>1</b>	<b>2</b>	<b>3</b>
Empirical formula	(Pb <sub>2</sub> Cu <sup>2+</sup> <sub>9</sub> O <sub>4</sub> )(SeO <sub>3</sub> ) <sub>4</sub> (Cu <sup>+</sup> Cl <sub>2</sub> )Cl <sub>5</sub>	(PbCu <sup>2+</sup> <sub>5</sub> O <sub>2</sub> )(SeO <sub>3</sub> ) <sub>2</sub> (Cu <sup>+</sup> Cl <sub>2</sub> )Cl <sub>3</sub>	(Pb <sub>x</sub> Cu <sup>2+</sup> <sub>(6–x)</sub> O <sub>2</sub> )(SeO <sub>3</sub> ) <sub>2</sub> (Cu <sup>+</sup> Cl <sub>2</sub> ) K <sub>(1–x)</sub> Cl <sub>(4–x)</sub> , <i>x</i> = 0.20
Crystal system		Monoclinic	
Space group		<i>C2/m</i>	
<i>a</i> (Å)	18.605(17)	18.4956(4)	15.116(1)
<i>b</i> (Å)	6.204(6)	6.1454(1)	6.1850(4)
<i>c</i> (Å)	12.673(11)	15.2985(4)	9.2672(9)
<i>β</i> (deg)	109.87(2)	119.311(1)	95.965(5)
<i>V</i> (Å <sup>3</sup> )	1376(2)	1516.25(6)	861.72(12)
<i>ρ</i> <sub>calc</sub> (g cm <sup>–3</sup> )	4.514	4.607	3.840
<i>μ</i> (mm <sup>–1</sup> )	25.78	25.02	15.52
Reflection collected	7722	6910	4817
Independent reflections ( <i>R</i> <sub>int</sub> )	1301 (0.069)	1924 (0.024)	974 (0.029)
Goodness-of-fit	0.791	1.231	1.121
<i>R</i> <sub>1</sub> [ <i>I</i> > 2σ( <i>I</i> )] <sup>a</sup>	0.0257	0.0260	0.0412
<i>wR</i> <sub>2</sub>	0.0349	0.0761	0.1172
<i>R</i> <sub>1</sub> (all data)	0.0475	0.0267	0.0496
<i>wR</i> <sub>2</sub>	0.0378	0.0761	0.1176
Largest diff. peak and hole [e Å <sup>–3</sup> ]	0.951, –0.988	3.783, –2.942	4.244, –1.592

<sup>a</sup> *R*<sub>1</sub> = ∑||*F*<sub>o</sub>| – |*F*<sub>c</sub>||/∑|*F*<sub>o</sub>|; *wR*<sub>2</sub> = {∑[*w*(*F*<sub>o</sub><sup>2</sup> – *F*<sub>c</sub><sup>2</sup>)<sub>2</sub>]/∑[*w*(*F*<sub>o</sub><sup>2</sup>)]<sup>1/2</sup>.

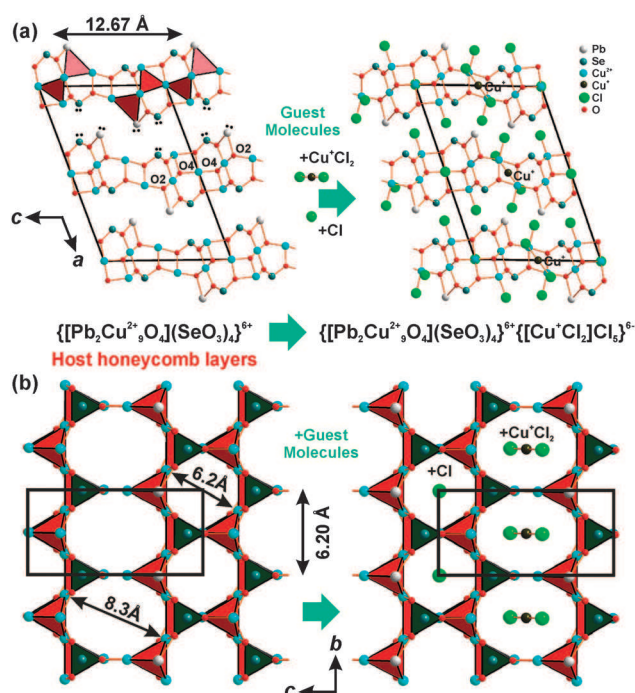
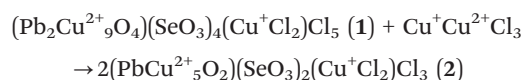


Fig. 2 General projections of the structure of **1** along the *b* and *a* axes – (a) and (b). Honeycomb layers of  $\{[\text{Pb}_2\text{Cu}^{2+}_9\text{O}_4](\text{SeO}_3)_4\}^{6+}$  composition are hosts for the  $[\text{Cu}^+\text{Cl}_2]^-$  guest species localized in the layer cavities. The  $\{[\text{Pb}_2\text{Cu}^{2+}_9\text{O}_4](\text{SeO}_3)_4\}^{6+}$  layers are formed via interconnection of the  $[\text{Pb}_2\text{Cu}^{2+}_9\text{O}_4]$  oxo-centered chains (red) and isolated  $\text{SeO}_3$  groups (dark-green). The O(2) and O(4) designated in (a) are central oxygen atoms in  $\text{OCu}_4$  and  $\text{OCu}_5\text{Pb}$  tetrahedra, respectively.

compositions, respectively (Fig. 1f and g). Together with  $\text{SeO}_3$  groups, these chains form 1-dimensional  $\{[\text{O}_2\text{M}_6](\text{SeO}_3)_2\}^{4+}$  metal-oxide ( $\text{M} = \text{Cu}$  or  $\text{Pb}$ ) backbones of the structures that are arranged to form pseudo honeycomb layers. Due to the elementary single-chains, only large honeycomb windows are created that accommodate the  $[\text{Cu}^+\text{Cl}_2]^-$  guest anions (Fig. 3) as observed in **1**. The structure of **3** contains additional  $\text{K}^+$  cations located in the interlayer space between the metal oxoselenite chloride layers. In all three structures, lone electron pairs on the  $\text{Pb}^{2+}$  and  $\text{Se}^{4+}$  cations are oriented toward the interlayer space, thus conforming the ‘chemical scissor’ principle of structural organization in compounds with lone-electron-pair cations.<sup>10</sup>

It is noteworthy that compounds **1** and **2** are closely chemically related, which can be described by the equation:



From the structural viewpoint, transition from **1** to **2** is associated with the reconstruction of the metal-oxide backbone, *i.e.* in depolymerization of anion-centered tetrahedra and splitting of the double  $[\text{O}_4\text{Pb}_2\text{Cu}^{2+}_9]^{14+}$  chains into single  $[\text{O}_2\text{PbCu}_5]^{8+}$  chains. This kind of structural reconstruction accompanied by the inclusion of imaginary ionic component  $\text{Cu}^+\text{Cu}^{2+}\text{Cl}_3$  into the metal-oxide matrix is in good agreement with the principle of dimensional reduction.<sup>11</sup> It should also be noted that **2** is a synthetic analogue of

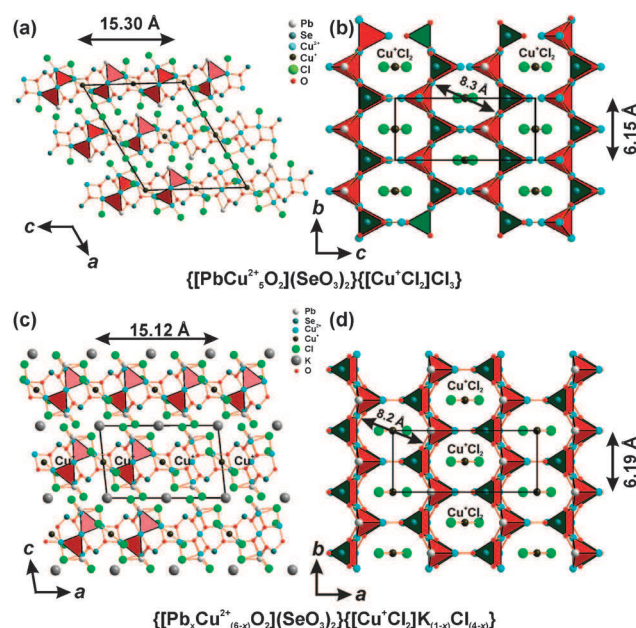


Fig. 3 General projections of the structure of **2** (a, b) and **3** (c, d). In **2**, the  $\text{OCu}_4$  and  $\text{OCu}_5\text{Pb}$  tetrahedra (red) form single  $[\text{O}_2\text{PbCu}_5]$  chains, which results in the enlargement of the *c*-parameter value from 12.67 Å (in **1**) to 15.30 Å (in **2**). In **3**, K atoms are located in the interlayer under and above the pseudohexagonal voids filled by the  $[\text{Cu}^+\text{Cl}_2]$  groups. The layers (b, d) are characterized by only one type of pore with 8.3 Å and 8.2 Å diameter in **2** and **3**, respectively.

allochalcocelite, the mineral first described to be obtained from volcanic fumaroles of the Tolbachik volcano (Kamchatka peninsula, Russia).<sup>3d</sup>

To summarize, three novel  $\text{Cu}^{2+}$ – $\text{Cu}^+$  Pb oxoselenite chlorides were obtained by the chemical vapor transport reactions, which proves the efficiency of this method for the synthesis of new mixed  $\text{Cu}^{2+}$ – $\text{Cu}^+$  based oxyhalide compounds. These compounds described herein are based upon oxocentered mixed  $\text{Pb}$ – $\text{Cu}^{2+}$  one-dimensional units of different architectures. These units determine basic topologies of the structures and influence their stability and properties. For instance, in the three compounds only corner-sharing  $\text{OCu}_4$  and  $\text{OCu}_5\text{Pb}$  are found in chains and double chains forming hollow voids. It follows that in all the compounds, the role of the tightly bonded  $[\text{Cu}^+\text{Cl}_2]^-$  anions is that of guest complexes incorporated inside metal oxide chloride units. The present study also points out that the  $\text{Cu}^+\text{Cl}_2$  groups may serve as transport agents of  $\text{Cu}^+$  in Cl-rich gaseous environments such as that observed in natural volcanic fumaroles.

This work was financially supported by the Russian Science Foundation through the grant 14-17-00071. Technical support by the SPbSU X-ray Diffraction Resource Centre is gratefully acknowledged. This work was carried out under the framework of the Multi-InMaDe project supported by the ANR (Grant ANR 2011-JS-08 003 01). V.M.K. thanks l’Ambassade de France en Russie and l’Agence Campus France (contracts no. 768231K, 779116K 794852B, 808399A, and 808400J) for the partial support of this work.

## Notes and references

- (a) N. V. Kuratieva, M. Banki, A. A. Tsirlin, J. Eckert, H. Ehrenberg and D. Mikhailova, *Inorg. Chem.*, 2013, **52**, 13974; (b) A. A. Tsirlin, O. Janson, S. Lebernegg and H. Rosner, *Phys. Rev. B: Condens. Matter Mater. Phys.*, 2013, **B87**, 064404; (c) S. Tamilarasan, D. Sarma, S. Bhattacharjee, U. V. Waghmare, S. Natarajan and J. Gopalakrishnan, *Inorg. Chem.*, 2013, **52**, 5757; (d) P. S. Berdonosov, O. Janson, A. V. Olenev, S. V. Krivovichev, H. Rosner, V. A. Dolgikh and A. A. Tsirlin, *Dalton Trans.*, 2013, **42**, 9547; (e) T.-T. Zhu, W. Sun, Y.-X. Huang, Z.-M. Sun, Y. Pan, L. Balents and J.-X. Mi, *J. Mater. Chem. C*, 2014, **2**, 8170; (f) H. L. Feng, M. Arai, Y. Matsushita, Y. Tsujimoto, Y. Yuan, C. I. Sathish, J. He, M. Tanaka and K. Yamaura, *J. Solid State Chem.*, 2014, **217**, 9; (g) S. Hu, A. Mace, M. Johnsson, V. Gnezdilov, P. Lemmens, J. Tapp and A. Moeller, *Inorg. Chem.*, 2014, **53**, 7661.
- (a) S. V. Krivovichev, S. K. Filatov and L. P. Vergasova, *Mineral. Petrol.*, 2013, **107**, 235; (b) I. V. Pekov, M. E. Zelenski, V. O. Yapaskurt, Y. S. Polekhovskiy and M. N. Murashko, *Eur. J. Mineral.*, 2013, **25**, 91; (c) I. V. Pekov, N. V. Zubkova, M. E. Zelenski, V. O. Yapaskurt, Y. S. Polekhovskiy, O. A. Fadeeva and D. Y. Pushcharovskiy, *Mineral. Mag.*, 2013, **77**, 107; (d) I. V. Pekov, O. I. Siidra, N. V. Chukanov, V. O. Yapaskurt, D. I. Belakovskiy, M. N. Murashko and E. G. Sidorov, *Eur. J. Mineral.*, 2014, **26**, 597; (e) I. V. Pekov, N. V. Zubkova, V. O. Yapaskurt, D. I. Belakovskiy, I. S. Lykova, M. F. Vigasina, E. G. Sidorov and D. Yu. Pushcharovskiy, *Mineral. Mag.*, 2014, **78**, 905; (f) I. V. Pekov, N. V. Zubkova, V. O. Yapaskurt, P. M. Kartashov, Yu. S. Polekhovskiy, M. N. Murashko and D. Yu. Pushcharovskiy, *Eur. J. Mineral.*, 2014, **26**, 667; (g) L. P. Vergasova, T. F. Semenova, S. V. Krivovichev, S. K. Filatov, A. A. Zolotarev, Jr. and V. V. Ananiev, *Eur. J. Mineral.*, 2014, **26**, 439.
- (a) S. V. Krivovichev, S. K. Filatov, T. F. Semenova and I. V. Rozhdstvenskaya, *Z. Kristallogr.*, 1998, **213**, 645; (b) S. V. Krivovichev, R. R. Shuvalov, T. F. Semenova and S. K. Filatov, *Z. Kristallogr.*, 1999, **214**, 135; (c) P. C. Burns, S. V. Krivovichev and S. K. Filatov, *Can. Mineral.*, 2002, **40**, 1587; (d) S. V. Krivovichev, S. K. Filatov, P. C. Burns and L. P. Vergasova, *Can. Mineral.*, 2006, **44**, 507; (e) S. V. Krivovichev, S. K. Filatov, P. C. Burns and L. P. Vergasova, *Can. Mineral.*, 2007, **45**, 929; (f) R. R. Shuvalov, L. P. Vergasova, T. F. Semenova, S. K. Filatov, S. V. Krivovichev, O. I. Siidra and N. S. Rudashevsky, *Am. Mineral.*, 2013, **98**, 463.
- M. Binnewies, R. Glaum, M. Schmidt and P. Schmidt, *Z. Anorg. Allg. Chem.*, 2013, **639**, 219.
- A. Aliev, V. M. Kovrugin, M. Colmont, C. Terryn, M. Huvé, O. I. Siidra, S. V. Krivovichev and O. Mentré, *Cryst. Growth Des.*, 2014, **14**, 3026.
- O. I. Siidra, D. S. Zenko and S. V. Krivovichev, *Am. Mineral.*, 2014, **99**, 817.
- (a) S. V. Krivovichev, O. I. Siidra, E. V. Nazarchuk, P. C. Burns and W. Depmeier, *Inorg. Chem.*, 2006, **45**, 3846; (b) O. I. Siidra, D. O. Zinyakhina, A. I. Zadoya, S. V. Krivovichev and R. W. Turner, *Inorg. Chem.*, 2013, **52**, 2799; (c) O. I. Siidra, S. V. Krivovichev, R. W. Turner, M. S. Rumsey and J. Spratt, *Am. Mineral.*, 2013, **98**, 248; (d) O. I. Siidra, S. V. Krivovichev, R. W. Turner, M. S. Rumsey and J. Spratt, *Am. Mineral.*, 2013, **98**, 256; (e) O. I. Siidra, D. S. Zenko, A. N. Suknotova and S. V. Krivovichev, *Mineral. Mag.*, 2013, **77**, 3239.
- (a) N. E. Brese and M. O'Keeffe, *Acta Crystallogr.*, 1991, **B47**, 192; (b) S. V. Krivovichev and I. D. Brown, *Z. Kristallogr.*, 2001, **216**, 245.
- S. V. Krivovichev, O. Mentré, O. I. Siidra, M. Colmont and S. K. Filatov, *Chem. Rev.*, 2013, **113**, 6459.
- (a) R. Becker, M. Johnsson, R. K. Kremer and P. Lemmens, *Solid State Sci.*, 2003, **5**, 1411; (b) Z. Mayerova, M. Johnsson and S. Lidin, *Angew. Chem., Int. Ed.*, 2006, **45**, 5602; (c) V. Jo, M. K. Kim, D. W. Lee, I. W. Shim and K. M. Ok, *Inorg. Chem.*, 2010, **49**, 2990.
- E. G. Tulskey and J. R. Long, *Chem. Mater.*, 2001, **13**, 1149.

# Oxocentered Cu(II) Lead Selenite Honeycomb Lattices Hosting Cu(I)Cl<sub>2</sub> Groups Obtained by Chemical Vapor Transport Reactions

Vadim M. Kovrugin,<sup>a,b</sup> Marie Colmont,<sup>b</sup> Olivier Mentré,<sup>b</sup> Alexander Al-Shuray,<sup>a</sup> Oleg I. Siidra,<sup>a</sup> Vladislav V. Gurzhiy<sup>a</sup> and Sergey V. Krivovichev<sup>\*a</sup>

<sup>a</sup> Department of Crystallography, St. Petersburg State University, University Emb. 7/9, 199034 St. Petersburg, Russia.

E-mail: s.krivovichev@spbu.ru

<sup>b</sup> UCCS, UMR 8181, Université Lille Nord de France, USTL, F-59655 Villeneuve d'Ascq, France.

## Electronic Supplementary Information

### Experimental

#### Syntheses

SeO<sub>2</sub> (powder, 99%, Alfa Aesar), CuO (powder, 99%, Aldrich), CuCl<sub>2</sub> (powder, 99%, Aldrich), CuCl (powder, 90%, Sigma-Aldrich), PbO (powder, 99%, Aldrich), NaCl (powder, 99%, Alfa Aesar), and KCl (powder, 99%, Carlo Erba) were used as received.

Single crystals of three new Pb-containing mixed-valent copper oxoselenite chlorides have been prepared by the CVT reactions. The reagents were grounded in an agate mortar and loaded into a silica tube (*ca.* 15 cm), which was further evacuated to 10<sup>-2</sup> mbar and sealed. The tubes were placed horizontally into a tubular two-zone furnace, heated to 723K for 4 days (1) and 823 K for 3 days (2 and 3), and then slowly cooled to room temperature. The temperature difference between the hot zone with initial reagents mixture and cold zone of the tube in furnace was about 50 K. Likely, during these reactions the selenites and metal halides play the role of transport agent. The compounds obtained are only partially stable and deteriorate in air within several tens of hours, which prevented their detailed chemical characterization by electron microprobe analysis.

#### (Pb<sub>2</sub>Cu<sup>2+</sup><sub>9</sub>O<sub>4</sub>)(SeO<sub>3</sub>)<sub>4</sub>(Cu<sup>+</sup>Cl<sub>2</sub>)Cl<sub>5</sub> (**1**)

Red-brown prismatic crystals of **1** have been observed in the cold zone of the tube with a mixture of SeO<sub>2</sub> (0.111 g, 1 mmol), CuCl (0.124 g, 1.25 mmol), CuCl<sub>2</sub> (0.303 g, 2.25 mmol), PbO (0.167 g, 0.75 mmol), and NaCl (0.029 g, 0.50 mmol). Black block-shaped single crystals of synthetic georgbokiite, [Cu<sub>5</sub>O<sub>2</sub>](SeO<sub>3</sub>)<sub>2</sub>Cl<sub>2</sub>, were found in all zones of the tube.

#### (PbCu<sup>2+</sup><sub>5</sub>O<sub>2</sub>)(SeO<sub>3</sub>)<sub>2</sub>(Cu<sup>+</sup>Cl<sub>2</sub>)Cl<sub>3</sub> (**2**)

Brown platy crystals of **2** were obtained by CTR from SeO<sub>2</sub> (0.111 g, 1 mmol), CuCl<sub>2</sub> (0.202 g, 1.5 mmol), CuO (0.159 g, 2 mmol), PbO (0.112 g, 0.5 mmol), and NaCl (0.059 g, 1 mmol). The crystals of **2** were found in association with dark-green prismatic crystals of Na<sub>2</sub>[Cu<sub>7</sub>O<sub>2</sub>](SeO<sub>3</sub>)<sub>4</sub>Cl<sub>4</sub> in the hot zone of the tube. Black

block-shaped single crystals of synthetic georgbokiite,  $[\text{Cu}_5\text{O}_2](\text{SeO}_3)_2\text{Cl}_2$ , and orange needle-like crystals of synthetic chloromenite,  $[\text{Cu}_9\text{O}_2](\text{SeO}_3)_4\text{Cl}_6$  were found in the middle part of the tube. Greenish transparent prismatic crystals of  $\text{Cu}_2\text{O}(\text{SeO}_3)$  and  $\text{Na}_2\text{CuO}_2$  were also observed in the cold zone of the tube.



Ruby-red crystals of **3** were observed in the cold zone of the tube. The following mixture was used:  $\text{SeO}_2$  (0.111 g, 1 mmol),  $\text{CuCl}$  (0.124 g, 1.25 mmol),  $\text{CuCl}_2$  (0.303 g, 2.25 mmol),  $\text{PbO}$  (0.167 g, 0.75 mmol), and  $\text{NaCl}$  (0.029 g, 0.50 mmol). Black block-shaped crystals of synthetic georgbokiite,  $[\text{Cu}_5\text{O}_2](\text{SeO}_3)_2\text{Cl}_2$ , were also observed in all zones of the tube.

### Chemical analysis

The electron-microprobe analyses (Hitachi TM 3000 EDS system) were performed for **1–3**. Qualitative electron microprobe analysis revealed no other elements, except Cu, Pb, Se, Cl and K (**3**), with the atomic number greater than 11 (Na). The compounds are unstable under an electron beam, which did not allow detailed chemical characterization.

### X-ray crystallography

Single crystals of all compounds were mounted on thin glass fibers for X-ray diffraction analysis using Bruker APEX II DUO X-ray diffractometer with a micro-focus X-ray tube operated with  $\text{MoK}\alpha$  radiation at 50 kV and 40 mA. The data were integrated and corrected for absorption using a multi-scan type model using the Bruker programs APEX and SADABS. More than a hemisphere of X-ray diffraction data were collected for each crystal. Crystallographic information for all obtained phases is summarized in Table 1. Atomic coordinates and additional structural information are provided in the Supporting Information (CIF).

### Infrared spectroscopy

Infrared spectra of **2** and **3** were measured between 4000 and 400  $\text{cm}^{-1}$  with a Perkin–Elmer Spectrum Two spectrometer equipped with a diamond attenuated total reflectance (ATR) accessory. The vibrational bands of selenite groups and ethanol have been established in the studied range (Figs. S2–3). Stretching vibrations  $\nu(\text{SeO}_3)$  and deformation modes  $\delta(\text{SeO}_3)$  of selenite oxoanions appear in range 831–712, 665  $\text{cm}^{-1}$ , and 571–411  $\text{cm}^{-1}$ , respectively. The observed bands are in good agreement with those reported in the literature for similar natural and synthetic selenite phases<sup>1,2</sup>. The presence of the bands of the ethanol molecules in the IR



spectra is a consequence of the use of ethanol for cleaning of the ATR accessory of the spectrometer between the measurements of the samples of different phases. Stretching and deformation modes of the ethanol molecules appear at 2988, 2901, 1490, 1250, and 1066  $\text{cm}^{-1}$ . The observed positions of the bands are consistent with published data for ethanol<sup>3</sup>.

- 1 K. Nakamoto, in *Handbook of Vibrational Spectroscopy*, eds. J. M. Chalmers and P. R. Griffiths, John Wiley & Sons Ltd., 2006, vol. 3, pp. 1872–1892.
- 2 N. V. Chukanov, *Infrared spectra of mineral species*, Springer Netherlands, Dordrecht, 2014, vol. 1., 1726 p.
- 3 Coblenz Society Inc., in *NIST Chemistry WebBook, NIST Standard Reference Database Number 69*, eds. P. J. Linstrom and W. G. Mallard, National Institute of Standards and Technology, Gaithersburg MD, 2009.

**Table S1** Bond-valence analysis (in valence units = v.u.) for the structure of **1** =

	O1	O2	O3	O4	O5	O6	Cl1	Cl2	Cl3	Cl4	$\Sigma$
Pb1		0.45			0.40 <sup>2x→</sup>		0.28, 0.08 <sup>2x→↓</sup>	0.21	0.06		1.96
Cu1		0.51 <sup>2x↓</sup>		0.56 <sup>2x↓</sup>	0.45	0.41			0.06 <sup>2x↓</sup>	0.05 <sup>4x↓</sup>	2.04
Cu2			0.43 <sup>2x→</sup>	0.58 <sup>2x→</sup>						0.05 <sup>2x→↓</sup>	2.12
Cu3	0.47, 0.40	0.55					0.44		0.05 <sup>2x→↓</sup>		1.96
Cu4			0.32	0.53		0.34 <sup>2x→</sup>		0.57			2.10
Cu5									0.51 <sup>2x→</sup>		1.02
Se1			1.39		1.32 <sup>2x→</sup>						4.03
Se2	1.28					1.44 <sup>2x→</sup>					4.16
$\Sigma$	2.15	2.02	2.14	2.23	2.17	2.19	0.88	0.78	0.79	0.30	

**Table S2** Bond-valence analysis (in valence units = v.u.) for the structure of **2** =

	O1	O2	O3	O4	O5	O6	Cl1	Cl2	Cl3	Cl4	Cl5	$\Sigma$
Pb1		0.39 <sup>2x→</sup>				0.44	0.23		0.30, 0.10 <sup>2x→↓</sup>			1.95
Cu1			0.32 <sup>2x→</sup>		0.53		0.56	0.32				2.05
Cu2	0.47, 0.41				0.56			0.49			0.05 <sup>2x→↓</sup>	2.03
Cu3				0.47, 0.42		0.55			0.45	0.05 <sup>2x→↓</sup>		1.99
Cu4		0.47	0.44		0.52 <sup>2x↓</sup>	0.51 <sup>2x↓</sup>				0.07 <sup>2x↓</sup>	0.12 <sup>2x↓</sup>	2.13
Cu5											0.58 <sup>2x→</sup>	1.16
Cu6										0.50 <sup>2x→</sup>		1.00
Se1	1.32	1.37 <sup>2x→</sup>										4.06
Se2			1.42 <sup>2x→</sup>	1.29								4.13
$\Sigma$	2.20	2.23	2.18	2.18	2.13	2.01	0.79	0.81	0.95	0.74	0.92	

**Table S3** Bond-valence analysis (in valence units = v.u.) for the structure of **3** =

$K_{(1-x)}[Cu^+Cl_2][Cu^{2+}_{(6-x)}Pb_xO_2](SeO_3)_2Cl_{(4-x)}$  ( $x \approx 0.20$ ). Site occupancy factors (s.o.f.) are shown in brackets. The Pb1 site is only 10% occupied and its bond-valence characteristics are omitted in the table.

	O1 (1.0)	O2 (1.0)	O3 (1.0)	Cl1 (1.0)	Cl2 (1.0)	Cl3 (0.9)	$\Sigma$
K1 (0.8)				0.08 <sup>2x→</sup>	0.07 <sup>4x→2x↓</sup>	0.18 <sup>2x→</sup>	0.80
Cu1 (1.0)	0.50, 0.41		0.57	0.05 <sup>2x→↓</sup>	0.47		2.06
Cu2 (1.0)		0.46 <sup>2x→</sup>	0.54 <sup>2x→↓</sup>	0.07 <sup>2x→↓</sup>			2.14
Cu3 (1.0)				0.55 <sup>2x→</sup>			1.10
Cu4 (0.9)		0.29 <sup>2x→</sup>	0.54		0.29	0.61	2.02
Se1 (1.0)	1.26	1.39 <sup>2x→</sup>					4.04
$\Sigma$	2.17	2.14	2.19	0.87	0.90	0.79	

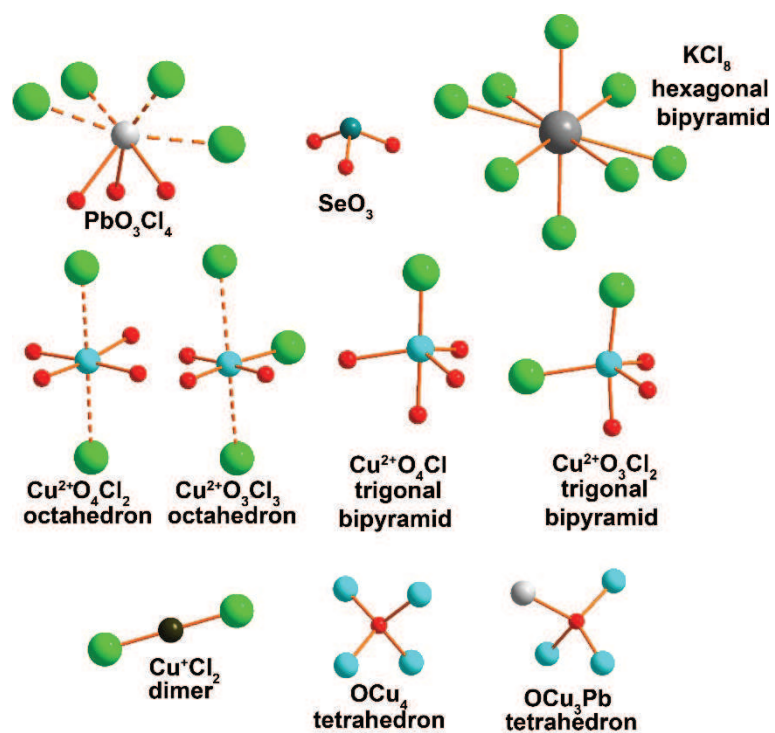


**Fig. S1** General representation of coordination environments of cations and additional oxygen atoms ( $\text{O}_a$ ) coordination in the crystal structures of 1–3. The Pb–Cl and  $\text{Cu}^{2+}$ –Cl bonds longer than 3 Å are shown as dashed lines.

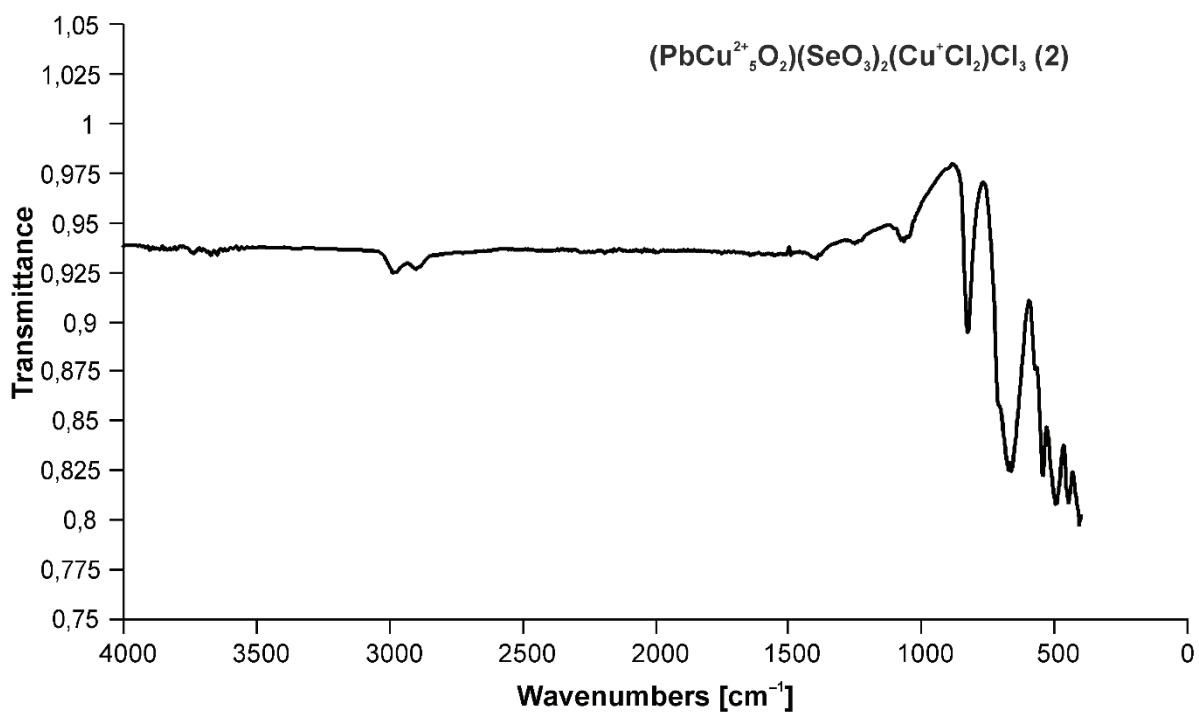


**Fig. S2** Infrared spectrum of (PbCu<sup>2+</sup><sub>5</sub>O<sub>2</sub>)(SeO<sub>3</sub>)<sub>2</sub>(Cu<sup>+</sup>Cl<sub>2</sub>)Cl<sub>3</sub> (2).

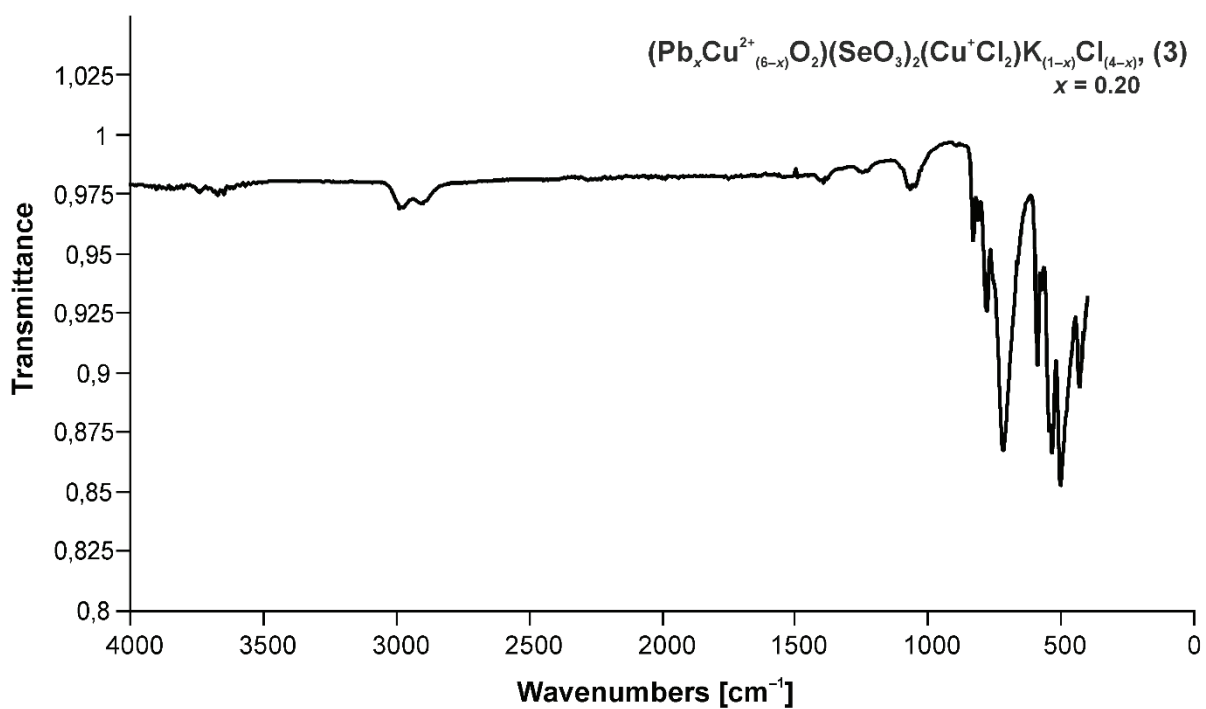


**Fig. S3** Infrared spectrum of  $(\text{Pb}_x\text{Cu}^{2+}_{(6-x)}\text{O}_2)(\text{SeO}_3)_2(\text{Cu}^+\text{Cl}_2)\text{K}_{(1-x)}\text{Cl}_{(4-x)}$ ,  $x = 0.20$  (3).





## **A-VI**

# **Topologically and geometrically flexible structural units in seven new organically templated uranyl selenates and selenite-selenates**

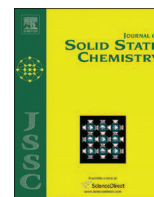
Vladislav V. Gurzhiy, Vadim M. Kovrugin, Pavel A. Mikhaylenko, Olga S. Tyumentseva,  
Sergey V. Krivovichev, and Ivan G. Tananaev

Published in: *Journal of Solid State Chemistry*, 2015, Vol. 229, 32–40.

DOI: 10.1016/j.jssc.2015.04.040

Reprinted with kind permission from Elsevier Inc.





# Topologically and geometrically flexible structural units in seven new organically templated uranyl selenates and selenite–selenates



Vladislav V. Gurzhiy<sup>a,\*</sup>, Vadim M. Kovrugin<sup>a</sup>, Olga S. Tyumentseva<sup>a</sup>,  
Pavel A. Mikhaylenko<sup>a</sup>, Sergey V. Krivovichev<sup>a</sup>, Ivan G. Tananaev<sup>b</sup>

<sup>a</sup> Department of Crystallography, St. Petersburg State University, University Emb. 7/9, 199034 St. Petersburg, Russia

<sup>b</sup> National Research Nuclear University MEPhI, pr. Pobedy 48, 456783 Ozersk, Russia

## ARTICLE INFO

### Article history:

Received 6 March 2015

Received in revised form

24 April 2015

Accepted 27 April 2015

Available online 8 May 2015

### Keywords:

Uranyl

Selenate

Crystal structure

Topology

Isomerism

X-ray diffraction

## ABSTRACT

Single crystals of seven novel uranyl oxysalts of selenium with protonated methylamine molecules,  $[\text{C}_2\text{H}_8\text{N}]_2[(\text{UO}_2)(\text{SeO}_4)_2(\text{H}_2\text{O})]$  (**I**),  $[\text{C}_2\text{H}_8\text{N}]_2[(\text{UO}_2)_2(\text{SeO}_4)_3(\text{H}_2\text{O})]$  (**II**),  $[\text{C}_4\text{H}_{15}\text{N}_3][\text{H}_3\text{O}]_{0.5}[(\text{UO}_2)_2(\text{SeO}_4)_{2.93}(\text{SeO}_3)_{0.07}(\text{H}_2\text{O})](\text{NO}_3)_{0.5}$  (**III**),  $[\text{C}_2\text{H}_8\text{N}]_3[\text{H}_5\text{O}_2][(\text{UO}_2)_2(\text{SeO}_4)_3(\text{H}_2\text{O})_2]_2(\text{H}_2\text{O})_5$  (**IV**),  $[\text{C}_2\text{H}_8\text{N}]_2[\text{H}_3\text{O}][(\text{UO}_2)_3(\text{SeO}_4)_4(\text{HSeO}_3)(\text{H}_2\text{O})](\text{H}_2\text{SeO}_3)_{0.2}$  (**V**),  $[\text{C}_4\text{H}_{12}\text{N}_3][\text{H}_3\text{O}][(\text{UO}_2)_3(\text{SeO}_4)_5(\text{H}_2\text{O})]$  (**VI**), and  $[\text{C}_2\text{H}_8\text{N}]_3(\text{C}_2\text{H}_7\text{N})[(\text{UO}_2)_3(\text{SeO}_4)_4(\text{HSeO}_3)(\text{H}_2\text{O})]$  (**VII**) have been prepared by isothermal evaporation from aqueous solutions. Their crystal structures have been solved by direct methods and their uranyl selenate and selenite–selenate units investigated using black-and-white graphs from the viewpoints of topology of interpolyhedral linkages and isomeric variations. The crystal structure of **IV** is based upon complex layers with unique topology, which has not been observed previously in uranyl selenates. Investigations of the statistics and local distribution of the U–O<sub>br</sub>–Se bond angles demonstrates that shorter angles associate with undulations, whereas larger angles correspond to planar areas of the uranyl selenite layers.

© 2015 Elsevier Inc. All rights reserved.

## 1. Introduction

Within the last decade actinide oxysalts attracted significant attention due to their importance in mineralogy, uranium mining technologies and studies related to the advanced nuclear fuel cycle. The diversity of polyhedral units found in uranyl compounds is unique, starting from isolated complexes [1–3] and clusters [4–7] to cage compounds [8–11] and nanotubules [12–14]. Selenium-containing uranyl oxysalts are known for both mono- and divalent inorganic cations [15–19], as well as for organic template molecules of various charge and structure [20–24]. The crystal structures of uranyl selenates and selenites are based upon a variety of complex units formed by polymerization of U and Se coordination polyhedra. The topology and geometry of these units is controlled by a number of factors, governing interactions between organic and inorganic substructures. The principles that describe these interactions include hydrophilic–hydrophobic interactions, charge-density matching and weak hydrogen bonding that nevertheless may induce distortions of particular geometries of U–O–Se links. Herein we report on the syntheses and structural characterization of seven novel Se-containing uranyl

oxysalts that contain protonated organic molecules as interlayer species.

## 2. Experimental

### 2.1. Synthesis

*N,N*-dimethylformamide (99%, Sigma-Aldrich), dimethylamine (40 wt% in H<sub>2</sub>O, Aldrich), diethylenetriamine (99%, Sigma-Aldrich), diethylamine (99%, Sigma-Aldrich), selenic acid (40 wt% in H<sub>2</sub>O, 99.95%, Aldrich), and UO<sub>2</sub>(NO<sub>3</sub>)<sub>2</sub>·6H<sub>2</sub>O (Vekton) were used as received.  $[\text{C}_2\text{H}_8\text{N}]_2[(\text{UO}_2)(\text{SeO}_4)_2(\text{H}_2\text{O})]$  (**I**),  $[\text{C}_2\text{H}_8\text{N}]_2[(\text{UO}_2)_2(\text{SeO}_4)_3(\text{H}_2\text{O})]$  (**II**),  $[\text{C}_4\text{H}_{15}\text{N}_3][\text{H}_3\text{O}]_{0.5}[(\text{UO}_2)_2(\text{SeO}_4)_{2.93}(\text{SeO}_3)_{0.07}(\text{H}_2\text{O})](\text{NO}_3)_{0.5}$  (**III**),  $[\text{C}_2\text{H}_8\text{N}]_3[\text{H}_5\text{O}_2][(\text{UO}_2)_2(\text{SeO}_4)_3(\text{H}_2\text{O})_2]_2(\text{H}_2\text{O})_5$  (**IV**),  $[\text{C}_2\text{H}_8\text{N}]_2[\text{H}_3\text{O}][(\text{UO}_2)_3(\text{SeO}_4)_4(\text{HSeO}_3)(\text{H}_2\text{O})](\text{H}_2\text{SeO}_3)_{0.2}$  (**V**),  $[\text{C}_4\text{H}_{12}\text{N}_3][\text{H}_3\text{O}][(\text{UO}_2)_3(\text{SeO}_4)_5(\text{H}_2\text{O})]$  (**VI**), and  $[\text{C}_2\text{H}_8\text{N}]_3(\text{C}_2\text{H}_7\text{N})[(\text{UO}_2)_3(\text{SeO}_4)_4(\text{HSeO}_3)(\text{H}_2\text{O})]$  (**VII**) have been prepared by evaporation from aqueous solutions of uranyl nitrate, 40%–solution of selenic acid, *N,N*-dimethylformamide, 40%–solution of methylamine, diethylenetriamine, diethylamine, and deionized distilled water. Yellow–green homogeneous liquid solutions were left in a fumehood at the room temperature. The crystals of compound **I**, and **II** were synthesized through the reaction 0.198 g (0.4 mmol) of uranyl nitrate, 0.094 g (1.3 mmol) of *N,N*-dimethylformamide,

\* Corresponding author. Tel.: +7 9119749592.

E-mail addresses: [vladgeo17@mail.ru](mailto:vladgeo17@mail.ru) (V.V. Gurzhiy), [vladgeo17@mail.ru](mailto:vladgeo17@mail.ru) (I.G. Tananaev).

0.590 g (4.1 mmol) of selenic acid and 2.001 g (110.2 mmol) of deionized distilled water. The crystals of compound **IV**, and **V** were synthesized through the reaction 0.0502 g (0.1 mmol) of uranyl nitrate, 0.009 g (0.2 mmol) of dimethylamine, 0.102 g (0.7 mmol) of selenic acid and 2.002 g (110.2 mmol) of deionized distilled water. The crystals of compound **VII** were synthesized through the reaction 0.0502 g (0.1 mmol) of uranyl nitrate, 0.018 g (0.4 mmol) of dimethylamine, 0.072 g (0.5 mmol) of selenic acid and 2.001 g (110.2 mmol) of deionized distilled water. The crystals of compound **III** were synthesized through the reaction 0.100 g (0.2 mmol) of uranyl nitrate, 0.010 g (0.1 mmol) of diethylenetriamine, 0.102 g (0.7 mmol) of selenic acid and 2.002 g (110.2 mmol) of deionized distilled water. The crystals of compound **VI** were synthesized through the reaction 0.059 g (0.1 mmol) of uranyl nitrate, 0.010 g (0.1 mmol) of diethylamine, 0.679 g (4.7 mmol) of selenic acid and 2.002 g (110.2 mmol) of deionized distilled water. The solid products were formed after three days in small amount. The pH values of the solutions described above are in the range from 1 to 0, moreover for the newly prepared solutions the values tend closer to 1, whereas precipitation of crystals increases acidity.

## 2.2. Single crystal X-ray study

Single crystals of **I–VII** have been selected for data collection under an optical microscope, encased in epoxy and mounted on glass fibres. Data were collected using monochromatic MoK $\alpha$  radiation ( $\lambda[\text{MoK}\alpha]=0.71073 \text{ \AA}$ ) by means of a Bruker SMART APEX II CCD (**I–VI**) and STOE IPDS II (**VII**) diffractometers. The unit-cell parameters were refined by least-squares techniques. Data were integrated and corrected for background, Lorentz, and polarization effects using an empirical spherical model by means of the Bruker programs APEX2 and XPREP (**I–VI**) and STOE X-AREA (**VII**). Absorption correction was applied using the SADABS program [25] for (**I–VI**) and STOE X-RED & X-SHAPE [26] for **VII**. The structures were solved by direct methods and refined using the SIR-92 [27] and SHELXL-97 programs [28] incorporated in the OLEX2 program package [29]. Due to the low quality of crystals (especially phases **IV–VII**), their metastability and sensitivity to air, only rather rough structural models could be obtained, which is manifested in the presence of high residual electron-density peaks, low bond precision, and refinement of organic molecules in isotropic

approximation only (**VII**), as well as in the impossibility to localize the positions of several H atoms. However, the hydrogen bonding system in such cases can be inferred from the short O–O contacts involving sites occupied by water and hydronium molecules. The final models included coordinates and anisotropic displacement parameters for all non-hydrogen atoms. The carbon-bound H atoms were placed in calculated positions and were included in the refinement in the 'riding' model approximation, with  $U_{\text{iso}}(\text{H})$  set to  $1.5U_{\text{eq}}(\text{C})$  and C–H 0.96 Å for CH<sub>3</sub> groups, with  $U_{\text{iso}}(\text{H})$  set to  $1.2U_{\text{eq}}(\text{C})$  and C–H 0.97 Å for CH<sub>2</sub> groups,  $U_{\text{iso}}(\text{H})$  set to  $1.2U_{\text{eq}}(\text{N})$  and N–H 0.89 Å for the NH<sub>3</sub> groups, and  $U_{\text{iso}}(\text{H})$  set to  $1.2U_{\text{eq}}(\text{N})$  and N–H 0.86 Å for the NH<sub>2</sub> groups. Positions of H atoms of H<sub>2</sub>O molecules, hydronium cations and OH<sup>−</sup> groups were localized from difference Fourier maps and kept fixed during refinement. Relevant crystallographic data are listed in Table 1. Selected interatomic distances are listed in Tables S1–S7. CCDC files 901940, 901941, 901942, 901943, 901944, 901945, and 901946 contain the supplementary crystallographic data for the compounds **I–VII**, respectively. These data can be obtained free of charge from The Cambridge Crystallographic Data Centre via [www.ccdc.cam.ac.uk/data\\_request/cif](http://www.ccdc.cam.ac.uk/data_request/cif)

## 3. Results

### 3.1. Structural descriptions

The crystal structures of all seven compounds reported in this paper contain uranyl pentagonal bipyramids and selenate tetrahedra. The structures of **V** and **VII** also contain selenite trigonal pyramids. The polyhedra are linked into inorganic structural units. The structures contain one (**I**), two (**II**, **III**, **V**, **VI** and **VII**), or four (**IV**) crystallographically unique U<sup>VI</sup> cations forming approximately linear uranyl ions, [UO<sub>2</sub>]<sup>2+</sup>, with the U=O bond lengths varying from 1.711(10) Å to 1.787(7) Å. These basic uranyl entities are coordinated in their equatorial planes by four oxygen atoms and one H<sub>2</sub>O molecule to form UO<sub>7</sub> pentagonal bipyramids with the average (U–O<sub>eq</sub>) bond lengths equal to 2.390 Å. The U–H<sub>2</sub>O bond lengths lie in range of 2.424(12)–2.554(7) Å. In the structure of **I** there are two symmetrically independent Se<sup>VI</sup> atoms. The structures of **II**, **III**, **IV**, and **VI** contain three Se<sup>VI</sup> atoms each, whereas the structure of **IV** contains six

**Table 1**  
Crystallographic data for **I**, **II**, **III**, **IV**, **V**, **VI** and **VII**.

Compound	<b>I</b>	<b>II</b>	<b>III</b>	<b>IV</b>	<b>V</b>	<b>VI</b>	<b>VII</b>
Formula mass	666.15	1079.14	2256.03	2267.28	1685.05	1770.70	1685.07
Space group	<i>P</i> 2 <sub>1</sub> 2 <sub>1</sub> 2 <sub>1</sub>	<i>P</i> 2 <sub>1</sub> 2 <sub>1</sub> 2 <sub>1</sub>	<i>P</i> 2 <sub>1</sub> / <i>c</i>	<i>P</i> 2 <sub>1</sub> / <i>c</i>	<i>P</i> 2 <sub>1</sub> / <i>m</i>	<i>P</i> 2 <sub>1</sub> / <i>m</i>	<i>Pnma</i>
<i>a</i> (Å)	7.5363(7)	11.2154(5)	11.1679(4)	12.451(5)	8.3116(4)	8.941(2)	11.6591(11)
<i>b</i> (Å)	12.2021(11)	11.2263(5)	10.9040(4)	31.126(5)	18.6363(8)	19.300(4)	14.9556(17)
<i>c</i> (Å)	16.7601(16)	16.9138(8)	17.9913(6)	14.197(4)	11.5623(5)	11.377(3)	22.194(2)
$\beta$ (°)	90.00	90.00	98.019(1)	120.39(2)	97.582(1)	97.510(4)	90.00
<i>V</i> (Å <sup>3</sup> )	1541.2(2)	2129.57(17)	2169.57(17)	4746(2)	1775.31(14)	1946.5(7)	3870.0(7)
Size (mm <sup>3</sup> )	0.21 × 0.17 × 0.09	0.21 × 0.17 × 0.07	0.23 × 0.19 × 0.08	0.23 × 0.18 × 0.07	0.19 × 0.14 × 0.08	0.22 × 0.20 × 0.06	0.26 × 0.20 × 0.09
$\mu$ (mm <sup>−1</sup> )	15.306	20.394	20.036	18.323	19.286	17.217	17.310
<i>Z</i>	4	4	2	4	2	2	4
2 $\theta$ range (°)	4.13–60.00	4.35–60.00	4.38–55.00	2.62–55.00	4.17–60.00	4.18–54.98	3.28–39.10
<i>D</i> <sub>calc</sub> (g/cm <sup>3</sup> )	2.871	3.366	3.457	3.173	3.152	3.021	2.892
Total ref.	13,644	17,184	23,671	34,682	23,753	18,435	10,911
Unique ref.	4492	6112	4988	10896	5323	4597	1680
Unique   <i>F</i> <sub>o</sub>   ≥ 4 $\sigma$ <sub><i>F</i></sub>	4117	5340	3855	5379	3940	2459	1221
<i>R</i> <sub>int</sub>	0.0564	0.0651	0.0723	0.0963	0.0762	0.1196	0.1116
<i>R</i> <sub><math>\sigma</math></sub>	0.0562	0.0684	0.0574	0.0993	0.0605	0.1609	0.0714
<i>R</i> <sub>1</sub> (  <i>F</i> <sub>o</sub>   ≥ 4 $\sigma$ <sub><i>F</i></sub> )	0.0311	0.0283	0.0330	0.0482	0.0362	0.0396	0.0602
<i>wR</i> <sub>2</sub> (  <i>F</i> <sub>o</sub>   ≥ 4 $\sigma$ <sub><i>F</i></sub> )	0.0629	0.0484	0.0735	0.1060	0.0935	0.0583	0.0962
GOF	0.940	0.934	0.964	0.875	1.083	0.737	1.127
$\rho_{\text{min}}$ , $\rho_{\text{max}}$ , <i>e</i> (Å <sup>−3</sup> )	−1.497, 2.339	−1.199, 1.099	−1.997, 2.824	−4.340, 4.608	−2.216, 2.793	−1.383, 1.651	−1.210, 1.054
CCDC	901940	901941	901942	901943	901944	901945	901946

Note:  $R_1 = \sum ||F_o| - |F_c|| / \sum |F_o|$ ;  $wR_2 = \{ \sum [w(F_o^2 - F_c^2)]^2 / \sum [w(F_o^2)]^2 \}^{1/2}$ ;  $w = 1 / [ \sigma^2(F_o^2) + (aP)^2 + bP ]$ , where  $P = (F_o^2 + 2F_c^2) / 3$ ;  $GOF = \{ \sum [w(F_o^2 - F_c^2)] / (n-p) \}^{1/2}$  where *n* is the number of reflections and *p* is the number of refined parameters.

independent  $\text{Se}^{\text{VI}}$  atoms. In the structures of **V** and **VII** there are three independent Se positions of which two sites [Se1 and Se2] correspond to  $\text{Se}^{\text{VI}}$ , whereas the Se3 site is occupied by  $\text{Se}^{\text{IV}}$ . The  $\text{Se}^{\text{VI}}$  cations in each structure are tetrahedrally coordinated by four O atoms, forming  $[\text{SeO}_4]^{2-}$  tetrahedra with the average  $\langle \text{Se-O} \rangle$  bond length equals to 1.634 Å. In the structure of **V** and **VII**, the Se3 site has a trigonal pyramidal coordination with an apex occupied by the  $\text{Se}^{\text{IV}}$  atom. This coordination type is typical for  $\text{Se}^{\text{IV}}$  cations possessing stereoactive lone electron pairs. In the structure of **III**, the Se3 site is occupied by both  $\text{Se}^{\text{VI}}$  (site-occupation factor (s.o.f.)=0.93) and  $\text{Se}^{\text{IV}}$  (s.o.f.=0.07) atoms with the total s.o.f. equal to 1.0. The  $\text{Se}_3\text{O}_3$  trigonal pyramids in **V** and **VII** are strongly distorted: two short equivalent bonds [1.645(6) Å and 1.653(16) Å in **V** and **VII**, respectively] and one longer bond [1.78(2) Å and 1.78(4) Å in **V** and **VII**, respectively]. The observed elongation is the result of relatively strong hydrogen bonding to the nearby terminal methyl cations of the protonated dimethylamine molecule in the structure of **V**, and by protonation of the selenite group in the structure of **VII**. The asymmetric  $[\text{SeO}_3]^{2-}$  and  $[\text{HSeO}_3]^{2-}$  selenite groups were observed, in particular, in the structures of  $(\text{NH}_4)[\text{UO}_2(\text{HSeO}_3)(\text{SeO}_3)]$  [30],  $M[(\text{UO}_2)(\text{HSeO}_3)(\text{SeO}_3)]$  ( $M=\text{K}, \text{Rb}, \text{Cs}, \text{Ti}$ ) [31],  $[\text{C}_5\text{H}_{14}\text{N}][(\text{UO}_2)(\text{SeO}_4)(\text{SeO}_2\text{OH})]$  [32], and  $[\text{C}_5\text{H}_{14}\text{N}]_4(\text{UO}_2)_3(\text{SeO}_4)_4(\text{HSeO}_3)(\text{H}_2\text{O})(\text{H}_2\text{SeO}_3)(\text{HSeO}_4)$  [33].

In the crystal structure of **I**, the  $[\text{UO}_6(\text{H}_2\text{O})]^{6-}$  pentagonal bipyramids share corners with two adjacent  $[\text{SeO}_4]^{2-}$  tetrahedra to form  $[(\text{UO}_2)(\text{SeO}_4)_2(\text{H}_2\text{O})]^{2-}$  chains running parallel to the  $b$  axis. The chains are arranged into the pseudo layers parallel to the (0 0 1) plane

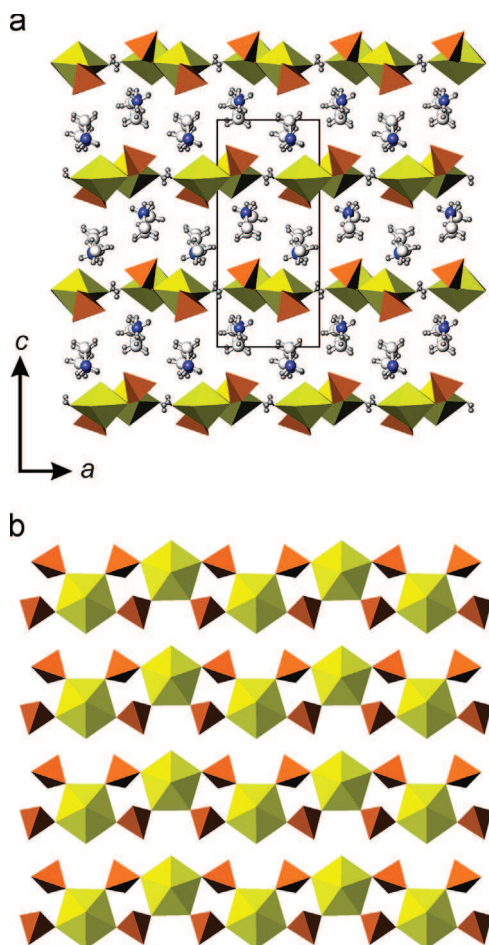


**Fig. 1.** The crystal structure of **I** projected along the  $b$  axis (a), and the  $[(\text{UO}_2)(\text{SeO}_4)_2(\text{H}_2\text{O})]^{2-}$  chains in the crystal structure of **I** (b). Legend: U polyhedra=yellow; Se polyhedra=orange; C and N atoms are white and blue, respectively; hydrogen atoms are small grey circles. (For interpretation of the references to color in this figure legend, the reader is referred to the web version of this article.)

(Fig. 1a). Two protonated dimethylamine cations  $[\text{C}_2\text{H}_8\text{N}]^+$  are arranged between the chains and provide their linkage into a three-dimensional structure.

The crystal structures of **II**, **IV** and **III**, are based upon complex 2D layers with the composition  $[(\text{UO}_2)_2(\text{SeO}_4)_3(\text{H}_2\text{O})_n]^{2-}$ . The topology of the U and Se polyhedral linkage is different for the different values of  $n$ . The layers are parallel to (0 0 1) in **II** and **III**, and to (0 1 0) in **IV** (Figs. 2 and 3). The uranyl selenate layers present in **II** and **III** are slightly corrugated. The interpolyhedral  $\text{U-O}_{\text{br}}\text{-Se}$  angles in **II**, **III** and **IV** have the average values of 135.6°, 136.1° and 135.6°, respectively, which are in general agreement with the average value of 136.8° reported in [34]. The structure of **II** contains two protonated linear dimethylamine molecules  $[\text{C}_2\text{H}_8\text{N}]^+$  as interlayer species. Diprotonated diethylenetriamine cation  $[\text{C}_4\text{H}_{15}\text{N}_3]^{2+}$ , hydronium cation  $[\text{H}_3\text{O}]^+$  and disordered nitrate group  $[\text{NO}_3]^-$  are arranged between the layers in the structure of **III**. In the interlayer space of **IV**, there are three crystallographically independent protonated  $[\text{C}_2\text{H}_8\text{N}]^+$  cations, one Zundel  $[\text{H}_5\text{O}_2]^+$  cation, and five water molecules.

The crystal structures of **V**, **VI**, and **VII** are based upon the layers with  $\text{U}:\text{Se}=3:5$  formed as a result of condensation of the  $[\text{UO}_2]^{2+}$ ,  $[\text{UO}_2(\text{H}_2\text{O})]^{2+}$ ,  $[\text{Se}^{\text{VI}}\text{O}_4]^{2-}$ ,  $[\text{Se}^{\text{IV}}\text{O}_3]^{2-}$  and  $[\text{HSe}^{\text{IV}}\text{O}_3]^-$  coordination polyhedra by sharing common oxygen atoms. In the structures of **V** and **VI** the inorganic layers are parallel to (1 0 0) (Fig. 4). The layers in **VII** are parallel to (0 0 1) and are strongly undulated along the  $c$  axis (Fig. 5). The undulation vector is parallel to [0 1 0] and is equal to  $b$  (14.956 Å). The undulation amplitude is about 15 Å. The undulations in the adjacent sheets have an anti-phase character, which means that large elliptical channels are created along the  $a$  axis. The structure

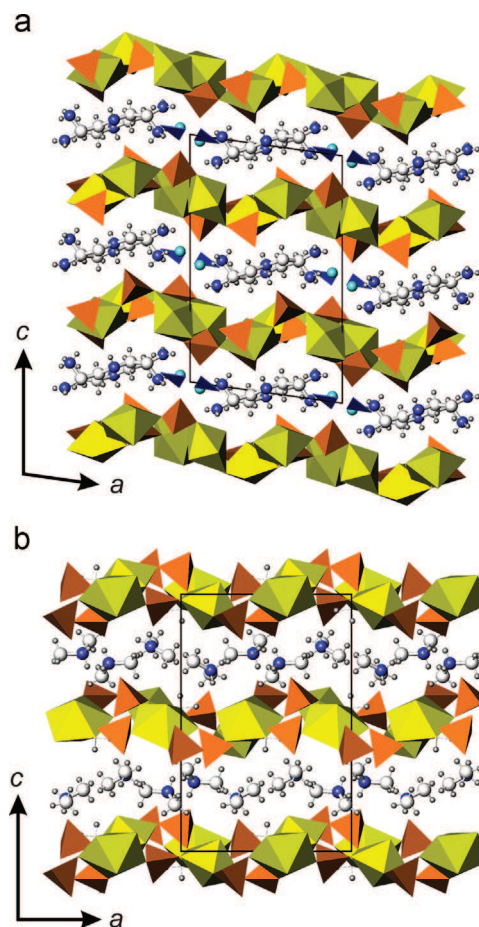


**Fig. 2.** The crystal structures of **II** and **III** projected along the  $b$  axis, (a) and (b), respectively. Legend is as in Fig. 1;  $[\text{H}_3\text{O}]^+$  groups=cyan circles,  $[\text{NO}_3]^-$ =blue triangles. (For interpretation of the references to color in this figure legend, the reader is referred to the web version of this article.)

with similar undulated layers was observed previously [35]. In the structure of **V**, two protonated dimethylamine molecules  $[\text{C}_2\text{H}_8\text{N}]^+$  and one hydronium cation  $[\text{H}_3\text{O}]^+$  are located in the interlayer space, and form hydrogen bonds to the O atoms of uranyl groups and selenium oxyanions. The structure of **VI** contains three protonated diethylamine molecules  $[\text{C}_4\text{H}_{12}\text{N}]^+$  and one hydronium cation  $[\text{H}_3\text{O}]^+$  as interlayer species. The charge of the inorganic layer in **VII** is compensated by three disordered protonated dimethylamine molecules  $[\text{C}_2\text{H}_8\text{N}]^+$  located in the interlayer space. It is of interest

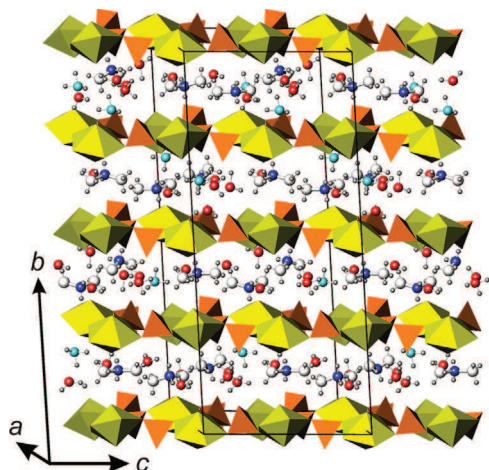


**Fig. 3.** The crystal structure of **IV**. Legend is as in Fig. 1;  $[\text{H}_3\text{O}]^+$  groups and water molecules = cyan and red circles, respectively. (For interpretation of the references to color in this figure legend, the reader is referred to the web version of this article.)

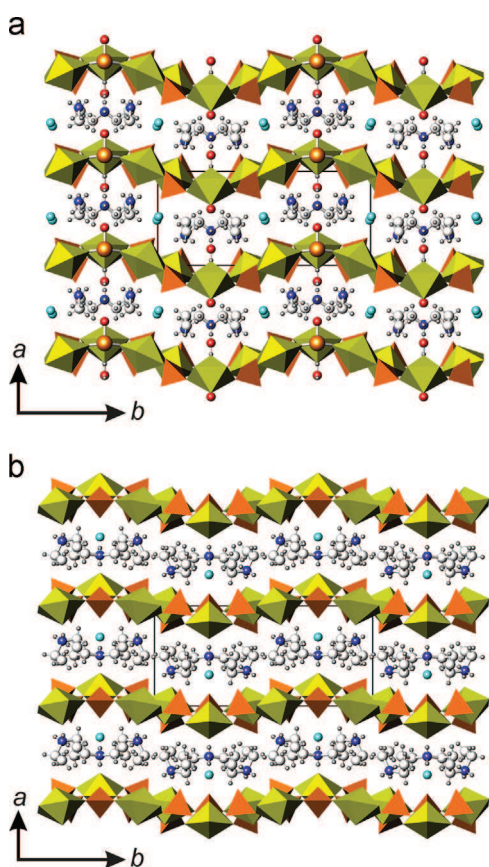


**Fig. 4.** The crystal structures of **V** and **VI** projected along the *b* axis, (a) and (b), respectively. Legend is as in Fig. 1.  $[\text{H}_3\text{O}]^+$  groups and oxygen atoms = cyan and red circles;  $\text{Se}^{\text{IV}}$  atoms = big orange circles. (For interpretation of the references to color in this figure legend, the reader is referred to the web version of this article.)

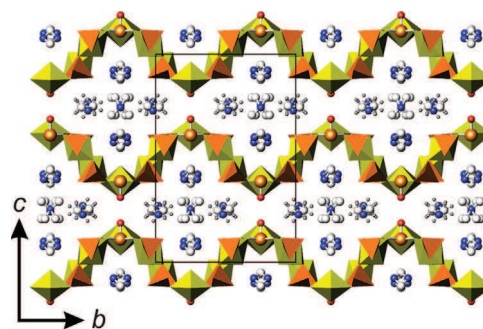


**Fig. 5.** The crystal structure of **VII** projected along the *b* axis. Legend is as in Fig. 1; oxygen atoms = circles;  $\text{Se}^{\text{IV}}$  atoms = big orange circles.

that there is also one electroneutral dimethylamine molecule  $(\text{C}_2\text{H}_7\text{N})^0$  in the centre of the elliptical channels.

### 3.2. Topological analysis

Topological structure of uranyl selenate units in the structures under consideration can be visualized using the nodal representation. In the framework of this approach [36–38], the U and Se coordination polyhedra are symbolized by black and white nodes, respectively. The vertices are linked by an edge if two respective polyhedra share a common oxygen atom. The resulting graph is used to investigate topological relations between similar structures.

Fig. 1b shows the topological structure of the 1D-units of **I**. The  $[(\text{UO}_2)(\text{SeO}_4)_2(\text{H}_2\text{O})]^{2-}$  chain observed in the structure of **I** corresponds to the simple 1D graph. Chains of this type are quite common for uranyl compounds with the  $[\text{TO}_4]^{n-}$  tetrahedra ( $T = \text{S}, \text{Se}, \text{P}, \text{As}$ ). They have been observed first in the structure of  $\text{Mn}[(\text{UO}_2)(\text{SO}_4)_2(\text{H}_2\text{O})](\text{H}_2\text{O})_5$  [39] and later in a number of amine-templated uranyl sulfates [40–45] and other compounds, including  $[(\text{UO}_2)(\text{H}_2\text{PO}_4)_2(\text{H}_2\text{O})](\text{H}_2\text{O})_2$  [46],  $[(\text{UO}_2)(\text{H}_2\text{AsO}_4)_2(\text{H}_2\text{O})]$  [47],  $M[(\text{UO}_2)(\text{SeO}_4)_2(\text{H}_2\text{O})](\text{H}_2\text{O})_4$  ( $M = \text{Mg}, \text{Zn}$ ) [48],  $[\text{C}_5\text{H}_{16}\text{N}_2]_2[(\text{UO}_2)(\text{SeO}_4)_2(\text{H}_2\text{O})](\text{NO}_3)_2$  [49],  $[\text{CH}_3\text{NH}_3]_2[(\text{UO}_2)(\text{SeO}_4)_2(\text{H}_2\text{O})](\text{H}_2\text{O})$  [50].

Fig. 6a and b shows uranyl selenate layers in the structures of **II**, **III**, and **IV**. The corresponding black-and-white graphs are depicted in Fig. 6c and d. In the crystal structure of **II** and **III**, the topology of the  $[(\text{UO}_2)_2(\text{SeO}_4)_3(\text{H}_2\text{O})_n]^{2-}$  layers with  $n = 1$  is based upon 4- and 6-membered rings of alternating black and white nodes. The graph has been observed in uranyl sulfates  $[\text{N}_2\text{C}_3\text{H}_{12}][(\text{UO}_2)_2(\text{H}_2\text{O})(\text{SO}_4)_3]$  [44],  $[\text{N}_2\text{C}_4\text{H}_{14}][(\text{UO}_2)_2(\text{H}_2\text{O})(\text{SO}_4)_3](\text{H}_2\text{O})$  [51], and uranyl selenates  $[\text{C}_4\text{H}_{12}\text{N}]_2[(\text{UO}_2)_2(\text{SeO}_4)_3(\text{H}_2\text{O})]$ ,  $[\text{C}_4\text{H}_{14}\text{N}_2][(\text{UO}_2)_2(\text{SeO}_4)_3(\text{H}_2\text{O})](\text{H}_2\text{O})_2$ ,  $[\text{C}_3\text{H}_{10}\text{N}][(\text{UO}_2)_2(\text{SeO}_4)_3(\text{H}_2\text{O})](\text{H}_2\text{O})$ ,  $[\text{C}_5\text{H}_{16}\text{N}_2][(\text{UO}_2)_2(\text{SeO}_4)_3(\text{H}_2\text{O})](\text{H}_2\text{O})$  [52],  $\text{K}(\text{H}_5\text{O}_2)[(\text{UO}_2)_2(\text{SeO}_4)_3(\text{H}_2\text{O})]$  [53]. The topology of the  $[(\text{UO}_2)_2(\text{SeO}_4)_3(\text{H}_2\text{O})_n]^{2-}$  layer with  $n = 2$  in **IV** contains 4- and 8-membered rings. This topology is rare and has previously been observed only in two uranyl chromates  $(\text{NH}_4)_2(\text{UO}_2)_2(\text{CrO}_4)_3(\text{H}_2\text{O})_6$  [54] and  $\text{K}_2[(\text{UO}_2)_2(\text{CrO}_4)_3(\text{H}_2\text{O})_2](\text{H}_2\text{O})_4$  [55], but has never been observed in uranyl selenates.

The crystal structures of **V**, **VI**, and **VII** are based upon the layers with  $\text{U}:\text{Se} = 3:5$  (Fig. 7a). These structures have the same topology of inorganic layers. The corresponding graph (Fig. 7b) is built from 4- and 6-membered rings. This topology of inorganic complexes is typical for uranyl selenite–selenates such as  $[\text{C}_5\text{H}_{14}\text{N}]_4[(\text{UO}_2)_3(\text{SeO}_4)_4(\text{HSeO}_3)(\text{H}_2\text{O})](\text{H}_2\text{SeO}_3)(\text{HSeO}_4)$  [33],  $(\text{H}_3\text{O})[\text{C}_5\text{H}_{14}\text{N}]_2[(\text{UO}_2)_3(\text{SeO}_4)_4(\text{HSeO}_4)(\text{H}_2\text{O})]$ ,  $(\text{H}_3\text{O})[\text{C}_5\text{H}_{14}\text{N}]_2[(\text{UO}_2)_3(\text{SeO}_4)_4(\text{HSeO}_4)(\text{H}_2\text{O})]$ , and has also been observed in some uranyl selenates:  $\text{Rb}_4[(\text{UO}_2)_3(-\text{SeO}_4)_5(\text{H}_2\text{O})]$  [57],  $(\text{H}_5\text{O}_2)(\text{H}_3\text{O})_2[(\text{C}_{10}\text{H}_{20}\text{O}_5)_2][(\text{UO}_2)_3(\text{SeO}_4)_5(\text{H}_2\text{O})]$  and  $(\text{H}_5\text{O}_2)(\text{H}_3\text{O})_3[\text{C}_{10}\text{H}_{20}\text{O}_5]_5[(\text{UO}_2)_3(\text{SeO}_4)_5(\text{H}_2\text{O})]$  [58].

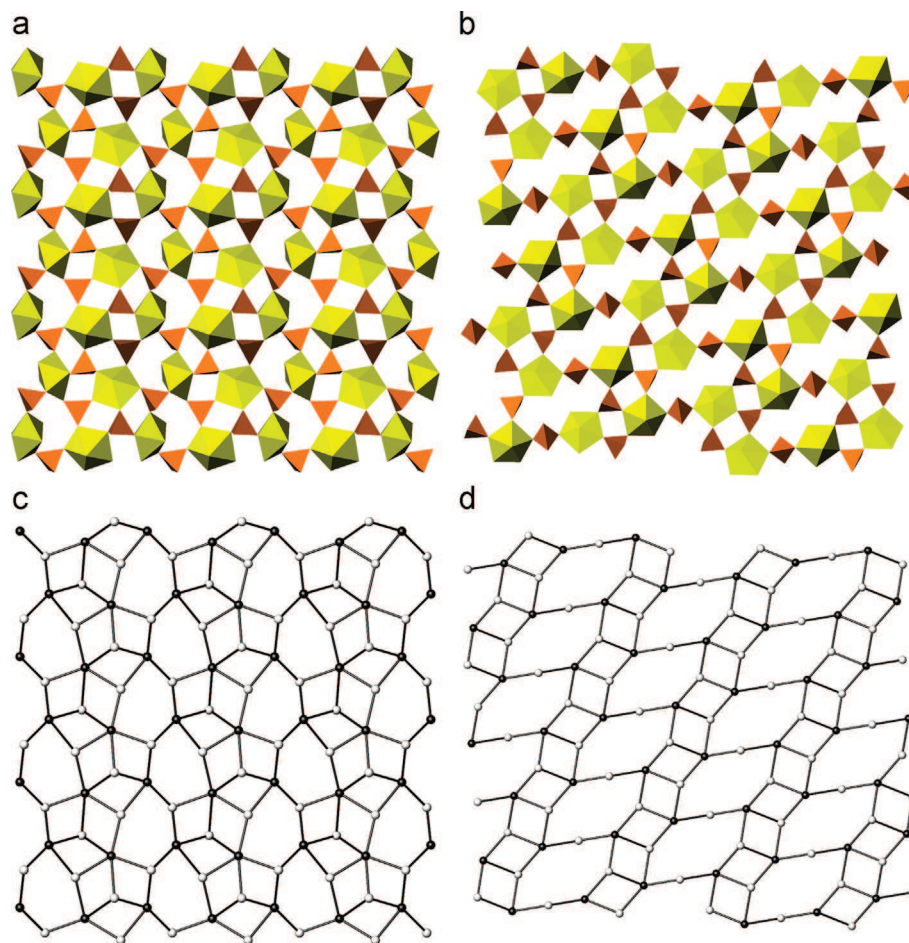


**Fig. 6.** The  $[(\text{UO}_2)_2(\text{SeO}_4)_3(\text{H}_2\text{O})_n]^{2-}$  layers in the crystal structures of **II**, **III**—(a) ( $n=1$ ), and in the crystal structure of **IV**—(b) ( $n=2$ ) in polyhedral representations; their graphs (c and d, respectively). Legend is as in Fig. 1; white vertices=Se, black vertices=U.

### 3.3. Geometrical isomerism

To define a topology of the layer by means of its nodal representation is not enough to define its complete topological structure. The detailed examination of orientations of structural units may reveal geometrical difference between the layers with the same black-and-white graph, which led Krivovichev and Burns [57] to the definition of geometrical isomerism. It is important to note that the isomers cannot be transformed one into another by simple rotations without breaking of chemical bonds. To distinguish between the layers with the same graph observed in the structures of **II**, **III**, and **V**, **VI**, **VII**, one has to analyse orientations of selenium polyhedra relative to the planes of the layers.

The analysis of the black-and-graph of the topology of layers of **V**, **VI** and **VII** (Fig. 7d–f) indicates that its white vertices are either 2- or 3-connected: 2-connected white vertices correspond to selenite trigonal pyramids, whereas 3-connected correspond to selenate tetrahedra. These selenite–selenate polyhedra share three of its corners with adjacent 4- or 5-connected uranyl pentagonal bipyramids. The non-shared corners may have either up-, down- or disordered (up-or-down) orientations relative to the plane of the layer. This ambiguity gives rise to geometric isomers with various orientations of the selenium polyhedra. To identify and classify the isomers of this type, we use their orientation matrices [58]. According to this approach, as applied to the structures in hand, the symbols **u** (up), **d** (down), **m** (orientation up-down topologically equivalent) or  $\square$  (white vertex is missing in the graph) are assigned to each white vertex.

The graphs shown in Fig. 8 have the **u**, **d** and **m** symbols written near white vertices. It can be seen that the systems of the

**u**, **d** and **m** symbols are different for the layers, which therefore should be considered as different geometrical isomers. The isomers can be distinguished by their orientation matrices that provide short notations of the translational independent rectangular system of the **u**, **d**, **m** and  $\square$  symbols. The orientation matrices of the layers in the crystal structures of **V**, **VI** and **VII** shown in Figs. 8d–f have  $6 \times 2$  dimensions and can be written in row as (**duuudd**)(**ud** $\square$ **du** $\square$ ), (**dumudm**)(**ud** $\square$ **du** $\square$ ) and (**ududud**)(**ud** $\square$ **du** $\square$ ), respectively. Thus, the uranyl selenite layers observed in the crystal structures of **V**, **VI** and **VII** correspond to different geometrical isomers.

Using the above procedure, we can constitute the equivalence of the orientation matrices of the inorganic layers of the crystal structures of **II** and **III**. The same orientation matrix for these structures may be written as (**u** $\square$ **dd**)(**uu** $\square$ **d**) (Fig. 9).

### 3.4. Flexibility of structural units

An interesting feature of the substantial number of uranyl compounds [37,59], including seven structures reported herein, is the connection of adjacent coordination polyhedra through the common bridging vertices that can be depicted as a sort of a flexible ball-in-socket arrangement. This flexibility results in the relative ease of adaptation of layered  $[(\text{UO}_2)_x(\text{TO}_4)_y]^{z-}$  systems to variable cations and other species present in the solutions during crystallization. As it has been observed in multiple experiments, there is no direct correlation between the size of the cation and the degree of the layer distortion (corrugation). The presence of large cations or molecules may lead to minor tiltings of coordination polyhedra at their connections, i.e.

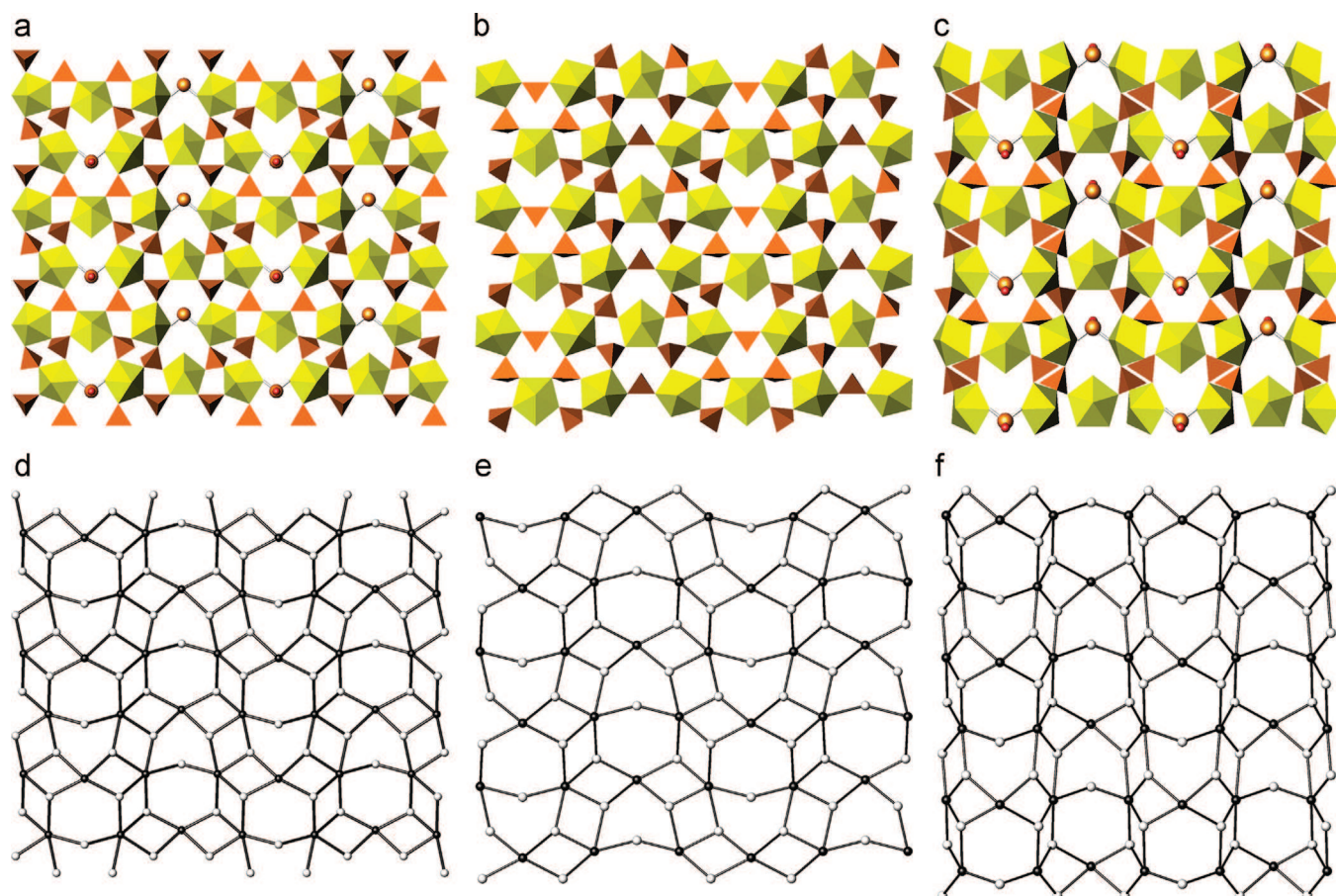


**Fig. 7.** The inorganic layers with U:Se=3:5 in the crystal structures of **V**, **VI**, and **VII**—(a), (b), and (c), respectively; their graphs—(d), (e) and (f), respectively. Legend is as in Fig. 5. See text for details.

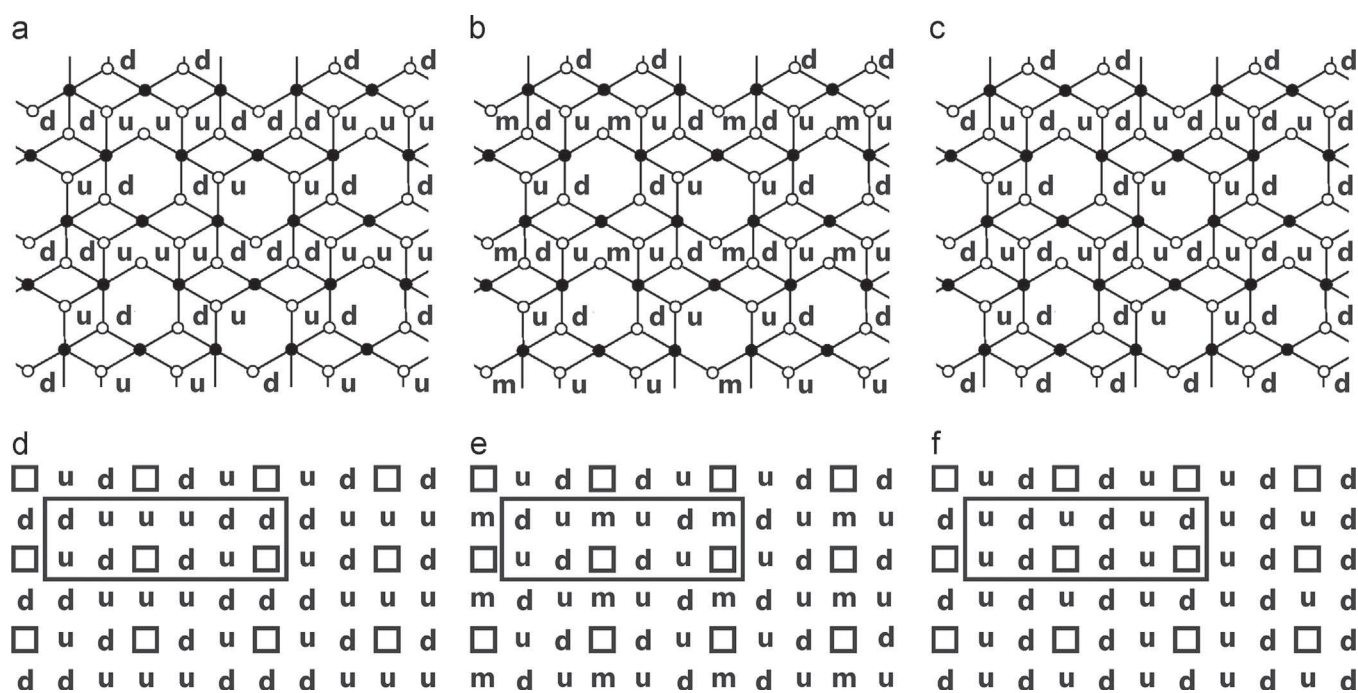


**Fig. 8.** Black-and-white graphs of the inorganic layers in the structures of **V**, **VI**, and **VII**—(a), (b) and (c), respectively, with the orientation symbols of selenium polyhedra; extended tables of orientation symbols (d), (e) and (f), respectively. Translational independent orientation matrices are selected in extended tables by rectangular areas.

around bridging oxygen atoms, to result in a symmetry reduction [60] compared to the ideal symmetry of structural units. In some cases, interactions between interlayer species and uranyl oxysalt units result

in distortion of the layer planes and, in rare cases, formation of tubular structures [12–14]. The total effect of the 2-D unit bending includes rotation and displacements of individual  $U-O_{br}-T$  fragments (Fig. 10).



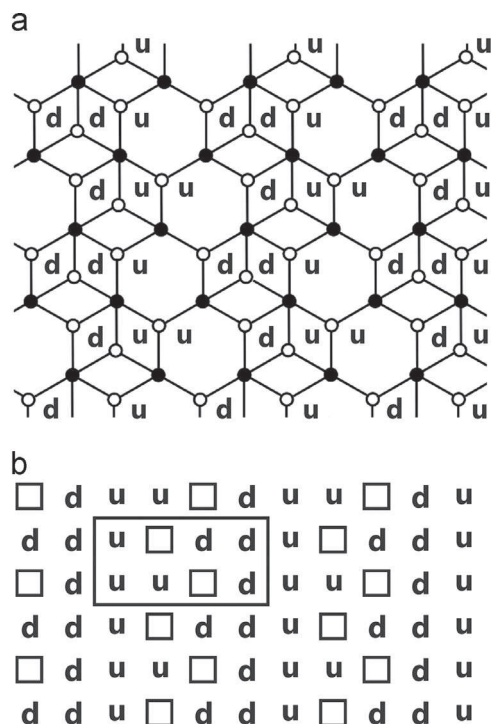


**Fig. 9.** Black-and-white graph of the inorganic layers in the structures of **II**, and **III** (a) with the orientation symbols of selenium polyhedra; extended tables of orientation symbols—(b). Translational independent orientation matrices are selected in (b) by rectangular areas.

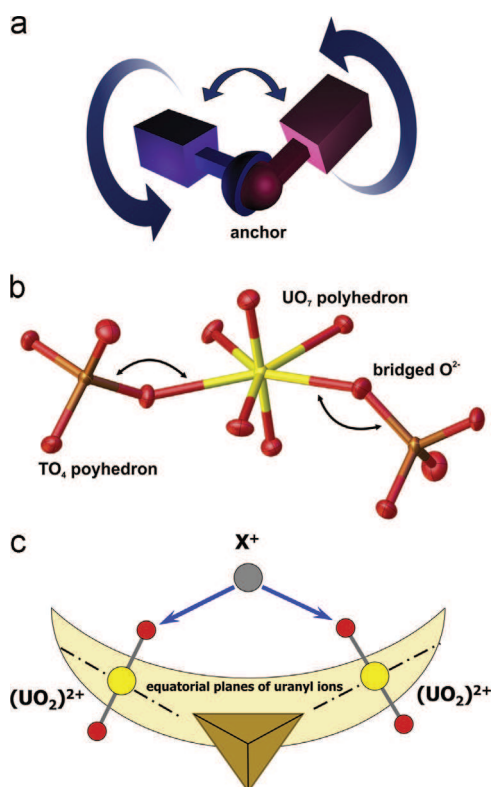


**Fig. 10.** Ball-in-socket joint model (a) and its working principle in the structures of uranyl containing compounds (b and c).

Therefore, it can be assumed that the value of the layer distortion can be determined by analyzing the bond angles at bridging oxygen atoms. This principle has a restricted application and works only locally, because of the fact that polyhedral tiltings are often occur in

**Table 2**  
The  $U-O_{br}-Se$  bond angles ( $^{\circ}$ ) in the structures of **I–VII**.

<b>I</b>			
$U1-O3-Se1$	138.0 (4)	$U3-O4-Se4$	141.2 (6)
$U1-O5-Se1$	137.4 (4)	$U3-O17-Se4$	132.3 (6)
$U1-O7-Se2$	141.6 (3)	$U3-O8-Se5$	132.8 (6)
$U1-O9-Se2$	137.1 (4)	$U3-O29-Se6$	135.7 (6)
$\langle U-O_{br}-Se \rangle$	138.5	$U4-O12-Se4$	133.8 (6)
		$U4-O5-Se5$	132.2 (6)
		$U4-O10-Se5$	143.2 (7)
<b>II</b>		$U4-O16-Se6$	134.4 (6)
$U1-O3-Se1$	134.0 (4)	$\langle U-O_{br}-Se \rangle$	135.6
$U1-O5-Se1$	143.3 (4)		
$U1-O8-Se2$	137.1 (4)	<b>V</b>	
$U1-O9-Se2$	133.8 (3)	$U1-O1-Se1$	134.3 (3)
$U1-O16-Se3$	132.5 (3)	$U1-O4-Se2$	141.3 (4)
$U2-O6-Se1$	128.7 (4)	$U1-O12-Se1$	131.4 (3)
$U2-O10-Se2$	133.8 (3)	$U1-O8-Se2$	142.9 (4)
$U2-O14-Se3$	143.6 (4)	$U1-O9-Se3$	136.8 (3)
$U2-O15-Se3$	134.0 (4)	$U2-O2-Se1$	142.9 (3)
$\langle U-O_{br}-Se \rangle$	135.6	$U2-O5-Se2$	161.0 (5)
		$\langle U-O_{br}-Se \rangle$	141.5
<b>III</b>			
$U1-O4-Se1$	140.9 (3)	<b>VI</b>	
$U1-O5-Se1$	143.6 (4)	$U1-O4-Se1$	150.3 (4)
$U1-O6-Se2$	133.8 (3)	$U1-O14-Se2$	136.1 (4)
$U1-O3-Se3$	132.9 (3)	$U2-O5-Se1$	133.7 (4)
$U1-O7-Se3$	133.4 (4)	$U2-O6-Se1$	132.7 (4)
$U2-O13-Se1$	131.2 (3)	$U2-O10-Se2$	134.5 (4)
$U2-O10-Se2$	138.1 (3)	$U2-O12-Se2$	153.4 (4)
$U2-O11-Se2$	136.5 (3)	$U2-O11-Se3$	135.3 (4)
$U2-O12-Se3$	134.6 (3)	$\langle U-O_{br}-Se \rangle$	139.4
$\langle U-O_{br}-Se \rangle$	136.1		
<b>IV</b>		<b>VII</b>	
$U1-O7-Se1$	132.3 (5)	$U1-O9-Se1$	132.8 (10)
$U1-O11-Se1$	133.4 (6)	$U1-O14-Se1$	132.6 (13)
$U1-O2-Se2$	140.9 (6)	$U1-O1-Se2$	157.2 (13)
$U1-O18-Se3$	135.5 (6)	$U1-O5-Se2$	139.4 (10)
$U2-O6-Se1$	140.2 (7)	$U1-O11-Se3$	124.9 (11)
$U2-O1-Se2$	133.5 (6)	$U2-O15-Se1$	137.0 (11)
$U2-O3-Se2$	133.5 (6)	$U2-O6-Se2$	139.2 (11)
$U2-O13-Se3$	134.0 (6)	$\langle U-O_{br}-Se \rangle$	137.6

the layer plane. It might be assumed that the lower the average  $U-O-T$  angle, the higher the degree of the layer distortion. However, **Table 2** and **Fig. 11** show that the average value of the bridging angles for the most flat layers (**IV**) is less than the average value for the most distorted ones (**VII**). However, the smallest angle in the structure of **VII** [124.9(11)  $^{\circ}$ ] matches the “wave’s crest”, while the biggest angle (157.2(13)  $^{\circ}$ ) stretches along the “wave’s wall” (**Fig. 12**). The same observation could be also attributed, for instance, to the structure of **II**, where the similar pair of angles [128.7(4) and 143.3(4)  $^{\circ}$ ] arranged in the similar way. Thus, the local distribution of the  $U-O-Se$  links supports the suggestion that the lower  $U-O_{br}-T$  angles correspond to the direction of the higher layer undulation. Another point is that the average angles arranged in the middle part of the interval even for highly distorted layers, which could be explained by the tendency of the layer to flatten itself at least partially.

#### 4. Conclusion

In this paper, we have reported seven new uranyl oxysalts with selenium and organic amines. The observed topologies of the structural units of new compounds have been investigated using graphs, and the special approach based upon construction of orientation matrices has been applied to distinguish different geometrical isomers of uranyl selenates and selenite-selenates with the same structural topologies. The statistical analysis of the  $U-O_{br}-Se$  bond angles in selenium polyhedra in the crystal structures showed the possibility for the specification of the undulation of crystal complexes. Further analysis of the data accumulated for uranyl oxysalts may

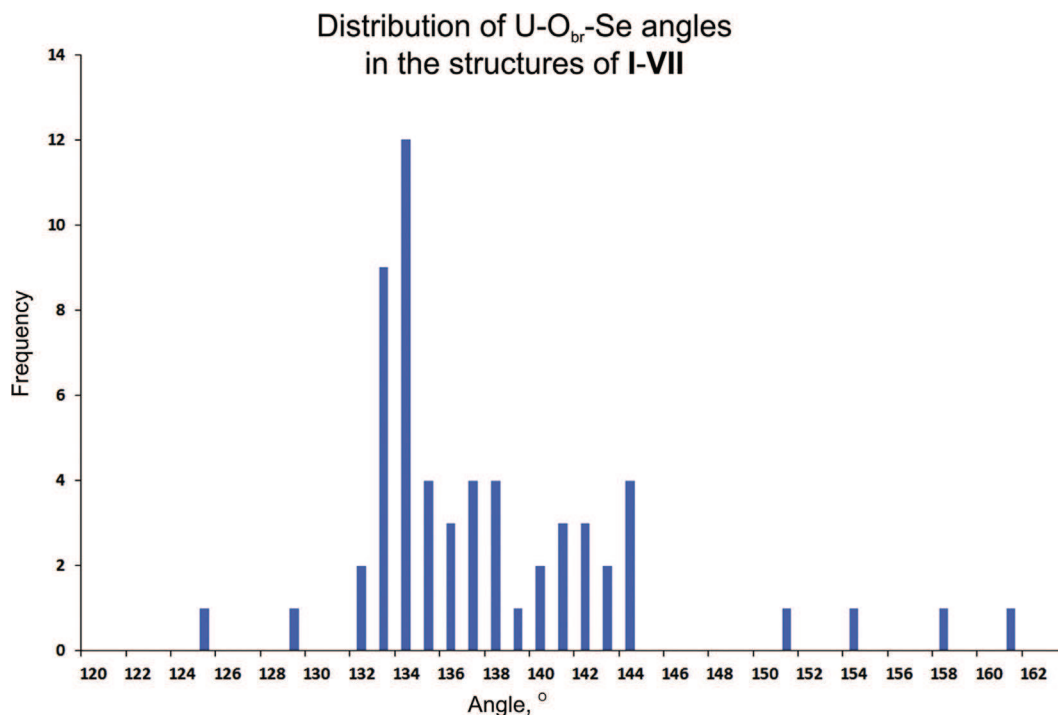


Fig. 11. Distribution of U-O<sub>br</sub>-Se angles in the structures of I-VII.

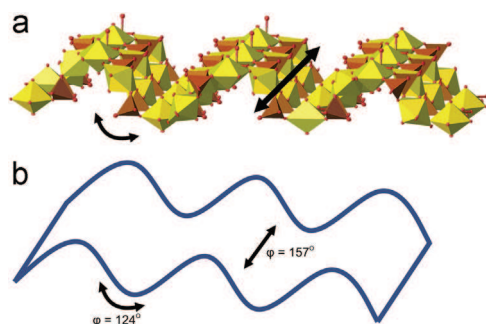


Fig. 12. The smallest angle (124.9(11) Å) in the structure of VII matches the “wave’s crest” while the biggest angle (157.0(13) Å) stretches along the “wave’s wall”; fragment of the structure of VII (a) and its schematic view (b).

provide more details for understanding of how cations of various shape and dimensionality influence topology and geometry of complex inorganic substructures.

### Acknowledgments

This work was supported by St. Petersburg State University (internal grant 3.38.136.2014), President of Russian Federation grant for young scientists (no. MK-1737.2014.5 to VVG) and Russian Foundation for Basic Research (grant 12-05-33097 to VMK). X-ray diffraction studies were carried out in the X-ray Diffraction Centre of St. Petersburg State University.

### Appendix A. Supporting information

Supplementary data associated with this article can be found in the online version at <http://dx.doi.org/10.1016/j.jssc.2015.04.040>.

### References

- [1] S.V. Krivovichev, P.C. Burns, *Can. Mineral.* 43 (2005) 713–720.
- [2] S.V. Krivovichev, P.C. Burns, *Can. Mineral.* 41 (2003) 707–719.
- [3] S.V. Krivovichev, P.C. Burns, *Can. Mineral.* 40 (2002) 201–209.
- [4] G.E. Sigmon, P.C. Burns, *J. Am. Chem. Soc.* 133 (2011) 9137–9139.
- [5] P.C. Burns, *C.R. Chim.* 13 (2010) 737–746.
- [6] G.E. Sigmon, B. Weaver, K.A. Kubatko, P.C. Burns, *Inorg. Chem.* 48 (2009) 10907–10909.
- [7] P.C. Burns, K.A. Kubatko, G.E. Sigmon, B.J. Fryer, J.E. Gagnon, M.R. Antonio, L. Soderholm, *Angew. Chem. Int. Ed.* 44 (2005) 2135–2139.
- [8] J. Ling, M. Ozga, M. Stoffer, P.C. Burns, *Dalton Trans.* 41 (2012) 7278–7284.
- [9] J. Ling, J. Qiu, P.C. Burns, *Inorg. Chem.* 51 (2012) 2403–2408.
- [10] P.C. Burns, *Mineral. Mag.* 75 (2011) 1–25.
- [11] J. Ling, J. Qiu, J.E.S. Szymanowski, P.C. Burns, *Chem. Eur. J* 17 (2011) 2571–2574.
- [12] S.V. Krivovichev, V. Kahlenberg, R. Kaindl, E. Mersdorf, I.G. Tananaev, B.F. Myasoedov, *Angew. Chem. Int. Ed.* 44 (2005) 1134–1136.
- [13] S.V. Krivovichev, V. Kahlenberg, I.G. Tananaev, R. Kaindl, E. Mersdorf, B.F. Myasoedov, *J. Am. Chem. Soc.* 127 (2005) 1072–1073.
- [14] E.V. Alekseev, S.V. Krivovichev, W. Depmeier, *Angew. Chem. Int. Ed.* 47 (2008) 549–551.
- [15] V.V. Gurzhiy, S.V. Krivovichev, *Vestn S.-Peterb. Univ., Ser. : Geol., Geogr.* 7 vol. 3 (2008) 33–40.
- [17] S.V. Krivovichev, V. Kahlenberg, *J. Alloys Compd.* 395 (2005) 41–47.
- [18] S.V. Krivovichev, V. Kahlenberg, *J. Alloys Compd.* 389 (2005) 55–60.
- [19] S.V. Krivovichev, V. Kahlenberg, *Z. Anorg. Allg. Chem.* 630 (2004) 2736–2742.
- [20] L.J. Joffret, E.M. Wylie, P.C. Burns, *Z. Anorg. Allg. Chem.* 638 (2012) 1796–1803.
- [21] V.V. Gurzhiy, P.A. Mikhailenko, S.V. Krivovichev, I.G. Tananaev, B.F. Myasoedov, *Russ. J. Gen. Chem.* 82 (2012) 23–26.
- [22] V.M. Kovrugin, V.V. Gurzhiy, S.V. Krivovichev, I.G. Tananaev, B.F. Myasoedov, *Mendeleev Commun.* 22 (2012) 11–12.
- [23] S.V. Krivovichev, V.V. Gurzhiy, I.G. Tananaev, B.F. Myasoedov, *Z. Kristallogr.* 224 (2009) 316–324.
- [24] S.V. Krivovichev, V.V. Gurzhiy, I.G. Tananaev, B.F. Myasoedov, *Russ. J. Gen. Chem.* 79 (2009) 2723–2730.
- [25] G.M. Sheldrick, *SADABS*, Univ. Gottingen, Germany, 2004.
- [26] Stoe & Cie, (Darmstadt, Germany): Stoe & Cie GmbH, 2005.
- [27] A. Altomare, G. Cascarano, C. Giacovazzo, A. Guagliardi, M.C. Burla, G. Polidori, M. Camalli, *J. Appl. Crystallogr.* 27 (1994) 435.
- [28] G.M. Sheldrick, *Acta Crystallogr. A* 64 (2008) 112–122.
- [29] O.V. Dolomanov, L.J. Bourhis, R.J. Gildea, J.A.K. Howard, H. Puschmann, *Appl. Crystallogr.* 42 (2009) 339–341.
- [30] M. Koskenlinna, I. Mutikainen, T. Leskela, M. Leskela, *Acta Chem. Scand.* 51 (1997) 264–269.
- [31] P.M. Almond, T.E. Albrecht-Schmitt, *Inorg. Chem.* 41 (2002) 1177–1183.

- [32] S.V. Krivovichev, I.G. Tananaev, V. Kahlenberg, B.F. Myasoedov, *Dokl. Phys. Chem.* 403 (2005) 124–127.
- [33] S.V. Krivovichev, I.G. Tananaev, V. Kahlenberg, B.F. Myasoedov, *Radiochemistry* 48 (2006) 217–222.
- [34] S.V. Krivovichev, *Radiochemistry* 46 (2004) 434–437.
- [35] S.V. Krivovichev, V. Kahlenberg, E.Yu. Avdontseva, E. Mersdorf, R. Kaindl, *Eur. J. Inorg. Chem.* 2005 (2005) 1653–1656.
- [36] S.V. Krivovichev, *Crystallogr. Rev.* 10 (2004) 185–232.
- [37] S.V. Krivovichev, *Structural Crystallography of Inorganic Oxysalts*, Oxford University Press, Oxford, 2008.
- [38] S.V. Krivovichev, *Eur. J. Inorg. Chem.* 2010 (2010) 2594–3437.
- [39] V.V. Tabachenko, V.N. Serezhkin, L.B. Serezhkina, L.M. Kovba, *Zh. Neorg. Khim.* 5 (1979) 1563–1568.
- [40] Yu.N. Mikhailov, Yu.E. Gorbunova, E.A. Demchenko, L.B. Serezhkina, V.N. Serezhkin, *Zh. Neorg. Khim.* 45 (2000) 1711–1713.
- [41] A.J. Norquist, P.M. Thomas, M.B. Doran, D. O'Hare, *Chem. Mater.* 14 (2002) 5179–5184.
- [42] A.J. Norquist, M.B. Doran, P.M. Thomas, D. O'Hare, *Dalton Trans.* 2003 (2003) 1168–1175.
- [43] A.J. Norquist, M.B. Doran, *Solid State Sci.* 5 (2003) 1149–1158.
- [44] P.M. Thomas, A.J. Norquist, M.B. Doran, *J. Mater. Chem.* 13 (2003) 88–92.
- [45] C.L. Stuart, M.B. Doran, A.J. Norquist, D. O'Hare, *Acta Crystallogr. E* 59 (2003) m446–m448.
- [46] R. Mercier, T.M. Pham, P. Colomban, *Solid State Ionics* 15 (1985) 113–126.
- [47] T.M. Gesing, C.H. Rüscher, *Z. Anorg. Chem.* 626 (2000) 1414–1420.
- [48] S.V. Krivovichev, V. Kahlenberg, *Z. Naturforsch.* 60b (2005) 538–542.
- [49] S.V. Krivovichev, V. Kahlenberg, *Z. Anorg. Chem.* 631 (2005) 2352–2357.
- [50] V.M. Kovrugin, V.V. Gurzhiy, S.V. Krivovichev, *Struct. Chem.* 23 (2012) 2003–2017.
- [51] M.B. Doran, A.J. Norquist, D. O'Hare, *Inorg. Chem.* 42 (2003) 6989–6995.
- [52] S.V. Krivovichev, V.V. Gurzhiy, I.G. Tananaev, B.F. Myasoedov, *Dokl. Phys. Chem.* 409 (2006) 228–232.
- [53] V.V. Gurzhiy, O.S. Tyumentseva, S.V. Krivovichev, I.G. Tananaev, B.F. Myasoedov, *Radiochemistry* 54 (2012) 43–47.
- [54] Yu.N. Mikhailov, Yu.E. Gorbunova, L.B. Serezhkina, V.N. Serezhkin, *Zh. Neorg. Khim.* 42 (1997) 734–738.
- [55] S.V. Krivovichev, P.C. Burns, *Z. Kristallogr.* 218 (2003) 725–732.
- [56] S.V. Krivovichev, I.G. Tananaev, B.F. Myasoedov, *Radiochemistry* 48 (2006) 552–560.
- [57] S.V. Krivovichev, V. Kahlenberg, *Z. Anorg. Allg. Chem.* 631 (2005) 739–744.
- [58] S.V. Krivovichev, P.C. Burns, *Z. Kristallogr.* 218 (2003) 683–690.
- [59] S.V. Krivovichev, P.C. Burns, I.G. Tananaev, *Structural Chemistry of Inorganic Actinide Compounds*, Elsevier, The Netherlands (2007) 494.
- [60] V.V. Gurzhiy, D.V. Tyshchenko, S.V. Krivovichev, I.G. Tananaev, *Z. Kristallogr.* 229 (2014) 368–377.

**Topologically and geometrically flexible structural units in seven new organically templated uranyl selenates and selenite–selenates**

Vladislav V. Gurzhiy<sup>1,\*</sup>, Vadim M. Kovrugin<sup>1</sup>, Olga S. Tyumentseva<sup>1</sup>,

Pavel A. Mikhaylenko<sup>1</sup>, Sergey V. Krivovichev<sup>1</sup>, Ivan G. Tananaev<sup>2</sup>

<sup>1</sup> *Department of Crystallography, St. Petersburg State University, University Emb. 7/9, 199034 St. Petersburg, Russia.*

<sup>2</sup> *National Research Nuclear University MEPhI, pr. Pobedy 48, 456783 Ozersk, Russia.*

**Table S1**  
Selected interatomic distances (Å) in **I**.

Distance		Distance	
U1–O2	1.772(5)	Se1–O6	1.617(7)
U1–O1	1.774(5)	Se1–O4	1.622(7)
U1–O7	2.287(5)	Se1–O3	1.647(6)
U1–O5	2.328(5)	Se1–O5	1.663(5)
U1–O9	2.372(5)	<Se1–O>	1.637
U1–O3	2.396(6)	Se2–O8	1.621(7)
U1–H <sub>2</sub> O11	2.489(6)	Se2–O10	1.628(7)
<U1–O <sub>Ur</sub> >	1.773	Se2–O9	1.642(5)
<U1–O <sub>eq</sub> >	2.374	Se2–O7	1.694(5)
		<Se2–O>	1.646

**Table S2**  
Selected interatomic distances (Å) in **II**.

Distance		Distance	
U1–O2	1.757(6)	Se1–O4	1.605(7)
U1–O1	1.757(7)	Se1–O3	1.633(7)
U1–O5	2.358(6)	Se1–O5	1.639(6)
U1–O3	2.365(6)	Se1–O6	1.661(6)
U1–O8	2.382(5)	<Se1–O>	1.635
U1–O9	2.424(6)	Se2–O7	1.593(7)
U1–O16	2.433(5)	Se2–O9	1.639(6)
<U1–O <sub>Ur</sub> >	1.757	Se2–O10	1.654(5)
<U1–O <sub>eq</sub> >	2.392	Se2–O8	1.654(6)
U2–O12	1.755(7)	<Se2–O>	1.635
U2–O11	1.760(7)	Se3–O17	1.614(6)
U2–O14	2.357(7)	Se3–O15	1.637(6)
U2–O10	2.365(6)	Se3–O14	1.639(6)
U2–O15	2.367(6)	Se3–O16	1.650(6)
U2–O6	2.413(7)	<Se3–O>	1.635
U2–H <sub>2</sub> O13	2.499(7)		
<U2–O <sub>Ur</sub> >	1.758		
<U2–O <sub>eq</sub> >	2.400		

**Table S3**Selected interatomic distances (Å) in **III**.

Distance		Distance	
U1–O2	1.743(6)	Se1–O17	1.616(6)
U1–O1	1.763(6)	Se1–O5	1.633(6)
U1–O3	2.362(5)	Se1–O13	1.640(6)
U1–O5	2.379(5)	Se1–O4	1.646(5)
U1–O7	2.381(6)	<Se1–O>	1.634
U1–O6	2.384(6)		
U1–O4	2.386(5)	Se2–O15	1.577(8)
<U1–O <sub>Ur</sub> >	1.753	Se2–O10	1.646(6)
<U1–O <sub>eq</sub> >	2.378	Se2–O11	1.653(6)
		Se2–O6	1.657(5)
U2–O8	1.752(6)	<Se2–O>	1.633
U2–O9	1.767(6)		
U2–O10	2.352(5)	Se3–O16	1.600(7)
U2–O11	2.355(6)	Se3–O12	1.643(6)
U2–O12	2.387(5)	Se3–O3	1.660(5)
U2–O13	2.407(7)	Se3–O7	1.660(6)
U2–H <sub>2</sub> O14	2.481(6)	<Se3–O>	1.641
<U2–O <sub>Ur</sub> >	1.760		
<U2–O <sub>eq</sub> >	2.396	Se3A–O7	1.528(10)
		Se3A–O3	1.587(10)
		Se3A–O12	1.653(11)
		<Se3A–O>	1.589

**Table S4**Selected interatomic distances (Å) in **IV**.

Distance		Distance	
U1–O14	1.752(12)	Se1–O20	1.617(12)
U1–O22	1.771(11)	Se1–O11	1.626(9)
U1–O18	2.358(10)	Se1–O7	1.644(9)
U1–O2	2.363(11)	Se1–O6	1.657(12)
U1–O11	2.392(8)	<Se1–O>	1.636
U1–O7	2.412(8)		
U1–H <sub>2</sub> O24	2.476(11)	Se2–O28	1.587(12)
<U1–O <sub>Ur</sub> >	1.762	Se2–O1	1.632(8)
<U1–O <sub>eq</sub> >	2.400	Se2–O3	1.636(9)
		Se2–O2	1.643(11)
U2–O23	1.766(11)	<Se2–O>	1.625
U2–O32	1.780(12)		
U2–O6	2.364(11)	Se3–O15	1.619(10)
U2–O13	2.372(9)	Se3–O9	1.622(10)
U2–O1	2.391(8)	Se3–O13	1.652(10)
U2–O3	2.400(7)	Se3–O18	1.666(10)

U2–H <sub>2</sub> O30	2.424(12)	<Se3–O>	1.640
<U2–O <sub>Ur</sub> >	1.773		
<U2–O <sub>eq</sub> >	2.90	Se4–O4	1.606(11)
		Se4–O33	1.638(11)
U3–O31	1.764(12)	Se4–O12	1.639(9)
U3–O27	1.770(11)	Se4–O17	1.640(10)
U3–O29	2.381(10)	<Se4–O>	1.631
U3–O4	2.390(11)		
U3–O8	2.396(8)	Se5–O34	1.610(12)
U3–O17	2.398(9)	Se5–O10	1.611(11)
U3–H <sub>2</sub> O35	2.470(11)	Se5–O5	1.644(9)
<U3–O <sub>Ur</sub> >	1.767	Se5–O8	1.645(9)
<U3–O <sub>eq</sub> >	2.407	<Se5–O>	1.628
U4–O26	1.730(13)	Se6–O19	1.611(11)
U4–O25	1.763(12)	Se6–O21	1.624(10)
U4–O10	2.369(11)	Se6–O29	1.631(10)
U4–O16 <sup>v</sup>	2.376(9)	Se6–O16	1.647(10)
U4–O5	2.398(9)	<Se6–O>	1.628
U4–O12	2.404(8)		
U4–H <sub>2</sub> O36	2.455(12)		
<U4–O <sub>Ur</sub> >	1.747		
<U4–O <sub>eq</sub> >	2.400		

**Table S5**

Selected interatomic distances (Å) in V.

Distance		Distance	
U1–O10	1.758(7)	Se1–O11	1.589(6)
U1–O6	1.787(7)	Se1–O2	1.635(5)
U1–O9	2.336(5)	Se1–O1	1.640(6)
U1–O8	2.364(6)	Se1–O12	1.643(5)
U1–O4	2.392(6)	<Se1–O>	1.627
U1–O1	2.393(5)		
U1–O12	2.445(5)	Se2–O5	1.600(7)
<U1–O <sub>Ur</sub> >	1.773	Se2–O8	1.603(6)
<U1–O <sub>eq</sub> >	2.386	Se2–O4	1.630(6)
		Se2–O14	1.650(10)
U2–O13	1.749(10)	<Se2–O>	1.621
U2–O3	1.765(9)		
U2–O2	2.336(5) 2×	Se3–O9	1.645(6) 2×
U2–O5	2.338(6) 2×	Se3–HO15	1.888(19)
U2–H <sub>2</sub> O7	2.554(7)	<Se3–O>	1.726
<U2–O <sub>Ur</sub> >	1.757		
<U2–O <sub>eq</sub> >	2.380		

**Table S6**Selected interatomic distances (Å) in **VI**.

Distance		Distance	
U1–O1	1.711(10)	Se1–O7	1.608(7)
U1–O2	1.734(10)	Se1–O5	1.632(7)
U1–O4	2.312(7) 2×	Se1–O6	1.646(7)
U1–O14	2.409(7) 2×	Se1–O4	1.655(7)
U1–H <sub>2</sub> O3	2.537(10)	<Se1–O>	1.635
<U1–O <sub>Ur</sub> >	1.723	Se2–O13	1.611(7)
<U1–O <sub>eq</sub> >	2.396	Se2–O12	1.633(7)
U2–O9	1.728(7)	Se2–O10	1.644(7)
U2–O8	1.748(7)	Se2–O14	1.663(7)
U2–O11	2.356(7)	<Se2–O>	1.638
U2–O12	2.369(7)	Se3–O16	1.54(4)
U2–O10	2.392(6)	Se3–O11	1.645(7) 2×
U2–O6	2.395(7)	Se3–O15	1.723(12)
U2–O5	2.441(7)	<Se3–O>	1.64
<U2–O <sub>Ur</sub> >	1.738		
<U2–O <sub>eq</sub> >	2.391		

**Table S7**Selected interatomic distances (Å) in **VII**.

Distance		Distance	
U1–O13	1.737(18)	Se1–O8	1.62(3)
U1–O2	1.749(17)	Se1–O9	1.66(2)
U1–O5	2.331(19)	Se1–O15	1.66(2)
U1–O1 <sup>i</sup>	2.35(2)	Se1–O14	1.67(3)
U1–O14	2.36(2)	<Se1–O>	1.65
U1–O11	2.365(17)	Se2–O12	1.57(3)
U1–O9	2.42(2)	Se2–O1	1.60(2)
<U1–O <sub>Ur</sub> >	1.743	Se2–O6	1.633(18)
<U1–O <sub>eq</sub> >	2.37	Se2–O5	1.67(2)
U2–O3	1.77(3)	<Se2–O>	1.62
U2–O10	1.78(3)	Se3–O11	1.653(16) 2×
U2–O15	2.334(16) 2×	Se3–HO4	1.78(4)
U2–O6	2.367(18) 2×	<Se3–O>	1.70
U2–H <sub>2</sub> O7	2.49(3)		
<U2–O <sub>Ur</sub> >	1.78		
<U2–O <sub>eq</sub> >	2.38		



**A-VII**  
**Emulating exhalative chemistry: synthesis and structural  
characterization of ilinskite, Na[Cu<sub>5</sub>O<sub>2</sub>](SeO<sub>3</sub>)<sub>2</sub>Cl<sub>3</sub>, and its K-  
analogue**

Vadim M. Kovrugin, Oleg I. Siidra, Marie Colmont, Olivier Mentré, and  
Sergey V. Krivovichev

Published in: *Mineralogy and Petrology*, 2015, Vol. 109, 421–430.

DOI: 10.1007/s00710-015-0369-3

Reprinted with kind permission from Springer-Verlag Wien.



# Emulating exhalative chemistry: synthesis and structural characterization of ilinskite, $\text{Na}[\text{Cu}_5\text{O}_2](\text{SeO}_3)_2\text{Cl}_3$ , and its K-analogue

Vadim M. Kovrugin · Oleg I. Siidra · Marie Colmont · Olivier Mentré · Sergey V. Krivovichev

Received: 11 November 2014 / Accepted: 6 February 2015  
© Springer-Verlag Wien 2015

**Abstract** The K- and Na-synthetic analogues of the fumarolic mineral ilinskite have been synthesized by the chemical vapor transport (CVT) reactions method. The  $A$ - $[\text{Cu}_5\text{O}_2](\text{SeO}_3)_2\text{Cl}_3$  ( $A^+ = \text{K}^+, \text{Na}^+$ ) compounds crystallize in the orthorhombic space group  $Pnma$ :  $a = 18.1691(6)$  Å,  $b = 6.4483(2)$  Å,  $c = 10.5684(4)$  Å,  $V = 1238.19(7)$  Å<sup>3</sup>,  $R_1 = 0.018$  for 1957 unique reflections with  $F > 4\sigma_F$  for  $\text{K}[\text{Cu}_5\text{O}_2](\text{SeO}_3)_2\text{Cl}_3$  (**KI**), and  $a = 17.7489(18)$  Å,  $b = 6.4412(6)$  Å,  $c = 10.4880(12)$  Å,  $V = 1199.0(2)$  Å<sup>3</sup>,  $R_1 = 0.049$  for 1300 unique reflections with  $F > 4\sigma_F$  for  $\text{Na}[\text{Cu}_5\text{O}_2](\text{SeO}_3)_2\text{Cl}_3$  (**NaI**). The crystal structures of **KI** and **NaI** are based upon the  $[\text{O}_2\text{Cu}_5]^{6+}$  sheets consisting of corner-sharing  $(\text{OCu}_4)^{6+}$  tetrahedra. The Na-for-K substitution results in the significant expansion of the interlayer space and changes in local coordination of some of the  $\text{Cu}^{2+}$  cations. The  $A^+$  cation coordination changes from fivefold (for  $\text{Na}^+$ ) to ninefold (for  $\text{K}^+$ ). The CVT reactions method provides a unique opportunity to model physicochemical conditions existing in fumarolic environments and may be used not only to model exhalative processes, but also to predict possible mineral phases that may form in fumaroles. In particular, the K analogue of ilinskite is not known in nature, whereas it may well form from volcanic gases in a K-rich local geochemical environment.

## Introduction

Exhalative geochemistry and mineralogy have attracted considerable attention recently, owing to the discovery of a wide range of minerals that form during condensation of volcanic gases in fumaroles (Demartin et al. 2013, 2014; Garavelli et al. 2013; Mitolo et al. 2013; Krivovichev et al. 2013a; Shuvalov et al. 2013; Pinto et al. 2014; Pekov et al. 2013a, b, c, d, 2014a, b, c; Murashko et al. 2013; Vergasova et al. 2014). Of particular interest are copper oxoselenite chlorides, which, in addition to their mineralogical interest, possess rich and unique structural chemistry and special magnetic properties (Burns and Hawthorne 1995; Bastide et al. 2000; Millet et al. 2001; Burns et al. 2002; Krivovichev et al. 2006; Zhang et al. 2010; Berdonosov et al. 2013).

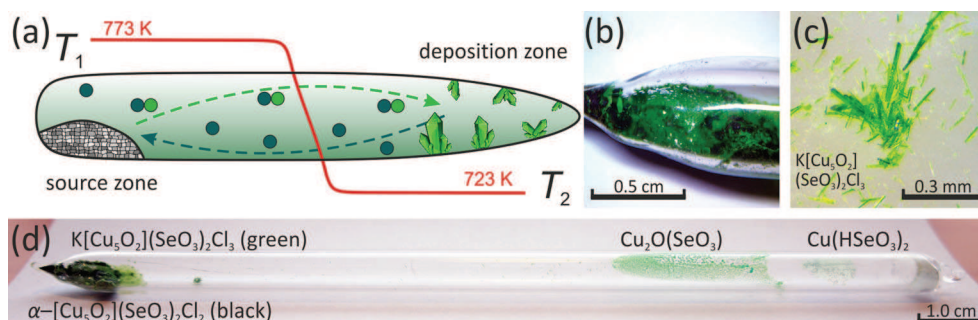
Most of naturally occurring copper selenite oxyhalide minerals contain “additional” oxygen atoms that are coordinated solely by  $\text{Cu}^{2+}$  cations, resulting in the formation of oxocentered  $(\text{OCu}_4)^{6+}$  tetrahedra: allochalcocelite,  $\text{Cu}^+[\text{PbCu}^{2+}_5\text{O}_2](\text{SeO}_3)_2\text{Cl}_5$  (Krivovichev et al. 2006), burnsite,  $\text{K}[\text{Cu}_7\text{O}_2](\text{SeO}_3)_2\text{Cl}_9$  (Burns et al. 2002), chloromenite  $[\text{Cu}_9\text{O}_2](\text{SeO}_3)_4\text{Cl}_6$  (Krivovichev et al. 1998), francisite,  $[\text{Cu}_3\text{BiO}_2](\text{SeO}_3)_2\text{Cl}$  (Pring et al. 1990), georgbokiite,  $\alpha$ - $[\text{Cu}_5\text{O}_2](\text{SeO}_3)_2\text{Cl}_2$  (Krivovichev et al. 1999a), nicksobolevite,  $[\text{Cu}_7\text{O}_2](\text{SeO}_3)_2\text{Cl}_6$  (Vergasova et al. 2014), parageorgbokiite  $\beta$ - $[\text{Cu}_5\text{O}_2](\text{SeO}_3)_2\text{Cl}_2$  (Krivovichev et al. 2007), prewittite  $\text{K}[\text{Pb}_{0.5}\text{Cu}[\text{PbCu}_5\text{O}_2]\text{Zn}(\text{SeO}_3)_2\text{Cl}_{10}]$  (Shuvalov et al. 2013). It is the unique feature of  $\text{Cu}^{2+}$  to form anion-centered units of different dimensionalities reviewed recently by Krivovichev et al. (2013b). These minerals form as a result of volcanic exhalative processes that can be modeled using gas transport reactions as was originally suggested by Filatov et al. (1992) and confirmed by a number of successful syntheses of mineral analogues under laboratory conditions by chemical vapor transport (CVT)

Editorial handling: A. Beran

V. M. Kovrugin · M. Colmont · O. Mentré  
UCCS, ENSCL, Université Lille 1, CNRS, UMR 8181,  
59652 Villeneuve d'Ascq, France

V. M. Kovrugin · O. I. Siidra · S. V. Krivovichev (✉)  
Department of Crystallography, Institute of Earth Sciences,  
St. Petersburg State University, University emb. 7/9, 199034  
St. Petersburg, Russia  
e-mail: s.krivovichev@spbu.ru

**Fig. 1** General scheme of the CVT method (a), the source zone of the tube (b), the crystals of  $\text{K}[\text{Cu}_5\text{O}_2](\text{SeO}_3)_2\text{Cl}_3$  picked out from the source zone (c), and a common view of the sealed silica tube after the CVT synthesis (d)



reactions method (Millet et al. 2001; Krivovichev et al. 2004; Berdonosov et al. 2009; Zhang et al. 2010; Kovrugin et al. 2015).

In this paper, we report on the synthesis and crystal structures of K- and Na-synthetic analogues of ilinskite (Vergasova et al. 1997; Krivovichev et al. 2013c), a rare mineral from volcanic fumaroles of the Tolbachik volcano (Kamchatka peninsula, Russia).

## Experimental

Single crystals of  $\text{K}[\text{Cu}_5\text{O}_2](\text{SeO}_3)_2\text{Cl}_3$  (**KI**) and  $\text{Na}[\text{Cu}_5\text{O}_2](\text{SeO}_3)_2\text{Cl}_3$  (**NaI**) were prepared by the chemical vapor transport (CVT) reactions method (Binnewies et al. 2013). In the course of the CVT reactions a precursor is partially transported by a gaseous agent from a source zone to a deposition zone under the action of a temperature gradient.

**Table 1** Crystallographic data and refinement parameters for **KI** and **NaI**

	$\text{K}[\text{Cu}_5\text{O}_2](\text{SeO}_3)_2\text{Cl}_3$	$\text{Na}[\text{Cu}_5\text{O}_2](\text{SeO}_3)_2\text{Cl}_3$
Crystal data:		
Temperature	293 K	293 K
Radiation	$\text{MoK}\alpha$ , 0.71073 Å	$\text{MoK}\alpha$ , 0.71073 Å
Crystal system	orthorhombic	orthorhombic
Space group	<i>Pnma</i>	<i>Pnma</i>
<i>a</i> (Å)	18.1691(6)	17.7489(18)
<i>b</i> (Å)	6.4483(2)	6.4412(6)
<i>c</i> (Å)	10.5684(4)	10.4880(12)
Volume (Å <sup>3</sup> )	1238.19(7)	1199.0(2)
<i>Z</i>	4	4
<i>D</i> <sub>calc</sub> (g/cm <sup>3</sup> )	4.018	4.060
$\mu$ (mm <sup>-1</sup> )	15.333	15.523
Crystal size (mm <sup>3</sup> )	0.25 × 0.10 × 0.08	0.21 × 0.11 × 0.08
Data collection:		
$\theta$ range	2.23 – 31.54°	2.27 – 31.02°
<i>h</i> , <i>k</i> , <i>l</i> ranges	–26 → 26, –8 → 9, –14 → 15	–17 → 25, –9 → 6, –15 → 15
Total reflections collected	9584	7946
Unique reflections ( <i>R</i> <sub>int</sub> )	2233 (0.0265)	2042 (0.0984)
Unique reflections <i>F</i> > 4σ <sub><i>F</i></sub>	1957	1300
Structure refinement:		
Refinement method	Full-matrix least-squares on <i>F</i> <sup>2</sup>	
Weighting scheme	$w = 1/[\sigma^2(F_o^2) + (0.023P)^2]$ , where $P = (F_o^2 + 2F_c^2)/3$	
Extinction coefficient	0.00079(8)	none
<i>R</i> <sub>1</sub> [ <i>F</i> > 4σ <sub><i>F</i></sub> ], <i>wR</i> <sub>2</sub> [ <i>F</i> > 4σ <sub><i>F</i></sub> ]	0.018, 0.040	0.049, 0.065
<i>R</i> <sub>1</sub> all, <i>wR</i> <sub>2</sub> all	0.023, 0.041	0.099, 0.077
Goodness-of-fit	1.035	0.991
Largest diff. peak and hole, e Å <sup>-3</sup>	0.735, –0.765	1.617, –1.668

The general scheme of the CVT method is shown in Fig. 1a. A mixture of CuO (0.318 g, 4 mmol), CuCl<sub>2</sub> (0.134 g, 1 mmol), SeO<sub>2</sub> (0.222 g, 2 mmol) and KCl (0.075 g, 1 mmol) for **KI** (NaCl (0.058 g, 1 mmol) for **NaI**) were grounded and loaded into a silica tube (*ca.* 15 cm), which was further evacuated to 10<sup>-2</sup> mbar and sealed. The tubes were placed horizontally into a tubular two-zone furnace, heated to 773 K for 3 days and subsequently slowly cooled to room temperature. The temperature gradient between the source (hot) and deposition (cold) zones of the tube in the furnace was about 50 K. Green needle-like single crystals of **KI** (Fig. 1c) and **NaI** were observed in the source zones of the tubes (Fig. 1b) in association with black block-shaped crystals of synthetic georgbokiite, α-[Cu<sub>5</sub>O<sub>2</sub>](SeO<sub>3</sub>)<sub>2</sub>Cl<sub>2</sub> (Krivovichev et al. 1999a). Green platy

crystals of Cu<sub>2</sub>O(SeO<sub>3</sub>) (Effenberger and Pertlik 1986) were found in the middle part, while transparent elongated crystals of Cu(HSeO<sub>3</sub>)<sub>2</sub> (Effenberger 1985) occurred in the deposition zone of the tubes (Fig. 1d).

The crystals of **KI** and **NaI** selected for the X-ray diffraction data collection were mounted on a Bruker APEX II X-ray diffractometer equipped with a microfocus MoK<sub>α</sub> (λ = 0.71073 Å) X-ray tube operated at 50 kV and 40 mA. The unit-cell dimensions (Table 1) for both compounds were refined by the least-squares techniques. The data were integrated and corrected for absorption and background effects using the Bruker program packages. The solution and refinement of the crystal structures of **KI** and **NaI** were performed using the SHELXL program package (Sheldrick 2008). Both

**Table 2** Atomic coordinates and equivalent isotropic displacement parameters of atoms in the structures of A[Cu<sub>5</sub>O<sub>2</sub>](SeO<sub>3</sub>)<sub>2</sub>Cl<sub>3</sub> (A<sup>+</sup> = K<sup>+</sup>, Na<sup>+</sup>) and ilinskite (Krivovichev et al. 2013c).  $U_{eq} = (1/3)\sum_i \sum_j U_{ij} a_i a_j$

Atom	A = K	A = Na	ilinskite	Atom	A = K	A = Na	ilinskite
Cu1	x	0.40349(4)	0.4076(3)	Cl2	x	0.54316(5)	0.53659(16)
	y	1/4	1/4	y	1/4	1/4	1/4
	z	0.74241(7)	0.7359(5)	z	-0.12462(11)	-0.1356(3)	-0.13445(17)
	$U_{eq}/\text{Å}^2$	0.02347(15)	0.0502(15)	$U_{eq}/\text{Å}^2$	0.0431(3)	0.0375(8)	0.0361(4)
Cu2	x	0.59855(2)	0.59928(6)	Cl3	x	0.74081(5)	0.75484(16)
	y	1/4	1/4	y	1/4	1/4	1/4
	z	0.49282(3)	0.49980(11)	z	0.76767(9)	0.7729(3)	0.77233(15)
	$U_{eq}/\text{Å}^2$	0.01207(8)	0.0123(3)	$U_{eq}/\text{Å}^2$	0.0347(2)	0.0330(7)	0.0339(3)
Cu3	x	0.64034(2)	0.63266(7)	O1	x	0.76868(10)	0.7730(3)
	y	1/4	1/4	y	-1/4	-1/4	-1/4
	z	-0.00210(4)	-0.00159(11)	z	0.59776(18)	0.5958(5)	0.5962(3)
	$U_{eq}/\text{Å}^2$	0.01364(8)	0.0135(3)	$U_{eq}/\text{Å}^2$	0.0099(4)	0.0088(13)	0.0095(5)
Cu4	x	0.71965(2)	0.71861(7)	O2	x	0.70183(10)	0.7041(3)
	y	1/4	1/4	y	1/4	1/4	1/4
	z	0.27638(3)	0.27544(11)	z	0.45476(18)	0.4551(6)	0.4560(3)
	$U_{eq}/\text{Å}^2$	0.01261(8)	0.0131(3)	$U_{eq}/\text{Å}^2$	0.0094(3)	0.0089(13)	0.0104(5)
Cu5	x	0.73299(2)	0.73701(5)	O3	x	0.65743(7)	0.6516(2)
	y	0.00432(4)	0.00171(13)	y	-0.0537(2)	-0.0522(6)	-0.0515(4)
	z	0.53549(2)	0.53098(8)	z	0.01066(14)	0.0075(4)	0.0081(2)
	$U_{eq}/\text{Å}^2$	0.01281(6)	0.01442(19)	$U_{eq}/\text{Å}^2$	0.0136(3)	0.0124(10)	0.0147(4)
s	x	0.43000(2)	0.43047(6)	O4	x	0.49551(10)	0.4939(3)
	y	1/4	1/4	y	1/4	1/4	1/4
	z	0.41824(3)	0.42166(9)	z	0.53153(19)	0.5421(6)	0.5412(3)
	$U_{eq}/\text{Å}^2$	0.01051(6)	0.0106(2)	$U_{eq}/\text{Å}^2$	0.0158(4)	0.0149(15)	0.0161(7)
Se2	x	0.62105(2)	0.61514(5)	O5	x	0.67294(11)	0.6697(4)
	y	-1/4	-1/4	y	-1/4	-1/4	-1/4
	z	-0.08073(3)	-0.08525(9)	z	-0.21020(19)	-0.2131(6)	-0.2130(3)
	$U_{eq}/\text{Å}^2$	0.01014(6)	0.0101(2)	$U_{eq}/\text{Å}^2$	0.0166(4)	0.0168(15)	0.0169(7)
Cl1	x	0.59034(4)	0.58643(15)	O6	x	0.37690(7)	0.3753(2)
	y	1/4	1/4	y	0.0512(2)	0.0508(6)	0.0504(4)
	z	0.24841(7)	0.2508(3)	z	0.47371(15)	0.4727(5)	0.4733(3)
	$U_{eq}/\text{Å}^2$	0.01870(15)	0.0261(6)	$U_{eq}/\text{Å}^2$	0.0168(3)	0.0187(11)	0.0189(5)

structures were solved by direct methods in the orthorhombic *Pnma* space group and refined to the  $R_1$  values of 0.018 for **KI** and 0.049 for **NaI**. The crystal quality of **NaI** was relatively poor that most probably results from a local intergrowth of twinned domains. Atom coordinates and displacement parameters are given in Table 2 and selected distances are in Table 3. The results of the bond-valence sum (BVS) analysis for **KI**, **NaI** and ilinskite are given in Table 4. All empirical bond-valence parameters required for the BVS calculations were taken from (Brese and O’Keeffe 1991). The BVS values obtained for Cl(3) are rather low (0.42 and 0.46 valence units (v.u.) for **KI** and **NaI**, respectively). This phenomenon is rather typical for copper oxoselenite chlorides (Krivovichev et al. 2013c; Kovrugin et al. 2015). Additional structural information is provided in the Supporting Information as Crystallographic information files (CIFs).

## Results

$K[Cu_5O_2](SeO_3)_2Cl_3$  (**KI**) and  $Na[Cu_5O_2](SeO_3)_2Cl_3$  (**NaI**) are isotypic and crystallize in the *Pnma* space group. The structural data for **NaI** are in full agreement with the data reported for natural ilinskite by (Krivovichev et al. 2013c). The differences between the structures of synthetic K- and Na-ilinskites are discussed below.

The crystal structures of **KI** and **NaI** contain four symmetrically independent Cu sites with different mixed-ligand coordination environments (Fig. 2). The Cu(1) site is coordinated by five ligands to form [(4O)+Cl] square pyramids. The similar coordination geometries have previously been reported in the crystal structures of nabokoite,  $K_2Cu_7(TeO_4)(SO_4)_5Cl$  (Pertlik and Zemmann 1988), and bobkingite,  $Cu_5Cl_2(OH)_8(H_2O)_2$  (Hawthorne et al. 2002). The average <Cu(1)–O> distances are 1.971 and 1.965 Å for **KI** and **NaI**, respectively, whereas the Cu(1)–Cl(1) bond lengths are 2.587 and 2.621 Å for **KI** in **NaI**, respectively. The Cu(3) site has a distorted square coordination by three oxygen and one chlorine atom. This type of coordination geometry, [3O+Cl], has been observed recently in the crystal structure of  $Na_2[Cu_7O_2](SeO_3)_4Cl_4$  (Kovrugin et al. 2015). The Cu(3)–O bond lengths are in the ranges of 1.900–1.957 Å in **KI** and of 1.890–1.985 Å in **NaI**. The Cu(3)–Cl1 bonds are 2.368 Å and 2.360 Å in **KI** and **NaI**, respectively.

The coordinations of the Cu(2) and Cu(4) sites in **KI** and **NaI** are different due to the shift of the Cl(3) site induced by the greater size of the  $K^+$  cations compared to  $Na^+$ . The Cu(2) site has a distorted square pyramidal [(3O+Cl)+Cl] coordination in **NaI**, similar to the one observed in  $Cu_3(MoO_4)(TeO_3)Cl_2(H_2O)_{0.5}$  (Takagi et al. 2006). In the crystal structure of **KI**, the Cu–Cl distance to the sixth nearest neighboring site Cl(3) (3.042 Å (0.06 v.u.)) is shorter than that in **NaI** (3.209 Å (0.04 v.u.)). Thus Cl(3) anion can be

considered as a sixth ligand of a Jahn-Teller-distorted [(3O+Cl)+2Cl] octahedral environment of the Cu2 atom in the structure of **KI**, but not in the structure of **NaI**. The same coordinations were observed in the crystal structures of belloite,  $Cu(OH)Cl$  (Effenberger 1984), avdoninite,  $K_2Cu_5Cl_8(OH)_4(H_2O)_2$  (Kahlenberg 2004; Chukanov et al. 2007),  $SrCu_2(SeO_3)_2Cl_2$  (Berdonosov et al. 2009), and nicksobolevite,  $Cu_7(SeO_3)_2O_2Cl_6$  (Vergasova et al. 2014). The opposite apical Cl(1) atom of the Cu(2) octahedron is located at the distance of 2.780 Å and 2.772 Å in **KI** and **NaI**, respectively. In the square plane of the polyhedron, the average <Cu(2)–O> bond length is equal to 1.979 Å in **KI** and

**Table 3** Selected interatomic distances (Å) in the structures of  $A[Cu_5O_2](SeO_3)_2Cl_3$  ( $A^+ = K^+, Na^+$ ) and ilinskite (Krivovichev et al. 2013c). The italicized values are not considered as bonds owing to their bond-valences smaller than 0.05 v.u

	$K[Cu_5O_2](SeO_3)_2Cl_3$	$Na[Cu_5O_2](SeO_3)_2Cl_3$	ilinskite
A1–O4	2.786(2)	2.545(8)	2.585(4)
A1–Cl2	2.9009(11)	2.657(6)	2.688(3)
A1–Cl3	2.9575(11)	2.713(6)	2.702(3)
A1–Cl1	3.2276(1) 2x	3.2253(4) 2x	3.230(1) 2x
	3.1529(18) 2x	3.098(7) 2x	3.095(5) 2x
	3.1043(16) 2x	3.157(7) 2x	3.150(4) 2x
Cu1–O2	1.9163(19)	1.919(6)	1.910(3)
Cu1–O4	1.9191(18)	1.922(6)	1.921(3)
Cu1–O6	2.0238(15) 2x	2.010(4) 2x	2.009(2) 2x
Cu1–Cl1	2.5874(8)	2.621(3)	2.628(2)
Cu2–O1	1.9611(18)	1.961(6)	1.964(3)
Cu2–O3	1.9876(15) 2x	1.977(4) 2x	1.975(2) 2x
Cu2–Cl2	2.1896(9)	2.210(3)	2.211(2)
Cu2–Cl1	2.7989(8)	2.772(3)	2.779(2)
Cu2–Cl3	3.0419(9)	3.209(3)	3.208(2)
Cu3–O1	1.8996(19)	1.890(6)	1.897(3)
Cu3–O2	1.9128(19)	1.902(6)	1.914(3)
Cu3–O5	1.957(2)	1.985(7)	1.972(3)
Cu3–Cl1	2.3680(7)	2.360(3)	2.360(2)
Cu3–Cl3	3.3045(2) 2x	3.2550(5) 2x	3.260(3) 2x
Cu4–O1	1.8823(9)	1.871(3)	1.876(2)
Cu4–O2	1.8863(10)	1.879(3)	1.878(2)
Cu4–O3	2.0333(13)	2.019(4)	2.022(2)
Cu4–O6	2.0307(14)	2.022(4)	2.023(2)
Cu4–Cl3	2.9242(9)	3.016(3)	3.012(2)
Cu4–Cl3	3.3057(9)	3.159(3)	3.179(2)
Se1–O4	1.688(2)	1.692(6)	1.695(3)
Se1–O6	1.7083(14) 2x	1.701(4) 2x	1.705(2) 2x
<Se1–O>	1.702	1.698	1.702
Se2–O5	1.662(2)	1.655(6)	1.665(4)
Se2–O3	1.7238(14) 2x	1.729(4) 2x	1.734(2) 2x
<Se2–O>	1.703	1.704	1.711

1.972 Å in **NaI**; the Cu(2)–Cl(2) is 2.190 Å and 2.210 Å in **KI** and **NaI**, respectively.

In the crystal structure of **NaI**, the Cu(4) atom possesses an octahedral environment with four short equatorial Cu–O and two longer axial Cu–Cl bonds. The [(4O)+(2Cl)] type of an octahedral environment of Cu<sup>2+</sup> cations is commonly

observed in Pb–Cu oxyhalides, and has been described *e.g.*, in the crystal structures of leningradite, PbCu<sub>3</sub>(VO<sub>4</sub>)<sub>2</sub>Cl<sub>2</sub> (Siidra et al. 2007), and chloroxiphite, Pb<sub>3</sub>CuO<sub>2</sub>(OH)<sub>2</sub>Cl<sub>2</sub> (Siidra et al. 2008). The shift of the Cl(3) atoms is influenced by the larger size of K<sup>+</sup> cations in the structure of **KI** and results in the change of the two symmetrically inequivalent

**Table 4** Bond-valence analysis (in valence units = v.u.) for the crystal structures of  $A[\text{Cu}_5\text{O}_2](\text{SeO}_3)_2\text{Cl}_3$  ( $A^+ = \text{K}^+, \text{Na}^+$ ) and ilinskite (Krivovichev et al. 2013c). The italicized values in brackets are given for interatomic distances that are not considered as bonds, and do not sum up in total

Compound	Site	O1	O2	O3	O4	O5	O6	Cl1	Cl2	Cl3	Σ
<b>KI</b>	A1			0.07 <sup>2x→</sup>	0.17		0.06 <sup>2x→</sup>	0.13 <sup>x2→↓</sup>	0.23	0.20	1.12
<b>NaI</b>				(0.03 <sup>2x→</sup> )	0.14		(0.03 <sup>2x→</sup> )	0.07 <sup>x2→↓</sup>	0.31	0.26	0.85
ilinskite				(0.03 <sup>2x→</sup> )	0.12		(0.03 <sup>2x→</sup> )	0.07 <sup>x2→↓</sup>	0.28	0.27	0.81
<b>KI</b>	Cu1		0.53		0.52		0.39 <sup>2x→</sup>	0.20			2.03
<b>NaI</b>			0.52		0.52		0.41 <sup>2x→</sup>	0.19			2.05
ilinskite			0.54		0.52		0.41 <sup>2x→</sup>	0.18			2.06
<b>KI</b>	Cu2	0.47		0.43 <sup>2x→</sup>				0.12	0.60	0.06	2.11
<b>NaI</b>		0.47		0.45 <sup>2x→</sup>				0.12	0.57	(0.04)	2.06
ilinskite		0.46		0.45 <sup>2x→</sup>				0.12	0.57	(0.04)	2.05
<b>KI</b>	Cu3	0.55	0.53			0.47		0.37		(0.03 <sup>2x→↓</sup> )	1.92
<b>NaI</b>		0.57	0.55			0.44		0.38		(0.03 <sup>2x→↓</sup> )	1.94
ilinskite		0.55	0.53			0.45		0.38		(0.03 <sup>2x→↓</sup> )	1.91
<b>KI</b>	Cu4	0.58 <sup>2x↓</sup>	0.57 <sup>2x↓</sup>	0.38			0.39			0.08 <sup>2x↓</sup> , (0.03 <sup>2x↓</sup> )	2.00
<b>NaI</b>		0.60 <sup>2x↓</sup>	0.58 <sup>2x↓</sup>	0.40			0.40			0.06 <sup>2x↓</sup> , 0.04 <sup>2x↓</sup>	2.08
ilinskite		0.59 <sup>2x↓</sup>	0.58 <sup>2x↓</sup>	0.39			0.40			0.06 <sup>2x↓</sup> , 0.04 <sup>2x↓</sup>	2.06
<b>KI</b>	Se1				1.39		1.32 <sup>2x→</sup>				4.03
<b>NaI</b>					1.38		1.35 <sup>2x→</sup>				4.08
ilinskite					1.37		1.33 <sup>2x→</sup>				4.03
<b>KI</b>	Se2			1.27 <sup>2x→</sup>		1.50					4.04
<b>NaI</b>				1.25 <sup>2x→</sup>		1.52					4.02
ilinskite				1.23 <sup>2x→</sup>		1.48					3.94
<b>KI</b>	Σ	2.18	2.20	2.15	2.09	1.97	2.16	0.95	0.83	0.42	
<b>NaI</b>		2.24	2.23	2.10	2.04	1.96	2.16	0.83	0.88	0.46	
ilinskite		2.19	2.23	2.07	2.01	1.93	2.14	0.82	0.85	0.47	

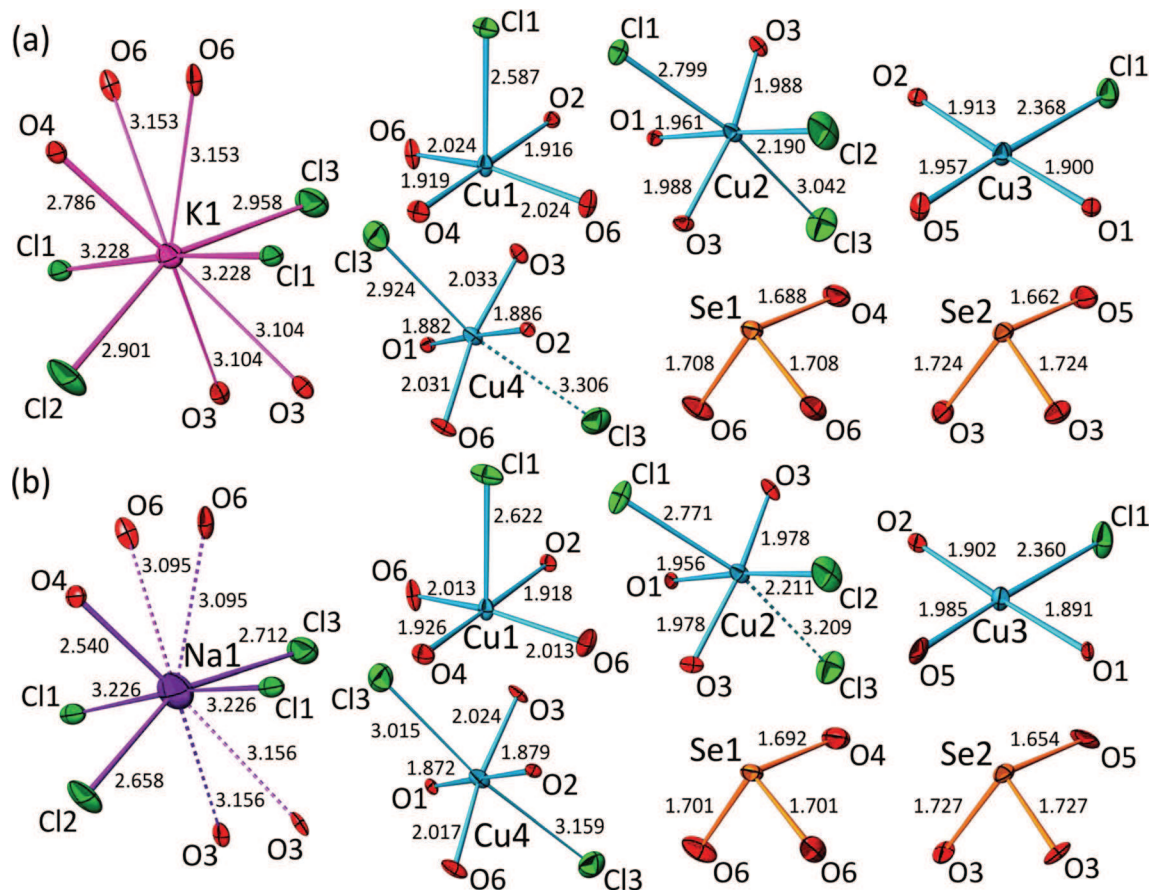


**Fig. 2** Coordination of cations in the crystal structures of  $K[Cu_5O_2](SeO_3)_2Cl_3$  (a) and  $Na[Cu_5O_2](SeO_3)_2Cl_3$  (b). Legend:  $K^+$  = pink;  $Na^+$  = violet;  $Cu^{2+}$  = cyan;  $Se^{4+}$  = orange;  $O^{2-}$  = red;  $Cl^-$  = green. Displacement ellipsoids are drawn at the 50 % probability level

axial Cu(4)–Cl(3) bonds within the Cu(4) polyhedron: 2.924 Å (0.08 v.u.) and 3.306 Å (0.03 v.u.) in **KI** in contrast to 3.016 Å (0.06 v.u.) and 3.159 Å (0.04 v.u.) in **NaI**. Thus, the coordination of the Cu(4) site in **KI** can be regarded as a five-fold square [(4O)+(Cl)] pyramid with one axial Cu(4)–Cl(3) bond, analogous to the environment of the Cu(1) sites in both structures. The average  $\langle Cu(4)–O \rangle$  bond lengths within the square plane of the Cu(4) polyhedron are equal to 1.958 Å and 1.948 Å in **KI** and **NaI**, respectively.

There are two symmetrically independent selenium sites in the crystal structures of **KI** and **NaI**. The  $Se^{4+}$  cations have typical oxygen coordination of triangular pyramid with a stereochemically active lone pair of electrons as a complementary ligand. The average  $\langle Se–O \rangle$  distances are equal 1.702 Å and 1.703 Å for Se1 and Se2 sites, respectively in **KI**, and 1.698 Å and 1.704 Å for Se1 and Se2 sites, respectively in **NaI**.

According to the calculated BVSS (Table 4), the arrangement of alkali cations in the crystal structures of **KI** and **NaI** is different. The arrangement of coordinating ligands of  $Na^+$  in **NaI** consists of one oxygen and four chlorines, forming a distorted [(O+2Cl)+2Cl] trigonal bipyramid (Fig. 2b).  $K^+$  cations in **KI** are surrounded by five oxygen and four chlorine atoms each (Figs. 2a and 3).

The crystal structures of **KI** and **NaI** contain “additional” oxygen atoms, which are coordinated solely by  $Cu^{2+}$  cations,

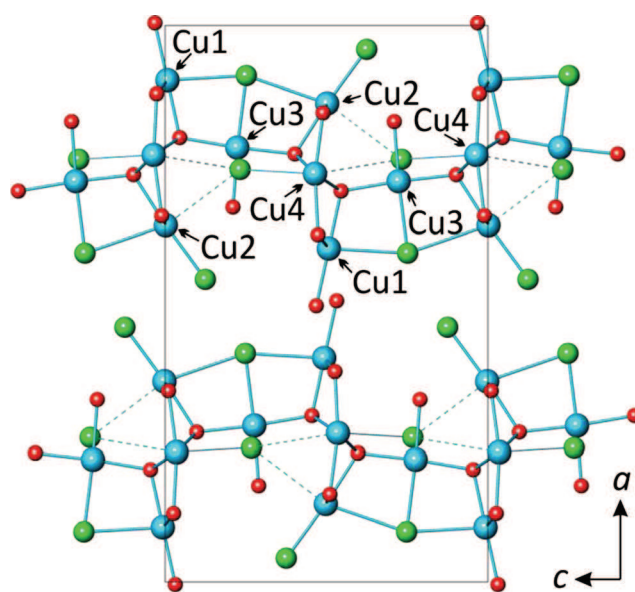
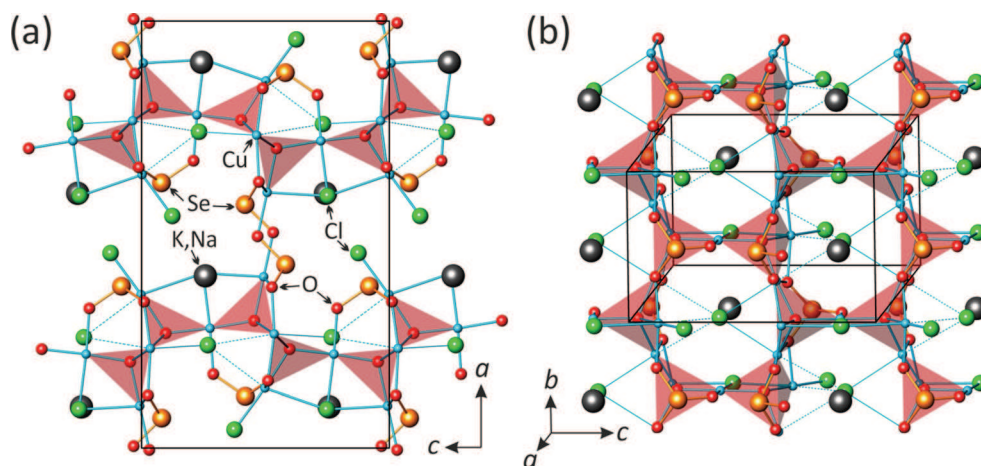


**Fig. 3** Mode of linkage of the Cu coordination polyhedra in the crystal structures of  $A[Cu_5O_2](SeO_3)_2Cl_3$  ( $A^+ = K^+, Na^+$ ). Legend:  $Cu^{2+}$  = cyan;  $O^{2-}$  = red;  $Cl^-$  = green



**Fig. 4** The crystal structures of  $A[\text{Cu}_5\text{O}_2](\text{SeO}_3)_2\text{Cl}_3$  ( $A^+ = \text{K}^+$ ,  $\text{Na}^+$ ) in two different projections featuring side and top view of the  $[\text{O}_2\text{Cu}_5]^{6+}$  layer of oxocentered  $(\text{OCu}_4)^{6+}$  tetrahedra. Legend:  $A^+ = \text{black}$ ;  $\text{Cu}^{2+} = \text{cyan}$ ;  $\text{Se}^{4+} = \text{orange}$ ;  $\text{O}^{2-} = \text{red}$ ;  $\text{Cl}^- = \text{green}$ ; the  $(\text{OCu}_4)^{6+}$  tetrahedra are highlighted by red. The  $A\text{--O}$  and  $A\text{--Cl}$  bonds are omitted for clarity



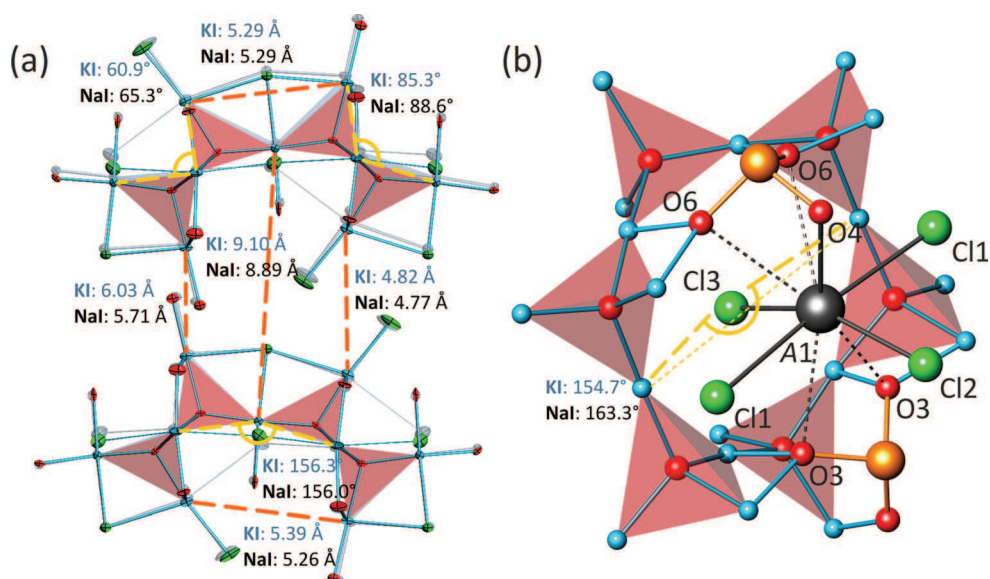
resulting in the formation of oxocentered  $(\text{OCu}_4)^{6+}$  tetrahedra. The  $(\text{OCu}_4)^{6+}$  tetrahedra share common corners to form the  $[\text{Cu}_5\text{O}_2]^{6+}$  sheets parallel to (100) (Fig. 4a). These two-dimensional (2D) structural units resemble the  $[\text{Si}_2\text{O}_5]^{2-}$  groups in phyllosilicates, where the cations and anions are inverted. Similar copper-oxide sheets with large pseudohexagonal pores were observed in the crystal structure of averievite,  $[\text{Cu}_5\text{O}_2](\text{VO}_4)_2\cdot M\text{Cl}$  ( $M = \text{Cu}^+$ ,  $\text{Rb}^+$ ,  $\text{Cs}^+$ ) (Starova et al. 1997), and synthetic  $[\text{Pb}_2\text{Cu}_3\text{O}_2](\text{SeO}_3)_2(\text{NO}_3)_2$  (Effenberg 1986). An important topological distinction between these 2D units is that the non-bonded apices of the  $(\text{OCu}_4)^{6+}$  tetrahedra in 6-membered rings have different “up” and “down” orientations relative to the plane of the sheet. The sheet in the crystal structures of ilinskite-type compounds,  $A[\text{Cu}_5\text{O}_2](\text{SeO}_3)_2\text{Cl}_3$  ( $A^+ = \text{K}^+$ ,  $\text{Na}^+$ ), is based upon **UUDUUD** rings (Fig. 4b), whereas the structure of averievite and synthetic  $[\text{Pb}_2\text{Cu}_3\text{O}_2](\text{SeO}_3)_2(\text{NO}_3)_2$  consist of the sheets with **UDUDUD** topology (the **U** and **D** symbols identify the “up” and “down” orientations of the  $\text{O}\text{--}\text{Cu}_{\text{terminal}}$  bond relative to the plane of the sheet).

The  $[\text{Cu}_5\text{O}_2]^{6+}$  sheets in the crystal structures of **KI** and **NaI** are surrounded by selenite triangular pyramids and chlorine anions to produce a microporous framework. The pores are filled with alkali metal cations and lone pairs of electrons of selenite groups. It is noteworthy that two crystallographically independent selenite groups play different roles in the structural architecture. The  $\text{O}\text{--}\text{O}\text{--}\text{O}$  triangular planes of the  $(\text{Se}(2)\text{O}_3)$  pyramids are parallel and attached to the  $\text{Cu}\text{--}\text{Cu}\text{--}\text{Cu}$  face of the  $(\text{O}(2)\text{Cu}_4)^{6+}$  tetrahedra according to the ‘face-to-face’ principle (Krivovichev and Filatov 1999; Krivovichev et al. 1999b). The  $(\text{Se}(1)\text{O}_3)$  groups are oriented perpendicular to the copper-oxide  $[\text{Cu}_5\text{O}_2]^{6+}$  sheets and link them into a three-dimensional (3D) framework through strong  $\text{Se}\text{--}\text{O}\text{--}\text{Cu}$  bonds (Fig. 4a).

## Discussion

The size of alkali cations in the crystal structures of **KI** and **NaI** has a significant influence upon their organization. The

**Fig. 5** Comparison of the superimposed crystal structures of  $\text{Na}[\text{Cu}_5\text{O}_2](\text{SeO}_3)_2\text{Cl}_3$  (on top in color) and  $\text{K}[\text{Cu}_5\text{O}_2](\text{SeO}_3)_2\text{Cl}_3$  (below in greyscale) (a:  $\text{Na}^+$  and  $\text{K}^+$  are omitted for clarity) and the coordination environments of the  $A1$  atoms (b). Legend is the same as in Fig. 4. Displacement ellipsoids in (a) are drawn at the 50 % probability level



substitution of smaller  $\text{Na}^+$  cations ( $R_{\text{ion}} = 1.02 \text{ \AA}$ , Shannon (1976)) by larger  $\text{K}^+$  cations ( $R_{\text{ion}} = 1.38 \text{ \AA}$ ) leads to the expansion of alkali metal coordination polyhedra and, as a result, in the enlarged unit-cell parameters of  $\text{K}[\text{Cu}_5\text{O}_2](\text{SeO}_3)_2\text{Cl}_3$  compared to its Na analogue.

The  $a$  parameter value is most seriously influenced by the increased size of an alkali metal atom: it enlarges by  $0.420 \text{ \AA}$  from  $17.749 \text{ \AA}$  in **NaI** to  $18.169 \text{ \AA}$  in **KI**, whereas the  $b$  and  $c$  unit-cell parameters do not undergo significant changes ( $\Delta = +0.071 \text{ \AA}$  and  $\Delta = +0.080 \text{ \AA}$  for the  $b$  and  $c$  parameters, respectively). It can be explained by the fact that the major size-effect occurs in separating further the complex copper oxide-selenite sheets parallel to (100). One of the shortest distance between the two closest copper cations from the adjacent sheets changes from  $5.705 \text{ \AA}$  in **NaI** to  $6.034 \text{ \AA}$  in **KI** ( $\Delta = +0.329 \text{ \AA}$ ). The longest Cu–Cu distance increases from  $8.891 \text{ \AA}$  in **NaI** to  $9.102 \text{ \AA}$  in **KI** ( $\Delta = +0.211 \text{ \AA}$ ) as shown in Fig. 5a. Geometry of the linkage of the corner-sharing  $(\text{OCu}_4)^{6+}$  tetrahedra varies in both structures due to the difference in the interlayer distance. The dihedral angles between triangular Cu–Cu–Cu faces of the adjacent  $(\text{OCu}_4)^{6+}$  tetrahedra with alternating orientations of the ‘pendant’ vertices relative to the sheet plane differ significantly ( $60.87^\circ$  in **KI** and  $65.30^\circ$  in **NaI**), whereas the adjacent faces of the tetrahedra oriented in the same direction are inclined to each other at approximately the same angle in both structures ( $156.27^\circ$  in **KI**, and  $155.97^\circ$  in **NaI**).

The shift of the Cl(3) site (Fig. 5b) relative to its coordination environment is influenced by the cation size and deserves a special remark. The  $A(1)$ –Cl(3) bond length increases from  $2.713 \text{ \AA}$  in **NaI** to  $2.956 \text{ \AA}$  in **KI** ( $\Delta = +0.243 \text{ \AA}$ ). The Cu(3)–Cl(3)–Cu(3) angle between the chlorine anion and the plane of the  $[\text{O}_2\text{Cu}_5]^{6+}$  sheet is smaller in **KI**:  $154.68^\circ$  versus  $163.33^\circ$  in **NaI**.

The  $[\text{O}_2\text{Cu}_5]_n^{6n+}$  sheets in the crystal structures of **KI** and **NaI** are slightly bent due to the Na→K substitution. The planes formed by the oxygen atoms of the parallel adjacent  $(\text{OCu}_4)^{6+}$  tetrahedra are inclined one to each other at  $16.17^\circ$  and  $12.31^\circ$  in **KI** and **NaI**, respectively.

The present work further demonstrates that CVT reactions method provides a unique opportunity to model physicochemical conditions existing in fumarolic environments and may be used not only to model exhalative processes, but also to predict possible mineral phases that may form in fumaroles. In particular, the K analogue of ilinskite is not known in nature, whereas it may well be formed from volcanic gases. The similar case of the Na→K substitution is present in many fumarolic minerals, e.g. euchlorine ( $\text{NaKCu}_3\text{O}(\text{SO}_4)_3$ ) – fedotovite ( $\text{K}_2\text{Cu}_3\text{O}(\text{SO}_4)_3$ ) (Scordari and Stasi 1990; Vergasova et al. 1988; Starova et al. 1991), wulfite ( $\text{K}_3\text{NaCu}_4\text{O}_2(\text{SO}_4)_2$ ) – parawulfite ( $\text{K}_5\text{Na}_3\text{Cu}_8\text{O}_4(\text{SO}_4)_4$ ) (Pekov et al. 2013c, d; Karpov et al. 2013). It is therefore well-probable that the K analogue of ilinskite,  $\text{K}[\text{Cu}_5\text{O}_2](\text{SeO}_3)_2\text{Cl}_3$ , may form in nature in a K-rich fumarolic environment.

**Acknowledgements** We are grateful to two anonymous referees and Associate Editor Anton Beran for helpful comments on the manuscript. This work was carried out under the framework of the Multi-InMaDe project supported by the ANR (Grant ANR 2011-JS-08 00301). VMK, OIS and SVK have been supported in this work by the Russian Science Foundation (grant 14-17-00071). The Fonds Européen de Développement Régional (FEDER), CNRS, Région Nord Pas-de-Calais, and Ministère de l’Éducation Nationale de l’Enseignement Supérieur et de la Recherche are acknowledged for funding the X-ray diffractometers.

## References

- Bastide B, Millet P, Johnsson M, Galy J (2000) Synthesis of copper(II) and selenium(IV) oxochlorides by chemical transport reaction: crystal structure of  $\text{Cu}_9\text{O}_2(\text{SeO}_3)_4\text{Cl}_6$ . *Mater Res Bull* 35:847–855
- Berdonov PS, Janson O, Olenev AV, Krivovichev SV, Rosner H, Dolgikh VA, Tsirlin AA (2013) Crystal structures and variable magnetism of  $\text{PbCu}_2(\text{XO}_3)_2\text{Cl}_2$  with  $X = \text{Se}, \text{Te}$ . *Dalton Trans* 42:9547–9554
- Berdonov PS, Olenev AV, Dolgikh VA (2009) Strontium–copper selenite–chlorides: synthesis and structural investigation. *J Solid State Chem* 182:2368–2373
- Binnewies M, Glaum R, Schmidt M, Schmidt P (2013) Chemical vapor transport reactions—a historical review. *Z Anorg Allg Chem* 639: 219–229
- Brese NE, O’Keeffe M (1991) Bond-valence parameters for solids. *Acta Crystallogr B* 47:192–197
- Burns PC, Hawthorne FC (1995) Coordination-geometry structural pathways in  $\text{Cu}^{2+}$  oxysalt minerals. *Can Mineral* 33:889–905
- Burns PC, Krivovichev SV, Filatov SK (2002) New  $\text{Cu}^{2+}$  coordination polyhedra in the crystal structure of burnsite,  $\text{KCu}_2\text{O}_2(\text{SeO}_3)_2\text{Cl}_9$ . *Can Mineral* 40:1587–1595
- Chukanov NV, Murashko MN, Zadov AE, Bushmakin AF (2007) Avdoninite,  $\text{K}_2\text{Cu}_5\text{Cl}_8(\text{OH})_4 \cdot \text{H}_2\text{O}$ , a new mineral species from volcanic exhalations and the technogenic zone at volcanic-hosted massive sulfide deposits. *Geol Ore Depos* 49:505–508
- Demartin F, Castellano C, Campostrini I (2013) Aluminopyracmonite,  $(\text{NH}_4)_3\text{Al}(\text{SO}_4)_3$ , a new ammonium aluminium sulfate from La Fossa Crater, Vulcano, Aeolian Islands, Italy. *Mineral Mag* 77: 443–451
- Demartin F, Castellano C, Campostrini I (2014) Therasiaite,  $(\text{NH}_4)_3\text{KNa}_2\text{Fe}^{2+}\text{Fe}^{3+}(\text{SO}_4)_3\text{Cl}_5$ , a new sulfate chloride from La Fossa Crater, Vulcano, Aeolian islands, Italy. *Mineral Mag* 78: 203–213
- Effenberger H (1984) Verfeinerung der Kristallstruktur von Kupfer(II)-hydroxichlorid,  $\text{Cu}(\text{OH})\text{Cl}$ . *Monatsh Chem* 115:725–730
- Effenberger H (1985)  $\text{Cu}(\text{SeO}_2\text{OH})_2$ : synthesis and crystal structure. *Z Kristallogr* 173:167–272
- Effenberger H (1986)  $\text{PbCu}_3(\text{OH})(\text{NO}_3)(\text{SeO}_3)_3 \cdot 1/2\text{H}_2\text{O}$  und  $\text{Pb}_2\text{Cu}_3\text{O}_2(\text{NO}_3)_2(\text{SeO}_3)_2$ : synthese und Kristallstrukturuntersuchung. *Monatsh Chem* 117:1099–1106
- Effenberger H, Pertlik F (1986) Die Kristallstrukturen der Kupfer(II)-oxo-selenite  $\text{Cu}_2\text{O}(\text{SeO}_3)$  (kubisch und monoklin) und  $\text{Cu}_4\text{O}(\text{SeO}_3)_3$  (monoklin und triklin). *Monatsh Chem* 117:887–896
- Filatov SK, Semenova TF, Vergasova LP (1992) Types of polymerization of  $[\text{OCu}_4]^{6+}$  in inorganic compounds with ‘‘additional’’ oxygen atoms. *Dokl Akad Nauk SSSR (in russian)* 322:539–539
- Garavelli A, Mitolo D, Pinto D, Vurro F (2013) Lucabindiite,  $(\text{K}, \text{NH}_4)\text{As}_4\text{O}_6(\text{Cl}, \text{Br})$ , a new fumarole mineral from the ‘‘La Fossa’’ crater at Vulcano, Aeolian Islands, Italy. *Am Mineral* 98:470–477
- Hawthorne FC, Cooper MA, Grice JD, Roberts AC, Hubbard N (2002) Description and crystal structure of bobkingite,  $\text{Cu}^{2+}_5\text{Cl}_2(\text{OH})_8(\text{H}_2\text{O})_2$ , a new mineral from New Cliffe Hill

- Quarry, Stanton-under-Bardon, Leicestershire, UK. *Mineral Mag* 66:301–311
- Kahlenberg V (2004) On the crystal structure of  $K_2Cu_5Cl_8(OH)_4 \cdot 2H_2O$ . *Z Anorg Allg Chem* 630:900–903
- Karpov GA, Krivovichev SV, Vergasova LP, Chernyat'eva AP, Anikin LP, Moskaleva SV, Filatov SK (2013) Oxysulfates of copper, sodium, and potassium in the lava flows of the 2012–2013 Tolbachik Fissure Eruption. *J Volcanol Seismol* 7:362–370
- Kovrugin VM, Colmont M, Mentré O, Siidra OI, Krivovichev SV (2015) Dimers of oxocentered  $[OCu_4]^{6+}$  tetrahedra in two novel copper selenite chlorides,  $K[Cu_5O](SeO_3)_2Cl$  and  $Na_2[Cu_7O_2](SeO_3)_4Cl_4$ , and related minerals and inorganic compounds. *Mineral Mag*: submitted
- Krivovichev SV, Filatov SK (1999) Structural principles for minerals and inorganic compounds containing anion-centered tetrahedra. *Am Mineral* 84:1099–1106
- Krivovichev SV, Filatov SK, Semenova TF, Rozhdestvenskaya IV (1998) Crystal chemistry of inorganic compounds based on chains of oxocentered tetrahedra. I. Crystal structure of chloromenite,  $Cu_9O_2(SeO_3)_4Cl_6$ . *Z Krist* 213:645–649
- Krivovichev SV, Shuvalov RR, Semenova TF, Filatov SK (1999a) Crystal chemistry of inorganic compounds based on chains of oxocentered tetrahedra. III. Crystal structure of georgbokiite,  $Cu_5O_2(SeO_3)_2Cl_2$ . *Z Krist* 214:135–138
- Krivovichev SV, Starova GL, Filatov SK (1999b) “Face-to-face” relationships between oxocentered tetrahedra and cation-centred tetrahedral oxyanions in crystal structures of minerals and inorganic compounds. *Mineral Mag* 63:263–266
- Krivovichev SV, Filatov SK, Armbruster T, Pankratova OY (2004) Crystal structure of  $Cu^{(I)}Cu^{(II)}_4O(SeO_3)Cl_5$ , a new heterovalent copper compound. *Dokl Chem* 399:226–228
- Krivovichev SV, Filatov SK, Burns PC, Vergasova LP (2006) The crystal structure of allochalcocelite,  $Cu^+Cu^{2+}_5PbO_2(SeO_3)_2Cl_5$ , a mineral with well-defined  $Cu^+$  and  $Cu^{2+}$  positions. *Can Mineral* 44:507–514
- Krivovichev SV, Filatov SK, Burns PC, Vergasova LP (2007) The crystal structure of parageorgbokiite,  $\beta$ - $Cu_5O_2(SeO_3)_2Cl_2$ . *Can Mineral* 45: 929–934
- Krivovichev SV, Vergasova LP, Filatov SK, Rybin DS, Britvin SN, Ananiev VV (2013a) Hatertite,  $Na_2(Ca, Na)(Fe^{3+}, Cu)_2(AsO_4)_3$ , a new alluaudite-group mineral from Tolbachik fumaroles, Kamchatka peninsula, Russia. *Eur J Mineral* 25:683–691
- Krivovichev SV, Mentré O, Siidra OI, Colmont M, Filatov SK (2013b) Anion-centered tetrahedra in inorganic compounds. *Chem Rev* 113: 6459–6535
- Krivovichev SV, Filatov SK, Vergasova LP (2013c) The crystal structure of ilinskite,  $NaCu_5O_2(SeO_3)_2Cl_3$ , and review of mixed-ligand  $CuO_mCl_n$  coordination geometries in minerals and inorganic compounds. *Mineral Petrol* 107:235–242
- Millet P, Bastide B, Pashchenko V, Gnatchenko S, Ksari Y, Stepanov A (2001) Syntheses, crystal structures and magnetic properties of francisite compounds  $Cu_3Bi(SeO_3)_2O_2X$  ( $X = Cl, Br$  and  $I$ ). *J Mater Chem* 11:1152–1157
- Mitolo D, Demartin F, Garavelli A, Campostrini I, Pinto D, Gramaccioli CM, Acquafredda P, Kolitsch U (2013) Adranosite-(Fe),  $(NH_4)_4NaFe_2(SO_4)_4Cl(OH)_2$ , a new ammonium sulfate chloride from La Fossa Crater, Vulcano, Aeolian Islands, Italy. *Can Mineral* 51:57–66
- Murashko MN, Pekov IV, Krivovichev SV, Chernyat'eva AP, Yapaskurt VO, Zadov AE, Zelenski ME (2013) Steklite,  $KAl(SO_4)_2$ : a finding at the Tolbachik Volcano, Kamchatka, Russia, validating its status as a mineral species and crystal structure. *Geol Ore Depos* 55:594–600
- Pekov IV, Zelenski ME, Yapaskurt VO, Polekhovskiy YS, Murashko MN (2013a) Starovaita,  $KCu_5O(VO_4)_3$ , a new mineral from fumarole sublimates of the Tolbachik volcano, Kamchatka, Russia. *Eur J Mineral* 25:91–96
- Pekov IV, Zubkova NV, Yapaskurt VO, Belakovskiy DI, Chukanov NV, Lykova IS, Sidorov EG, Pushcharovskiy DY (2013b) Wulffite. IMA 2013-035. *CNMNC Newsletter* No. 17. *Mineral Mag* 77:2998
- Pekov IV, Zubkova NV, Yapaskurt VO, Belakovskiy DI, Chukanov NV, Lykova IS, Sidorov EG, Pushcharovskiy DY (2013c) Parawulffite, IMA 2013-036. *CNMNC Newsletter* No. 17. *Mineral Mag* 77:2998
- Pekov IV, Zubkova NV, Zelenski ME, Yapaskurt VO, Polekhovskiy YS, Fadeeva OA, Pushcharovskiy DY (2013d) Yaroshevskite,  $Cu_9O_2(VO_4)_4Cl_2$ , a new mineral from the Tolbachik volcano, Kamchatka, Russia. *Mineral Mag* 77:107–116
- Pekov IV, Siidra OI, Chukanov NV, Yapaskurt VO, Belakovskiy DI, Murashko MN, Sidorov EG (2014a) Kaliochalcite,  $KCu_2(SO_4)_2[(OH)(H_2O)]$ , a new tsumcorite-group mineral from the Tolbachik volcano, Kamchatka, Russia. *Eur J Mineral* 26:597–604
- Pekov IV, Zubkova NV, Yapaskurt VO, Belakovskiy DI, Lykova IS, Viskasina MF, Sidorov EG, Pushcharovskiy DY (2014b) New arsenate minerals from the Arsenatnaya fumarole, Tolbachik volcano, Kamchatka, Russia. I. Yurmarinite,  $Na_7(Fe^{3+}, Mg, Cu)_4(AsO_4)_6$ . *Mineral Mag* 78:905–917
- Pekov IV, Zubkova NV, Yapaskurt VO, Kartashov PM, Polekhovskiy YS, Murashko MN, Pushcharovskiy DY (2014c) Koksharovite,  $CaMg_2Fe^{3+}_4(VO_4)_6$ , and grigorievite,  $Cu_3Fe^{3+}_2Al_2(VO_4)_6$ , two new howardevansite-group minerals from volcanic exhalations. *Eur J Mineral* 26:667–677
- Pertlik F, Zemann J (1988) The crystal structure of nabokoite,  $Cu_7TeO_4(SO_4)_5 \cdot KCl$ : the first example of a  $Te^{(IV)}O_4$  pyramid with exactly tetragonal symmetry. *Mineral Petrol* 38:291–298
- Pinto D, Garavelli A, Mitolo D (2014) Baličžuničite,  $Bi_2O(SO_4)_2$ , a new fumarole mineral from La Fossa crater, Vulcano, Aeolian Islands, Italy. *Mineral Mag* 78:1043–1055
- Pring A, Gatehouse BM, Birch WD (1990) Francisite,  $Cu_3Bi(SeO_3)_2O_2Cl$ , a new mineral from Iron Monarch, South Australia: description and crystal structure. *Am Mineral* 75:1421–1425
- Scordari F, Stasi F (1990) The crystal structure of euchlorine,  $NaKCu_3O(SO_4)_3$ . *N Jb Mineral Abh* 161:241–253
- Shannon RD (1976) Revised effective ionic radii and systematic studies of interatomic distances in halides and chalcogenides. *Acta Crystallogr* A32:751–767
- Sheldrick GM (2008) A short history of SHELX. *Acta Crystallogr* A64: 112–122
- Shuvalov RR, Vergasova LP, Semenova TF, Filatov SK, Krivovichev SV, Siidra OI, Rudashevskiy NS (2013) Prewittite,  $KPb_{1.5}Cu_6Zn(SeO_3)_2O_2Cl_{10}$ , a new mineral from Tolbachik fumaroles, Kamchatka peninsula, Russia: description and crystal structure. *Am Mineral* 98:463–469
- Siidra OI, Krivovichev SV, Armbruster T, Pekov IV (2007) The crystal structure of leningradite,  $PbCu_3(VO_4)_2Cl_2$ . *Can Mineral* 45:445–449
- Siidra OI, Krivovichev SV, Turner RW, Rumsey MS (2008) Chloroxiphite  $Pb_3CuO_2(OH)_2Cl_2$ : structure refinement and description in terms of oxocentered  $OPb_4$  tetrahedra. *Mineral Mag* 72:793–798
- Starova GL, Filatov SK, Vergasova LP (1991) The crystal structure of fedotovite,  $K_2Cu_3O(SO_4)_3$ . *Mineral Mag* 55:613–616
- Starova GL, Krivovichev SV, Fundamenskiy VS, Filatov SK (1997) The crystal structure of averievite,  $Cu_5O_2(VO_4)_2 \cdot nMX$ ; comparison with related compounds. *Mineral Mag* 61:441–446
- Takagi R, Duc F, Johnsson M (2006)  $MoCu_3TeO_7Cl_2 \cdot 0.5H_2O$ . *Acta Crystallogr* C62:i16–i18
- Vergasova LP, Filatov SK, Serafimova YK, Varaksina TV (1988) Kamchatkite  $KCu_3OCl(SO_4)_2$ —a new mineral from volcanic sublimates. *Zap VMO* 117:459–461
- Vergasova LP, Semenova TF, Shuvalov RR, Filatov SK, Ananiev VV (1997) Ilinskite  $NaCu_5O_2(SeO_3)_2Cl_3$ —a new mineral of volcanic exhalations. *Dokl Akad Nauk (in russian)* 353:641–644

Vergasova LP, Semenova TF, Krivovichev SV, Filatov SK, Zolotarev Jr AA, Ananiev VV (2014) Nicksobolevite,  $\text{Cu}_7(\text{SeO}_3)_2\text{O}_2\text{Cl}_6$ , a new complex copper oxoselenite chloride from Tolbachik fumaroles, Kamchatka peninsula, Russia. *Eur J Mineral* 26:439–449

Zhang D, Berger H, Kremer RK, Wulfering D, Lemmens P, Johnsson M (2010) Synthesis, crystal structure, and magnetic properties of the copper selenite chloride  $\text{Cu}_5(\text{SeO}_3)_4\text{Cl}_2$ . *Inorg Chem* 49:9683–9688

## A-VIII

# **[NaCl][Cu(HSeO<sub>3</sub>)<sub>2</sub>], NaCl-intercalated Cu(HSeO<sub>3</sub>)<sub>2</sub>: synthesis, crystal structure and comparison with related compounds**

Vadim M. Kovrugin, Sergey V. Krivovichev, Olivier Mentré, and Marie Colmont

Published in: *Zeitschrift für Kristallographie - Crystalline Materials*, 2015, Vol. 230, 573–577.

DOI: 10.1515/zkri-2015-1849

Reprinted with kind permission from Walter de Gruyter GmbH.



Vadim M. Kovrugin, Sergey V. Krivovichev\*, Olivier Mentré and Marie Colmont

# [NaCl][Cu(HSeO<sub>3</sub>)<sub>2</sub>], NaCl-intercalated Cu(HSeO<sub>3</sub>)<sub>2</sub>: synthesis, crystal structure and comparison with related compounds

DOI 10.1515/zkri-2015-1849

Received March 2, 2015; accepted May 29, 2015

**Keywords:** copper; crystal structure; intercalated structures; layered compounds; selenite.

**Abstract:** Single crystals of [NaCl][Cu(HSeO<sub>3</sub>)<sub>2</sub>] have been prepared by the chemical vapor transport reactions. Its crystal structure (monoclinic, *C2/c*, *a* = 13.9874(7), *b* = 7.2594(4), *c* = 9.0421(5) Å, β = 127.046(2)°, *V* = 732.81(7) Å<sup>3</sup>) is based upon electroneutral [Cu(HSeO<sub>3</sub>)<sub>2</sub>] sheets formed by corner sharing between the [CuO<sub>4</sub>] squares and (HSeO<sub>3</sub>) groups that are parallel to the (100) plane. Each (SeO<sub>2</sub>OH)<sup>−</sup> group forms the O<sub>h</sub>1–O2 hydrogen bond to an adjacent hydroselenite group to constitute a [(SeO<sub>2</sub>OH)<sub>2</sub>]<sup>2−</sup> dimer that provides additional stabilization of the copper diselenite sheet. The [Cu(HSeO<sub>3</sub>)<sub>2</sub>] sheets alternate with the sheets consisting of zigzag–Na–Cl–Na–Cl–chains formed by Cl atoms and disordered Na sites. The chains are parallel to the *c* axis. The linkage between the alternating electroneutral [Cu(HSeO<sub>3</sub>)<sub>2</sub>] and [NaCl] sheets is provided by the Cu–Cl and Na–O bonds. The coordination of Na is fivefold and consists of three O and two Cl atoms. [NaCl][Cu(HSeO<sub>3</sub>)<sub>2</sub>] is a new member of the group of compounds based upon the M(HSeO<sub>3</sub>)<sub>2</sub> layers (M<sup>2+</sup> = Cu, Co, Cd). The prototype structure for this group is [Cu(HSeO<sub>3</sub>)<sub>2</sub>] that does not have any chemical species separating the copper hydroselenite layers. In other compounds, the interlayer space between the [Cu(HSeO<sub>3</sub>)<sub>2</sub>]<sup>0</sup> layers is occupied by structural units of different complexity. [NaCl][Cu(HSeO<sub>3</sub>)<sub>2</sub>] can be considered as [Cu(HSeO<sub>3</sub>)<sub>2</sub>] intercalated with the NaCl layers consisting of one-dimensional–Na–Cl–Na–Cl–chains.

## Introduction

Transition metal selenites have been the focus of a number of recent studies due to their interesting physical properties, arising in part due to the interplay between the stereochemical activity of lone pairs of electrons on the Se<sup>4+</sup> cations and electronic properties of transition metal cations [1–9]. The interest has also been stimulated by the attempts to understand purely fundamental reasons for structural diversity in selenites and its underlying crystal chemical mechanisms [10–12]. In this regard, copper selenite chlorides are of particular importance, due to their natural occurrences as minerals [13–17] and the structures featuring ‘scissor’-type disruption of a bonding network induced by the well-localized stereochemically active but chemically inactive lone electron pairs [18–22].

In this paper, we report on the synthesis and crystal structure of [NaCl][Cu(HSeO<sub>3</sub>)<sub>2</sub>], a novel compound prepared by the chemical vapor techniques (CVT) and a new member of the family of inorganic and organic-inorganic compounds based upon the electroneutral M(HSeO<sub>3</sub>)<sub>2</sub> layers (M<sup>2+</sup> = Cu, Co, Cd) [23–29].

## Experimental

### Synthesis

Single crystals of [NaCl][Cu(HSeO<sub>3</sub>)<sub>2</sub>] have been prepared by the CVT method. Mixture of CuO, CuCl<sub>2</sub>, SeO<sub>2</sub>, and NaCl taken in the 4:1:2:3 molar ratio were loaded into a fused silica tube (*ca.* 15 cm), which was evacuated to 10<sup>−2</sup> mbar before sealing. The tubes were placed horizontally into a tubular two-zone furnace, and heated to 500°. The temperature difference between the source and deposition zones of the tube was about 50 °C. After 3 days, the tubes were cooled down to room temperature over 24 h. The products of the synthesis consisted of green crystals of Na<sub>2</sub>[Cu<sub>2</sub>O<sub>2</sub>](SeO<sub>3</sub>)<sub>4</sub>Cl<sub>4</sub> [30] and few

\*Corresponding author: Sergey V. Krivovichev, Department of Crystallography, St. Petersburg State University, Universitetskaya nab. 7/9, 199034 St. Petersburg, Russia; and Institute of Silicate Chemistry, Russian Academy of Sciences, Makarova Emb. 6, 199034 St. Petersburg, Russia, E-mail: skrivovi@mail.ru

Vadim M. Kovrugin: Department of Crystallography, St. Petersburg State University, Universitetskaya nab. 7/9, 199034 St. Petersburg, Russia; and UCCS, ENSCL, Université Lille 1, CNRS, UMR 8181, 59652 Villeneuve d’Ascq, France

Olivier Mentré and Marie Colmont: UCCS, ENSCL, Université Lille 1, CNRS, UMR 8181, 59652 Villeneuve d’Ascq, France

pale blue translucent block-shaped crystals of [NaCl][Cu(HSeO<sub>3</sub>)<sub>2</sub>] (Figure 1).

### X-ray experiment

Single crystals of [NaCl][Cu(HSeO<sub>3</sub>)<sub>2</sub>] selected for data collection were examined under an optical microscope and mounted on a glass fiber with epoxy for single crystal X-rays diffraction analysis. More than a hemisphere of the X-ray diffraction data were collected with the frame width of 0.5° in  $\omega$ , and 45 s spent counting for each frame using a Bruker APEX DUO diffractometer equipped with a micro-focus X-ray tube operated with MoK $\alpha$  radiation at 50 kV and 40 mA. The data were integrated and corrected for absorption using a multi-scan type model using the Bruker programs APEX and SADABS. The crystal structure was solved by direct methods and refined to the crystallographic agreement factor  $R_1 = 0.021$  by means of the SHELX program package [31]. Relevant crystallographic information is listed in Table 1. The final atomic coordinates, site-occupation factors (SOFs) and anisotropic displacement parameters are given in Table 2. Selected interatomic distances are in Table 3. Hydrogen atom positions have been determined from difference Fourier map.

Further details of the crystal structure investigation are available from the Fachinformationszentrum Karlsruhe, D-76344 Eggenstein-Leopoldshafen, Germany, on quoting the depository number CSD-429287, the names of the authors and the citation of the paper.

## Results

The crystal structure of the title compound contains one symmetrically independent Cu site octahedrally coordinated by four O and two Cl atoms. The coordination is typical for the mixed-metal CuO<sub>n</sub>Cl<sub>m</sub> configurations occurring in inorganic copper oxysalts [14]. The Cu site forms four short Cu–O bonds (1.967–1.968 Å) that define a [CuO<sub>4</sub>] square complemented by two long Cu–Cl bonds. This type of coordination (four short equatorial and two long apical bonds) is a consequence of the Jahn–Teller distortion of octahedral geometry. The similar [CuO<sub>4</sub>Cl<sub>2</sub>]

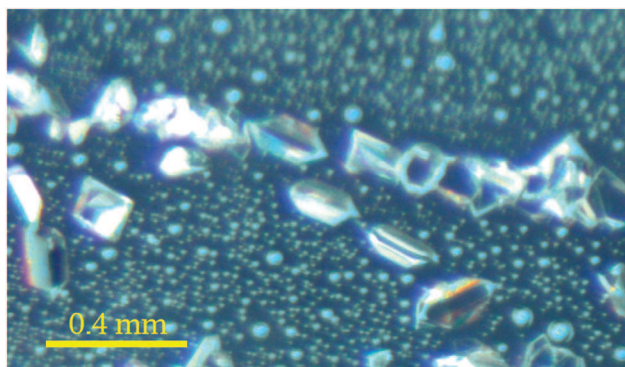


Fig. 1: Crystals of [NaCl][Cu(HSeO<sub>3</sub>)<sub>2</sub>] under optical microscope.

Tab. 1: Crystallographic data and refinement parameters for [NaCl][Cu(HSeO<sub>3</sub>)<sub>2</sub>].

Crystal data	
Crystal system	monoclinic
Space group	C2/c
<i>a</i> (Å)	13.9874(7)
<i>b</i> (Å)	7.2594(4)
<i>c</i> (Å)	9.0421(5)
$\beta$ (°)	127.046(2)
Unit-cell volume (Å <sup>3</sup> )	732.81(7)
<i>Z</i>	2
Calculated density (g/cm <sup>3</sup> )	3.425
Absorption coefficient (mm <sup>-1</sup> )	13.313
Crystal size (mm)	0.17 × 0.12 × 0.09
Data collection	
Temperature	293 K
Radiation, wavelength (Å)	MoK $\alpha$ , 0.71073
<i>F</i> (000)	700
$\theta$ range (°)	3.35–30.97
<i>h</i> , <i>k</i> , <i>l</i> ranges	–20 → 11, –9 → 10, –12 → 13
Total reflections collected	3926
Unique reflections ( $R_{int}$ )	1170 (0.026)
Unique reflections $F > 4\sigma_F$	989
Structure refinement	
Refinement method	Full-matrix least-squares on $F^2$
Weighting coefficients <i>a</i> , <i>b</i> *	0.0232, 1.3732
Data/restraints/parameters	1170/0/62
$R_1[F > 4\sigma_F]$ , $wR_2[F > 4\sigma_F]$	0.021, 0.051
$R_1$ all, $wR_2$ all	0.030, 0.053
Goodness-of-fit on $F^2$	1.081
Largest diff. peak and hole	0.702, –0.645 eÅ <sup>-3</sup>

octahedra have been observed, e.g. in atacamite, Cu<sub>2</sub>(OH)<sub>3</sub>Cl [32], and leningradite, PbCu<sub>3</sub>(VO<sub>4</sub>)<sub>2</sub>Cl<sub>2</sub> [33]. There is one Se site coordinated by three O atoms to form a trigonal (SeO<sub>3</sub>) pyramid characteristic for selenites. One of the three Se–O bonds is elongated (Se–O<sub>h1</sub> = 1.751 Å) compared to two other bonds (1.671 and 1.680 Å), owing to the protonation of the O<sub>h1</sub> site. The [CuO<sub>4</sub>] squares and (HSeO<sub>3</sub>) groups share O atoms to form electroneutral [Cu(HSeO<sub>3</sub>)<sub>2</sub>] sheets parallel to the (100) plane (Figure 2a). The (SeO<sub>2</sub>OH)<sup>–</sup> group form the O<sub>h1</sub>···O2 hydrogen bond to an adjacent hydroselenite group to form a [(SeO<sub>2</sub>OH)<sub>2</sub>]<sup>2–</sup> dimer that provides additional stabilization of the copper diselenite sheet.

In the crystal structure, the [Cu(HSeO<sub>3</sub>)<sub>2</sub>] sheets alternate with the sheets consisting of zigzag–Na–Cl–Na–Cl–chains formed by Cl atoms and disordered Na sites (Figure 2b). The chains are parallel to the *c* axis. The Na–Cl distances are 2.917 and 2.881 Å, which is comparable to the distance 2.82 Å observed in halite, NaCl. The Na–Cl–Na angle is equal to 97.1–110.5°, which can be compared to the ideal angle of 90° observed in halite.



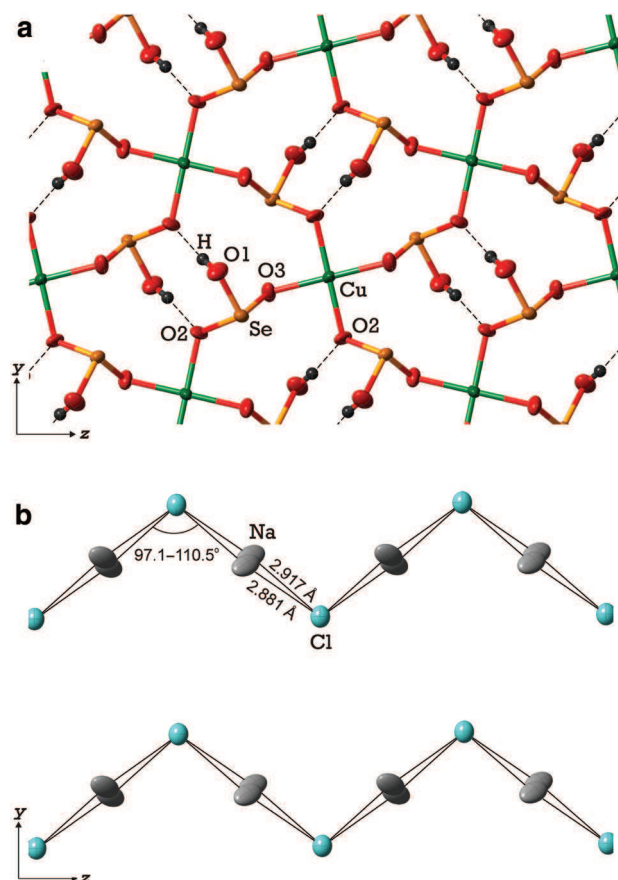
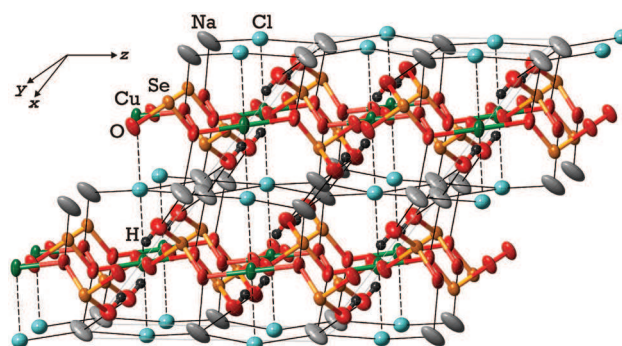
**Tab. 2:** Atomic coordinates, site-occupation factors (SOFs) and displacement parameters ( $\text{\AA}^2$ ) of atoms in the crystal structure  $[\text{NaCl}][\text{Cu}(\text{HSeO}_3)_2]$ .

Atom	x	y	z	$U_{\text{eq}}$	$U_{11}$	$U_{22}$	$U_{33}$	$U_{23}$	$U_{13}$	$U_{12}$
Se	0.16713(2)	0.41354(4)	0.11467(3)	0.01585(8)	0.0205(1)	0.0116(1)	0.0198(1)	0.00158(9)	0.0145(1)	0.00050(9)
Cu	3/4	1/4	0	0.0180(1)	0.0319(3)	0.0103(2)	0.0187(2)	-0.0005(2)	0.0189(2)	-0.0028(2)
Cl	0	0.2461(2)	1/4	0.0271(2)	0.0217(4)	0.0334(6)	0.0243(4)	0.000	0.0129(4)	0.000
O <sub>h1</sub>	0.3996(2)	0.2790(3)	0.0302(3)	0.0278(5)	0.029(1)	0.024(1)	0.035(1)	-0.0110(9)	0.022(1)	-0.0101(9)
O2	0.7484(2)	-0.0146(3)	0.0451(3)	0.0226(4)	0.034(1)	0.0122(9)	0.037(1)	0.0044(8)	0.029(1)	0.0005(8)
O3	0.2755(2)	0.3130(3)	0.3144(3)	0.0230(4)	0.030(1)	0.026(1)	0.0189(9)	0.0072(8)	0.0174(8)	0.0089(9)
Na*	0.5242(4)	0.4802(9)	0.0326(10)	0.0437(13)	0.047(3)	0.029(3)	0.079(5)	-0.017(2)	0.051(4)	-0.017(2)
H	0.350(5)	0.333(8)	0.034(7)	0.069(16)						

\*Site-occupation factor = 0.5.

**Tab. 3:** Selected bond lengths ( $\text{\AA}$ ) and angles (deg) in the crystal structure  $[\text{NaCl}][\text{Cu}(\text{HSeO}_3)_2]$ .

Se–O3	1.671(2)	Na–O <sub>h1</sub>	2.265(7)
Se–O2	1.680(2)	Na–O <sub>h1</sub>	2.290(7)
Se–O <sub>h1</sub>	1.751(2)	Na–O3	2.562(4)
<Se–O>	1.701	Na–Cl	2.881(8)
		Na–Cl	2.918(8)
Cu–O2	1.967(2) 2×		
Cu–O3	1.968(2) 2×	O <sub>h1</sub> –H	0.81(5)
Cu–Cl	2.7954(2) 2×	H–O2	1.85(5)

**Fig. 2:** Projections of the  $[\text{Cu}(\text{HSeO}_3)_2]^0$  layer (a) and the layer of the  $\dots\text{Na-Cl-Na-Cl}\dots$  chains (b) onto the (100) plane.**Fig. 3:** Crystal structure of  $[\text{NaCl}][\text{Cu}(\text{HSeO}_3)_2]$  featuring two-dimensional  $[\text{Cu}(\text{HSeO}_3)_2]^0$  layers with intercalated  $\dots\text{Na-Cl}\dots$  chains.

The linkage between the alternating electroneutral  $[\text{Cu}(\text{HSeO}_3)_2]$  and  $[\text{NaCl}]$  sheets is provided by the Cu–Cl and Na–O bonds (Figure 3). The coordination of Na is five-fold and consists of three O and two Cl atoms.

## Discussion

According to the results of this study, the title compound can be considered as a member of the group of compounds based upon the  $M(\text{HSeO}_3)_2$  layers ( $M^{2+} = \text{Cu}, \text{Co}, \text{Cd}$ ) [23–29]. Crystallographic data and geometrical parameters of the layers are given in Table 4. The prototype structure for this group is  $[\text{Cu}(\text{HSeO}_3)_2]$  [23] that does not have any chemical species separating the copper hydroselenite layers. In other compounds, the interlayer space between the  $[\text{Cu}(\text{HSeO}_3)_2]^0$  layers is occupied by structural units of different complexity. In all Cu compounds, the  $[\text{Cu}(\text{HSeO}_3)_2]^0$  layers have approximately the same linear parameters, except for  $[\text{Cu}(\text{HSeO}_3)_2](\text{H}_2\text{O})_2$ , where the layers are strongly corrugated.

In general, the compound  $[\text{NaCl}][\text{Cu}(\text{HSeO}_3)_2]$  reported herein can be considered as  $[\text{Cu}(\text{HSeO}_3)_2]^0$  intercalated

**Tab. 4:** Crystallographic data for inorganic compounds containing electroneutral [M(HSeO<sub>3</sub>)<sub>2</sub>] layers (M = Cu, Co).

Chemical formula	Space group	a, Å	b, Å/β, °	c, Å	Layer orientation: parameters	References
[Cu(HSeO <sub>3</sub> ) <sub>2</sub> ]	P2 <sub>1</sub> /n	5.766	7.352/93.28	6.447	(101): 8.892 × 7.352 Å <sup>2</sup>	[23]
[Cu(HSeO <sub>3</sub> ) <sub>2</sub> ](H <sub>2</sub> O) <sub>2</sub>	P2 <sub>1</sub> /c	6.279	6.258/90.97	9.091	(100): 9.091 × 6.258 Å <sup>2</sup>	[25]
[(NH <sub>4</sub> )(NO <sub>3</sub> ) <sub>3</sub> ][Cu(HSeO <sub>3</sub> ) <sub>2</sub> ]	Pnma	8.881	24.010/90	7.220	(010): 8.881 × 7.220 Å <sup>2</sup>	[25]
[Mn(H <sub>2</sub> O) <sub>4</sub> Cl <sub>2</sub> ][Cu(HSeO <sub>3</sub> ) <sub>2</sub> ]	Pnma	9.125	18.179/90	7.188	(010): 9.125 × 7.188 Å <sup>2</sup>	[26]
[(NH <sub>4</sub> )Cl][Cu(HSeO <sub>3</sub> ) <sub>2</sub> ]	Pnma	8.975	12.118/90	7.265	(010): 8.975 × 7.265 Å <sup>2</sup>	[27]
[Cu(H <sub>2</sub> O) <sub>4</sub> Cl <sub>2</sub> ][Cu(HSeO <sub>3</sub> ) <sub>2</sub> ]	Pnma	9.149	17.835/90	7.229	(010): 9.149 × 7.229 Å <sup>2</sup>	[28]
[Co(H <sub>2</sub> O) <sub>4</sub> Cl <sub>2</sub> ][Co(HSeO <sub>3</sub> ) <sub>2</sub> ]	Pnma	9.338	17.345/90	7.320	(010): 9.338 × 7.320 Å <sup>2</sup>	[29]
[NaCl][Cu(HSeO <sub>3</sub> ) <sub>2</sub> ]	C2/c	13.987	7.259/127.05	9.042	(100): 9.042 × 7.259 Å <sup>2</sup>	this work

with the NaCl layers consisting of one-dimensional –Na–Cl–Na–Cl–chains.

**Acknowledgments:** VMK and SVK have been supported in this work by the Russian Science Foundation (grant 14-17-00071). This work was carried out under the framework of the Multi-InMaDe project supported by the ANR (Grant ANR 2011-JS-0800301). The Fonds Européen de Développement Régional (FEDER), CNRS, Région Nord Pas-de-Calais, and Ministère de l'Éducation Nationale de l'Enseignement Supérieur et de la Recherche are acknowledged for funding the X-ray diffractometers. VMK also thanks l'Ambassade de France en Russie and l'Agence Campus France (Contract Nos. 768231K, 779116K, 794852B, 808399A, and 808400J) for the partial support of this work.

## References

- [1] S. Hu, M. Johnsson, Synthesis and crystal structure of two synthetic oxofluoride framework compounds – Co<sub>2</sub>TeO<sub>3</sub>F<sub>2</sub> and Co<sub>2</sub>SeO<sub>3</sub>F<sub>2</sub>, *Dalton Trans.* **2012**, 41, 12786.
- [2] P. S. Berdonosov, O. Janson, A. V. Olenev, S. V. Krivovichev, H. Rosner, V. A. Dolgikh, A. A. Tselin, Crystal structures and variable magnetism of PbCu<sub>2</sub>(XO<sub>3</sub>)<sub>2</sub>Cl<sub>2</sub> with X = Se, Te, *Dalton Trans.* **2013**, 42, 9547.
- [3] Y. H. Kim, D. W. Lee, K. M. Ok, α-ScVSe<sub>2</sub>O<sub>8</sub>, β-ScVSe<sub>2</sub>O<sub>8</sub>, and ScVTe<sub>2</sub>O<sub>8</sub>: new quaternary mixed metal oxides composed of only second-order Jahn-Teller distortive cations. *Inorg. Chem.* **2013**, 52, 11450.
- [4] Y. Shin, D. W. Lee, K. Y. Choi, H.-J. Koo, K. M. Ok, VSb(SeO<sub>3</sub>)<sub>4</sub>, first selenite containing V<sup>3+</sup> cation: synthesis, structure, characterization, magnetic properties, and calculations. *Inorg. Chem.* **2013**, 52, 14224.
- [5] Y. H. Kim, D. W. Lee, K. M. Ok, Noncentrosymmetric YVSe<sub>2</sub>O<sub>8</sub> and centrosymmetric YVTe<sub>2</sub>O<sub>8</sub>: macroscopic centricities influenced by the size of lone pair cation linkers. *Inorg. Chem.* **2014**, 53, 1250.
- [6] T. Eaton, J. Lin, J. N. Cross, J. T. Stritzinger, T. E. Albrecht-Schmitt, Th(VO<sub>3</sub>)<sub>2</sub>(SeO<sub>3</sub>) and Ln(VO<sub>3</sub>)<sub>2</sub>(IO<sub>3</sub>) (Ln = Ce, Pr, Nd, Sm, and Eu): unusual cases of aliovalent substitution. *Chem. Comm.* **2014**, 50, 3668.
- [7] S. Hu, M. Johnsson, J. M. Law, J. L. Bettis, M.-H. Whangbo, R. K. Kremer, Crystal structure and magnetic properties of FeSeO<sub>3</sub>F – alternating antiferromagnetic S = 5/2 chains. *Inorg. Chem.* **2014**, 53, 4250.
- [8] X.-L. Cao, F. Kong, C.-L. Hu, X. Xu, J.-G. Mao, Pb<sub>2</sub>V<sub>6</sub>O<sub>16</sub>(SeO<sub>3</sub>)<sub>3</sub>(H<sub>2</sub>O), Pb<sub>2</sub>VO<sub>2</sub>(SeO<sub>3</sub>)<sub>2</sub>Cl, and PbVO<sub>2</sub>(SeO<sub>3</sub>)F: new lead(II)-vanadium(V) mixed-metal selenites featuring novel anionic skeletons. *Inorg. Chem.* **2014**, 53, 8816.
- [9] K. L. Kilminster, F. J. Lincoln, B. W. Skelton, A. H. White, A barium vanadium(V) selenite hydrate, Ba(VO<sub>2</sub>)<sub>2</sub>(SeO<sub>3</sub>)<sub>2</sub>·H<sub>2</sub>O: a novel 3D polymer of cross-linked sheets with embedded ...V-O-V... 2<sub>1</sub> helices. *Austr. J. Chem.* **2014**, 67, 1878.
- [10] J. H. Koffer, J. H. Olshansky, M. D. Smith, K. J. Hernandez, M. Zeller, G. M. Ferrence, J. Schrier, A. J. Norquist, Formation principles for templated vanadium selenite oxalates. *Cryst. Growth Des.* **2013**, 13, 4504.
- [11] A. Aliev, V. M. Kovrugin, M. Colmont, C. Terry, M. Huve, O. I. Siidra, S. V. Krivovichev, O. Mentre, Revised bismuth chloroselenite system: evidence of a noncentrosymmetric structure with a giant unit cell. *Cryst. Growth Des.* **2014**, 14, 3026.
- [12] J. H. Olshansky, K. J. Wiener, M. D. Smith, A. Nourmahnad, M. J. Charles, M. Zeller, J. Schrier, A. J. Norquist, Formation principles for vanadium selenites: the role of pH on product composition. *Inorg. Chem.* **2014**, 53, 12027.
- [13] M. Gemmi, I. Campostrini, F. Demartin, T. E. Gorelik, C. M. Gramaccioli, Structure of the new mineral sarrabusite, Pb<sub>5</sub>CuCl<sub>4</sub>(SeO<sub>3</sub>)<sub>4</sub>, solved by manual electron-diffraction tomography. *Acta Crystallogr.* **2012**, B68, 15.
- [14] S. V. Krivovichev, S. K. Filatov, L. P. Vergasova, The crystal structure of ilinskite, NaCu<sub>5</sub>O<sub>2</sub>(SeO<sub>3</sub>)<sub>2</sub>Cl<sub>3</sub>, and review of mixed-ligand Cu<sub>m</sub>Cl<sub>n</sub> coordination geometries in minerals and inorganic compounds. *Mineral. Petrol.* **2013**, 107, 235.
- [15] R. R. Shuvalov, L. P. Vergasova, T. F. Semenova, S. K. Filatov, S. V. Krivovichev, O. I. Siidra, N. S. Rudashevsky, Prewittite, KPb<sub>1.5</sub>Cu<sub>6</sub>Zn(SeO<sub>3</sub>)<sub>2</sub>O<sub>2</sub>Cl<sub>10</sub>, a new mineral from Tolbachik fumaroles, Kamchatka Peninsula, Russia: description and crystal structure. *Amer. Mineral.* **2013**, 98, 463.
- [16] S. J. Mills, A. R. Kampf, A. G. Christy, R. M. Housley, B. Thorne, Y.-S. Chen, I. M. Steele, Favreuite, a new selenite mineral from the El Dragon mine, Bolivia. *Eur. J. Mineral.* **2014**, 26, 771.
- [17] L. P. Vergasova, T. F. Semenova, S. V. Krivovichev, S. K. Filatov, A. A. Zolotarev, Jr., V. V. Ananiev, Nicksobolevite, Cu<sub>7</sub>(SeO<sub>3</sub>)<sub>2</sub>O<sub>2</sub>Cl<sub>6</sub>, a new complex copper oxoselenite chloride from Tolbachik fumaroles, Kamchatka peninsula, Russia. *Eur. J. Mineral.* **2014**, 26, 439.

- [18] Z. Mayerová, M. Johnsson, S. Lidin, Lone-pair interfaces that divide inorganic materials into ionic and covalent parts. *Angew. Chem. Int. Ed.* **2006**, *45*, 5602.
- [19] V. Jo, M. K. Kim, D. W. Lee, I. W. Shim, K. M. Ok, Lone pairs as chemical scissors in new antimony oxychlorides,  $\text{Sb}_2\text{ZnO}_3\text{Cl}_2$  and  $\text{Sb}_{16}\text{Cd}_8\text{O}_{25}\text{Cl}_{14}$ . *Inorg. Chem.* **2010**, *49*, 2990.
- [20] S. Hu, M. Johnsson, Synthesis and crystal structure of  $\text{Fe}_6\text{Ca}_2(\text{SeO}_3)_9\text{Cl}_4$  – a porous oxohalide. *Dalton Trans.* **2013**, *42*, 7859.
- [21] I. Zimmermann, M. Johnsson, A synthetic route toward layered materials: introducing stereochemically active lone-pairs into transition metal oxohalides. *Cryst. Growth Des.* **2014**, *14*, 5252.
- [22] I. Zimmermann, A. Corgnet, M. Johnsson, S. Lidin, Synthesis and crystal structure of a series of incommensurately modulated composite oxohalide compounds. *Dalton Trans.* **2014**, *43*, 15812.
- [23] H. Effenberger,  $\text{Cu}(\text{SeO}_2\text{OH})_2$ : synthesis and crystal structure. *Z. Kristallogr.* **1985**, *173*, 267.
- [24] L. Hiltunen, M. Leskela, L. Niinisto, M. Tammenmaa, Crystal structure of copper hydrogenselenite monohydrate. *Acta Chem. Scand.* **1985**, *A39*, 809.
- [25] A. M. Lafront, J. C. Trombe, 'Layered hydrogenselenites'. I. Synthesis, structure redetermination of  $\text{Cu}(\text{HSeO}_3)_2(\text{H}_2\text{O})_2$  and determination of  $(\text{Cu}(\text{HSeO}_3)_2(\text{NO}_3)_2)^{2-} \cdot 2(\text{NH}_4)^+$ ,  $\text{NH}_4\text{NO}_3$ . Structural relationships of these complexes with  $(\text{Cu}(\text{HSeO}_3)_2)$ . *Inorg. Chim. Acta* **1995**, *234*, 19.
- [26] A. M. Lafront, J. C. Trombe, J. Bonvoisin, 'Layered hydrogenselenites'. II. Synthesis, structure studies and magnetic properties of a novel series of bimetallic hydrogenselenites:  $\text{Cu}(\text{HSeO}_3)_2\text{MCl}_2(\text{H}_2\text{O})_4$ ,  $\text{M}(\text{II}) = \text{Mn}, \text{Co}, \text{Ni}, \text{Cu}, \text{Zn}$ . *Inorg. Chim. Acta* **1995**, *238*, 15.
- [27] J. C. Trombe, A. M. Lafront, J. Bonvoisin, Synthesis, structure and magnetic measurement of a new layered copper hydrogenselenite:  $(\text{Cu}(\text{HSeO}_3)_2) \cdot (\text{NH}_4)\text{Cl}$ . *Inorg. Chim. Acta* **1997**, *262*, 47.
- [28] W. T. A. Harrison, M. G. Johnston, Syntheses and structures of two selenite chloride hydrates:  $\text{Co}(\text{HSeO}_3)\text{Cl} \cdot 3(\text{H}_2\text{O})$  and  $\text{Cu}(\text{HSeO}_3)\text{Cl} \cdot 2(\text{H}_2\text{O})$ . *Z. Anorg. Allg. Chem.* **2000**, *626*, 2487.
- [29] M. G. Johnston, W. T. A. Harrison, Cobalt hydrogen selenite chloride dihydrate,  $\text{Co}(\text{HSeO}_3)\text{Cl} \cdot 2(\text{H}_2\text{O})$ . *Acta Crystallogr.* **2003**, *E59*, i62.
- [30] V. M. Kovrugin, M. Colmont, O. Mentré, O. I. Siidra, S. V. Krivovichev, Dimers of oxocentered  $[\text{OCu}_4]^{6+}$  tetrahedra in two novel copper selenite chlorides,  $\text{K}[\text{Cu}_3\text{O}](\text{SeO}_3)_2\text{Cl}$  and  $\text{Na}_2[\text{Cu}_7\text{O}_2](\text{SeO}_3)_4\text{Cl}_4$ , and related minerals and inorganic compounds. *Mineral. Mag.* **2015**, submitted.
- [31] G. M. Sheldrick, A short history of SHELX. *Acta Crystallogr.* **2008**, *A64*, 112.
- [32] J. B. Parise, B. G. Hyde, The structure of atacamite and its relationships to spinel. *Acta Crystallogr.* **1986**, *B42*, 1277.
- [33] O. I. Siidra, S. V. Krivovichev, T. Armbruster, S. K. Filatov, I. V. Pekov, The crystal structure of leningradite,  $\text{PbCu}_3(\text{VO}_4)_2\text{Cl}_2$ . *Can. Mineral.* **2007**, *45*, 445.



## A-IX

### **Dimers of oxocentered $[\text{OCu}_4]^{6+}$ tetrahedra in two novel copper selenite chlorides, $\text{K}[\text{Cu}_3\text{O}](\text{SeO}_3)_2\text{Cl}$ and $\text{Na}_2[\text{Cu}_7\text{O}_2](\text{SeO}_3)_4\text{Cl}_4$ , and related minerals and inorganic compounds**

Vadim M. Kovrugin, Marie Colmont, Olivier Mentré, Oleg I. Siidra, and Sergey V. Krivovichev

Published in: *Mineralogical Magazine*, accepted.

Reprinted with kind permission from The Mineralogical Society.



**Dimers of oxocentered [OCu<sub>4</sub>]<sup>6+</sup> tetrahedra in two novel copper selenite chlorides,  
K[Cu<sub>3</sub>O](SeO<sub>3</sub>)<sub>2</sub>Cl and Na<sub>2</sub>[Cu<sub>7</sub>O<sub>2</sub>](SeO<sub>3</sub>)<sub>4</sub>Cl<sub>4</sub>, and related minerals and inorganic compounds**

Vadim M. Kovrugin<sup>1,2</sup>, Marie Colmont<sup>2</sup>, Olivier Mentré<sup>2</sup>, Oleg I. Siidra<sup>1</sup>, Sergey V. Krivovichev<sup>1,\*</sup>

<sup>1</sup> *Department of Crystallography, St. Petersburg State University, Universitetskaya nab. 7/9, 199034 St. Petersburg, Russia*

<sup>2</sup> *UCCS, ENSCL, Université Lille 1, CNRS, UMR 8181, 59652 Villeneuve d'Ascq, France*

\* Corresponding author: s.krivovichev@spbu.ru

## Abstract

Two novel copper selenite chlorides,  $\text{K}[\text{Cu}_3\text{O}](\text{SeO}_3)_2\text{Cl}$  (**I**) and  $\text{Na}_2[\text{Cu}_7\text{O}_2](\text{SeO}_3)_4\text{Cl}_4$  (**II**), have been synthesized by the chemical vapor transport reactions (CVT method). The crystal structures have been solved by direct methods and refined by least-square techniques: **I** is triclinic, space group  $P\bar{1}$ ,  $a = 7.6821(5)$  Å,  $b = 8.1179(5)$  Å,  $c = 8.7836(6)$  Å,  $\alpha = 113.193(3)^\circ$ ,  $\beta = 108.735(4)^\circ$ ,  $\gamma = 98.245(4)^\circ$ ,  $V = 453.32(5)$  Å<sup>3</sup>,  $R_1 = 0.0481$  for 1210 unique reflections with  $|F_o| \geq 4\sigma_F$ ; **II** is triclinic, space group  $P\bar{1}$ ,  $a = 7.4362(6)$  Å,  $b = 8.3361(7)$  Å,  $c = 9.1343(11)$  Å,  $\alpha = 110.277(6)^\circ$ ,  $\beta = 106.212(6)^\circ$ ,  $\gamma = 105.158(4)^\circ$ ,  $V = 467.94(8)$  Å<sup>3</sup>,  $R_1 = 0.0265$  for 2498 unique reflections with  $|F_o| \geq 4\sigma_F$ . The structures of **I** and **II** can be described in terms of dimers of copper oxocentered tetrahedra. In the crystal structure of **I**, two  $(\text{OCu}_4)^{6+}$  tetrahedra share a common  $\text{Cu}\cdots\text{Cu}$  edge to form the  $[\text{O}_2\text{Cu}_6]^{8+}$  dimer, whereas the crystal structure of **II** is based upon two  $(\text{OCu}_4)^{6+}$  tetrahedra linked together by one common Cu atom resulting in the formation of the  $[\text{O}_2\text{Cu}_7]^{10+}$  dimer. A comparison with related minerals and inorganic compounds is given.

*Keywords:* crystal structure, oxocentered tetrahedra, lone electron pair, stereoactivity, euchlorine, fedotovite, prewittite, burnsite



## Introduction

The crystal chemistry of selenium-containing natural and synthetic oxocompounds of copper is of special interest owing to the specific structural features of both  $\text{Cu}^{2+}$  and  $\text{Se}^{4+}$  cations.  $\text{Cu}^{2+}$  cations may possess different and flexible coordination geometries (Burns and Hawthorne, 1995a, b; Rosner *et al.*, 2007; Melník *et al.*, 2011; Burrows *et al.*, 2012; Krivovichev *et al.*, 2012), while  $\text{Se}^{4+}$  cations form asymmetric  $(\text{SeO}_3)^{2-}$  groups due to the stereochemically active behaviour of the  $s^2$  lone electron pairs resulting in structurally complex architectures and interesting physical properties (Mao *et al.*, 2008; Zhang *et al.*, 2010; Berdonosov *et al.*, 2013).

Most of the naturally occurring copper selenite chlorides have been reported from the fumaroles of the Tolbachik volcano (Kamchatka peninsula, Russia): ilinskite,  $\text{Na}[\text{Cu}_5\text{O}_2](\text{SeO}_3)_2\text{Cl}_3$  (Vergasova *et al.*, 1997; Krivovichev *et al.*, 2012), georgbokiite,  $\alpha\text{-}[\text{Cu}_5\text{O}_2](\text{SeO}_3)_2\text{Cl}_2$  (Krivovichev *et al.*, 1999a), chloromenite,  $[\text{Cu}_9\text{O}_2](\text{SeO}_3)_4\text{Cl}_6$  (Vergasova *et al.*, 1999), burnsite,  $\text{KCd}[\text{Cu}_7\text{O}_2](\text{SeO}_3)_2\text{Cl}_9$  (Burns *et al.*, 2002; Krivovichev *et al.*, 2002), allochalcoseelite,  $\text{Cu}^+[\text{PbCu}^{2+}_5\text{O}_2](\text{SeO}_3)_2\text{Cl}_5$  (Krivovichev *et al.*, 2006), parageorgbokiite,  $\beta\text{-}[\text{Cu}_5\text{O}_2](\text{SeO}_3)_2\text{Cl}_2$  (Krivovichev *et al.*, 2007), prewittite,  $\text{KPb}_{0.5}\text{Cu}[\text{PbCu}_5\text{O}_2]\text{Zn}(\text{SeO}_3)_2\text{Cl}_{10}$  (Shuvalov *et al.*, 2013), and nicksobolevite,  $[\text{Cu}_7\text{O}_2](\text{SeO}_3)_2\text{Cl}_6$  (Vergasova *et al.*, 2014). The crystal structures of these mineral species contain so-called “additional” or “extra” oxygen atoms, which are coordinated solely by copper atoms to form oxocentered  $(\text{OCu}_4)^{6+}$  tetrahedra. A number of experimental and theoretical works on structural description of anion-centered tetrahedra in inorganic compounds have been recently summarized by Krivovichev *et al.* (2013).

According to the original idea proposed by Filatov *et al.* (1992), polynuclear clusters based upon the oxocentered copper tetrahedra can perform the role of transport agents of copper in high-temperature environments in volcanic fumaroles. Further experimental works on preparation of mineral analogues by using of chemical vapor transport reactions (CVT method) provided additional (though indirect) evidence in favor of this hypothesis and demonstrated the suitability of the CVT method for the synthesis of copper oxoselenites with various structural architectures (Millet *et al.*, 2001; Krivovichev *et al.*, 2004; Becker *et al.*, 2007; Berdonosov *et al.*, 2009; Zhang *et al.*, 2010).

In this paper, we report on the syntheses and crystal structures of two novel copper oxoselenite chlorides,  $\text{K}[\text{Cu}_3\text{O}](\text{SeO}_3)_2\text{Cl}$  (**I**) and  $\text{Na}_2[\text{Cu}_7\text{O}_2](\text{SeO}_3)_4\text{Cl}_4$  (**II**), that have been obtained during exploration of synthetic copper selenite chloride systems close to ilinskite and prewittite. The structures of the new compounds are based upon topologically different types of dimers of  $[\text{OCu}_4]^{6+}$  tetrahedra, and herein we provide a short review of related minerals and inorganic compounds.

## Experimental

### *Synthesis*

Single crystals of two novel copper selenite chlorides,  $\text{K}[\text{Cu}_3\text{O}](\text{SeO}_3)_2\text{Cl}$  (**I**) and  $\text{Na}_2[\text{Cu}_7\text{O}_2](\text{SeO}_3)_4\text{Cl}_4$  (**II**), have been prepared by the CVT method. Mixtures of  $\text{CuO}$ ,  $\text{CuCl}_2$ ,  $\text{SeO}_2$ , and  $\text{KCl}$  for **I** ( $\text{NaCl}$  for **II**) taken in the 4:1:2:3 molar ratio were loaded into a fused silica tube (*ca.* 15 cm), which was evacuated to  $10^{-2}$  mbar before sealing. The tubes were placed horizontally into a tubular two-zone furnace, and heated to  $500^\circ$ . The temperature difference between the source and deposition zones of the tube was about  $50^\circ\text{C}$ . After three days, the tubes were cooled down to room temperature over 24 hours. Tiny rifle green block-shaped crystals of **I** and **II** were observed in the middle parts of tubes.

### *X-ray diffraction single-crystal analysis*

Crystals selected for the X-ray data collection were mounted on glass fibers, and studied on a Bruker X8 APEX II three-circle diffractometer equipped with a microfocus X-ray tube with the  $\text{MoK}_\alpha$  radiation at 50 kV and 40 mA. The unit-cell parameters ([Table 1](#)) were refined by the least-squares techniques. The data were integrated and corrected for absorption using a multiscan type model implemented in the Bruker programs APEX and SADABS.

The crystal structures of **I** and **II** have been solved by direct methods in the space group  $P\bar{1}$ , and refined using least-squares techniques to the  $R_1$  value of 0.048 for **I** and 0.027 for **II**, calculated for 1210 and 2498 observed unique reflections for **I** and **II**, respectively, using the SHELXL ([Sheldrick, 2008](#)) program package. Atomic coordinates and displacement parameters are given in [Tables 2 and 3](#); selected interatomic

distances are in [Tables 4 and 5](#). The result of bond-valence analysis for **I** and **II** is given in [Tables 6 and 7](#). All empirical parameters required for bond-valence calculations were taken from [\(Brese and O’Keeffe 1991\)](#). In both structures the values of bond-valence sums of Cl anions are rather low (0.53 v.u. for Cl1 in **I**; 0.69 v.u. and 0.70 v.u. for Cl1 and Cl2 in **II**, respectively), which is typical for copper oxoselenite chlorides [\(Krivovichev \*et al.\*, 2012\)](#). Additional structural information is provided in the Supporting Information (CIF).

## Results

### *Cation polyhedra and their arrangement*

The review of the mixed-ligand  $\text{CuO}_m\text{Cl}_n$  atomic environments of  $\text{Cu}^{2+}$  cations was given in [\(Krivovichev \*et al.\*, 2012\)](#). The coordination polyhedra of  $\text{Cu}^{2+}$  cations observed in the crystal structures of **I** and **II** have been already described in other natural and synthetic copper compounds.

The structure of **I** contains three symmetrically independent Cu sites ([Fig. 1a](#)). The Cu1 site is surrounded by four O and one Cl atoms to form an unusual distorted  $[\text{CuO}_4\text{Cl}]^{7-}$  trigonal bipyramid with the O7, O2 and Cl1 atoms forming an equatorial triangular plane. This type of coordination geometry,  $[(2\text{O}+\text{Cl})+2\text{O}]$ , has previously been reported for the structure of  $\beta\text{-Cu}_3(\text{SeO}_3)_2\text{Cl}_2$  [\(Becker \*et al.\*, 2007\)](#). The Cu1–O bond lengths vary from 1.892 Å to 2.144 Å; the Cu1–Cl1 bond length is equal to 2.400 Å. The Cu2 atom has a typical planar-square  $[\text{CuO}_4]^{6-}$  coordination, which had been observed, *e.g.* in the structure of francisite,  $[\text{Cu}_3\text{BiO}_2](\text{SeO}_3)_2\text{Cl}$  [\(Pring \*et al.\*, 1990\)](#). Four oxygen atoms are located at a distance from the Cu2 atom ranging between 1.932 Å and 2.003 Å. The coordination polyhedron of Cu3 can be described as a distorted  $[(4\text{O})+(\text{O}+\text{Cl})]$  octahedron, and is similar to that observed in the crystal structures of georgbokiite,  $\alpha\text{-}[\text{Cu}_5\text{O}_2](\text{SeO}_3)_2\text{Cl}_2$  [\(Krivovichev \*et al.\*, 1999a\)](#), kamchatkite,  $\text{K}[\text{Cu}_3\text{O}](\text{SO}_4)_2\text{Cl}$  [\(Varaksina \*et al.\*, 1990\)](#), and nabokoite,  $\text{K}_2\text{Cu}_7(\text{TeO}_4)(\text{SO}_4)_5\text{Cl}$  [\(Pertlik and Zemmann, 1988\)](#). The average  $\langle\text{Cu3-O}_{\text{eq}}\rangle$  bond length within the equatorial plane of the octahedron is 1.952 Å. The apical O7 and Cl1 atoms are located at 2.749 Å and 3.046 Å from the Cu3 site, respectively. Various Cu coordination polyhedra are combined into layers parallel to (001) ([Fig. 2a](#)). The structure of **I** contains two symmetrically independent  $\text{Se}^{4+}$  cations that form the

(SeO<sub>3</sub>)<sup>2-</sup> triangular pyramids with Se located at its apical corner and a stereoactive lone pair acting as a complementary ligand. The average <Se–O> distance equals 1.687 Å and 1.701 Å for the Se1 and Se2 sites, respectively. The K<sup>+</sup> cation is coordinated by seven O<sup>2-</sup> and two Cl<sup>-</sup> anions in a distorted arrangement (Fig. 1a).

In the crystal structure of **II**, there are four symmetrically independent Cu sites (Fig. 1b). The Cu1 site forms a [CuO<sub>4</sub>]<sup>6-</sup> square with the average <Cu1–O> bond length of 1.940 Å, similar to the Cu2 site in the structure of **I**. The Cu2 and Cu4 sites are coordinated by three O (<Cu2–O> = 1.934 Å, <Cu4–O> = 1.945 Å) and one Cl atom (Cu2–Cl2 = 2.363 Å, Cu4–Cl1 = 2.284 Å) to form [CuO<sub>3</sub>Cl]<sup>5-</sup> planar squares. The same [(3O+Cl)] coordination has been observed previously in the crystal structure of ilinskite, Na[Cu<sub>5</sub>O<sub>2</sub>](SeO<sub>3</sub>)<sub>2</sub>Cl<sub>3</sub> (Vergasova *et al.*, 1997; Krivovichev *et al.*, 2012). The Cu3 site in the crystal structure of **II** has a triangular bipyramidal [(2O+Cl)+2O] coordination with the bond Cu3–O bond lengths in range 1.902–2.156 Å, and the Cu3–Cl2 distance of 2.407 Å. The copper polyhedra form the arrangement shown in Fig. 2b. Two symmetrically independent Se sites form (SeO<sub>3</sub>)<sup>2-</sup> trigonal pyramids with the average <Se–O> bond lengths of 1.699 Å and 1.697 Å for Se1 and Se2, respectively. The symmetrically unique Na<sup>+</sup> cation is surrounded by six O<sup>2-</sup> and one Cl<sup>-</sup> anion. The Na1–O6 contact corresponds to a weak interaction and its distance is rather long (3.169 Å), but it helps to form an approximately triangular prismatic oxygen environment of Na<sup>+</sup>.

#### *Dimers of [OCu<sub>4</sub>]<sup>6+</sup> tetrahedra and their linkage*

By analogy with many copper minerals of fumarolic origin (see, e.g. Pekov *et al.* (2013a,b)), the analysis of the crystal structures of **I** and **II** in terms of oxocentered tetrahedra seems appropriate to describe the structural organization and to reveal relations between different structures with similar chemical composition.

In the crystal structure of **I**, two [OCu<sub>4</sub>]<sup>6+</sup> tetrahedra share a common Cu··Cu edge to form the [O<sub>2</sub>Cu<sub>6</sub>]<sup>8+</sup> dimer shown in Fig. 3a. The selenite groups and Cl atoms surround these dimers to form the {[O<sub>2</sub>Cu<sub>6</sub>](SeO<sub>3</sub>)<sub>4</sub>Cl<sub>2</sub>}]<sup>2-</sup> structural units shown in Fig. 3b, which are further interconnected into layers parallel to (001) (Fig. 4). The interlayer space is occupied by the K<sup>+</sup> cations. The (SeO<sub>3</sub>)<sup>2-</sup> triangular

pyramids are attached to the  $[\text{O}_2\text{Cu}_6]^{8+}$  finite cluster in such a way that four selenite triangular O–O–O bases are parallel to the four triangular Cu–Cu–Cu faces of the oxocentered tetrahedra (Fig. 4b). This mode of atomic interactions between oxocentered tetrahedra and cation-centered groups is known as a ‘face-to-face’ principle and it had been previously reported by Krivovichev and Filatov (1999) and Krivovichev *et al.* (1999b). It is of interest that the same geometry of linkage between copper oxocentered dimers and selenite triangular pyramids have been observed previously in the monoclinic polymorph of  $\text{Cu}[\text{Cu}_3\text{O}](\text{SeO}_3)_3\text{--I}$  (Effenberger and Pertlik, 1986).

It is noteworthy that, despite of the similarity in their similar chemical formulae, kamchatkite,  $\text{K}[\text{Cu}_3\text{O}](\text{SO}_4)_2\text{Cl}$  (Varaksina *et al.*, 1990), is not isotypic to the compound **I**,  $\text{K}[\text{Cu}_3\text{O}](\text{SeO}_3)_2\text{Cl}$ . In contrast to the latter, the former is based upon chains of corner-sharing  $(\text{OCu}_4)^{6+}$  tetrahedra.

The crystal structure of **II** is based upon the  $[\text{O}_2\text{Cu}_7]^{10+}$  dimeric units shown in Fig. 3c and formed by two  $(\text{OCu}_4)^{6+}$  tetrahedra sharing a common Cu atom. The dimers are linked by the  $(\text{SeO}_3)^{2-}$  groups to produce layers parallel to (100) with interlayer space filled by the  $\text{Na}^+$  cations,  $\text{Cl}^-$  anions and lone electron pairs of the  $\text{Se}^{4+}$  cations (Fig. 5). The  $[\text{O}_2\text{Cu}_7]^{10+}$  dimers are coordinated by selenite groups and Cl atoms to form  $\{[\text{O}_2\text{Cu}_7](\text{SeO}_3)_4\text{Cl}_4\}^{2-}$  structural unit shown in Fig. 3d. Note that the selenite anions play different structural roles in the crystal structure of **II**. Whereas the  $(\text{Se}_2\text{O}_3)$  triangular pyramids is in ‘face-to-face’ orientation relative to  $(\text{O}_1\text{Cu}_4)$  tetrahedra, the  $(\text{Se}_1\text{O}_3)$  groups are located in between the copper oxoselenite clusters and provide their linkage into the metal-oxide layers through the formation of the Se–O–Cu links.

## Discussion

The novel compounds **I** and **II** reported herein are the new members of the structural family of minerals and synthetic compounds that are based upon the dimers composed from  $(\text{OCu}_4)^{6+}$  groups (Krivovichev *et al.*, 2013) (Table 8). Fig. 6 provides an overview of the observed coordination environments of the dimers of oxocentered tetrahedra in the crystal structures of related copper minerals and synthetic compounds.

The structures based upon dimers of edge-sharing oxocentered tetrahedra have been observed previously in the crystal structures of two polymorphs of  $\text{Cu}[\text{Cu}_3\text{O}](\text{SeO}_3)_3$  (Effenberger and Pertlik, 1986). Here the

$[\text{O}_2\text{Cu}_6]^{8+}$  dimers are surrounded by the selenite groups and Cu atoms not bonded to “additional” O atoms. The coordination environments of the dimers in the two polymorphs are different. In the monoclinic structure, four selenite anions attach to four faces of the  $(\text{OCu}_4)^{6+}$  tetrahedra in a ‘face-to-face’ orientation (Fig. 6a), very similar to the arrangement observed in **I**. In the crystal structure of the triclinic phase, in addition to the four ‘face-to-face’-attached selenite groups, the dimers are surrounded by two other selenite groups each (Fig. 6b).

Euchlorine,  $\text{NaK}[\text{Cu}_3\text{O}](\text{SO}_4)_3$  (Scordari and Stasi, 1990), and fedotovite,  $\text{K}_2[\text{Cu}_3\text{O}](\text{SO}_4)_3$  (Starova *et al.*, 1991), were the first minerals described as based upon the  $[\text{O}_2\text{Cu}_6]^{8+}$  dimers. In the crystal structures of these minerals, four sulfate tetrahedra are ‘face-to-face’ attached to the dimers, whereas two other sulfate tetrahedra groups provide their linkage in two dimensions (Fig. 6d). Very similar copper oxosulfate clusters have recently been observed in the crystal structures of novel Cu metal–organic polymers:  $(\text{NMe}_2\text{H}_2)_4[\text{Cu}_6\text{O}_2](\text{SO}_4)_6(\text{DMF})_4$  (Fig. 6e) and  $(\text{NMe}_2\text{H}_2)_4[\text{Cu}_6\text{O}_2](\text{SO}_4)_6(\text{DMF})_2$  (Fig. 6f) (Burrows *et al.*, 2012).

In the crystal structure of prewittite,  $\text{KPb}_{0.5}\text{Cu}[\text{PbCu}_5\text{O}_2]\text{Zn}(\text{SeO}_3)_2\text{Cl}_{10}$  (Shuvalov *et al.*, 2013), two adjacent heterometallic oxocentered  $(\text{OCu}_3\text{Pb})^{6+}$  tetrahedra share of a common  $\text{Cu}\cdots\text{Pb}$  edge to form the  $[\text{O}_2\text{Cu}_5\text{Pb}]^{8+}$  dimer (Fig. 6c). Two selenite groups are in ‘face-to-face’ position relative to the oxocentered tetrahedra.

The  $[\text{O}_2\text{Cu}_7]^{10+}$  dimer formed by two corner-sharing  $(\text{OCu}_4)^{6+}$  tetrahedra has been described in the crystal structure of burnsite,  $\text{KCd}[\text{Cu}_7\text{O}_2](\text{SeO}_3)_2\text{Cl}_9$  (Burns *et al.*, 2002; Krivovichev *et al.*, 2002), and the compound **II** described here is the second example. In contrast to the crystal structure of **II**, where the selenite groups are attached to the lateral faces of the oxocentered tetrahedra (Fig. 6g), in the structure of burnsite, selenite groups are in the ‘face-to-face’ orientation relative to the opposite  $\text{Cu}\text{--}\text{Cu}\text{--}\text{Cu}$  faces of the dimer so that they are parallel to each other (Fig. 6h). The resulting copper oxoselenite complexes are linked via  $\text{Cu}\text{--}\text{O}$  bonds into a 3D-framework that contains large channels filled by the  $(\text{KCl}_6)^{5-}$  triangular prisms and the  $(\text{CdCl}_6)^{4-}$  octahedra.

The interesting case of a  $[\text{O}_4\text{Cu}_{13}]^{18+}$  tetramer formed by successive linkage of two  $[\text{O}_2\text{Cu}_7]^{10+}$  dimers has recently been reported for nicksobolevite,  $\text{Cu}[\text{Cu}_{13}\text{O}_4](\text{SeO}_3)_4\text{Cl}_{12}$  (Vergasova *et al.*, 2014). The tetramers are interconnected by selenite groups and additional copper cations into ladder-like layers.

The observed complex clusters consisting of oxocentered tetrahedral units surrounded by selenite groups form metal-oxide backbones of many copper oxoselenite chlorides. Whereas Cu coordination is diverse and is changing from structure to structure, the oxocentered units appear to be relatively robust. Their existence and frequent occurrence in different structures provides an indirect evidence for the importance of such units as pre-nucleation building blocks existing in gaseous media as it occurs in volcanic fumaroles or evacuated silica ampoules used in the CVT method. The two new compounds,  $\text{K}[\text{Cu}_3\text{O}](\text{SeO}_3)_2\text{Cl}$  and  $\text{Na}_2[\text{Cu}_7\text{O}_2](\text{SeO}_3)_4\text{Cl}_4$ , reported herein, are very similar in their chemistry and structure to the natural copper oxoselenite chlorides and one may predict their possible formation in fumarolic environments under appropriate physical and chemical conditions.

## Acknowledgements

This work was carried out under the framework of the Multi-InMaDe project supported by the ANR (Grant ANR 2011-JS-08 00301). The Fonds Européen de Développement Régional (FEDER), CNRS, Région Nord Pas-de-Calais, and Ministère de l'Education Nationale de l'Enseignement Supérieur et de la Recherche are acknowledged for funding the X-ray diffractometers. VMK, OIS and SVK have been supported in this work by the Russian Science Foundation (grant 14-17-00071).

## References

- Becker, R., Berger, H. and Johnsson, M. (2007) Monoclinic  $\text{Cu}_3(\text{SeO}_3)_2\text{Cl}_2$ : an oxohalide with an unusual  $\text{CuO}_4\text{Cl}$  trigonal-bipyramidal coordination. *Acta Crystallographica*, **C63**, i4–6.
- Berdonosov, P.S., Olenov, A.V. and Dolgikh, V.A. (2009) Strontium–copper selenite–chlorides: Synthesis and structural investigation. *Journal of Solid State Chemistry*, **182**, 2368–2373.
- Berdonosov, P.S., Janson, O., Olenov, A.V., Krivovichev, S.V., Rosner, H., Dolgikh, V.A. and Tsirlin, A.A. (2013) Crystal structures and variable magnetism of  $\text{PbCu}_2(\text{XO}_3)_2\text{Cl}_2$  with  $X = \text{Se}, \text{Te}$ . *Dalton transactions*, **42**, 9547–9554.
- Brese, N.E. and O’Keeffe, M. (1991) Bond-valence parameters for solids. *Acta Crystallographica*, **B47**, 192–197.
- Burns, P.C. and Hawthorne, F.C. (1995a) Coordination-geometry pathways in  $\text{Cu}^{2+}$  oxysalt minerals. *The Canadian Mineralogist*, **33**, 889–905.

- Burns, P.C. and Hawthorne, F.C. (1995b) Mixed-ligand  $\text{Cu}^{2+}\Phi_6$  octahedra in minerals: observed stereochemistries and HartreFock calculations. *The Canadian Mineralogist*, **33**, 1177–1188.
- Burns, P.C., Krivovichev, S.V. and Filatov, S.K. (2002) New  $\text{Cu}^{2+}$  coordination polyhedra in the crystal structure of burnsite,  $\text{KCdCu}_7\text{O}_2(\text{SeO}_3)_2\text{Cl}_9$ . *The Canadian Mineralogist*, **40**, 1587–1595.
- Burrows, A.D., Mahon, M.F., Sebestyen, V.M., Lan, Y. and Powell, A.K. (2012) Synthesis, structures, and magnetic behavior of new anionic copper(II) sulfate aggregates and chains. *Inorganic Chemistry*, **51**, 10983–10989.
- Effenberger, H. and Pertlik, F. (1986) Die Kristallstrukturen der Kupfer(II)-oxo-selenite  $\text{Cu}_2\text{O}(\text{SeO}_3)$  (kubisch und monoklin) und  $\text{Cu}_4\text{O}(\text{SeO}_3)_3$  (monoklin und triklin). *Monatshefte für Chemie*, **117**, 887–896.
- Filatov, S.K., Semenova, T.F. and Vergasova, L.P. (1992) Types of polymerization of  $[\text{OCu}_4]^{6+}$  in inorganic compounds with “additional” oxygen atoms. *Doklady Akademii Nauk SSSR (in Russian)*, **322**, 539–539.
- Krivovichev, S.V., Vergasova, L.P., Starova, G.L., Filatov, S.K., Britvin, S.N., Roberts, A.C. and Steele, I.M. (2002) Burnsite,  $\text{KCdCu}_7\text{O}_2(\text{SeO}_3)_2\text{Cl}_9$ , a New Mineral Species from the Tolbachik Volcano, Kamchatka Peninsula, Russia. *The Canadian Mineralogist*, **40**, 1171–1175.
- Krivovichev, S.V., Filatov, S.K., Burns, P.C. and Vergasova, L.P. (2007) The crystal structure of parageorgbokiite,  $\beta\text{-Cu}_5\text{O}_2(\text{SeO}_3)_2\text{Cl}_2$ . *The Canadian Mineralogist*, **45**, 929–934.
- Krivovichev, S.V. and Filatov, S.K. (1999) Structural principles for minerals and inorganic compounds containing anion-centered tetrahedra. *American Mineralogist*, **84**, 1099–1106.
- Krivovichev, S.V., Shuvalov, R.R., Semenova, T.F. and Filatov, S.K. (1999a) Crystal chemistry of inorganic compounds based on chains of oxocentered tetrahedra. III. Crystal structure of georgbokiite,  $\text{Cu}_5\text{O}_2(\text{SeO}_3)_2\text{Cl}_2$ . *Zeitschrift für Kristallographie*, **214**, 135–138.
- Krivovichev, S.V., Starova, G.L. and Filatov, S.K. (1999b) ‘Face-to-face’ relationships between oxocentred tetrahedra and cation-centred tetrahedral oxyanions in crystal structures of minerals and inorganic compounds. *Mineralogical Magazine*, **63**, 263–266.
- Krivovichev, S.V., Filatov, S.K., Armbruster, T. and Pankratova, O.Y. (2004) Crystal structure of  $\text{Cu}(\text{I})\text{Cu}(\text{II})_4\text{O}(\text{SeO}_3)\text{Cl}_5$ , a new heterovalent copper compound. *Doklady Chemistry*, **399**, 226–228.
- Krivovichev, S.V., Filatov, S.K., Burns, P.C. and Vergasova, L.P. (2006) The crystal structure of allochalcoseelite,  $\text{Cu}^+\text{Cu}^{2+}_5\text{PbO}_2(\text{SeO}_3)_2\text{Cl}_5$ , A mineral with well-defined  $\text{Cu}^+$  and  $\text{Cu}^{2+}$  positions. *The Canadian Mineralogist*, **44**, 507–514.
- Krivovichev, S.V., Filatov, S.K. and Vergasova, L.P. (2012) The crystal structure of ilinskite,  $\text{NaCu}_5\text{O}_2(\text{SeO}_3)_2\text{Cl}_3$ , and review of mixed-ligand  $\text{CuO}_m\text{Cl}_n$  coordination geometries in minerals and inorganic compounds. *Mineralogy and Petrology*, **107**, 235–242.
- Krivovichev, S.V., Mentré, O., Siidra, O.I., Colmont, M. and Filatov, S.K. (2013) Anion-centered tetrahedra in inorganic compounds. *Chemical Reviews*, **113**, 6459–6535.
- Mao, J.-G., Jiang, H.-L. and Kong, F. (2008) Structures and properties of functional metal selenites and tellurites. *Inorganic Chemistry*, **47**, 8498–8510.
- Melník, M., Koman, M. and Ondrejovič, G. (2011) Tetramers  $\text{Cu}_4(\mu_4\text{-O})(\eta\text{-X})_6(\text{L}_4)$ : Analysis of structural data. *Coordination Chemistry Reviews*, **255**, 1581–1586.



- Millet, P., Bastide, B., Pashchenko, V., Gnatchenko, S., Gapon, V., Ksari, Y. and Stepanov, A. (2001) Syntheses, crystal structures and magnetic properties of francisite compounds  $\text{Cu}_3\text{Bi}(\text{SeO}_3)_2\text{O}_2\text{X}$  ( $\text{X} = \text{Cl}, \text{Br}$  and  $\text{I}$ ). *Journal of Materials Chemistry*, **11**, 1152–1157.
- Pekov, I.V., Zelenski, M.E., Yapaskurt, V.O., Polekhovskiy, Y.S. and Murashko, M.N. (2013a): Starovaite,  $\text{KCu}_5\text{O}(\text{VO}_4)_3$ , a new mineral from fumarole sublimates of the Tolbachik volcano, Kamchatka, Russia. *European Journal of Mineralogy*, **25**, 91-96.
- Pekov, I.V., Zubkova, N.V., Zelenski, M.E., Yapaskurt, V.O., Polekhovskiy, Yu.S., Fadeeva, O.A. and Pushcharovskiy, D.Yu. (2013b): Yaroshevskite,  $\text{Cu}_9\text{O}_2(\text{VO}_4)_4\text{Cl}_2$ , a new mineral from the Tolbachik volcano, Kamchatka, Russia. *Mineralogical Magazine*, **77**, 107-116.
- Pertlik, F. and Zemann, J. (1988) The crystal structure of nabokoite,  $\text{Cu}_7\text{TeO}_4(\text{SO}_4)_5\text{KCl}$ : The first example of a  $\text{Te}(\text{IV})\text{O}_4$  pyramid with exactly tetragonal symmetry. *Mineralogy and Petrology*, **38**, 291–298.
- Pring, A., Gatehouse, B.M. and Birch, W.D. (1990) Francisite,  $\text{Cu}_3\text{Bi}(\text{SeO}_3)_2\text{O}_2\text{Cl}$ , a new mineral from Iron Monarch, South Australia: Description and crystal structure. *American Mineralogist*, **75**, 1421–1425.
- Rosner, H., Johannes, M.D., Drechsler, S.-L., Schmitt, M., Janson, O., Schnelle, W., Liu, W., Huang, Y.-X. and Kniep, R. (2007)  $\text{Cu}^{\text{II}}$  materials – from crystal chemistry to magnetic model compounds. *Science and Technology of Advanced Materials*, **8**, 352–356.
- Scordari, F. and Stasi, F. (1990) The crystal structure of euchlorine,  $\text{NaKCu}_3\text{O}(\text{SO}_4)_3$ . *Neues Jahrbuch für Mineralogie Abhandlungen*, **161**, 241–253.
- Sheldrick, G.M. (2008) A short history of SHELX. *Acta Crystallographica*, **A64**, 112–22.
- Shuvalov, R.R., Vergasova, L.P., Semenova, T.F., Filatov, S.K., Krivovichev, S.V., Siidra, O.I. and Rudashevskiy, N.S. (2013) Prewittite,  $\text{KPb}_{1.5}\text{Cu}_6\text{Zn}(\text{SeO}_3)_2\text{O}_2\text{Cl}_{10}$ , a new mineral from Tolbachik fumaroles, Kamchatka peninsula, Russia: Description and crystal structure. *American Mineralogist*, **98**, 463–469.
- Starova, G.L., Filatov, S.K. and Vergasova, L.P. (1991) The crystal structure of fedotovite,  $\text{K}_2\text{Cu}_3\text{O}(\text{SO}_4)_3$ . *Mineralogical Magazine*, **55**, 613–616.
- Varaksina, T.V., Fundamenskiy, V.S., Filatov, S.K. and Vergasova, L.P. (1990) The crystal structure of kamchatkite, a new naturally occurring oxychloride sulphate of potassium and copper. *Mineralogical Magazine*, **54**, 613–616.
- Vergasova, L.P., Semenova, T.F., Shuvalov, R.R., Filatov, S.K. and Ananiev, V.V. (1997) Ilinskite  $\text{NaCu}_5\text{O}_2(\text{SeO}_3)_2\text{Cl}_3$  - a new mineral of volcanic exhalations. *Doklady Akademii Nauk SSSR (in Russian)*, **353**, 641–644.
- Vergasova, L.P., Krivovichev, S.V., Semenova, T.F., Filatov, S.K. and Ananiev, V.V. (1999) Chloromenite,  $\text{Cu}_9\text{O}_2(\text{SeO}_3)_4\text{Cl}_6$ , a new mineral from the Tolbachik Volcano, Kamchatka, Russia. *European Journal of Mineralogy*, **11**, 119–123.
- Vergasova, L.P., Semenova, T.F., Krivovichev, S.V., Filatov, S.K., Zolotarev Jr, A.A. and Ananiev, V.V. (2014) Nicksobolevite,  $\text{Cu}_7(\text{SeO}_3)_2\text{O}_2\text{Cl}_6$ , a new complex copper oxoselenite chloride from Tolbachik fumaroles, Kamchatka peninsula, Russia. *European Journal of Mineralogy*, **26**, 439–449.
- Zhang, D., Berger, H., Kremer, R.K., Wulferding, D., Lemmens, P. and Johnsson, M. (2010) Synthesis, crystal structure, and magnetic properties of the copper selenite chloride  $\text{Cu}_5(\text{SeO}_3)_4\text{Cl}_2$ . *Inorganic Chemistry*, **49**, 9683–8.

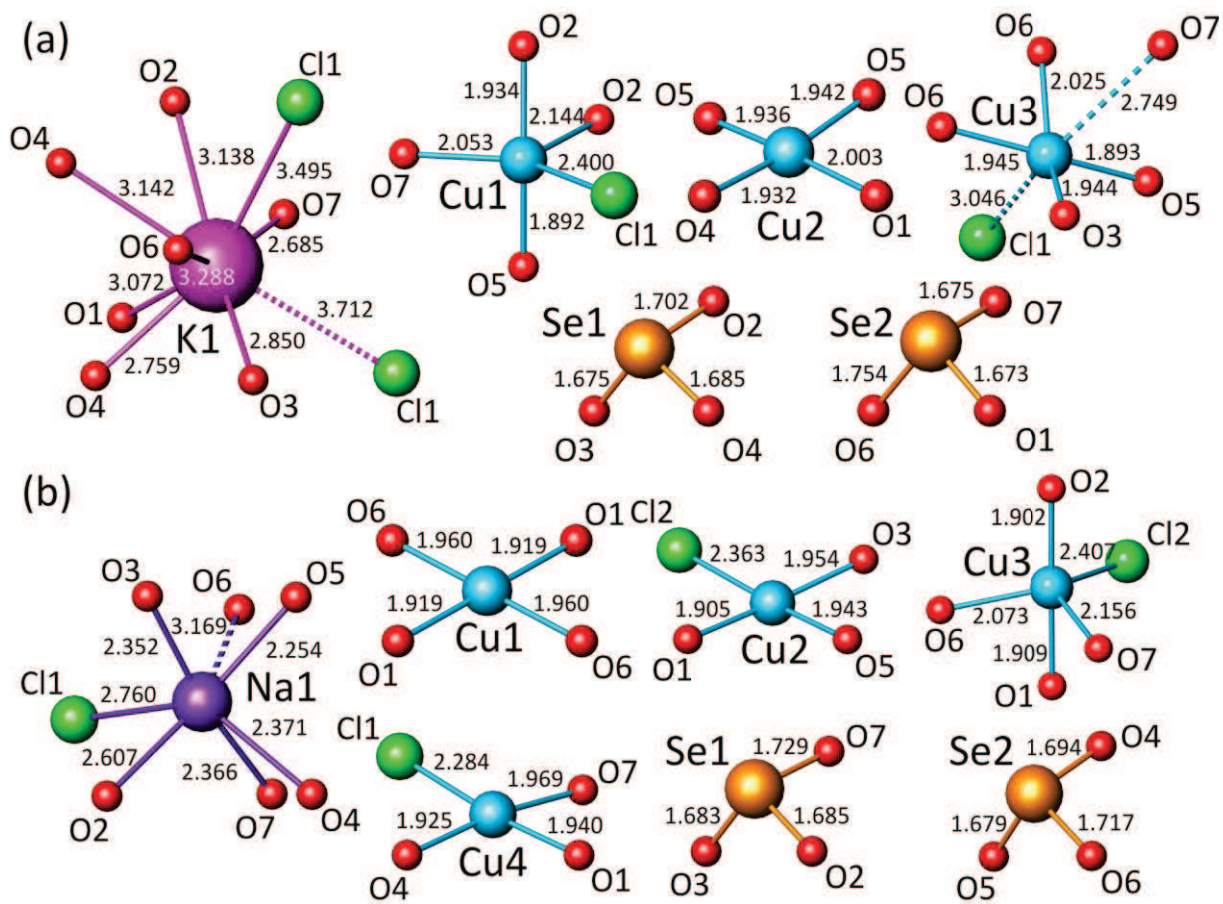


**Fig. 1.** Coordination of cations in the crystal structures of  $K[Cu_3O](SeO_3)_2Cl$  (a) and  $Na_2[Cu_7O_2](SeO_3)_4Cl_4$  (b). Legend:  $K^+$  = pink;  $Cu^{2+}$  = cyan;  $Se^{4+}$  = orange;  $O^{2-}$  = red;  $Cl^-$  = green.

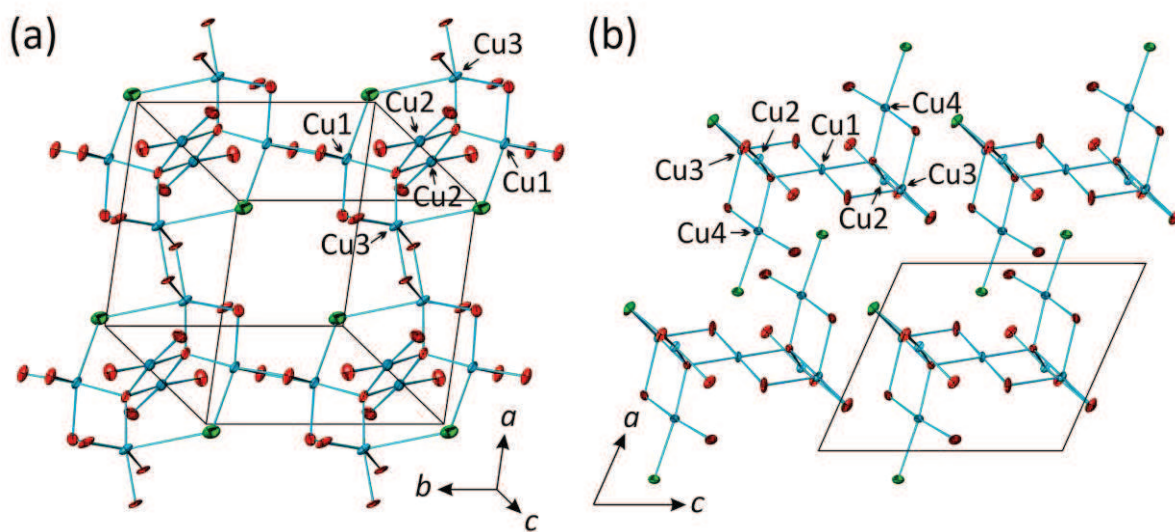


**Fig. 2.** Mode of linkage of the Cu coordination polyhedra in the crystal structures of  $K[Cu_3O](SeO_3)_2Cl$  (a) and  $Na_2[Cu_7O_2](SeO_3)_4Cl_4$  (b). Legend:  $Cu^{2+}$  = cyan;  $O^{2-}$  = red;  $Cl^-$  = green. Displacement ellipsoids are drawn at 50 % probability level.

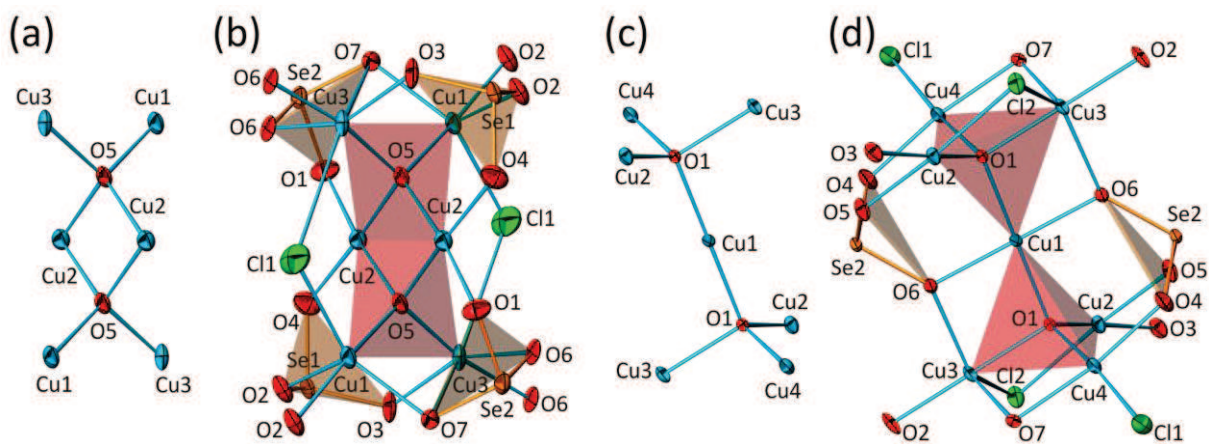


**Fig. 3.** Structural units based upon oxocentered  $(OCu_4)^{6+}$  tetrahedra and their environment in the crystal structures of  $Na_2[Cu_7O_2](SeO_3)_4Cl_4$  (a, b) and  $K[Cu_3O](SeO_3)_2Cl$  (c, d). Legend as in Fig. 2. Displacement ellipsoids are drawn at 50 % probability level.

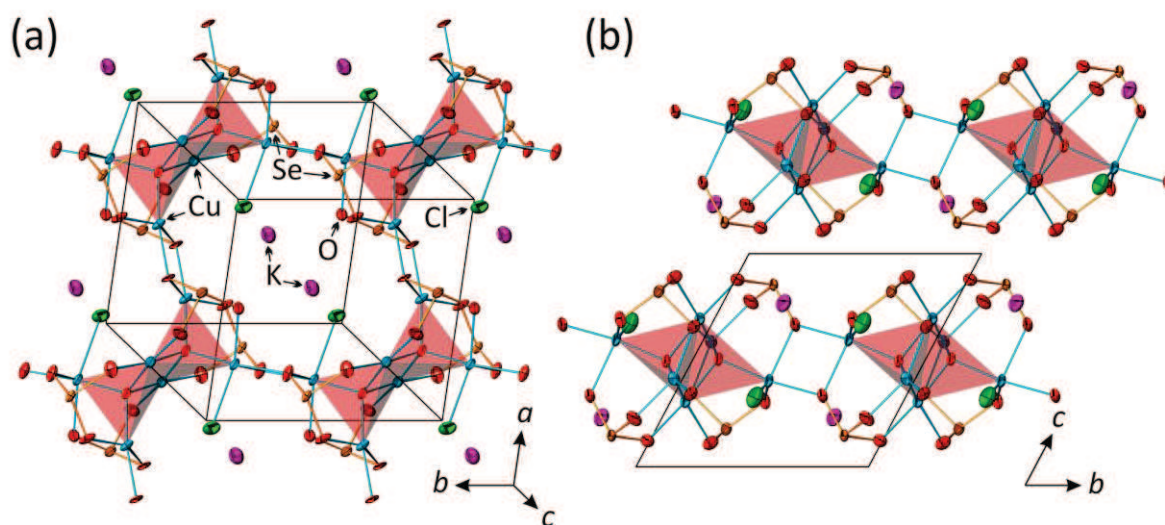


**Fig. 4.** The crystal structures of  $\text{K}[\text{Cu}_3\text{O}](\text{SeO}_3)_2\text{Cl}$  in two different projections. Legend:  $\text{K}^+$  = pink;  $\text{Cu}^{2+}$  = cyan;  $\text{Se}^{4+}$  = orange;  $\text{O}^{2-}$  = red;  $\text{Cl}^-$  = green; the  $[\text{OCu}_4]^{6+}$  tetrahedra are highlighted by red. K–O, K–Cl and Cu–Cl bonds are omitted for clarity. Displacement ellipsoids are drawn at 50 % probability level.

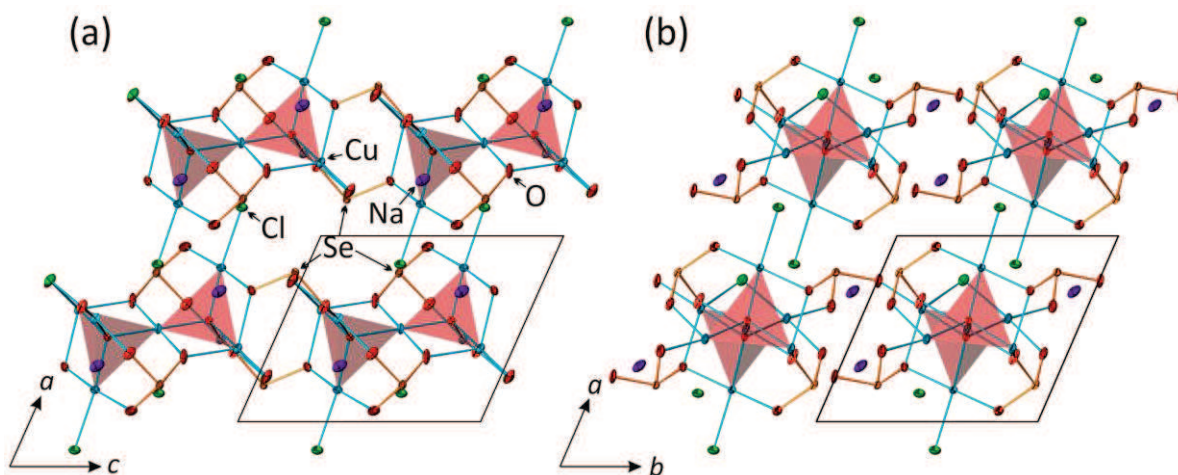


**Fig. 5.** The crystal structure of  $\text{Na}_2[\text{Cu}_7\text{O}_2](\text{SeO}_3)_4\text{Cl}_4$  projected along the  $b$  (a) and  $c$  (b) axes. Legend as in Fig. 4. Na–O, Na–Cl and Cu–Cl bonds are omitted for clarity. Displacement ellipsoids are drawn at 50 % probability level.

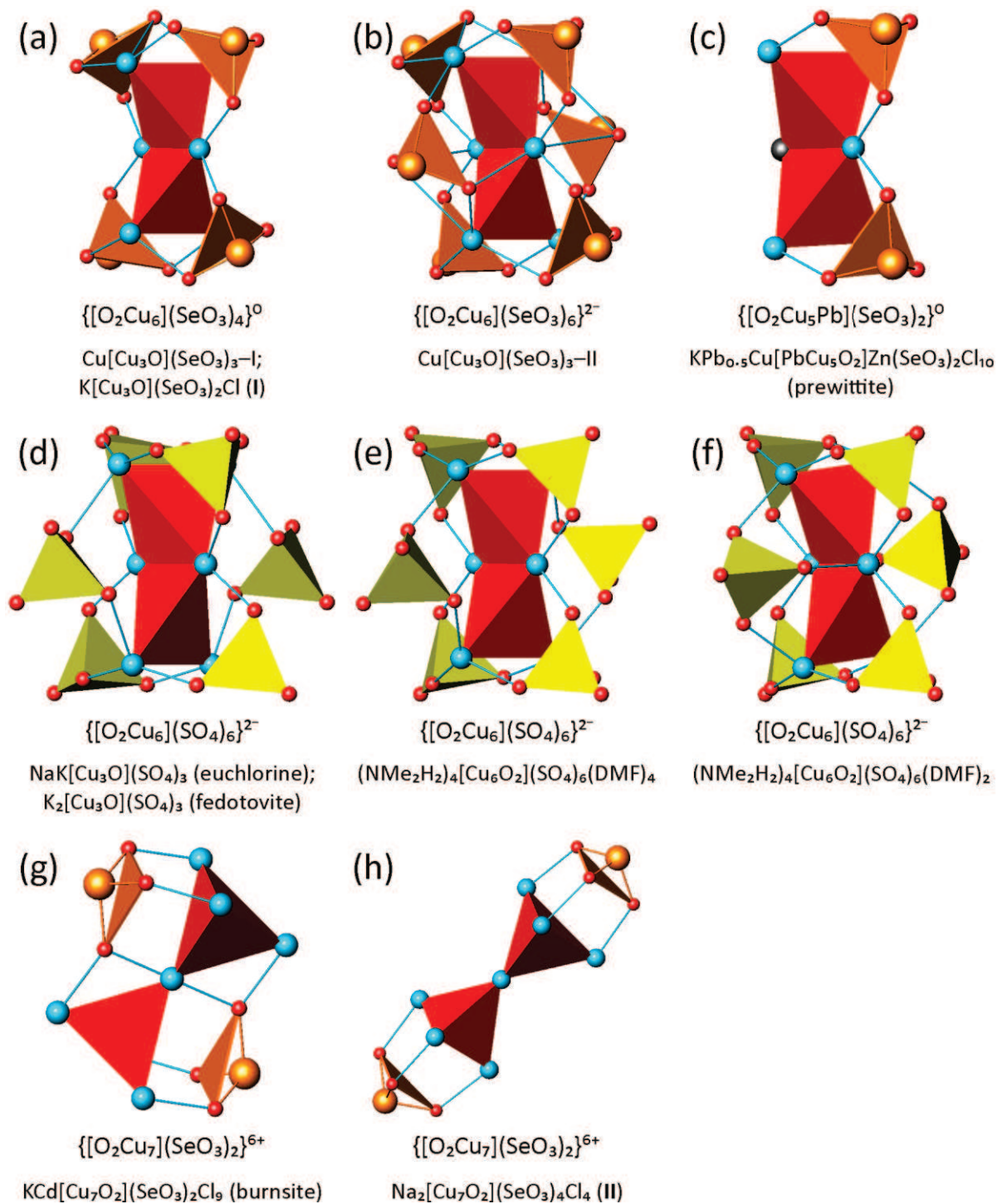


**Fig. 6.** Coordination environment of the dimers composed of  $[OCu_4]^{6+}$  tetrahedra in the crystal structures of different minerals and synthetic compounds. See text for details.

Table 1. Crystallographic data and refinement parameters for **I** and **II**.

	K[Cu <sub>3</sub> O](SeO <sub>3</sub> ) <sub>2</sub> Cl	Na <sub>2</sub> [Cu <sub>7</sub> O <sub>2</sub> ](SeO <sub>3</sub> ) <sub>4</sub> Cl <sub>4</sub>
<b>Crystal data</b>		
Crystal system	triclinic	triclinic
Space group	<i>P</i> -1	<i>P</i> -1
Unit-cell dimensions <i>a</i> , <i>b</i> , <i>c</i> (Å), <i>α</i> , <i>β</i> , <i>γ</i> (°)	7.6821(5), 8.1179(5), 8.7836(6), 113.193(3), 108.735(4), 98.245(4)	7.4362(6), 8.3361(7), 9.1343(11), 110.277(6), 106.212(6), 105.158(4)
Unit-cell volume (Å <sup>3</sup> )	453.32(5)	467.94(8)
<i>Z</i>	2	1
Calculated density (g/cm <sup>3</sup> )	3.920	4.160
Absorption coefficient (mm <sup>-1</sup> )	15.757	16.263
Crystal size (mm)	0.13×0.09×0.07	0.25×0.21×0.20
<b>Data collection</b>		
Temperature	293 K	293 K
Radiation, wavelength (Å)	MoK <sub>α</sub> , 0.71073	MoK <sub>α</sub> , 0.71073
<i>F</i> (000)	494	541
θ range (°)	2.95 – 27.46	2.60 – 30.52
<i>h</i> , <i>k</i> , <i>l</i> ranges	-8→9, -10→6, -11→10	-10→10, -11→11, -12→13
Total reflections collected	5607	11190
Unique reflections ( <i>R</i> <sub>int</sub> )	1749 (0.0501)	2842 (0.0474)
Unique reflections <i>F</i> >4σ <sub><i>F</i></sub>	1210	2498
<b>Structure refinement</b>		
Refinement method	Full-matrix least-squares on <i>F</i> <sup>2</sup>	Full-matrix least-squares on <i>F</i> <sup>2</sup>
Weighting coefficients <i>a</i> , <i>b</i> *	0.0766, 0.0	0.0202, 0.0999
Extinction coefficient	0.0046(13)	0.0069(5)
Data/restraints/parameters	1749/0/128	2842/0/143
<i>R</i> <sub>1</sub> [ <i>F</i> >4σ <sub><i>F</i></sub> ], <i>wR</i> <sub>2</sub> [ <i>F</i> >4σ <sub><i>F</i></sub> ]	0.0481, 0.1170	0.0265, 0.0601
<i>R</i> <sub>1</sub> all, <i>wR</i> <sub>2</sub> all	0.0800, 0.1328	0.0322, 0.0621
Goodness-of-fit on <i>F</i> <sup>2</sup>	1.014	1.070
Largest diff. peak and hole	1.620, -1.617 e Å <sup>-3</sup>	0.851, -0.954 e Å <sup>-3</sup>

$R_{\text{int}} = \sum |F_o^2 - F_o^2(\text{mean})| / \sum [F_o^2]$ .  $\text{GoF} = S = \{ \sum [w(F_o^2 - F_c^2)^2] / (n-p) \}^{1/2}$  where *n* = no. of reflections, *p* = no. of refined parameters.  $R_1 = \sum |F_o| - |F_c| / \sum |F_o|$ .  $wR_2 = \{ \sum [w(F_o^2 - F_c^2)^2] / \sum [w(F_o^2)^2] \}^{1/2}$ .  $w^* = 1 / [\sigma^2(F_o^2) + (aP)^2 + bP]$  where *P* is  $[2F_c^2 + \text{Max}(F_o^2, 0)] / 3$ .



Table 2. Coordinates and displacement parameters ( $\text{\AA}^2$ ) of atoms in the structure of  $\text{K}[\text{Cu}_3\text{O}](\text{SeO}_3)_2\text{Cl}$ .

Atom	$x$	$y$	$z$	$U_{\text{iso}}$	$U_{11}$	$U_{22}$	$U_{33}$	$U_{12}$	$U_{13}$	$U_{23}$
Se1	1.23517(15)	1.17635(13)	0.64629(15)	0.0174(3)	0.0193(6)	0.0140(5)	0.0202(6)	0.0009(4)	0.0090(5)	0.0102(5)
Se2	0.71723(15)	0.69809(14)	0.67694(15)	0.0189(3)	0.0198(6)	0.0162(5)	0.0215(6)	0.0024(4)	0.0119(5)	0.0082(5)
Cu1	0.49212(18)	0.62544(17)	0.90290(18)	0.0192(4)	0.0216(8)	0.0128(6)	0.0247(8)	0.0014(5)	0.0122(7)	0.0096(6)
Cu2	1.46001(18)	0.93661(17)	0.80631(18)	0.0186(4)	0.0211(8)	0.0157(6)	0.0217(8)	0.0048(6)	0.0113(6)	0.0096(6)
Cu3	1.12983(18)	1.03779(18)	0.91313(19)	0.0204(4)	0.0179(8)	0.0221(7)	0.0228(8)	-0.0004(6)	0.0105(6)	0.0125(6)
K1	0.7620(4)	0.2614(4)	0.7322(4)	0.0354(7)	0.0420(18)	0.0280(14)	0.0405(17)	0.0170(13)	0.0221(15)	0.0139(13)
Cl1	0.1696(4)	0.6465(5)	0.8255(5)	0.0419(9)	0.0211(17)	0.0347(17)	0.060(2)	0.0014(13)	0.0139(16)	0.0175(17)
O1	0.5028(10)	0.7348(10)	0.6123(11)	0.0265(18)	0.020(4)	0.025(4)	0.026(4)	0.008(3)	0.005(4)	0.008(4)
O2	1.4202(11)	1.3595(10)	0.8331(11)	0.0266(18)	0.039(5)	0.020(4)	0.025(4)	0.005(4)	0.014(4)	0.015(4)
O3	1.0784(10)	1.1176(11)	0.7258(11)	0.0264(18)	0.018(4)	0.036(5)	0.027(5)	-0.001(4)	0.009(4)	0.020(4)
O4	1.3468(11)	1.0094(11)	0.6216(10)	0.0274(18)	0.038(5)	0.027(4)	0.021(4)	0.014(4)	0.012(4)	0.014(4)
O5	1.4020(10)	1.1104(9)	0.9949(10)	0.0176(16)	0.022(4)	0.010(3)	0.023(4)	0.003(3)	0.013(3)	0.008(3)
O6	0.8557(9)	0.9306(10)	0.8422(10)	0.0198(16)	0.008(4)	0.019(4)	0.025(4)	-0.005(3)	0.007(3)	0.008(3)
O7	0.7045(11)	0.5981(10)	0.8090(11)	0.0251(18)	0.036(5)	0.025(4)	0.037(5)	0.019(4)	0.028(4)	0.022(4)

Table 3. Coordinates and displacement parameters ( $\text{\AA}^2$ ) of atoms in the structure of  $\text{Na}_2[\text{Cu}_7\text{O}_2](\text{SeO}_3)_4\text{Cl}_4$ .

Atom	$x$	$y$	$z$	$U_{\text{eq}}$	$U_{11}$	$U_{22}$	$U_{33}$	$U_{12}$	$U_{13}$	$U_{23}$
Se1	0.80394(5)	0.70487(4)	0.03921(4)	0.00933(9)	0.01006(16)	0.00726(15)	0.00905(15)	0.00281(12)	0.00426(12)	0.00214(12)
Se2	0.19751(5)	0.58188(4)	0.38951(4)	0.01030(9)	0.01288(16)	0.00626(15)	0.00850(15)	0.00156(12)	0.00387(12)	0.00191(12)
Cu1	1/2	0	1/2	0.01074(12)	0.0159(3)	0.0073(3)	0.0074(2)	0.0024(2)	0.0058(2)	0.0024(2)
Cu2	0.44487(6)	0.16460(5)	0.22254(5)	0.01188(10)	0.0153(2)	0.00841(19)	0.01058(18)	0.00455(16)	0.00297(15)	0.00480(15)
Cu3	0.39381(6)	0.75727(5)	0.13594(5)	0.01176(10)	0.0152(2)	0.00709(18)	0.00861(18)	0.00344(15)	0.00260(15)	0.00141(15)
Cu4	0.82861(6)	0.05631(5)	0.35240(5)	0.01161(10)	0.00888(18)	0.00882(19)	0.01261(19)	0.00299(15)	0.00376(14)	0.00093(15)
Cl1	0.15293(12)	0.09108(12)	0.37902(10)	0.01866(18)	0.0110(4)	0.0195(4)	0.0193(4)	0.0053(3)	0.0051(3)	0.0036(3)
Cl2	0.23806(12)	-0.11216(11)	-0.03503(10)	0.01686(17)	0.0189(4)	0.0131(4)	0.0135(3)	0.0035(3)	0.0017(3)	0.0064(3)
Na1	0.7002(2)	0.59122(19)	0.31681(18)	0.0223(3)	0.0213(7)	0.0159(7)	0.0211(7)	-0.0011(6)	0.0008(6)	0.0117(6)
O1	0.5442(3)	0.0106(3)	0.3057(3)	0.0084(4)	0.0097(10)	0.0063(10)	0.0092(10)	0.0031(8)	0.0045(8)	0.0029(8)
O2	0.7574(4)	0.4941(3)	0.0353(3)	0.0170(5)	0.0261(13)	0.0071(10)	0.0092(10)	0.0067(10)	-0.0002(9)	0.0002(9)
O3	0.3796(4)	0.3415(3)	0.1450(3)	0.0166(5)	0.0238(13)	0.0119(11)	0.0120(11)	0.0077(10)	0.0038(9)	0.0055(9)
O4	0.0590(3)	0.6979(3)	0.4600(3)	0.0184(5)	0.0134(11)	0.0121(11)	0.0184(11)	0.0034(9)	0.0034(9)	-0.0013(10)
O5	0.6337(4)	0.3922(3)	0.4289(3)	0.0168(5)	0.0219(12)	0.0087(11)	0.0142(11)	0.0041(10)	0.0015(9)	0.0054(9)
O6	0.3492(4)	0.7335(3)	0.3429(3)	0.0182(5)	0.0319(14)	0.0086(11)	0.0106(10)	0.0013(10)	0.0118(10)	0.0031(9)
O7	0.7057(3)	0.7911(3)	0.1854(3)	0.0114(4)	0.0134(11)	0.0095(10)	0.0120(10)	0.0051(9)	0.0076(9)	0.0033(9)

Table 4. Selected bond lengths (Å) in the structure of  $\text{K}[\text{Cu}_3\text{O}](\text{SeO}_3)_2\text{Cl}$ .

K1–O7	2.685(7)	Cu2–O1 <sup>iv</sup>	2.003(8)
K1–O4 <sup>v</sup>	2.759(8)		
K1–O3 <sup>vi</sup>	2.850(8)	Cu3–O5	1.893(7)
K1–O1 <sup>vii</sup>	3.072(8)	Cu3–O3	1.944(7)
K1–O2 <sup>ii</sup>	3.138(8)	Cu3–O6	1.945(7)
K1–O4 <sup>ii</sup>	3.142(8)	Cu3–O6 <sup>i</sup>	2.025(7)
K1–O6 <sup>vi</sup>	3.288(7)	Cu3–O7 <sup>i</sup>	2.749(8)
K1–Cl1 <sup>viii</sup>	3.495(5)	Cu3–Cl1	3.046(8)
K1–Cl1 <sup>iv</sup>	3.712(4)		
		Se1–O3	1.675(7)
Cu1–O5 <sup>i</sup>	1.892(6)	Se1–O4	1.685(8)
Cu1–O2 <sup>ii</sup>	1.934(7)	Se1–O2	1.702(8)
Cu1–O7	2.053(7)	<Se1–O>	1.687
Cu1–O2 <sup>i</sup>	2.144(8)		
Cu1–Cl1	2.400(3)	Se2–O1	1.673(7)
		Se2–O7	1.675(7)
Cu2–O4	1.932(7)	Se2–O6	1.754(7)
Cu2–O5	1.936(7)	<Se2–O>	1.701
Cu2–O5 <sup>iii</sup>	1.942(7)		

Symmetry codes: (i)  $-x+2, -y+2, -z+2$ ; (ii)  $x-1, y-1, z$ ; (iii)  $-x+3, -y+2, -z+2$ ; (iv)  $x+1, y, z$ ; (v)  $-x+2, -y+1, -z+1$ ; (vi)  $x, y-1, z$ ; (vii)  $-x+1, -y+1, -z+1$ ; (viii)  $-x+1, -y+1, -z+2$ .

Table 5. Selected bond lengths (Å) in the structure of Na<sub>2</sub>[Cu<sub>7</sub>O<sub>2</sub>](SeO<sub>3</sub>)<sub>4</sub>Cl<sub>4</sub>.

Na1–O5	2.253(3)	Cu3–O1 <sup>v</sup>	1.909(2)
Na1–O3	2.352(3)	Cu3–O6	2.073(2)
Na1–O7	2.365(3)	Cu3–O7	2.156(2)
Na1–O4 <sup>vi</sup>	2.371(3)	Cu3–Cl2 <sup>v</sup>	2.4067(9)
Na1–O2	2.607(3)		
Na1–Cl1 <sup>ii</sup>	2.7603(16)	Cu4–O4 <sup>ii</sup>	1.925(2)
Na1–O6	3.169(3)	Cu4–O1	1.940(2)
		Cu4–O7 <sup>iv</sup>	1.969(2)
Cu1–O1	1.919(2)	Cu4–Cl1 <sup>vi</sup>	2.2842(9)
Cu1–O1 <sup>iii</sup>	1.919(2)		
Cu1–O6 <sup>ii</sup>	1.960(2)	Se1–O2	1.685(2)
Cu1–O6 <sup>iv</sup>	1.960(2)	Se1–O3 <sup>i</sup>	1.683(2)
		Se1–O7	1.729(2)
Cu2–O1	1.905(2)	<Se1–O>	1.699
Cu2–O5	1.943(2)		
Cu2–O3	1.954(2)	Se2–O5 <sup>ii</sup>	1.679(2)
Cu2–Cl2	2.3633(9)	Se2–O4	1.694(2)
		Se2–O6	1.717(2)
Cu3–O2 <sup>i</sup>	1.902(2)	<Se2–O>	1.697

Symmetry codes: (i)  $-x+1, -y+1, -z$ ; (ii)  $-x+1, -y+1, -z+1$ ; (iii)  $-x+1, -y, -z+1$ ; (iv)  $x, y-1, z$ ; (v)  $x, y+1, z$ ; (vi)  $x+1, y, z$ .

Table 6. Bond-valence analysis (in valence units = v.u.) for the structures of  $\text{K}[\text{Cu}_3\text{O}](\text{SeO}_3)_2\text{Cl}$ . The italicized values in brackets are given for interatomic distances that are not considered as bonds, and do not sum up in total.

	O1	O2	O3	O4	O5	O6	O7	Cl1	$\Sigma$
K1	0.08	0.07	0.14	0.18, 0.07		<i>(0.04)</i>	0.22	0.08, 0.05	0.89
Cu1		0.50, 0.28			0.56		0.36	0.34	2.04
Cu2	0.42			0.50	0.50, 0.49				1.91
Cu3			0.49		0.56	0.49, 0.39	0.06	0.06	2.05
Se1		1.34	1.44	1.41					4.19
Se2	1.45					1.17	1.44		4.06
$\Sigma$	1.95	2.19	2.07	2.16	2.11	2.05	2.08	0.53	

Table 7. Bond-valence analysis (in valence units = v.u.) for the structures of Na<sub>2</sub>[Cu<sub>7</sub>O<sub>2</sub>](SeO<sub>3</sub>)<sub>4</sub>Cl<sub>4</sub>. The italicized values in brackets are given for interatomic distances that are not considered as bonds, and do not sum up in total.

	O1	O2	O3	O4	O5	O6	O7	Cl1	Cl2	Σ
Na1		0.11	0.23	0.22	0.30	<i>(0.02)</i>	0.22	0.23		1.31
Cu1	0.52 <sup>2x→</sup>					0.47 <sup>2x→</sup>				1.98
Cu2	0.54		0.48		0.49				0.37	1.88
Cu3	0.54	0.55				0.34	0.28		0.33	2.04
Cu4	0.49			0.51			0.46	0.46		1.92
Se1		1.41	1.41				1.25			4.07
Se2				1.37	1.43	1.29				4.09
Σ	2.09	2.07	2.12	2.10	2.22	2.10	2.21	0.69	0.70	

Table 8. Crystallographic data for minerals and inorganic copper compounds based upon dimers composed of  $[\text{OCu}_4]^{6+}$  tetrahedra.

O:Cu	Chemical formula	Mineral name	Space group	$a$ (Å); $\alpha$ (°)	$b$ (Å); $\beta$ (°)	$c$ (Å); $\gamma$ (°)	$V$ (Å <sup>3</sup> )	Ref.
2:6	$\text{NaK}[\text{Cu}_3\text{O}](\text{SO}_4)_3$	euchlorine	$C2/c$	18.41	9.43; 113.7	14.21	2259	1
	$\text{K}_2[\text{Cu}_3\text{O}](\text{SO}_4)_3$	fedotovite	$C2/c$	19.037	9.479; 111.0	14.231	2397	2
	$\text{KPb}_{0.5}\text{Cu}[\text{PbCu}_5\text{O}_2]\text{Zn}(\text{SeO}_3)_2\text{Cl}_{10}$	prewittite	$Pnmm$	9.132	19.415	13.213	2343	3
	$\text{Cu}[\text{Cu}_3\text{O}](\text{SeO}_3)_3\text{--I}$		$P2_1/a$	15.990	13.518; 90.5	17.745	3836	4
	$\text{Cu}[\text{Cu}_3\text{O}](\text{SeO}_3)_3\text{--II}$		$P-1$	7.992; 77.3	8.141; 66.6	8.391; 81.4	484	4
	$\text{K}[\text{Cu}_3\text{O}](\text{SeO}_3)_2\text{Cl}$		$P-1$	7.682; 113.2	8.118; 108.7	8.784; 98.2	453	*
2:7	$\text{KCd}[\text{Cu}_7\text{O}_2](\text{SeO}_3)_2\text{Cl}_9$	burnsite	$P6_3/mmc$	8.781	8.781	15.521	1036	5
	$\text{Na}_2[\text{Cu}_7\text{O}_2](\text{SeO}_3)_4\text{Cl}_4$		$P-1$	7.436; 110.3	8.336; 106.2	9.134; 105.2	468	*

References: 1 – (Scordari and Stasi, 1990); 2 – (Starova *et al.*, 1991); 3 – (Shuvalov *et al.*, 2013); 4 – (Effenberger and Pertlik, 1986); 5 – (Burns *et al.*, 2002; Krivovichev *et al.*, 2002); \* – this work.







## ABSTRACT

This work deals with the synthesis and characterization of novel oxide materials containing selenium in the oxidation states of +4 or +6. The structural types occurring in 33 known oxoselenite minerals have an amazing variety, and cover the whole field from *0D* isolated complexes to *3D* frameworks, which offer unexploited potentialities in terms of physical properties. This thesis aims to synthesize and investigate new Se based compounds, essentially using methods inspired by mineralogical processes. Information based on original building units assembled into original architectures have been deduced and compared to related inorganic phases of the literature. In the present study, our innovative so-called “geo-inspired” approach is applied in order to obtain complex novel crystalline compounds. This approach assumes emulation and modelling of natural crystal growth processes. Herein, we used either a traditional descriptive procedure based on consideration of the crystal structures in terms of coordinations of cations, or the modern theory of anion-centered tetrahedra developed by the St. Petersburg school of crystallography and the UCCS group of solid-state chemistry in Lille, in cases when the traditional structural interpretation does not reflect basic principles of crystal chemistry. Thus, several metal-oxide chemical systems with  $\text{Se}^{4+/6+}$  and various metals ( $\text{Cu}^{+2+}$ ,  $\text{Ni}^{2+}$ ,  $\text{Co}^{2+}$ ,  $\text{V}^{4+/5+}$ ,  $\text{Mn}^{2+}$ ,  $\text{Fe}^{3+}$ ,  $\text{Pb}^{2+}$ ,  $\text{Bi}^{3+}$ ,  $\text{U}^{6+}$ ) were studied in the context of the present work. The thesis contains results of synthetic procedures, and crystal chemical characterization of 39 new metal selenites, selenates, and selenite-selenates. The analogy of selenite groups with phosphites was also investigated. Main results are described with references to more detailed publications given in the appendices.

## RÉSUMÉ

Ce manuscrit est consacré à la synthèse et la caractérisation de nouveaux matériaux d'oxyde à base de sélénium dans les états d'oxydation +4 ou +6. Les types structuraux rencontrés parmi les 33 oxy sélénites minéraux montrent une diversité structurale étonnante, et couvrent le champ des dimensionnalités *0D* à *3D*, offrant ainsi des potentialités inexploitées en termes des propriétés physiques. Cette thèse a visé la synthèse de l'étude de nouveaux composés du Se, en utilisant des méthodes de synthèse essentiellement inspirées des conditions de croissance des minéraux. Les informations basées sur l'assemblage de briques élémentaires originales dans des architectures structurales ont été déduites et comparées aux données de la littérature sur des phases proches. Lors de ce travail, notre approche « géo-inspirée » innovante été appliquée afin d'obtenir de nouveaux polytypes complexes. Nous avons donc utilisé des procédés simulant les conditions de croissance des minéraux. En termes de description, nous avons également utilisé soit le modèle « standard » basé sur l'examen des structures cristallines en termes de coordinations de cations, soit des outils plus modernes basés sur l'assemblage de tétraèdres anions-centrés développée par l'école de la cristallographie de Saint-Petersbourg et par le groupe de chimie du solide de l'UCCS, à Lille, et ce dans les cas où l'interprétation structurale traditionnelle ne reflète pas les principes de base de la cristalochimie. Finalement, plusieurs systèmes chimiques métal-oxyde avec du  $\text{Se}^{4+/6+}$  et divers métaux ( $\text{Cu}^{+2+}$ ,  $\text{Ni}^{2+}$ ,  $\text{Co}^{2+}$ ,  $\text{V}^{4+/5+}$ ,  $\text{Mn}^{2+}$ ,  $\text{Fe}^{3+}$ ,  $\text{Pb}^{2+}$ ,  $\text{Bi}^{3+}$ ,  $\text{U}^{6+}$ ) ont été étudiés dans le cadre de ce manuscrit. La thèse contient les résultats des procédures synthétiques et de la caractérisation cristalochimique des 39 nouveaux sélénites, sélénates et sélénite-sélénates des métaux. Les principaux résultats sont donnés et font référence aux publications plus détaillées données en annexe.